DECISION MAKING TOOLS FOR SUSTAINABLE TRANSITION TOWARD LOW CARBON ENERGY TECHNOLOGIES IN THE RESIDENTIAL SECTOR

Mohamed Abokersh

UNIVERSITAT ROVIRA i VIRGILI

Decision Making Tools for Sustainable Transition Toward Low Carbon Energy Technologies in the Residential Sector

Mohamed Hany Abokersh

DOCTORAL THESIS

2021

UNIVERSITAT ROVIRA I VIRGILI
DECISION MAKING TOOLS FOR SUSTAINABLE TRANSITION TOWARD LOW CARBON ENERGY TECHNOLOGIES IN THE RESIDENTIAL SECTOR
Mohamed Abokersh

UNIVERSITAT ROVIRA I VIRGILI
DECISION MAKING TOOLS FOR SUSTAINABLE TRANSITION TOWARD LOW CARBON ENERGY TECHNOLOGIES IN THE RESIDENTIAL SECTOR
Mohamed Abokersh

UNIVERSITAT ROVIRA I VIRGILI
DECISION MAKING TOOLS FOR SUSTAINABLE TRANSITION TOWARD LOW CARBON ENERGY TECHNOLOGIES IN THE RESIDENTIAL SECTOR
Mohamed Abokersh

Mohamed Hany Abokersh

Decision Making Tools for Sustainable Transition Toward Low Carbon Energy Technologies in the Residential Sector

Doctoral Thesis

Supervised by: Dr. Dieter Boer

Dr. Manel Vallès

Department of Mechanical Engineering

SUSCAPE Research Group

University of Rovira i Virgili

Tarragona

2021

UNIVERSITAT ROVIRA I VIRGILI
DECISION MAKING TOOLS FOR SUSTAINABLE TRANSITION TOWARD LOW CARBON ENERGY TECHNOLOGIES IN THE RESIDENTIAL SECTOR
Mohamed Abokersh

UNIVERSITAT ROVIRA I VIRGILI
DECISION MAKING TOOLS FOR SUSTAINABLE TRANSITION TOWARD LOW CARBON ENERGY TECHNOLOGIES IN THE RESIDENTIAL SECTOR
Mohamed Abokersh

UNIVERSITAT ROVIRA i VIRGILI

We state that the presented study, entitled, “Decision Making Tools for Sustainable Transition Toward Low Carbon Energy Technologies in the Residential Sector” Mohamed Hany Abokersh for the award of the degree of Doctor, has been carried out under our supervision at the Department of Mechanical Engineering of this university.

Tarragona, 23th February 2021

Doctoral Thesis Supervisor/s

Dr. Dieter Boer

UNIVERSITAT ROVIRA i VIRGILI
Firmado digitalmente por BOER DIETER THOMAS - X1992293X
Nombre de reconocimiento (DN): c=ES, serialNumber=IDCES-X1992293X, givenName=DIETER THOMAS, sn=BOER, cn=BOER DIETER THOMAS - X1992293X
Fecha: 2021.03.02 14:16:35 +01'00'

Dr. Dieter Boer

Dr. Manel Valles

VALLES RASQUERA JOAN MANEL - 39680747C
Firmado digitalmente por VALLES RASQUERA JOAN MANEL - 39680747C
Fecha: 2021.03.02 14:49:21 +01'00'

Dr. Manel Valles

UNIVERSITAT ROVIRA I VIRGILI
DECISION MAKING TOOLS FOR SUSTAINABLE TRANSITION TOWARD LOW CARBON ENERGY TECHNOLOGIES IN THE RESIDENTIAL SECTOR
Mohamed Abokersh

Acknowledgement

First and foremost, I would like to express my deepest gratitude to my supervisor Dr. Dieter Boer for giving me the opportunity to undertake my PhD research as a member of his group and for offering me his continuous support and vision through my research and thesis writing stages. Additionally, I would also like to express my greatest appreciation to my co-supervisor Dr. Manel Valles for his support, his patience and the invaluable advice he offered me at every stage of my PhD. The door to his office was always open and he always had time for me whenever I had a question about my research, my writing or any other minor or major issue that came to my mind.

During the course of my PhD research, I also received advice, guidance and help from a group of significant people to whom I am very grateful. Firstly, I would like to thank Dr. Victor Tulus for introducing me to the field of Climate Systems Modelling and pointing me towards climate change projection data. Additionally, I must thank Dr. Hatem Rashwan for supporting me by answering multiple questions I had regarding methodological and computational aspects of Machine learning.

My sincerest thanks go to Prof. Jose Caballero and Prof. Philip Griffiths for agreeing to participate as co-examiners in my Doctoral Examination and for offering their valuable comments on this PhD thesis. Additionally, I would like to thank Prof. Laureano Jiménez for chairing my PhD defense.

My deepest appreciation also goes to Dr. Marleen Spiekman and Dr. Linda Hoes from the building physics department in TNO, Delft who gave me the opportunity to work as a scientific researcher in their group. Working closely with them and the members of their research group was in many ways an immensely educational experience regarding the energy in buildings.

The support and the funding of this PhD research by the European Union's Horizon 2020 research and innovation programme under the Marie Skłodowska-Curie grant agreement No. 713679 and from the Universitat Rovira i Virgili (URV) is also appreciable.

I would also like to extend my warmest gratitude towards my parents, my wife Sara and the rest of my family who have been extremely supportive of me during all those years and they always were there for me whenever I needed them and whatever I needed them for.

Mohamed Hany Abokersh

Tarragona, February 2021

UNIVERSITAT ROVIRA I VIRGILI
DECISION MAKING TOOLS FOR SUSTAINABLE TRANSITION TOWARD LOW CARBON ENERGY TECHNOLOGIES IN THE RESIDENTIAL SECTOR
Mohamed Abokersh

UNIVERSITAT ROVIRA I VIRGILI
DECISION MAKING TOOLS FOR SUSTAINABLE TRANSITION TOWARD LOW CARBON ENERGY TECHNOLOGIES IN THE RESIDENTIAL SECTOR
Mohamed Abokersh

Summary

The global tendency for changing the world energy map is a booming topic, and more efforts should be scaled up to shift the current energy production systems towards the use of cleaner and less carbon-intensive sources. Currently, fossil fuels share about 80% of the primary energy use. The International Energy Outlook forecasts a significant increase in the world energy demand over the next decades. It is projected that global energy consumption will evolve by 48% in 2040 with a growth in the usage of crude oil and natural gas by 30% and 53.2%, respectively. This outlook trend leads to serious environmental problems such as more greenhouse gas (GHG) emissions and the subsequent impact on the climate.

Europe is one of the relevant players in this scenario contributing 21.6% to the overall energy consumption. Additionally, in the European Union (EU) the building stock accounts for about 40% of the total energy demand, while the residential sector consumes 63% of this energy. According to estimations of the US Energy Information Administration (EIA), the energy consumption demand for the residential section in the EU increases by an average of 0.9% per year. Along with all of these figures, the residential buildings are the fourth most important source of GHG in the EU, and it accounted for about 10% of the total GHG in 2016. In response to this challenge, the EU has adopted the 2020 climate and energy package which includes requisite legislation to tackle the environmental concerns and support the energy security and independence. The package sets three main targets: (i) reduce by 20% the GHG emissions compared to the 1990 levels, (ii) increase the renewable energy share and (iii) improve its energy efficiency by 20%. In 2013, the EU approved a new ambitious framework for the climate and energy between 2020 and 2030. This strategy plans to cut the GHG emissions by 40%, to achieve a share of at least 32% of renewable energies, and to improve the energy efficiency by at least 32.5%. In addition, in February 2016 the European Commission published its first action plan to tackle the massive amount of energy used to heat and cool Europe's Buildings. The Heating and Cooling Strategy includes actions to increase renewable energy use and the integration of district heating (DH) systems, providing flexibility to the energy systems by reducing and shifting demand through thermal energy storage (TES) systems. Providing energy services via renewable energy through DH networks can be simpler, more efficient, and less expensive than direct integration into each individual building. Thus, to reduce the energy dependence and emissions in the building sector, efficient DH systems based on low-carbon energy (LCE) are identified as key technologies for a sustainable energy transition.

A range of potential barriers (technical, financial, and administrative) are still obstructing the wide deployment of DH based on LCE in Europe. One of the most important challenges associated with the DH is the significant performance variations. Besides the performance variation, the high capital costs of this technology represent a challengeable barrier and make it more difficult to obtain the required funding. Also, there are primarily political and legal barriers which include: lack of a standardized model of the system which could help the European 2030 climate and energy framework achieve its targets; the sudden change in the renewable energy legal framework in some EU countries. All these

technical, economic, and legal barriers promote high variation in quantifying the DH benefits over its lifetime and add more difficulties for the EU members to state their forecast plans for future deployment of the DH in the heating fields.

In order to expand the benefits of DH systems based on LCE, the optimal designing and sizing of DH and their relative relevant components (e.g., charging/discharging devices) should be adequately planned [29]. Substantially, six major contributions are made in this thesis, first, a systematic multi-objective optimization (MOO) framework for optimizing the design of DH plants considering economic and environmental aspects simultaneously. To this end, a simulation-optimization methodology was developed based on a DH plant modeled in TRNSYS 18 that was optimized by a generic optimization tool (i.e., GenOpt) according to economic and environmental indicators. The latter objective was assessed through life cycle assessment (LCA) principles, which quantify the impact caused in all the stages in the life cycle of the energy system. Second, In the direction of mathematical programming research line stays the development of surrogate models computationally much cheaper to solve then our rigorous TRNSYS simulation models. In this context, a complete multi-objective optimization framework using a robust machine learning approach to inherent sustainability principles in the design of SDHS is proposed. Moreover, the framework investigates the uncertainty in the context of DH design, in which the Global Sensitivity Analysis is combined with the heuristic's optimization approach. Third, with the help of key performance indicators related to the 4th generation district heating (4GDH) characteristics and key stakeholders for possible market growth, the possibility of integrating heat pump (HP) into DH with seasonal thermal energy storage is investigated to support stabilization of its performance and assist in the sustainable transition towards 4GDH. Furthermore, the 4GDH economic feasibly is dependent on the circularly of TES due to its large contribution in the 4GDH investment. Thus, the fourth section presents a framework for the circularity assessment of the TES which can be useful for the sustainable assessment of the 4GDH. Fifth, this part lies in demonstrating the sustainable aspects for integrating 4GDH at various residential community sizes to achieve Nearly Zero Energy Building (NZEB) targets. However, achieving the NZEB is a dependent process in the building performance as well. Thus, in the sixth section, a diagnostic tool is developed to improve and guarantee the performance of NZEB buildings during its operation stage which can be useful for the construction and installation companies to maintain the performance of their products proactively.

In summary, this thesis provides sound systematic mathematical programming tools to support decision and policy-making on the path to sustainability EU targets, which are flexible and practical enough to contribute towards sustainable transition toward LCE. Although there will be major sustainability challenges ahead, contributions such as those sought in this thesis, although even small steps, may bring major strides in the transition towards a new era where the economy, society and the environment coexist as key pillars of sustainable development.

Resumen

La necesidad de cambiar el modelo energético mundial es un tema que cada vez cobra mayor importancia e interés. Se deben redoblar los esfuerzos para cambiar los sistemas de producción de energía actuales hacia el uso de fuentes más limpias y menos intensivas en carbono.

Actualmente, los combustibles fósiles representan alrededor del 80% del uso de energía primaria. Por otro lado, el International Energy Outlook prevé un aumento significativo de la demanda mundial de energía durante las próximas décadas. Se proyecta que el consumo global de energía se incrementará en un 48% en 2040 con un crecimiento en el uso de petróleo y gas natural de un 30% y 53,2%, respectivamente. Esta tendencia de las perspectivas conduciría a graves problemas ambientales, como el aumento de emisiones de gases de efecto invernadero (GEI) y el consiguiente impacto en el clima.

Europa es uno de los actores relevantes en este escenario, contribuyendo con un 21,6% al consumo total de energía. Además, en la Unión Europea (UE) el parque de edificios representa alrededor del 40% de la demanda total de energía, con el sector residencial consumiendo el 63% de esta energía. Según estimaciones de la Administración de Información Energética (EIA), la demanda de consumo de energía para el sector residencial en la UE aumenta en una media del 0,9% anual. Junto con todas estas cifras, los edificios residenciales son la cuarta fuente más importante de GEI en la UE y representaron alrededor del 10% del total de GEI en 2016. En respuesta a este desafío, la UE ha adoptado el paquete de medidas sobre clima y energía hasta 2020 que incluye la legislación necesaria para abordar las preocupaciones medioambientales y apoyar la seguridad e independencia energética. El paquete establece tres objetivos principales: (i) reducir en un 20% las emisiones de GEI en comparación con los niveles de 1990, (ii) aumentar la participación de las energías renovables y (iii) mejorar la eficiencia energética en un 20%. En 2013, la UE aprobó un nuevo y ambicioso marco para el clima y la energía entre 2020 y 2030. Esta estrategia prevé reducir las emisiones de GEI en un 40%, lograr una participación de al menos el 32% de las energías renovables y mejorar la energía eficiencia en al menos un 32,5%. Además, en febrero de 2016, la Comisión Europea publicó su primer plan de acción para abordar la enorme cantidad de energía utilizada para calentar y enfriar los edificios europeos. La estrategia de calefacción y refrigeración incluye acciones para aumentar el uso de energía renovable y la integración de sistemas de calefacción urbana (DH), proporcionando flexibilidad a los sistemas de energía al reducir y cambiar la demanda a través de sistemas de almacenamiento de energía térmica (TES). Brindar servicios de energía con energías renovables a través a través de redes de distrito (DH) puede ser más simple, más eficiente y menos costoso que la integración directa en cada edificio individual. Así, para reducir la dependencia energética y las emisiones en el sector de la construcción, los sistemas de DH eficientes basados en energía baja en carbono (LCE) se identifican como tecnologías clave para una transición energética sostenible.

Una serie de posibles barreras (técnicas, financieras y administrativas) todavía obstruyen el amplio despliegue de DH basado en LCE en Europa. Uno de los desafíos más importantes asociados con el DH son las variaciones significativas de prestaciones

observadas. Además de la variación en las prestaciones, los altos costos de capital de esta tecnología representan una barrera desafiante y dificultan la obtención del financiamiento requerido. Por otro lado, existen barreras principalmente políticas y legales que incluyen: la falta de un modelo estandarizado del sistema que pueda ayudar al marco europeo de clima y energía 2030 a alcanzar sus objetivos; el repentino cambio en el marco legal de las energías renovables en algunos países de la UE. Todas estas barreras técnicas, económicas y legales provocan una gran variación en la cuantificación de los beneficios de la DH a lo largo de su vida útil y agregan más dificultades para que los miembros de la UE establezcan sus planes de previsión para el futuro despliegue de la DH.

Para ampliar los beneficios de los sistemas DH basados en LCE, el diseño y dimensionamiento óptimos de la DH y sus componentes relevantes (por ejemplo, dispositivos de carga / descarga) deben planificarse adecuadamente [29]. Para contribuir a este objetivo, se realizan seis contribuciones destacables en esta tesis. En primer lugar, se propone un marco de optimización multiobjetivo sistemático (MOO) para optimizar el diseño de plantas de DH considerando simultáneamente los aspectos económicos y ambientales. Para ello, se desarrolló una metodología de simulación-optimización basada en una planta DH modelada en TRNSYS 18 que fue optimizada mediante una herramienta de optimización genérica (i.e., GenOpt) de acuerdo a indicadores económicos y ambientales. Este último objetivo se evaluó a través de los principios de evaluación del ciclo de vida (LCA), que cuantifican el impacto causado en todas las etapas del ciclo de vida del sistema energético. En segundo lugar, siguiendo la línea de investigación de programación matemática, se desarrollaron modelos sustitutos computacionalmente mucho menos costosos de resolver que los rigurosos modelos de simulación con TRNSYS. En este contexto, se propone un marco de optimización multiobjetivo completo que utiliza un enfoque robusto de aprendizaje automático para los principios de sostenibilidad inherentes en el diseño de SDHS. Además, el marco investiga la incertidumbre en el contexto del diseño de DH, en el que el Análisis de Sensibilidad Global se combina con el enfoque de optimización heurístico. En tercer lugar, con la ayuda de indicadores clave de rendimiento relacionados con las características de calefacción urbana de cuarta generación (4GDH) y los actores clave para un posible crecimiento del mercado, se investiga la posibilidad de integrar la bomba de calor (HP) en la DH con almacenamiento de energía térmica estacional para apoyar la estabilización de su rendimiento y ayudar en la transición sostenible hacia 4GDH. Además, la viabilidad económica de 4GDH depende de la circularidad del TES debido a su gran contribución en la inversión de 4GDH. Así, la cuarta sección presenta un marco para la evaluación de circularidad del TES que puede ser útil para la evaluación sostenible de la 4GDH. La quinta sección se centra en mostrar los aspectos sostenibles clave para integrar 4GDH en varios tamaños de comunidades residenciales para lograr los objetivos de edificios de energía casi nula (NZEB). Sin embargo, lograr el NZEB también es un proceso dependiente del funcionamiento del edificio. Así, en el sexto apartado, se desarrolla una herramienta de diagnóstico para mejorar y garantizar el desempeño de los edificios NZEB durante su etapa de operación que puede ser útil para que las empresas constructoras e instaladoras mantengan las prestaciones de sus productos de manera proactiva.

En resumen, esta tesis proporciona herramientas sólidas y sistemáticas de programación matemática para respaldar la toma de decisiones y la formulación de políticas en el camino hacia los objetivos de sostenibilidad de la UE, que son lo suficientemente flexibles y prácticas para contribuir a una transición sostenible hacia la LCE.

Si bien habrá importantes retos de sostenibilidad por delante, aportes como los que se buscan en esta tesis, aunque aparentemente insignificantes, pueden dar grandes pasos en la transición hacia una nueva era donde la economía, la sociedad y el medio ambiente coexistan como pilares clave del desarrollo sostenible.

Resum

La necessitat de canviar el model energètic mundial és un tema que cada cop cobra més importància i interès. S'han de redoblar els esforços per canviar els sistemes de producció d'energia actuals cap a l'ús de fonts més netes i menys intensives en carboni. Actualment, els combustibles fòssils representen al voltant del 80% de l'ús d'energia primària. D'altra banda, l'International Energy Outlook preveu un augment significatiu de la demanda mundial d'energia durant les properes dècades. Es preveu que el consum global d'energia s'incrementarà en un 48% pel 2040 amb un creixement en l'ús de petroli i gas natural d'un 30% i 53,2%, respectivament. Aquesta tendència de les perspectives conduiria a greus problemes ambientals, com l'augment d'emissions de gasos d'efecte hivernacle (GEH) i el consegüent impacte en el clima.

Europa és un dels actors rellevants en aquest escenari, contribuint amb un 21,6% al consum total d'energia. A més, a la Unió Europea (UE) el parc d'edificis representa al voltant del 40% de la demanda total d'energia, amb el sector residencial consumint el 63% d'aquesta energia. Segons estimacions de l'Administració d'Informació Energètica (EIA), la demanda de consum d'energia per al sector residencial a la UE augmenta en una mitjana del 0,9% anual. Juntament amb totes aquestes xifres, els edificis residencials són la quarta font més important de GEH a la UE i van representar al voltant del 10% del total de GEH el 2016. En resposta a aquest desafiament, la UE ha adoptat el paquet de mesures sobre clima i energia fins a 2020 que inclou la legislació necessària per abordar les preocupacions mediambientals i donar suport a la seguretat i independència energètica. El paquet estableix tres objectius principals: (i) reduir en un 20% les emissions de GEH en comparació amb els nivells de 1990, (ii) augmentar la participació de les energies renovables i (iii) millorar l'eficiència energètica en un 20%. El 2013, la UE va aprovar un nou i ambiciós marc per al clima i l'energia entre 2020 i 2030. Aquesta estratègia preveu reduir les emissions de GEH en un 40%, aconseguir una participació de al menys el 32% de les energies renovables i millorar l'energia eficiència al menys un 32,5%. A més, al febrer de 2016, la Comissió Europea va publicar el seu primer pla d'acció per abordar l'enorme quantitat d'energia utilitzada per escalfar i refredar els edificis europeus. L'estratègia de calefacció i refrigeració inclou accions per augmentar l'ús d'energia renovable i la integració de sistemes de calefacció urbana (DH), proporcionant flexibilitat als sistemes d'energia al reduir i canviar la demanda a través de sistemes d'emmagatzematge d'energia tèrmica (TES). Brindar serveis d'energia amb energies renovables a través a través de xarxes de districte (DH) pot ser més simple, més eficient i menys costós que la integració directa en cada edifici individual. Així, per reduir la dependència energètica i les emissions en el sector de la construcció, els sistemes de DH eficients basats en energia baixa en carboni (LCE) s'identifiquen com a tecnologies clau per a una transició energètica sostenible.

Una sèrie de possibles barreres (tècniques, financeres i administratives) encara obstrueixen l'ampli desplegament de DH basat en LCE a Europa. Un dels reptes més importants associats amb el DH són les variacions significatives de prestacions observades. A més de la variació en les prestacions, els alts costos de capital d'aquesta tecnologia representen una barrera desafiant i dificulten l'obtenció del finançament requerit. Per altre banda, hi ha barreres principalment polítiques i legals que inclouen: la manca d'un model estandarditzat de sistema que pugui ajudar al marc europeu de clima i energia 2030 a assolir els seus objectius; el sobtat canvi en el marc legal de les energies renovables en alguns països de la UE. Totes aquestes barreres tècniques, econòmiques

i legals provoquen una gran variació en la quantificació dels beneficis de la DH al llarg de la seva vida útil i afegeixen més dificultats perquè els membres de la UE estableixin els seus plans de previsió per al futur desplegament de la DH.

Per ampliar els beneficis dels sistemes DH basats en LCE, el disseny i dimensionament òptims de la DH i els seus components rellevants (per exemple, dispositius de càrrega / descàrrega) s'han de planificar adequadament [29]. Per contribuir a aquest objectiu, es realitzen sis contribucions destacades en aquesta tesi. En primer lloc, es proposa un marc d'optimització multiobjectiu sistemàtic (MOO) per optimitzar el disseny de plantes de DH considerant simultàniament els aspectes econòmics i ambientals. Per a això, es va desenvolupar una metodologia de simulació-optimització basada en una planta DH modelada en TRNSYS 18 que va ser optimitzada mitjançant una eina d'optimització genèrica (i.e., GenOpt) d'acord a indicadors econòmics i ambientals. Aquest últim objectiu es va avaluar a través dels principis d'avaluació del cicle de vida (LCA), que quantifiquen l'impacte causat en totes les etapes del cicle de vida de el sistema energètic. En segon lloc, seguint la línia d'investigació de programació matemàtica, es van desenvolupar models substituts computacionalment molt menys costosos de resoldre que els rigorosos models de simulació amb TRNSYS. En aquest context, es proposa un marc d'optimització multiobjectiu complet que utilitza un enfocament robust d'aprenentatge automàtic per als principis de sostenibilitat inherents en el disseny de SDHS. A més, el marc investiga la incertesa en el context del disseny de DH, en què l'Anàlisi de Sensibilitat Global es combina amb l'enfocament d'optimització heurístic. En tercer lloc, amb l'ajuda d'indicadors clau de rendiment relacionats amb les característiques de calefacció urbana de quarta generació (4GDH) i els actors clau per a un possible creixement de mercat, s'investiga la possibilitat d'integrar la bomba de calor (HP) a la DH amb emmagatzematge d'energia tèrmica estacional per donar suport a la estabilització del seu rendiment i ajudar a la transició sostenible cap a 4GDH. A més, la viabilitat econòmica de la 4GDH depèn de la circularitat del TES a causa de la seva gran contribució en la inversió de la 4GDH. Així, la quarta secció presenta un marc per a l'avaluació de circularitat del TES que pot ser útil per a l'avaluació sostenible de la 4GDH. La cinquena secció es centra en mostrar els aspectes sostenibles clau per integrar 4GDH en diverses mides de comunitats residencials per assolir els objectius d'edificis d'energia gairebé nul·la (NZEB). No obstant això, aconseguir el NZEB també és un procés dependent del funcionament de l'edifici. Així, en el sisè apartat, es desenvolupa una eina de diagnòstic per millorar i garantir l'acompliment dels edificis NZEB durant la seva etapa d'operació que pot ser útil perquè les empreses constructores i instal·ladores mantinguin les prestacions dels seus productes de manera proactiva.

En resum, aquesta tesi proporciona eines sòlides i sistemàtiques de programació matemàtica per recolzar la presa de decisions i la formulació de polítiques en el camí cap als objectius de sostenibilitat de la UE, que són prou flexibles i pràctiques per contribuir a una transició sostenible cap la LCE.

Si bé hi haurà importants reptes de sostenibilitat per davant, aportacions com les que es busquen en aquesta tesi, encara que aparentment insignificants, poden donar grans passos en la transició cap a una nova era on l'economia, la societat i el medi ambient coexisteixin com a pilars clau del desenvolupament sostenible.

UNIVERSITAT ROVIRA I VIRGILI
DECISION MAKING TOOLS FOR SUSTAINABLE TRANSITION TOWARD LOW CARBON ENERGY TECHNOLOGIES IN THE RESIDENTIAL SECTOR
Mohamed Abokersh

Table of Contents

List of Figures

List of Tables

Chapter I

Introduction

I. Introduction

I.1 Background and motivation

There are a new series of social hurdles, owing to the massive stress on organizational resources and the massive expansion of the worldwide population. The consumption of oil, food, water, components and other resources has risen, and suppliers are, of course, coping with this development [1]. The exponential progress of the world and the rapid growth of developing markets indicate that energy demand is growing, and costs have typically risen after the new century [2]. Despite the global tendency in shifting the current energy production toward a more clean, economical and sustainable energy options, the gap between the observed emissions and the desirable reduction to fulfill the international energy and climate legislation is widening where the carbon dioxide (CO_2) emissions grow by 6.5% over the last five years [3].

In Europe, the Governance of the Energy Union approved new clean energy for all Europeans package [4]. This plan comprehensively updates the European Union (EU) energy policy framework to facilities the sustainable transaction from fossil fuel toward the deployment of low carbon energy technologies to follow up the EU's 2030 targets for climate and energy consistently with delivering the EU´s Paris agreement commitments toward the reduction in greenhouse gas emissions (GHG) [5]. An important step to spread on the clean energy transition in the European Union and its Member States is the energy efficiency in the building sector. The buildings represent one of the biggest energy consumers in the EU, accounting for more than 40% of the final energy consumption [6], where the residential buildings consume 63% of this energy [7]. Moreover, more than 75% of residential energy consumption is utilized for space and domestic hot water heating [8]. Along with all these figures, the residential sector counts for about 10% of the total GHG in 2017 [9]. Thus, the residential buildings present excellent energy efficiency opportunities with measures aimed at reducing their heating and cooling requirements or their energy consumption for lighting, appliances, and other equipment. Apart from the energy demand side, residential buildings are also expected to contribute to the supply side of the energy system by incorporating various renewable sources, such as solar, thermal energy storages and efficient technologies like biomass, heat pumps and cogeneration, both at the building and at the district scale. In response to this opportunity, the EU promotes Energy efficiency directive plan 2012/27/EU [10]. This plan tends to boost the energy performance of the buildings and introduce energy certificates, taking into account the external climatic conditions and defining the Net Zero Energy Building (NZEB). Even though these actions plan led to decline the final energy consumption of the residential section by 9.3% over the last 15 years, still the average energy consumption still increases by 0.4% per year due to the growth in the urbanization area and dispersion of the central heating [11]. Aligning with this growth, various types

of renewable energy systems are installed in the building sector for electricity and thermal loads coverage.

Among all renewable sources, the solar energy seems to be the most promising alternative for fossil fuel due its unique benefits which comprises [12]: (i) reduction in the primary energy consumption at the end-user level, (ii) increment in the power generation and transmission capacities, (iii) hybrid feature with almost all kind of back up heating sources, and (iv) high availability with some limitation in the high latitudes. For these reasons, solar energy can be utilized for satisfying the large heating demand in the building sector. However, the main drawback of solar energy, as well as the other renewable energy sources, is the intermittency and fluctuation based on short and long term basis [13,14] which causes a gap between the energy demand and supply. Between several storage techniques, the thermal energy storage (TES) systems seem to be the most promising technique that fulfills this gap issue. The thermal energy storage (TES) technique stores the excess generated power and provides it on-demand [15]. Considering its storage capacity, the TES systems comprise two main categories; these categories are short and long-term systems. The first type has a charge-discharge capacity for a few days and is widely known as diurnal storage [16]. In general, this type suffers from demand coverage problems during the winter season, especially in the high latitude countries. This is due to the difference in solar availability between summer and winter seasons [17]. On the other hand, the long-term storage can last up for several months, and it is known as seasonal TES. Accordingly, the seasonal TES can efficiently contribute to solve the demand issue during the winter season, and consequently improve the usage of the renewables in district heating systems aligning with the building decarbonization concept [18,19]. Even though the seasonal TES has been developed for chemical and latent heat storage, the existing seasonal TES mainly uses sensible storage due to its stability [20].

In Europe, the begin of developing solar assisted district heating system (SDHS) based on low-carbon energy coupled with sensible seasonal TES began in the 1970s with the energy crisis [21]. Such these district heating communities have been established in the 1990s and 2000s, mostly in Denmark and Germany [22]. Since then, the SHDS market has been grown practically in the northern and the Northern and central of Europe [23]. Within 2016, 37 SDHS were installed in Europe compared to only 25 plants installation in 2015. With few exceptions, the real performance of the SDHS has met with the estimated or predicted results. In Friedrichshafen-Germany, the estimate performance in terms of the solar fraction could reach up to 43%. However, the monitoring data under realistic operation conditions showed that a solar fraction between 21% to 33% could be reached [24]. The higher estimated solar fraction value has not been reached due to several issues comprises higher heating demand compared the excepted, higher thermal losses in the seasonal storage, and lower solar collector and heat exchanger efficiencies [25]. The same

issue has been noticed in other SDHS installed in the Neckarsulm, and Rockstock [26]. Moreover, in the installed plants in Steinfurt-Borghorst, Hamburg, and Neckarsulm II, a considerable deviation between the design and monitored performance is noticed due to the high thermal losses in the seasonal and other tanks, high net return temperature, and smaller solar collector area than the planned [27]. In Crailsheim-Hirtenwiesen, a SDHS was built to cover 50% of the heating requirement in a residential area comprises 260 apartments, a school, and a gym. To ensure the system accessibility throughout the year, a borehole seasonal storage with volume of 10,000 m^3 is added to the system [28]. The performance monitoring showed a variation between the estimated and real solar fraction up to 60%. This huge gap is due to the ground losses combined with higher operating temperature in the space heating network [29]. The most famous solar community is the Drake Landing Solar Community in Canada. This plant has been able to cover 98% of the space heating demand through solar energy [30]. However, a high-performance variation faces this solar community during a five year of monitoring. According to ASHRAE report [31], the reason behind this underperformance of the system compared to the simulation results is the high thermal losses throughout the network, the storage tank stratification, and pump control. Other than the problems mentioned above, Claudia Weissmann et al.[32] mentioned that the building orientation, the thermal collector orientation combined with the pipe leakages could adversely affect the SHDS performance. Besides the performance variation, the high capital costs of this technology represent a challengeable barrier and make it more difficult to obtain the required funding [33]. Also, there are primarily political and legal barriers which include: lack of a standardized model of the system which could help the European 2030 climate and energy framework achieve its targets; the sudden change in the renewable energy legal framework in some EU countries such as Spain [34]. All these technical, economic, and legal barriers promote high variation in quantifying the SDHS benefits over its lifetime and add more difficulties for the EU members to state their forecast plans for future deployment of the SDHS in district heating fields.

In addition to the integration of potential of SDHS to achieve Nearly Zero Energy Buildings (NZEB) and improve the energy performance in the residential sector, the construction companies that lead the development of NZEB itself in Europe indicate a substantial obstacle to guarantee the nZEB performance and thus to improve their market position. An additional challenge is that the guarantee of building data quality where monitoring a thousand of homes simultaneously isn't feasible since sensors may not function properly and it can be out of budget. Therefore, the need for a generic approach to monitor and guarantee the building performance is essential. Furthermore, this approach should be based on minimal monitoring data for individual homes to find out what is the cause for the current situation of the deviations between the actual and expected performance as analyses based on wrong data lead to wrong conclusions, wrong decisions, extra costs and loss of support.

I.2 General Objectives

All the performance, economical and legal barriers mentioned before promote a high variation in quantifying the sustainable transformation to NZEB and subsequently improve the energy efficiency in the residential sector to fulfill the EU's 2030 targets. Thus, this thesis aims to propose tools and methodology frameworks to address the shortcomings associate with the low carbon energy technologies represented by the SDHS via the following contributions:

- Develop and verify a detailed simulation of the SDHS performance considering seasonal and short-term storage systems and their respective load profiles based on the explored climates.
- Develop systematic multi-objective optimization approach for the designing of SDHS with seasonal storage capable of simultaneously minimizing the system life cycle cost and its environmental impact for different European climatic conditions.
- Formulate a novel mathematical programming framework based on machine learning adept to assist the operator, inventors and policy makers in development of policies that encourage sustainable practices and decisions in response to the deployment of the SDHS at the residential sector.
- Investigate the uncertainty associate with SDHS performance for the economic parameters (investment costs, energy carrier prices, etc.) through taking advantage of the low computational cost feature associated with the development of machine learning.
- Demonstrate the sustainable potential of efficient technologies such as heat pump integration into a residential community sized SDHS to stabilize its performance.
- Develop a method for sustainable circular system design (SCSD) that ecologically assesses the sustainability of TES technologies. The method can be utilized to increase circularity and the sustainability of those derived measures.

Furthermore, from the building side, this thesis attempt to tackle the challenges facing the construction companies in ensuring the NZEB performance via the following contributions:

- Develop a diagnostic tool to guarantee and proactively maintain the indoor climate performance of nZEBs with consideration for the temporal variation associate with the climate data and occupant behavior.
- Develop a modelling scheme for defining the difference between the predicted and actual energy and indoor performance at an individual nZEB based on uncertainty analysis.
- Use the data analysis based on uncertainty model and sensitivity analysis to have an additional knowledge in the future regarding the building

performance which can be added to the builders, installers and occupants, and subsequently bridge the NZEB concept with the client anticipations.

The capability of the proposed methodologies and tools for both, the supply and building sides, is illustrated through case studies, some of them directly based on existing applications in order to demonstrate how they can support decision and policy makers to design effective strategies towards sustainability.

I.3 The simulation tools

A computer simulation is an attempt to model a real-life or hypothetical system on a computer so that it can be studied in order to get insights into how the system works. It is a tool used to virtually investigate the behaviour of the system. Simulation is used in many contexts. It can be used to simulate the eventual real effects of alternative conditions and courses of action. It is used when a real system cannot be engaged with because it is inaccessible, or it may be dangerous. Key issues in the simulations include the acquisition of valid source information about the important selection of key characteristics and behaviour. Within the simulations, simplification, approximations, and assumptions are made. Afterwards, the simulation outcome needs to be validated.

Energy and building simulation software is an important tool used by designers to analyse system feasibility and cost. The energy simulation software allows a designer to predict, measure, optimize and design systems and buildings with some accuracy. It also allows designers to identify important variables that can support their decisions when building a new or redesigning an existing system [1].

The tools can be useful in building complex systems and simulations without investing a lot in building such systems. Nowadays, tools are needed to answer very specific questions during the initial phase. Designers can also predict the energy system's behaviour and building before they are constructed and simulate the investments and operational costs of the systems in their current and future conditions.

Energy simulation software can also consider all the regulations in force and provide appropriate suggestions for a better energy system design. Energy simulation software tools have developed over the years. At the moment, there are many energy simulations tools with different complexity and responses to different variables [1]. Generally, in all energy simulations software tools, three steps have to be performed (for instance: the creation of the model, building simulations and analysis of the results). Different commercially available simulation tools are available, such as IDA Indoor Climate and Energy (IDA ICE), Integrated Environmental solutions (IES), Energy Plus and TRNSYS (stands for transient system simulation programme). These software tools have been used in various studies [2].

I.3.1 TRNSYS dynamic simulation software

TRNSYS is a complete and extensible simulation. It is quite a flexible tool, especially in performing transient simulation of an energy system. TRNSYS was first developed jointly by the University of Wisconsin-Madison's Solar Energy Lab and Colorado State University's Solar Energy Applications Lab [3].

TRNSYS is an algebraic and differential equation solver in which components are connected graphically in the simulation studio. The software has a modular structure that has been designed to develop complex systems. The components may range from a heat pump to the multi-zone of a building complex. The components are configured through the graphical user interface known as TRNSYS Simulation Studio. In solar district heating network simulations, all the mechanical components are solved simultaneously at each time step. The time step may vary from an hour to 0.1 of second. The library in the software tool allows the use of various components like, solar panels, PV panels, HVAC (heating, ventilation and air conditioning) systems, cogeneration systems etc. It also provides different weather data. The simulation results can show the performance of an individual component which can be selected from the simulation studio. It assists understanding complicated systems. Logical programming or simple equations can be written on open-source code to accomplish system control strategies.

In the simulation tool, the construction of the building can be achieved by the introduction of data on a dedicated visual interface known as TRNBuild. TRNSYS also provides TRNEdit, which is an editor for reading and writing TRNSYS inputs and outputs. TRNEdit can also perform parametric TRNSYS simulation and plot data. In addition, this energy simulation tools allows the user to incorporate other components developed in software tools, such as Matlab, Excel, and Visual Basic (VBA) etc. [4].

I.3.2 Machine learning modeling approach

Due to the high computational expenses of using TRNSYS to simulate large energy systems, machine learning (metamodel) may overcome these computational obstacles [5]. The metamodel is a generated model of the sequential model, which is typically fast compared to the original detailed TRNSYS model. One of the most widely used metamodel technique is artificial neural networks (ANN) to solve complex engineering problems [6]. The main ANN advantage is the replicate the detailed model through approximate an implicit relationship based on the training data.

The ANN is a supervised learning technique which covers a board range of models and learning algorithm. Generally, the neural network consists of several hidden layers where each layer consists of several neurons; these neurons propagate information using weighted connections and transfer functions. The number of neurons in the input and output layers is equal to the number of the model input and output, respectively. Since the number of hidden layers and its relative neurons

selection increase the overfitting risk, the hidden layers are interpreted based on an optimization algorithm which can be used to interpret other ANN settings [7]. The outline for the ANN model is shown in Figure I-1.

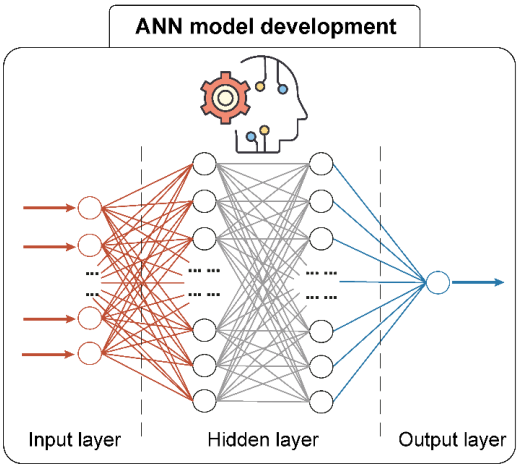

Figure I-1: Structure of the ANN model

In addition to the hidden layers and its relative neurons, the ANN architecture is also defined through other settings comprises the training/learning method, the activation functions, momentum mean, and the learning rate. Thus, we construct the neural network based on investigating the optimal setting for the following hyperparameters:

- Number of the hidden layers.
- Number of neurons in the hidden layer.
- Training function.
- Activation function, hidden layer.
- Activation function, output layer.
- Learning rate.
- Momentum mean.

I.4 Mathematical programming

In order to expand the benefits of energy systems, the optimal designing and sizing of system and its relative relevant components (e.g., charging/discharging devices) should be adequately planned [8]. Substantially, planning and construction of large-scale energy system coupled is a complex process. Furthermore, the vast options evolve the optimization approach as a viable option to obtain the optimal design and operation conditions. The formulation of the optimization problem has two main approaches: single objective optimization and Multi-objective optimization.

I.4.1 Single objective optimization

Generic single-objective optimization problem is generally stated in compact form [9] as follows:

$$\begin{aligned} &\min \{f(x,y)\} \\ &s.t.\ h(x,y) = 0 \\ &\quad g(x,y) \geq 0 \\ &x \in R,\ y \in Z \end{aligned} \qquad \text{Eq.I-1}$$

where $f(x,y)$ represents the objective function to be minimized and x and y represent the vectors of continuous and integer decision variables (if any), respectively. The feasible set of solutions is defined by the set of constraints imposing restrictions on variables where $h(x,y)$ represents equality constraints whereas $g(x,y)$ refers to inequality constraints.

A point (x,y) satisfying all constraints is a feasible solution to the problem. All feasible solutions constitute the feasible regions. The aim of the optimization is to satisfy the optimality criteria by selecting the best point from available feasible solutions. A point (x^*,y^*) from the feasible region ω is deemed as local minimum if the objective function takes the smallest value in some feasible neighbourhood, that is, there exists a δ>0 such that $f(x^*,y^*) \leq f(x,y) \forall x,\ y \in \{\omega: |x - x^*| \leq \delta\}$. Often, in an optimization problem, there can be many local minima but only one global minimum is possible. A point (x^*,y^*) is a global minimum when the objective function takes the smallest value in all the feasible region, that is, $f(x^*,y^*) < f(x,y) \forall x,\ y \in \omega$.

I.4.2 Multi-objective optimization

To optimize problems considering more than one criterion (i.e., economic, and environmental) multi-objective optimization (MOO) techniques are required.

$$\begin{aligned} &\min \{f_1(x), \dots \dots f_n(x)\} \\ &s.t.\ h(x) = 0 \\ &g(x) \geq 0 \\ &x \in R,\ y \in Z \end{aligned} \qquad \text{Eq.I-2}$$

In MOO problems usually there is not only one optimal solution but rather a set of Pareto solutions that represent the optimal trade-off between the conflicting objectives considered in the analysis. A solution is said to be Pareto optimal when it cannot be improved simultaneously in all the objectives without necessarily worsening at least one of them. Therefore, all the Pareto solutions are considered to be equally optimal (see [10] for further information) as shown in Figure I-2.

The optimized solution in the multi-objective problem provides a set of non-dominated solutions (Pareto frontier points), which represent optimal trade-off solutions between different objectives that satisfy the technical performance constraints. The extreme points in the Pareto frontier called the anchor points, and it corresponds to the minimum economic and environmental impact solutions in our case studies. In the MOO problems using the classical methods based on point by point approach (weighted sum or the ε-constraint method) [11], the optimization outcome represents a single optimized solution based on a particular search direction, which often delivers local information (suboptimal solution). Furthermore, due to the dependency of the optimal solutions on the initial chosen solution, these approaches fail in solving different optimization problems type [12]. Aligning with these limitations, an evolutionary approach based on a technique called Pareto-ranking [13] is utilized to estimate approximate Pareto-optimal solutions based on the objective functions. The main advantage of evolutionary algorithms is the fact that they typically generate sets of solutions, allowing computation of an approximation of the entire Pareto front. The main drawback of evolutionary algorithms is their lower speed, and that the Pareto optimality of the solutions cannot be mathematically guaranteed. There are many different tools to optimize energy systems designs. GenOpt [14] and MATLAB environment [15] are the widely used tools.

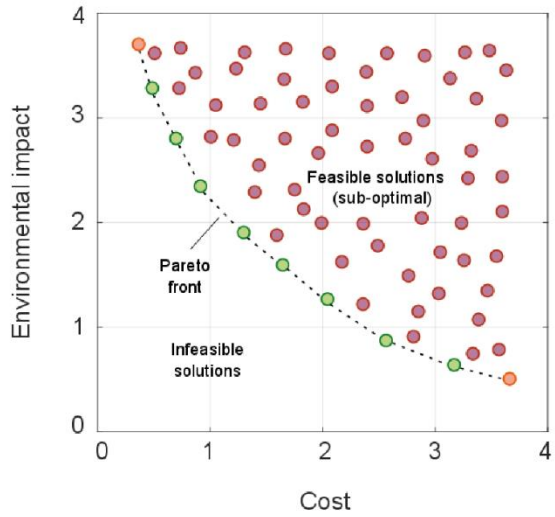

Figure I-2: Schematic representation of the Pareto frontier for a two criteria multi-objective optimization problem

I.4.3 Simulation-based optimization methods

I.4.3.1 Single point or population-based search

The number of solutions attained by the algorithm at the same time can be the other

characteristic of classification. The algorithms which work on single solutions are also referred to as trajectory methods. Here are included all the metaheuristics based on local search. On the other hand, population-based metaheuristics perform search processes similar to the evolution of the set of points in the search space.

I.4.3.2 Dynamic or static objective function

Some algorithms use static objective functions during run-time, others (e.g. guided local search) modify the objective function during the search. The idea behind the dynamic approach is to escape from local minimum by modifying the search "landscape".

I.4.3.3 One or various neighborhood structures

Many algorithms use one invariable neighborhood structure during the optimization. Some metaheuristics (e.g. variable neighborhood search) use different landscape topologies which make them more likely to escape the local minimum solutions.

I.4.3.4 Memory-based or memory-less methods.

The use of memory is recognized as one of the most important elements of a powerful metaheuristic. Memory-less algorithms perform a Markov process, they use memory slots only to decide the next action. There are also short-term algorithms which refer to recently performed moves or recently taken decisions. The long-term algorithms accumulate information about the whole search.

I.4.3.5 Genetic algorithm

In complex models, an analytical formulation is unavailable, and it is infeasible to use classical methods (grid search). With such a problem, meta-heuristic methods can be used, such as a genetic algorithm. A genetic algorithm is an optimization method that is based on the evolution principle. After a set of solutions has been found, they are compared, and the best ones are combined by way of exchanging some of their variable values. After this the solutions are compared with new variables to find the better solution set. NSGA-II is a popular genetic algorithm that utilizes solution sorting based on function values. It helps to find solutions on the Pareto front.

In this work, fast sorting and elite multi objective genetic algorithm (NSGA-II) is used because it can handle multi-objective problems, while at the same time handling both the discrete and continuous design variables. Furthermore, NSGA-II provides a parallel computing facility that can reduce the time needed to reach optimal solutions [16].

I.4.3.6 Bayesian optimization

As in other kinds of optimization, in Bayesian optimization we are interested in finding the minimum of a function $f(x)$ on some bounded set X. What makes Bayesian optimization different from other procedures is that it constructs a probabilistic model for $f(x)$ and then exploits this model to make decisions about where in X to next evaluate the function, while integrating out uncertainty. The essential philosophy is to use all of the information available from previous evaluations of $f(x)$ and not simply rely on local gradient and Hessian approximations. This results in a procedure that can find the minimum of difficult non-convex functions with relatively few evaluations, at the cost of performing more computation to determine the next point to try. When evaluations of $f(x)$ are expensive to perform — as is the case when it requires training a machine learning algorithm — then it is easy to justify some extra computation to make better decisions. For an overview of the Bayesian optimization formalism and a review of previous work, see, e.g., Snoek J et al. [17].

I.5 Optimization solutions post analysis

The Multi-objective optimization presents us with a Pareto front of the optimal solutions which are then subjected to multi-criteria decision making (MCDM) to facilitate the selection of suitable optimal solution according to the need of stakeholders. For MCDM, we have used TOPSIS methodology, which ranks the solutions based on the desired criteria. To illustrate the significance of uncertainty on the optimized objectives, we performed the uncertainty and the sensitivity analysis [18].

I.5.1 TOPSIS method

A widely used MCDM algorithm presented by Hwang et al. [19] is TOPSIS. This method uses the normalized values obtained from (Eq.I-3-Eq.I-4) and assumes a distance-based criterion signifying that ideal solution lies at the shortest distance from the positive ideal solution and the longest distance from the negative ideal solution. The calculated distances then compared to find out the best plausible solution. The advantage of TOPSIS is that it can provide a ranking of each solution for each criterion [20].

To determine the rank, first, we identify the positive ideal solution (A^+) and negative ideal solution (A^-) as below:

$$A^{+} = \left\{\left(\underbrace{max}_{i} v_{ij} | j \in I\right), \left(\underbrace{min}_{i} v_{ij} | j \in I'\right), i = 1,2,\dots,m\right\} = \{v_1^{+}, v_2^{+}, \dots, v_m^{+}\} \quad \text{Eq.I-3}$$

$$A^{-} = \left\{\left(\underbrace{min}_{i} v_{ij} | j \in I\right), \left(\underbrace{max}_{i} v_{ij} | j \in I'\right), i = 1,2,\dots,m\right\} = \{v_1^{-}, v_2^{-}, \dots, v_m^{-}\} \quad \text{Eq.I-4}$$

Here, $I = \{j = 1, 2,\dots, n\}$ and $I' = \{j = 1, 2,\dots, n\}$ represents the sets of economic and environmental criterion in our case studies. Then, we measure the Euclidean distance for each solution from positive and negative ideal solutions using following equations:

$$S_i^{+} = \sqrt{\sum_{j=1}^{n} \left(v_{ij} - v_j^{+}\right)^2}, \qquad for\ i = 1,2,\dots,m \quad \text{Eq.I-5}$$

$$S_i^{-} = \sqrt{\sum_{j=1}^{n} \left(v_{ij} - v_j^{-}\right)^2}, \qquad for\ i = 1,2,\dots,m \quad \text{Eq.I-6}$$

Lastly, proximity index ($C_i \in [0;1]$ for $i = 1, 2,\dots, m$) is calculated to find the remoteness from the positive and negative ideal solutions for ranking, as:

$$C_i = \frac{S_j^{-}}{S_j^{+} + S_j^{-}} \quad \text{Eq.I-7}$$

I.5.2 Uncertainty Analysis (UA)

Uncertainty Analysis (UA) aims to investigate the variability of the model's output given uncertain inputs. UA essentially allows the modeler to answer the question: "How uncertain is my model output?" In an energy system design problem, for instance, UA would allow us to examine how the optimal design outcome varies for different realizations of the uncertain model inputs. Hence, we could learn more about the design's robustness to change. The most common approach to perform UA is to execute a deterministic model multiple times by propagating Monte Carlo (MC) samples of the uncertain parameters through the model in order to obtain an uncertain model response. UA focuses solely on this uncertain model output, which can be used to perform statistical calculations, such as computing the mean and standard deviation of the output, statistical moments, estimates of the probability that the output will exceed a specific threshold etc., but also to plot histograms and empirical cumulative distribution functions (CDF), among others. By analyzing the statistical properties of the model's uncertain response, the impacts of uncertainty can be quantified. More information on MC-based UA can be found in [21].

I.5.3 Sensitivity Analysis (SA)

Sensitivity Analysis (SA) is a related practice to UA and is commonly applied in succession to it. In fact, SA has a different goal than UA which defines SA as "the study of how uncertainty in the output of a model (numerical or otherwise) can be apportioned to different sources of uncertainty in the model input". In other words, SA aims to quantify the importance of the input parameters with regards to their contribution to the model output variability. SA techniques are often divided into Local SA (LSA) and Global SA (GSA) techniques. In the following sections, a brief introduction will be given to the main computational methods that can be applied to perform SA. More information and up-to-date reviews of SA methods can be found [22].

I.5.3.1 Local Sensitivity Analysis (LSA)

Local Sensitivity Analysis (LSA) is the simplest and most commonly used approach to perform SA. The technique provides a measure of the effect of input parameters on the model output by varying one parameter of the model at a time, while all the other parameters remain fixed at their nominal point. That is why LSA is also referred to as one-at-a-time (OAT) analysis. The popularity of LSA in modelling activities is explained by a series of reasons given by Saltelli and Annoni [18] with the most important ones associated with the method's simplicity and ease of understanding. However, the same authors, as well as many others, have argued that LSA is inadequate practice. Firstly, LSA is informative only around the point of the calculation and does not adequately cover the input parameter space. In addition, any available probabilistic knowledge on the inputs is not taken into account and the values for the input parameters are considered equiprobable. Finally, the interaction effects among factors cannot be detected as these would require simultaneous inputs variation and not OAT. These shortfalls of LSA have been addressed with the development of Global Sensitivity Analysis (GSA) techniques, which are introduced below.

I.5.3.2 Global Sensitivity Analysis (GSA)

In contrast to LSA, GSA extends the field of investigation of the uncertain parameters from the base point to the whole input parameter space, allowing the interactions between parameters to be studied. GSA contains a series of different methods that are applicable in different settings and their main ideas are briefly described below. More detailed information to carry out the GSA are the following:

1. **Screening analysis**: Computational models might have hundreds or even thousands of uncertain parameters, but practice has shown that often only a small subset of these parameters might be influential. Thus, screening techniques aim specifically to identify the set of least influential model parameters that can be fixed to any given value within their uncertain range,

without significantly affecting the output variance. The advantage of screening methods is their low computational cost; hence, they are very well suited to models that have a large number of uncertain parameters and/or are computationally expensive. The main representative of screening analysis and the one that is the most widely used is the method of Morris [23]. The main disadvantage of the method of Morris is that its results can only be interpreted qualitatively. The method can provide a rank of importance for the input parameters but cannot quantify how much more important one parameter is over another.

2. **Variance-based methods**: The last group of methods are based on the variance decomposition of the model output. Unlike screening techniques, these methods quantify the contribution of each parameter to the output's variance as a measure of parameter importance. For this task, they calculate the first-order and total-order Sobol indices per parameter on the basis of Monte Carlo simulations. The first-order index quantifies the effect on the output variance that can be attributed to the parameter examined alone, while the total-order also considers the interactions with other model parameters. Variance-based techniques require no assumption regarding the model's form, such as linearity or monotonicity, and they can be used with black-box simulation tools as well. The main drawback of these methods is that they require a large number of Monte Carlo model runs per uncertain model parameter, therefore, it is commonly suggested that a screening analysis precedes a variance-based SA to reduce the dimensionality of the problem [23].

3. **Bayesian analysis of computer code outputs (BACCO)**: The main advantage of this approach is its ability to cover a wide range of uncertain parameters and interactions with consideration for their relative distributions [24]. Furthermore, it offers a substantial computational improvement compared to using expensive GSA based on Variance-based methods [25]. The BACCO method entails two main key stages. In the first step, a statistical representative model (i.e., an emulator) is built based on a set of training data points derived from the developed simulation-based optimization model. The training data is ideally cover the feasible design domain using a multidimensional space-filling algorithm (Latin hypercube design). Prior to the second stage, the cross-validation approach is applied automaticity to estimate the emulator accuracy. The second stage uses the constructed emulator (which is efficient in covering a multidimensional design domain in low computational expenses in comparison to the original optimized model) in quantifying the importance of parameters in interest [26].

I.6 Sustainability evaluation criteria

In current thesis, two main sustainable criteria comprise: the economic performance with details regarding the construction and operation of the equipment in the proposed plant, as well the environmental performance throughout the system lifetime.

I.6.1 Economic analysis

In the current work, the economic evaluation follows the work of Tulus et al. [27] which is carried out based on the life cycle costing (LCC) methodology [28,29].

The LCC methodology is a valuable monetary approach for assessing the energy system designs in terms of the initial purchase cost and the operational costs throughout the expected lifetime of the system. The LCC perspective in the early stages of design empowers the decision-makers to deeply comprehend the lifetime costs of the system [30], and subsequently enhance the possibility of an additional reduction in the system operational cost even if more investment cost is required [31].

The main principle of the LCC methodology is the future cost approach. Its feature is to discount the summation of all expenses during the lifetime of the system to its present value where the net present cost (*NPC*) can be estimated by adding the initial capital cost (C_C), the operational cost (C_O) and the total replacement cost of the equipment (C_R):

$$NPC = C_C + C_O + C_R \qquad \text{Eq.I-8}$$

I.6.1.1 Initial capital cost

The initial capital cost is the investment cost at the project starting point. It takes into consideration the actual equipment cost, the installation labor and transportation costs along with any possible contingency expenses:

$$C_C = (1+\alpha_{CF})\sum_k (PEC_k \cdot FBM_k) \qquad \text{Eq.I-9}$$

where PEC_k is the initial purchase cost of equipment unit k, FBM_k denotes the bare module factor, which represents the installation labour and transportation costs, and α_{CF} denotes the contingency fees factor.

The PEC_k is brought to its present worth value from the base year (*year A*) to the year of installation (*year B*) using the Chemical Engineering Plant Cost Index (*CEPCI*) [32] as follows:

$$PEC_k = PEC_k^{yearA} \frac{CEPCI^{yearB}}{CEPCI^{yearA}} \quad \forall k \qquad \text{Eq.I-10}$$

I.6.1.2 Operational cost

The operational cost refers to the sum of all the annual operating costs such as maintenance costs of the different equipment units and facilities, the consumption of electricity by hydraulic equipment and the consumption of natural gas by auxiliary heaters. It can be expressed as follows:

$$C_O = C_M PWF_M + C_P PWF_P + C_{AUX} PWF_{AUX} \qquad \text{Eq.I-11}$$

where C_M, C_P and C_{AUX} represent the annual maintenance cost, hydraulic equipment (*i.e.* pumps) and auxiliary consumption costs, respectively. The present worth factor (*PWF*) counts for the time value of money considering the inflation rate (i), discount rate (d), and lifetime of the proposed system (N_e) as expressed in following:

$$PWF = \begin{cases} \frac{1}{d-i}\left[1-\left(\frac{1+i}{1-d}\right)^{N_e}\right] & \forall i \neq d \\ \frac{N_e}{1+i} & \forall i = d \end{cases} \qquad \text{Eq.I-12}$$

I.6.1.3 Replacement cost

Several equipment units have a high depreciation rate and subsequently need to be replaced during the plant operation. The replacement cost can be expressed as following with consideration for the equipment present value:

$$C_R = PVF_n \sum_k (PEC_k \cdot FMB_k) \qquad \text{Eq.I-13}$$

where PVF_n is the present value factor of a future cash flow at year n and it can be expressed as follows:

$$PVF_n = \frac{(1+i)^n}{(1+d)^n} \qquad \text{Eq.I-14}$$

I.6.2 Life cycle assessment

The LCA is a methodology for the environmental evaluation connected with material, products, or operation under which resources, energy, and atmosphere (from the cradle to the grave) are defined and quantified [33]. LCA contributes, including the production, utilization, and landfill process, for all resource and energy inputs and

outputs of a product over its lifetime. The environmental impact measured by conducting an LCA practice must be transformed into a singular dimensionless value. The proposed procedure includes two sub-processes: standardization and weighting, two additional components of the LCA method of life-cycle impact assessment, as defined in the ISO 14044 International Standard [34]. Standardization is the magnitude measurement for the reference information of the section indicating findings. This will also help convey details on the relative value of the effects of the indicator [35]. Weighting is a procedure using numerical variables to transform the findings of the impact category metrics, enabling the converted metrics to be aggregated further [36]. LCA intends to examine the unique influence of a product or service to the environmental burdens in its various life cycle phases. The ISO 14040:2006 and ISO 14044:2006 [34,37,38] set out four interrelated measures: (1) Goal and scope definition; (2) inventory analysis; (3) impact assessment; (4) interpretation which identifies relevant issues and formulate recommendations. These phases are explained in detail in the next subsections.

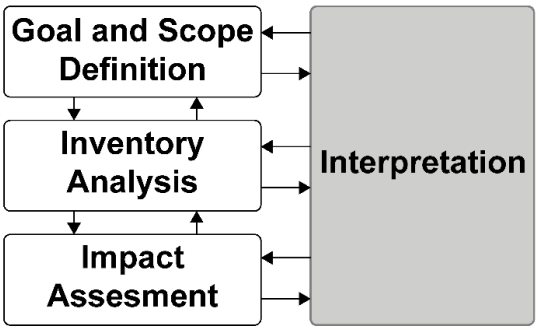

Figure I-3: The life cycle assessment guidelines

I.6.2.1 Goal and scope definition

Three key regions, system borders, impact groups and the functional unit are included in this process. The whole product development (cradle to grave idea) must be evaluated on the system border. The environmental effects of the impact groups are measured using indicators as the ReCiPe 2016 [39] impact value. The ReCiPe is a measure that is broadly utilized for comprehending damage. Eighteen metrics of middle point effect are chosen and clustered in three groups of endpoint damage. They are (1) ecological quality that covers acidification & eutrophication, ecological toxicity, and land use; (2) cancer-causing issues, environmental issues, cosmic rays, deteriorating ozone levels and breathing impacts, and (3) fossil fuel and mineral mining raw material. These results are given in classifications of impact and by specific measures determine the environmental burden. The decision-maker

considers this kind of measure more comprehensible than the so-called mid-point concept [40].

I.6.2.2 Inventory analysis

It considers input, performance, and energy usage in connection with product in the second phase of the LCA sequence. In the impact evaluation step, they are further interpreted in waste and pollution. The material distribution and delivery to the factory are regarded during the entire project time. Besides the energy usage in the framework, the related impact during its lifespan can be obtained from databases as Ecoinvent [41].

I.6.2.3 Impact assessment

During this step, the inventory records are transcribed into sustainability reports. As already stated, three separate areas of damage are covered: health care, the environment, and risk to infrastructure centred on the 2016 ReCiPe framework [39]. The assisted system classification may be carried out for either or not the midpoints depending on the endpoints scale. The loss can be represented as follows numerically for each impact section.

$$IMP_e = \sum_i \theta_{ei}.LCI_i^{ToT} \quad \forall e \qquad \text{Eq.I-15}$$

Where LCI_i^{ToT} is the life cycle inventory related to production, resource logistics and plant execution, correlated with the primary flow *i*. θ_{ei} showed the damage component with respect to the elementary flow *i* impact factor *e*. This aspect encourages a connection between the inventory and the classifications of damage.

$$DAM_d = \sum_{e \in ID_d} IMP_e \quad \forall d \qquad \text{Eq.I-16}$$

$$RCP_d = \sum_d \delta_d \varepsilon_d DAM_d \quad \forall d \qquad \text{Eq.I-17}$$

Where DAM_d describes a classification of endpoint effects in damage classification *d*. RCP is the standardized ReCiPe 2016 measure and δ_d, and ε_d are the specific weight and normalization elements. The element of normalization is calculated based on the EU damage computations for land use and emissions calculations [42]. The weighting variables are calculated based on suggested values, as described in the ReCiPe 2016.

I.6.2.4 Interpretation

In addition to several suggestions which help to improve system efficiency, this step offers an evaluation of the findings. In this sense, policymakers can recognize the weak points conveniently along the way, where additional effort must be made to decrease the environmental impact. Even so, there are no specific boundaries on how the decrease can be achieved. Besides, because of the range of possibilities and differing targets (i.e., impact classifications) in many situations, assessment is highly complicated. The LCA findings can be implemented as variables in the statistical model in order to address these constraints.

I.7 Outline: Low carbon technologies case studies

The simulation-based optimization methods have a great potential for solving computationally expensive real-world sustainability problems. These methods can aid decision-makers and policymakers in their struggle of taking correct actions towards a more sustainable future. In the next lines we briefly comment on the problems we have addressed in this thesis.

I.7.1 Sustainable SDHS potential in EU (article 1)

Aligning with the ambitions EU 2030 climate & energy package for cutting the greenhouse emission and replacing conventional heat sources through the presence of renewable energy share inside efficient district heating fields, central solar heating plant coupled with seasonal storage (CSHPSS) can have a viable contribution to this goal. However, the performance uncertainty combined with the inadequate assessment regarding the financial potential and the greenhouse gas emission reduction associated with the deployment of those innovate district heating systems represents a big challenge for sufficiently applying the CSHPSS in Europe.

In this context, this paper presents a comprehensive evaluation for the possibility of integrating CSHPSS in the residential sector at various EU states members through the formulation for a multiple objective optimization problem. This problem comprises the life-cycle cost analysis (LCC) for the economic evaluation and the Life Cycle Assessment (LCA) for the environmental impact simultaneously with consideration for both the space heating (SH) demand and the domestic hot water (DHW) services. The methodology framework is applied to a residential neighborhood community of 1120 apartment under various EU climate zones that comprise Madrid, Athens, Berlin, and Helsinki as a representative for the Mediterranean continental, Mediterranean, central European, and Nordic climates, respectively. The environmental assessment shows a significant improvement when using the CSPHSS in comparison to the natural gas heating systems where the environmental impact associated with the CSPHSS is reduced 82-87%. On the other hand, an extensive economic improvement is limited especially in the Mediterranean climate

zone (Athens) with low heating demand and prices for the non-renewable resources where the total economic cost of the CSHPSS plants can increase up to 50.8%. However, aligning with the increment tendency in natural gas price in EU nowadays, the future development in the plant cost confirms its favorable economic feasibility at the long term. Figure I-4 shows a graphical summary for article 1.

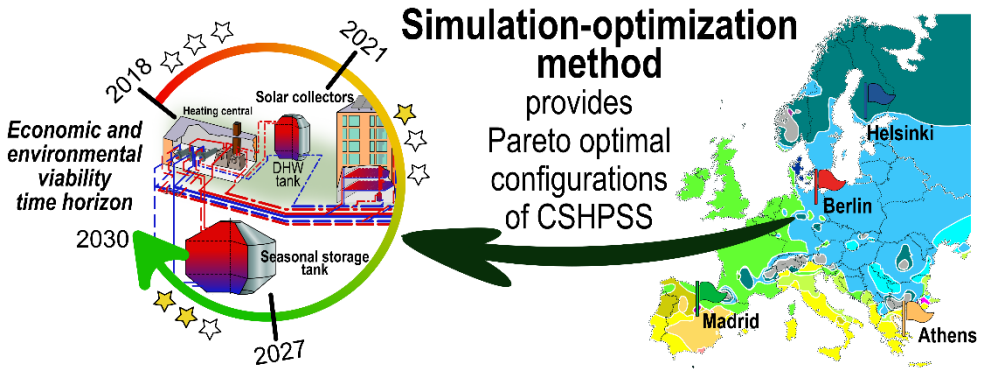

Figure I-4: Graphical abstract of article 1: Economic and environmental potential for solar assisted central heating plants in the EU residential sector: Contribution to the 2030 climate and energy EU agenda

I.7.2 Machine learning approach to improve SDHS sustainability (article 2)

A promising pathway towards sustainable transaction to clean energy production lies in the adoption of solar assisted district heating systems (SDHS), which are placed in the end-user sector and hence reduce energy transmission losses. However, SDHS technical barriers during their design and operation phases, combined with their economic limitation, promote a high variation in quantifying SDHS benefits over their lifetime. This study proposes a complete framework using a robust machine learning approach based on an artificial neural network (ANN) to inherent sustainability principles in the design of SDHS. These principles comprising the life cycle cost analysis and the life cycle assessment are formulated in a multi-objective optimization problem to assess the SDHS beneficial performance in comparison to conventional heating systems based on natural gas. Moreover, the methodological framework investigates the uncertainty in the context of SDHS design, in which the Global Sensitivity Analysis (GSA) based on Bayesian analysis of computer code outputs is combined with the Heuristics optimization frameworks using the low computational expenses benefits of the ANN model.

Figure I-5: Graphical abstract of article 2: a framework for the optimal integration of solar assisted district heating in different urban sized communities: a robust machine learning approach incorporating global sensitivity analysis

The application of the framework is illustrated through a case study for the optimal design of SHDS at different urban community sizes (10, 25, 50, and 100 buildings) located in Madrid. The optimization problem is formulated under two optimizations setting where the first setting includes only the system equipment sizing, whereas the other setting embraces the seasonal storage tank (SST) construction materials as well in the optimization problem. Results reveal a substantial improvement in environmental benefits for deploying SDHS instead of the natural gas boilers with the increment in the community size, especially with including the SST construction properties in the optimization problem, and it can achieve an improvement up to 89.3% in the community size of 100 buildings. Moreover, SDHS can reduce the greenhouse gas payback period up to 3 years for all community sizes. These benefits are extended to the economic objective and are reduced up to 30.7-66% based on the community size. In terms of the economic payback period, SDHS show their feasibility when increasing the community size; the payback period can reach 13.7 years at the community size of 100 buildings. Regarding the technical performance, optimization results show that the solar fraction did not fall below 82.1 % for the investigated community sizes with efficiency for the SST above 69.5%. Finally, GSA results indicate the initial investment cost of the SST and its relevant construction materials, in addition to the annual natural gas inflation rate, are primarily responsible for the variability in the optimal system feasibility. The proposed framework based on the robust machine learning approach can provide a good starting point to solve the enormous computational expenses drawbacks associated with the heuristics optimization approach. Furthermore, it can function as a decision support tool that retrofits efforts toward the most effective action plans to fulfill the European Union energy targets regarding clean energy production. Figure I-5 shows a graphical summary for article 2.

I.7.3 Sustainable integration of heat pump in SDHS (article 3)

The movement toward the 4th generation district heating (4GDH) embrace a great opportunity to support the future smart energy development concept. However, its development is addressing technological and economic obstacles aligning with the need for a reformation of the energy market to ensure the quality of service. In this context, our paper presents a comprehensive analysis based on a multi-objective optimization framework incorporating artificial neural network-based model for the possibility of integrating heat pump (HP) into solar assisted district heating (SDHS) with seasonal thermal energy storage to support the sustainable transition toward 4GHD. The study evaluates the performance of the proposed system with the help of key performance indicators (KPI) related to the 4GDH characteristics and key stakeholders for possible market growth with consideration for the environmental benefits.

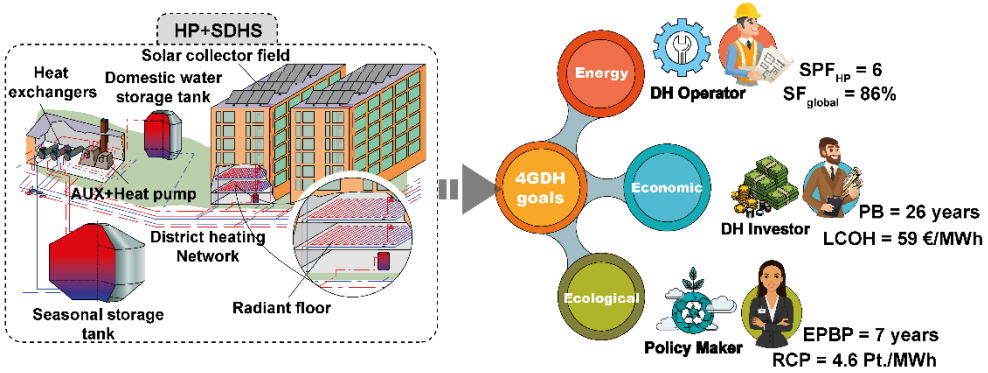

Figure I-6: Graphical abstract of article 3: Flexible Heat Pump Integration to Improve Sustainable Transition Toward 4th Generation District Heating

The framework application is illustrated through a case study for an optimal integrating of HP under different control strategy into a SDHS located in Madrid to cover the heating demand of a small neighbourhood of 10 buildings. Inherent the SDHS operator stakeholder perspective, the results reveal a significant improvement in the stabilization of the SDHS performance due to the HP integration where the solar field temperature never exceeds 80^{o}C and seasonal storage tank (SST) temperature stands at 85.4^{o}C. Furthermore, the solar fraction never falls below 86.1% with an efficiency of 73.9% for the SST. While the seasonal HP performance factor stands above 5.5 for all optimal scenarios. From the investor viewpoint, a 59.1 Euro/MWh can be achieved for the proposed system with a payback period of 26 years. Finally, from the policymaker perspective, along with the significant economic and sustainable improvement in the SDHS performance, a substantial environmental improvement of 82.5% is achieved in comparison to the conventional natural gas heating system. The proposed analysis reflects a great motivation for different

stakeholders to propose this system as a path toward the 4GDH in the future district energy systems. Figure I-6 shows a graphical summary for article 3.

I.7.4 Thermal Energy Storage in Circular Economy (article 4)

The present study develops a methodology framework for Sustainable Circular System Design (SCSD), aiming to assess Thermal Energy Storage (TES) technologies from an ecological point of view. To this end, a composite indicator, namely, Environmental Sustainability and Circularity indicator (ESC) is provided. This indicator combines the environmental impacts of the TES system, via the conduction of an LCA, and its circulatory performance using product-level Material Circularity Indicator (MCI). The developed methodology is applied to a case study of a liquid (molten salts) thermal storage media. The SCSD embraces the analysis for the most relevant processes through proposing different ecological scenarios including, increasing the recycling rates (Modest Scenario), increasing the reuse rates (Medium Scenario), and a combination of both (Optimistic scenario).

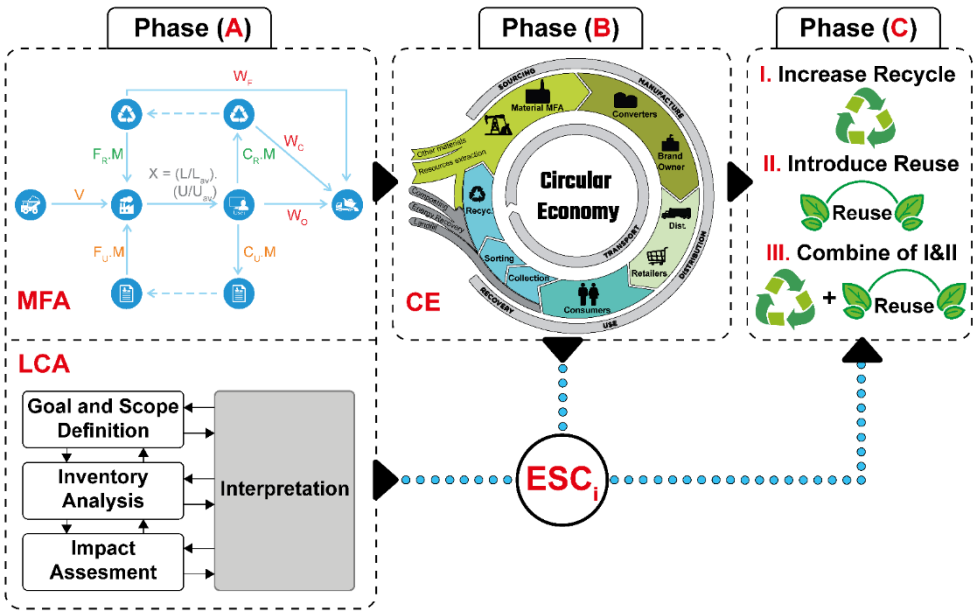

Figure I-7: Graphical abstract of article 5: A Framework for Sustainable Evaluation of Thermal Energy Storage in Circular Economy

The circularity analysis showed that for the scenarios Modest, Medium and optimistic, the MCI moves from 20.6% for the current situation to 30.3%, 38.6%, and 46.4%, respectively. The results also revealed that improving circularity generally reduces environmental impacts. Accordingly, the optimistic scenario showed the most environmentally sustainable and circular scenario with ESC of 7.89%, where Modest

and Medium scenarios exhibited ESCs of 1.20% and 2.16%, respectively. A major obstacle for substantial improvement of the circulatory and ESC is the high share of unrecyclable molten salts in the system and therefore, any effort to improve the circulatory and the environmental benefits of this system can be reached by using more environmentally friendly alternative materials. The study concludes that the integration of reusing and recycling at the initial design should be sought in order to achieve a more environmentally sustainable and circular outcome. Figure I-7 shows a graphical summary for article 4.

I.7.5 SDHS potential to achieve Zero Energy Buildings (article 5)

Arising Nearly Zero Energy Buildings (NZEB) concept in Europe, the solar district heating systems (SDHS) present a potential solution to meet the European energy performance directive for the buildings sector. Nevertheless, current practices face several technological and economical barriers to ensure service quality. In this context, our work presents a sustainability analysis (technical, economic, environmental, and social) for SDHS integration in the residential sector to meet the NZEB and positive energy building goals.

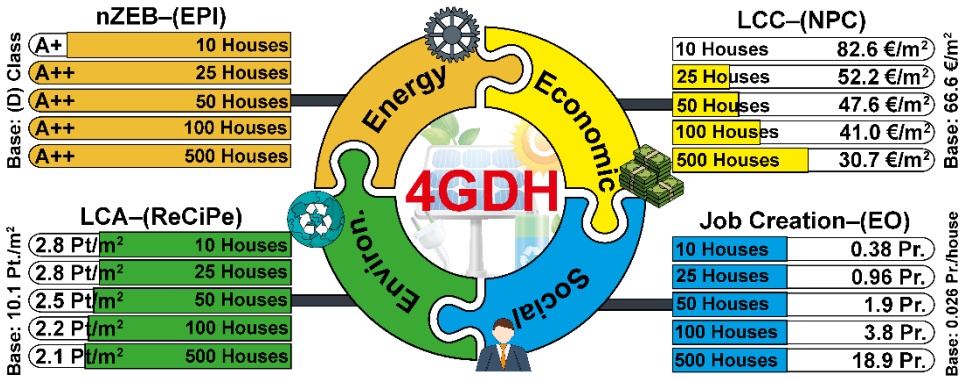

Figure I-8: Graphical abstract of article 5: Sustainable Insights on Emerging Solar District Heating Technologies to Boost the Nearly Zero Energy Building Concept

This paper proposes an application of the machine learning model based incorporating a multi-objective optimization and multi-criteria decision making to facilitate a sustainability index for the decision-making stakeholders and policymakers. The proposed analysis application is illustrated through retrofitted residential communities with building energy rating (D) at different sizes (10, 25, 50, 100, and 500 houses) located in Emmen (Netherlands) and compared to a standard decentralized heat pump. The optimization results show the ability of SDHS to provide a solar fraction up to 95% at the community of 500 houses. Furthermore, achieving a NZEB status is only approved economically at community size ≥ 100 houses with life cycle cost of 41 €/m^2 and a payback period of 25 years. These results align with a substantial environmental and social improvement of 78.2% and 29.7%, respectively compared to the decentralized heat pump. Overall, this study provides policy decision

making with an evaluation for positive energy communities and suggests the SDHS integration to meet the global sustainability goals. Figure I-8 shows a graphical summary for article 5.

I.7.6 Allocation for Nearly Zero Energy Building Constraints (article 6)

The nearly zero-energy buildings (nZEB) present a promising contribution to fulfill the EU sustainable future targets. However, the construction industry that leads the development of nZEB is facing challenges to guarantee its performance. In this context, this paper proposes a methodology framework based on Multizone Resistance–Capacitance Model to trace the nZEB performance challenges with quantifications for the time-dependent variables comprising occupant behaviors as well as the dynamic behavior of weather conditions and building operations. This approach incorporates Bayesian optimization for calibration purposes to minimize the required monitoring data. Moreover, the proposed framework integrates the uncertainty analysis (UA) with two-step global sensitivity analysis (GSA) in order to quantify and assess the uncertainty associate with the performance of the developed digital dwelling.

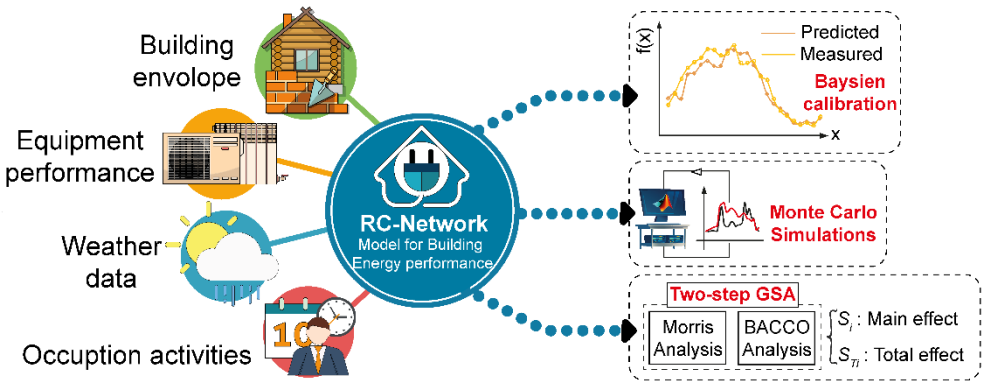

Figure I-9: Graphical abstract of article 6: a real-time diagnostic tool for evaluating the thermal performance of nearly zero energy buildings

The methodology application is demonstrated through a case study for a newly renovated two-story dwelling located in a district of Emmen at the Netherlands. The results confirm a high accuracy for the digital dwelling performance where the model offers a prediction accuracy of 2.2% and 7.03% for the thermal energy consumption and indoor zone temperature, respectively. On the other hand, the UA confirms a high uncertainty associate with the nZEB performance where the total thermal energy consumption can increase up to 100 kWh/m^2/yr. This variation is driven by the infiltration rates followed by the building envelope characteristics. The proposed framework can serve a diagnostic tool to assist the construction and installation companies to maintain the performance of their products proactively. Figure I-9 shows a graphical summary for article 6.

I.8 General conclusions

This thesis has been devoted to develop mathematical programming models to support sustainable decision and policy making. Different methodology frameworks have been developed to tackle some sustainability challenges with emphasis on sustainable energy systems modelling in the residential sector. We next present a summary of the knowledge derived from the study of five problems addressed in this thesis which is covering the low carbon energy technologies problem represented by the SDHDS, and its application to achieve NZEB. Note that further discussions and particular conclusions can be found in each corresponding chapter. The general conclusions are listed below:

- A systematic multi-objective optimization approach is proposed to design a complex SDHS which is applied to optimize the cost and the aggregated environmental metric throughout the life cycle of the system in comparison to conventional heating systems using natural gas boilers. This approach proposes guidelines for different stakeholders to evaluate the SDHS potential at different EU climate conditions.
- The proposed methodological framework successes in reducing the technical variation the system performance when introduced in various EU climate zones. Furthermore, the overall trend indicates that for the installation to be more profitable from the economic point of view, a better distribution of available and demanded energy is preferable (and this strongly depends on the climate conditions). On the other hand, from the environmental point of view all the cases showed great long-term reduction comparing to a natural gas system. However, the low heating demand and low prices of the natural gas and g optimization problem and investigate the possible market growth with consideration for the environmental benefits.
- Taking advantage of the low computational cost feature associated with the robust ANN model, the uncertainty associated with the economic parameters (investment costs, energy carrier prices, etc.) is investigated through global sensitivity analysis based on Bayesian analysis of computer code outputs.
- With including the seasonal TES design parameters in the optimization problem, a large improvement in both the economic and environmental performance of the SDHS is indicated. Furthermore, the uncertainty analysis reveals that the variation in the optimal SDHS cost and its relative impact is due to the initial investment cost of the SST and its relevant construction materials in addition to the annual natural gas inflation rate.
- With including the heat pump technology in the SDHS design to stabilize its performance and assist in the sustainable transition towards 4th generation district heating (4GDH), a novel methodology with the help of key performance indicators (KPI) related to the 4GDH characteristics and key stakeholders for possible market growth and expansion is proposed. This

multi-perspective analysis can be used by the key stakeholders as a starting point to develop necessary business models which will allow the full competitiveness of SDHS for the sustainable energy transition.

- With arising for the NZEB concept in Europe, a complete sustainability analysis (technical, economic, environmental, and social) for SDHS integration in the residential sector to meet the NZEB and positive energy building goals is proposed. This approach comprises an application of the machine learning model based incorporating a multi-objective optimization and multi-criteria decision making to facilitate a sustainability index for the decision-making stakeholders and policymakers.
- To trace the economic failure of the seasonal TES, a methodology framework is developed for Sustainable Circular System Design (SCSD), aiming to assess TES from an ecological point of view. To this end, a composite indicator, namely, Environmental Sustainability and Circularity indicator (ESC) is provided. This indicator combines the environmental impacts of the TES system, via the conduction of an LCA, and its circulatory performance using product-level Material Circularity Indicator (MCI).
- With the NZEB performance challenges, a novel diagnostic tool to guarantee and proactively maintain the indoor climate performance of NZEB with consideration for the temporal variation associate with the climate data and occupant behavior during the operation stage of the building. Furthermore, with the data analysis model based on uncertainty incorporating global sensitivity analysis, additional knowledge in the future can be added to the builders, installers, and occupants, which can bridge the NZEB concept with the client anticipations.

I.9 Future work

A wide range of issues as well as potential improvements and new ideas have been revealed in the course of this thesis that may be focus of further investigation. Here we present some of the potential research lines to be explored in future work:

- The relevance of the work presented in this thesis extends beyond the research field of district heating systems and can relate to multiple environmental and economic aspects. A potential barrier to the wider adoption of distributed heating systems in urban environments is the uncertainty surrounding the wider energy landscape, causing investors to be more hesitant towards these systems. Thus, the investigation of uncertainty's impacts should importantly be addressed. Therefore, the adoption of these methods from practitioners can assist in designing systems that are robust against uncertainty, hence, increasing their attractiveness.
- Future research can focus on investigating uncertainty in different energy system contexts. In fact, in any part of the energy modelling spectrum uncertainty sources can most likely be traced. Therefore, any modelling

activity that takes place in a deterministic context can be extended to include uncertainty considerations. For instance, it would be of interest to investigate the impacts of uncertainty for multi-site energy system configurations. In that way, we could determine whether interconnections between multiple sites allow systems to better hedge against uncertainty and to what degree this would be favourable. Additionally, the focus could also be placed on isolated systems e.g., in remote areas. If grid interconnection is not available or cannot fully support the needs of remote communities, useful insights can be obtained by designing systems that are robust against uncertainty. Finally, the design of systems that aim to achieve specific goals could also be investigated, such as zero-energy or zero-carbon communities. If such systems are designed deterministically, there is always the risk of failing to meet the targets under uncertainty. Therefore, it would be interesting to investigate how systems that can achieve their targets under any conditions or with high probability should be designed.

- For the building performance, the modelling of stochastic occupancy and activity patterns in buildings is an important aspect. Therefore, more advanced models following the ones mentioned in Chapter VII can be coupled with BPS tools to better reproduce the stochastic occupancy and activity patterns.
- Social indicators were almost neglected in our approach. Enlarge the scope of the sustainability encompassing more social aspects together with the economic and environmental criteria will be a major focus for future research. Although it might probe challenging from the parameter gathering perspective, there are some emerging methodologies recently proposed (i.e., Social Life Cycle Assessment initiative) that may be used to include social aspects.
- A comprehensive circular economy analysis with consideration for the recycling impact as well as the potential for reuse concept in the design and manufacturing of the SDHS can enhance its feasibly with meeting the EU 2030 targets.

I.10 References

[1] Sousa J. Energy simulation software for buildings: Review and comparison. CEUR Workshop Proc., vol. 923, 2012, p. 57–68.

[2] Behrendt, B., Raimondo, D., Zhang, Y., Schwarz, S., Christensen, J. E., & Olesen BW. A system for the comparison of tools for the simulation of water-based radiant heating and cooling systems. 12th Conf. Int. Build. Perform. Simul. Assoc., http://www.bs2011.org/; 2011.

[3] Klein SA et al. TRNSYS Version. 18, Solar Energy Laboratory, University of Wisconsin-Madison, Website: <http://sel.me.wisc.edu/ trnsys> 2004.

[4] Crawley DB, Hand JW, Kummert M, Griffith BT. Contrasting the capabilities of building energy performance simulation programs. Build Environ 2008;43:661–73. doi:10.1016/j.buildenv.2006.10.027.

[5] Bornatico R, Hüssy J, Witzig A, Guzzella L. Surrogate modeling for the fast optimization of energy systems. Energy 2013;57:653–62. doi:10.1016/j.energy.2013.05.044.

[6] Wong SL, Wan KKW, Lam TNT. Artificial neural networks for energy analysis of office buildings with daylighting. Appl Energy 2010;87:551–7. doi:10.1016/j.apenergy.2009.06.028.

[7] Østergård T, Jensen RL, Maagaard SE. A comparison of six metamodeling techniques applied to building performance simulations. Appl Energy 2018;211:89–103. doi:10.1016/j.apenergy.2017.10.102.

[8] Yang Y, Zhang S, Xiao Y. Optimal design of distributed energy resource systems coupled withenergy distribution networks. Energy 2015;85:433–48. doi:10.1016/j.energy.2015.03.101.

[9] Grossmann IE, Caballero JA, Yeomans H. Advances in mathematical programming for the synthesis of process systems. Lat Am Appl Res 2000;30:263–84.

[10] Hany M, Vallès M, Cabeza LF, Boer D. A framework for the optimal integration of solar assisted district heating in different urban sized communities : A robust machine learning approach incorporating global sensitivity analysis. Appl Energy 2020;267:114903. doi:10.1016/j.apenergy.2020.114903.

[11] Ehrgott M. Multicriteria optimization. Heidelberg: Springer; 2005.

[12] Deb K. Multiobjective Optimization Using Evolutionary Algorithms. New York, NY: John Wiley & Sons, Inc; 2001.

[13] Konak A, Coit DW, Smith AE. Multi-objective optimization using genetic

algorithms : A tutorial. Reliab Eng Syst Saf 2006;91:992–1007. doi:10.1016/j.ress.2005.11.018.

[14] Wetter M. GenOpt. Generic Optimization Program. User Manual. California: 2011. doi:10.2172/962948.

[15] Bava F, Furbo S. Development and validation of a detailed TRNSYS-Matlab model for large solar collector fields for district heating applications. Energy 2017;135:698–708. doi:10.1016/j.energy.2017.06.146.

[16] Abokersh, Mohamed Hany, Kangkana Saikia, Luisa F cabeza, Dieter Boer MV. Flexible heat pump integration to improve sustainable transition toward 4th generation district heating. Energy Convers Manag 2020.

[17] Snoek J, Larochelle H. Practical Bayesian Optimization of Machine Learning Algorithms. Adv. neural Inf. Process. Syst., 2012, p. 2951–2959. doi:10.1016/S2468-2667(17)30214-1.

[18] Saltelli A, Annoni P. How to avoid a perfunctory sensitivity analysis. Environ Model Softw 2010;25:1508–17. doi:10.1016/j.envsoft.2010.04.012.

[19] Hwang C-L, Yoon K. Methods for Multiple Attribute Decision Making, 1981, p. 58–191. doi:10.1007/978-3-642-48318-9_3.

[20] Sari F. Forest fire susceptibility mapping via multi-criteria decision analysis techniques for Mugla, Turkey: A comparative analysis of VIKOR and TOPSIS. For Ecol Manage 2021;480:118644. doi:10.1016/j.foreco.2020.118644.

[21] Montgomery DC. Design and Analysis of Experiments, Eighth Edition. John Wiley & Sons, Inc.; 2013.

[22] Borgonovo E, Plischke E. Sensitivity analysis: A review of recent advances. Eur J Oper Res 2016;248:869–87. doi:10.1016/j.ejor.2015.06.032.

[23] Yang J. Convergence and uncertainty analyses in Monte-Carlo based sensitivity analysis. Environ Model Softw 2011;26:444–57. doi:10.1016/j.envsoft.2010.10.007.

[24] Kennedy MC, O'Hagan A. Bayesian calibration of computer models. J R Stat Soc Ser B (Statistical Methodol 2001;63:425–64. doi:10.1111/1467-9868.00294.

[25] Uusitalo L, Lehikoinen A, Helle I, Myrberg K. An overview of methods to evaluate uncertainty of deterministic models in decision support. Environ Model Softw 2015;63:24–31. doi:10.1016/j.envsoft.2014.09.017.

[26] Petropoulos G, Wooster MJ, Carlson TN, Kennedy MC, Scholze M. A global Bayesian sensitivity analysis of the 1d SimSphere soil-vegetation-

atmospheric transfer (SVAT) model using Gaussian model emulation. Ecol Modell 2009;220:2427–40. doi:10.1016/j.ecolmodel.2009.06.006.

[27] Tulus V, Boer D, Cabeza LF, Jiménez L, Guillén-Gosálbez G. Enhanced thermal energy supply via central solar heating plants with seasonal storage: A multi-objective optimization approach. Appl Energy 2016;181:549–61. doi:10.1016/j.apenergy.2016.08.037.

[28] Kalogirou SA. Solar energy engineering: processes and systems. 1st Ed. Academic Press; 2009. doi:10.1016/B978-0-12-374501-9.00014-5.

[29] Duffie, J.A., Beckman WA. Solar Engineering of Thermal Processes. 3rd ed. John Wiley & Sons, Inc; 2006.

[30] Pavičević M, Novosel T, Pukšec T, Duić N. Hourly optimization and sizing of district heating systems considering building refurbishment – Case study for the city of Zagreb. Energy 2017;137:1264–76. doi:10.1016/j.energy.2017.06.105.

[31] Gluch P, Baumann H. The life cycle costing (LCC) approach: A conceptual discussion of its usefulness for environmental decision-making. Build Environ 2004;39:571–80. doi:10.1016/j.buildenv.2003.10.008.

[32] Chemical Engineering Plant Cost Index (CEPCI): Economic Indicator. Chem Eng J 2015.

[33] Nemerow NL, Agardy FJ, Sullivan P, Salvato JA. ENVIRONMENTAL ENGINEERING: Environmental Health and Safety for Municipal Infrastructure, Land Use and Planning, and Industry. 6th ed. John Wiley & Sons, Inc; 2009.

[34] International Organization for Standardization (ISO). ISO 14040: Environmental management - Life Cycle Assessment - Principles and framework. 2006. doi:10.1002/jtr.

[35] Mantalovas K, Di Mino G. Integrating circularity in the sustainability assessment of asphalt mixtures. Sustain 2020;12:9–12. doi:10.3390/su12020594.

[36] International Organization for Standardization. SO 14040-Environmental Management—Life Cycle Assessment—Principles and Framework. Geneva, Switzerland: 2006.

[37] International Organization for Standardization (ISO). ISO 14041: Environmental Management - Life Cycle Assessment: Goal and Scope Definition and Inventory Analysis. 1997.

[38] International Organization for Standardization (ISO). ISO 14042:Environmental management - Life cycle assessment - Life cycle impact. 2000.

[39] Goedkoop M, Heijungs R, Huijbregts M, Schryver A De, Struijs J, Zelm R Van. ReCiPe: A LCIA method which comprises harmonised category indicators at the midpoint and the endpoint level. Report I: Characterisation 2008. 2009. doi:10.029/2003JD004283.

[40] Tulus V, Abokersh MH, Cabeza LF, Vallès M, Jiménez L, Boer D. Economic and environmental potential for solar assisted central heating plants in the EU residential sector: Contribution to the 2030 climate and energy EU agenda. Appl Energy 2019. doi:10.1016/j.apenergy.2018.11.094.

[41] Weidema BP, Bauer C, Hischier R, Mutel C, Nemecek T, Reinhard J, et al. Data quality guideline for the ecoinvent database version 3. vol. 3. 2013.

[42] JRC European commission (JRC-IES). ILCD Handbook: Recommendations for Life Cycle Impact Assessment in the European context. 1st editio. Luxemburg: Office of the European Union; 2011. doi:10.278/33030.

Chapter II

Sustainable SDHS potential in EU

II. Sustainable SDHS potential in EU

Economic and environmental potential for solar assisted central heating plants in the EU residential sector: Contribution to the 2030 climate and energy EU agenda

Victor Tulus [a], Mohamed Hany Abokersh [b], Luisa F. Cabeza [c], Manel Vallès [b], Laureano Jiménez [a], Dieter Boer [b,*]

[a] Departament d'Enginyeria Química, Universitat Rovira i Virgili, Av. Països Catalans 26, 43007 Tarragona, Spain

[b] Departament d'Enginyeria Mecànica, Universitat Rovira i Virgili, Av. Països Catalans 26, 43007 Tarragona, Spain

[c] GREiA Research Group, INSPIRES Research Centre, Universitat de Lleida, Pere de Cabrera s/n, 25001 Lleida, Spain

[*] *Corresponding author: dieter.boer@urv.cat*

E-mail addresses: victor.tulus@urv.cat (V.Tulus), mohamed.abokersh@urv.cat (M.H.Abokersh), lcabeza@diei.udl.cat (L.F.Cabeza), manel.valles@urv.cat (M.Vallès), laureano.jimenez@urv.cat (L.Jiménez)

Keywords: Central solar heating plant with seasonal storage, Solar community, Life cycle assessment (LCA), Life cycle cost (LCC), Multi-objective optimization, 2030 climate and energy EU targets

II.1 Introduction

The global tendency for changing the world energy map is a booming topic, and more efforts should be scaled up to shift the current energy production systems towards the use of cleaner and less carbon-intensive sources. Currently, fossil fuels share about 80% of the primary energy use [1]. The International Energy Outlook [2] forecasts a significant increase in the world energy demand over the next decades.

It is projected that global energy consumption will evolve by 48% in 2040 with a growth in the usage of crude oil and natural gas by 30% and 53.2%, respectively. This outlook trend leads to serious environmental problems such as more greenhouse gas (GHG) emissions and the subsequent impact on the climate [3].

Europe is one of the relevant players in this scenario contributing 21.6% to the overall energy consumption [4]. Additionally, in the European Union (EU) the building stock accounts for about 40% of the total energy demand [5], while the residential sector consumes 63% of this energy [6]. According to estimations of the US Energy Information Administration (EIA) [2], the energy consumption demand for the residential section in the EU increases by an average of 0.9% per year. Along with all of these figures, the residential buildings are the fourth most important source of GHG in the EU, and it accounted for about 10% of the total GHG in 2016 [7]. In response to this challenge, the EU has adopted the 2020 climate and energy package [8] which includes requisite legislation to tackle the environmental concerns and support the energy security and independence. The package sets three main targets: (i) reduce by 20% the GHG emissions compared to the 1990 levels, (ii) increase the renewable energy share and (iii) improve its energy efficiency by 20%. In 2013, the EU approved a new ambitious framework for the climate and energy between 2020 and 2030. This strategy plans to cut the GHG emissions by 40%, to achieve a share of at least 27% of renewable energies, and to improve the energy efficiency by at least 27% [9].

Among all of the renewable energy resources, the solar thermal energy obtained considerable attention since it is a CO_2 neutral and it can be used for both space and water heating [10,11]. It was reported that solar thermal technologies could substantially satisfy the heat demand in the residential sector in many countries [12]. Furthermore, it has several advantages which include [13] (i) savings in the primary energy consumption at the end user and country planning level, (ii) increase in energy security against the fluctuations in the prices of the conventional energy resources, (iii) decrease the dependency on the electricity from the network, and (iv) contribute to the network stabilization. These solar thermal energy systems continue to increase their market share across whole Europe. More than 1.2 $GW_{thermal}$ was installed within 2015 to raise the total installed capacity to 34.4 $GW_{thermal}$ [14].

However, the solar thermal systems are facing a significant challenge of intermittency and predictability, which cause a gap between the supply and the energy demand [15,16]. The thermal energy storage (TES) systems can effectively solve this issue [17]. There are three main categories of the TES. These categories include the sensible TES through a temperature gradient, the latent TES based on the phase change materials, and the thermo-chemical TES through chemical reactions [18]. Currently, sensible storage is the most common system to be used in the residential sector, while latent and chemical systems are promising technologies under development [19].

The specific heat and energy density are the two main characteristics that evaluate the thermal capacity of the sensible TES. Besides thermal capacity characteristics, the TES cost also has a vital role in the selection process. Therefore, water, rock material, and soil/ground are the usually employed storage media in sensible TES systems. The energy storage in the sensible TES systems can be classified into long-term (seasonal) and short-term (diurnal) [20]. The main difference between these two systems is the solar collector and storage volume sizing where the investment per square meter of collector area is almost doubled in the long-term seasonal storage systems [21]. In addition to that, seasonal storage is always coupled with an auxiliary heater to cover the shortage in supply [22]. On the contrary, short-term storage allows direct usage in the heating district network.

The solar district heating system coupled with sensible seasonal storage has been subjected to several investigations, and it has already been introduced as a feasible alternative. Initially, in the 1950's, Speyer [23] assesses theoretically the potential of the central solar heating plant coupled with seasonal storage (CSHPSS) to benefit from the excess of solar energy in summer during the winter period. The first proof of concept for this system was developed in Sweden in the 1970's to address the energy shortage crisis [24], followed by Denmark and Germany in the 1990's [25]. Since then, the market for solar heating plants has grown throughout Europe [26], particularly in Northern and Central European countries. During 2016, 37 large heating plants were installed in Europe compared to 21 new installed in 2015. Within these installations, 31 systems were added to the Denmark district heating networks, four systems in Germany, one system in Sweden and one system in France [27]. In the southern European countries, some positive signs of growth of solar thermal energy are noticed from Spain and Greece. These evolution signs are due to the legislation imposed by the governments to scale up the utilization of renewable energy technologies [28].

Several research entities such as the IEA's Task 32 and Task 45 [29] has paid attention to the solar district heating energy systems. Additionally, numerous articles discuss the principal methods available for the seasonal storage of the central solar heating system. Xu et al. [30] and Rad and Fung [31] presented an extensive review on the solar district energy system and its different types of TES. Shah et al. [32] conducted a comparative review to demonstrate the potential contribution of different TES options with a goal of building a decision support flowchart for the selection of TES based on the required application. In this context, Sibbitt et al. [33] and Antoniadis and Martinopoulos [34] developed several useful guidelines for the design of the CSHPSS. Rehman et al. [35], and Rämä and Mohammadi [36] conducted investigations toward the different options for community-sized solar thermal storage system configurations for the Nordic European climate zones. Also, Rad et al. [37], and Panno et al. [38] assessed the techno-economic promising performance of the

seasonal solar thermal storage in the residential sector. Finally, Ciampi et al. [39] demonstrated its environmental potentials.

In order to maximize the benefits from the centralized solar heating plants with seasonal storage in the residential sector, the optimal sizing of the system components and their operation should be adequately planned. This process can turn into a computationally requesting task. Li et al. [40] explored the optimal operation strategy for the CSHPSS based on the orthogonal schedule using real data. Durão et al. [41] and Rehman et al. [42] lean towards optimizing the design parameters of CSHPSS for different locations from an economical point of view using Genetic Algorithms, whereas Hirvonen et al. [43] also consider the community size effect. Buoro et al. [44] formulated a Mixed Integer Linear Programming (MILP) approach for optimizing the CSHPSS plant together with a conventional power unit for a large district heating network. Recently, several studies emphasized on the importance of taking into account the techno-economic parameters and the environmental impact simultaneously which expands the optimization approach for designing a new CSHPSS plant from a single objective optimization to a multi-objective optimization (MOO) problem. Tulus et al. [45] proposed a systematic MOO approach for designing CSHPSS plants based on a generic optimization tool according to economic and environmental indicators. The optimization of the environmental indicators become especially important as the main impact weight shifts from the fossil fuel consumption to the materials used for the installation of the system. Equally, Pavičević et al. [46] developed and demonstrated a long-term MILP optimization model based on SCIP (Solving Constraint Integer Program) solver for district heating systems. This model is capable of handling the operation strategy and system component sizing in the planning and evaluation process with considerations for the cost and the environmental impacts throughout the project lifetime. In addition, Welsch et al. [47] proposed an MOO approach for investigating solar district heating systems under various economic and environmental boundary conditions. Projection of the results promotes the influence of CSHPSS in increasing the feasibility of renewable energy technologies in the building sector.

Even though the tendency of the CSHPSS plants is promising, a range of potential barriers (technical, financial and administrative) are still obstructing the wide deployment of CSHPSS in Europe. One of the most important challenges associated with the CSHPSS is the significant performance variations. According to several large-scale seasonal energy storage systems, the solar fraction of the plants has a quite wide variation [48] which suggests a high degree of variation in the quantifiable costs and benefits. In German and Spanish CSHPSS projects [31, 36] the combination of seasonal heat storage with a central solar heating system enables solar fractions of over 50%. While in a CSHPSS project for a residential area in Alberta (Canada) 97% of solar fraction was achieved in the fifth year of operation [33]. A simulation study for district solar heating combined with seasonal borehole storage

in Helsinki showed that high solar fraction of 96% is feasible [51]. Besides the performance variation, the high capital costs of this technology represent a challengeable barrier and make it more difficult to obtain the required funding [52,53]. Also, there are primarily political and legal barriers which include: lack of a standardized model of the system which could help the European 2030 climate and energy framework achieve its targets; the sudden change in the renewable energy legal framework in some EU countries such as Spain [54]. All these technical, economic and legal barriers promote high variation in quantifying the CSHPSS benefits over its lifetime and add more difficulties for the EU members to state their forecast plans for future deployment of the CSHPSS in district heating fields.

Aligning with the challenges facing the wide deployment of CSHPSS in Europe combined with the ambitious EU 2030 climate and energy package for cutting the greenhouse emissions and increasing the share of renewable energies. The potential evaluation of a refurbished or a new solar district heating system requires not only its technical specification but its potential contribution when integrated into the end-user supply network taking into account the renewable source availability during various seasons of the year and the weather and ground conditions [55]. Thus, such issues call for developing an adaptive methodological framework to the local weather and ground conditions [56].

Due to the complexity of the CSHPSS design and its inconsistencies in the energy production combined with the challenges associated with its economic and environmental impact. The novelty in this work is to develop a methodological framework that supports the climate and energy goals of the EU through a comprehensive analysis for the techno-economic advantages and environmental impacts of CSHPSS plants in various EU member states with a comparison to a conventional heating system using natural gas as the primary heat source. In this context, a simulation-optimization methodology is developed with a detailed simulation of the CSHPSS plant performance using TRNSYS 18 software [57] considering seasonal and short-term storage systems and their respective load profiles based on the explored climates. Then a multi-objective optimization is performed by an external generic optimization toolbox (GenOpt [58]). The proposed methodology can serve as a supportive tool for decision-makers helping them assess the potential of the CSHPSS plants in Europe and subsequently, promote a clear statement towards the possibility of achieving the 2030 European climate and energy framework targets.

The article organization is the following: in Section II.2 a general overview of the CSHPSS system is provided. The mathematical formulation of the simulation-optimization methodology together with the mathematical basis of the CSHPSS market forecasting is provided in Section II.3. Section II.4 describes the application of the methodology to four EU climate zones, and Section II.5 offers the necessary

results and discussions. Finally, the conclusions of the work are presented in Section II.6.

II.2 Overview of the CSHPSS system

Central solar heating plants with seasonal thermal energy storage are designed to fulfill energy demands for space heating (SH) and DHW in a residential sector (see Figure II-1). Usually, these systems are designed to supply district heating for more than 100 apartments with a solar fraction of approximately 50% [49]. The main components of the CSHPSS system are the thermal solar collector, the seasonal storage tank (SST), and the DHW storage tank (DHWT). The solar collector transfers the heat gained from the solar radiation to the storage tanks which is then supplied to the customer on demand. The mismatching between the energy supply and demand in the daily and seasonal bases is balanced through the storage tanks. Auxiliary natural gas heaters are installed to back up the required heat demand in case the solar heating system failed to cover it.

The SST facilitates long-term storage of thermal energy used to cover the SH demand during a winter season with solar energy stored during a summer period. The long-term storage implies relatively large dimensions for the SST which favors slow charging and discharging processes. On the other hand, the DHWT is a short-term independent storage tank which is used to cover the daily DHW service at a temperature of 60ºC.

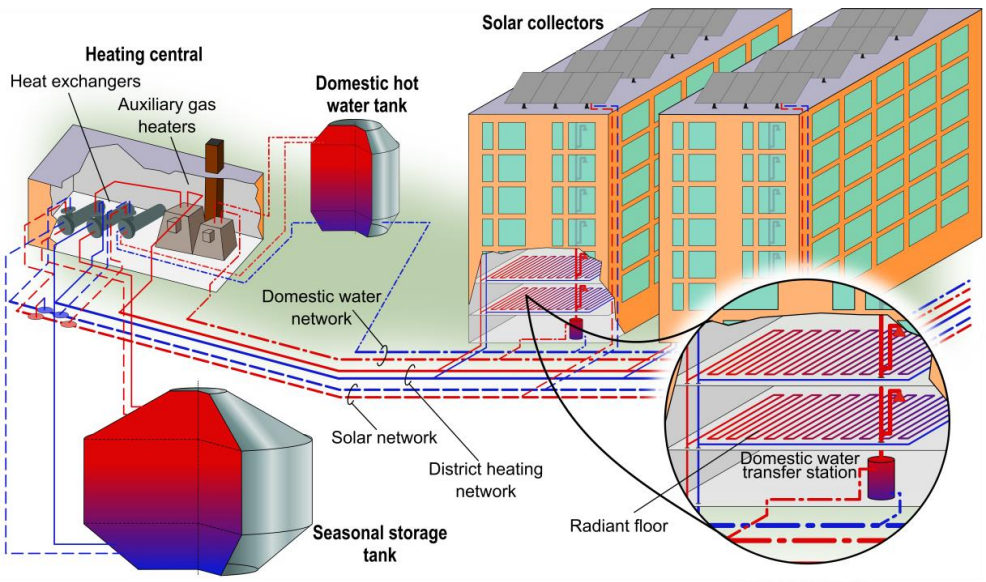

Figure II-1: Overview of the central solar heating system with long and short-term storage tanks coupled to a district heating network.

The proposed CSHPSS system is divided into four circuits, three of them are closed: solar field circuit, seasonal storage circuit, and SH distribution circuit; and the last one, DHW distribution circuit, is open (*i.e.*, fed from the water main) as shown in Figure II-2. The water-glycol mixture is the primary heat transfer fluid in the solar field circuit. The solar energy is collected through the field of solar collectors (COL), and a centrifugal pump (P_1) impulses the fluid to reach the heat exchangers (HE_1) and (HE_2). These heat exchangers connect the solar field circuit to the seasonal storage circuit or DHW distribution circuit depending on the selected control mode through Y-type valves. The heat exchangers separate the solar field circuit from the SST and DHWT to protect the solar collectors from damage [59].

In the DWH operation mode (priority 1) the monitored variables are the average DHWT temperature and the COL output temperature. Once the mode is triggered, the centrifugal pumps P_1 and P_4 are activated, and the water is sent towards the DHWT through HE_2. A natural gas boiler AUX_2 is installed to cover any occasional shortages in the thermal energy supply to the DHW network. Two Y-type valves regulate the water temperature which arrives at the DHW network through the mixing of fresh water from the water main with the hot water coming from the AUX_2.

In the SH operation mode (priority 2) the monitored variables are the SST temperatures, the average DHWT temperature, and the COL output temperature. Once the average DHWT temperature hits its setpoint and the COL output temperature is higher than the SST bottom temperature, the mode is activated by starting pumps P_1 and P_2 and allowing the heat transfer through HE_1 in order to charge the SST. During the heat demand period, a variable speed pump P_3 impulses the cold water to the bottom of the SST and discharges the hot water to the HE_3 that connects the seasonal storage circuit to the SH distribution circuit. Downstream the HE_3 a natural gas boiler AUX_1 is installed. This boiler operates when the SST cannot reach the setpoint. The combination of two Y-type valves regulates the water temperature arriving at the heating network through back-mixing of the returned water from the network with the hot water coming from the AUX_1.

Beside these two operation modes, the simultaneous SH and DWH mode (priority 3) is also established and regulated based on the controlling system when the conditions of the two previous modes are satisfied. Additional control loops regulate the operation of the Y-type valves in the SH and DHW distribution circuits in order to maintain the established setpoints at the entrances of the heating and DHW networks.

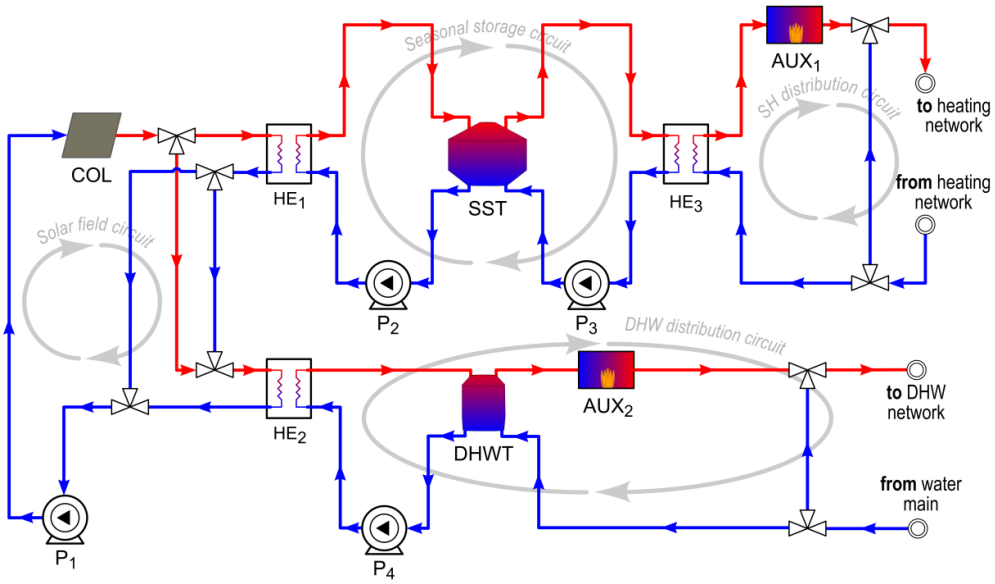

Figure II-2: Process flow diagram of the CSHPSS plant simulated in TRNSYS 18, where COL is the field of solar collectors, SST is the seasonal storage tank, DHWT is the domestic hot water tank, AUX_i are the auxiliary heaters, HE_i are the heat exchangers, and P_i are the centrifugal pumps.

II.3 Methodological framework

Our simulation-optimization approach [60–62] incorporates the evaluation of a CSHPSS plant performance at various EU locations and the definition of a set of optimal configurations of the plant from both techno-economic and environmental aspects simultaneously. Thus, the proposed methodology is a multi-objective optimization problem. The transient performance of the CSHPSS plant is modeled in TRNSYS 18, simulation software which allows interconnecting available standard equipment units to obtain more complex systems. The optimization is performed externally using a generic optimization toolbox, GenOpt. The first subsection of the methodology illustrates the developed TRNSYS model and its input and output data. The second subsection shows the techno-economic and environmental criteria for assessing the proposed CSHPSS. Finally, the third subsection dives deeper into the optimization framework itself and the implemented algorithm.

II.3.1 TRNSYS simulation model

TRNSYS 18, transient simulation software, is employed to analyze the dynamic behavior of the proposed CSHPSS. The software operates by solving partial differential equations of the mass and energy balances within previously defined boundaries.

The dynamic nature of the program intends to offer a realistic simulation of the CSHPSS plant. On the other hand, to reduce the computational cost, the model is simulated over a typical year of operation, and the solution is extrapolated over the plant lifetime assuming same climatic conditions and demand profiles year after year.

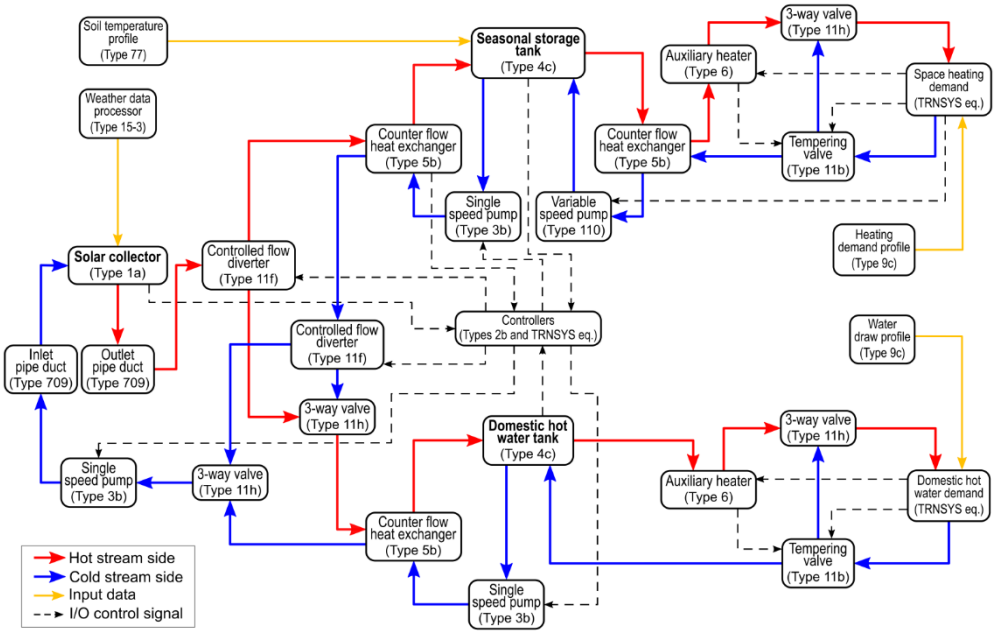

Figure II-3: Information flow diagram of the CSHPSS system modeled in TRNSYS 18 with the representation of the software components and their interconnections.

The proposed simulation model follows the models previously developed by Guadalfajara et al. [50] and Tulus et al. [45] with modifications to include the DHW distribution circuit and a more sophisticated controlling loop. See the information flow diagram presented in Figure II-3 for details about the individual components (called Types inside the software) used in TRNSYS. Each type has three main information boxes which include the component-specific parameters, input variables, and output variables.

The main types used in our CSHPSS model are: flat plate solar collectors (Type 1a) with an optical efficiency of 0.817, heat loss coefficient of 2.205 W/m^2·K; sensible storage tanks (Type 4c) with heat loss coefficient of 0.06 W/m^2·K and 0.3125 W/m^2·K for the SST and DHWT, respectively; counterflow heat exchangers (Type 5b) with overall heat transfer coefficient of 3931 W/m^2·K; and auxiliary heaters (Type 6) with an efficiency of 93%. The secondary model types are: single speed centrifugal pumps (Type 3b), inlet and outlet pipe ducts (Type 709), three-way valves (Type 11h),

controlled flow diverters (Type 11f), tempering valves (Type 11b), soil temperature profile for the SST (Type 77), weather data processor (Type 15-3), time-dependent forcing functions for the heating and DHW demand profiles (Type 9c), and controllers (Type 2b).

II.3.2 Technical criteria

The technical evaluation of the dynamic behaviour of the CSHPSS plant is described through several parameters that include the energy supplied by the SST, DHWT, and auxiliary boilers.

The storage tank has a vital role in the CSHPSS plant performance. Thus, the energy provided by the fully stratified seasonal and DHW storage tanks are described in Eq. II-1 - Eq. II-2 , respectively [63]:

$$Q_{SST} = \int_0^t \dot{m}_{SH} c_p \Delta T_{SST} \quad \text{Eq. II-1}$$

$$Q_{DHW} = \int_0^t \dot{m}_{DHW} c_p \Delta T_{DHW} \quad \text{Eq. II-2}$$

where $\dot{m}_{SH}$ and $\dot{m}_{DHW}$ are the mass flow rates of the recirculated water inside the SH and the DHW distribution circuits, respectively, c_p is the specific heat capacity, ΔT_{SST} and ΔT_{DHW} are the temperature differences between the extracted and replaced water at storage tanks to cover the SH and DHW load, respectively.

Auxiliary boilers are utilized to cover the SH demand and the DHW demand when the solar system is unable to reach the set temperature point. The auxiliary energy rate supplied to the SH and DHW networks can be expressed as shown in Eq. II-3 - Eq. II-4, respectively [64]:

$$\dot{Q}_{AUX1} = \dot{m}_{SH} c_p \Delta T_L \quad \text{Eq. II-3}$$

$$\dot{Q}_{AUX2} = \dot{m}_{DHW} c_p \Delta T_L \quad \text{Eq. II-4}$$

where ΔT_L is the temperature difference between the exit and entrance of the auxiliary heater. Annual solar fraction [65,66] for the SH and DHW distribution

circuits are introduced as technical performance indicators. These indicators can be computed using
Eq. II-5 -
Eq. II-6 as a function of the heating network demand ($Q_{heating\ load}$), and the DHW network demand ($Q_{DHW\ load}$).

$$SF_{SH} = 1 - \frac{\int_0^t \dot{Q}_{AUX1}}{Q_{\text{heating load}}} \qquad \text{Eq. II-5}$$

$$SF_{DHW} = 1 - \frac{\int_0^t \dot{Q}_{AUX2}}{Q_{\text{DHW load}}} \qquad \text{Eq. II-6}$$

II.3.3 Economic criteria

In the current study, the economic evaluation of the CSHPSS system follows the work of Tulus et al. [45] which is carried out based on the life cycle costing (LCC) methodology [67,68].

The LCC methodology is a valuable monetary approach for assessing the energy system designs in terms of the initial purchase cost and the operational costs throughout the expected lifetime of the system. The LCC perspective in the early stages of design empowers the decision-makers to deeply comprehend the lifetime costs of the system [46], and subsequently enhance the possibility of an additional reduction in the system operational cost even if more investment cost is required [69].

The main principle of the LCC methodology is the future cost approach. Its feature is to discount the summation of all expenses during the lifetime of the system to its present value where the net present cost (*NPC*) can be estimated by adding the initial capital cost (C_C), the operational cost (C_O) and the total replacement cost of the equipment (C_R):

$$NPC = C_C + C_O + C_R \qquad \text{Eq. II-7}$$

II.3.3.1 Initial capital cost

The initial capital cost is the investment cost at the project starting point. It takes into consideration the actual equipment cost, the installation labor, and transportation costs along with any possible contingency expenses:

$$C_C = (1 + \alpha_{CF}) \sum_k (PEC_k \cdot FBM_k) \qquad \text{Eq. II-8}$$

where PEC_k is the initial purchase cost of equipment unit k, FBM_k denotes the bare module factor, which represents the installation labor and transportation costs, and α_{CF} denotes the contingency fees factor.

The PEC_k is brought from the base year (*year A*) to the year of installation (*year B*) using the Chemical Engineering Plant Cost Index (*CEPCI*) [70] as follows:

$$PEC_k = PEC_k^{yearA} \frac{CEPCI^{yearB}}{CEPCI^{yearA}} \quad \forall k \qquad \text{Eq. II-9}$$

The initial purchase cost of equipment unit *k* at year A can be estimated as shown in Eq. II-10 to Eq. II-12 [71–74]:

$$PEC_k^{yearA} = \alpha_k CAP_k^{\beta k} \quad \forall k = COL, SST, DHW, AUX \qquad \text{Eq. II-10}$$

$$PEC_k^{yearA} = CAP_k^{\beta k} \cdot 10^{\left[\alpha_k \left(\log_{10} CAP_k\right)^{\beta_k}\right]} \quad \forall k = HE_1, HE_2 \qquad \text{Eq. II-11}$$

$$PEC_k^{yearA} = \alpha_k \ln\left(\frac{CAP_k}{1000}\right) + \beta_k \quad \forall k = P_1, P_2, P_3, P_4 \qquad \text{Eq. II-12}$$

where α_k and β_k are the equipment purchase parameters of unit *k* and CAP_k is the design variable of unit *k*. In the current study, the design variables are the solar collector area (A_{COL}), the volume of the storage tanks (V_{SST}, V_{DHW}), the capacity of the auxiliary heaters (AUX_1, AUX_2), the effective heat transfer area of the heat exchangers (HE_1, HE_2, HE_3) and the mass flow rates of the pumps ($\dot{m}_1$, $\dot{m}_2$, $\dot{m}_3$).

II.3.3.2 Operational cost

The operational cost refers to the sum of all the annual operating costs such as maintenance costs of the different equipment units and facilities, the consumption of electricity by hydraulic equipment and the consumption of natural gas by auxiliary heaters. It can be expressed as follows:

$$C_O = C_M PWF_M + C_P PWF_P + C_{AUX} PWF_{AUX} \qquad \text{Eq. II-13}$$

where C_M, C_P, and C_{AUX} represent the annual maintenance cost, hydraulic equipment (*i.e.*, pumps) and auxiliary consumption costs, respectively. The present worth factor (*PWF*) counts for the time value of money considering the inflation rate (*i*), the discount rate (*d*), and the lifetime of the proposed system (N_e) as expressed in Eq. II-14:

$$PWF = \begin{cases} \dfrac{1}{d-i}\left[1-\left(\dfrac{1+i}{1-d}\right)^{N_e}\right] & \forall i \neq d \\ \dfrac{N_e}{1+i} & \forall i = d \end{cases} \qquad \text{Eq. II-14}$$

II.3.3.3 Replacement cost

Several equipment units in the CSHPSS plant have a high depreciation rate and subsequently, need to be replaced during the plant operation. These units are the

field of solar collectors, the heat exchangers, and the auxiliary heaters. The replacement cost can be expressed as shown in Eq. II-15 with consideration for the present equipment value:

$$C_R = PVF_n \sum_k (PEC_k \cdot FMB_k) \quad \text{Eq. II-15}$$

where PVF_n is the present value factor of future cash flow at year n, and it can be expressed as follows:

$$PVF_n = \frac{(1+i)^n}{(1+d)^n} \quad \text{Eq. II-16}$$

II.3.4 Environmental criteria

The LCC is purely based on an economic approach not considering the environmental performance of the CSHPSS plant. In this context, the environmental impact is assessed by using the life cycle assessment (LCA) methodology. This methodology enables a comprehensive estimation of the local environmental impacts by analysing the product lifecycle from a global perspective. Thus, LCA assesses the product based on the "cradle-to-grave" concept [75] taking into account a range of environmental categories. The LCA methodology was standardized through ISO 14040 series [76–78], and it comprises four main phases which trail a specific sequence: goal and scope definition, inventory analysis, impact assessment, and interpretation. These phases are depicted in details in the next subsections as mentioned previously by Guillén-Gosálbez et al. [79].

II.3.4.1 Goal and scope definition

This phase comprises three main scopes: the system, its boundaries, and the functional unit. In the system boundary, the entire product life cycle should be analysed ("cradle-to-grave" concept). However, this study focuses on the CSHPSS plant itself, which is connected to an existing district heating network. Therefore, the system boundary would be drawn based on the "cradle-to-gate" concept with exclusion for the end user distribution networks, that is, from the extraction of raw materials for equipment units manufacturing to delivery of hot water to the district heating network. The functional unit in this study is the energy amount demanded by the end user in order to cover his heating and hot water necessities over the entire time horizon.

II.3.4.2 Inventory analysis

Inventory analysis is the second phase in the LCA sequence which quantifies the input and output materials and the energy consumption associated with the CSHPSS plant construction and operation. In the current problem, several sources of impact

are considered: equipment manufacturing and utility energy consumption (natural gas and electricity) by the system during the whole lifetime (LCI_i^{MP}); transportation to the site of material and finished equipment units (LCI_i^{TR}); plant operation during the entire time horizon (LCI_i^{OP}).

These resources consumption associated with the whole elementary flows during its lifetime has been retrieved from the Ecoinvent 3.0 database [80]. Mathematically, the inventory entries can be expressed as follows:

$$LCI_i^{TOT} = LCI_i^{MP} + LCI_i^{TR} + LCI_i^{OP} \quad \forall i \qquad \text{Eq. II-17}$$

where LCI_i^{TOT} is the total life cycle inventory associated with the elementary flow *i*. LCI_i^{MP}, LCI_i^{TR}, and LCI_i^{OP} refer to the manufacturing processes, the transportation tasks and the plant operation associated with the elementary flow *i*, respectively.

II.3.4.3 Impact assessment

In this phase, the inventory data are translated into environmental impacts. As mentioned previously, three different damage categories include the human health, the ecosystem, and the resources damages based on the ReCiPe 2008 framework [81]. The characterization of the promoted framework has been carried out based on the endpoints level not considering the midpoints. Mathematically, the impact values associated with each impact category can be expressed as follows:

$$IMP_e = \sum_i \theta_{ei} \cdot LCI_i^{TOT} \quad \forall e \qquad \text{Eq. II-18}$$

where θ_{ei} denotes the characterization factor which links the elementary flow *i* with endpoint impact category *e*.

Finally, the endpoint impact categories *e* are aggregated into damage categories (DAM_d), which are further normalized and aggregated into a single final indicator *RCP* as stated in Eq. II-19 - Eq. II-20:

$$DAM_d = \sum_{e \in ID_d} IMP_e \quad \forall d \qquad \text{Eq. II-19}$$

$$RCP = \sum_d \delta_d \varepsilon_d DAM_d \quad \forall d \qquad \text{Eq. II-20}$$

where ID_d represents a set of endpoint impacts *e* that contribute to the damage category *d*, *RCP* is the ReCiPe 2008 aggregated metric, and δ_d, ε_d are the specific normalization and weighting factors, respectively. The normalization factors are estimated based on the damage calculations for relevant European land uses, emissions and extractions [82], whereas the weighting factors are specified based on the recommended values defined in the ReCiPe 2008.

II.3.4.4 Interpretation

This phase provides an analysis of the results in addition to a set of recommendations that assist in improving the system performance. In this context, the environmental impact indicator *RCP* for different design alternatives is coupled with the LCC methodology which uses *NPC* for evaluating the future cost through a multi-objective optimization algorithm. This framework assists in optimizing the economic and environmental impacts simultaneously. As a result, a set of Pareto optimal solutions is obtained which give further insight into different design alternatives, and subsequently promote various solutions for the decision-makers that best fit their legislation.

II.3.5 Future market development criteria

In order to try to anticipate the future development of the CSHPSS technology in monetary terms taking into consideration the actual effect of the technology deployment, we performed a CSHPSS market projection up to 2030 [83–85]. The obtained learning curve by definition [86,87] tends to develop a relationship between the cumulative market size and the production cost of the CSHPSS plant (Eq. II-21).

$$C(x_t) = C(x_o) - \left(\frac{x_t}{x_o}\right)^{-b} \qquad \text{Eq. II-21}$$

Here $C(x_t)$ is the marginal cost of the CSHPSS plant production (x) at a specific time t, $C(x_o)$ is the cost production at the reference point (x_o), and b is the learning parameter which is estimated based on the fractional reduction in the CSHPSS plant cost represented by the learning rate (LR). The values for the LR are estimated based on the stated recommendation in the European Energy Scenario [85]. In addition to the market projection for the next decade, several specific annual figures can be assigned so the CSHPSS cost reduction can be anticipated on a chronological index.

II.3.6 Optimization procedure

The main goal of the optimization procedure is to simultaneously reduce the total cost of the plant (*NPC*) and its environmental impact (*RCP*) while still satisfying the technical requirements. The decision variables in our model are the area of solar collectors (A_{COL}), and the volume of the seasonal storage tank (V_{SST}), the dimensions of the other equipment units are related to the decision variables through mathematical equations. It is worth noting that our methodology is general enough to incorporate additional decision variables.

The developed TRNSYS model is connected to the GenOpt optimization toolbox, which integrates several predefined optimization algorithms. The general mathematical representation of the simulation-optimization model can be seen below:

$$\begin{aligned} &\min_{x}\{f_1(x), f_2(x)\} \\ &\text{s.t. } h(x) = 0 \\ &\quad x^L \le x \le x^U \\ &\quad x \in \mathbb{R} \end{aligned} \tag{M1}$$

where $f_1(x)$ and $f_2(x)$ are the objective functions, in this case net present cost, $NPC(x)$, and ReCiPe 2008 aggregated impact factor, $RCP(x)$, and x denotes the continuous variables of the simulation model, which can vary between their lower and upper bounds x^L and x^U, respectively. The equality constraints $h(x) = 0$, that model mass and energy balances as well as thermodynamic correlations, are implicitly solved in TRNSYS.

The correct technical performance of the model during the optimization process is achieved by implementing a constraint to model M1. This constraint must maintain the global annual solar fraction of the system (SF) above 50% for all the optimized solutions. The modified simulation-optimization model which includes the big-M reformulation [88] is shown next:

$$\begin{aligned} &\min_{x} WS = (1-\lambda)\bar{f}_1(x) + \lambda \bar{f}_2(x) \\ &\text{s.t. } h(x) = 0 \\ &\quad x^L \le x \le x^U \\ &\quad 0 \le \lambda \le 1 \\ &\quad x \in \mathbb{R}, \lambda \in \mathbb{R} \end{aligned} \tag{M2}$$

where y_1 and y_2 are the binary variables which are activated when the SF is lower than 50%, M_1 and M_2 are the big-M values corresponding to every objective function. The tightest values for the big-M are approximated using Eq. II-22, where M_c stands for big-M values implemented in model M2.

$$M_c = \max\left\{f_c(x) \mid x^L \le x \le x^U\right\} \quad \forall c = 1,2 \tag{Eq. II-22}$$

The solution of the multi-objective problem introduced in model M2provides a set of Pareto points, which represent the optimal trade-off between economic and environmental objectives. The extreme points of this Pareto frontier are the so-called anchor points, which correspond to the individual minimum of each objective. The Pareto solutions are calculated here via the weighted-sum method [89], which relies on formulating an auxiliary single-objective model that optimizes a linear weighted-sum (WS) of the original objectives (M3). Note that the weighted-sum method cannot generate solutions lying on the nonconvex part of the Pareto set.

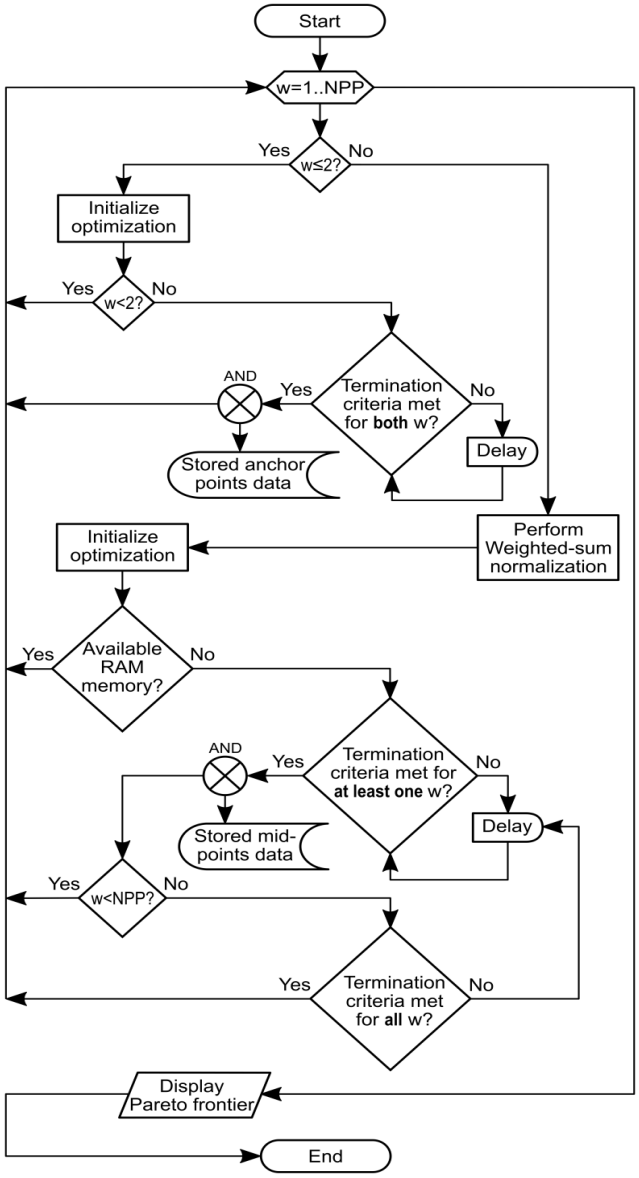

Figure II-4: Flowchart of the solution procedure performed in MATLAB environment, where NPP is the number of points of the Pareto frontier specified by the user

$$\min_{x} WS = (1-\lambda)\bar{f}_1(x) + \lambda\bar{f}_2(x)$$
$$\text{s.t.} \quad h(x) = 0$$
$$x^L \le x \le x^U$$
$$0 \le \lambda \le 1$$
$$x \in \mathbb{R}, \lambda \in \mathbb{R} \qquad \text{(M3)}$$

Here, $\bar{f}_1(x)$ and $\bar{f}_2(x)$ are the normalized objectives with the implemented big-M reformulation, and λ is the non-negative weight given to $\bar{f}_2(x)$, *i.e.*, the normalized $RCP(x)$ function. We normalize the objectives as shown below:

$$\bar{f}_c(x) = \frac{f_c(x) - f_c^{UT}}{f_c^{PN} - f_c^{UT}} \quad \forall c = 1,2 \qquad \text{Eq. II-23}$$

where f_c^{UT} denotes the c^{th} coordinate of the utopia points and f_c^{PN} denotes the c^{th} coordinate of the pseudo nadir point. These points, f_c^{UT} and f_c^{PN}, are the anchor points.

The solution procedure was integrated via a MATLAB routine designed to speed up the optimization process. The routine would launch several GenOpt toolboxes or start TRNSYS simulations whenever required.

The procedure starts with the determination of the anchor points. To obtain the individual minimum of the $RCP(x)$ function, M2 & M3 is solved for λ=1. Next, to determine the individual minimum of the $NPC(x)$ function, M3M2 is solved for λ=0. The two previous cases run simultaneously sharing all the available RAM of the computer. Once the anchor points are identified, the WS normalization is performed. Afterward, M3M2 is solved a finite number of times for different weight values between 0 and 1 (see details in Figure II-4) to generate the desired number of Pareto points. The MATLAB routine launches simultaneously various optimizations with different λ weights until there is no available memory. Once all the memory slots are occupied, the routine is halted until necessary RAM is liberated and then the next points are launched. The procedure ends with the display of the full Pareto frontier after all the optimization runs have met the termination criteria.

To perform the separate single-objective optimization steps we used a hybrid metaheuristic optimization algorithm [58], known as the Generalized Pattern Search algorithm with Particle Swarm Optimization with Construction Coefficient and Hooke-Jeeves (GPSPSOCCHJ). This algorithm uses the combined benefits of the Particle Swarm Optimization (PSO) algorithm [90,91] and the Hooke-Jeeves (HJ) algorithm [92]. The details of this hybrid metaheuristic algorithm are discussed in Wetter [58].

The PSO algorithm is in charge of performing a global search over the feasible space of possible solutions. Since PSO is a population-based probabilistic algorithm, it generates several particles uniformly scattered over the feasible space, where each of the particles is a potential optimal solution. These potential solutions are obtained by performing runs with randomly generated values for the decision variables. On the other hand, the HJ is a local generalized pattern search algorithm, and it explores the feasible space following paths of potential minimization of the objective function. The best particle found by PSO, the potential optimal solution, is used as a starting point for the HJ algorithm, which exhaustively explores its neighborhood in an attempt to

improve the solution. In order to reduce the probability of falling in a local optimum, we included multiple starts of the HJ algorithm.

This combined PSO-HJ architecture is used to avoid possible local optimal solutions which may exist due to the nonconvex nature of the problem. Note that our methodology is not limited to be used only with GPSPSOCCHJ algorithm; any other algorithm can be easily implemented.

II.4 Case studies (four EU climate zones)

In this section, the proposed methodology procedure was applied to four climatic zones in Europe. The objective is to assess the feasibility of the CSHPSS plant in the residential sector of these countries in techno-economic and environmental terms.

The CSHPSS plant is connected to a reference residential neighborhood community of 1120 apartments [45] which is placed in various European countries. Each apartment of this neighborhood community has a useful area of 90 m^2 [93]. The buildings are equipped with a radiant underfloor heating system and a domestic hot water system in order to meet the SH and DHW demand at 50ºC and 60ºC, respectively. The CSHPSS model validation is performed based on the implemented work by Guadalfajara et al. [50] and Tulus et al. [45].

Besides, a boiler fueled with natural gas is considered as a base case for comparison purposes. This conventional system is designed to satisfy the heating and DHW demand alone independently on the CSHPSS plant.

II.4.1 Specifications of the simulation model

A field of flat plate solar collectors supplies thermal heat to the CSHPSS model. These collectors are coupled in series and oriented to the south with a specific inclination based on the respective latitude of the cities [94] as shown in Table II-1. The primary working fluid in the solar field circuit is a $67/33_{w/w}$ mixture of a water-glycol solution with a flow rate of 20 $kg/h \cdot m^2$. Whereas the other three circuits (seasonal storage, SH distribution, DHW distribution circuits) are operated with water.

A partially buried tank with a cylindrical cross-section is used for a seasonal storage purpose. This tank has a fixed height to diameter ratio of 0.6, insulated with 0.5 m of extruded polystyrene and divided into 20 equally stratified levels. On the other hand, the DHW tank is relatively small since it covers only the daily DHW service. The DHWT has a height to diameter ratio of 1.7 with ten equally stratified levels.

Natural gas boilers with 93% efficiency are utilized as auxiliary heaters in both the SH and DHW distribution circuits. The boilers are designed to satisfy up to 100% of the heat demand when required.

The TRNSYS simulation predicts the transient response of the CSHPSS plant based on a simulation time step of 15 min. The system evaluation was performed over three years of simulation (28,260 hrs.). Then the performance of the third year was extrapolated over the total lifetime of the CSHPSS plant. Due to initial homogeneity assumption of 30ºC inside the storage tanks, the first two years of simulation were performed to eliminate the initial assumption effect. The lifetime of the CSHPSS is 40 years [95]. However, the solar collectors, the DHWT, the heat exchanger, and the auxiliary heaters need to be replaced after 20 years of operation, while the lifespan of the SST is considered to reach 80 years [96].

II.4.2 Meteorological data

Various climate zones were selected in order to evaluate the application performance of the CSHPSS plants in the EU. In Europe, the climate can be categorized into three major climate types [97,98]: Mediterranean climate, central European climate, and Nordic climate. Four cities were selected to represent these major climatic types:

- Mediterranean climate: Madrid and Athens represent this climatic type with the difference in the daylight hours, the daily ambient temperature and the humidity due to their geographical location. Madrid is considered a Continental Mediterranean climate, while Athens is considered a Mediterranean climate.
- Central European climate: Berlin is selected as representative for this climate type. In comparison with the Mediterranean climate, a moderate reduction in the ambient temperature and daylight hours is noticed.
- Nordic climate: Helsinki is chosen as an example of this climate type. This type of weather is elected as an opposite to the Mediterranean climate with a drastic reduction in both the ambient temperature and the daylight hours.

The geographic information including the latitude and the solar collector inclination angle for the four cities are illustrated in Table II-1 whereas the climate conditions of the four cities including the average ambient temperature and the annual incident solar radiation per area are extracted from the EnergyPlus database [99] as shown in Figure II-5.

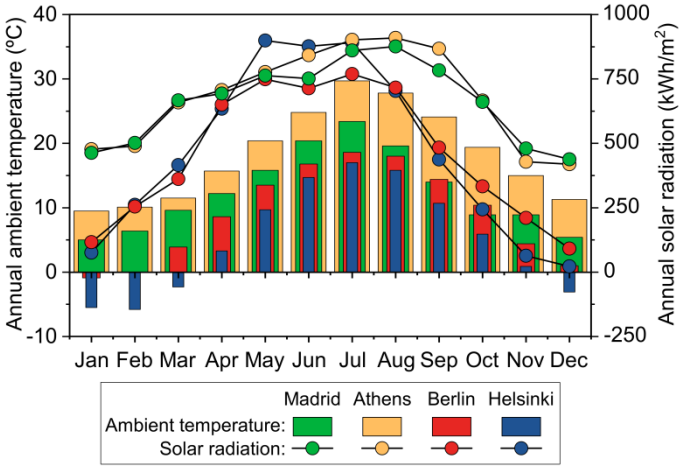

Figure II-5: Climatic conditions in the four European cities taken as representatives for the different EU climate zones.

Table II-1. Latitudes and relative inclination angles of the solar collectors in the four European cities taken as representatives for the different EU climate zones.

City	Latitude (º)	Inclination angle (º)
Madrid	40	50
Athens	37	50
Berlin	52	60
Helsinki	60	70

Several parameters need to be defined based on the climate conditions of the cities. These parameters include the SH and DHW consumption, the economic [100] and the environmental [101] data which are defined in the following sections.

II.4.3 Space heating and DHW profiles

The heating demand for the residential neighborhood community follows Guadalfajara et al. [50] and Tulus et al. [45] studies. A 3-D building model was generated using a graphical tool SketchUp [102] and imported into the TRNSYS model. In TRNSYS, the occupation profiles of the apartments and physical properties of the construction materials were included. A typical hourly heating load over a year of operation depending on the climatic conditions of the city was simulated in this TRNSYS building model. These data were then extrapolated to the whole neighborhood of 40 buildings (see the profiles in Figure II-6).

The DHW demand for the residential neighborhood community depends on four main factors which comprise:

- The daily water consumption per person: Ahmed et al. [103] indicated that water consumption is highly dependent on the geographical location. Therefore, DHW consumption has a high level of diversity from one city to another. The DHW consumption per capita is 28, 30, 35, and 35 liters/capita·day in Madrid, Athens, Berlin, and Helsinki, respectively [104].
- Monthly water temperature from the public distribution network: The water temperature was calculated depending on the city and the month of the year using EnergyPlus database [99].
- The number of people living in each household: The DHW consumption is dependent on the people/property value, and it is considered as a constant value (4 people/property) referring to the European average [105,106].

The daily DHW consumption profiles are simulated using computer software, DHWcalc [107]. This software assists in developing a realistic and detailed hourly DHW consumption profiles with consideration for the main factors controlling the DHW demand (see the profiles in Figure II-6).

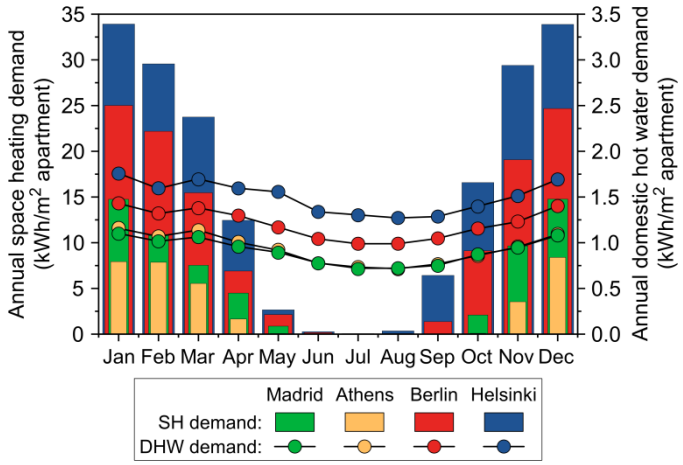

Figure II-6: Annual space heating and DHW demand profiles in the four European cities taken as representatives for the different EU climate zones.

II.4.4 Economic and environmental data

The parameters for the initial purchase cost estimation of the main equipment units of the CSHPSS are summarized in Table II-2 following Tulus et al. [45], while the operational cost is estimated at 1.5% of the initial purchase cost based on Kalogirou [67] recommendation. The cost for both the electricity and natural gas are dependent on the country policies. Therefore, the electricity and natural gas costs were extracted from the EUROSTAT database [100] and summarized in Table II-4. Furthermore, the

inflation rate associated with the price of these power resources is set to 5%, and 5.9% for the electricity and natural gas, respectively [45]. Additionally, the inflation rate associated with the proposed system during its life cycle is set to 2.3% [108], while the annual discount rate is set to 3.5% [109].

Table II-2. Purchase cost parameters of the CSHPSS equipment units [45]

Unit	α_k	β_k	CAP_k	**Range**	**Base year**	FBM_k
Solar collector	974.2	0.8330	Aperture area (m^2)	4000-150,00 m^2	2007	1.00
Storage tank	3955	0.6500	Volume (m^3)	1-100,000 m^3	2007	1.00
Auxiliary heater	225.0	0.7460	Duty (kW)	600-100,00 kW	2001	2.10
Heat exchanger	3.133	-0.3310	Exchange area (m^2)	10-1000 m^2	2001	3.29
Pump (P_1, P_2)	389.0	-283.2	Mass flow rate (kg/h)	15000-100,000 kg/h	2009	3.24
Pump (P_3, P_4)	389.0	717.0	Mass flow rate (kg/h)	15000-100,000 kg/h	2009	3.24

The LCA data are retrieved from the Ecoinvent database [101]. These data include the impact of various CSHPSS equipment units (Table II-3) and utilities (Table II-4) based on the ReCiPe 2008 methodology.

Table II-3.ReCiPe 2008 aggregated impact factor for the CSHPSS equipment units, in ReCiPe points (Pt) per characteristic dimension

Unit	**Impact factor (ReCiPe 2008)**
Solar collector	17.0 Pt/m^2
Storage tank	117 Pt/m^3
Auxiliary boiler	$1.57 \cdot 10^3$ Pt/unit
Heat exchanger	9.00 Pt/m^2
Pump	82.0 Pt/unit

The pollution associated with the extraction of natural gas from the underground reserves should be limited in the proposed system. On the other hand, the pollution associated with the electricity generation is highly dependent on the electricity mix of the specific country. Therefore, the natural gas environmental impact is considered the same for the selected cities, while the electricity impacts are variable, as indicated in Table II-4.

Table II-4. Specific costs and ReCiPe 2008 aggregated impact factors for the utilities in the four European cities taken as representatives for the different EU climate zones.

City	Electricity		Natural gas	
	Cost (€/kWh)	***Impact (Pt*/kWh)**	**Cost (€/kWh)**	***Impact (Pt*/kWh)**
Madrid	0.101	0.0357	0.0294	0.0230
Athens	0.0862	0.0193	0.0242	0.0230
Berlin	0.0761	0.0529	0.0277	0.0230
Helsinki	0.0596	0.0261	0.0296	0.0230

II.4.5 Future market development data

By the end of 2016, the cumulative capacity of the installed solar heating systems in Europe increased by 2.6% compared to the previous year to achieve a total installed capacity of 34.5 GW_{th}. Germany has the lead in the solar heating systems installation in Europe where a 0.52 GW_{th} within 2016 was added to a total capacity of 13.14 GW_{th}. Elsewhere in Europe, Spain added a 0.146 GW_{th} to achieve a total capacity of 2.4 GW_{th}, whereas Greece and Finland added 0.19 GW_{th} and 0.0028 GW_{th} [14].

The future market of the CSHPSS based on an in-depth analysis of solar heating energy systems from the technical, social and political perspectives, shows different expansion scenarios for this technology in Europe. Greenpeace international [110] proposed the EU 27 energy scenario for the CSHPSS expansion up to the year 2030 as shown in Table II-5.

Besides, the natural gas price trends are assumed to increase in a moderated manner based on the recommendations of the Federal Ministry of Environment of Germany [111] (see Table II-5). These trends are motivated by the shortage in the CO_2 allowance [112].

Table II-5. Estimated growth of CSHPSS installed capacity according to Greenpeace international and projected increase of the natural gas price up to 2030.

Parameter	**2017**	**2020**	**2025**	**2030**
Total installed capacity (GW_{th})	34.50	40.66	52.77	67.16
Average natural gas price in the EU (Euro/kWh)	0.02700	0.03200	0.03415	0.03630

The forecast cost for the CSHPSS technology can be generated based on the observed historical learning rate of solar thermal collector systems over the forecasted period between 2020 and 2030. The learning rate of such systems is 0.90 according to Greenpeace international [85].

II.5 Results and discussions

In this study, the results are presented in four main parts. The first part depicts the behavior of CSHPSS in one of the proposed EU climate zones. Then, in the second part, the discussion is extended to the other three cities. These two parts provide a detailed analysis of techno-economic and environmental characteristics based on a set of Pareto optimal solutions in comparison to a conventional heating system fuelled by natural gas (base case). Next, the main results are expressed along with an appropriate sensitivity analysis for the proposed optimal solutions of the system. Finally, the market projection forecast for the CSHPSS is portrayed using historical learning rates.

II.5.1 Application analysis (Madrid case study)

The capabilities of the formulated multi-objective optimization model are illustrated through Madrid case study that addresses the design of CSHPSS in the Mediterranean EU climate zone. A set of optimal solutions that define the Pareto frontier are obtained as a result of the optimization process (see Figure II-7). Each point of the Pareto front comprises a defined configuration of the CSHPSS plant under a set of operational conditions. The average computation time for the anchor points was 15,700 CPU seconds (8 execution units of 2.0 GB RAM each for every anchor point, optimizing both simultaneously) and 47,000 CPU seconds for the intermediate Pareto solutions (2 execution units of 2.0 GB RAM each for every intermediate point, optimizing all of them simultaneously) using an Intel® Xeon® E5-2620 v4 2.10 GHz processor with 32.0 GB RAM.

As observed in Figure II-7, there is a clear trade-off between the proposed objective functions since the reduction in the environmental impact can be only achieved through an increment in the expenses of the CSHPSS plant. The projected optimal solutions, following our methodological framework, visibly improve the environmental impact in comparison to the base case. Point A and B are the optimal design Pareto points with minimum cost and impact, respectively. Note that these points consider the integration of solar thermal energy storage. Replacing the base case with a CSHPSS plant following point A configuration can reduce the environmental impact by 81.1%, whereas point B reduces it even more, by 86.5%. On the other hand, the Pareto optimal systems could not provide a marginal economic reduction compared to the base case. The installation of a CSHPSS in these cases corresponds to an increase in the cost of approximately 1% and 6.1% in A and B cases, respectively compared to the base case.

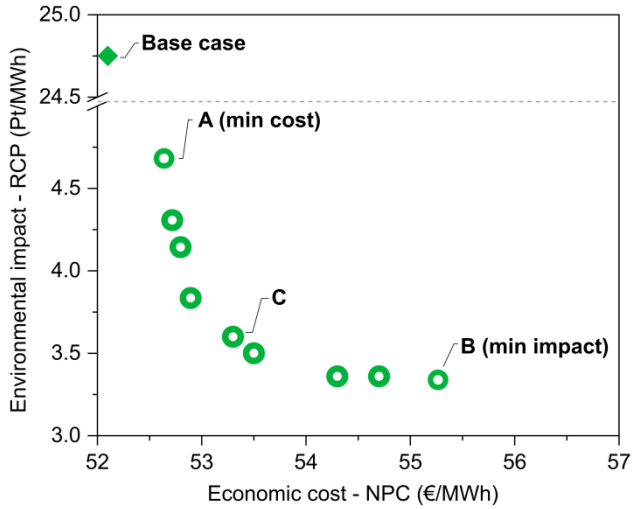

Figure II-7: Pareto set of optimal solutions for the CSHPSS in Madrid which covers 7654 MWh/year of combined SH and DHW demand during its lifetime. Anchor point A is the minimum cost solution, anchor point B is the minimum impact solution, and the intermediate point C is one of the trade-off solutions with λ = 0.44 (weight) given to the normalized environmental impact objective function, the *RCP*(*x*); the base case represents a natural gas heating system.

In the optimal minimum cost solution (point A), the *NPC* is equal to 52.6 €/MWh which is smaller than solution B by 4.7%, whereas in the minimum impact solution (point B), the *RCP* is 3.34 Pt/MWh which is smaller than solution A by 28.6%. Besides, point C embodies one possible intermediate Pareto optimal solution where the *NPC* is equal to 53.3 €/MWh, and the *RCP* reaches 3.6 Pt/MWh, this intermediate point increases the economic cost by 1.25% compared to the point A, but simultaneously reduces the environmental impact by 23.1%. It is worth noting that point C is selected as an example solution for comparison purposes. Likewise, any other intermediate solution could be selected since all of them are Pareto optimal.

Following that, each point in the Pareto set represents a different configuration of the CSHPSS plant. The proposed methodology offers the possibility to perform a detailed analysis of any Pareto optimal solution. Here we analyzed the anchor points (point A and B) from the economic and environmental perspectives comparing them to the base case.

II.5.2 Economic cost analysis

To facilitate detailed economic analysis, Figure II-8 provides a comprehensive breakdown of the cost contribution of each parameter for the Pareto optimal solutions A and B during their operation life together with the base case solution.

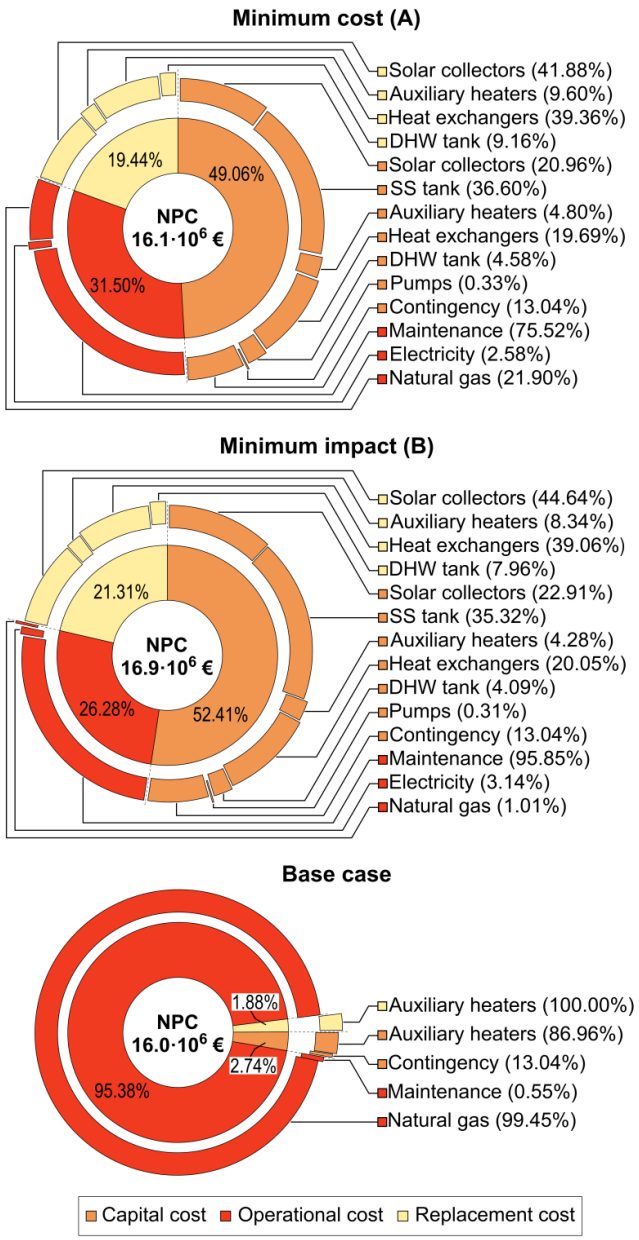

Figure II-8: Distribution of the net present costs of two Pareto optimal solutions (point A and B in Figure II-7) for the CSHPSS in Madrid which covers 7654 MWh/year of combined SH and DHW demand during its lifetime and the base case, which represents a natural gas heating system.

In this figure, the initial capital cost, associated with both A and B solutions, has a significant contribution compared to the base case. This contribution is 49.06% and

52.4 % in solution A and B, respectively, whereas in the base case, it is only 2.73%. This marginal capital cost contribution is commonly arisen in the CSHPSS plants due to the deployment of the solar energy in a district heating field which requires a high investment cost [22]. To be more specific, the solar collectors and SST represent 28.24% and 30.52% of the capital cost for the Pareto optimal solution A and B, respectively. The minimum cost solution (A) has solar collector field of 6888 m^2 and SST of 65784 m^3, whereas the minimum impact solution (B) has solar collector field 8802 m^2 and SST of 74322 m^3. Since the DHWT is used only for the daily services without seasonal storage, it represents almost about 4.5% of the initial capital cost in both the Pareto optimal solution A and B with a tank size of 109.6 m^3. The same behavior was noticed for replacement cost which represents 19.4% and 21.3% in solution A and B compared to only 1.88% in the base case. On the contrary, the operational cost has a predominant contribution of 95.4% in the base case compared to 31.5% and 26.3% in the optimal solutions A and B, respectively. Such a high operational cost is due to the dependency of the base case on natural gas cost. In general, solution A and B have a similar distribution for the *NPC* components. However, the minimum cost solution (A) has a slightly higher contribution of 6.9% for the natural gas compared to the minimum impact solution with only 0.27% which will be reflected in the environmental impact analysis.

II.5.3 Environmental impact analysis

As shown in Figure II-9, solution A and B success in declining the environmental impact up to 7 times compared to the base case due to the deployment of the solar water heating systems and the saving of non-renewable energy systems (i.e., natural gas and electricity). In the base case, the natural gas represents almost 100% of the environmental damage ($1.88 \cdot 10^5$ Pt). While this contribution is reduced to 38.8% ($1.39 \cdot 10^4$ Pt) in the minimum cost solution (A) and it becomes almost negligible in the minimum impact solution (B) where it counts only for 2.20% ($5.60 \cdot 10^4$ Pt).

Following the economic analysis of the anchor points (A and B), the solar collector and the SST share most of the contribution to the total environmental impact [64]. In solution A, the solar collector counts for 16.7% of the total damage to the environment, whereas this fraction increases up to 30% in the solution B due to the limitation of using natural gas as the primary fuel. On the other hand, the impact fraction of the SST represents 37.9 % in solution A, and it increases to 57.7% in solution B.

As the latest highlight, the impact of the heat exchangers increased by 40.1% from solution A to B. This is due to the further deployment of the solar collectors in the minimum impact solution (B), and subsequently extra supplement of heat exchange is required to cover the additional solar energy.

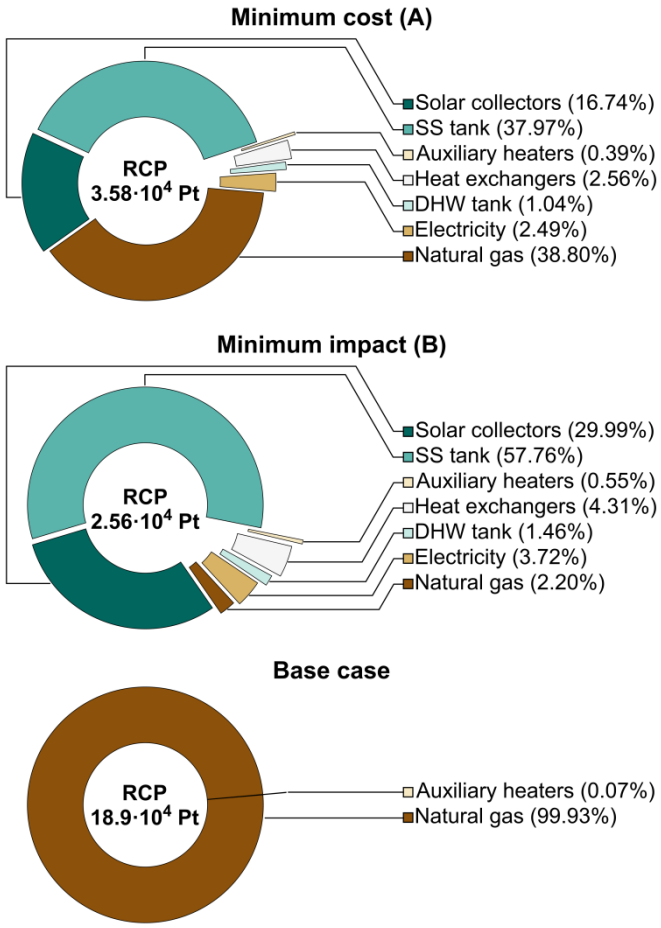

Figure II-9: Distribution of the environmental impact into its single impact categories of two Pareto optimal solutions (point A and B in Figure II-7) for the CSHPSS in Madrid which covers 7654 MWh/year of combined SH and DHW demand during its lifetime and the base case, which represents a natural gas heating system.

II.5.4 Energy analysis of an intermediate Pareto optimal solution (C)

The thermal performance characteristics of the optimized CSHPSS plant configuration based on the proposed methodological framework is presented through an intermediate Pareto optimal solution (point C in Figure II-7). This solution is designed to fulfill a total SH and DHW demand of approximately 6555 MWh/year and 1099 MWh/year, respectively. Note that any other intermediate point in the proposed Pareto set would be similarly comparable in this analysis.

As shown in Figure II-10, the monthly amount of SH and DHW demands are mainly covered by the solar collectors and the thermal energy stored in the SST and the DHWT. In Figure II-10 the energy supplied by the CSHPSS plant is represented as a positive input, whereas the energy stored in the SST is depicted as a negative input.

In summer and autumn seasons (*i.e.*, April to October), when the solar radiation is relatively high, and the SH demand is small, most of the provided energy from the solar collectors are directly stored into the SST, and the remaining is utilized to cover the instant heating demand. On the contrary, the solar radiation decreases, and the heating load significantly increases during the winter season (*i.e.*, November to January), therefore the total demand is covered through a combination of the energy supplied by the DHWT, the solar collectors and the stored energy in the SST. Moreover, in extreme cases when the proposed solar system fails in fulfilling the required heating demand, the auxiliary heaters fuelled by natural gas deliver the necessary energy. These cases happen during February and March where most of the stored energy in the SST is already discharged during the coldest months. This can be reflected in the solar fraction of the distribution circuits during these months. In February, the solar fraction declines by 5.84% and 1.22% for the SH and DHW circuits, respectively. While in March, this value changes a bit for the DHW distribution circuit and the solar fraction increases by only 2.81% due to the increment in the solar radiation. On the other hand, the solar fraction for the SH circuit keep deteriorating, and it drops by 10.1% due to the absence of the seasonal storage and the limited direct energy provided by the solar collectors.

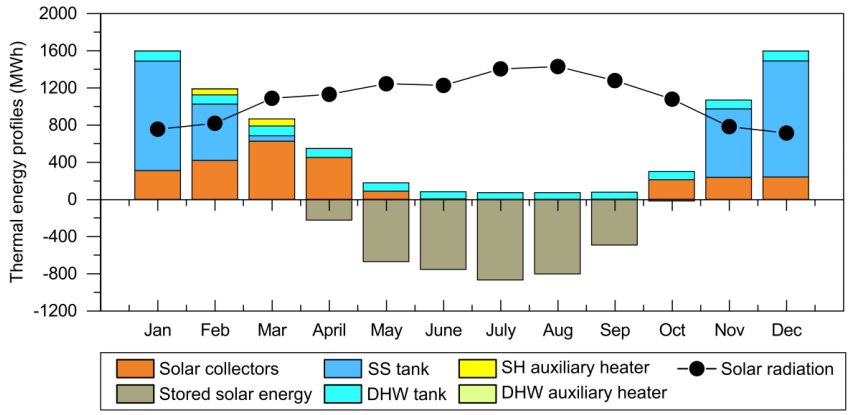

Figure II-10: Monthly thermal energy profiles of an intermediate Pareto optimal solution (point C in Figure II-7) for the CSHPSS in Madrid which covers 7654 MWh/year of combined SH and DHW demand during its lifetime.

II.5.5 Application analysis on the selected climate zones in the EU

Following Madrid case analysis combined with the main objective of assessing the CSHPSS plant feasibility in the residential sector at various climate zones in the EU,

the proposed methodological framework correspondingly based on the multi-objective approach is applied to optimize the cost against an aggregated environmental metric in Athens, Berlin and Helsinki as a representative for the Mediterranean, central European, and Nordic climates, respectively. The problem is formulated to cover annual SH and DHW demands of 4661 MWh, 14180 MWh, and 20896 MWh for Athens, Berlin, and Helsinki, respectively.

As shown in Figure II-11, a clear trend is observed for the deployment of the CSHPSS which causes a rise in the economic cost under various EU climate zones compared to the base cases. The optimal economic solutions in the nominated locations depend on several factors including the climate condition, the heating demand, and the natural gas and electricity prices. In Athens, the *NPC* in the minimum cost and impact optimal points have been raised by 33.3% and 50.8%, respectively compared to their base case. This high growth is due to the low cost of non-renewable energy resources in Athens compared to Madrid. Following the observed tendency in Athens, the *NPC* in Berlin case raised by 16.9% and 25.3% compared to their base case. On the other hand, the *NPC* increase only by 3.12% and 8.11% in Helsinki due to several factors including, the high price of natural gas and electricity, and the high heating demand.

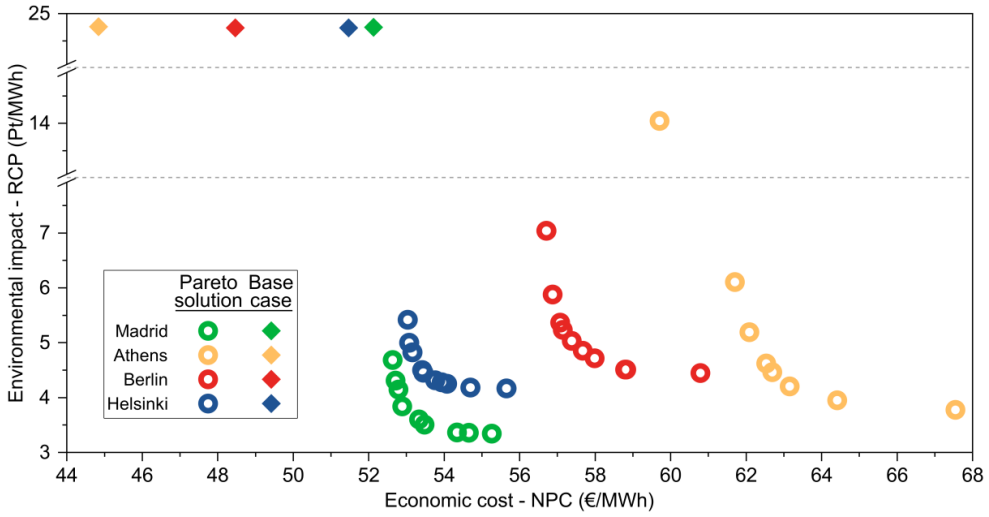

Figure II-11. Pareto sets depicted a range of optimal solutions for the CSHPSS compared to its base case under various EU climate zones.

The optimal environmental solutions for the four locations follows the minimum impact solution of Madrid case where the *RCP* improves by 84.7%, 82.1%, and 82.9% for Athens, Berlin, and Helsinki cases, respectively. The same tendency was found for Berlin and Helsinki at the minimum cost solution since the *RCP* improved by 71.3% and 77.9% for Berlin and Helsinki. On contrary, the low natural gas and electricity prices in Athens restrict substantial improvement in the *RCP*, and it is improved only

by 42.9%. This marginal improvement in the minimum cost optimal solution of Athens case will be mirrored in its breakdown for the *NPC* and *RCP*.

II.5.5.1 Economic cost analysis for the EU climate zones

Figure II-12 shows a comprehensive breakdown of the *NPC* of various CSHPSS plants during their lifetime under different EU climate zones. Similar contributions can be observed for each component of the *NPC* comparing among Madrid, Berlin and Helsinki cases. Furthermore, the results show that the capital and replacement costs for the presented optimal solutions (minimum cost and minimum impact) of Berlin and Helsinki are quite large in comparison to their base cases as mentioned in Madrid case study. Moreover, the results confirm the dependency of the CSHPSS plant configuration on the heating demand where the capital and replacement costs ascending increases with the heating demand based on the climate zone [51] as shown in Madrid, Berlin, and Helsinki, respectively.

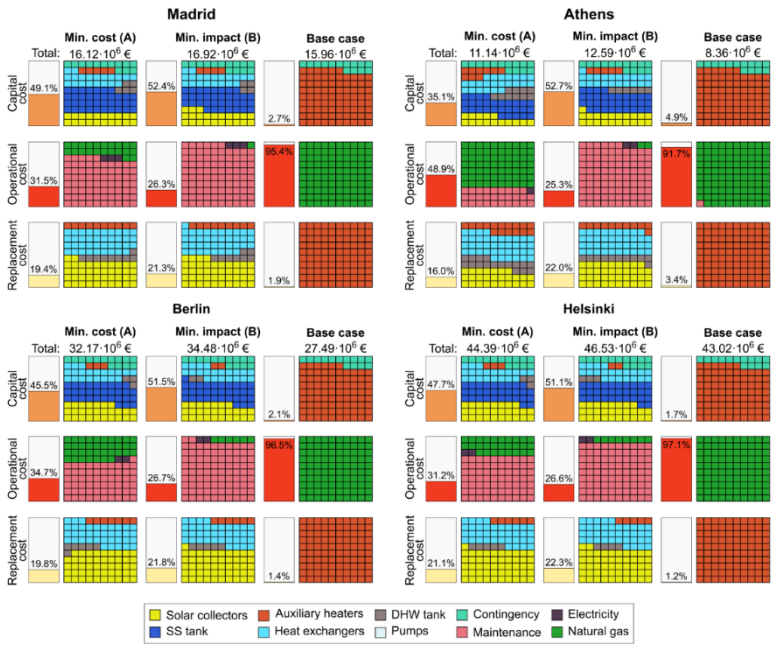

Figure II-12: Breakdown of the net present cost including initial capital cost, operational cost, and replacement cost for Pareto optimal solutions (minimum cost and impact) of a CSHPSS plant under different climate zones in comparison with its base case.

On the contrary, the low heating demand combined with the low prices for the natural gas and electricity in Athens contribute to change the distribution for the *NPC* of the minimum cost optimal solution in this Mediterranean zone. The operational cost has

a significant contribution of 48.9% compared to only 35.3% of the initial capital cost and 16% of the replacement cost. This is due to the dependency of the system on natural gas which almost represents 69.6% of the operational cost and the limited involvement for the solar water heating system. More precisely, the solar collectors and SST represent only 15.7% and of the initial capital and 28.6% of the replacement costs. In term of the renewable energy equipment sizing at the proposed climate zones, Table II-6 shows a summary for the proposed sizing the renewable energy equipment based on the Pareto optimal solution in various EU climate zones. It is noticed that for all the minimum impact optimum solutions under different EU climate zones, the ratio between the SST volume and the solar collector field area is around 8 ± 0.5 m^3/m^2 for the minimum impact solutions based on the climate zone.

Table II-6. Optimal renewable energy equipment sizing in various EU climate zones.

City	Optimal solution	Solar collectors (10^3 m^2)	Seasonal storage tank (10^3 m^3)	Domestic hot water tank (m^3)	Seasonal storage volume/ collectors area ratio (m^3/m^2)
Madrid	A	6.888	65.78	109.7	9.55
	B	8.802	74.32	109.7	8.44
Athens	A	2.097	15.25	117.6	7.27
	B	5.593	44.39	117.6	7.94
Berlin	A	21.00	149.2	137.2	7.10
	B	25.50	198.0	137.0	7.76
Helsinki	A	32.91	230.4	168.5	7.00
	B	38.13	287.9	168.5	7.55

II.5.5.2 Environmental impact analysis for the EU climate zones

Figure II-13 shows a breakdown for the environmental impact into its categories for the minimum cost and impact Pareto optimal solutions of a CSHPSS plant under different climate zones in comparison with its base case. The results follow the environmental impact breakdown of Madrid where the optimal solutions can reduce the environmental impact up to 5.5 and 5.8 times for Berlin and Helsinki cases, respectively. In Athens case, the minimum cost optimal solution reduces the environmental impact only by 1.75 times. This relatively small reduction is due to the significant contribution of the natural gas ($5.7 \cdot 10^4$ Pt) which represents almost 87.5% of the total environmental impact.

Following the environmental impact in Madrid case, the solar collector and SST are the main contributor to the total environmental impact in the minimum cost optimal solution with a contribution of 39.6%, and 52.7% in Berlin and Helsinki, respectively.

This contribution increases significantly for the minimum impact optimum solutions, where they share 87.2%, 80.2%, and 78.9% in Athens, Berlin and Helsinki solutions, respectively.

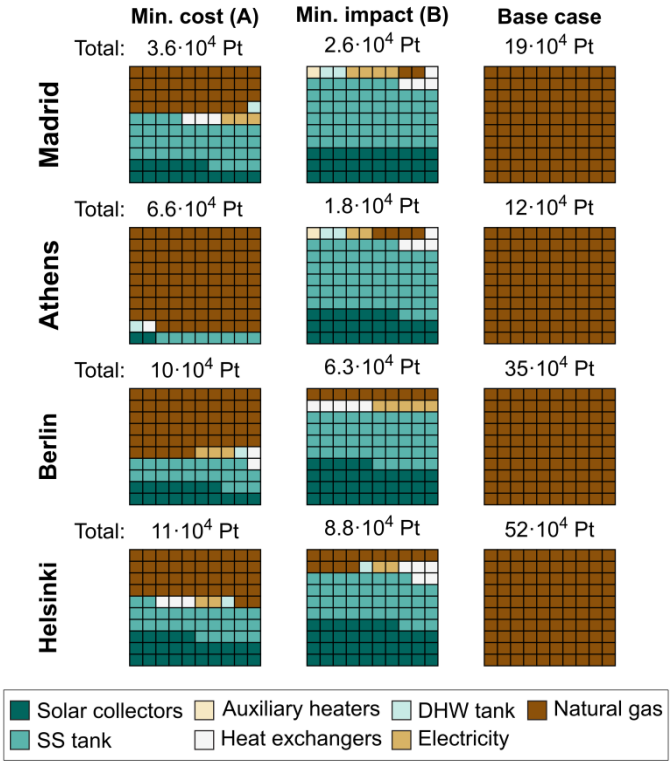

Figure II-13: Breakdown for the environmental impact of Pareto optimal solutions (Minimum cost and Minimum impact) of a CSHPSS plant under different climate zones in comparison with its base case.

II.5.5.3 Energy analysis for the EU climate zones

Following the energy analysis in Madrid case study, an intermediate Pareto optimal solution with λ = 0.44 is presented to evaluate the thermal performance of the CSHPSS plant in different EU climate zones as shown in Figure II-14.

Based on the limitation of the solar heating system in covering the heating demand during several months in Berlin and Helsinki, the AUX_1 operated from February until April due to the full discharging of the SST during the winter period. Furthermore, the AUX_2 almost operates throughout the year except the summer months (June to August) for these climates since the DHW tank is designed to cover only the daily services. In Athens, limited seasonal storage is projected between April and October where high solar radiation and low heating demand are observed due to the

Mediterranean weather conditions (see Figure II-5 and Figure II-6). This limited heating demand reduces the usage of auxiliary heaters throughout the whole year.

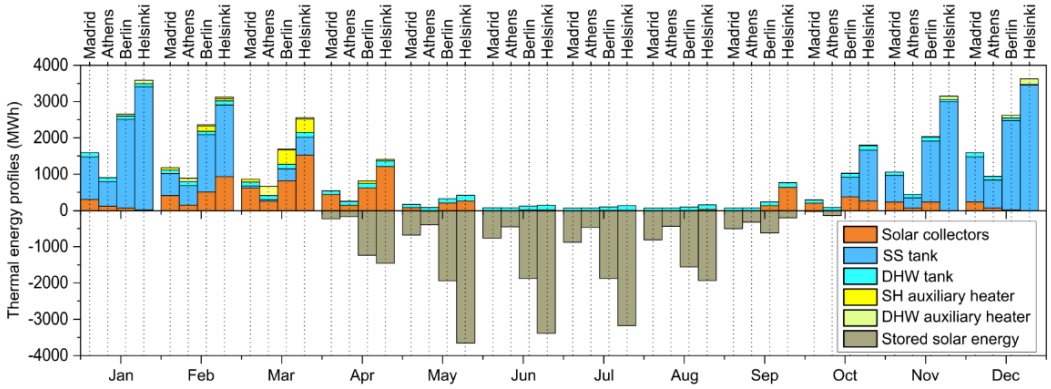

Figure II-14: Monthly thermal energy profile of an intermediate Pareto optimal solution under various EU climate zones.

Based on normalizing the technical performance of the CSHPSS plant, the solar fraction was presented, and its minimum value was noticed during January and March for the DHW and SH circuits, respectively. In the DHW distribution circuit, the solar fraction is 62.1% and 47.5% for Berlin and Helsinki, respectively. While the solar fraction for the SH distribution circuit becomes 74.1% and 84.5% in Berlin and Helsinki, respectively. On the other hand, due to the low price of natural gas in Athens in comparison to the other EU countries, an extensive usage for the auxiliary heaters in March is shown where the solar fraction has reduced to 54.6% for the SH circuit and sustain around 98.7% for DHW circuit due to low DHW heating demand. Even though the literature shows a high variation in the solar fraction when the CSHPSS plants introduced under different climate zones, the proposed methodological framework succeeds in reducing the solar fraction variation when introduced in various climate zones as shown in Table II-7. In the SH distribution circuit, which has a substantial contribution to the life cycle of the CSHPSS plant, the solar fraction never goes below than 90% for different EU climate zones. While due to the DHW distribution circuit functionally in covering only the daily services, the solar fraction diminishes up to 74.7% in Helsinki due the high demand in the winter period.

Table II-7. The yearly solar fraction of the intermediate Pareto optimal solution under various EU climate zones.

City	SF_{SH} (%)	SF_{DHW} (%)
Madrid	97.8	98.9
Athens	90.1	97.4
Berlin	95.2	84.9
Helsinki	97.5	74.7

Remarking that the proposed optimal solutions for the CSHPSS plants in different EU climate zones are high sensitivity for their geographical locations and economic parameters comprise energy prices. Therefore, the influence of the most relevant economic parameters should be assessed in a sensitivity analysis to give an estimate for the uncertainty associated with the results.

II.5.6 Sensitivity analysis for the methodological framework

A sensitivity analysis for the most critical economic parameters is implemented to understand their influence on both the *NPC* and *RCP* objective functions. This analysis is carried out based on One-factor-at-a-time (OFAT) approach [113] in which each economic parameter is varied by up to 20% after another in comparison to a reference case. The Pareto optimal solution (A) of Madrid case study is selected as the reference case. The assessment includes the influence of the natural gas price, electricity price, discount rate, inflation rate, investment cost, operational cost, and replacement cost. The sensitivity analysis not only comprises the influence of the selected parameters on the *NPC* and *RCP*, but it also proposes a detailed breakdown for the economic cost and the environmental impact for the influence of each of these parameters.

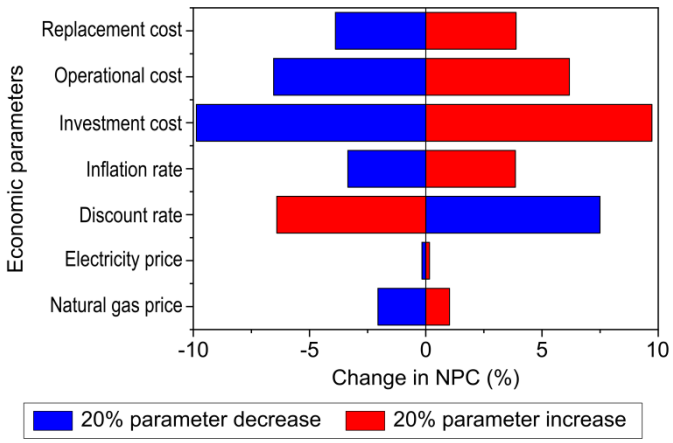

Figure II-15: Sensitivity analysis for the minimum cost Pareto optimal solution of Madrid case study (point A in Figure II-7)

Aligning with the financial challenges facing the CSHPSS plant, Figure II-15 shows the sensitivity analysis for a CSHPSS plant configured based on the optimal solution A (minimum cost) under Madrid climate zone demonstrates a high dependency for the *NPC* on the investment cost followed by the discount rate and the operational cost in which it can changes up to 9.8%. This change can be explained through the change in the system configuration where the reduction in the discount rate and the investment cost aggravate a slight more dependency on using renewable energy

sources. Furthermore, a non-linear effect for both the natural gas price and the discount rate is noticed. The *NPC* changes by 1.02% and 2.05% for increasing and decreasing the *NPC* by 20%, respectively. On the hand, the *NPC* increases by 7.49% for decreasing the discount rate by 20%, whereas it decreases only by 4.30% for increasing the discount rate by 20%. The inflation rate and the replacement cost have a limited contribution to the *NPC* since it changes only by 3.8% for both. The electricity price has a minor influence on the *NPC* since it has a marginal share of the total cost in the reference case.

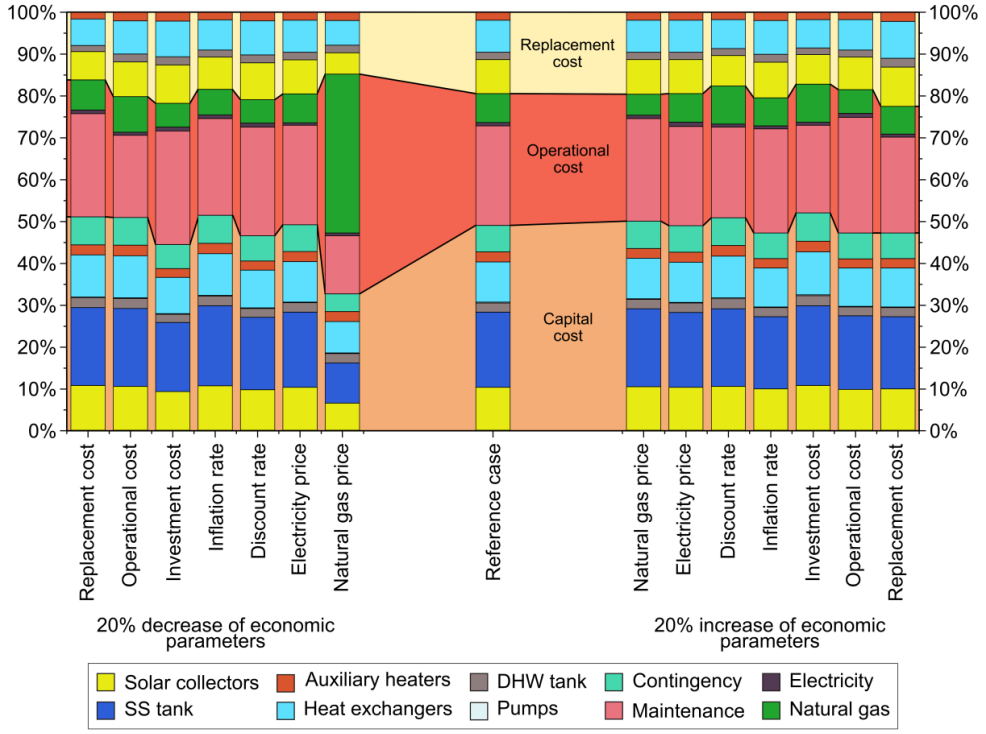

Figure II-16: Breakdown for the *NPC* where to the left of the reference case is depicted the breakdown when each economic parameter decreases 20%, whereas to the right of the reference case is depicted the breakdown when each economic parameter increases 20%.

Figure II-16 (to the left of the reference case) shows a breakdown for reducing the economic parameters of the optimal solution A by 20% where each component of the bar comprises the share percentage of a certain cost parameter in the *NPC* breakdown. The *NPC* breakdown shows the changes in the system configuration due to the reduction in the natural gas price. This reduction intends to propose the natural gas usage as a visible solution instead of the solar water heating system in covering the heating demand. Therefore, a large share of 38% is observed when the natural

gas price decrease 20%, respectively. On the contrary, the natural gas in the reference case shares only 6.89%. Furthermore, the large share of natural gas reduces the use of solar collectors to only 11.9% and the SST to 9.87%, whereas the reference case shares up to 18.4% and 17.9% of the total shared solar collectors and SST, respectively. For the breakdown of increasing the economic parameters of the optimal solution A by 20% shown in Figure II-16 (to the right of the reference case), almost the same pattern is observed for changing the discount rate and the investment and operational costs with a slight change in the natural gas share.

Following the sensitivity analysis for the *NPC* objective function, Figure II-17 shows the sensitivity analysis for the *RCP* when the economic parameters vary by 20%. Recalling the sharp influence for the natural gas price in presenting the natural gas usage as a valid solution with a limited share for the solar collectors and SST, the *RCP* increases 195.7% for reducing the natural gas price. Moreover, when this parameter increases 20% and due to the non-linear noticed effect, the *RCP* decreases by 12.2%. On the other hand, the discount rate and the investment and operational costs have a slight effect in the *RCP* since it increases by 15.14% when the investment cost and discount rate increased by 20%. While increasing the operational cost promote a reduction in the *RCP* by 15.14% due to the slight dependency of using renewable energy sources.

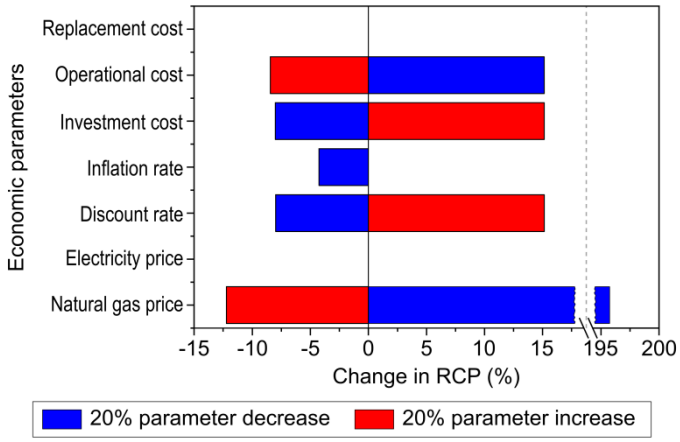

Figure II-17: A sensitivity analysis for the environmental impact objective of Pareto optimal solutions A (Minimum cost) under Madrid climate zone.

The dramatic increase in the *RCP* for the reducing the natural gas price can be observed in the *RCP* breakdown which is shown in Figure II-18 (to the left of the reference case). A high dependency is noticed when using natural gas instead of the solar water heating system where the natural gas shares 88.4% for varying the natural gas price down 20%, whereas the natural gas shares only 38.8% in the reference case. On the other hand, increasing the economic parameters 20% keeps almost the share for each parameter as the reference case with a marginal change in the natural gas share when the natural gas increases 20%, as shown in the *RCP* breakdown Figure II-18 (to the right of the reference case).

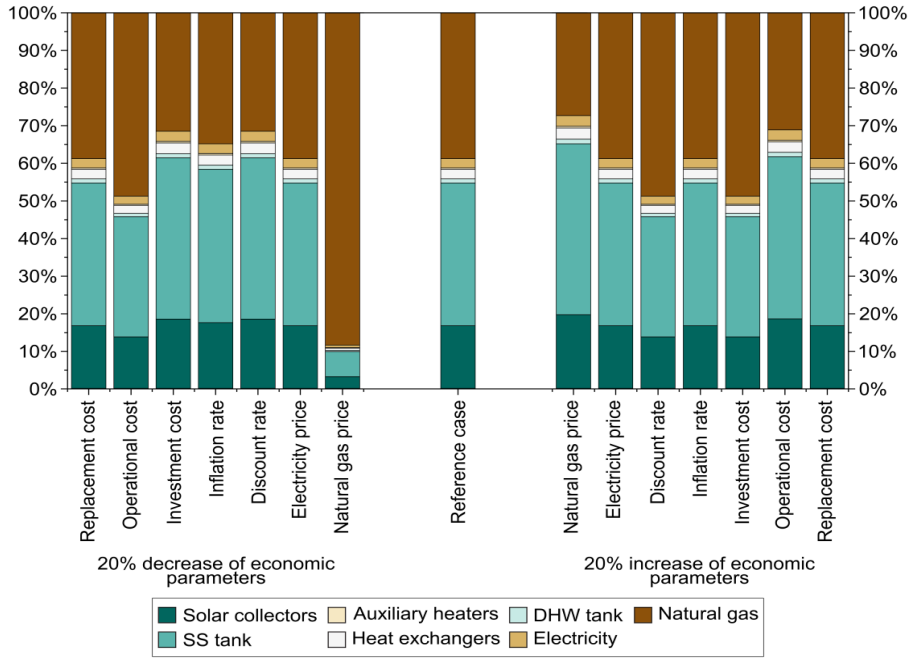

Figure II-18: Breakdown for the RCP where to the left of the reference case is depicted the breakdown when each economic parameter decreases by 20%, whereas to the right of the reference case is depicted the breakdown when each economic parameter increases by 20%.

II.5.7 Discussion and future market development

The future potential of CSHPSS plants in different EU climate zones is assessed through various Pareto optimal solutions offered by the proposed methodological framework in which both the techno-economic and environmental impact is considered. Generally, the CSHPSS system succeeded in decreasing the environmental impact in the investigated climate zones. However, the high investment cost of the CSHPSS plants compared to the conventional heating systems that use natural gas as fuel limit the extended benefit of wide-spreading the CSHPSS plants in different EU climate zones.

This limitation becomes more substantial in Athens (Mediterranean climate zone) where heating demand is low due to the high solar radiation throughout the year, and the prices of the non-renewable energy resources are low. However, the growing tendency for the natural gas price in the EU [111] would positively affect the economic feasibility of the CSHPSS plants in different EU climate zones. Therefore, as a part of the methodological framework, the future development in the plant cost with consideration for the actual effect of the technology deployment is evaluated for the proposed EU climate zones based on the historically observed learning curves.

As shown in Figure II-19, a clear trade-off for the increment in the conventional systems price is observed, this price raise associates with a gradual declination in the CSHPSS plants prices. In the long term, the CSHPSS plants in various EU climate zones can significantly under price the *NPC* in comparison to the conventional system using natural gas by 2030. This development can significantly assist in improving the competitiveness of the CSHPSS plant as a sustainable alternative solution in comparison to the conventional systems.

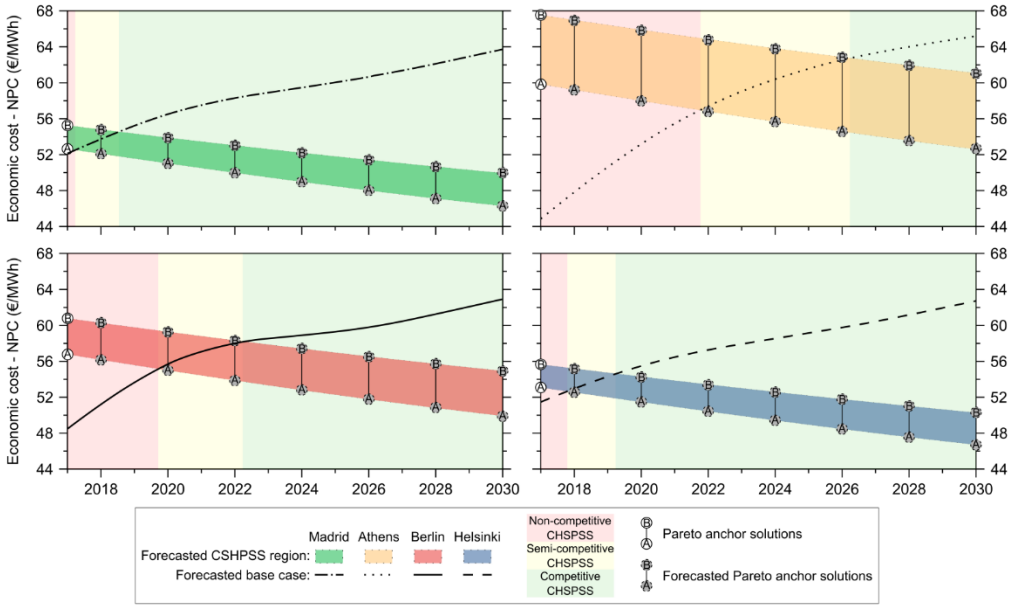

Figure II-19: Forecast for the development of *NPC* of the CSHPSS plant in different EU climate zones along with their base cases by 2030.

Currently, in Madrid, the CSHPSS plants can cover the heating demand for less than 52.6 €/MWh, whereas its base case covers it at 52.1 €/MWh. With this minor difference, the feasibility of the CSHPSS plant under Madrid climate conditions can be proved. In 2030, the *NPC* will range from 46.3 to 49.9 €/MWh for the CSHPSS while its base case 63.7 €/MWh. In Athens where the CSHPSS plant can cover the

heating demand at high price ranged between 59.7 and 67.5 €/MWh. Beyond 2022, the CSHPSS plants will be able to cover the heating demand at a lower cost than the conventional system, at which the heating demand is covered at a price of 56.7 to 64.8 €/MWh. The CSHPSS plant in Athens will continue decreasing to less than 52.5 €/MWh by 2030, whereas the base case will increase to 65.2 €/MWh. In Berlin, a slight cost reduction would be available in the CSHPSS plants by 2020 where the *NPC* will range from 54.9 to 59.3 €/MWh. By 2030, the CSHPSS plant *NPC* drops to 49.9 €/MWh compared to a rise in the *NPC* of the base case to 62.9 €/MWh. In Helsinki, the *NPC* ranges between 53.1 and 55.7 €/MWh, while its base case covers the heating demand at 51.5 €/MWh. These prices embody the CSHPSS plant in Helsinki as a competitive solution due to the high heating demand and high the non-renewable energy resources prices. By 2030, the *NPC* is expected to decrease below 46.7 €/MWh, while its base case continues to increase up to 62.7 €/MWh.

II.6 Conclusions

The EU ambitious plan to cut the GHG up to 40% simultaneously with increasing the share of the renewable energy resource at least 27% by 2030 encourages the prevalent methodology to quantify the renewable energy systems performance including its economic and environmental aspects. This work attempts to explore the prospects for wide-scale deployment of the central solar heating plants coupled with seasonal storage (CSHPSS) in the residential sector under various EU climate zones in order to solve its challenges. The proposed methodological framework correspondingly based on a multi-objective approach which is applied to optimize the cost against an aggregated environmental metric throughout the life cycle of the proposed system in comparison to their relative conventional heating systems. In this context, the proposed methodology is applied to various EU climates comprising Madrid, Athens, Berlin and Helsinki as representative for the Mediterranean, central European, and Nordic climates, respectively with consideration for the seasonal and short-term storage systems and their relative load profiles based on the explored climate zones.

Based on the life cycle assessment, the calculated optimal solutions demonstrate an environmental advancement for the CSHPSS plants at the considered EU climate zones in comparison to a heating system fueled by natural gas. The minimum impact solutions reduce the total environmental impact by 86.5%, 84.7%, 82.1%, and 82.9% for Madrid, Athens, Berlin, and Helsinki cases, respectively. While this improvement becomes only 42.9% for the Athens climate zone at the minimum cost optimal solution due to the dependency on using natural gas as a competitive solution in comparison to the deployment of the solar energy equipment. On the other hand, the life cycle costing analysis shows a clear tendency for increasing the net present cost (*NPC*) under various EU climate zones compared to their base cases due to the high initial capital cost of CSHPSS plants. In the minimum cost solutions, the *NPC* raised by 1%, 33.3%, 16.9% and 3.12% for Madrid, Athens, Berlin, and Helsinki cases,

respectively. This increment proofs dependency for the CSHPSS plants on the climate zone condition, the heating demand, and the natural gas and electricity prices.

Furthermore, this raise relatively increases in the minimum impact solution, and it becomes more substantial in Athens, and Berlin since the *NPC* increases by 50.8%, and 25.3% for these cities respectively due to the low price of non-renewable energy resources. Recalling the optimal solutions dependency on the design parameters, a detailed sensitivity analysis for the most relevant economic parameters in Madrid case study is presented. The sensitivity results aggravate a high dependency for the CSHPSS plant *NPC* objective on the natural gas price, the discount rate, the investment cost, the operational cost, where decreasing these parameters by 20% contribute to a significant change in the *NPC* up to 10%. While the total environmental impact increases by 196% for the reducing the natural gas price by 20%.

Following the challenges facing the CSHPSS in EU member states include high investment costs and the variation in the technical benefits. The proposed methodological framework successes in reducing this variation the system performance when introduced in various EU climate zones. Thus, the yearly solar fraction never goes below than 90.1% in the investigated climate zones where the ratio of seasonal storage tank volume to solar collector field area is around 8 ± 0.5 m^3/ m^2. From the economic point of view, the future development of the CSHPSS plant cost based on the historically observed learning curves combined with the clear tendency for the increment in the natural gas prices at various EU member states proposes a significant economic improvement in the competitiveness of the CSHPSS plant in comparison to the conventional system by 2020. However, the low heating demand and low prices of the natural gas and electricity in Athens (Mediterranean climate zone) provokes a limited improvement in the CSHPSS plant competitiveness until 2022.

In the real application of sizing community solar district heating network, the present framework can be beneficial for obtaining the right combination of design variables with maximizing its environmental impact incorporation with eliminating the oversizing system equipment. Furthermore, the proposed framework initiates a proportional optimal value regarding the seasonal storage tank and solar collector field of 8 ± 0.5 m^3/ m^2 which can serve as a guide for developing business models or establishing pilot storage plant.

Overall this study provides an effective tool for the techno-economic and environmental assessment of the CSHPSS at the residential sector which can be applied to plan its integration into the existing district heating fields. Furthermore, our study highlights the broad applicability of using CSHPSS in different EU climate as a sustainable alternative solution to the conventional systems based on natural gas. Even though in the real applications, such solar district heating systems are highly sensitive to the fluctuation in the fossil fuel prices and other economic parameters.

Therefore, the competitiveness cannot be approved without clear and effective policies based on a longer-term view for the deployment of renewable energy systems in the EU with a goal of establishing a more sustainable energy infrastructure.

II.7 Acknowledgments

The authors would like to acknowledge financial support from Martí i Franquès COFUND Fellowship program. This project has received funding from the European Union's Horizon 2020 research and innovation programme under the Marie Skłodowska-Curie grant agreement No. 713679 and the Spanish Ministry of Education and Competitiveness (CTQ2016-77968, MINECO/FEDER). In addition, this work was partially funded by the Ministerio de Economía y Competitividad de España (ENE2015-64117-C5-1-R (MINECO/FEDER) and ENE2015-64117-C5-3-R (MINECO/FEDER)). The authors at the University of Lleida would like to thank the Catalan Government for the quality accreditation given to their research group (2017 SGR 1537). GREA is certified agent TECNIO in the category of technology developers from the Government of Catalonia.

II.8 Nomenclature

A_{COL}	total aperture area of the solar collectors (m^2)
$C(x_0)$	cost production of a reference point (€/MWh)
$C(x_t)$	marginal cost of the CSHPSS plant at a certain particular time (€/MWh)
CAP_k	design variable of equipment unit *k*
C_{AUX}	annual operational cost of the auxiliary heaters (€)
C_C	total initial capital cost (€)
$CEPCI^{year\ A}$	chemical Engineering Plant Cost Index in the base year
$CEPCI^{year\ B}$	chemical Engineering Plant Cost Index in the installation year
C_M	annual cost of equipment unit *k* (€)
C_O	total discounted operational cost (€)
C_P	annual operational cost of a pump (€)
c_p	specific heat capacity (kJ/kg. k·K)
C_R	total discounted replacement cost (€)

d	annual discount rate (%)
DAM_d	indicator result for damage category d
FBM_k	bare module factor of equipment unit k
$f_c(x)$	original objective function [$NPC(x)$ or $RCP(x)$]
$\overline{f}_c(x)$	normalized objective function [$NPC(x)$ or $RCP(x)$]
f_m	maintenance factor
$f^{PN}(x)$	pseudo nadir point
$f^{UT}(x)$	utopia point
i	annual inflation rate (%)
IMP_e	indicator result for endpoint impact category e
LCI_i^{MP}	life cycle inventory of the elementary flow i related to the manufacturing process
LCI_i^{OP}	life cycle inventory of the elementary flow i related to operation activities
LCI_i^{TOT}	total life cycle inventory of the elementary flow i
LCI_i^{TR}	life cycle inventory of the elementary flow i related to transportation
LR	learning rate
$\dot{m}_{DHW}$	mass flow rate of the fluid in the DHW distribution circuit recirculate water pumps (kg/s)
$\dot{m}_{SH}$	mass flow rate of the recirculated fluid in the SH distribution circuit (kg/s)
M_c	big-M values used in the reformulated optimization model
NPC	net present cost (€/MWh)
PEC_k	purchase cost of equipment unit k
PVF_n	present value factor of a single future cash flow at the beginning of the n^{th} time period
PWF_n	present worth factor of periodic future cash flows
$\dot{Q}_{AUX}$	natural gas boiler duty rate (MW)

Q_{DHW}	total energy supplied by a domestic hot water tank (MWh)
$Q_{DHW\ load}$	total domestic hot water heating demand (MWh)
$Q_{SH\ load}$	total space heating demand (MWh)
Q_{SST}	total energy supplied by Seasonal seasonal storage tank (MWh)
RCP	ReCiPe 2008 aggregated impact factor (Pt/MWh)
SF_{DHW}	annual solar fraction for the DHW distribution circuit (%)
SF_{SH}	annual solar fraction for the SH distribution circuit (%)
V_{DHW}	volume of the domestic hot water tank (m^3)
V_{SST}	volume of the seasonal storage tank (m^3)
WS(x)	weighted-sum objective function
x	continuous variables of the simulation model
x_0	capacity at the reference point (MW)
x^L	lower bounds of the continuous variables of the simulation model
x_t	capacity at a certain time (MW)
x^U	upper bounds of the continuous variables of the simulation model
y	binary variable used in the reformulated optimization model

Greek symbols

α_{CF}	factor of contingency fees
α_k	purchase cost coefficient of equipment unit *k*
β_k	purchase cost exponent of equipment unit *k*
δ_d	normalization factor for damage category *d*
ΔT_{DHW}	temperature difference between the extracted and replaced water inside the DHWT (ºC)
ΔT_L	temperature difference between the exit and entrance of the auxiliary heater (ºC)
ΔT_{SST}	temperature difference between the extracted and replaced water inside the SST (ºC)

ε_d	weighting factor for damage category *d*
θ_{ei}	characterization factor that connects the elementary flow *i* with endpoint impact category *e*
λ	non-negative weight for the weighted-sum method

Abbreviations

AUX	auxiliary heater fueled by natural gas
COL	field of solar collectors
CSHPSS	central solar heating plant coupled with seasonal storage
DHW	domestic hot water
DHWT	domestic hot water storage tank
GHG	greenhouse gas
GenOpt	generic optimization program
GPSPSOCCHJ	generalized pattern search algorithm with particle swarm optimization with construction coefficient and Hooke-Jeeves algorithm
HE	heat exchanger
HJ	Hooke-Jeeves algorithm
LCA	life cycle assessment
LCC	life cycle costing
MOO	multi-objective optimization
P_i	centrifugal pump
PSO	particle swarm optimization algorithm
SH	space heating
SST	seasonal storage tank
TES	thermal energy storage
TRNSYS	transient system simulation program

Indices

c	objective function
d	damage category
e	endpoint impact category
i	elementary factor
k	equipment unit

Sets

ID_d	set of endpoint impact categories *e* that contribute to damage *d*

II.9 References

[1] Renewable Energy Policy Network for 21st Century (REN21). Renewables 2016-Global Status Report. 2016.

[2] U.S. Energy Information Administration. International Energy Outlook 2016. 2016. doi:www.eia.gov/forecasts/ieo/pdf/0484(2016).pdf.

[3] Rezaie B, Rosen MA. District heating and cooling: Review of technology and potential enhancements. Appl Energy 2012;93:2–10. doi:10.1016/j.apenergy.2011.04.020.

[4] British Petroleum. BP Statistical Review of World Energy 2017. 2017. doi:http://www.bp.com/content/dam/bp/en/corporate/pdf/energy-economics/statistical-review-2017/bp-statistical-review-of-world-energy-2017-full-report.pdf.

[5] European Energy Agency. Final energy consumption by sector and fuel. Denmark: 2017. doi:CSI 027/ENER 016.

[6] Balaras CA, Gaglia AG, Georgopoulou E, Mirasgedis S, Sarafidis Y, Lalas DP. European residential buildings and empirical assessment of the Hellenic building stock, energy consumption, emissions and potential energy savings. Build Environ 2007;42:1298–314. doi:10.1016/j.buildenv.2005.11.001.

[7] European Environment Agency. Annual European Union greenhouse gasinventory 1990–2016 and inventory report 2018. Copenhagen: 2018.

[8] European Commision. Memo on the Renewable Energy and Climate Change Package. Brussels: 2008.

[9] European Commision. Communication from the commission to the European parliament, the council, the European economic and social committee and the committee of the regions - a policy framework for climate and energy in the period from 2020 to 2030. Brussels: 2014.

[10] Olsthoorn D, Haghighat F, Mirzaei PA. Integration of storage and renewable energy into district heating systems: A review of modelling and optimization. Sol Energy 2016;136:49–64. doi:10.1016/j.solener.2016.06.054.

[11] Jamar A, Majid ZAA, Azmi WH, Norhafana M, Razak AA. A review of water heating system for solar energy applications. Int Commun Heat Mass Transf 2016;76:178–87. doi:10.1016/j.icheatmasstransfer.2016.05.028.

[12] Pinel P, Cruickshank CA, Beausoleil-Morrison I, Wills A. A review of available methods for seasonal storage of solar thermal energy in residential applications. Renew Sustain Energy Rev 2011;15:3341–59. doi:10.1016/j.rser.2011.04.013.

[13] Raluy R, Serra L, Guadalfajara M, Lozano M. Life Cycle Assessment of Central Solar Heating Plants with Seasonal Storage. Energy Procedia 2014;48:966–76. doi:10.1016/j.egypro.2014.02.110.

[14] European Solar Thermal Industry Federation (ESTIF). Solar heat markets in Europe: Trends and Market Statistics 2016. Brussels: 2016.

[15] Carrilho da Graça G, Augusto A, Lerer MM. Solar powered net zero energy houses for southern Europe: Feasibility study. Sol Energy 2012;86:634–46. doi:10.1016/j.solener.2011.11.008.

[16] Abokersh M, Osman M, El-Baz O, El-Morsi M, Sharaf O. Review on the Use of Phase Change Material in Domestic Solar Water Heating Systems. Int J Energy Res 2018;42:329–57. doi:10.1002/er.3765.

[17] McDaniel B, Kosanovic D. Modeling of combined heat and power plant performance with seasonal thermal energy storage. J Energy Storage 2016;7:13–23. doi:10.1016/j.est.2016.04.006.

[18] Ibrahim NI, Al-Sulaiman FA, Rahman S, Yilbas BS, Sahin AZ. Heat transfer enhancement of phase change materials for thermal energy storage applications: A critical review. Renew Sustain Energy Rev 2017;74:26–50. doi:10.1016/j.rser.2017.01.169.

[19] Antoniadis CN, Martinopoulos G. Simulation of Solar Thermal Systems with Seasonal Storage Operation for Residential Scale Applications. Procedia Environ Sci 2017;38:405–12. doi:10.1016/j.proenv.2017.03.124.

[20] Dincer I. On thermal energy storage systems and applications in buildings. Energy Build 2002;34:377–88. doi:10.1016/S0378-7788(01)00126-8.

[21] Fisch M, Guigas M, Dalenbäck J. A review of large-scale solar heating systems in Europe. Sol Energy 1998;63:355–66. doi:10.1016/S0038-092X(98)00103-0.

[22] Hesaraki A, Holmberg S, Haghighat F. Seasonal thermal energy storage with heat pumps and low temperatures in building projects - A comparative review. Renew Sustain Energy Rev 2015;43:1199–213. doi:10.1016/j.rser.2014.12.002.

[23] Speyer E. Optimum storage of heat with a solar house. Sol Energy 1959;3:24–48. doi:10.1016/0038-092X(59)90004-0.

[24] Ochs F, Heidemann W, Müller-Steinhagen H. Performance of Large-Scale Seasonal Thermal Energy Stores. J Sol Energy Eng 2009;131:041005. doi:10.1115/1.3197842.

[25] Bankston CA. The status and potential of central solar heating plants with seasonal storage: An international Report. Adv. Sol. Energy, New York: Plenum Press; 1988, p. 352–444.

[26] Tian Z, Perers B, Furbo S, Fan J. Annual measured and simulated thermal performance analysis of a hybrid solar district heating plant with flat plate collectors and parabolic trough collectors in series. Appl Energy 2017;205:417–27. doi:10.1016/j.apenergy.2017.07.139.

[27] Weiss W, Spörk-Dür M, Mauthner F. Solar Heat Worldwide: Global Market

Development and Trends in 2016. Gleisdorf, Austria: 2017.

[28] European Solar Thermal Industry Federation. Solar Thermal Markets in Europe. Trends and Market Statistics 2014. Brussel - Belgium: 2015.

[29] Schultz J, Andersen E, Furbo S. Advanced storage concepts for solar and low energy buildings, IEA-SHC Task 32. Copenhagen: 2008.

[30] Xu J, Wang RZ, Li Y. A review of available technologies for seasonal thermal energy storage. Sol Energy 2014;103:610–38. doi:10.1016/j.solener.2013.06.006.

[31] Rad FM, Fung AS. Solar community heating and cooling system with borehole thermal energy storage - Review of systems. Renew Sustain Energy Rev 2016;60:1550–61. doi:10.1016/j.rser.2016.03.025.

[32] Shah SK, Aye L, Rismanchi B. Seasonal thermal energy storage system for cold climate zones: A review of recent developments. Renew Sustain Energy Rev 2018;97:38–49. doi:10.1016/j.rser.2018.08.025.

[33] Sibbitt B, McClenahan D, Djebbar R, Thornton J, Wong B, Carriere J, et al. The performance of a high solar fraction seasonal storage district heating system - Five years of operation. Energy Procedia 2012;30:856–65. doi:10.1016/j.egypro.2012.11.097.

[34] Antoniadis CN, Martinopoulos G. Simulation of Solar Thermal Systems with Seasonal Storage Operation for Residential Scale Applications. Procedia Environ Sci 2017;38:405–12. doi:10.1016/j.proenv.2017.03.124.

[35] Rehman H ur, Hirvonen J, Sirén K. A long-term performance analysis of three different configurations for community-sized solar heating systems in high latitudes. Renew Energy 2017;113:479–93. doi:10.1016/j.renene.2017.06.017.

[36] Rämä M, Mohammadi S. Comparison of distributed and centralised integration of solar heat in a district heating system. Energy 2017;137:649–60. doi:10.1016/j.energy.2017.03.115.

[37] Rad FM, Fung AS, Rosen MA. An integrated model for designing a solar community heating system with borehole thermal storage. Energy Sustain Dev 2017;36:6–15. doi:10.1016/j.esd.2016.10.003.

[38] Panno D, Buscemi A, Beccali M, Chiaruzzi C, Cipriani G, Ciulla G, et al. A solar assisted seasonal borehole thermal energy system for a non-residential building in the Mediterranean area. Sol Energy 2018:0–1. doi:10.1016/j.solener.2018.06.014.

[39] Ciampi G, Rosato A, Sibilio S. Thermo-economic sensitivity analysis by dynamic simulations of a small Italian solar district heating system with a seasonal borehole thermal energy storage. Energy 2018;143:757–71. doi:10.1016/j.energy.2017.11.029.

[40] Li X, Liu M, Duanmu L, Ji Y. The Optimization of Solar Heating System with

Seasonal Storage Based on a Real Project. Procedia Eng 2015;121:1341–8. doi:10.1016/j.proeng.2015.09.017.

[41] Durão B, Joyce A, Mendes JF. Optimization of a seasonal storage solar system using Genetic Algorithms. Sol Energy 2014;101:160–6. doi:10.1016/j.solener.2013.12.031.

[42] Rehman H ur, Hirvonen J, Sirén K. Influence of technical failures on the performance of an optimized community-size solar heating system in Nordic conditions. J Clean Prod 2018;175:624–40. doi:10.1016/j.jclepro.2017.12.088.

[43] Hirvonen J, ur Rehman H, Sirén K. Techno-economic optimization and analysis of a high latitude solar district heating system with seasonal storage, considering different community sizes. Sol Energy 2018;162:472–88. doi:10.1016/j.solener.2018.01.052.

[44] Buoro D, Pinamonti P, Reini M. Optimization of a Distributed Cogeneration System with solar district heating. Appl Energy 2014;124:298–308. doi:10.1016/j.apenergy.2014.02.062.

[45] Tulus V, Boer D, Cabeza LF, Jiménez L, Guillén-Gosálbez G. Enhanced thermal energy supply via central solar heating plants with seasonal storage: A multi-objective optimization approach. Appl Energy 2016;181:549–61. doi:10.1016/j.apenergy.2016.08.037.

[46] Pavičević M, Novosel T, Pukšec T, Duić N. Hourly optimization and sizing of district heating systems considering building refurbishment – Case study for the city of Zagreb. Energy 2017;137:1264–76. doi:10.1016/j.energy.2017.06.105.

[47] Welsch B, Göllner-Völker L, Schulte DO, Bär K, Sass I, Schebek L. Environmental and economic assessment of borehole thermal energy storage in district heating systems. Appl Energy 2018;216:73–90. doi:10.1016/j.apenergy.2018.02.011.

[48] Paiho S, Hoang H, Hukkalainen M. Energy and emission analyses of solar assisted local energy solutions with seasonal heat storage in a Finnish case district. Renew Energy 2017;107:147–55. doi:10.1016/j.renene.2017.02.003.

[49] Bauer D, Marx R, Nußbicker-Lux J. German central solar heating plants with seasonal heat storage. Sol Energy 2010;84:612–23. doi:10.1016/j.solener.2009.05.013.

[50] De Guadalfajara M, Lozano MA, Serra LM. Evaluation of the potential of large solar heating plants in Spain. Energy Procedia 2012;30:839–48. doi:10.1016/j.egypro.2012.11.095.

[51] Flynn C, Sirén K. Influence of location and design on the performance of a solar district heating system equipped with borehole seasonal storage. Renew Energy 2015;81:377–88. doi:10.1016/j.renene.2015.03.036.

[52] Edenhofer O, Pichs-Madruga R, Sokona Y, Seyboth K, Eickemeier P,

Matschoss P, et al. Renewable Energy Sources and Climate Change Mitigation: Summary for Policymakers and Technical Summary. 2011. doi:10.5860/CHOICE.49-6309.

[53] Bauer D, Marx R, Drück H. Solar district heating for the built environment technology and future trends within the european project Einstein. Energy Procedia 2014;57:2716–24. doi:10.1016/j.egypro.2014.10.303.

[54] Teske S, Janis L, Luis C, Marcel B, Elena D, Christoph R, et al. Solar Thermal Electricity Global Outlook 2016. Amsterdam: 2016.

[55] Carpaneto E, Lazzeroni P, Repetto M. Optimal integration of solar energy in a district heating network. Renew Energy 2015;75:714–21. doi:10.1016/j.renene.2014.10.055.

[56] Hassam ur Rehman; Janne Hirvonen; Kai Sirén. Performance comparison between optimized design of a centralized and semi-decentralized community size solar district heating system. Appl Energy 2018;229:1072–94. doi:https://doi.org/10.1016/j.apenergy.2018.08.064.

[57] Klein SA et al. TRNSYS Version. 18, Solar Energy Laboratory, University of Wisconsin-Madison, Website: <http://sel.me.wisc.edu/ trnsys> 2004.

[58] Wetter M. GenOpt. Generic Optimization Program. User Manual. California: 2011. doi:10.2172/962948.

[59] Raab S, Mangold D, Müller-Steinhagen H. Validation of a computer model for solar assisted district heating systems with seasonal hot water heat store. Sol Energy 2005;79:531–43. doi:10.1016/j.solener.2004.10.014.

[60] Gebreslassie B, Guillén-Gosálbez G. Design of environmentally conscious absorption cooling systems via multi-objective optimization and life cycle assessment. Appl Energy 2009;86:1712–22. doi:10.1016/j.apenergy.2008.11.019.

[61] Sameti M, Haghighat F. A two-level multi-objective optimization for simultaneous design and scheduling of a district energy system. Appl Energy 2017;208:1053–70. doi:10.1016/j.apenergy.2017.09.046.

[62] Di Somma M, Yan B, Bianco N, Graditi G, Luh PB, Mongibello L, et al. Multi-objective design optimization of distributed energy systems through cost and exergy assessments. Appl Energy 2017;204:1299–316. doi:10.1016/j.apenergy.2017.03.105.

[63] Duffie, J.A., Beckman WA. Solar Engineering of Thermal Processes. 3rd ed. John Wiley & Sons, Inc; 2006.

[64] Allouhi A, Agrouaz Y, Benzakour Amine M, Rehman S, Buker MS, Kousksou T, et al. Design optimization of a multi-temperature solar thermal heating system for an industrial process. Appl Energy 2017;206:382–92. doi:10.1016/j.apenergy.2017.08.196.

[65] Hobbi A, Siddiqui K. Optimal design of a forced circulation solar water heating

system for a residential unit in cold climate using TRNSYS. Sol Energy 2009;83:700–14. doi:10.1016/j.solener.2008.10.018.

[66] Hang Y, Qu M, Ukkusuri S. Optimizing the design of a solar cooling system using central composite design techniques. Energy Build 2011;43:988–94. doi:10.1016/j.enbuild.2010.12.024.

[67] Kalogirou SA. Solar energy engineering: processes and systems. 1st Ed. Academic Press; 2009. doi:10.1016/B978-0-12-374501-9.00014-5.

[68] Duffie JA, Beckman WA, Worek WM. Solar Engineering of Thermal Processes, 2nd ed. J Sol Energy Eng 1994;116:67. doi:10.1115/1.2930068.

[69] Gluch P, Baumann H. The life cycle costing (LCC) approach: A conceptual discussion of its usefulness for environmental decision-making. Build Environ 2004;39:571–80. doi:10.1016/j.buildenv.2003.10.008.

[70] Chemical Engineering Plant Cost Index (CEPCI): Economic Indicator. Chem Eng J 2015.

[71] Turton R, Bailie RC, Whiting WB, Shaeiwitz JA, Bhattacharyya D. Analysis, synthesis, and design of chemical processes. 3rd ed. Prentice Hall; 2008.

[72] Ellehauge K, Pedersen TE. Solar heat storages in district heating networks. Energinet.dk, PREHEAT project no. 2006-2-6750. 2007.

[73] Schmidt T MD. Status of solar thermal seasonal storage in Germany. 2009.

[74] Calise F, Dentice d'Accadia M, Palombo A. Transient analysis and energy optimization of solar heating and cooling systems in various configurations. Sol Energy 2010;84:432–49. doi:10.1016/j.solener.2010.01.001.

[75] Nemerow NL, Agardy FJ, Sullivan P, Salvato JA. ENVIRONMENTAL ENGINEERING: Environmental Health and Safety for Municipal Infrastructure, Land Use and Planning, and Industry. 6th ed. John Wiley & Sons, Inc; 2009.

[76] ISO/TC 207/SC 5. ISO 14040:2006 Environmental management — Life cycle assessment — Principles and framework 2006.

[77] International Organization for Standardization (ISO). ISO 14041: Environmental Management - Life Cycle Assessment: Goal and Scope Definition and Inventory Analysis. 1997.

[78] International Organization for Standardization (ISO). ISO 14042:Environmental management - Life cycle assessment - Life cycle impact. 2000.

[79] Guillén-Gosálbez G, Caballero JA, Jiménez L. Application of Life Cycle Assessment to the Structural Optimization of Process Flowsheets. Ind Eng Chem Res 2008;47:777–89. doi:10.1016/S1570-7946(07)80218-5.

[80] Weidema BP, Bauer C, Hischier R, Mutel C, Nemecek T, Reinhard J, et al. Data quality guideline for the ecoinvent database version 3. vol. 3. 2013.

[81] Goedkoop M, Heijungs R, De Schryver A, Struijs J, van Zelm R. ReCiPe 2008. A LCIA method which comprises harmonised category indicators at the midpoint and the endpoint level. Report I: Characterisation 2009:1–133. doi:http://www.lcia-recipe.net.

[82] JRC European commission (JRC-IES). ILCD Handbook: Recommendations for Life Cycle Impact Assessment in the European context. 1st editio. Luxemburg: Office of the European Union; 2011. doi:10.278/33030.

[83] Weiss W, Biermayr P. Potential of Solar Thermal in Europe. 2010.

[84] Paul Hutchens. Solar Heating Roadmap: Strategy and Measures of the Solar Heating Industry for Accelerated Market Growth to 2030. Berlin: 2012.

[85] Greenpeace international. Energy Revolution: A sustainable pathway to a clean energy future for europe. 2005.

[86] Rout UK, Blesl M, Fahl U, Remme U, Voß A. Uncertainty in the learning rates of energy technologies: An experiment in a global multi-regional energy system model. Energy Policy 2009;37:4927–42. doi:10.1016/j.enpol.2009.06.056.

[87] Rubin ES, Azevedo IML, Jaramillo P, Yeh S. A review of learning rates for electricity supply technologies. Energy Policy 2015;86:198–218. doi:10.1016/j.enpol.2015.06.011.

[88] Vecchietti A, Lee S, Grossmann IE. Modeling of discrete/continuous optimization problems: characterization and formulation of disjunctions and their relaxations. Comput Chem Eng 2003;27:433–48. doi:10.1016/S0098-1354(02)00220-X.

[89] Ehrgott M. Multicriteria optimization. Heidelberg: Springer; 2005.

[90] Kennedy J, Eberhart R. Particle swarm optimization. Neural Networks, 1995 Proceedings, IEEE Int Conf 1995;4:1942–8 vol.4. doi:10.1109/ICNN.1995.488968.

[91] Kennedy J, Eberhart RC. A discrete binary version of the particle swarm algorithm. 1997 IEEE Int Conf Syst Man, Cybern Comput Cybern Simul 1997;5:4–8. doi:10.1109/ICSMC.1997.637339.

[92] Hooke R, Jeeves TA. “Direct Search” Solution of Numerical and Statistical Problems. J ACM 1961;8:212–29. doi:10.1145/321062.321069.

[93] IDAE. Análisis del consumo energético del sector residencial en España. INFORME FINAL. 2011.

[94] Shariah A, Al-Akhras MA, Al-Omari I a. Optimizing the tilt angle of solar collectors. Renew Energy 2002;26:587–98. doi:10.1016/S0960-1481(01)00106-9.

[95] United Nations Environment Programme, Solar Thermal Energy Technology Fact Sheet. 2014.

[96] Colclough S, McGrath T. Net energy analysis of a solar combi system with Seasonal Thermal Energy Store. Appl Energy 2015;147:611–6. doi:10.1016/j.apenergy.2015.02.088.

[97] Kottek M, Grieser J, Beck C, Rudolf B, Rubel F. World map of the Köppen-Geiger climate classification updated. Meteorol Zeitschrift 2006;15:259–63. doi:10.1127/0941-2948/2006/0130.

[98] Rubel F, Kottek M. Observed and projected climate shifts 1901-2100 depicted by world maps of the Köppen-Geiger climate classification. Meteorol Zeitschrift 2010;19:135–41. doi:10.1127/0941-2948/2010/0430.

[99] U.S. Department of Energy. EnergyPlus. Energy Simulation Software: Weather Data n.d. 2015.

[100] European Commission. Eurostat. Energy database n.d.

[101] Weidema BP, Bauer C, Hischier R, Mutel C, Nemecek T, Reinhard J, et al. The ecoinvent database: Overview and methodology, Data quality guideline for the ecoinvent database version 3 2013.

[102] Trimble. SketchUp 2012. http://www.sketchup.com.

[103] Ahmed K, Pylsy P, Kurnitski J. Hourly consumption profiles of domestic hot water for different occupant groups in dwellings. Sol Energy 2016;137:516–30. doi:10.1016/j.solener.2016.08.033.

[104] Instituto de Estadística. Trends in households in the European Union: 1995-2025 2003. http://www.madrid.org/iestadis/fijas/efemerides/ue171203.htm (accessed March 11, 2018).

[105] Parakosta K, Papageorgiou N, Sotiropoulos B. Residential hot water use pattern in Greece. Sol Energy 1995;54:369–74.

[106] Ahmed K, Pylsy P, Kurnitski J. Monthly domestic hot water profiles for energy calculation in Finnish apartment buildings. Energy Build 2015;97:77–85. doi:10.1016/j.enbuild.2015.03.051.

[107] Jordan U, Vajen K. DHWcalc: program to generate domestic hot water profiles with statistical means for user defined conditions. Proc. ISES Sol. World Congr., Orlando (US): n.d., p. 8–12.

[108] Eurostat. Inflation in the euro area 2018. http://ec.europa.eu/eurostat/statistics-explained/index.php/Inflation_in_the_euro_area (accessed March 12, 2018).

[109] Braungardt S, Eichhammer W, Elsland R, Fleiter T, Klobasa M, Krail M, et al. Study evaluating the current energy efficiency policy framework in the EU and providing orientation on policy options for realising the cost-effective energy-efficiency/saving potential until 2020 and beyond. 2014.

[110] Greenpeace international. Energy [R]evolution - A sustainable EU 27 energy outlook. 2012.

[111] Joachim Nitsch, Thomas Pregger, Scholz Y, Naegler T, Sterner M, Gerhardt N, et al. Langfristszenarien und Strategien für den Ausbau der Erneuerbaren Energien in Deutschland bei Berücksichtigung der Entwicklung in Europa und global. 2012. doi:BMU - FKZ 03MAP146.

[112] Kost C, Mayer JN, Thomsen J, Hartmann N, Senkpiel C, Philipps S, et al. Levelized Cost of Electricity Renewable Energy Technologies. Freiburg, Germany: 2013. doi:10.1613/jair.301.

[113] Montgomery DC. Design and Analysis of Experiments, Eighth Edition. John Wiley & Sons, Inc.; 2013.

Chapter III

Machine learning approach to improve SDHS sustainability

III. Machine learning approach to improve SDHS sustainability

A framework for the optimal integration of solar assisted district heating in different urban sized communities: a robust machine learning approach incorporating global sensitivity analysis

Mohamed Hany Abokersh [a], Manel Vallès [a], Luisa F. Cabeza [b], Dieter Boer [a, *]

a Departament d'Enginyeria Mecànica, Universitat Rovira i Virgili, Av. Països Catalans 26, 43007 Tarragona, Spain

b GREiA Research Group, INSPIRES Research Centre, Universitat de Lleida, Pere de Cabrera s/n, 25001 Lleida, Spain

** Corresponding author: dieter.boer@urv.cat*

E-mail addresses: mohamed.abokersh@urv.cat (M.H. Abokersh), manel.valles@urv.cat (M. Vallès), lcabeza@diei.udl.cat (L.F. Cabeza)

Keywords: Solar assist district heating system; Artificial Neural Network; Bayesian optimization approach; Life cycle assessment; Multi-objective optimization; Global sensitivity analysis

III.1 Introduction

Despite the global tendency in shifting the current energy production towards more and sustainable energy options, the carbon dioxide (CO_2) emissions keep growing by 6.5% over the last five years [1].

In Europe, the Governance of the Energy Union approved new clean energy for all Europeans package [2]. This plan comprehensively updates the European Union (EU) energy policy framework to facilitate the sustainable transaction from fossil fuel towards the deployment of renewable energy to follow up the EU 2030 targets for climate and energy consistently with delivering the EU Paris agreement commitments towards the reduction in greenhouse gas emissions (GHG) [3]. An important step to spread on the clean energy transition in the European Union and its Member States is the energy efficiency in the building sector. Buildings represent one of the biggest

energy consumers in the EU, accounting for more than 40% of the final energy consumption [4], where the residential buildings consume 63% of this energy [5]. Moreover, more than 75% of residential energy consumption is utilized for space and domestic hot water heating [6]. Along with all these figures, the residential sector counts for about 10% of the total GHG in 2017 [7]. In response to this issue, the EU promoted the Energy Efficiency Directive plan 2012/27/EU [8]. This plan tends to boost the energy performance of the buildings and introduce energy certificates, taking into account the external climatic conditions and defining Net Zero Energy Buildings. Even though these actions plan led to decrease the final energy consumption of the residential section by 9.3% over the last 15 years, still the average energy consumption still increases by 0.4% per year due to the growth in the urbanization area and dispersion of the central heating [9]. Aligning with this growth, various types of renewable energy systems are installed in the building sector for electricity and thermal loads coverage.

Among all renewable sources, solar energy seems to be the most promising alternative for fossil fuel due its unique benefits [10]. However, the main drawback of solar thermal energy, as well as the other renewable energy sources, is the intermittency and fluctuation based on short and long term basis [11,12], which causes a gap between the energy demand and supply. Between several storage techniques, the thermal energy storage (TES) systems seem to be the most promising technologies that fulfill this gap issue. TES systems store the excess generated power and provides it on-demand [13]. Considering their storage capacity, TES systems comprise two main categories; these categories are short- and long-term systems. Short-term systems have a charge-discharge capacity for a few days and they are widely known as diurnal storage [14]. In general, these systems suffer from demand coverage problems during the winter season, especially in the high latitude countries. This is due to the difference in solar availability between summer and winter seasons [15]. On the other hand, long-term storage can last up for several months, and it is known as seasonal TES. Accordingly, seasonal TES can efficiently contribute to solve the demand issue during the winter season, and consequently improve the usage of renewable energy source in district heating systems aligning with the building decarbonization concept [16,17]. Even though seasonal TES has been developed for chemical and latent heat storage, the existing seasonal TES mainly uses sensible storage due to its stability [18].

In Europe, the begin of developing solar assisted district heating systems (SDHS) coupled with sensible seasonal TES began in the 1970s with the energy crisis [19]. Such district heating communities have been established in the 1990s and 2000s, mostly in Denmark and Germany [20]. Since then, the SHDS market has been growing practically in Northern and Central Europe [21]. With few exceptions (detailed below), the real performance of the SDHS has met with the estimated or predicted results. In Friedrichshafen (Germany), the estimated performance in terms of the

solar fraction could reach up to 43%. However, the monitoring data under realistic operation conditions showed that only a solar fraction between 21% to 33% could be reached [22]. A higher estimated solar fraction value has not been reached due to several issues that comprise higher heating demand compared to the excepted, higher thermal losses in the seasonal storage, and lower solar collector and heat exchanger efficiencies [23]. The same issue has been noticed in other SDHS installed in Neckarsulm and Rostock [24]. Moreover, in the installed plants in Steinfurt-Borghorst, Hamburg, and Neckarsulm II, a considerable deviation between the design and monitored performance due to the high thermal losses in the seasonal and other tanks, high net return temperature, and smaller solar collector area than the planned [25]. The most famous solar community is the Drake Landing Solar Community in Canada. This plant has been able to cover 98% of the space heating demand through solar energy [26]. However, a high-performance variation faces this solar community during a five year of monitoring. According to ASHRAE report [27], the reason behind this underperformance of the system compared to the simulation results is the high thermal losses throughout the network, the storage tank stratification, and pump control. Other than the problems mentioned above, Weissmann et al. [28] stated that the building orientation and the thermal collector orientation combined with the pipe leakages could adversely affect the SHDS performance.

In order to expand the benefits of SDHS, the optimal designing and sizing of SDHS and their relative relevant components (e.g., charging/discharging devices) should be adequately planned [29]. Substantially, planning and construction of large-scale SDHS coupled with seasonal TES is a complex process. Furthermore, the vast options of seasonal TES combined evolve the optimization approach as a viable option to obtain the optimal design and operation conditions of SDHS. The formulation of the optimization problem has two main approaches, the first is to use equation-oriented approach, which leads to non-convex mixed-integer non-linear programming (MINLP) and it can be solved through software packages (e.g., GAMS, MATLAB, etc.) [30]. According to Klatt and Marquardt [31], however, MINLP is still not a suitable method for reasonably sized models. Therefore, MINLP models are often reformulated and solved using mixed-integer linear programming (MILP). This approach relies on simpler and less accurate methods. In this context, Buoro et al. [32] and Welsch et al. [33] formulated a MILP for optimizing SDHS together with conventional power units to emphasize on the renewable energies rule in the residential sector. On the other hand, the second approach refers to the sequential models which rely on detailed equations with accurate results [34]. Therefore, this approach is used in commercial software (e.g., TRNSYS, EnergyPlus, etc.). In this context, Tian et al. [21] and Rehman et al. [35] set up a TRNSYS-GenOpt model to optimize the key design parameters of a SDHS in a multi-objective optimization (MOO) framework. Their results approve the techno-economic feasibility of district heat networks in Nordic climates. Lined up with the environmental benefits of SDHS,

Tulus et al. [36] proposed a framework to optimize SDHS design parameters according to economic and environmental indicators based on a generic optimization tool combined with TRNSYS. Even though the sequential models have great potential in developing validated models [37], the optimization based on sequential models (Heuristics optimization) is computationally costly and have many limitations regarding the optimization process to consider several decision variables comprises the operation, configuration, and sizing of the SDHS in the same framework. Moreover, these Heuristics optimization frameworks failed in considering the stochastic nature of renewable energy sources [38]. In this context, several studies performed a sensitivity analysis in order to investigate the contribution of various parameters to the SDHS model output [38,39]. However, due to the high computational expenses of the Heuristics optimization problems, the most common approach is the Local Sensitivity Analysis (LSA), where the importance of the parameters is investigated by varying one parameter at a time whereas the remain parameters are fixed [40]. This approach is an inadequate practice to cover the input parameters domain and its interactions. Alternatively, the Global Sensitivity Analysis (GSA) approach solve these drawback, where it can offer better coverage for the parameter design space and its relative interactions [41], but it required thousands of simulations in order to cover the design parameters domain sufficiently which does not fit with the Heuristics optimization approach.

This computational obstacle of SDHS simulation may be overcome by using the surrogate model (metamodel) [42]. The metamodel is a generated model of the sequential model, which is typically fast compared to the original detailed model. One of the most widely used metamodel technique is artificial neural networks (ANN) to solve complex engineering problems [43]. The main advantage of ANN is to replicate the detailed model through approximate an implicit relationship based on the training data. In the SDHS context, Yaïci and Entchev [44] utilized ANN to predict the yearly performance of SDHS that covers the domestic hot water and space heating demand in a residential application. While Xia et al. [45] combined the ANN model with a genetic algorithm to optimize the performance of SDHS in a multi-objective framework. Despite the ANN potential in developing accurate metamodels, the generation of an adequate training set required large simulation number. Moreover, the large set of tuning parameters in the ANN model combined with the requirement of large simulation for generating an adequate training set represents a significant limitation in using ANN [46].

All the performance, modelling, economical and legal barriers promote a high variation in quantifying the SDHS benefits over its lifetime [38,47], especially in different community size [48]. Thus, this study aims to propose a methodology framework to address these shortcomings via the following contributions:

1. To develop a robust approach for establishing an ANN model that covers the drawbacks associated with the surrogate modelling technique.

2. To integrate this robust ANN model to solve the computational obstacle associated with heuristics optimization models for SDHS in a MOO framework.

3. To trace the technical failure of the seasonal TES through expanding the decision variables by presenting its geometry and construction design parameters in the optimization problem due to its potential importance, as reported in several established projects [22,24].

4. To examine the community size effect on the performance of the SDHS in a techno-economic optimization framework with consideration for its environmental impact.

5. To investigate the uncertainty using the GSA approach for the economic parameters (investment costs, energy carrier prices, etc.) through taking advantage of the low computational cost feature associated with the robust ANN model.

Hence, the main novelty of the work is to develop a sustainable pathway to trace the techno-economic failures of the SDHS in the residential communities with consideration for its environmental impact. This path is implemented through developing a complete methodological optimization framework based on a robust ANN to showcase the full system potential throughout its lifetime when introduced in different urban community sizes. Moreover, another novelty of this paper is the integration of Global Sensitivity Analysis (GSA) with the Heuristics optimization frameworks; it is the first effort to bridge the heuristics optimization approach and the uncertainty associated with the SDHS design from a global perspective. In this context, the framework starts with developing a detailed simulation for the SDHS based on TRNSYS 18 software [49], the model includes seasonal and short term storages to fulfill both energy demands for the space heating (SH) and the domestic hot water (DHW). The developed TRNSYS model is combined with MATLAB to develop the robust surrogate model and then introduced in a multi-objective optimization problem that comprises the community size effect and the seasonal TES design parameters under two main different optimization settings. The first optimization setting considers only the SDHS equipment sizes, whereas the other setting includes the SST construction materials in the optimization problem. The developed framework can serve as a supportive decision-making tool that assesses the potential of SDHS in Europe and subsequently, accelerating the clean energy transition with promoting a clear statement regarding the new clean energy for all Europeans packages.

III.2 System description

The study is performed for a virtual residential community with a dedicated solar-assisted district network. The SDHS is modelled in a dynamic simulation software TRNSYS 18, which is introduced earlier in [38]. The main components of the SDHS are the solar collector field, the seasonal storage tank (SST), and the DHW storage tank (DHWT). The solar collector field can be either installed in the residential community roofs or the ground nearby the storages and its relative distribution systems. The SST is a large-scale sensible water insulated reservoir, which is usually half-buried, and it is mainly utilized to accumulate energy for an extended period. The SST is able to cover the SH demand during the winter season through the stored energy during the summer season. On the contrary, the DHWT is relatively a small water TES tank dedicated to supply energy on a daily bases to cover the DHW demand at a temperature of 60ºC. The mismatch between the supply and the customer demand in a daily or seasonal base is covered by auxiliary natural gas heaters. A schematic representation for the analysed SDHS in this work, and its main inputs/outputs are shown in Figure III-1

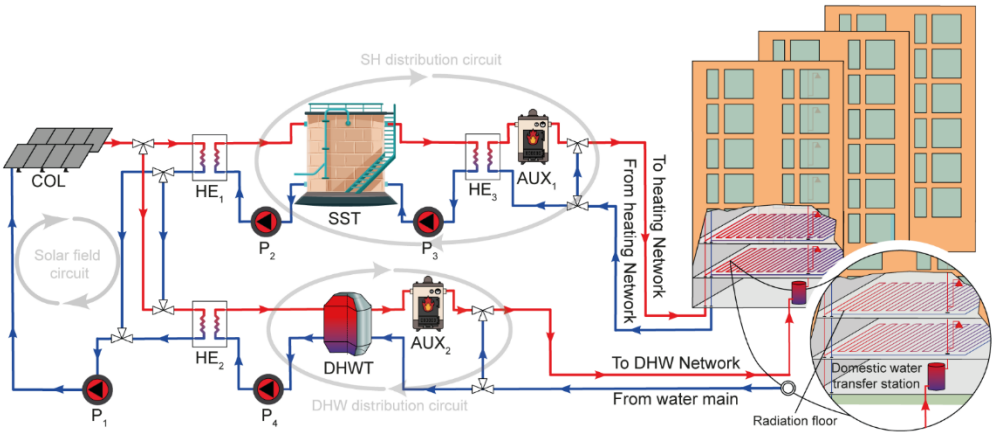

Figure III-1: Simple schematic representation for the SDHS

The proposed SDHS is divided into three primary circuits; these circuits comprise the solar field circuit, the SH distribution circuit, and the DHW distribution circuit. The solar collector field (COL) is connected to the short- and long-term storages through heat exchangers (HE_1) and (HE_2). These heat exchangers impulse the captured heat through the solar collector to the SH distribution circuit or DHW distribution circuit based on the selected control mode using the Y-type valves. The blue line shows the heat flows in the cold side of the SHDS, whereas the red line represents the hot side, as illustrated in Figure III-1.

The control strategy is designed to maximize the solar contribution where solar energy is utilized to meet the SH and DHW demand. In the DHW operation mode (priority 1), the COL output temperature and the average DHW temperature are the monitoring variables. When this mode is activated, the centrifugal pumps P_1 and P_4 are triggered to transfer the accumulated solar heat to the DHWT through the HE_2. An auxiliary heater using natural gas AUX_2 is installed to cover any shortage in the DHW network supply. Two Y-valves are installed to regulate the water temperature at the DHW distribution circuit by mixing the hot water from the AUX_2 with fresh water from the mainstream.

In the SH operation mode (priority 2), the COL output temperature, the average DHW temperature, and the temperature at the bottom of the SST are the monitoring variables. When the temperature in the DHWT achieved its set point, and the temperature in the COL is higher than the SST bottom temperature, the SH operation mode is activated. In this mode, pump P_1 and P_2 allow the heat transfer from the solar collector field to the SST through the HE_1. During the demand periods, P_3 impulse the hot water from the bottom of the SST to the SH network through HE_3. Downstream this heat exchanger, a natural gas boiler AUX_1 is installed to cover any failure of the solar system.

In addition to these two control strategies, the simultaneous SH and DHW operation mode (priority 3) is activated when both the previous two modes of control are satisfied. Beside these control operation modes, control loops are developed to regulate the Y-type values in the SH and DHW distribution circuits in order to maintain the set-point temperature at the heating and DHW network.

III.3 Methodology framework

The proposed methodology framework for the sustainable assessment of the SHDS is outlined in Figure III-2. The first step in the framework is the simulation for the SDHS process through a commercial simulator (TRNSYS 18). Then defining the suitable decision variables range and their relative output, which reflect the thermal performance of the SDHS. Once the decision variables are set, MATLAB creates scenarios based on the decision variables range to cover the process feasibility and automatically launches TRNSYS in a parallel manner to simulate these scenarios. With computationally demanding processes, the machine learning approach based on ANN is utilized to alleviate the computationally effort during the optimization phase. Before the MOO stage, the ANN model is coupled with the Bayesian optimization approach to develop a robust ANN model-independent on its tuning parameters (Hyperparameter). To solve the MOO problem, a multi-objective genetic algorithm (MOGA) is introduced to quantify the economic and environmental benefits of the SHDS in the different community sizes, and it is coupled with the developed ANN model. Once the Pareto frontier is generated based on the objective functions, the

GSA is presented to illustrate the significant impacts of uncertainty on the economic and environmental indicators [41,50].

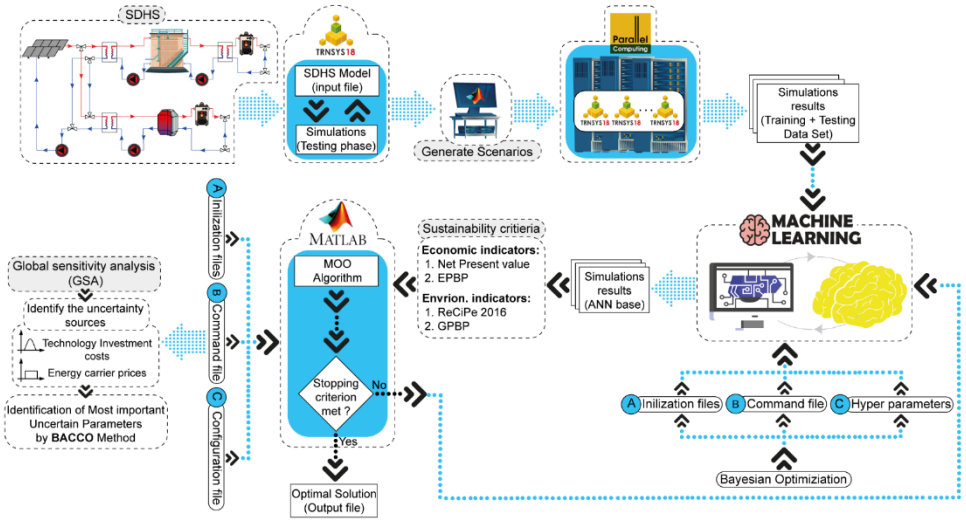

Figure III-2: Sustainable framework for the optimal design of SDHS

III.3.1 Energy system modelling

The developed SDHS simulation model is built based on TRNSYS18, following the models previously developed by Guadalfajara et al. [51] and Tulus et al. [36]. This software mainly solves the partial differential equations, mainly apply the mass and energy balances equations within the SDHS boundaries. The dynamic nature of TRNSYS simulation environmental assists in introducing the simulation of SHDS more realistically. Aligning with the simplicity idea in calculations, a typical year of operation based on hourly timescale is introduced and then extrapolated in order to show the performance of the system throughout its lifetime with assuming the same climatic conditions and demands over the years of operation.

A part of the methodology framework is to tackle the technical failure of the SDHS comprising the construction, sizing, and operation of its equipment when introduced in various community sizes. Thus, being the solar collector, storages tanks are the key decision variables in designing an optimal SDHS [36], 15 decision variables including the orientation of solar collectors and the construction and sizing of the storage tanks are introduced in the optimization problem. For each simulation, 19 aggregated outputs are considered; these outputs comprise the energy production in the solar field, the energy stored in the storage tanks, the supplied energy by the auxiliary heaters, and the energy consumption by the pumps.

III.3.2 Robust ANN solution procedure

As stated in the introduction, some barriers limit the using of the ANN. Aligning with these drawbacks, this section explains the approach carried out in this study to develop a robust metamodel that eliminates them. The proposed methodology starts with the data generation (known as sampling) in which a vast range of training points are introduced to testify the metamodels accuracy converges and its time consumption. The Bayesian optimization approach is then combined with the sensitivity analysis to test the variety of the metamodel settings. Once the metamodel settings are nominated, the ANN model is developed with testing the balance between the model accuracy and the time consumption.

III.3.2.1 General Background on ANN modeling

The ANN is a supervised learning technique which covers a board range of models and learning algorithm. This study is mainly focussed on the feedforward neural network with multi hidden layers. Generally, the neural network consists of several hidden layers where each layer consists of several neurons; these neurons propagate information using weighted connections and transfer functions. The number of neurons in the input and output layers is equal to the number of the model input and output, respectively. Since the number of hidden layers and their relative neurons selection increase the overfitting risk, the hidden layers are interpreted based on an optimization algorithm that can be used to interpret other ANN settings [52].

In addition to the hidden layers and its relative neurons, the ANN architecture is also defined through other settings comprising the training/learning method, the activation functions, momentum mean, and the learning rate. Thus, the neural network is based on investigating the optimal setting for the hyperparameters number of the hidden layers, number of neurons in the hidden layer, training function, activation function-hidden layer, activation function- output layer, learning rate, and momentum mean.

III.3.2.2 Data generation and preparation

The process of building the training data for the surrogate model is known as sampling. The performance of the surrogate mainly depends on the quality of the sampling strategy as well as its size. In order to maintain the quality of the surrogate model without high computational cost, the sampling strategy represents significant importance [53].

The sampling strategy can rely on the grid pattern where this sampling method is derived from the design of experiment literature (factorial, Box-Behnken designs), space-filling design (Latin hypercube design, low-discrepancy sequences), and sequential sampling approach where the samples are generated adaptively where information is required [54]. In this context, the low-discrepancy sequences (Sobol's LP_{τ}) are utilized to create the training data since it is assumed to cover the space

design domain more efficiently in comparison to the Latin hypercube design [55]. The generation process starts with generating N samples in an n-dimensional unit where n represents the number of decision variables. Then the generated points turned into n×N input matrix where each row represents a set of decision variables to obtain the thermal performance of SDHS. The data generation process is built automatically in MATLAB and connected to TRNSYS to perform the required simulations in a parallel manner.

The appropriate sampling size mainly depends on the size of decision variables along with the computational budget. At some points, increasing the size of samples has a negative effect on improving the performance of the surrogate model with an excessive computational cost. Thus, aligning with building a surrogate model independently on the sampling size at a suitable computational cost, the metamodel is trained using different sample sizes in a range between 32 – 8192, which is within our acceptable computational limits (10,000 simulations). In the process of the ANN model setting selection, the k-fold cross-validation process is presented in order to avoid the overfitting issue [56]. This process involves splitting the generated samples into k subsets, where each subset includes an equal set of samples. The ANN model is trained on k-1 subsets and tested on the remain k subset. The process is repeated k times. Thus, each k subset will be used as a testing set.

III.3.2.3 Assessing Model Setting and convergence

The robust surrogate model building process has been divided into two main steps; the model setting selection and the model convergence testing, as shown in Table III-1. In the first step, model settings and its relative hyperparameters through using the Bayesian optimization approach at different training set sizes are emphasized. The optimization approach is combined with the sensitivity analysis to estimate the importance of the hyperparameters. In the second step, the convergence of the ANN model is assessed through testing the develop a surrogate model based on the optimal model settings under a wide range of training set to define the optimal sample size.

Table III-1.Building the Robust ANN model steps

Investigation	Model settings	Convergence
Training sets	64, 256, 1024	32, 64, 128, 256, 512, 1024, 2048, 4096, 8192
Purpose	To find suitable model settings	To assess model accuracy in balance with its computing time

Corresponding to the importance of tuning the ANN model hyperparameters in determining the model accuracy, different approaches, including the naive gird search and random search can be utilized in this context. However, these approaches exhaustively time-consuming; thus, limited decision variables can be investigated based on these methods [57]. In addition to these approaches, the optimization workflow can succeed in solving the drawbacks associated with the traditional methods. In this regard, a few generic optimization algorithms, including genetic and particle swarm algorithms, have been applied to optimize the metamodels hyperparameters [58,59]. However, these algorithms have dimensionality problems [60]. Among these approaches, the Bayesian optimization algorithm demonstrates better performance in several cases [61].

In our case, it is applied due to its beneficial advantage in solving computationally intensive cases since it can include binary, continuous, and discrete hyperparameters in the optimization problem [62]. Moreover, the Bayesian hyperparameter optimization algorithm is capable of handling the optimization problem in parallel computing manner using a cluster of computers [63]. This approach aims to constructs a probabilistic model using the Gaussian process, which is updated with each new observation and has a definitive goal of improving the metamodel accuracy. Table III-2 lists the hyperparameters settings options in the two stages of the development of the Robust ANN model in comparison to the default setting of the ANN.

Table III-2. The model setting in the two stages of developing a Robust ANN model

Model setting (hyperparameter)	Model settings	Convergence	Default
1. Number of the hidden layers	1:10	3	1
2. Number of neurons	1:50	14	10
3. Training function	a. Levenberg Marquardt b. Bayesian regularization c. Scaled conjugate gradient d. Resilient backpropagation	b	a
4. Activation function, hidden layer	i. logsig, ii. tansig, iii. purelin	i	ii
5. Activation function, output layer	i. satlin, ii. logsig, iii. tansig, iv. purelin	iv	iv
6. Learning rate	0.001:0.5	0.001	0.01
7. Momentum mean	0.001:1	0.004	0.9

In addition to the hypermeters tuning through using the Bayesian optimization algorithm. A sensitivity analysis based on screening design is attractive to eliminate irrelative hyperparameters from the second stage (B. Convergence). Often fractional factorial designs with resolution III or IV are introduced in the early stages of screening designs. However, these design types required a broad set of runs and have no capability of capturing the quadratic terms [64]. Thus, using the definitive screening design proposes efficient properties in minimizing the number of the required runs, and estimating the quadratic terms. The evaluation of the definitive screening design is conducted through ANOVA, where a Pareto chart is constructed to rank the significant hyperparameters [65].

When the least significant hyperparameters are identified through the definitive screening design, an interactive parallel coordinate plot is presented. This plot is then combined with histograms for each hypermeter showing its setting distribution in providing an accurate metamodel.

In order to characterize the performance of the developed metamodels, a group of metamodel performance metric are utilized to evaluate its accuracy. These metrics include three standard evaluation measures; (i) adjusted R-squared ($R^2{-}adj$), (ii) Coefficient of Variation ($C.V$), and (iii) Symmetric mean absolute percentage error ($SMAPE$), their formulas are expressed in .

$$R^2 = 1 - \frac{\sum_{i=1}^{n}\left(y_{predict,i} - y_{data,i}\right)^2}{\sum_{i=1}^{n}\left(y_{data,i} - \overline{y}_{data}\right)^2} \quad \text{Eq. III-1}$$

$$Adjusted - R^2 = 1 - \frac{(1-R^2)(n-1)}{n-k-1} \quad \text{Eq. III-2}$$

$$CV(\%) = \sqrt{\frac{\sum_{i=1}^{n}\left(y_{predict,i} - y_{data,i}\right)^2}{\overline{y}_{data}}} \times 100 \quad \text{Eq. III-3}$$

$$SMAPE(\%) = \frac{1}{n}\sum_{t=1}^{n}\frac{\left|y_{data} - y_{predict}\right|}{\left|y_{predict}\right| + \left|y_{data}\right|/2} \times 100 \quad \text{Eq. III-4}$$

where $y_{predict,i}$ is the predicted value at time point i, $y_{data,i}$ is the actual data at time point i, n is the sample size, and k is the number of regressors. Following the proposed standard accuracy evaluators. The CV is used as an objective function in the model setting stage for two main reasons. First, it´s recommended by ASHRAE for evaluating the energy systems. Second, it´s a normalized value, which can be more convenient for comparison purposes [66].

III.3.3 Sustainable assessment

The developed framework evaluates the proposed SHDS based on three main criteria comprise: the technical performance with details regarding the construction and operation of the equipment in the proposed plant, as well as the economic and environmental performance throughout the system lifetime.

III.3.3.1 Technical assessment

The technical analysis of the SHDS, coupled with sensible seasonal TES in the proposed framework, can be implemented in two main stages. The first stage examines the thermal performance of the sensible seasonal TES based on the storage dimension and its construction materials. While the second stage proposes several indicators to assess the overall performance of the SDHS.

Within the SST analysis, a large water cylindrical tank built over the ground and filled with water to serve as a seasonal storage unit in the SHDS is investigated. The SST constructed based on reinforced concrete and insulation from the top, side, and bottom based on various insulation material to reduce its heat loss to the environment. The SST characterization is evaluated based on the storage heat capacity and heat loss during its operation [67]. The energy provided by the fully stratified SST can be expressed, as shown in Eq. III-5:

$$Q_{SST} = \int_0^t \dot{m}_{SH} C_p \Delta T_{SST} \qquad \text{Eq. III-5}$$

where $\dot{m}_{SH}$ is the water mass flow rate in the SH distribution circuit, C_P is the specific heat, and ΔT_{SST} is a temperature difference between the extracted and replaced water from the storage tank to cover SH demand.

Another characterization key of the SST performance is the thermal heat losses, and it can be evaluated based on heat losses through the top (U_{Roof}), sideways (U_{Wall}) , and bottom of the storage (U_{Gnd}). The thermal heat loss through these surfaces depends on the construction material, the insulation material, the ground properties, and the height to diameter ratio [68], A set of a nominal performance metric is introduced to evaluate the technical performance of the solar field circuit, and SH and DHW distribution circuits. These indicators comprise the solar collector, SST, and DHWT efficiencies [69,70], and the annual solar fraction for both the SH and DHW distribution circuits [71,72]. These performance indicators are calculated using Eq.III-9 to Eq.III-13 as a function of the energy flow over the solar field and the distribution circuits:

$$\eta_{COL} = \frac{\int_0^t \dot{Q}_{Useful}}{\int_0^t \dot{Q}_{SOL}} \quad \text{Eq.III-6}$$

$$\eta_{SST} = 1 - \frac{\int_0^t \dot{Q}_{SST\ loss}}{\int_0^t \dot{Q}_{HE_1}} \quad \text{Eq.III-7}$$

$$\eta_{DHWT} = 1 - \frac{\int_0^t \dot{Q}_{DHW\ loss}}{\int_0^t \dot{Q}_{HE_3}} \quad \text{Eq.III-8}$$

$$S.F_{SH} = 1 - \frac{\int_0^t \dot{Q}_{AUX_1}}{Q_{SH\ load}} \quad \text{Eq.III-9}$$

$$S.F_{DHW} = 1 - \frac{\int_0^t \dot{Q}_{AUX_2}}{Q_{DHW\ load}} \quad \text{Eq.III-10}$$

where $\dot{Q}_{Useful}$ and $\dot{Q}_{SOL}$ are the useful energy produced and received by the solar collector field, respectively. $\dot{Q}_{SST\ loss}$ and $\dot{Q}_{DHW\ loss}$ represent the heat loss in the SST and DHWT, whereas the $\dot{Q}_{HE_1}$ and $\dot{Q}_{HE_3}$ are the heat transfer rate through the heat exchangers HE_1 and HE_3. Moreover, $\dot{Q}_{AUX_1}$ and $\dot{Q}_{AUX_2}$ states for the auxiliary energy rate provided by the natural gas boilers in the SH and DHW distribution circuits to cover the SH load ($Q_{SH\ load}$) and DHW load ($Q_{DHW\ load}$) demand when the solar system fails in reaching the set temperature point.

III.3.3.2 Economic assessment

In the current study, the economic performance of the system configuration is implemented through the life cycle costing (LCC) methodology [73,74].

The LCC approach is a valuable technique for assessing the economic performance of the energy system in terms of the initial investment cost combined with its operational and replacement cost throughout the system lifetime. The LCC approach assists the decision-makers in comprehensively interpreting the energy system's economic performance throughout its life cycle and subsequently avoiding extra expenses in the early stages of design even though additional investment cost is required [75].

The main principle of the LCC methodology is the future system value, where all system expenses throughout its lifetime are discounted to its present value. The total present value (NPC) can be estimated by considering the initial investment cost (C_C), the operational cost (C_O), and the replacement cost (C_R):

$$NPC = C_C + C_O + C_R \quad \text{Eq.III-11}$$

The initial investment cost states for the initial capital cost at the project starting point. It considers the equipment cost, installation, and transportation cost. In addition to any possible contingency expenses, and it can be expressed as follows:

$$C_C = (1 + \alpha_{CF}) \sum_k (PCE_k . FBM_k) \quad \text{Eq.III-12}$$

where PCE_k represents the initial capital cost of purchased unit k, FBM_k is the bare module factor, which states for the installation and transportation cost of unit k, and α_{CF} donates for the contingency factor.

PCE_k fetched the initial purchased cost from the base year (year A) to the year of installation (year B) based on the Chemical Engineering Plant Cost Index (CEPCI) using the following equation:

$$PEC_k = PEC_k^{yearA} \frac{CEPCI^{yearB}}{CEPCI^{yearA}} \quad \forall k \quad \text{Eq.III-13}$$

The initial purchased cost of unit k at year A can be estimated using Eq.III-14 to Eq.III-17):

$$PEC_k^{yearA} = \alpha_k CAP_k^{\beta_k} \quad \forall k = COL, DHW, AUX \quad \text{Eq.III-14}$$

$$PEC_k^{yearA} = CAP_k^{\beta_k} . 10^{[\alpha_k (log_{10} CAP_k)^{\beta_k}]} \quad \forall k = HE_1, HE_2, HE_3 \quad \text{Eq.III-15}$$

$$PEC_k^{yearA} = \alpha_k \, ln\left(\frac{CAP_k}{1000}\right) + \beta_k \quad \forall k = P_1, P_2, P_3, P_4 \quad \text{Eq.III-16}$$

$$PEC_k^{yearA} = Ins_{SST} + Con_{SST} \quad \forall k = SST \quad \text{Eq.III-17}$$

Where:

$$Ins_{SST} = \alpha_k CAP_k^{\beta_k} \quad \forall k = XPS, MW, FG \quad \text{Eq.III-17.1}$$

$$Con_{SST} = \alpha_k CAP_k^{\beta_k} \quad \forall k = NC, HPC \quad \text{Eq.III-17.2}$$

$$Con_{SST} = \alpha_k e^{\left(\frac{\beta_k}{10^5} CAP_k\right)} \quad \forall k = UHPC \quad \text{Eq.III-17.3}$$

where α_k and β_k are the equipment or material purchase cost parameters, CAP_k is the design variables of equipment k. The design variables are the solar collector field area (A_{COL}), the storage tank volume (V_{SST}, V_{DHW}), the SST insulation type (XPS, MW, FG) comprising extruded polystyrene, mineral wool, and foam glass gravel, respectively, the construction material type ($NC, HPC, UHPC$) comprising Normal concrete, high performance concrete, and ultra-high performance concrete,

respectively, the heat exchanger areas ($HE_1,\ HE_2,\ HE_3$), and the pumps discharge mass flow rates ($\dot{m}_1,\ \dot{m}_2,\ \dot{m}_3,\ \dot{m}_4$).

The operational cost states for the annual maintenance cost of different equipment, the electricity consumption by the centrifugal pumps, and energy consumption by the natural gas auxiliary heaters. It can be expressed as follows:

$$C_O = C_M PWF_M + C_P PWF_P + C_{AUX} PWF_{AUX} \quad \text{Eq.III-18}$$

where the C_M, C_P, and C_{AUX} donate for the annual maintenance cost, the recirculation pumps, and the auxiliary heater consumption cost. While PWF tends for the time value of the money with consideration for the inflation rate (i) and discount rate (d) throughout the proposed system lifetime.

The replacement cost counts for the depreciation associated with several equipment during the lifetime of the SDHS. This equipment is the solar collector field, the DHW storage tank, the heat exchangers, and the auxiliary heaters. The replacement cost can be calculated using Eq.Eq.III-19) with consideration for the equipment present value:

$$C_R = PVF_n \sum_k (PEC_k . FMB_k) \quad \text{Eq.III-19}$$

where PVF_n is the present value factor of future cash flow at year n.

The economic viability of the SDHS can be specified as well based on the economic payback period ($EPBP$) [76]. It is widely used for evaluating energy system performance throughout its lifetime, and it´s usually expressed in years. The shorter the payback period, the more favourably a project is ensured. The computation of the ($EPBP$) can be obtained by dividing the future system value (NPC) by the yearly cost saving for using the SDHS as follows:

$$EPBP = \frac{NPC}{Annual\ cost\ saving} \quad \text{Eq.III-20}$$

III.3.3.3 Environmental assessment

In addition to the LCC approach for assessing the economic performance of the SHDS. The system environmental impact is evaluated using a life cycle assessment approach (LCA) [77]. This approach empowers a comprehensive analysis of the system components during its production as well as their operation and disposal based on the “cradle to grave” concept [78]. The LCA, as standardized in the ISO

14040 series [79–81] comprises several phases that trail a specific sequence; the goal and the scope definition, life cycle inventory, and impact assessment.

The LCA conducted within this study proposes the goal and scope stage for defining the system boundary and its functional unit. In this context, the functional unit was defined as the annual heating demand for the SH and DHW over the system time horizon. The SDHS boundary is drawn based on the “cradle to gate” concept since this study focus on the existing district heating with excluding the disposal phase (end of life). This is a common practice in the LCA approach as the disposal phase is negligible compared to the production and use phases. Moreover, the recycling phase is insignificant as well due to its advance and difficulty in prediction [33].

In the life cycle inventory and impact assessment stage, based on several databases, the material input, output, and their relative energy consumption are compiled during the construction and operation of the plant. In the current study, the impact of equipment manufacturing, as well as the utility energy consumption (natural gas by electricity) by the SHDS, are considered throughout the whole lifetime. Furthermore, the material transportation to the site as well as the plant components impact during its operation is also considered. These impact data are retrieved from the Ecoinvent 3.5 database [82].

Afterwards, the inventory data are weighted and translated into impact categories. These damages comprise; the damage to human health, the damage to the ecological system, and resources damage. In this work, the ReCiPe 2016 framework is promoted to evaluate different environmental categories based on the aggregated endpoint indicator metric (RCP) rather than using the mid-point indicators, which would be misleading in interpreting the overall SDHS environmental performance with different sized systems. The RCP can be expressed as follows:

$$RCP = \sum_{d} \delta_d \varepsilon_f DAM_d \qquad \forall d \qquad \text{Eq.III-21}$$

where DAM_d represents the endpoint of the damage category d, and δ_d, ε_d are the specific normalization and weighting factors. The normalized factors are specified based on the damage to the European land uses, and their relative material extractions [83]. On the other hand, the weighting factors are estimated based on the ReCiPe 2016 recommendation [38].

In addition to the LCA indicator, the greenhouse gas payback period ($GPBP$) is used to measure the system sustainability of the system [84]. Even though the SDHS is almost a free greenhouse gas emissions during its operation, the environmental damage of such this system is generated during the production and disposal processes [85]. The ($GPBP$) is defined as the environmental impact reduction potential as a result of the SDHS installation, and it can be expressed as follows:

$$GPBP = \frac{RCP}{Annual\ RCP\ saving} \qquad \text{Eq.III-22}$$

III.3.4 Optimization problem

This stage focusses on solving the computational obstacle associated with heuristics optimization models through using the developed robust ANN model in a MOO problem. Moreover, it tends to trace the technical failure of the SDHS through expanding its decision variables by presenting the SST geometry and construction design parameters as well in an optimization framework. Therefore, the energy performance is optimized to cooperate with the economic and environmental system requirements using the MOO framework to deal with the multi-objective conflict nature. Lastly, the community size effect on the performance of the SDHS was examined in separate optimization problems.

In the solar district heating system, the formulation of an optimization problem always deals with the conflicting nature associated with such these energy systems. Therefore, researches are often concern about the technical performance aligning with its economic profiles [23,35]. In this study, we add more real-world nature objective by considering the environmental impact in the problem formulation. Therefore, the current study emphasis on optimizing the LCC of the SHDS presented by the total plant cost (NPC) simultaneously with the LCA presented the eco-points (RCP) to satisfy the technical requirement, and it is given as:

$$\min \{f_1(x), f_2(x)\}$$

$$s.t.\ h(x) = 0$$
$$g(x) \geq 0$$

$$lb_i \leq x_i \leq ub_i \qquad i \in \{1, \dots, 15\} \qquad \text{Eq.III-23}$$

where f_1 is the plant net present value (NPC) and f_2 is the ReCiPe 2016 aggregated impact factor (RCP), h donates for the equality constraints, which corresponding to the mass and energy balance equation solved implicitly in TRNSYS in the first stage. While g donates for the inequality constraints, which correspond to the correct technical performance of SDHS. These constraints must maintain the annual solar collector efficiency above 60%, whereas SH annual solar fraction and SST efficiency should be maintained above 50% based on Bauer et al.[22] and Solites [86] recommendations.

The optimized solution in the multi-objective problem provides a set of non-dominated solutions (Pareto frontier points), which represent optimal trade-off solutions between the economic and environmental objectives that satisfy the technical performance constraints. The extreme points in the Pareto frontier called the anchor points, and it

corresponds to the minimum economic and environmental impact solutions. In the MOO problems using the classical methods based on point by point approach (weighted sum or the ε-constraint method) [87], the optimization outcome represents a single optimized solution based on a particular search direction, which often delivers local information (suboptimal solution). Furthermore, due to the dependency of the optimal solutions on the initial chosen solution, these approaches fail in solving different optimization problems type [88]. Aligning with these limitations, an evolutionary approach based on a technique called Pareto-ranking [89] is utilized to estimate approximate Pareto-optimal solutions based on the (NPC) and (RCP) objective functions.

Table III-3. Decision variables for the SHDS categorized by circuit name

Circuit name	Decision variable	Unit	Uniform	Discrete	Ref.
Solar field circuit	A_{COL}	m^2/MWh/a	0.1:2		[38,90]
	β_{COL}	^{o}	20:70		[48]
	N_{COL}	-	1:5		
SH distribution circuit	V_{SST}	m^3/MWh/a	1:20		[22,91]
	HDR	m/m	0.3:1.5		[68,92]
	d_{Roof}	m	0.2:0.7		
	d_{Wall}	m	0.2:0.7		[93,94]
	d_{Gnd}	M	0.2:0.7		
	λ_{con}	W/m. K	-	NC =1.5 W/m. K HPC =2.5 W/m. K $UHPC$ =1.6 W/m. K	[95,96]
	λ_{ins}	W/m. K	-	XPS =0.032 W/m. K MW =0.04 W/m. K FG =0.06 W/m. K	[97,98]
	$\lambda_{ins\ gnd}$	W/m. K	-	XPS =0.032 W/m. K MW =0.04 W/m. K FG =0.06 W/m. K	
	FC_{AUX1}	%	0.1:1		
DHW distribution circuit	V_{DHWT}	m^3/MWh/a	0.05:0.25		[38,69]
	HDR_{DHWT}	m/m	1:2		[93,99]
	FC_{AUX2}	%	0.1:1		

The SDHS performance is examined in four different community sizes (10, 25, 50, and 100) based on 15 decision variables; these decision variables describe various components in the SDHS, including its sizing as well its relative orientation and

construction. These variables can be categorized based on the circuit name. In the solar field circuit, (i) COL area (A_{COL}), (ii) COL inclination angle (β_{COL}), and (iii) number of COL in series (N_{COL}) are considered. In the SH distribution circuit, (i) SST volume (V_{SST}), (ii) SST aspect ratio (HDR), (iii) SST construction material (λ_{con}), (iv) SST roof, wall, and ground insulation material type (λ_{ins}), (v) ground insulation material type ($\lambda_{ins\ gnd}$), (vi) roof, wall, and ground insulation material thickness (T_{Roof}), (T_{Wall}), and (T_{Gnd}), respectively, and (vii) AUX_1 fraction (FC_{AUX1}) are considered. Finally, in the DHW distribution circuit, (i) DHWT volume (V_{DHWT}), (ii) DHWT aspect ratio (HDR_{DHW}), and (iii) AUX_2 fraction (FC_{AUX2}) are considered. A wide range of these decision variables is estimated for simulation and optimization processes based on real implemented projects in EU and recommendation for various articles, as shown in Table III-3. On the other hand, the sizing of other equipment units in the SDHS is determined through mathematical equations that relate them to the decision variables.

In the current framework, the Multi-Objective Genetic Algorithm (MOGA) is introduced, as it can be coupled easily with a simulator, Blackbox models or even models based on algebraic equations. The MOGA is particularly able to handle a set of points simultaneously, which would empower the user to obtain several Pareto frontiers in a single run [30]. An elitist genetic algorithm (a variant of NSGA-II [100]) is nominated. This algorithm can handle a multi-objective problem in a parallel computing manner. Moreover, it can handle discrete and continues variables, along with equality and inequality constraints [101]. Following the evolutionary approach, the solutions are iteratively modified according to the internal ranking of each population. These populations are generated based on the mutation and crossover functions [30]. An automated simulation-based optimization model is performed by combining the generated robust metamodel based on ANN with the NSGA-II algorithm. The MOGA uses the NSGA-II algorithm with 1000 initial population due for 300 generations based on Alajmi et al. [102] recommendation.

III.3.5 Sensitivity analysis

The final step in the methodology framework is to perform a sensitivity analysis, which is a common approach that offers an insight into the important model parameters. Given the drawbacks in the LSA, the GSA approach based on Bayesian analysis of computer code outputs (BACCO) [103] is employed. The main advantage of this approach is its ability to cover a wide range of uncertain parameters and interactions with consideration for their relative distributions. Furthermore, it offers a substantial computational improvement compared to using expensive GSA based on Monte Carlo simulations [104].

The BACCO method entails two main key stages. In the first step, a statistical representative model (i.e., an emulator) is built based on a set of training data points derived from the developed simulation-based optimization model. The training data

are ideally cover the feasible design domain using a multidimensional space-filling algorithm (Latin hypercube design). Prior to the second stage, the cross-validation approach is applied to automaticity to estimate the emulator accuracy. The second stage uses the constructed emulator (which is efficient in covering a multidimensional design domain in low computational expenses in comparison to the original optimized model) in quantifying the importance of parameters in interest [105]. The performed sensitivity analysis is presented in terms of the percentage variance contribution of each input with respect to the economic (NPC) indicator and environmental indictor (RCP).

III.4 Case study

To better illustrate the capabilities of the proposed framework, the methodology procedure is applied to a SDHS located in Madrid (Spain) to meet the heating demand of different sized neighbourhood community (10, 25, 50, and 100 buildings). Each building comprises 28 apartments with 90 m^2 of useful area [106] per apartment and equipped with a radiant underfloor heating system and a domestic hot water system to meet the SH and DHW demand at 50°C and 60°C, respectively. The SDHS model validation and heating demand comparison were implemented in comparison to Guadalfajara et al. [107] and Tulus et al. [38].

For comparison purposes, a base case using only a natural gas boiler is considered. This conventional system is able to fulfil the SH and DHW demand alone independently from the SDHS.

III.4.1 SDHS model specification

The solar collector field in the SDHS consists of flat-plate collectors (type ARCON HT-SA 28/10) designed for large applications [36]. These collectors are connected in series and oriented toward the south. A 33% mixture of glycol in water (C_p= 3.8 kJ/kg·ºC at 50ºC) is initiative as a working fluid in the solar field circuit with a nominal recirculation flow rate of 20 kg/h·m^2. On the other hand, the SH and DHW distribution circuits are operated with water.

The SST is a partially buried tank with a cylindrical section. Since the tank construction is a part of the optimization problem, the seasonal storage design parameters are initialized based on the constructed project in Friedrichshafen (Germany) [96], where normal concrete with a thickness of 0.5 m was selected as a construction material. For the storage insulation, the mineral wool was placed outside the concrete with a thickness of 0.3 and 0.2 m for the roof, wall, and ground, respectively. On the other hand, the DHW is a relatively small tank compared to the SST since it is utilized for only daily services, the DHWT constructed with an overall heat coefficient of 0.3 W/(m^2·K) [107]. To cover any shortage of the solar system,

natural gas boilers with efficiency 93% are utilized as auxiliary heaters for both SH and DHW distribution circuits.

To reproduce the transient behaviour associated with the simulation process, all the TRNSYS simulations were implemented with a time step of 15 min [108]. The system assessment was performed over three years of simulation (28,260 h), and the results after the third year are extrapolated over the SDHS lifetime. The three years of simulation idea is due to the homogeneous assumption inside the SST where SST temperature is equal to 30°C at the beginning of the first year of simulation. Therefore, after two years of simulations, this initial assumption is eliminated, and the change in temperature becomes insignificant in the following years [23]. According to the United Nations Environment Programme [109], the lifetime of the SDHS is 40 years, where several equipment include the solar collectors, heat exchanger DHWT and auxiliary heaters need to be replaced after only 20 years of operation.

III.4.2 Climate and demand profiles

The climate data for Madrid is obtained from the EnergyPlus database [110]. These data include the incident solar radiation, ambient temperature, relative humidity, and other relative information. The monthly average ambient temperature and its relative incident solar radiation per solar collector area are shown in *Figure* III-3.

The space heating demand is established based on the implemented work by Guadalfajara [107] in order to develop a 7-story building that meets the minimum requirement of the Spanish regulations for residential buildings. A 3D building model is developed using SketchUp [111] and imported into TRNSYS, where the occupancy densities and building materials comprising its windows and insulations are defined. By simulating the developed building in TRNSYS, the annual space heating demand profile is generated based on an hourly timescale. The generated SH demand is then extrapolated for the different urban community sizes, and the monthly SH demand is shown in *Figure* III-3*.*

On the other hand, to generate the DHW demand for the investigated residential buildings, Tulus et al. [38] was followed, where the DHW demand is based on three main factors: (i) the daily water consumption per person, (ii) monthly water temperature from the public distribution network, and (iii) the number of occupations per household. These data are imported into computer software, DHWcalc [112]. This software can generate a realistic hourly DHW consumption profiles with consideration for main controlling factors, as shown in Figure III-3.

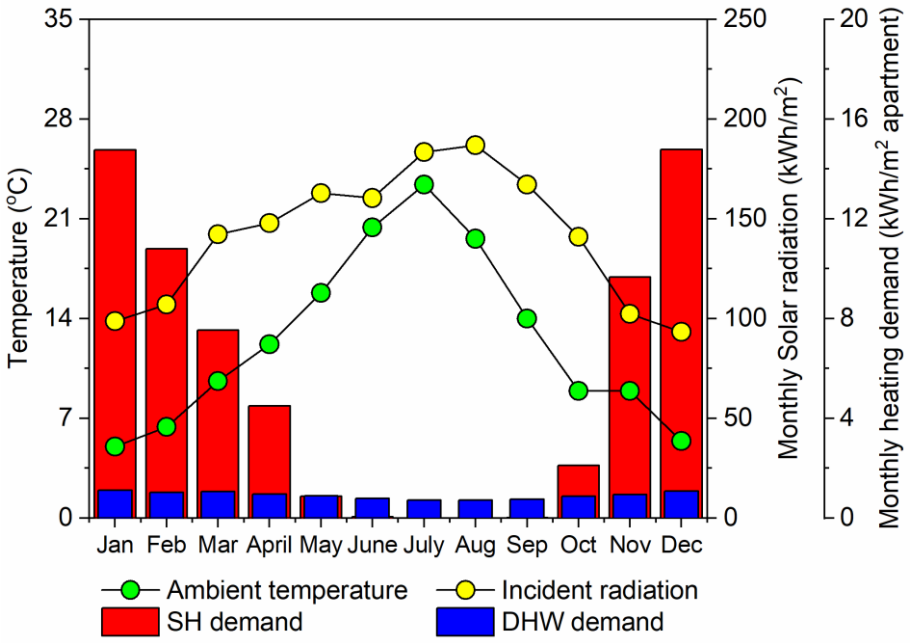

Figure III-3: The climate conditions in Madrid and energy demand per apartment

III.4.3 Economic and environmental input data

The parameters for the initial investment cost are outlined in Table III-4. Following Tulus et al. [36], the maintenance cost is estimated to be 1.5% of the initial purchase cost of the equipment. The prices of natural gas and electricity are 0.0526 and 0.1873 Euro/kWh, respectively, based on the EUROSTAT database [113]. Moreover, the inflation rate associated with natural gas and electricity is 5.9% and 5%, respectively [38]. According to Braungardt et al. [114], the inflation rate associated with the proposed system throughout its lifetime is set to be 2.3%, with a discount rate of 3.5%.

Table III-4. The economic parameters of SDHS equipment

Unit	*Options*	α_k	β_k	CAP_k	Range	Base year	*Ref.*	FBM_k
Solar collector		974.2	0.8330	Aperture area (m^2)	4,000-15,000 m^2	2007	[115]	1.00
DHWT		3955	0.6500	Volume (m^3)	1-100,000 m^3	2007	[116]	1.00
Auxiliary heater		225.0	0.7460	Duty (kW)	600-10,000 kW	2001	[36]	2.10
Heat exchanger		3.133	0.3310	Exchange area (m^2)	10-1000 m^2	2001	[36]	3.29
Pump (P_1, P_2)		389.0	283.2	Mass flow rate (kg/h)	15,000-100,000 kg/h	2009	[117]	3.24
Pump (P_3, P_4)		389.0	717.0	Mass flow rate (kg/h)	15,000-100,000 kg/h	2009	[117]	3.24
SST insulation	XPS	561.09	0.397	Material thickness (m)	0.05-0.8	2017	[118]	1.00
	MW	1902.7	0.942	Material thickness (m)	0.05-0.8	2018	[119]	1.00
	FG	311.41	0.968	Material thickness (m)	0.05-0.8	2014	[120]	1.00
STT construction	NC	4178.1	-0.394	Volume (m^3)	1-100,000 m^3	2000		1.00
	HPC	2575	-0.363	Volume (m^3)	1-100,000 m^3	2004	[97]	1.00
	$UHPC$	90.83	-3	Volume (m^3)	1-100,000 m^3	2004		1.00

The LCA data were retrieved from the Ecoinvent database [82]. This database comprises the damage categories caused by the SDHS main equipment and their relative utilities based on the ReCiPe 2016 methodology.

Table III-5. Specific ReCiPe 2016 aggregated impact factor for the main SDHS equipment and utilities, in ReCiPe points (Pt) per characteristic dimension [82]

Unit	Option	Impact factor (ReCiPe 2016)
Solar collector		32.5Pt/m^2
DHWT		173.1 Pt/m^3
Auxiliary boiler		$1.57 \cdot 10^3$ Pt/kW
Heat exchanger		2.515 Pt/m^2
Pump		62.8 Pt/kW
SST insulation	XPS	0.773 Pt/kg
	MW	0.0016 Pt/kg
	FG	0.266 Pt/kg
SST construction	NC	0.008 Pt/kg
	HPC	0.002 Pt/kg
	$UHPC$	0.0206 Pt/kg
Natural gas		0.0245 Pt/kWh
Electricity		0.0380 Pt/kWh

III.4.4 Uncertainty characteristics

A correct quantification of the uncertainty is vital to obtain reliable results of the SHDS model. This analysis would support decision-makers in the early design stages. The probabilistic approach, which treats the uncertain parameters as a random variable, is the most common approach to quantify the uncertainty associated with parameters [121]. In the current study, we focus on the economic parameters and their corresponding uncertainty. In total, 13 individual uncertain economic parameters are identified in this study. These parameters are classified into three main categories:

- Investment cost: The solar collector field, the storage, and their relative utilities in the SDHS are considered uncertain since this equipment is a market-driven. Thus, the prices in the early stages of design might differ from the final investment cost [122].
- Economic factors: Aligning with the changes in the energy policies for accelerating the transformation toward clean energies, the economic parameters such as annual inflation rate, market discount, and maintenance factor can change during the long lifetime of SDHS.
- Energy carrier: Normally, the prices of natural gas and electricity are deterministic parameters. However, throughout the system lifetime, the SDHS energy carriers might change due to the market or the energy policies [123].

A summary of the uncertain economic parameters and their characteristic distribution is shown in Table III-6.

Table III-6. Summary of uncertain parameters in the SHDS model and their characterization approaches (The parameter μ (mean) for a normal distribution (N) and (U) refers to the discrete non-probabilistic scenario)

Uncertain parameter	Parameter description	Probability distribution	Ref.
$C_{C_{COL}}$	Investment cost of the solar collector	$N(\mu, 0.07\mu)$	[41]
$C_{C_{SST}}$	Investment cost of the SST	$N(\mu, 0.07\mu)$	[41]
$C_{C_{DHWT}}$	Investment cost of the DHWT	$N(\mu, 0.07\mu)$	[41]
$C_{C_{H.E}}$	Investment cost of the heat exchanger	$N(\mu, 0.07\mu)$	[41]
C_{C_P}	Investment cost of the pumps	$N(\mu, 0.07\mu)$	[41]
C_{C_f}	Investment cost of the gas boiler	$N(\mu, 0.07\mu)$	[41]
i_f	Annual natural gas inflation rate	$N(\mu, 0.166\mu)$	[122]
i_e	Annual electricity inflation rate	$N(\mu, 0.166\mu)$	[122]
i	Annual inflation rate	$N(\mu, 0.166\mu)$	[122]
d	Discount rate	$N(\mu, 0.137\mu)$	[124]
FBM	Maintenance factor	$D[1\%, 1.5\%, 2\%]$	[125]
c_f	Natural gas cost rate	$N(\mu, 0.166\mu)$	[124]
c_e	Electricity cost rate	$N(\mu, 0.166\mu)$	[124]

III.5 Results and discussion

In the current study, the results are divided into three main parts. The first part offers a deep analysis to build a robust ANN model by comprising the Bayesian optimization approach assisted sensitivity analysis. This part purposes an affordable metamodel that solves the computational obstacle associated with heuristics SDHS model built-in TRNSYS. Then the second part depicts the performance of SDHS in various urban community sizes in an optimization framework using the developed ANN model. This

framework intends to tackle the seasonal TES design parameters and its geometry effect to enhance the feasibility of the SDSH in various community sizes. Next, the SDHS optimal design is expressed adequately through including the uncertainty associated with several related economic parameters based on GSA to support the decision-making process.

III.5.1 Robust ANN results

III.5.1.1 Model setting

This is the first step (step A) of the two-step approach defined in Table III-1, which concerns to build a robust ANN model with an appropriate computational cost. In this stage, we evaluate the accuracy of the ANN model under three sample sizes (64, 256, 1024) using Bayesian optimization to produce an accurate metamodel independently on the model setting that can be extended to the large training set.

The solution of the Bayesian optimization is given by an interactive parallel coordinate plot to identify the suitable hyperparameters settings for the reduced number of configurations in step B (see Figure III-4). The top plot shows the total optimal Bayesian optimization results comprising 500 ANN model settings where each line represents one of these optimal solutions along with the achieved $C.V$ values. On the contrary, the bottom plot shows only the top 20% ranked optimal solutions based on $C.V$ criteria. The table below the interactive parallel coordinate plots shows the optimal metamodel setting that achieves the highest accuracy at step (A) training sets. In case of no agreement for selecting a certain optimal setting at different sample sizes, the histogram attached to each interactive parallel coordinate column is utilized to propose the most frequently setting at each hyperparameter. The hyperparameters, including the training function, number of layers, layer function, hidden function, and Momentum mean at each training set, have the same optimal setting at different training sets, whereas the number of neurons and learning rate change at each training set. As observed from the histogram, most of the optimal results setting for the learning rate are set in a range below 0.01. Thus, the learning rate is set to 0.001 for the convergence stage (step B) to sustain the training set converge. On the other hand, the number of neurons with the size of 3, 14, and 20 are set for the convergence stage (Step B) since its histogram is almost equally large for the training set size 64, 256, and 1024. A summary of the selected settings in the convergence stage (step B) is shown in the below table in Figure III-4, where the nominated settings are highlighted.

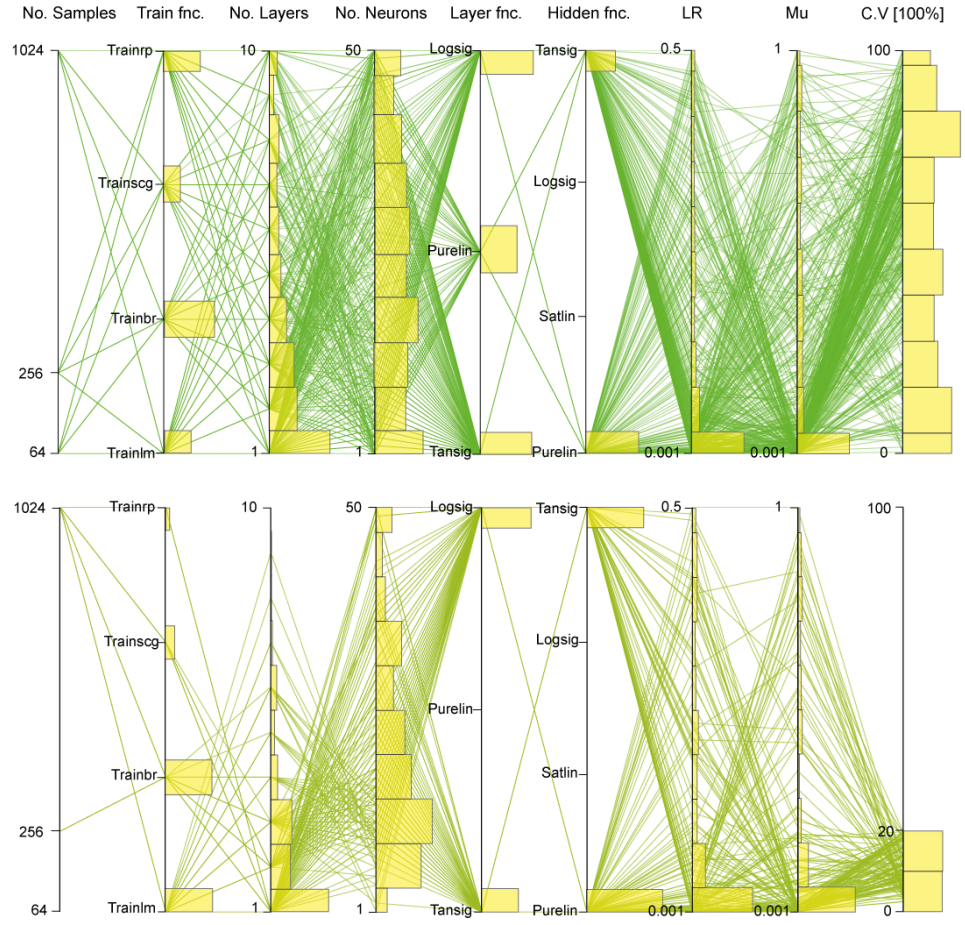

Optimal Hyperpar.	64	Trainbr	3	3	Logsig	Purelin	0.042	0.004	49.7%
	256	Trainbr	3	14	Logsig	Purelin	0.004	0.836	9.42%
	1024	Trainbr	3	20	Tansig	Purelin	0.001	0.004	2.49%

Figure III-4: Interactive parallel coordinate plots combined with histograms are utilized to identify the optimal hypermeters setting for the ANN model in step A. The top plot illustrates the total Bayesian optimal solutions without filtration, whereas the bottom plot shows the top 20% ranked ANN model settings. The table below shows the optimal hyperparameters that bounces the lowest $C.V$ value under different sample size where the selected setting for the convergence phase is highlighted

III.5.1.2 Sensitivity analysis

The next step is to perform the sensitivity analysis in order to investigate the relative importance of neurons sizes in step A and to eliminate the least influential variables

from the convergence step (step B), which include more training sets to develop an independent ANN model on the sample size. In the definitive screening design, we use three training sets with a size of 64, 256, and 1024 to rank the influence of hypermeters based on the $C.V$ criteria. The relative sensitivity of the ANN hyperparameters is shown in Figure III-5. The training set size, training function, and momentum mean are the most significant tuning parameter with a relative sensitivity of 28%, 26%, and 24%, respectively. These high impact parameters are followed by the number of neurons, which has a relative impact of 10% on the $C.V$. Thus, varying number of neurons may contribute to enhance in the performance of ANN model in step B. On the other hand, the activation functions, and the learning rate seems to be insignificant since they have only a contribution of 3% and 2%, respectively to the $C.V$ value. The results confirm the possibility of fixing the learning rate without affecting the surrogate model accuracy.

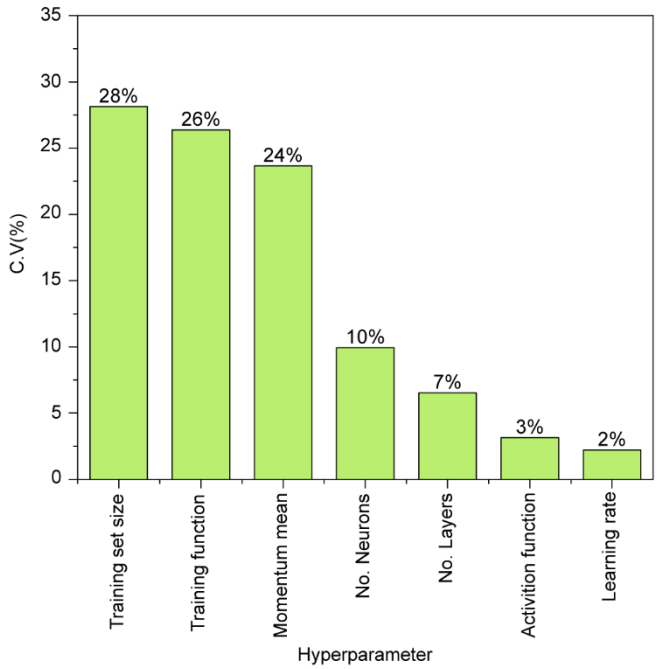

Figure III-5: The definitive screening design for the ANN hyperparameters

Following the sensitivity analysis results, a box plot (Figure III-6) is built to show the performance of the three-training sets (64, 256, and 1024) based on the $C.V$ rank under the optimal selected hyperparameters with considering for three neurons sizes comprising 3, 14, and 20 in comparison to the default settings. The box plot is characterized by the central mark, the upper and lower quartiles which correspond to the box edge. While the minimum and maximum optimal values are indicated at the whiskers. On the plot, the lined circles at each sample size show the results under

optimal settings at a different number of neurons, whereas the cross symbols represent the results at the default settings. In general, the default setting does not yield to build accurate ANN models that approve the importance of tuning the hyperparameters. Moreover, fixing the number of neurons at 14 provides the most accurate results with a $C.V$ value of 24.1% and 9.2% for the 256 and 1024 training set, respectively.

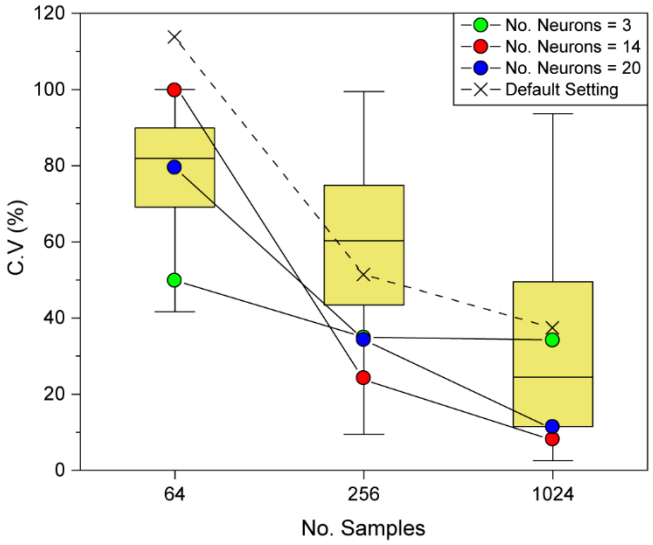

Figure III-6: Box plot for the output in step A including the ANN model performance under the optimal and default settings

III.5.1.3 Convergence with a variable training set

In step B, we test the performance of the selected optimal hyperparameters at various training sizes in order to choose the most accurate ANN model with consideration for its efficiency in terms of the computational cost, as shown in Figure III-7.In terms of convergence, as mentioned in the methodology section, three accuracy criteria comprising the $R^2{-}adj$, $C.V$ and $SMAPE$ are utilized to evaluate the performance of the ANN model. The results show that the $R^2{-}adj$ is a misleading criterion since most of the sample sizes excess 97%. Therefore, using $C.V$ and $SMAPE$ can be more efficient to measure the ANN model accuracy. Increasing the sample size has a clear tendency to improve the ANN model accuracy where the highest accurate value of 4.5% and 10% was indicated in a sample size of 2048 for the $C.V$ and $SMAPE$ criterion, respectively. In terms of the ANN model computational cost, an exponential behavior is indicated with increasing the sample size where the CPU time at 8192 sample size is $6{\times}10^4$ sec. Comprising the model accuracy with its efficiency simultaneously, the sample size 2048 provides the highest accuracy at an affordable

computational time of 8.9×10^3 sec using an Intel® Xeon® E5-2620 v4 2.10 GHz processor with 32.0 GB RAM.

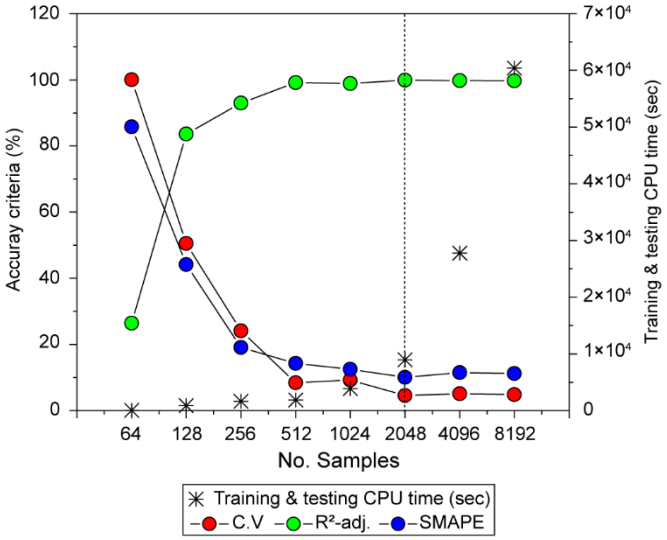

Figure III-7: Convergence of accuracy criteria at various training size with consideration for its relative computational cost

A breakdown for the ANN model performance in comparison to the rigorous model based on TRNSYS at a sample of the outputs is shown in Figure III-8.In general, an agreement between the rigorous and ANN model results is indicated for the 19 output where the R^2-adj is almost 99% for the whole outputs. To gain further confidence in the ANN model performance, the model accuracy is also presented through the $C.V$,which doesn't get below 5.3% for the model outputs.

The proposed robust surrogate model built based on the two-model steps comprising the sensitivity analysis offers a sufficient approach for the construction of fast metamodels to overcome the computational barrier related to design space exploration, design optimization, and sensitivity analysis of heuristics optimization models.

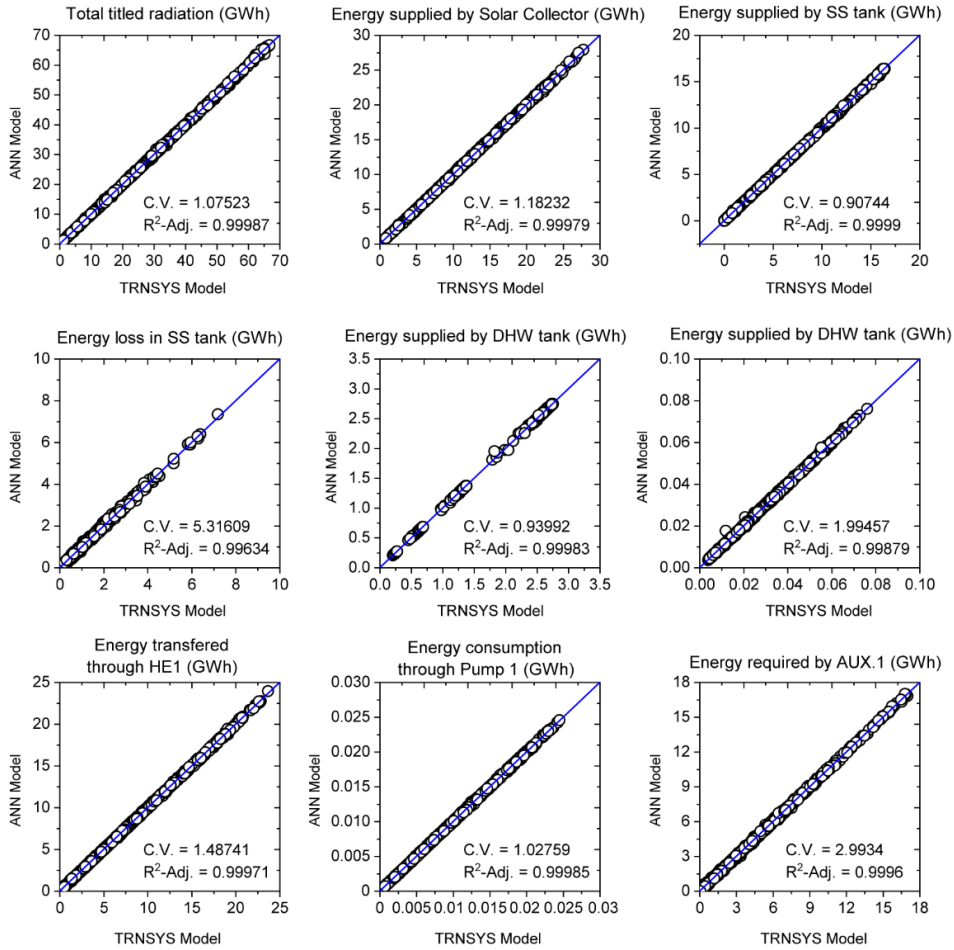

Figure III-8: Parity plots showing the performance sample of ANN model versus the TRNSYS model for the SDHS

III.5.2 Optimization results

Once a robust ANN model is built independently on its tuning parameters (Hyperparameter) with the consideration for the model accuracy simultaneously with its efficiency, the ANN model is coupled with a MOGA in order to investigate the capability of the develop simulation-optimization framework in tackling the technical performance of the SDHS in cooperate with its economic and environmental impact at various community sizes. The optimization problem has two main stages; the first stage is devoted to analyze the effect of expanding the decision variables through including the seasonal TES geometry and its construction design parameters in the optimization problem. While the second stage is dedicated to examine the community

size effect in the performance of the SDHS. In general, the optimization results are presented in five scenarios; these scenarios are:

- Scenario 1: No environmental damage limits (Min. cost).
- Scenario 2 to 4: 25%, 50%, and 75% damage reduction against the 1st scenario, respectively.
- Scenario 5: 100% of the environmental damage limits (Min. impact).

III.5.2.1 Influence of the SST design parameters (geometry & construction)

In this stage, the capability of the developed framework is tested through Madrid case study at a small community size of 10 buildings. The optimization problem is formulated under two main settings:

- Partial decision variables (PDV) – 8 decision variables: In this setting, only the equipment sizes are considered as decision variables in the optimization problem without consideration for the insulation material configuration and construction material of the SST. Thus, the construction of the SST is fixed based on the Friedrichshafen project [22], in which the NC has been used as the main construction material. While, the MW with a thickness of 0.3 m, 0.2m, and 0.2 m is utilized for the roof, wall, and ground, respectively.
- Full decision variables (FDV) – 15 decision variables: In this setting, the SST design variables are considered as well in formulating the optimization problem in order to investigate the impact of SST geometry and its construction in improving the SDHS optimal solutions.

Figure III-9 shows the optimal system cost in terms of NPC and its environmental impact in term of RCP under various scenarios. While the base case corresponds to the conventional system. A clear tradeoff between the proposed objective functions is indicated since the movement from scenario 1 to 5 at both PDV, and FDV settings increase the total cost while minimizing the environmental impact. Under the PDV setting, replacing the base case (Natural gas boiler) with SDHS can extensively minimize the environmental impact by 79.4% in scenario 1 (Min. cost). Using the latter value, the environmental impact for scenarios 2 to 5 improved by 80.8%, 83.3%, 85.1%, and 87%. On the other hand, the Pareto optimal solutions at small community size (10 buildings) under PDV setting couldn't provide a marginal economic benefit since only scenario 1 minimizes the economic cost by 22% whereas the economic cost increases by 10.2%, 35.5%, 49.9% and 61.7% for scenarios 2 to 5, respectively.

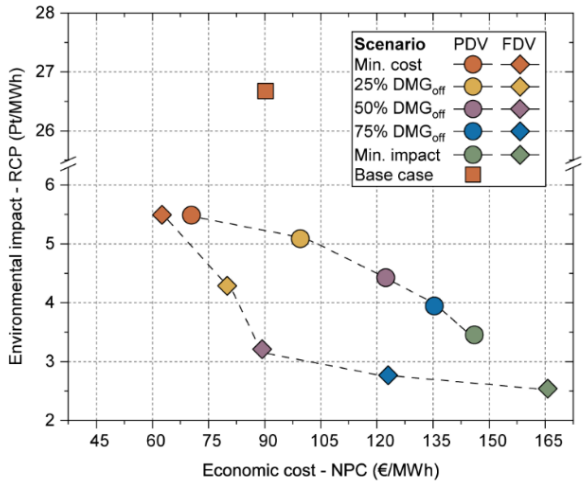

Figure III-9: Pareto sets for optimal SDHS solutions under PDV and FDV settings. These solutions cover the SH and DHW demand of 10 buildings located in Madrid at different scenarios in comparison to a conventional solution based on natural gas

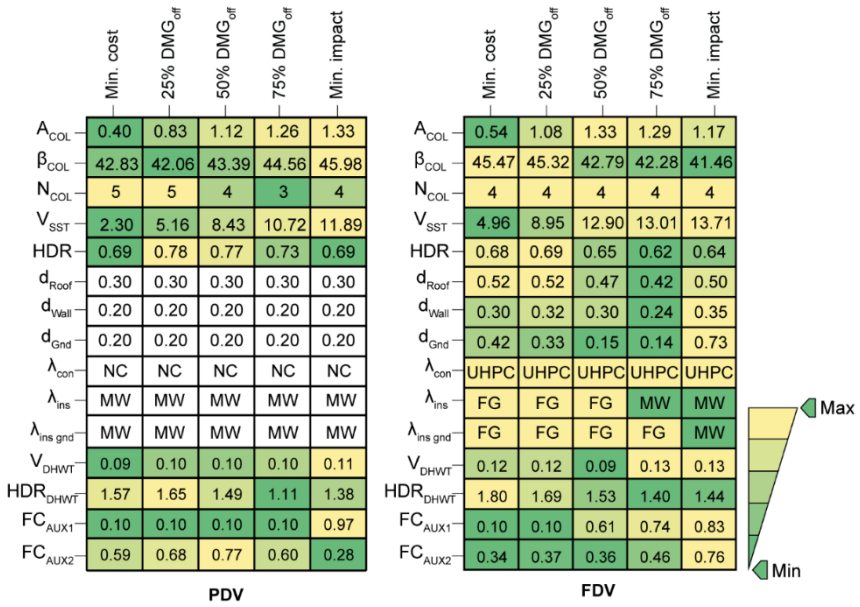

Figure III-10: Pareto optimal solutions of SDHS configuration to cover the demand of 10 buildings located in Madrid under PDV and FDV setting where the color map indicates the min and max value of each decision variable and the white boxes indicated the fixed parameters in the PDV optimization setting

Under the FDV setting, more enhancement is indicated in both objective functions in comparison to the PDV optimal Pareto solution due to including the SST design parameters in the optimization problem. In scenario 1, the NPC is equal to 62.5 €/MWh which is less than the PDV Min. cost solution by 11.1%, whereas the environmental impact (RCP) is 5.49 Pt/MWh which increases the RCP by 0.18% compared to the PDV setting. With increasing the environmental damage limits from scenario 2 to 4 under the FDV setting, the NPC decreases by 19.6%, 27%, and 9.4% whereas the Min. impact solution increase the total cost by 13.4% in comparison to the PDV setting. Furthermore, following scenario 1 under the FDV setting, the environmental impact is improved by 15.7%, 27.3%, 29.7%, and 26.4% for scenarios from 2 to 5. This improvement increases the competitivity of the SDHS compared to the conventional systems based on natural gas.

Following that, each Pareto optimal solution under PDV and FDV settings represents a specific configuration for the SDHS to cover the SH and DHW demand of a small urban community (10 buildings) located in Madrid. Figure III-10 shows the selected feature for each decision variable from scenario 1 to 5 under PDV and FDV settings. In both optimization settings, increasing the damage limitations causes an increment in the share of renewable energy equipment. Under the PDV setting, the solar collector share increases from 0.4 m^2/MWh/a at scenario 1 to 1.33 m^2/MWh/a at scenario 5.

Furthermore, the SST volume increases from 2.3 m^3/MWh/a for Min. cost solution to 11.9 m^3/MWh/a at the Min. impact solution. Including the SST design parameters in the optimization problem (FDV setting) shows a different configuration for SDHS where the solar collector share increases only from 0.54 m^2/MWh/a at scenario 1 to 1.17 m^2/MWh/a at scenario 5. While the SST volume share increases from 4.96 m^3/MWh/a at scenario 1 to 13.7 m^3/MWh/a at scenario 5 with an increment of 13.2% compared to the PDV optimization setting. Regarding the SST construction, the UHPC shows superiority over other construction materials at all scenarios under the FDV setting. Moreover, the foam glass gravel is utilized as an insulation material for all SST surfaces except the min impact solution, which uses mineral wool due to its lower environmental impact. For the insulation thickness, all Pareto optimal solutions under FDV settings increase the walls insulation thicknesses to be varying between 0.3 to 0.73 at all scenarios. Regarding the SST geometry, the HDR varies between 0.62 and 0.68 with a limited difference from the PDV settings. Moreover, the DHWT volume is almost constant for the proposed settings where its volume varies only between 0.09 and 0.13 m^3/MWh/a.

To facilitate a complete economic analysis of the SDHS, Figure III-11 shows a comprehensive breakdown for the cost contribution of each equipment in the SDHS throughout its operation lifetime under PDV and FDV optimization setting together with the base case solution. As shown in the figure, the contribution of the SDHS

initial capital cost under the PDV and FDV optimization settings is very high in comparison to the base case solution. This expansion is due to the deployment of solar energy equipment in the district heating system, which requires high investment cost. To be more specific, the solar collectors, heat exchangers, and SST have the main contribution to the initial capital cost. Under the PDV optimization setting, the movement from scenario 1 to 5 (Min cost to Min. impact optimal solution) expands the usage of solar collectors and SST due to its advantage in diminishing the contribution of using the auxiliary heater based on natural gas. In scenario 1, the solar collector and SST have contributions of 5.30% and 29.2%, respectively. These contributions are expanded to 6.94% and 39.7% in scenario 5. On the other hand, under the FDV optimization setting, with the opportunity to include the construction materials of the SST in the optimization framework, the initial investment cost can be relatively reduced compared to the PDV optimization Pareto solution where the SST contribution is only 22.5 % in the scenario 1 (Min. cost), and it expands to 44% in the scenario 5 (Min. impact). Furthermore, the solar collector has relatively more contribution under the FDV optimization setting, where the solar collector contribution expands from 7.60% in scenario 1 to 8.04% in scenario 4. However, this expansion bounds to only 5.50% in scenario 5 (Min. impact). In the replacement cost, the same behavior is noticed under the PDV and FDV optimization setting, where a significant contribution is observed due to the solar energy equipment in comparison to the base case solution. On the contrary, the operational cost has a predominant contribution of 98.2% in the base case solution due to usage of natural gas, these contribution shrinkages under the PDV and FDV optimization setting where the operational cost in scenario 1 represents around 39% in both optimization settings. With the increment in the environmental damage limits (scenario 2 to 5), less contribution to the operational expenses is noticed for both optimization settings where the operational cost in scenario 5 represents only 24% due to the reduction in using Natural gas. The reduction will be reflected in the environmental impact of the SDHS optimal solutions.

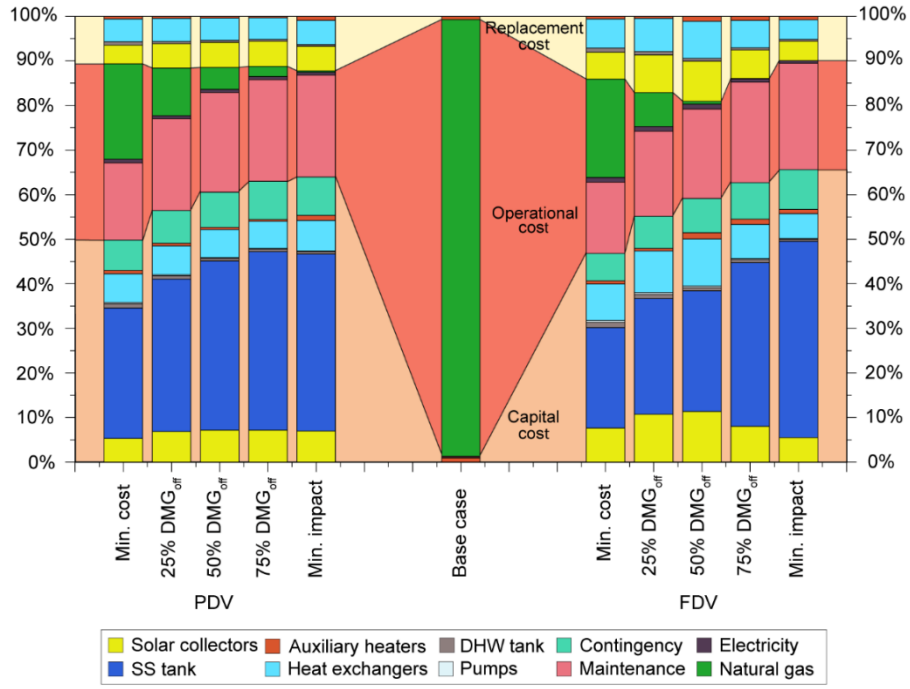

Figure III-11: Breakdown of the NPC including the shares of initial capital cost, operational cost, and replacement cost for Pareto optimal solutions under the PDV and FDV optimization settings at the 5 optimal scenarios in comparison to its relative base case. These solutions cover the SH and DHW demands of 10 residential building located in Madrid

In addition to the economic analysis, Figure III-12 offers a detailed analysis for each equipment in the SDHS based on the aggregated ReCiPe 2016 in comparison to the base case using natural gas. In this figure, the natural gas consumption in the base case represents almost 100% of the total impact. Under the PDV optimization setting, the SDHS optimal Pareto solutions are able to reduce the environmental impact up to 87.1%. This reduction value can increase up to 90.4% under the FDV setting. In scenario 1, the system relies heavily on natural gas, which corresponds to 81.9% and 74.9% of the environmental impact under the PDV and FDV optimization setting, respectively. From scenario 2 to 5, the natural gas impact diminutions progressively with the increment in the environmental limits. Along with the reduction in the natural gas impact share, a progressive rise is indicated in the renewable energy impact where the solar collectors and SST share the most contribution to the aggregated environmental impact especially with introducing the SST construction materials in the optimization problem (FDV optimization setting).

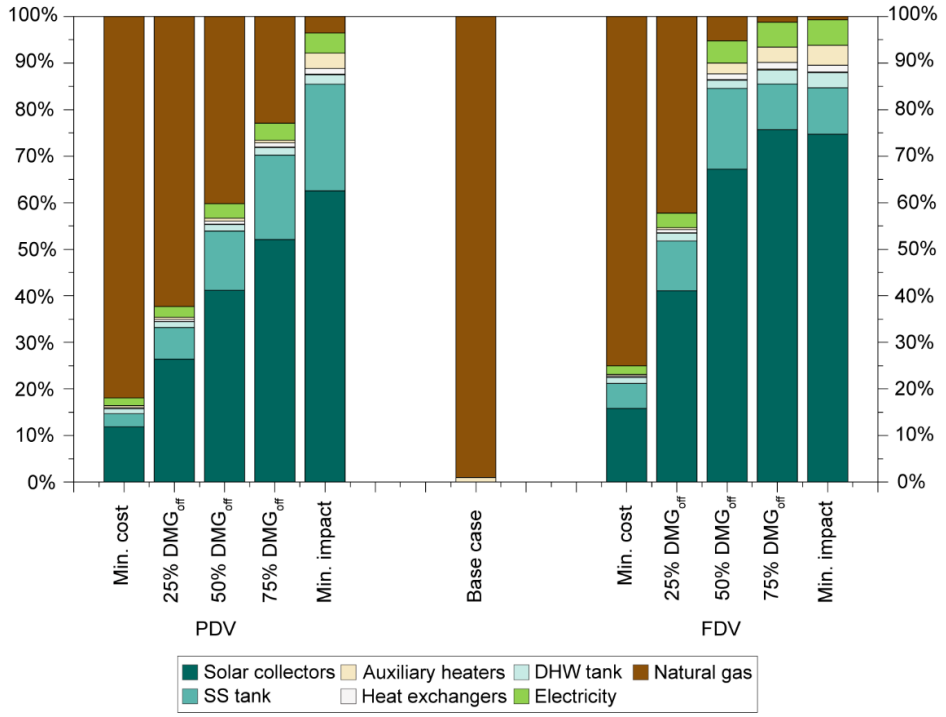

Figure III-12: A breakdown for the aggregated ReCiPe 2016 environmental impact of the optimal Pareto solutions under PDV and FDV optimization settings in comparison to their respective base case. These solutions comprise configurations to satisfy the SH and DHW demand of 10 residential building located in Madrid

As shown in Figure III-13, the thermal performance of the proposed SDHS is evaluated through a combination of nominal performance indicators; these indicators comprise the main renewable energy equipment efficiencies and their relative solar fractions. Under both optimization settings, a limited change in the η_{COL} is indicated with the change in scenarios, where the highest η_{COL} is indicated in the scenario 1 due to the limited utilization of solar collector. Moreover, the DHWT is utilized for daily purposes without storage; thus, a limited heat loss to the environment is indicated in all scenarios. This can be reflected in the DHWT efficiency, where η_{DHWT} is around 96% for all scenarios under both optimization settings. Regarding the SST performance, under the PDV optimization setting, with almost a constant value for the heat loss coefficient of around 0.16 W/m^2. K for all scenarios, the annual SST heat losses remain above 33 kWh/m^3 with a narrow variation with the increment in the environmental limits. Also, the η_{SST} remains around 71% for all scenarios except scenario 1 where the η_{SST} is 67%. In terms of the solar fraction, the contribution of the DHW distribution circuit remains above

98% for all scenarios, whereas the $S.F_{SST}$ rises progressively with the increment in the environmental damage limits (increment in the usage of renewable energy equipment) where solar fraction increases from 80% in scenario 1 (Min. cost) to 99% in scenario 5 (Min. impact).

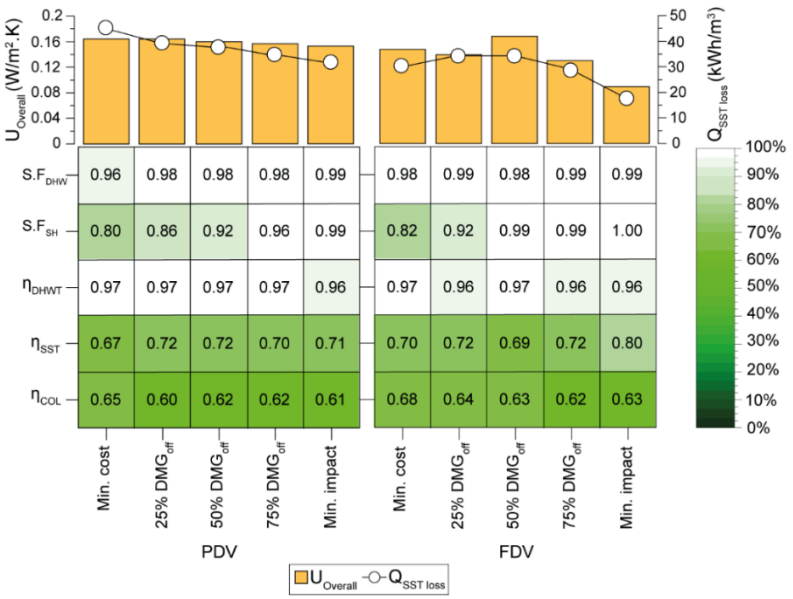

Figure III-13: Thermal performance indicators for the optimal Pareto SDHS solutions under PDV and FDV optimization settings. These designs satisfy the SH and DHW demand of the 10 residential buildings located in Madrid

Under the FDV optimization settings, with the change in the SST construction materials and its geometry, the heat loss coefficient of the SST reduces from 0.15 in scenario 1 to 0.08 W/m^2. K in scenario 5. This reduction is reflected in the SST heat losses, which diminish gradually with increasing the environmental damage limits, and it reaches 18 kWh/m^3 with an improvement of 45.2% compared to the same scenario under the PDV optimization setting. This improvement is emulated in the η_{SST} especially in the two extremes optimal scenarios (Min. cost and Min impact optimal solutions) where the η_{SST} improved by 4.5% and 12.3% in scenario 1 and 5, respectively. In terms of the solar fraction for both SH and DHW distribution circuits, the same progressive behavior is indicated under the FDV optimization setting with a slight improvement of 2.5 % in scenario 1 in comparison to the PDV optimization setting.

III.5.2.2 Influence of the community size

Following the performance analysis for the SDHS under PDV and FDV optimization settings in the small urban community with 10 buildings, the proposed framework

based on a MOO approach is expanded to be applied for different urban community sizes. This approach examines the community size effect (10, 25, 50, and 100 buildings) on the performance of the SDHS in a techno-economic optimization framework with consideration for its environmental impact.

Figure III-14 shows a clear tendency between the objective functions and the increment in the community size, where increasing the community size raises the economic and environmental benefits in comparison to their relative base cases. Following the small urban community size (10 building), under the PDV optimization setting, the NPC in the Min. cost solutions is improved by 26.8%, 34.7% and 53.9% for the 25, 50 and 100 buildings, respectively in comparison to their relative base cases. On the other hand, the economic competitivity of the Min. impact solution is restricted where at the 25-building community, the NPC increases by 21.3% in comparison to its base case. With increasing the community size above 25, the NPC of the Min. impact solution decreases by 2.3%, and 19.7% for 50 and 100 community size, respectively. Under the FDV optimization setting, a slight improvement is indicated in the NPC of the Min. cost optimal solution with increasing the community size where it improved by 18.1%, 35.9%, and 26.8% for building community size of 25, 50, and 100, respectively compared to the optimal solutions under PDV optimization setting. Furthermore, adding the construction materials of the SST in the optimization problem demonstrate a limited improvement in increasing the competitivity of SDHS against the natural gas solution where the Min. impact solution only improved by 1.85% at community size of 100 buildings compared to the same optimal solution under PDV optimization setting.

The optimal environmental impact of the SDHS in different community sizes follows the optimal solutions of the 10 buildings located in Madrid, where the SDHS is beneficially effective in reducing the environmental impact compared to the conventional system using natural gas. Under the PDV optimization setting, the optimal Min. cost solution reduces the environmental impact by 79.5%, 79.6%, and 79.7% for the urban community size of 25, 50, and 100 buildings, respectively. Besides, the optimal Min. impact solution extensively reduces the environmental damage by 87.4%, 87.7, and 88% for the 25, 50, and 100 buildings, respectively. These results approve a limited improvement in the environmental impact of the optimal SDSH solutions with the increment in the community size under the PDV optimization setting. Under the FDV optimization setting, the environmental benefits of replacing the conventional system based on natural gas with SDHS can progressively rise with increasing the community size compared to the optimization problem under the PDV setting. The optimal Min. cost solutions are improved by 87.4%, 88.4%, and 89.3% for an urban community of 25, 50, and 100 buildings, respectively. This improvement is expanded as well for the Min. impact solution where an improvement around 43.3% is indicated for all community sizes compared to the Min. impact optimal solutions under the PDV optimization setting.

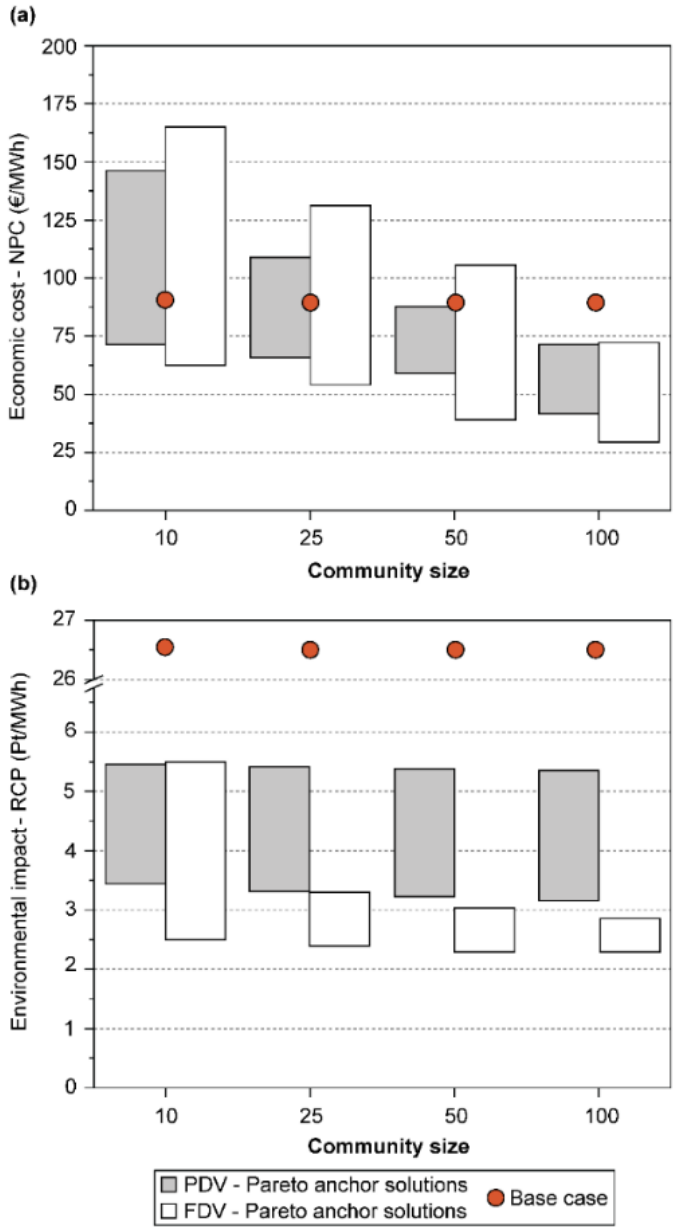

Figure III-14: Various Pareto optimal solutions for the SDHS in different community sizes covering the SH and DHW yearly demand in comparison to their respective base case using natural gas, (a) Economic optimal solution of SDHS at the different scenarios under PDV and FDV optimization setting, (b) Environmental optimal solution of SDHS at the different scenarios under PDV and FDV optimization setting

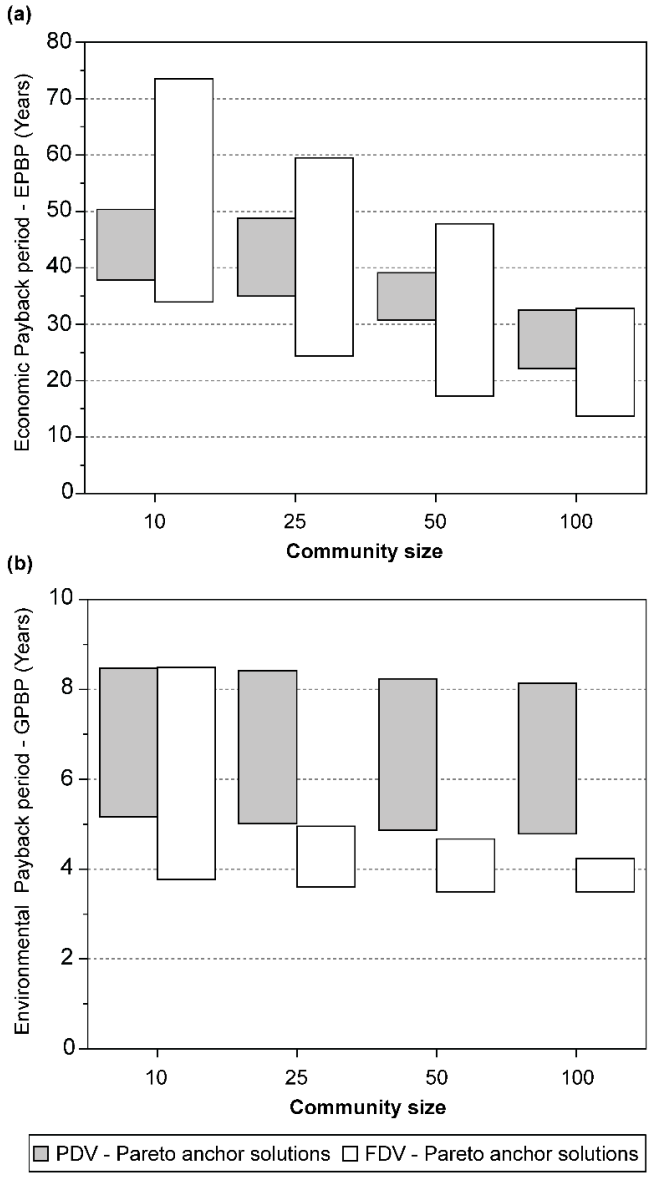

Figure III-15: Various Pareto optimal solutions for the SDHS in different community sizes covering the SH and DHW yearly demand in comparison to their respective base case using natural gas, (a) Economic payback period of the SDHS at the different scenarios under PDV and FDV optimization setting, (b) Environmental payback period of the SDHS at the different scenarios under PDV and FDV optimization setting

In addition to evaluating the economic and environmental performance of the SDHS based on the NPC and RPC indicators, respectively, the $EPBP$ and $GPBP$ are proposed to measure the system sustainability throughout its lifetime from the economic and environmental perspective under the PDV and FDV optimization settings at in different community sizes as shown in Figure III-15.In terms of the economic payback period, the SDHS could not approve its feasibility in the community size of 10 buildings, especially under the PDV optimization setting where the $EPBP$ is varying between 38 years and 51 years, which is higher than the lifetime of the SDHS. Under the FDV optimization setting, the SDHS feasibility increased, especially in the low environmental damage scenarios where the $EPBP$ in Min. cost optimal solution is 33 years. With increasing the community size, the $EPBP$ decreases progressively. Under the PDV optimization setting, the $EPBP$ at the Min. cost optimal solution reduces to 35, 31, and 22 years for the community size of 25, 50, and 100 buildings, respectively. While under the FDV optimization setting, more improvement in the $EPBP$ can be indicated where the $EPBP$ in the Min. impact optimal solution reduces to 25, 17, and 14 years for the community size of 25, 50, and 100 buildings, respectively. In terms of the $GPBP$, a limited improvement can be indicated with increasing the community size under the PDV optimization setting due to the absence of the SST construction materials in the optimization framework. In the Min. impact optimal solution, the $GPBP$ is around 5 years for all community sizes. While under the FDV optimization setting, the $GPBP$ reduces to only around 3 years for all community sizes. Moreover, an extensive improvement in the Min. cost solutions at the community size of 50 and 100 buildings are shown compared to its relative optimal solutions under the PDV optimization setting where the $GPBP$ reduces by 43.1% and 47.7% for the 50 and 100 buildings, respectively.

Following the advantage of including the SST construction materials in the optimization problem to improve the objective functions' performance, the proposed methodology offers a complete depiction of the features and configurations of the optimal Pareto solutions categorized by the circuit at different scenarios under the FDV optimization setting as shown Figure III-16. This figure tends to show the most frequent selected decision variables at different community sizes under various damage scenarios. This is implemented through combining the Interactive parallel coordinate, which shows the nominated decision variables under different damage scenarios with a histogram at each Interactive parallel coordinate column to show the most common size for each decision variable. In the solar circuit, most of the optimal Pareto solutions at different community sizes remain the A_{COL} at a narrow range of 1.1 ± 0.1 m^2/MWh/a. Following the previous recommendation by Tulus et al. [38], the optimal inclination angles of the solar collectors (β_{COL}) stayed at an angle of 43º for most of the community sizes, which is close to the latitude of Madrid. Moreover, the number of solar collectors connected in series remains at 4 for most of the scenarios. In the DHW circuit, since the DHWT is used only for the daily purposes without long

term storage, the histogram depicts that the V_{DHWT} is only around 0.15 m^3/MWh/a for most of the optimal solutions, whereas the HDR_{DHWT} diverge around 1.5 ± 0.1 m/m. In the SH circuit, the optimal characteristics of the SST geometry at various community sizes shows that the V_{SST} is around 15 ± 1 m^3/MWh/a, whereas the HDR is around 0.65±0.1 m/m for all environmental damage scenarios.

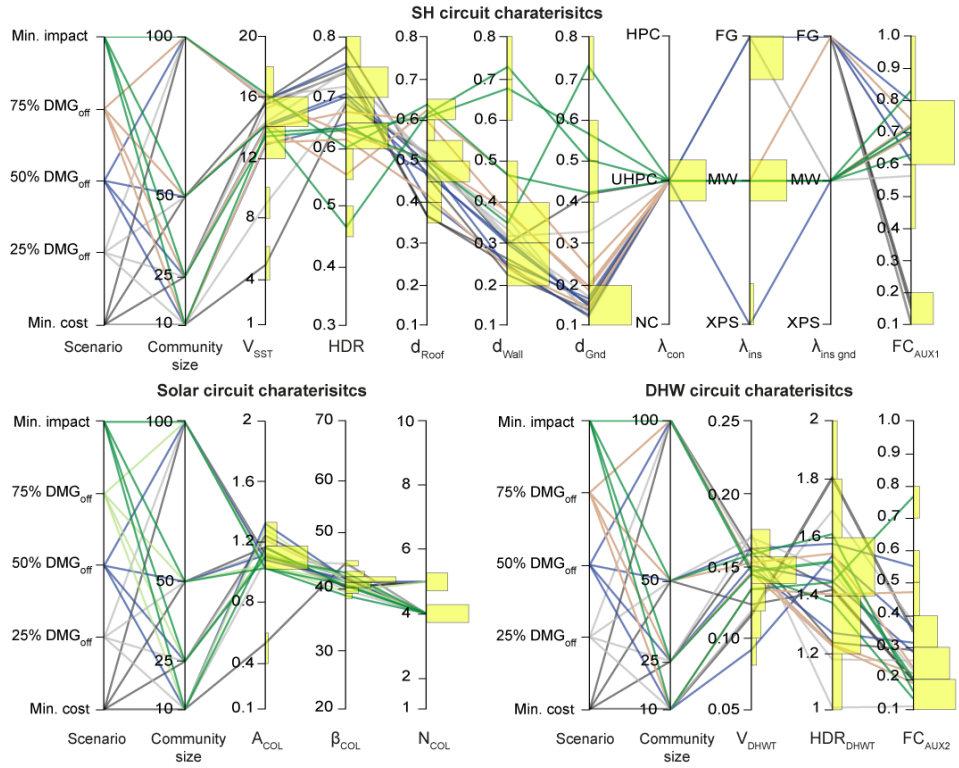

Figure III-16: Interactive parallel coordinate plots combined with histograms (Yellow bars) to identify the optimal range for the decision variables of the SHDS categorized by circuit name at different scenarios and different urban community sizes under the FDV optimization setting

In terms of the SST construction materials, the UHPC shows superior performance in all optimal solutions due to its techno-economic advantage combined with its limited environmental impact. For the insulation materials, no agreement can be indicated for all optimization scenarios. In scenarios 1 and 2 (low environmental damage limits), the foam glass gravel with thermal conductivity of 0.06 W/m. K is chosen as insulation material for all surfaces of the SST at each community size. While moving toward higher environmental limit scenarios, most of the optimal solutions insulate the SST surfaces using mineral wool with a thermal conductivity of 0.04 W/m. K, due to its limited environmental impact. Furthermore, the insulation thickness is around 0.5±0.05 m for the top roof of SST based on the scenario and the

community size. This range changes to 0.3±0.1 m for the SST wall, whereas it remains around 0.15±0.05 m for the SST ground. Regarding the capacity of the auxiliary heater, the FC_{AUX1} is varying around 0.7±0.1. These configurations of the SDHS circuit will be reflected in the NPC and RCP breakdown at different community sizes.

Figure III-17 shows a comprehensive economic breakdown for each component in the SDHS during its lifetime based on the NPC when applied at different community sizes under the FDV optimization setting. Similar to the small community size (10 buildings), the initial investment cost and the replacement at all other community sizes is a quite large cost component compared to their relative base cases. This cost contribution is ascending increases with raising the environmental damage limits. To be more specific, the solar collector and SST have the main contribution to the initial investment cost. Following the 10 buildings case, the community size of 25 buildings shows a significant contribution to the SST in all scenarios. This contribution declines with increasing the community size, especially in the Min. cost Pareto optimal solutions, where the SST represents only 21.9% and 16.3% of the initial investment cost for the community size of 50 and 100 buildings, respectively. This drop is due to the possibility of changing the SST construction, which can contribute to reduce the initial investment cost of the SST. For the operational cost, the Min. cost-optimal solution at a community size of 25 buildings represents 22.8% of the total cost. This is due to the dependency of the system on using renewable energy components, where the natural gas represents 12.7% of the total operational cost. With the increment in the community size, the dependency on using natural gas becomes less compared to the small community size (10 buildings) due to the feasibility of introducing the renewable energy components even in the Min. cost-optimal solutions. Thus, the operational cost due to natural gas represents only 16.9% and 13.8% for community size of 50 and 100 buildings, respectively.

Following the effect of introducing the SST construction materials in improving the performance of the objective functions, Figure III-18 depicts a detailed breakdown for the SST life cycle cost when introduced at different community sizes. For a community size of 10 buildings, all scenarios except the scenario 4 and 5 show almost the same contribution for the SST breakdown cost where the construction materials represent around 70%. While this value drops to only 40.6% and 25.6% in scenarios 4 and 5, respectively, and the remain contribution is dedicated to the insulation materials, especially the wall insulation materials, which represent around 33% of the total SST cost for both scenarios. In all other community sizes, the construction materials contribution is descending drops with the increment in the environmental damage limits and community size where it reduces from 59.8% to 11.4% at the community size of 25 buildings, and it drops to only 2.48% and 0.08% in Min. impact optimal solution at the 50 and 100 community size, respectively. This extensive reduction is due to the demand to hold the investment for the insulation materials.

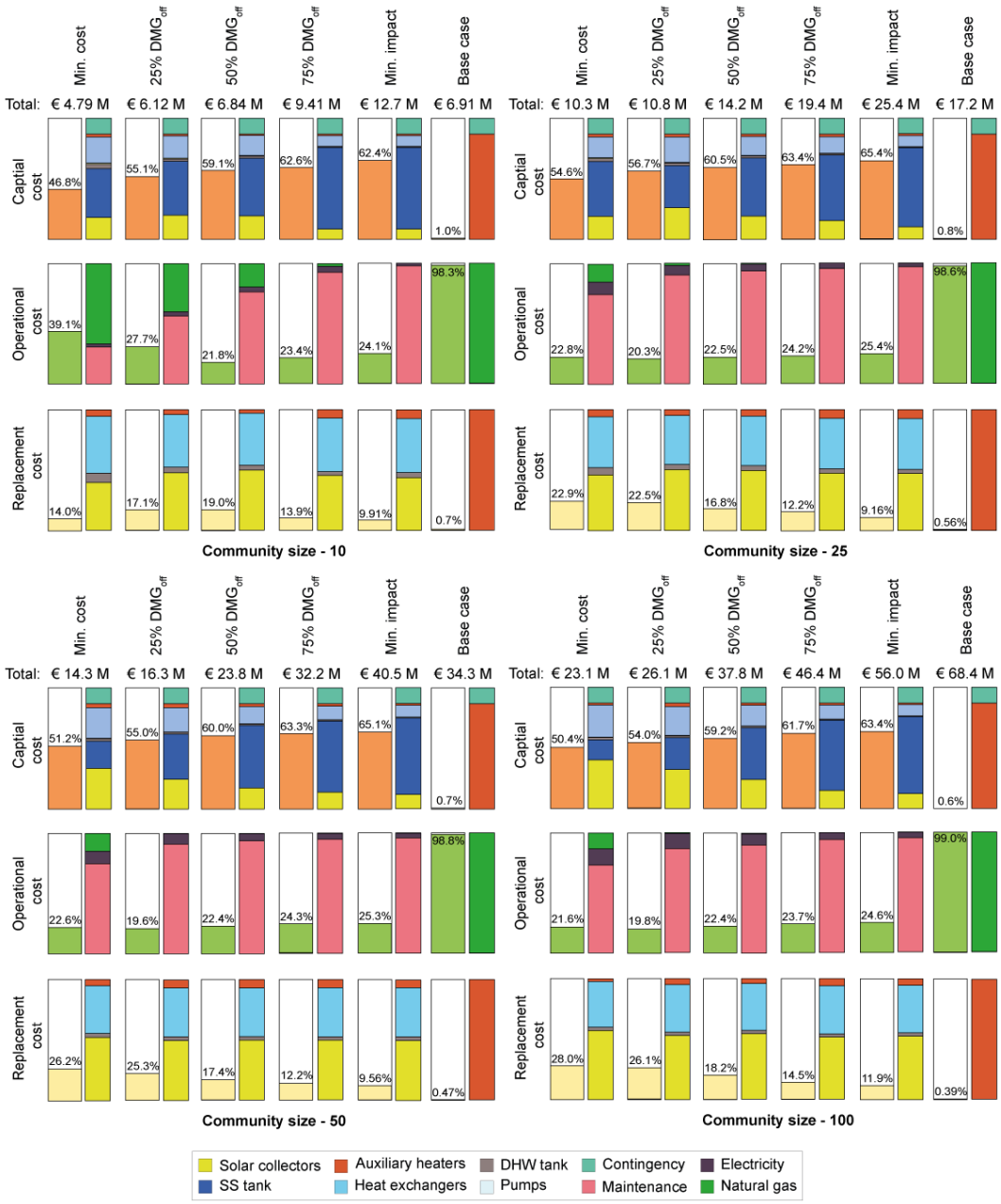

Figure III-17: Life cycle cost breakdown of Pareto optimal solutions at different scenarios for a SDHS system applied at various community sizes. The breakdown includes the shares of initial capital cost, operational cost, and replacement cost under the FDV optimization setting in comparison to their relative base case

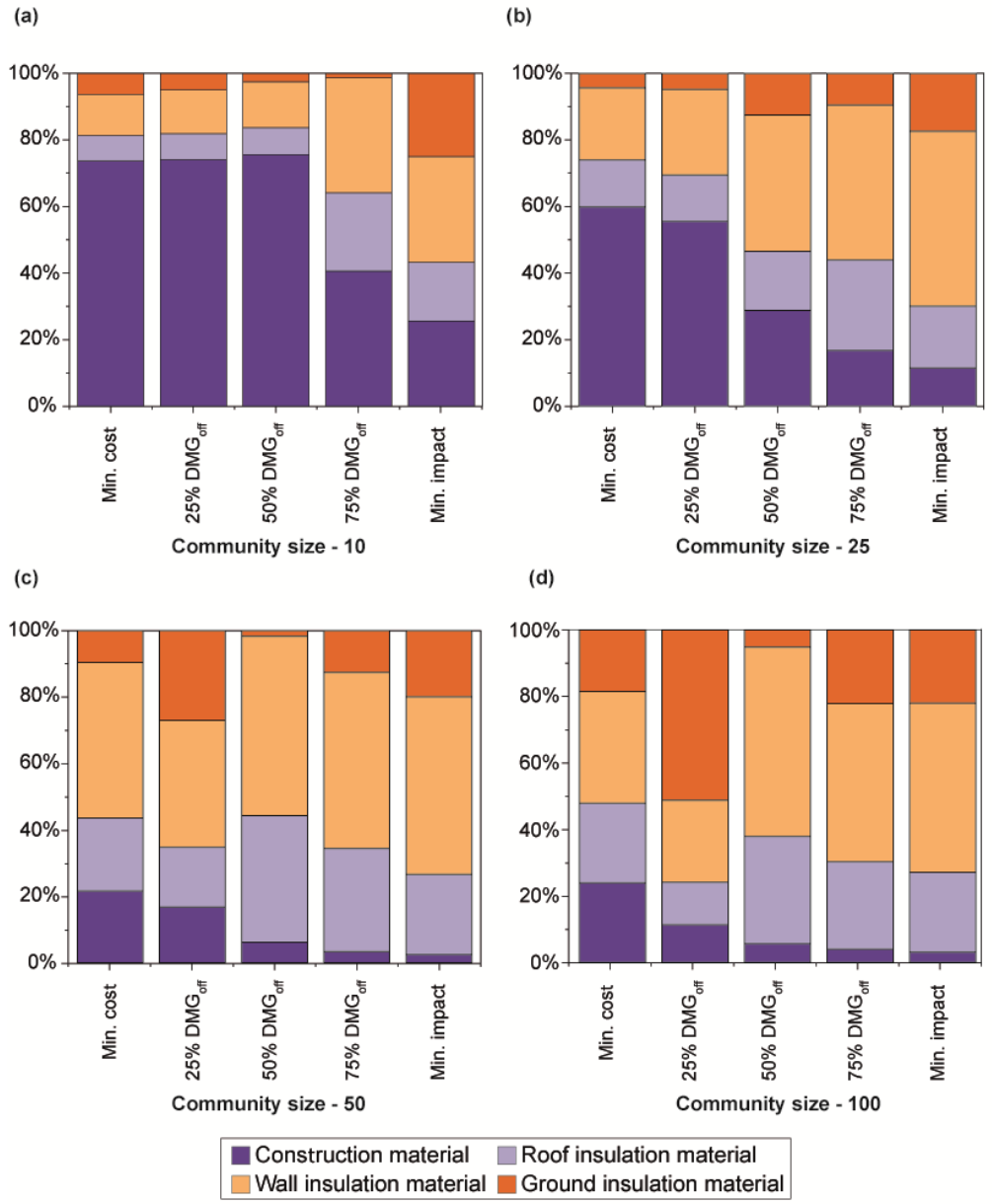

Figure III-18: Life cycle cost breakdown for the SST at different community sizes under different damage scenarios for (a) 10 buildings, (b) 25 buildings, (c) 50 buildings, and (d) 100 buildings

Figure III-19 shows a comprehensive environmental breakdown for each component in the SDHS during its lifetime based on the RCP when applied at different community sizes under the FDV optimization setting. On the contrary to the environmental impact

breakdown at the 10-buildings case, the Min. cost-optimal solution at the 25 buildings relays on renewable energy since the natural gas represents only 14.09% of the total impact. With the increment in the environmental damage limits, a progressive rise is indicated in the environmental impact due to introducing renewable energy components where the solar collector followed by the SST are the main contributors to the total environmental impact from scenario 2 to 5. With increasing the community size above 25 buildings, the environmental impact due to using natural extensively decrease where it represents only 13.9% and 9.60% in the Min. cost-optimal solution at the community size of 50 and 100 buildings, respectively.

In terms of the SST environmental impact, the construction material has the main contribution to the environmental impact of STT followed by the wall insulation material. It rises progressively with increasing the environmental damage limits, and it represents 32.1%, 23.1%, 23% and 18.7% for the community sizes of 10, 25, 50 and 100 building at the Min. optimal cost solution, this value increases to 99% at the Min. impact optimal solutions.

Following the energy analysis of the small urban community (10 buildings) located in Madrid, where the SST heat losses and its relative efficiency in addition to the solar fraction of the SH circuit are the key indicators in the SDHS, Figure III-20 shows the heat losses of the SST lining up with its coefficient under the PDV and FDV optimization setting at different community sizes. Under the PDV optimization setting, the heat loss coefficient remains almost at 0.15 W/m^2. K for all scenarios at different community sizes. While the heat loss coefficient reduces progressively with increasing the environmental damage limits under the FDV optimization setting where the heat loss coefficient reduces from 0.2 W/m^2. K in scenario 1 (Min cost-optimal solution) to 0.05 W/m^2. K in scenario 5 (Min impact optimal solution) at the community size 25. In the community size of 50 and 100, the heat loss coefficient declines from 0.18 W/m^2. K to 0.05 W/m^2. K in the Min. cost and impact optimal solutions, respectively.

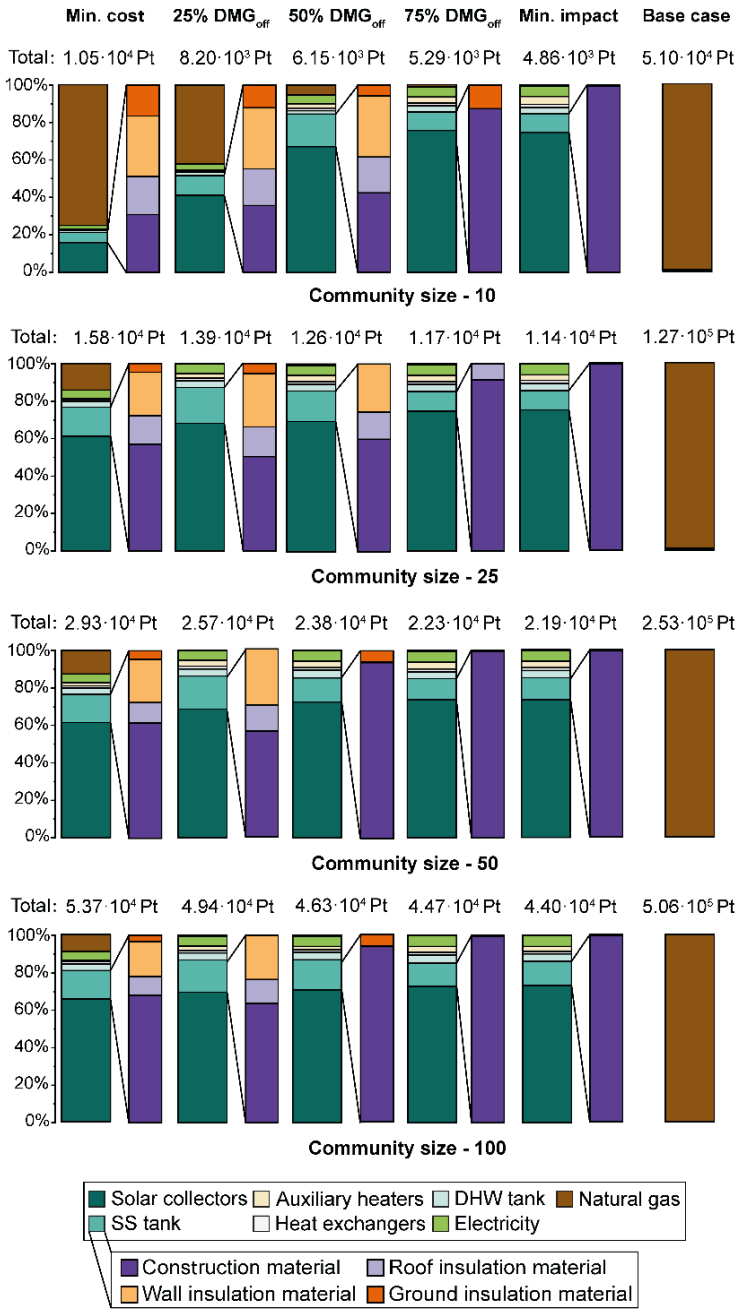

Figure III-19: A breakdown for the aggregated ReCiPe 2016 of Pareto optimal solutions at different scenarios for the SDHS system applied at various community sizes. The breakdown includes the share of the SST construction components under the FDV optimization setting in comparison to their relative base case

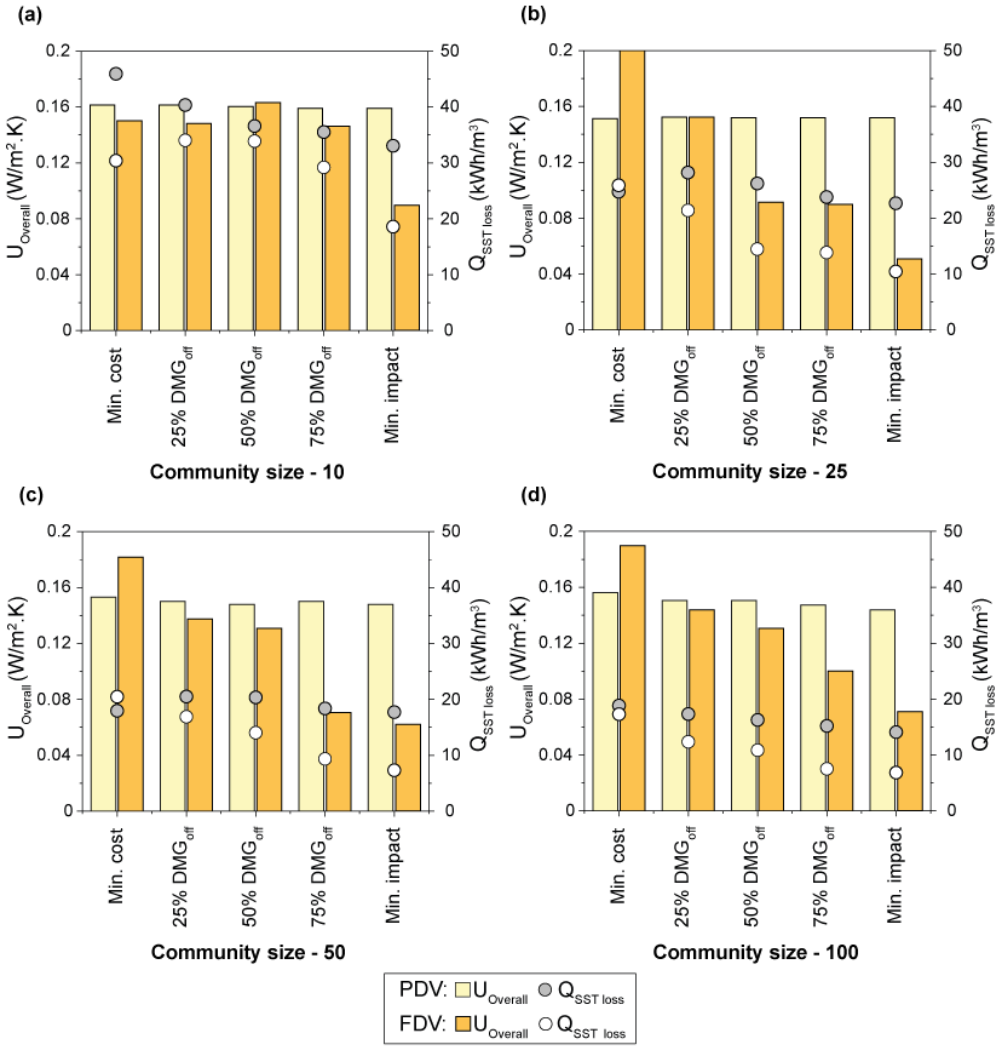

Figure III-20: Heat loss of the SST for the optimal Pareto SDHS solutions under PDV and FDV optimization settings. These designs satisfy the SH and DHW demand of different residential building sizes located in Madrid

The privilege of reducing the heat loss coefficient due to introducing the SST construction materials in the optimization problem is reflected in the annual heat losses of the SST. Following the small community size of 10 buildings, the Min. cost-optimal solution under FDV optimization setting fails to improve the heat losses in the SST at the community size of 25 buildings where the heat losses of the SST is higher by 7.14% compared to the same scenario under the PDV optimization setting at community size of 25 buildings, respectively. While increasing the environmental damage limits, the heat losses in SST reduce progressively under the FDV

optimization setting compared to its relative scenario under the PDV optimization setting where the SST heat losses reduced in the Min. impact optimal solution by 63.3%. The superiority of including the SST construction materials reveals in the community sizes of 50 and 100 at all optimal solutions except the Min. cost solution in the 50-community size where the SST heat losses increase by 15.8%. While in the community size of 100 buildings, the heat losses reduce by 11.8%. This improvement continues with increasing the environmental damage limits, and it is reduced by 58.2% and 52.3% for 50 and 100 buildings, respectively, at the min impact optimal solutions.

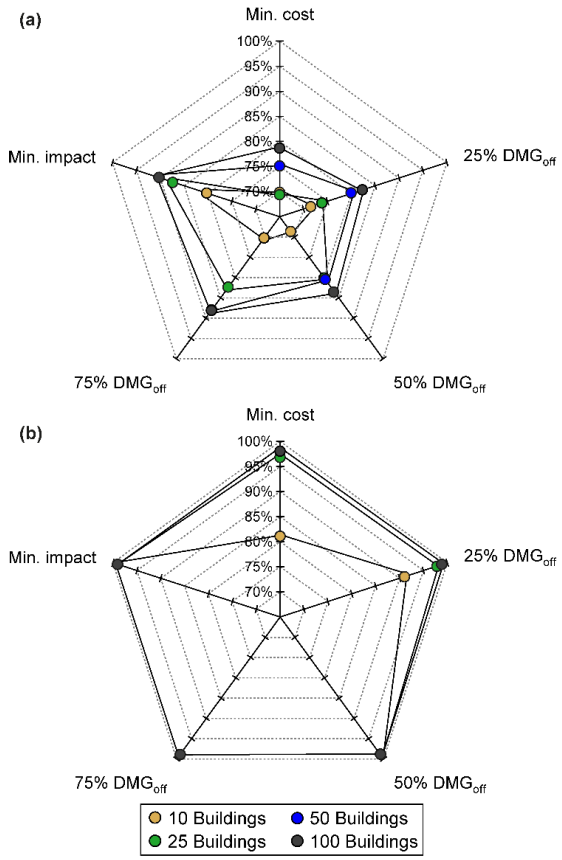

Figure III-21: The performance indicator including (a) η_{SST}, (B) $S.F_{SH}$ for the optimal Pareto SDHS solutions under the FDV optimization settings at different community size

The improvement in the SST heat loss due to introducing the SST construction materials in the optimization problem can be mirrored in the η_{SST} and the solar fraction of the SH circuit, as shown in Figure III-21. In term of the η_{SST}, the SST

efficiency rises with increasing the damage limits where the η_{SST} in the Min. cost optimal solution is 69.8%, 75.0%, and 78.9% for the community sizes of 25, 50, and 100 buildings, respectively. Moreover, this value increases in the Min. impact-optimal solutions to 87.8%, 90.4%, and 90.5% for the community size of 25, 50, and 100 buildings, respectively. Following the $S.F_{SH}$ of the Min. cost optimal solution in the 10 building, a $S.F_{SH}$ of 97.1% is indicated for a community size of 25 buildings. This value can be improved with the movement toward less environmental damage solution, and it achieves almost 100% in the Min. impact solution. With increasing the community size, a high $S.F_{SH}$ is indicated in all optimal solution where a $S.F_{SH}$ of 98% is indicated in the Min cost optimal solution, and it can reach almost 100% in the Min. impact optimal solution for both the 50 and 100 buildings.

III.5.3 Comparison of the optimal SDHS model to other projects

In this phase, our optimization framework results are compared with the results obtained by the framework proposed by Tulus et al. [38]. The main objective of this phase is to verify our optimization framework and indicate its advantage in enhancing the SDHS performance as well the computational expenses of the optimization process.

Aligning with the verification objective, the SDHS optimal solutions for a community size of 40 buildings located in Madrid is compared with Tulus et al. [38] results under an environmental damage of 50% scenario. The Tulus´s framework considered only the solar collector field area and SST volume as decision variables in the optimization problem while the remain decision variables were fixed based on the Friedrichshafen project [126] for the SST construction materials. In addition, Tulus´s setting was implemented in our framework to indicate the enhancement of including other decision variables as well as the SST construction properties in the optimization problem.

Table III-7. The Pareto optimal solution at environmental damage of 50% under different settings based on our simulation-optimization framework SDHS compared to Tulus et al. [38] results. This optimal solution covers SH and DHW demand of 40 buildings located in Madrid

	Circuit Name			Tulus et al. [38]	Tulus setting using our framework	FDV optimization setting
Decision variables	Solar Circuit	Heat demand	(MWh/a)	7654	7654	7654
		A_{COL}	(m^2/MWh/a)	0.89	1.16	1.09
		β_{COL}		50	50	42.3
		N_{COL}		1	1	5
	SH circuit	V_{SST}	m^3/MWh/a	10	10.6	14.3
		HDR	m/m	0.6	0.6	0.75
		d_{Roof}	m	-	0.3	0.44
		d_{Wall}	m	-	0.2	0.30
		d_{Gnd}	m	-	0.2	0.13
		λ_{con}	W/m. K	-	NC	UHPC
		λ_{ins}	W/m. K	-	MW	XPS
		$\lambda_{ins\ gnd}$	W/m. K	-	MW	XPS
		FC_{AUX1}	-	1	1	0.66
	DHW Circuit	V_{DWHT}	m^3	109.7	109.9	177.8
		HDR_{DHWT}	m/m	1.7	1.7	1.35
		FC_{AUX2}	-	1	1	0.45
Main Performance indicators	DHW Circuit	η_{DHWT}	%	98.1	98.2	97.2
		$S.F_{DHW}$	%	98.9	98.8	99.8
	SH Circuit	$U_{Overall}$	W/m^2. K	0.06	0.15	0.09
		$Q_{SST\ loss}$	kWh/m^3	3.11	21.6	12.4
		η_{SST}	%	96	81.2	85.3
		$S.F_{SH}$	%	97.8	96.3	99.9
	Economic indicators	NPC	Euro/MWh	53.3	91.1	58.5
	Environmental indicators	RCP	Pt/MWh	3.59	3.86	2.57

As shown in Table III-7, our framework results using Tulus et al. [52] setting, which only considers the solar collector field and SST volume as decision variables in the optimization problem agrees with the optimal results obtained by Tulus et al.[38] article where the optimal size for the decision variables comprising the solar collector field and SST are almost identical in both cases. Furthermore, this verification extends to the performance indicators including the η_{DHWT} , $S.F_{\mathrm{DHW}}$ and $S.F_{\mathrm{SH}}$. However, due to the low heat loss assumption in Tulus et al. [38] article for the SST, the heat loss coefficient is only 0.06 W/m^2·K, whereas in our optimization framework, where the SST construction materials were estimated based on the Friedrichshafen project [126], the heat loss coefficient is 0.15 W/m^2·K. This increment in the heat losses coefficient is reflected in the η_{SST} which is 81.2% compared to 96% in Tulus et al. [38]. Furthermore, the limitation in decision variables using our framework is reflected in the economic objective function where the NPC is 91.1 Euro/MWh. This extensive increment in the cost compared to Tulus et al. [38] is due to the usage of the mineral wool and Normal concert in the construction of the SST tank, and introducing the Auxiliary heaters with its full capacity as proposed in Tulus et al. [38]. On the other hand, the small cost of the SDHS in Tulus et al. [38] is due to estimating the SST cost as a function of the only its storage capacity without consideration for the cost of the SST construction materials.

After the verification stage, the developed methodology framework using the FDV optimization setting is tested against Tulus et al. [38] to approve the importance of including other decision variables comprising the SST properties in proposing a realistic estimation for the SDHS performance during its lifetime. The results under the FDV optimization setting shift the SST size to 14.3 m^3/MWh/a with a slight difference in its aspect ratio where the HDR is 0.75 compared to 0.6 proposed in Tulus et al. [38]. The difference in the SST volume is reflected in the $S.F_{\mathrm{DHW}}$ and $S.F_{\mathrm{SH}}$ which are almost 100% for both circuits. Furthermore, our framework achieves this high renewable energy fractions without losing its efficiency due to the larger size for the SST, where the SST heat loss coefficient is 0.09 W/m^2·K. and the η_{SST} is around 85.3%. Moreover, including the FDV optimization setting is reflect in the economic and environmental indicators where the NPC is 58.5 Euro/MWh with an increment of 9.7% compared to Tulus et al. [38]. While the RPC under the FDV optimization setting is improved by the 28.4% due to including the SST material and construction properties.

In addition to the SDHS optimal solution comparison to Tulus et al. [38], the capability of the methodological optimization framework based on a robust ANN in handling the Heuristics optimization is illustrated through comparing the computational expenses of the optimization process with the SDHS optimization problem mentioned by Tulus et al. [38]. In Tulus et al. study, the average computation time for the anchor points was 15,700 CPU seconds and 47,000 CPU seconds for intermediate Pareto solutions

using an Intel® Xeon® E5-2620 v4 2.10 GHz processor with 32.0 GB RAM. In this new framework, the average computational time for developing the full Pareto frontier is only around 600 CPU seconds using the same machine. This huge reduction is due to replacing the TRSNYS model with a robust ANN model and combining it in a MOO framework.

III.5.4 Global Sensitivity Analysis results

The GSA is implemented to identify the essential input parameters that responsible for the variation in both NPC and RPC objective functions. The analysis is carried out based on the BACCO analysis due to its low computational cost. The community of 10 buildings under the FDV optimization setting at different scenarios is selected as a reference case in the GSA due to its critical feasibility in comparison to the conventional system using natural gas.

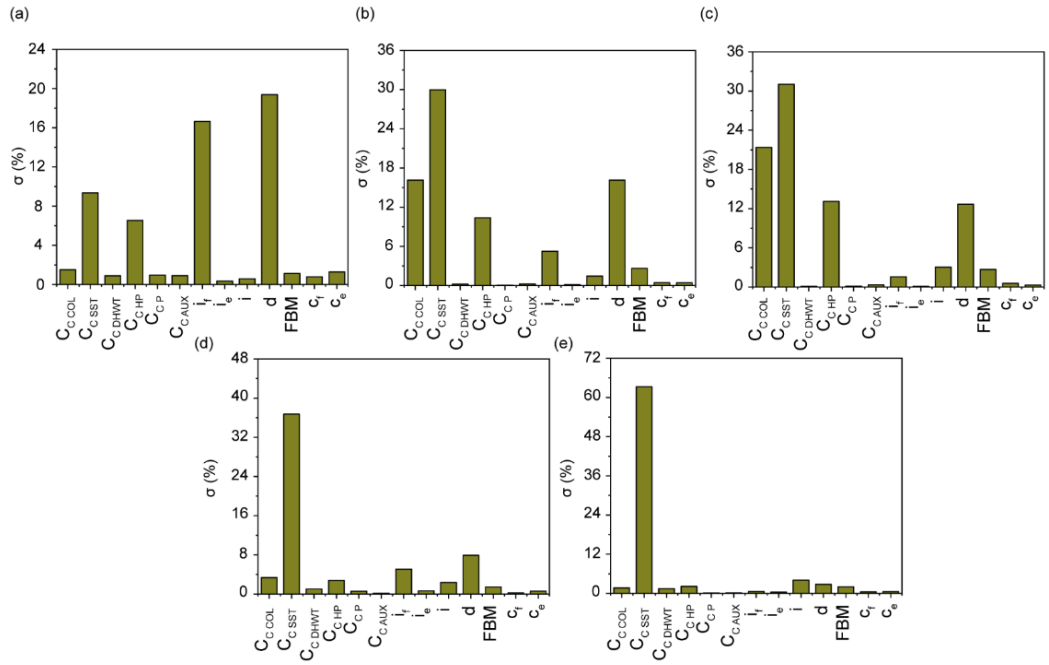

Figure III-22: Results of the BACCO analysis indicating the most influencing uncertain parameters with regards to the NPC under FDV optimization settings at different environmental damage scenarios where (a) Min. cost solution, (b) 25% damage off, (c) 50% damage off, (d) 75% damage off, (e) Min. impact solution

The evaluation assesses the economic parameters, including the investment cost of the SDHS equipment, the economic factors which would fasten the feasibility of SDHS deployment and the energy carriers. For the BACCO analysis, given a total

number of 400 sample points based on the Latin hypercube sampling (LHS) design, the sensitivity analysis problem is formulated and feed into the Gaussian emulator machine sensitivity analysis (GEM-SA) software to perform the analysis.

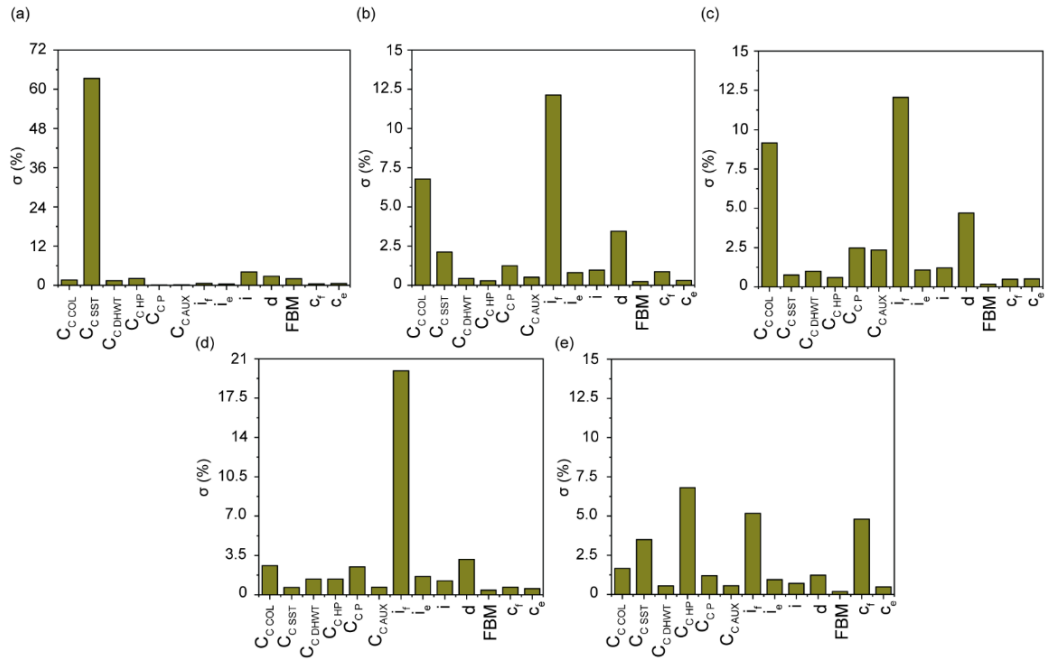

Figure III-23: Results of the BACCO analysis indicating the most influencing uncertain parameters with regards to the RPC under FDV optimization settings at different environmental damage scenarios where (a) Min. cost solution, (b) 25% damage off, (c) 50% damage off, (d) 75% damage off, (e) Min. impact solution

The results of the BACCO analysis for economic performance is shown in Figure III-22 In each plot, the most influential parameters are ranked based on their variance contribution to the NPC objective function, and it represented through their total effect, which comprises the main effect, interactions between these parameters, and their high order terms that can be involved in the emulator model. In scenario 1 (Min. cost-optimal solution), the discount rate, followed by the annual natural gas inflation rate and the investment cost of the SST, are responsible for the greatest portion of the output variance. Moreover, a limited distribution for the renewable energy equipment is due to the dependency of the SDHS under scenario 1 on using natural gas. With the movement toward a lower environmental damage solution, the contribution of the initial investment cost of the SST increases with diminishing the contribution of the discount rate. In scenarios 2 and 3, the investment cost of the SST and the investment cost of the solar collector are the most influential parameters.

While in scenarios 4 and 5, the investment cost of the SST is the only important uncertain parameter in designing SDHS. These results confirm the importance of including the SST construction materials, which can substantially improve the optimal solution and increase its competitivity against the conventional systems.

Following the sensitivity analysis for the economic performance of the SDHS based on BACCO analysis, Figure III-23 shows the sensitivity analysis for the RPC under different damage limits scenarios. In scenario 1, where the min possible change in the construction materials of the seasonal storage can be achieved due to the objective of minimizing the economic cost, the initial investment cost of the SST has the strongest influence in the RPC objective. With the possibly to change the construction materials due to increasing the environmental damage limits, the contribution of the investment cost of the SST starts to diminish, and the main contribution due to renewable energy equipment moves to the solar collector and natural gas. In scenarios 2 and 3, the annual natural gas inflation rate, followed by the investment cost of the solar collector field and discount rate, are the most influential parameters. While in scenario 4, the annual natural gas inflation rate appears to be the only relatively important parameter in this scenario. With moving toward the extensive environmental damage limit scenario (Min. impact solution), the investment cost of the heat exchangers followed by the annual natural gas inflation rate and the natural gas price represents the significant parameters that are affecting the RPC objective. Beside indicating the most influential parameters, the GSA based on BACCO analysis also indicates that the uncertainty due to the investment cost including the initial investment cost the DHWT, pumps and auxiliary heaters or due to the economic factors including the annual electricity inflation rate, inflation rate, and maintenance factor or due to the energy carrier including electricity prices can be neglected.

Overall, the GSA based on the BACCO analysis is a valuable decision-support technique that offers the SDHS designers' valuable information regarding the main driver parameters of uncertainty. In the proposed case study, the construction materials of the SST and the annual natural gas inflation rate would, in return, significantly contribute to the NPC and RPC objective functions.

III.6 Conclusions

The Governance of the Energy Union ambitious plan to updates the EU energy policy framework concerning the sustainable transaction from fossil fuel toward the deployment of renewable energy encourages the widespread of methodologies that can quantify the renewable energy systems performance with consideration for its economic and environmental impact. This paper presents a framework to evaluate the feasibility of deploying the SDHS at different urban community sizes with tracing its techno-economic failures as well as its environmental impact. This methodology

is implemented through developing a complete methodological optimization framework based on a robust ANN model to solve the computational obstacle associated with heuristics optimization models. The surrogate modelling approach empowers the feasibility of assessing the most influencing parameters driving the total cost of the SDHS based on GSA. The optimization framework correspondingly based on a multi-objective approach which is applied to optimize the SDHS life cycle cost with achieving progressively lower environmental impact throughout the system lifetime. In this context, the proposed framework is applied to four different urban community sizes comprising 10, 25, 50, and 100 buildings located in Madrid. In which the optimization problem is formulated under two different optimization settings (PDV and FDV) to investigate the effect of the seasonal TES geometry and its construction properties in enhancing the SDHS optimal design feasibility.

In the proposed framework, to overcome the ANN building computational barrier related to its design space exploration, and to optimize its tuning parameters (Hyperparameter), the ANN model is coupled with the Bayesian optimization approach assisted sensitivity analysis based on definitive screening. This procedure is utilized to develop a robust ANN model-independent on its hyperparameters and the training set size. Leading to create an accuracy ANN model that reflects the performance of the SDHS at affordable computational expenses, a summary of the robust ANN model key findings is the following:

- The default ANN model hyperparameters yield to poor accurate model that can predict the SDHS aggregated output. Thus, this result emphasizes the need for optimizing the hyperparameters.
- Relate to the ANN model settings, the hyperparameters comprising the number of hidden layers at 3, the number of neurons at 14, training function at Bayesian regularization, layer function at logsig, hidden function at purelin, learning rate at 0.001 and Momentum mean at 0.004 show the highest accurate ANN model at various training set size.
- Relate to the ANN model convergence at different training set sizes, the sample size of 2048 shows the highest accurate model prediction, where the $C.V$ criterion does not get below 5.3% for all model outputs at an affordable computational time of 8.9×10^3 sec.

Following the work objective in examining the effect of including the SST geometry and its construction material in enhancing the SDHS optimality when introduced at different urban community sizes. The following summarizes the key findings related to the MOO problem output under the PDV and FDV optimization setting in comparison to conventional heating systems using natural gas:

- The calculated Min. cost-optimal solutions demonstrate a progressive improvement in the economic and environment benefits for deploying SDHS

instead of the natural gas boilers with the increment in the community sizes where the NPC is improved by 22%, 26.7%, 34.7% and 53.9% for community size of 10, 25, 50 and 100 buildings, respectively, under the PDV optimization setting. These values further improved with including the SST construction properties in the optimization problem (FDV setting) where the NPC is diminished more by 11.1%, 15.7%, 27.3% and 29.7% for community size of 10, 25, 50 and 100 buildings, respectively compared to its relative scenario under the PDV optimization settings. On the other hand, the extensive environmental solution (Min. impact solution) increases the NPC by 62.1 %, 21.6% for the community size of 10, and 25 buildings, respectively, in comparison to the conventional system using natural gas. While increasing the community size to 50 and 100 buildings, increases the competitively of the SDHS, where the NPC is reduced by 2.13% and 19.7% for 50 and 100 buildings, respectively. With running the optimization problem under the FDV settings, further investment is required compared to the optimization problem under PDV setting where the NPC is increased by 13.4%, 21.6%, 20.8% and 1.84% for the community size of 10, 25, 50 and 100 building, respectively. This increment is due to the considerable reduction in the environmental impact for the FDV optimal solutions compared to its relative solutions under the PDV setting.

- In terms of the environmental benefits for deploying SDHS at different urban community sizes, the RPC at the Min. cost-optimal solution is reduced by 79.4%, 79.5%, 79.6%, and 79.7% for the community size of 10, 25, 50, and 100 buildings, respectively under the PDV setting in comparison to the natural gas boilers. Under the FDV optimization setting, a progressive improvement in the RPC is indicated with increasing the community size where the RPC is diminished more by 0.27%, 39.07%, 43%, and 47.7% for community size of 10, 25, 50 and 100 building compared to its relative solution under PDV setting. Moreover, with the movement toward an environmental solution, the improvement in the RPC is increased, and it achieved 88% in the community size of 100 building under the PDV setting, this improvement can be more extensive under the FDV setting where it reduced up 27.3% compared to its relative solution under the PDV setting.
- The effect of including the SST material properties in the optimization problem is reflected in the economic and environmental payback period where the EPBP at the Min. cost optimal-solution is reduced from 33.3 years at community size of 10 to 13.7 years at the community size of 100 buildings under the FDV setting. While the GPBP is only around 4 years for the Min. impact solutions at different community sizes.
- Aligning with tracing the technical failure of the SST in the optimization framework, the optimal solutions under the FDV settings show an extensive

improvement in the SST heat loss. This improvement is increased with the increment in the environmental damage limits, and it varies between 18.5 to 6.9 kWh/m^3 for community sizes 10 and 100 buildings. This reduction in the heat losses is reflected in the SST efficiency where all optimal solution at different community sizes never falls below 69.5% in the Min. cost-optimal solution, and it extends up to 90.5% at the Min. impact-optimal solution at community size of 100 building. Furthermore, the yearly solar fraction never falls below 82.1% for the investigated community sizes, and it expands to almost 100% in the high environmental damage limits scenarios.

- Finally, the GSA based on the BACCO analysis reveals that the variation in the optimal SDHS cost and its relative impact is due to the initial investment cost of the SST and its relevant construction materials in addition to the annual natural gas inflation rate. In contrast, the rest of the uncertain parameters have a limited influence.

In the real application of designing the SDHS, the present methodology can be beneficial to obtain the optimal sizing of the renewable energy equipment with consideration for the construction properties of the SST, and it initiates values of 1.1 ± 0.1 m^2/MWh/a and 15 ± 1 m^3/MWh/a for the solar collector field area and the SST volume, respectively at different community sizes. Furthermore, the proposed framework provokes the superiority of using the UHPC in the construction of SST and FG for insulation. These guiding can serve all project stakeholders to participate in the early design phases or developing business models for the SDHS.

The proposed framework can provide a good starting point to cover the drawbacks associated with the surrogate modeling technique and solve the enormous computational expenses of the heuristics optimization approach. Moreover, it is an effective tool to evaluate the techno-economic performance of the SDHS as well its environmental benefits with consideration for the market fluctuation regarding the investment cost and the energy carriers. Furthermore, it can assist in proposing the SDHS as a competitive solution instead of the conventional heating systems, and subsequently, it can promote a clear statement regarding the new clean energy for all Europeans packages.

III.7 Acknowledgments

The work is funded by the Spanish government RTI2018-093849-B-C31 and RTI2018-093849-B-C33. The authors would like to thank the Catalan Government for the quality accreditation given to their research group (GREiA - 2017 SGR 1537, AGACAPE - 2017 SGR 1409). GREiA is a certified agent TECNIO in the category of technology developers from the Government of Catalonia. This work is partially supported by ICREA under the ICREA Academia programme. This work is partially funded by the Ministerio de Ciencia, Innovación y Universidades - Agencia Estatal de Investigación (AEI) (RED2018-102431-T). This project has received funding from the

European Union's Horizon 2020 research and innovation programme under the Marie Skłodowska-Curie grant agreement No. 713679 and from the Universitat Rovira i Virgili (URV).

III.8 Nomenclature

A_{COL}	total aperture area of solar collectors (m^2/MWh/a)
β_{COL}	Inclination angle of the solar collectors (º)
C_C	total initial capital cost (€)
C_O	total discounted operational cost (€)
C_R	total discounted replacement cost (€)
CAP_k	design variable of equipment unit k
$CEPCI^{year\ A}$	Chemical engineering plant cost index in the base year
$CEPCI^{year\ B}$	Chemical Engineering Plant Cost Index in the installation year
Con_{SST}	purchase cost of the construction material of the seasonal storage tank (€)
C_M	annual cost of equipment unit k (€)
C_P	annual operational cost of a pump (€)
c_p	specific heat capacity (kJ/kg. k)
c_e	electricity price (€)
c_f	natural gas price (€)
$C.V$	coefficient of variation (%)
d	annual discount rate (%)
d_{Roof}	insulation material thickness for the seasonal storage tank roof (m)
d_{Wall}	insulation material thickness for the seasonal storage tank wall (m)
d_{Gnd}	insulation material thickness for the seasonal storage tank ground (m)
DAM_d	indicator result for damage category d
FBM_k	bare module factor of equipment unit k
FC_{AUX}	contribution of the auxiliary heater as a percentage of the maximum heating load (%)
$f_c(x)$	original objective function [NPC(x) or RCP(x)]
HDR	seasonal storage tank aspect ratio (m/m)
HDR_{DHWT}	domestic hot water storage aspect ratio (m/m)
i	annual inflation rate (%)

i_f	annual inflation rate of natural gas (%)
i_e	annual inflation rate of electricity (%)
Ins_{SST}	purchase cost of the insulation materials of the seasonal storage tank (€)
k	number of regressors
$\dot{m}$	mass flowrate of the recirculating water pumps (kg/s)
n	sample size
N_{COL}	number of solar collectors in series
NPC	net present cost (€/MWh)
PEC_k	purchase cost of equipment unit k (€)
PWF_n	present worth factor of periodic future cash flows (-)
PVF_n	present value factor of single future cash flow at the beginning of n^{th} time period (-)
$\dot{Q}_{SOL}$	useful energy rate received by the solar collector field (MW)
$\dot{Q}_{SST\ loss}$	heat loss rate through the seasonal storage tank (MW)
$\dot{Q}_{DHW\ loss}$	heat loss rate through the domestic hot water storage tank (MW)
$\dot{Q}_{HE}$	heat transfer rate through the heat exchanger (MW)
$\dot{Q}_{AUX}$	duty of auxiliary heater (MW)
$Q_{SH\ load}$	total space heating demand (MWh)
$Q_{DHW\ load}$	total domestic hot water demand (MWh)
$Q_{SST\ loss}$	total energy losses through the seasonal storage tank (MWh)
$SMAPE$	symmetric mean absolute percentage error
R^2	coefficient of determination
R^2-adj	adjusted coefficient of determination
RCP	ReCiPe 2016 aggregated impact factor (Pt/MWh)
$S.F_{DHW}$	annual solar fraction for the DHW distribution circuit (%)
$S.F_{SH}$	annual solar fraction for the SH distribution circuit (%)
U_{Roof}	The heat loss coefficient of the seasonal storage tank roof ($W/m^2.K$)
U_{Wall}	The heat loss coefficient of the seasonal storage tank wall ($W/m^2.K$)
U_{Gnd}	The heat loss coefficient of the seasonal storage tank ground ($W/m^2.K$)
$U_{Overall}$	The overall heat loss coefficient of the seasonal storage tank ($W/m^2.K$)
V_{DHWT}	volume of the domestic hot water tank (m^3/MWh/a)

V_{SST}	volume of the seasonal storage tank (m^3/MWh/a)
$y_{predict,i}$	predicted value
$y_{data,i}$	actual value

Greek symbols

α_{CF}	factor of contingency charges and fees
α_k	purchase cost coefficient of equipment unit k
β_k	purchase cost exponent of equipment unit k
η_{COL}	solar collector field efficiency (%)
η_{DHWT}	domestic hot water storage tank efficiency (%)
η_{SST}	seasonal storage tank efficiency (%)
λ_{con}	construction material thermal conductivity of the seasonal storage tank (W/m. K).
λ_{ins}	insulation material thermal conductivity for the seasonal storage tank roof and wall (W/m. K).
$\lambda_{ins\ gnd}$	insulation material thermal conductivity for the seasonal storage tank ground (W/m. K).
δ_d	normalization factor for damage category d
ε_d	weighting factor for damage category d
ΔT_{SST}	temperature difference between the extracted and replaced water inside the space heating circuit.

Abbreviations

ANN	Artificial Neural Network
AUX	auxiliary heater fueled by natural gas
COL	solar collector field
DHW	domestic hot water
DHWT	domestic hot water storage
DHWcalc	Domestic Hot Water profiles generator software
EPBP	economic payback period
GHG	greenhouse gas
GPBP	greenhouse gas payback period
GSA	global sensitivity analysis
FG	foam glass gravel
HE	heat exchanger
HPC	high-performance concrete

LCA	life cycle assessment
LCC	life cycle cost
LSA	local sensitivity analysis
MILP	mixed-integer linear programming
MINLP	mixed Integer Nonlinear Programming
MOO	multi-objective optimization
MOGA	multi-objective genetic algorithm
MW	mineral wool
NC	normal concrete
P	centrifugal pump
SDHS	solar assisted district heating system
SH	space heating
SST	seasonal storage tank
TES	thermal energy storage
TRNSYS	transient system simulation program
UHPC	ultra-high performance concrete
XPS	extruded polystyrene

Indices

d	damage category
i	elementary factor
k	equipment unit

III.9 References

[1] International Renewable Energy Agency (IRENA). Global Energy Transformation: A Roadmap to 2050. 2018.

[2] European Commission. Clean energy for all Europeans. Luxembourg: 2019. doi:10.2833/9937.

[3] European Commission. Communication from the commission to the European Parliament and the Council. Brussels: 2016.

[4] European Energy Agency. Final energy consumption by sector and fuel. 2015. doi:CSI 027/ENER 016.

[5] Balaras CA, Gaglia AG, Georgopoulou E, Mirasgedis S, Sarafidis Y, Lalas DP. European residential buildings and empirical assessment of the Hellenic building stock, energy consumption, emissions and potential energy savings. Build Environ 2007;42:1298–314. doi:10.1016/j.buildenv.2005.11.001.

[6] Eurostat. Final energy consumption in the residential sector by type of end-use 2016. https://ec.europa.eu/eurostat/statistics-explained/index.php?title=File:Final_energy_consumption_in_the_residential_sector_by_type_of_end-use,_EU-28,_2015.png&oldid=340063 (accessed June 27, 2019).

[7] European Environment Agency. Annual European Union greenhouse gas inventory 1990–2017 and inventory report 2019. 2019. doi:10.2800/41819.

[8] European Commission (Directive 2010/31/ EC). On the Energy Performance of Buildings. 2012.

[9] Antoniadis CN, Martinopoulos G. Optimization of a building integrated solar thermal system with seasonal storage using TRNSYS. Renew Energy 2019;137:56–66. doi:10.1016/j.renene.2018.03.074.

[10] Rad FM, Fung AS. Solar community heating and cooling system with borehole thermal energy storage - Review of systems. Renew Sustain Energy Rev 2016;60:1550–61. doi:10.1016/j.rser.2016.03.025.

[11] Carrilho da Graça G, Augusto A, Lerer MM. Solar powered net zero energy houses for southern Europe: Feasibility study. Sol Energy 2012;86:634–46. doi:10.1016/j.solener.2011.11.008.

[12] Gao L, Zhao J, Tang Z. A Review on Borehole Seasonal Solar Thermal Energy Storage. Energy Procedia 2015;70:209–18. doi:10.1016/j.egypro.2015.02.117.

[13] Cabeza LF, Martorell I, Miró L, Fernández AI, Barreneche C. Introduction to

thermal energy storage (TES) systems. Woodhead Publishing Limited; 2014. doi:10.1533/9781782420965.1.

[14] Dahash A, Ochs F, Janetti MB, Streicher W. Advances in seasonal thermal energy storage for solar district heating applications: A critical review on large-scale hot-water tank and pit thermal energy storage systems. Appl Energy 2019;239:296–315. doi:10.1016/j.apenergy.2019.01.189.

[15] Li Q, Tehrani SSM, Taylor RA. Techno-economic analysis of a concentrating solar collector with built-in shell and tube latent heat thermal energy storage. Energy 2017;121:220–37. doi:10.1016/j.energy.2017.01.023.

[16] International Renewable Energy Agency (IRENA). The Energy Technology Systems Analysis Programme (ESTAP): Technology Brief E17. 2013.

[17] Reed AL, Novelli AP, Doran KL, Ge S, Lu N, McCartney JS. Solar district heating with underground thermal energy storage: Pathways to commercial viability in North America. Renew Energy 2018;126:1–13. doi:10.1016/j.renene.2018.03.019.

[18] Xu J, Wang RZ, Li Y. A review of available technologies for seasonal thermal energy storage. Sol Energy 2014;103:610–38. doi:10.1016/j.solener.2013.06.006.

[19] Reuss M. Advances in Thermal Energy Storage Systems: Methods and Applications. United Kingdom: Woodhead Publishing Limited; 2015.

[20] Bankston CA. The status and potential of central solar heating plants with seasonal storage: An international Report. Adv. Sol. Energy, New York: Plenum Press; 1988, p. 352–444.

[21] Tian Z, Perers B, Furbo S, Fan J. Thermo-economic optimization of a hybrid solar district heating plant with flat plate collectors and parabolic trough collectors in series. Energy Convers Manag 2018;165:92–101. doi:10.1016/j.enconman.2018.03.034.

[22] Bauer D, Marx R, Nußbicker-Lux J, Ochs F, Heidemann W, Müller-Steinhagen H. German central solar heating plants with seasonal heat storage. Sol Energy 2010;84:612–23. doi:10.1016/j.solener.2009.05.013.

[23] Rehman H ur, Hirvonen J, Sirén K. Influence of technical failures on the performance of an optimized community-size solar heating system in Nordic conditions. J Clean Prod 2018;175:624–40. doi:10.1016/j.jclepro.2017.12.088.

[24] Urbaneck T, Oppelt T, Platzer B, Frey H, Uhlig U, Göschel T, et al. Solar District Heating in East Germany - Transformation in a Cogeneration

Dominated City. Energy Procedia 2015;70:587–94. doi:10.1016/j.egypro.2015.02.164.

[25] BINE Information Service. Solar-assisted District Heating [Online]. 2000.

[26] Sibbitt B, McClenahan D, Djebbar R, Thornton J, Wong B, Carriere J, et al. The performance of a high solar fraction seasonal storage district heating system - Five years of operation. Energy Procedia 2012;30:856–65. doi:10.1016/j.egypro.2012.11.097.

[27] Sibbit B, McClenahan D, Djebbar R, Paget K. GroundBreaking Solar. vol. Summer. Canada: 2015.

[28] Weissmann C, Hong T, Graubner CA. Analysis of heating load diversity in German residential districts and implications for the application in district heating systems. Energy Build 2017;139:302–13. doi:10.1016/j.enbuild.2016.12.096.

[29] Yang Y, Zhang S, Xiao Y. Optimal design of distributed energy resource systems coupled withenergy distribution networks. Energy 2015;85:433–48. doi:10.1016/j.energy.2015.03.101.

[30] Gonzalez-Garay A, Guillen-Gosalbez G. SUSCAPE: A framework for the optimal design of SUStainable ChemicAl ProcEsses incorporating data envelopment analysis. Chem Eng Res Des 2018;137:246–64. doi:10.1016/j.cherd.2018.07.009.

[31] Klatt KU, Marquardt W. Perspectives for process systems engineering-Personal views from academia and industry. Comput Chem Eng 2009;33:536–50. doi:10.1016/j.compchemeng.2008.09.002.

[32] Buoro D, Pinamonti P, Reini M. Optimization of a Distributed Cogeneration System with solar district heating. Appl Energy 2014;124:298–308. doi:10.1016/j.apenergy.2014.02.062.

[33] Welsch B, Göllner-Völker L, Schulte DO, Bär K, Sass I, Schebek L. Environmental and economic assessment of borehole thermal energy storage in district heating systems. Appl Energy 2018;216:73–90. doi:10.1016/j.apenergy.2018.02.011.

[34] Skiborowski M, Rautenberg M, Marquardt W. A Hybrid Evolutionary-Deterministic Optimization Approach for Conceptual Design. Ind Eng Chem Res 2015;54:10054–72. doi:10.1021/acs.iecr.5b01995.

[35] Rehman H ur, Hirvonen J, Sirén K. Performance comparison between optimized design of a centralized and semi-decentralized community size solar district heating system. Appl Energy 2018;229:1072–94.

doi:10.1016/j.apenergy.2018.08.064.

[36] Tulus V, Boer D, Cabeza LF, Jiménez L, Guillén-Gosálbez G. Enhanced thermal energy supply via central solar heating plants with seasonal storage: A multi-objective optimization approach. Appl Energy 2016;181:549–61. doi:10.1016/j.apenergy.2016.08.037.

[37] Bava F, Furbo S. Development and validation of a detailed TRNSYS-Matlab model for large solar collector fields for district heating applications. Energy 2017;135:698–708. doi:10.1016/j.energy.2017.06.146.

[38] Tulus V, Abokersh MH, Cabeza LF, Vallès M, Jiménez L, Boer D. Economic and environmental potential for solar assisted central heating plants in the EU residential sector: Contribution to the 2030 climate and energy EU agenda. Appl Energy 2019. doi:10.1016/j.apenergy.2018.11.094.

[39] Ciampi G, Rosato A, Sibilio S. Thermo-economic sensitivity analysis by dynamic simulations of a small Italian solar district heating system with a seasonal borehole thermal energy storage. Energy 2018;143:757–71. doi:10.1016/j.energy.2017.11.029.

[40] Saltelli A, Annoni P. How to avoid a perfunctory sensitivity analysis. Environ Model Softw 2010;25:1508–17. doi:10.1016/j.envsoft.2010.04.012.

[41] Mavromatidis G, Orehounig K, Carmeliet J. Uncertainty and global sensitivity analysis for the optimal design of distributed energy systems. Appl Energy 2018;214:219–38. doi:10.1016/j.apenergy.2018.01.062.

[42] Bornatico R, Hüssy J, Witzig A, Guzzella L. Surrogate modeling for the fast optimization of energy systems. Energy 2013;57:653–62. doi:10.1016/j.energy.2013.05.044.

[43] Wong SL, Wan KKW, Lam TNT. Artificial neural networks for energy analysis of office buildings with daylighting. Appl Energy 2010;87:551–7. doi:10.1016/j.apenergy.2009.06.028.

[44] Yaïci W, Entchev E. Performance prediction of a solar thermal energy system using artificial neural networks. Appl Therm Eng 2014;73:1348–59. doi:10.1016/j.applthermaleng.2014.07.040.

[45] Xia L, Ma Z, Kokogiannakis G, Wang Z, Wang S. A model-based design optimization strategy for ground source heat pump systems with integrated photovoltaic thermal collectors. Appl Energy 2018;214:178–90. doi:10.1016/j.apenergy.2018.01.067.

[46] Wang Z, Srinivasan RS. A review of artificial intelligence based building energy use prediction: Contrasting the capabilities of single and ensemble

prediction models. Renew Sustain Energy Rev 2017;75:796–808. doi:10.1016/j.rser.2016.10.079.

[47] Bauer D, Marx R, Drück H. Solar district heating for the built environment technology and future trends within the european project Einstein. Energy Procedia 2014;57:2716–24. doi:10.1016/j.egypro.2014.10.303.

[48] Hirvonen J, ur Rehman H, Sirén K. Techno-economic optimization and analysis of a high latitude solar district heating system with seasonal storage, considering different community sizes. Sol Energy 2018;162:472–88. doi:10.1016/j.solener.2018.01.052.

[49] Klein SA et al. TRNSYS Version. 18, Solar Energy Laboratory, University of Wisconsin-Madison, Website: <http://sel.me.wisc.edu/ trnsys> 2004.

[50] Guillén-gosálbez G, Grossmann I. A global optimization strategy for the environmentally conscious design of chemical supply chains under uncertainty in the damage assessment model 2010;34:42–58. doi:10.1016/j.compchemeng.2009.09.003.

[51] De Guadalfajara M, Lozano MA, Serra LM. Evaluation of the potential of large solar heating plants in Spain. Energy Procedia 2012;30:839–48. doi:10.1016/j.egypro.2012.11.095.

[52] Østergård T, Jensen RL, Maagaard SE. A comparison of six metamodeling techniques applied to building performance simulations. Appl Energy 2018;211:89–103. doi:10.1016/j.apenergy.2017.10.102.

[53] Bhosekar A, Ierapetritou M. Advances in surrogate based modeling, feasibility analysis, and optimization: A review. Comput Chem Eng 2018;108:250–67. doi:10.1016/j.compchemeng.2017.09.017.

[54] Wang GG, Shan S. Review of Metamodeling Techniques in Support of Engineering Design Optimization. J Mech Des 2007;129:370. doi:10.1115/1.2429697.

[55] Kucherenko S, Albrecht D, Saltelli A. Exploring multi-dimensional spaces: a Comparison of Latin Hypercube and Quasi Monte Carlo Sampling Techniques. 8th IMACS Semin. Monte Carlo methods, 2015, p. 1–32. doi:10.1016/j.ress.2017. 04.003.

[56] Robinson C, Dilkina B, Hubbs J, Zhang W, Guhathakurta S, Brown MA, et al. Machine learning approaches for estimating commercial building energy consumption. Appl Energy 2017;208:889–904. doi:10.1016/j.apenergy.2017.09.060.

[57] Carpenter J, Woodbury KA, O'Neill Z. Using change-point and Gaussian

process models to create baseline energy models in industrial facilities: A comparison. Appl Energy 2018;213:415–25. doi:10.1016/j.apenergy.2018.01.043.

[58] Huang CL, Chen MC, Wang CJ. Credit scoring with a data mining approach based on support vector machines. Expert Syst Appl 2007;33:847–56. doi:10.1016/j.eswa.2006.07.007.

[59] Lin SW, Ying KC, Chen SC, Lee ZJ. Particle swarm optimization for parameter determination and feature selection of support vector machines. Expert Syst Appl 2008;35:1817–24. doi:10.1016/j.eswa.2007.08.088.

[60] Xia Y, Liu C, Li YY, Liu N. A boosted decision tree approach using Bayesian hyper-parameter optimization for credit scoring. Expert Syst Appl 2017;78:225–41. doi:10.1016/j.eswa.2017.02.017.

[61] Snoek J, Larochelle H. Practical Bayesian Optimization of Machine Learning Algorithms. Adv. neural Inf. Process. Syst., 2012, p. 2951–2959. doi:10.1016/S2468-2667(17)30214-1.

[62] B MW, Runge-borchert G, Raatz A. Optimization of Neural Network Hyperparameters for Modeling of Soft Pneumatic Actuators. New Trends Med. Serv. Robot., vol. 48, Springer International Publishing; 2019, p. 199–206. doi:10.1007/978-3-319-59972-4.

[63] Bergstra J, Yamins D, Cox DD. Hyperopt : A Python Library for Optimizing the Hyperparameters of Machine Learning Algorithms. Proc. 12th Python Sci. Conf., 2013, p. 13–20.

[64] Jones B, Nachtsheim CJ, Jones B. A class of screening designs robust to active second-order effects a class of three-level designs for definitive screening in the presence of second-order effects. J Qual Technol 2011;43:1–15. doi:10.1007/978-3-7908-2410-0.

[65] Montgomery DC. Design and Analysis of Experiments, Eighth Edition. John Wiley & Sons, Inc.; 2013.

[66] Amasyali K, El-gohary NM. A review of data-driven building energy consumption prediction studies 2018;81:1192–205. doi:10.1016/j.rser.2017.04.095.

[67] Guadalfajara M, Lozano MA, Serra LM. Analysis of Large Thermal Energy Storage for Solar District Heating. Eurotherm Semin. #99 Adv. Adv. Therm. Energy Storage, 2014. doi:10.13140/2.1.3857.6008.

[68] Chung M, Park J, Yoon H. SIMULATION OF A CENTRAL SOLAR HEATING SYSTEM WITH SEASONAL STORAGE IN KOREA. Sol Energy

1998;64:163–78.

[69] Hobbi A, Siddiqui K. Optimal design of a forced circulation solar water heating system for a residential unit in cold climate using TRNSYS. Sol Energy 2009;83:700–14. doi:10.1016/j.solener.2008.10.018.

[70] Hui L, Edem NTK, Nolwenn LP, Lingai L. Evaluation of a seasonal storage system of solar energy for house heating using different absorption couples. Energy Convers Manag 2011;52:2427–36. doi:10.1016/j.enconman.2010.12.049.

[71] Hang Y, Qu M, Ukkusuri S. Optimizing the design of a solar cooling system using central composite design techniques. Energy Build 2011;43:988–94. doi:10.1016/j.enbuild.2010.12.024.

[72] Allouhi A, Agrouaz Y, Benzakour Amine M, Rehman S, Buker MS, Kousksou T, et al. Design optimization of a multi-temperature solar thermal heating system for an industrial process. Appl Energy 2017;206:382–92. doi:10.1016/j.apenergy.2017.08.196.

[73] Kalogirou SA. Solar energy engineering: processes and systems. 1st Ed. Academic Press; 2009. doi:10.1016/B978-0-12-374501-9.00014-5.

[74] Ximenes A, Barreneche C, Fernández AI, Cabeza LF. Life cycle costing as a bottom line for the life cycle sustainability assessment in the solar energy sector : A review. Sol Energy 2018:0–1. doi:10.1016/j.solener.2018.04.011.

[75] Gluch P, Baumann H. The life cycle costing (LCC) approach: A conceptual discussion of its usefulness for environmental decision-making. Build Environ 2004;39:571–80. doi:10.1016/j.buildenv.2003.10.008.

[76] Vikas K, Cheshta K, Savita N, Baredar P. Prefeasibility Assessment of a Tidal Energy System. Tidal Energy Syst. Des. Optim. Control, Elsevier; 2019, p. 115–88. doi:10.1016/B978-0-12-814881-5.00003-X.

[77] Guillén-Gosálbez G, Caballero JA, Jiménez L. Application of Life Cycle Assessment to the Structural Optimization of Process Flowsheets. Ind Eng Chem Res 2008;47:777–89. doi:10.1016/S1570-7946(07)80218-5.

[78] Nemerow NL, Agardy FJ, Sullivan P, Salvato JA. ENVIRONMENTAL ENGINEERING: Environmental Health and Safety for Municipal Infrastructure, Land Use and Planning, and Industry. 6th ed. John Wiley & Sons, Inc; 2009.

[79] ISO/TC 207/SC 5. ISO 14040:2006 Environmental management — Life cycle assessment — Principles and framework 2006.

[80] International Organization for Standardization (ISO). ISO 14041: Environmental Management - Life Cycle Assessment: Goal and Scope Definition and Inventory Analysis. 1997.

[81] International Organization for Standardization (ISO). ISO 14042:Environmental management - Life cycle assessment - Life cycle impact. 2000.

[82] Ecoinvent. Eco invent 2017. https://www.ecoinvent.org/home.html (accessed March 12, 2018).

[83] JRC European commission (JRC-IES). ILCD Handbook: Recommendations for Life Cycle Impact Assessment in the European context. 1st editio. Luxemburg: Office of the European Union; 2011. doi:10.278/33030.

[84] Li DHW, Lam TNT, Chan WWH, Mak AHL. Energy and cost analysis of semi-transparent photovoltaic in office buildings. Appl Energy 2009;86:722–9. doi:10.1016/j.apenergy.2008.08.009.

[85] Lu L, Yang HX. Environmental payback time analysis of a roof-mounted building-integrated photovoltaic (BIPV) system in Hong Kong 2010;87:3625–31. doi:10.1016/j.apenergy.2010.06.011.

[86] Solites. Guideline for Seasonal Thermal Energy Storage Systems in the Built Environment. Stuttgart: 2016.

[87] Ehrgott M. Multicriteria optimization. Heidelberg: Springer; 2005.

[88] Deb K. Multiobjective Optimization Using Evolutionary Algorithms. New York, NY: John Wiley & Sons, Inc; 2001.

[89] Konak A, Coit DW, Smith AE. Multi-objective optimization using genetic algorithms : A tutorial. Reliab Eng Syst Saf 2006;91:992–1007. doi:10.1016/j.ress.2005.11.018.

[90] Dalenbäck J-OG. LARGE-SCALE SOLAR HEATING. 1999.

[91] Rehman H ur, Hirvonen J, Sirén K. A long-term performance analysis of three different configurations for community-sized solar heating systems in high latitudes. Renew Energy 2017;113:479–93. doi:10.1016/j.renene.2017.06.017.

[92] Li X, Liu M, Duanmu L, Ji Y. The Optimization of Solar Heating System with Seasonal Storage Based on a Real Project. Procedia Eng 2015;121:1341–8. doi:10.1016/j.proeng.2015.09.017.

[93] Argiriouf A. CSHPSS SYSTEMS IN GREECE : TEST OF SIMULATION AND ANALYSIS OF TYPICAL SYSTEMS SOFTWARE 1997;60:159–70.

[94] Tao T, Zhang F, Zhang W, Wan P, Shen X, Li H. Low cost and marketable operational experiences for a solar heating system with seasonal thermal energy storage (SHSSTES) in Hebei. Energy Procedia 2015;70:267–74. doi:10.1016/j.egypro.2015.02.123.

[95] Shahedan NF, Mustafa M, Bakri A. Review on thermal insulation performance in various type of concrete. AIP Conf. Proc., AIP Publishing; 2017, p. 1–6. doi:10.1063/1.4981868.

[96] Reineck K, Prof A, Lichtenfels A, Engineers L. Concrete Hot Water Tanks for Solar Energy Storage. 2004.

[97] Reineck K, Greiner S, Reinhardt H. Dichte Heißwasser-Wärmespeicher aus ultrahochfestem Faserfeinkornbeton. Stuttgart: 2004.

[98] Oliveti G, Arcuri N. Prototype experimental plant for the interseasonal storage of solar energy for the winter heating of buildings: Description of plant and its functions. Sol Energy 1995;54:85–97.

[99] Hesaraki A, Halilovic A, Holmberg S. Low-temperature heat emission combined with seasonal thermal storage and heat pump. Sol ENERGY 2015;119:122–33. doi:10.1016/j.solener.2015.06.046.

[100] K. Deb, A. Pratap SA and TM. fast and elitist multiobjective genetic algorithm: NSGA-II. IEEE Trans Evol Comput 2002;6:182–97. doi:10.1109/4235.996017.

[101] Hassam ur Rehman; Janne Hirvonen; Kai Sirén. Performance comparison between optimized design of a centralized and semi-decentralized community size solar district heating system. Appl Energy 2018;229:1072–94. doi:https://doi.org/10.1016/j.apenergy.2018.08.064.

[102] Alajmi A, Wright J. Selecting the most efficient genetic algorithm sets in solving unconstrained building optimization problem. Int J Sustain Built Environ 2014;3:18–26. doi:10.1016/j.ijsbe.2014.07.003.

[103] Kennedy MC, O'Hagan A. Bayesian calibration of computer models. J R Stat Soc Ser B (Statistical Methodol 2001;63:425–64. doi:10.1111/1467-9868.00294.

[104] Uusitalo L, Lehikoinen A, Helle I, Myrberg K. An overview of methods to evaluate uncertainty of deterministic models in decision support. Environ Model Softw 2015;63:24–31. doi:10.1016/j.envsoft.2014.09.017.

[105] Petropoulos G, Wooster MJ, Carlson TN, Kennedy MC, Scholze M. A global Bayesian sensitivity analysis of the 1d SimSphere soil-vegetation-atmospheric transfer (SVAT) model using Gaussian model emulation. Ecol

Modell 2009;220:2427–40. doi:10.1016/j.ecolmodel.2009.06.006.

[106] Institute for Energy Diversification and Saving - IDAE. Análisis del consumo energético del sector residencial en España. INFORME FINAL; 2011.

[107] Guadalfajara M. Evaluación de centrales solares térmicas con acumulación estacional para el sector residencial en España. 2013. doi:10.1017/CBO9781107415324.004.

[108] Pahud D. Central solar heating plants with seasonal duct storage and short-term water storage: Design guidelines obtained by dynamic system simulations. Sol Energy 2000;69:495–509. doi:10.1016/S0038-092X(00)00119-5.

[109] United Nations Environment Programme, Solar Thermal Energy Technology Fact Sheet. 2014.

[110] U.S. Department of Energy. EnergyPlus. Energy Simulation Software: Weather Data n.d. 2015.

[111] Trimble. SketchUp 2012. http://www.sketchup.com.

[112] Jordan U, Vajen K. DHWcalc: program to generate domestic hot water profiles with statistical means for user defined conditions. Proc. ISES Sol. World Congr., Orlando (US): n.d., p. 8–12.

[113] European Commision. EuroStat 2018. http://ec.europa.eu/eurostat/web/energy/data/database (accessed March 12, 2018).

[114] Braungardt S, Eichhammer W, Elsland R, Fleiter T, Klobasa M, Krail M, et al. Study evaluating the current energy efficiency policy framework in the EU and providing orientation on policy options for realising the cost-effective energy-efficiency/saving potential until 2020 and beyond. 2014.

[115] Ellehauge K PT. Solar heat storages in district heating networks. Energinet.dk, PREHEAT project no. 2006-2-6750. 2007.

[116] Schmidt T MD. Status of solar thermal seasonal storage in Germany. 2009.

[117] Calise F, Dentice d'Accadia M, Palombo A. Transient analysis and energy optimization of solar heating and cooling systems in various configurations. Sol Energy 2010;84:432–49. doi:10.1016/j.solener.2010.01.001.

[118] austrotherm. General price list. 2017. doi:10.5962/bhl.title.138707.

[119] Specialist Insulation Supplies Ltd. Prices list. 2018.

[120] GLAPOR-Schaumglasprodukte. GLAPOR PRICE LIST. Belgium: 2014.

[121] Aven T. Interpretations of alternative uncertainty representations in a reliability and risk analysis context. Reliab Eng Syst Saf 2011;96:353–60. doi:10.1016/j.ress.2010.11.004.

[122] Burhenne S, Tsvetkova O, Jacob D, Henze GP, Wagner A. Uncertainty quantification for combined building performance and cost-benefit analyses. Build Environ 2013;62:143–54. doi:10.1016/j.buildenv.2013.01.013.

[123] Mirkhani S, Saboohi Y. Stochastic modeling of the energy supply system with uncertain fuel price - A case of emerging technologies for distributed power generation. Appl Energy 2012;93:668–74. doi:10.1016/j.apenergy.2011.12.099.

[124] Mavrotas G, Florios K, Vlachou D. Energy planning of a hospital using Mathematical Programming and Monte Carlo simulation for dealing with uncertainty in the economic parameters. Energy Convers Manag 2010;51:722–31. doi:10.1016/j.enconman.2009.10.029.

[125] Bustos F, Toledo A, Contreras J, Fuentes A. Sensitivity analysis of a photovoltaic solar plant in Chile. Renew Energy 2016;87:145–53. doi:10.1016/j.renene.2015.09.070.

[126] Bauer D, Marx R, Nußbicker-Lux J. German central solar heating plants with seasonal heat storage. Sol Energy 2010;84:612–23. doi:10.1016/j.solener.2009.05.013.

Chapter IV

Sustainable integration of heat pump in SDHS

IV. Sustainable integration of heat pump in SDHS

Flexible Heat Pump Integration to Improve Sustainable Transition Toward 4th Generation District Heating

Mohamed Hany Abokersh [a], Kangkana Saikia [a], Luisa F. Cabeza [b], Dieter Boer [a], Manel Vallès [a] *

[a] Departament d'Enginyeria Mecànica, Universitat Rovira i Virgili, Av. Països Catalans 26, 43007 Tarragona, Spain

[b] GREiA Research Group, Universitat de Lleida, Pere de Cabrera s/n, 25001 Lleida, Spain

* *Corresponding author: manel.valles@urv.cat*

*E-mail addresses: mohamed.abokersh@urv.cat (M.H. Abokersh),i*kangkana.saikia@gmail.com *(K. Saikia),* dieter.boer@urv.cat *(Dieter Boer), luisaf.cabeza@udl.cat (L.F. Cabeza)*

Keywords: Solar assist district heating system; Heat pump; Artificial Neural Network; Multi-objective optimization; Key performance indicators; 4th generation district heating

IV.1 Introduction

Energy infrastructure around the world is undergoing a transitional period to accommodate the highest possible share of renewable energy generation in the existing grid and provide reliable service to meet the demand in various sectors. With the revised EU directive on renewable energy, the European countries are focusing on delivering 32% of the total energy from renewable energy sources, such as wind, solar, and biomass, by the year 2030 [1]. In efforts to push this energy transition, the EU has also decided that beginning in 2021, the proportion of renewables in the heating/cooling sector will rise by 1.3% points annually. In this context, district heating (DH) networks have gained a great deal of attention with the possibility of integrating them into the future smart energy system.

The smart energy system concept is a broader definition of the smart grid moving the sole focus from the electrical power grid towards the integration of different energy sectors such as electricity, heating, cooling, industry, buildings, and transportation to achieve sustainable energy solutions [2]. In such a future energy vision, the district heating systems can play a crucial role by allowing the use of industrial waste heat and local renewables such as solar energy in combination with large scale thermal energy storage to transform into a low-temperature thermal grid which is also known as 4th generation district heating (4GDH) [3–6]. The 4GDH system has emerged as a promising technology because conventional high-temperature DH systems experience substantial heat losses and high installation costs [7] as well as the possibility of losing profit when the heating demand is decreased due to the renovation of existing buildings [8]. The key characteristic of 4GDH is considered to be the ability to deliver heat at a much lower temperature range (50 ~ 60°C) and significantly lowering the return temperature (25 ~ 30°C) [9],[10]. However, the implementation of a 4GDH needs further research in order to address technological and economic obstacles and reform the energy market framework to ensure the quality of service [11].

Different technologies can be combined with DH systems to improve efficiency and energy savings [12]. The large-scale solar thermal district heating plants are among the most interesting solutions that have already become a reality today in countries like Denmark, Sweden, Austria, Germany, Spain, and Greece [13], [14]. Such a system has the edge over the conventional heating system reducing the use of fossil fuels and emissions. Still, it deals with a higher degree of flexibility issues due to the fluctuating nature of solar radiation. The variation in heat load with changing seasons does not match with heat generation by the solar source creating an unfavourable condition for 4GDH [15]. This issue can be resolved by coupling seasonal thermal energy storage (STES) to solar thermal plants where the heat produced can be stored for later use [16]. Despite that, the solar heating system may fail to reach the expected level of solar fraction for seasonal storage (50-100%) and short term storage (10-20%) due to the high heating demand of the building, high return temperature to the storage, and high heat loss from thermal storage [17]. One way to reduce the storage heat loss is to maintain a low temperature inside the storage tank. Such control measures require a supporting device such as back up heat pumps for effective space heating (SH) [18]. With the aid of heat pumps, STES can be discharged to lower temperature levels, collectors under a low-temperature condition can reach higher solar fraction, and the whole system is less prone to fluctuating district heating network return temperature [19]. Heat pumps are also highly efficient when operated in low-temperature DH networks to supply temperatures below 70°C [20]. Therefore, introducing heat pumps into a solar assisted district heating with seasonal storage can be a promising technological intervention to improve the overall system efficiency and transform the existing plants into a 4GDH system [17] [21].

Heat pumps present low CO_2 emissions when used under high-efficiency conditions, in particular, the electrically powered heat pumps with electricity from renewable sources [22]. One way of using electric heat pumps for residential and commercial heating applications is to combine the technology with solar systems, i.e., solar thermal, solar photovoltaic [23], or both thermal and photovoltaic (PV/T) [24]. During recent years, a variety of solar-assisted heat pumps (SAHP) configurations are proposed and analyzed for the water heating application. Standard SAHP concepts such as direct expansion [25] and indirect expansion style [26] along with modified novel design such as SAHP with hybrid solar collectors [27], dual tank SAHP [28] have been investigated to show their feasibility from economy and energy conservation perspective. Concerning the integration of heat pumps into district heating networks, Kim et al. [29] designed a TRNSYS model consisting of a solar thermal system, seasonal storage, high temperature and low-temperature heat pumps which showed significant energy savings when the solar fraction is increased by varying the size of collectors and storage. Østergaard and Andersen [30] in another study assessed the potential of booster heat pumps to provide domestic hot water demand in a low-temperature district heating scheme. Hirvonen et al. [31] examined the influence of community size on the technical as well as the economic performance of a solar assisted district heating and a ground source heat pump for additional heat generation. Another optimization study compared a heat pump integrated centralized solar district heating with a semi-decentralized one and found that the decentralized system outperforms the centralized system in terms of life cycle cost [32]. These studies highlight that heat pumps can add more flexibility to the district heating network either by directly supplying SH and domestic hot water (DHW) load or charging up the storage tank. This allows shifting the use of electricity and reducing natural gas consumption, which leads to improved energy security.

The simulation-optimization studies on solar assisted district heating systems (SDHS) with storage and heat pumps are so far primarily focused on analyzing parameters associated with the solar source, storage technology, and energy demand profile of the community from the techno-economic point of view. However, efforts towards designing the whole SDHS framework to an optimal extent from the sustainability standpoint while fulfilling the targets of next-generation district heating are seldom found [33,34]. More importantly, the possible role that heat pumps can play in a SDHS network to address the issues related to storage heat loss and overall flexibility of the network has not been fully explored. This aspect of heat pump utilization to maintain an efficient low-temperature SDHS network may lead to high initial investment, electricity consumption, and related CO_2 emission. Hence, the optimization of the key design parameters of heat pump integrated SDHS becomes more important. It should consider energy efficiency, economic feasibility, and environmental impact simultaneously to ensure that such a system is walking hand in hand with the sustainable development goal. Nevertheless, such an optimization problem is complex enough to solve and takes more computational resources to take multiple

decision variables into account within the same framework. Therefore, we are introducing a meta-modeling method in this study to minimize computational effort while maintaining high accuracy rates.

The Artificial Neural Network (ANN) is one of the most widely used meta-model techniques for dealing with complex design problems in energy research compared to traditional algorithms when managing a large data set [35], [36]. ANN can find a relation between the input and output variables by studying previously recorded data and reproduce a comprehensive model based on that relationship [37]. In order to demonstrate the applicability of ANN, Esen et al. [38] used the backpropagation learning algorithm to predict the coefficient of performance of a horizontal ground-coupled heat pump system. Xia et al. [39] devised an ANN model using genetic algorithms to perform multi-objective optimization of a SDHS. Another proof of concept was developed by Hirvonen et al. [40], where neural network meta-modeling is used to optimize a solar community to supply the heating demand, and the proposed method provided better solutions compared to genetic algorithms.

This paper aims to analyze the techno-economic performance as well as the environmental impact of different control strategies for integrating heat pumps into SDHS equipped with seasonal thermal energy storage in the context of 4GDH. Emphasis is given mostly on district heating consumption for SH with less focus on DHW consumption. Two types of control strategy are proposed where the heat pump is connected in series with the solar collector. Each control concept is investigated through dynamic simulations in TRNSYS and multi-objective optimization based on an ANN model to determine the optimized combination of key design parameters based on energy performance, economic, and environmental impact. The results are used in a comparison of the seasonal storage enhanced SDHS with and without the inclusion of heat pumps. Furthermore, the study evaluates the performance of the proposed system with the help of key performance indicators (KPI) related to the 4GDH characteristics and key stakeholders for possible market growth and expansion.

Hence, the novelty of the work is to demonstrate the potential of heat pump integration into a community sized SDHS to stabilize its performance and assist in the sustainable transition towards 4GDH. Another novelty of this paper is the development of optimized control strategies for the heat pump operation to enhance the overall flexibility of the SDHS. The presented research, therefore, lays the groundwork for stakeholders of a SDHS with seasonal storage and heat pumps to navigate the next generation district heating transformation.

The structure of the article is as follows: A general outline of the SDHS and its mathematical definition is proposed in section 2. In section 3, both the techno-economic targets and environmental aspects are explained in terms of KPIs based on the stakeholder perspective. The design of an ANN-based optimization strategy is

introduced in section 4. Section 5 discusses the deployment of methodology in a community of 10 residential buildings in Madrid, Spain, and section 6 provides the relevant findings and discussions. The results of the study are eventually summarized in section 7.

IV.2 System description and simulation

IV.2.1 System development

A distinct typology of heat pump integrated into SDHS is designed to meet the space heating and domestic hot water demands for a hypothetical residential neighbourhood throughout the year as schematically shown in Figure IV-1. The system mainly consists of solar collectors, a half-buried sensible seasonal storage tank (SST), the DHW storage tank (DHWT), a water-to-water heat pump unit, and auxiliary natural gas heaters.

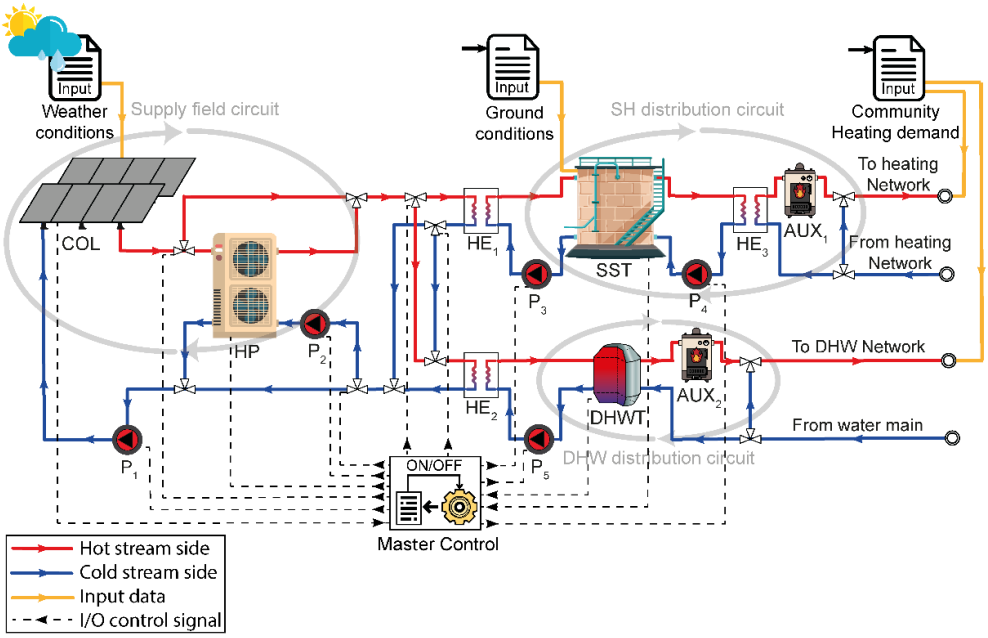

Figure IV-1: A schematic drawing for the HP integrated with SDHS.

The heat pump (HP) acts as a heat source for the SST when connected in the solar field circuit, as shown in Figure IV-1. In this configuration, the heat captured by the solar collector field (COL) can be directly used to fulfill the SH or DHW demand of the district or stored in the SST. The heat exchangers transfer the heat from the supply circuit to the distribution network using Y-type valves, depending on the mode of operation. Under a certain condition, the heat produced by the HP is either distributed directly for space heating or supplied to the SST for charging up the heat stored. The

SST is used during the winter season to supply the SH demand, while the short-term storage DHWT is used to supply the daily DHW demand. It is important to note here that the heat provided for SH corresponds to a low-temperature level (50°C), whereas the heat provided to the DHW is at high-temperature level (60°C). Finally, if the solar field, SST, and HP fail to meet the heat demand, the mismatch is covered by the auxiliary heater.

IV.2.2 Control logic

The developed system requires a good control strategy to operate under different modes to meet the district heating demand while maximizing the solar fraction and minimizing the heat losses. Four modes of control are designed based on the temperature levels at different points of SDHS, and these are achieved through on-off control of the isolation valves.

At first, when the DHW mode is triggered on, the heat gained by the solar collectors is transferred to the DHWT with the aid of the centrifugal pumps P_1, P_2 and P_5 via HE_2. The auxiliary heater is only enabled when the solar heat is not adequate to cover the demand in the DHW network. Under DHW mode, the heat pump unit is non-operational.

The SH mode is activated when an appropriate value of the temperature in the DHWT is reached, and the COL temperature is at a higher level than the bottom temperature of the SST. This operating mode uses the pumps P_1, P_2 and P_3 to deliver the heat to the SST from the solar collectors passing through the heat exchanger HE_1.

The third mode of control is for the simultaneous operation of DHW and SH circuits. This is activated only when the conditions for both DHW and SH operation are achieved, and the temperature in SST is higher than the DHWT.

Finally, the heat pump operation has two activated modes:

- *Control (A)* — In this mode, the heat pump works when the mean SST temperature (T_{SST}) is less than a reference temperature (T_{ref}).
- *Control (B)* — In this mode, the heat pump works if the solar collector temperature (T_{COL}) is less than the mean SST temperature (T_{SST}), which is, in turn, less than a reference temperature (T_{ref}).

In these modes of operation, the heat generated by the heat pump in Control (A) & (B) will be transferred either to the SST or the DHWT based on the demand. In case of insufficient supply from SST or DHWT, the auxiliary heater is turned on.

IV.2.3 System modeling

The concept is modeled using standard modules available on TRNSYS 18 environment based on the previous works by Tulus et al. [41], and Abokersh et al. [42]. Simulations are carried out for model training and performance assessment of the developed model. The major components of the TRNSYS model are explained in SI 1.

The SDHS model in TRNSYS is simulated considering a time step of 15 minutes. The simulations are carried out for a timeframe of three years, and the corresponding results are then extrapolated throughout the SDHS lifetime. This criterion is based on the assumption that the temperature within the SST remains at 30°C in the first year, and only after two years of simulation, the effect of the temperature change becomes negligible for the following years [43]. The lifetime of the SDHS is considered to be 40 years as set by the United Nations Environment Programme [44]. Replacements are required for the equipment such as the solar collectors, heat pump, heat exchangers, DHWT, auxiliary heaters, and centrifugal pumps after continuous operation for 20 years.

IV.3 Evaluation of System Performance

To evaluate the performance of the proposed heat pump integrated SDHS, a set of performance indicators was selected. The set includes indicators to provide information on energy efficiency as well as the economic and environmental performance over the entire lifetime of the system.

IV.3.1 Energy performance indicators

The energy evaluation indicators comprise of the efficiencies of the solar collector, SST, and DHWT [45], [46], seasonal performance factor (SPF) of the heat pump [47], and the overall solar fraction of the SDHS [48], [49]. The analysis is carried out using the following (Eq. IV-1 to Eq. IV-5) where the indicators are expressed in terms of the amount of energy flowing in the corresponding equipment unit:

$$\eta_{COL} = \frac{\int_0^t \dot{Q}_{Useful}}{\int_0^t \dot{Q}_{SOL}} \quad \text{Eq. IV-1}$$

$$\eta_{SST} = 1 - \frac{\int_0^t \dot{Q}_{SST\ loss}}{\int_0^t \dot{Q}_{HE_1}} \quad \text{Eq. IV-2}$$

$$\eta_{DHWT} = 1 - \frac{\int_0^t \dot{Q}_{DHW\ loss}}{\int_0^t \dot{Q}_{HE_2}} \quad \text{Eq. IV-3}$$

$$SPF_{HP} = \frac{\int_0^t Cap_{heating}}{\int_0^t \dot{P}_{heating}} \quad \text{Eq. IV-4}$$

$$SF_{global} = 1 - \frac{\int_0^t Cap_{heating} + \int_0^t \dot{Q}_{AUX_1} + \int_0^t \dot{Q}_{AUX_2}}{Q_{SH\ load} + Q_{DHW\ load}} \quad \text{Eq. IV-5}$$

where $\dot{Q}_{Useful}$ and $\dot{Q}_{SOL}$ are the useful solar energy produced and received by the solar collectors, respectively. The heat losses in the SST and DHWT are represented by $\dot{Q}_{SST\ loss}$ and $\dot{Q}_{DHW\ loss}$, while the rates of heat transfer through the heat exchangers HE_1 and HE_2 are given by $\dot{Q}_{HE_1}$ and $\dot{Q}_{HE_2}$. Moreover, $\dot{Q}_{AUX_1}$ and $\dot{Q}_{AUX_2}$ are the energy provided by the auxiliary heaters to supply the SH load ($Q_{SH\ load}$) and DHW load ($Q_{DHWload}$) under the condition of insufficient solar energy.

IV.3.2 Economic parameters

The Levelized cost of heat ($LCOH$) is adopted in our study for evaluating the economic competitiveness of the proposed SDHS, as demonstrated by Welsch et al. [50]. $LCOH$ in EUR per MWh is the minimum price at which the SDHS must supply heat to the customers at a pre-defined maximum temperature of the working fluid [51]. The $LCOH$ is performed by dividing the total discounted life cycle cost of the SDHS by the discounted thermal energy output $Q_a$of the SDHS as shown by the following formula [52]:

$$LCOH = \frac{\sum_{N=0}^{N_{end}} (C_C + C_O + C_R - R_a).(1+r)^{-N}}{\sum_{N=0}^{N_{end}} Q_a (1+r)^{-N}} \quad \text{Eq. IV-6}$$

Here $LCOH$ evaluation takes place over the assumed valuation period from $N = 0$ to N_{end} which takes into account of all costs associated with the SHDS during its lifespan, i.e., initial investment (C_C), operations and maintenance cost (C_O), equipment replacement cost (C_R) and the revenue of the system (R_a). An interest rate r is assumed. The $LCOH$ analysis requires all cost components to be converted into their present value. The revenue of the system (R_a) is not considered in this calculation. The details regarding the $LCOH$ components and their respective calculations can be

found in SI 2. In addition, the economic parameters for the initial cost and other life cycle cost inputs are mentioned in SI 3.

Another most commonly used cost-analysis methodology is the payback period (PB), which determines the number of years required to recover an initial investment through economic returns of the project. Therefore, the payback period of our proposed SDHS is the ratio of the total life cycle cost of the SDHS to the annual cost savings due to using SDHS instead of natural gas, as shown below [53]:

$$PB = \frac{LCOH}{Annual\ cost\ saving} \qquad \text{Eq. IV-7}$$

IV.3.3 Environmental assessment

For addressing the environmental impacts of coupling heat pumps with the SHDS system and comparing it with those of different district heating technologies, a life cycle assessment (LCA) approach is used [54]. The life cycle impact assessment (LCIA) can be performed using a variety of impact indicators. In this study, we follow the framework ReCiPe 2016 [55], which is considered as the most adaptable and uniform approach from a methodological point of view [56]. In this phase, the Life Cycle Inventory data are converted to endpoint impact indicators, which are again combined to represent three damage categories: human health, ecological systems, and resources. Afterwards, the three damages are aggregated and expressed as a normalized endpoint indicator metric (RCP) to interpret the overall environmental performance of the proposed SDHS configuration. The RCP can be expressed, as shown below:

$$RCP = \sum_{d} \delta_d \varepsilon_f DAM_d \qquad \forall d \qquad \text{Eq. IV-8}$$

Here $DAM_d$is the endpoint impact indicator for the damage category d. δ_d is the normalization factor based on land use and material extraction for the European setting while the weighting factor ε_d is based on recommended values by ReCiPe 2016. The environmental impact of SDHS components is found in SI 3.

Additionally, the environmental payback period ($EPBP$) is introduced to estimate the sustainability of the proposed SDHS model [57]. The $EPBP$ is the number of years of operation taken by the renewable energy plant until the total RCP savings due to the replacement of fossil energy by renewable energy equals the RCP during the life cycle [58]. It represents the potential of the SDHS model to reduce the environmental impact, and can be expressed as follows:

$$EPBP = \frac{RCP}{Annual\ RCP\ saving} \quad \text{Eq. IV-9}$$

IV.3.4 Key performance indicators (KPI) for successful 4GDH implementation

In the previous section, several performance indicators are described not only to evaluate the specific energy, economic and environmental characteristics of the proposed HP+SDHS but also to provide an appropriate identification of margins by which the system intends to meet the criteria of 4GDH concept. For this purpose, performance indicators that would demonstrate a successful representation of a specific target of 4GDH are used as KPIs in the current study and defined as shown in Table IV-1

Table IV-1: Key performance indicators for SDHS transition evaluation based on the 4th generation goals.

KPI	Symbol	Unit	4th generation goal
KPI$_1$— Share of renewable energy (solar)	-	%	Up to 100%
KPI$_2$— Seasonal Performance factor of the heat pump	SPF_{HP}	-	> 2.5[47]
KPI$_3$— District heating supply and return temperatures	T_{Supply}, T_{Return}	°C	50, 25
KPI$_4$— Thermal efficiency of the SST	η_{SST}	%	Up to 100%
KPI$_5$— Temperature level of the solar collector field	T_{COL}	°C	< 100 °C
KPI$_6$—Temperature level inside the SST	T_{SST}	°C	< 80 °C
KPI$_7$ — Levelized cost of heat	$LCOH$	€ /MWh	<Natural gas boiler cost
KPI$_8$ — Payback period	PB	Years	< 40 years
KPI$_9$—Recipe impact indicator	RCP	Pt./MWh	< Natural gas boiler impact
KPI$_{10}$—Environmental payback period	$EPBP$	Years	< 40 years

In order to attract the investors with environmental drivers as well the SDHS operators, the KPIs are associated to the stakeholders' perspectives [59]. Guidelines from [11] and [60] on the 4GDH concept have helped to select appropriate efficiency and sustainability indicators that complete a comprehensive assessment of the targeted solutions. Figure IV-2 summaries the proposed KPIs for respective stakeholders and their justification in a heat pump integrated SDHS.

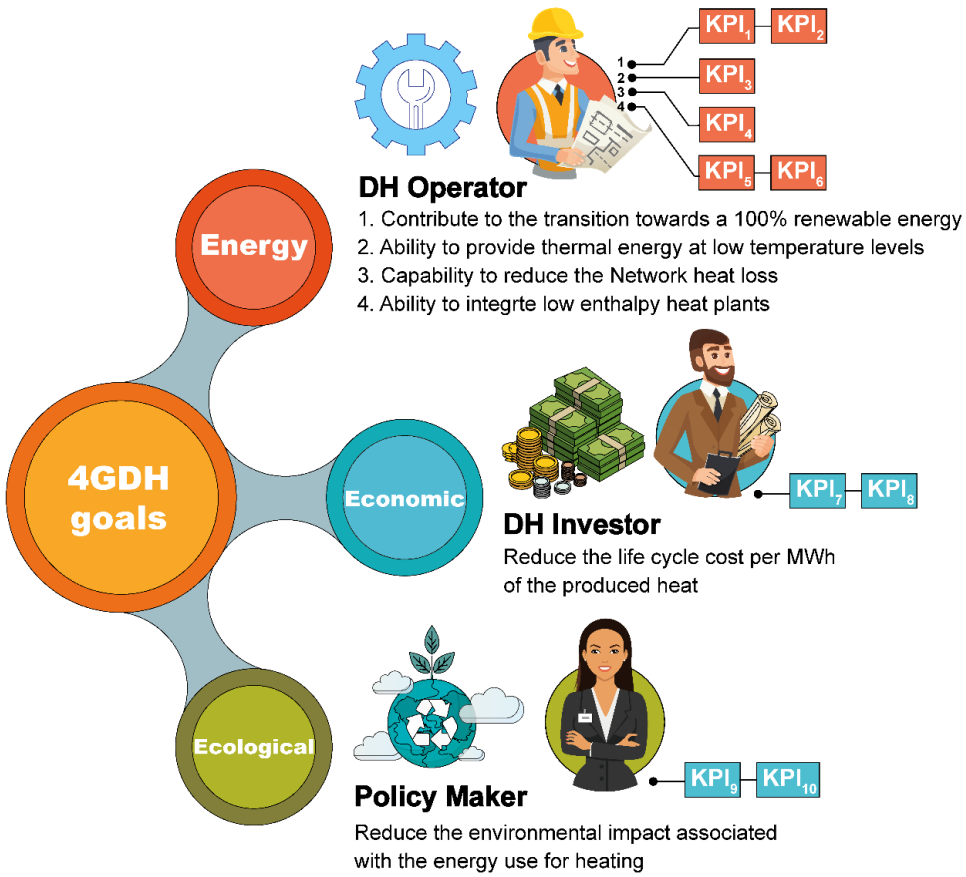

Figure IV-2: The 4GDH goals from the stakeholders' perspective connected to the KPIs.

IV.4 Development of design optimization strategy

IV.4.1 Outline for optimization approach

The main objective of the optimization approach is to minimize the life cycle cost ($LCOH$) simultaneously with the environmental impact (RCP) of the heat pump integrated into the SDHS. The outline of the optimization strategy is illustrated in Figure IV-3. This approach is developed based on the TRNSYS model mentioned in section 2. Once the TRNSYS model is built, we define the decision variables' range in the optimization problem, which, if changes reflect in the thermal output of the TRNSYS model. The software MATLAB is utilized to create the required scenarios where these scenarios cover the feasible range for the decision variables. Following that, MATLAB runs the scenarios automatically through TRNSYS in a parallel way. Once the feasible scenarios are built, the ANN model is trained using the developed

scenarios in order to predict the thermal performance of the SDHS. Finally, a genetic algorithm (GA) is coupled with the ANN to formulate a multi-objective optimization problem with an objective to minimize the cost functions aligning with the optimization problem constraints.

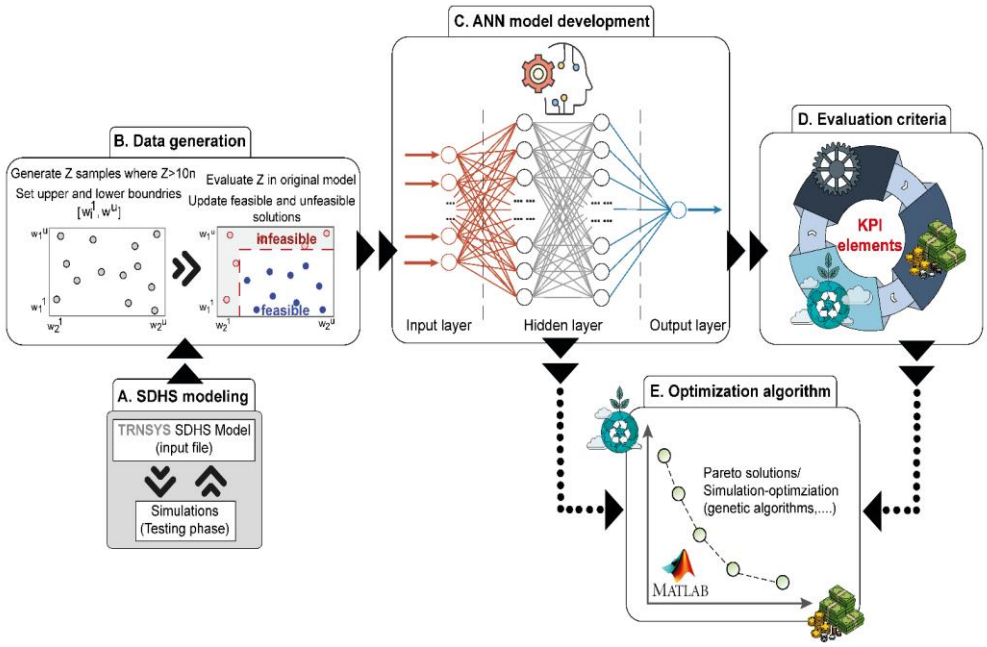

Figure IV-3: The optimization strategy outline.

IV.4.2 Development of the ANN performance model

IV.4.2.1 Data generation

The metamodel approach begins by generating an initial set of samples to train the metamodel. Aligning with the size of the decision variables and the computational budget, an appropriate size of the initial samples is selected. After that, the metamodel is trained using 2048 samples based on the Abokersh et al. [42] recommendation. In our framework, we apply the low-discrepancy sequences (Sobol's LP_T) for sampling due to its good space-filling feature [61]. The TRNSYS simulations are then evaluated based on the generated samples where the feasible solutions are utilized for training the metamodel, and the infeasible solutions are discarded.

IV.4.2.2 ANN model convergence criteria

The metamodel is built based on a multi-layer feedforward ANN model, where this model contains 14 neurons in the input layer and three hidden layers. The ANN

simulations are implemented based on the Bayesian regularization algorithm with a learning rate, and a Momentum mean of 0.001 and 0.004. The model structure is determined through the optimization approach proposed by Abokersh et al. [42] to provide a relatively good convergence. In the ANN model, 19 outputs are considered in the output layer. These outputs include the energy produced in the solar collector field, the energy supplied by the heat pumps, the energy supplied by the storage tanks, and finally, energy covered by the auxiliary heaters. To verify the performance of the metamodel, a set of performance metrics are proposed to assess the metamodel accuracy. These performance metrics are; (i) adjusted R-squared (R^2–$adj.$), and (ii) Coefficient of Variation ($C.V$), and they are estimated as shown in the Eq. IV-10 to Eq. IV-12:

$$R^2 = 1 - \frac{\sum_{i=1}^{n}\left(y_{predict,i} - y_{data,i}\right)^2}{\sum_{i=1}^{n}\left(y_{data,i} - \overline{y}_{data}\right)^2} \quad \text{Eq. IV-10}$$

$$R^2 - Adj. = 1 - \frac{(1-R^2)(n-1)}{n-k-1} \quad \text{Eq. IV-11}$$

$$C.V(\%) = \sqrt{\frac{\sum_{i=1}^{n}\left(y_{predict,i} - y_{data,i}\right)^2}{\overline{y}_{data}}} \times 100 \quad \text{Eq. IV-12}$$

Where $y_{predict,i}$ presents the estimated value at time point i, $y_{data,i}$ is the actual value at time point i, n is the size sample, and k is the number of regressors.

IV.4.3 Multi-objective optimization

In the formulation of the SDHS optimization problems, the cost functions usually create concerns about the energy performance and the economic profits [43]. However, in real problems, the environmental impact should be considered in the optimization framework to reflect the policy decision-makers' perspective. Therefore, our optimization problem tends to minimize the life cycle cost of the SDHS ($LCOH$) aligning with the environmental impact presented by the RCP to satisfy certain technical constraints. It is given as:

$$\begin{aligned} &min\ \{f_1(x), f_2(x)\} \\ &s.t.\ h(x) = 0 \\ &\quad g(x) \geq 0 \\ &lb_i \leq x_i \leq ub_i \qquad i \in \{1, \dots, 17\} \end{aligned} \quad \text{Eq. IV-13}$$

Where f_1 is the life cycle cost ($LCOH$) and f_2 is environmental impact aggregated by ReCiPe 2016 (RCP), while h represents the equality constraints solved implicitly in TRNSYS. The symbol $g$represents the inequality constraints, which reflects certain technical constraints comprising an annual solar collector field efficiency of 60%, SST

efficiency above 50%, and global solar fraction of 50%, as mentioned by Bauer et al. [62] and Solites [63].

In the current study, we utilized a Multi-Objective Genetic Algorithm (MOGA) [64] due to its capability to be coupled with metamodels easily [65]. In particular, the MOGA has the ability to handle several sets of Pareto points simultaneously. These sets of points are known as individuals in a population. Similar to the evolutionary algorithm, the initial populations can be modified with the proceedings of the iterations. These populations are generated with the application of the mutation and crossover functions [66]. The process is following the internal ranking of the population. For the available number of individuals in the population and iterates, the optimization is performed by evaluating the fitness function. The process is continued unless the criteria of convergence are met. All the information that is required for the evaluation of the sustainability metrics is available in the fitness function. The values of the fitness function for every sample point are used for the construction of the metamodel. Finally, the constraints associated with the metamodel simulator are handled through a penalty function [67]. A summary of the MOGA procedure is shown in Figure IV-4.

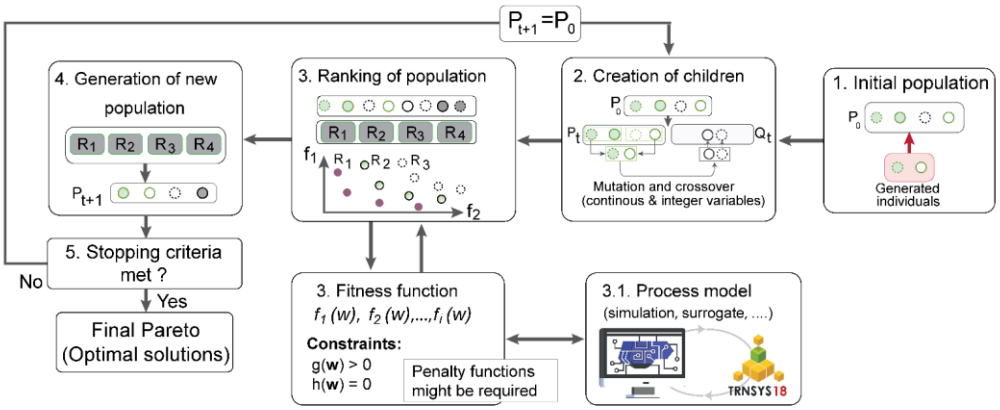

Figure IV-4: Flow diagram for the MOGA and TRNSYS simulations.

IV.4.4 Decision variables

In the current study, 17 decision variables are used in the formulation of the SDHS optimization problem. Different components of the SDHS comprising their relative orientation, construction, operational conditions, and sizing are included on the basis of these decision variables. The circuit name is used for the categorization of these decision variables. The decision variables in the supply field circuit comprise the solar collector field, its relative orientation, and the heat pump capacity with consideration for its operation criteria. In the SH distribution circuit, the SST and its relative construction materials are considered as decision variables in addition to the required auxiliary heater capacity in this circuit. In the DHW field, the DHWT volume and its relative construction ratio are considered aligning with the required auxiliary heater

capacity in this circuit. A summary of these decision variables and their relative range is shown in Figure IV-5. Furthermore, the sizing of other SDHS equipment is estimated based on mathematical equations linked with the decision variables.

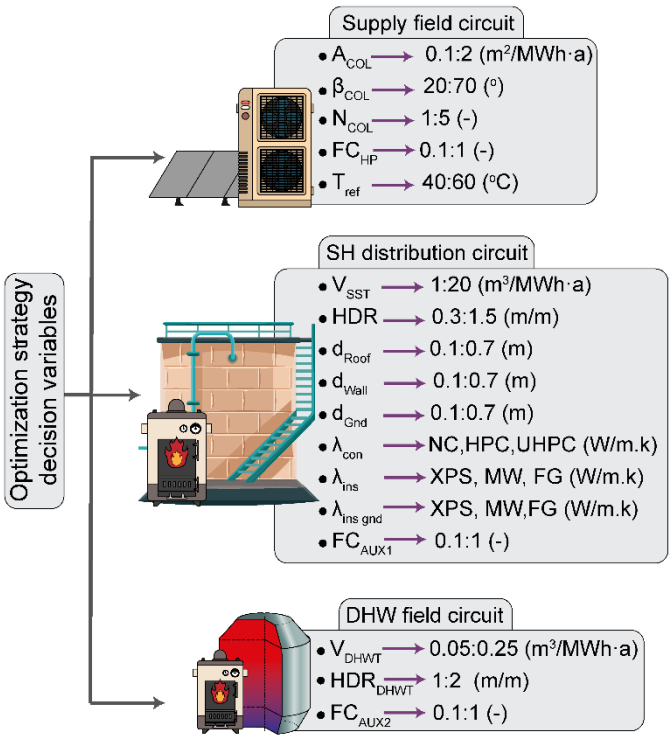

Figure IV-5: SDHS optimization decision variables.

IV.5 Case study

IV.5.1 Description

A small urban neighbourhood of 10 buildings located in Madrid (Spain) is utilized to illustrate the rule of the heat pump in enhancing the sustainable performance of SDHS under different control strategies. In the proposed community, every building consists of seven floors with 28 apartments where each one has a 90 square meter of a functional area [68]. The apartments are facilitated with a radiant underfloor heating and domestic hot water system. Therefore, the proposed system is designed to cover the SH and DHW demands at 50ºC and 60ºC, respectively. The comparison of the SDHS heating demand and model validation was carried out based on Tulus et al. [41].

To carry out a comparative study and showcase the benefits of the proposed configurations, two reference cases are also considered; a district heating system

fueled by natural gas (baseline 1) and a SDHS without integrated heat pumps (Baseline 2) as reported by Abokersh et al. [42].

IV.5.2 Meteorological data and energy demand profiles

The EnergyPlus database [69] is utilized to acquire the required climatic data for Madrid. These data comprise the incident solar radiation and the ambient temperature. The monthly average values for these climatic data are shown in Figure IV-6.

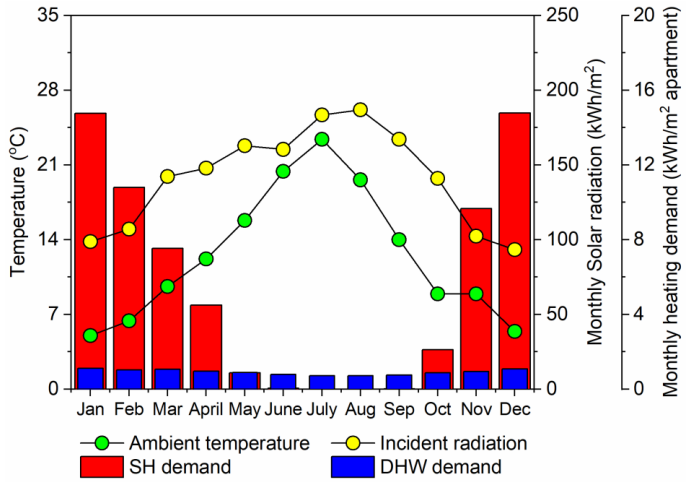

Figure IV-6: The monthly climate conditions as well the SH and DHW demand profile of the investigated neighbourhood located in Madrid.

Based on the Spanish regulation for residential buildings, a seven-floor building is simulated in the TRNSYS with consideration for the occupancy densities and the building material composition. The annual space heating demand profile is created based on the building simulation in TRNSYS following the work implemented by Guadalfajara [70]. The created space heating demand is then extrapolated for the whole neighbourhood where the total annual space heating for the neighbour is 1638.8 MWh. On the contrary, the DHW demand is generated based on DHWcalc [71]. This software generates representative DHW hourly demand profiles based on the daily water consumption per person and the number of occupants per household where the total annual DHW demand is 274.9 MWh for the specified neighbourhood. The monthly SH and DHW demands per apartment are shown in Figure IV-6, where the total neighbourhood demand is 1638.8 MWh for space heating and 274.9 MWh for the DHW.

IV.6 Results and discussion

In this study, the first part of the results offers an analysis of the ANN model to ensure the suitability of the metamodel for SDHS optimization. In the second part, the results obtained from the design optimization of the heat pump control strategy for integration with SDHS are presented via selected techno-economic and environmental performance indicators. A detailed analysis of the Pareto optimal solutions and the comparison between the results is carried out in this section. The third section provides a comparative study of the SDHS with and without HP to examine the possible effects of incorporating HP into SDHS for a small community. In the final stage of analysis, the capability of the developed system configuration is discussed in terms of the rate of achievements of 4GDH targets.

IV.6.1 The ANN performance analysis

In the current study, the overfitting problem associate with the ANN model is solved through K-fold cross-validation, where the 2048 sample is divided into k subsets. Each time the ANN model is trained by k-1 set, whereas the remaining k subset is utilized for testing.

A summary of the ANN model performance is shown in Table IV-2. The results showed that the ANN model prediction is agreed with the TRNSYS output where the $R^2 - Adj.$ never falls below 95.5%for all the output. To gather further confidence regarding the ANN model performance, the $C.V$ shows that model accuracy does not get below 8.83% for all ANN output. In general, these results indicate the ability of the ANN model to provide an acceptable prediction for the thermal performance of the SDHS within the training data range. Furthermore, the usage of metamodeling can offer a significant reduction in the computational expenses of heuristic optimization models.

Table IV-2: The performance sample of ANN model in predicting the TRNSYS output.

	Supply circuit			SH circuit		DHW circuit			
	Q_{SOL}	Q_{Usefui}	Q_{abs}	P_{elec}	Q_{SST}	$Q_{SST\ loss}$	Q_{AUX1}	Q_{DHW}	$Q_{DHW\ los}$	Q_{AUX2}
$R^2 - Adj.$	99.8 %	99.6 %	97.7 %	97.8 %	99.5 %	97.7 %	99.2 %	95.5 %	98.9%	99.4 %
$C.V$	1.98 %	1.99 %	8.83 %	8.16 %	2.87 %	8.54 %	8.15 %	0.49 %	2.70%	3.08 %

IV.6.2 The effect of HP control strategy on SDHS

From the results viewpoint, the multi-objective optimization procedure is devoted to analyze the effect of the decision variables on the design of SDHS with heat pump under the two designed control systems A and B. The set of Pareto optimal solutions

obtained from optimization process correspond to five scenarios. Scenario 1 represents the minimum cost solution with zero limits on possible environmental damage. The environmental damage limit of 25%, 50%, and 75% is allowed in scenario 2 up to 4 relative to scenario 1. In scenario 5, the SDHS model causes minimum environmental impact when 100% of the damage limit is hit.

It can be remarked from Figure IV-7 (a) that a clear trade-off exists between the proposed economic and environmental targets as we switch from scenario 1 to 5 under both control settings. The optimal cost of energy in terms of $LCOH$ is increased while the environmental impact of the SDHS (RCP) is minimized and vice versa. The baseline 1 represents a traditional heating system (natural gas boiler). It produces the maximum environmental impact of 26.6 Pt/MWh as well as a limited economic benefit (90.3 €/MWh) compared to the Pareto optimal system configurations.

Under the control scheme (A), where the HP in SDHS is turned on if T_{SST} is less than the reference temperature; it can extensively minimize the environmental impact compared to the baseline 1 while remaining to be cost-competitive at scenarios 1 and 2. The optimal Min. cost solution has $LCOH$ equal to 72.1 €/MWh, which is less than the base case by 20.1%, whereas the RCP reduces to 5.15 Pt/MWh, which is smaller than the baseline 1 solution by 80.6%. On the other hand, the Pareto optimal solutions from scenarios 3 to 5 could not provide any economic benefit, although they minimize the environmental impact by approximately 89.5% compared to baseline 1.

Under the control setting (B), more enhancements of both objective functions can be seen compared to the Pareto optimal solutions under control (A) as well as in baseline 1. This is due to the efficient control of the heat pump with respect to temperature levels in the solar collector and SST, as well as the reference temperature. In scenarios 1 and 2, the $LCOH$ with control setting (B) is remarkably less than that of control setting (A) along with marginal environmental benefits. At control setting (B), the Min. cost solution has $LCOH$ equal to 59.1 €/MWh which is less than (A) by 18% and base case by 34.5%, whereas the RCP value is reduced to 4.65 Pt/MWh which is smaller than the solution (A) by 9.7% and the base case by 82.5%. As the environmental damage limits are increased from scenarios 3 to 5 with control setting (B) in action, the decreasing environmental impact leads to an increment in the cost. If the Min. impact solutions are compared, control (B) has the upper hand over (A) with significant cost reduction as it is reduced by 28.9%. However, this optimal solution still fails to beat the baseline 1 economically where it higher than the baseline 1 by 40.6%.

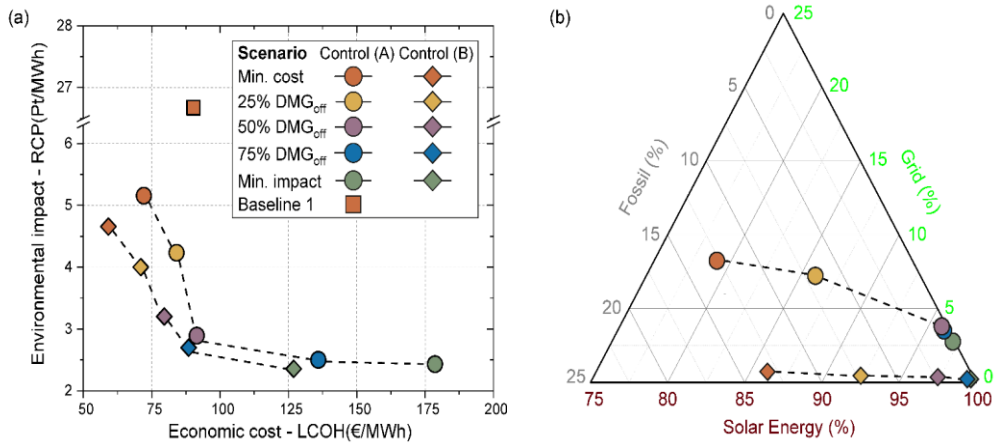

Figure IV-7: Various Pareto optimal solutions for the HP integrated with SDHS under two control strategies (A) and (B) to cover the SH and DHW yearly demand in comparison to their respective baseline 1 using natural gas, (a) Levelized cost of energy and environmental impact of the optimal configurations at the different scenarios, (b) Energy source and its share for the optimal system configurations for the different scenarios.

Since the proposed SDHS system comes with multiple energy sources to optimize the environmental and economic parameters, the share of different energy sources is an important aspect to ascertain the system's feasibility as a future 4GDH system. The ternary representation of energy shares in Figure IV-7(b) shows that as the Pareto front under the two control strategies (A) and (B) progress from generating the Min. cost-optimal solution to Min. impact, the SDHS can approach 100% solar energy input. For example, if the minimum cost solutions are compared, the Pareto optimal point under control (A) has 79.1% share of solar energy, 12.9% share of natural gas, and 7.98% share of grid electricity. Meanwhile, under control B, the optimal solution has 86.1% of solar energy, 13.1% share of fossil energy, and 0.73% share of grid proving that control mechanism (B) is more effective than (A). Regarding the rest of the scenarios (2-5), the share of solar energy in the system increases while the share of natural gas goes down when we move towards the minimum environmental impact solution. The control scheme (B) seems to be more successful with less percentage of electricity input from the grid for all the Pareto optimal solutions, and it reduces up to 3.5% and 0.3% for control (A) and (B), respectively.

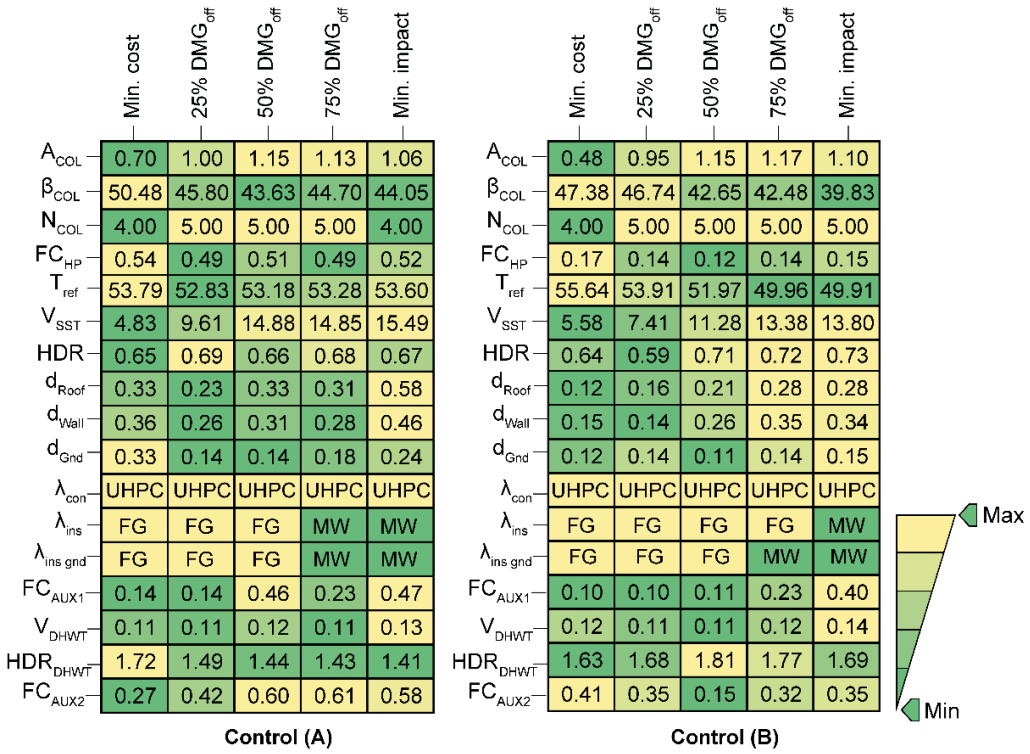

Figure IV-8: Pareto optimal solutions of the HP integrated SDHS configuration to cover the demand of 10 buildings located in Madrid under HP control strategy (A) and (B) where the colour map indicates the min and max value of each decision variable.

In order to enhance the understanding of the system performance, a breakdown is conducted for each Pareto optimal solution under both control strategies (A) and (B). In Figure IV-8, the optimal values for each decision variable are presented in a heat map in order to visualize how each design parameter changes under different optimization scenarios. Starting from the supply aspect, the design parameters related to the solar collector take similar values without any significant deviations except for the minimum cost scenario. In this case, the solar collector area decreases from 0.70 m^2/(MWh·a) under control (A) to 0.48 m^2/(MWh·a) under control (B). Similarly, the fractional capacity of the heat pump is significantly reduced under control (B), where the HP fraction is only 0.14±0.025 compared to 0.51±0.025 for control (A). This is expected since the heat pump is being operated only to stabilize the system, and it has a limited contribution to fulfill the thermal energy demand. Furthermore, the heat pump operation under control (A) keeps the reference operation temperature of the heat pump (T_{ref}) around 53.3±0.5°C for all optimal scenarios. While operating under control (B), the T_{ref} reduces from 55°C at the Min.

cost solution to 49.9ºC at the Min. impact solution due to the limited usage heat pump, especially when the damage limits are increased.

Comparing the design parameters related to the SST, it is seen that under control (A), the volume of the tank increase from 4.84 to 15.5 m^3/(MWh·a) with the movement toward Min. impact solution. While under control (B), a reduction in the seasonal storage tank volume is indicated by around 2.2 m^3/(MWh·a) for all the optimal configurations except for the Min. cost solution. On the other hand, significant changes are reflected in terms of the thickness of the insulation materials utilized in the SST. When the control (B) is used, the required thickness of the insulation for the roof, walls, and ground is reduced for all the Pareto optimal configurations. In case of the Min. cost solution, a thickness of around 0.3 m is selected for all SST walls under control strategy (A), whereas it is reduced to around 0.13 m under control strategy (B).

Regarding the SST construction, the material that exhibits superior performance in all the scenarios is found to be UHPC. In addition, all the surfaces of the SST select foam glass gravel for the insulation purpose. However, as damage limitations increase, mineral wool is chosen over foam glass, which has a lesser environmental impact. The SST aspect ratio HDR shows limited variations. The auxiliary heater used in the SH distribution circuit is operated less under control (B) which implies less consumption of natural gas. In addition, the DHWT parameters, as well as the auxiliary in the DHW distribution circuit, assume almost constant values under both the proposed control settings.

IV.6.2.1 Cost performance analysis

To perform a comprehensive economic analysis of the proposed SDHS+HP integration, Figure IV-9 shows the contributions of investment costs, operational, and replacement costs to the $LCOH$ by different components.

By comparing the two-control settings (A) and (B) against the baseline 1 solution, it is observed that the capital cost represents only 1.02% in the baseline 1. While under (A) and (B), the capital cost increases significantly, responsible for up to 65% of the $LCOH$ in case of the Min. impact solution. This high initial investment cost is expected owing to the utilization of solar energy and seasonal thermal energy storage as a heat source in the district heating system. This may be seen as one of the critical barriers to boost the market rollout. The optimal solutions show a noticeable variation from scenario 1 to 5 (from Min. cost to Min. impact), where the SST has the highest share in the $LCOH$, up to 40% in both (A) and (B) control strategies. The capital cost requirements for the SST decreases relatively under the settings (B), which can be attributed to the reduced thickness of the insulation materials used for the SST. Secondly, the investment cost for the heat pump also falls because of the less capacity requirement under (B) where it represents only around 2% compared to 12% in control (A) at the Min. cost solution. The composition of operation cost shows larger shares of natural gas cost under setting (B) compared to (A). This happens since the

auxiliary heater is operated more frequently to supply SH with the SST being at a low-temperature level. The replacement cost for the solar collectors shows a similar distribution in the optimization setting (A) and (B). The heat exchangers account for a marginally higher cost of replacement in (B) when the threshold for the environmental damage is increased. In contrast, the replacement cost for the heat pumps is higher in (A) due to its higher capacity.

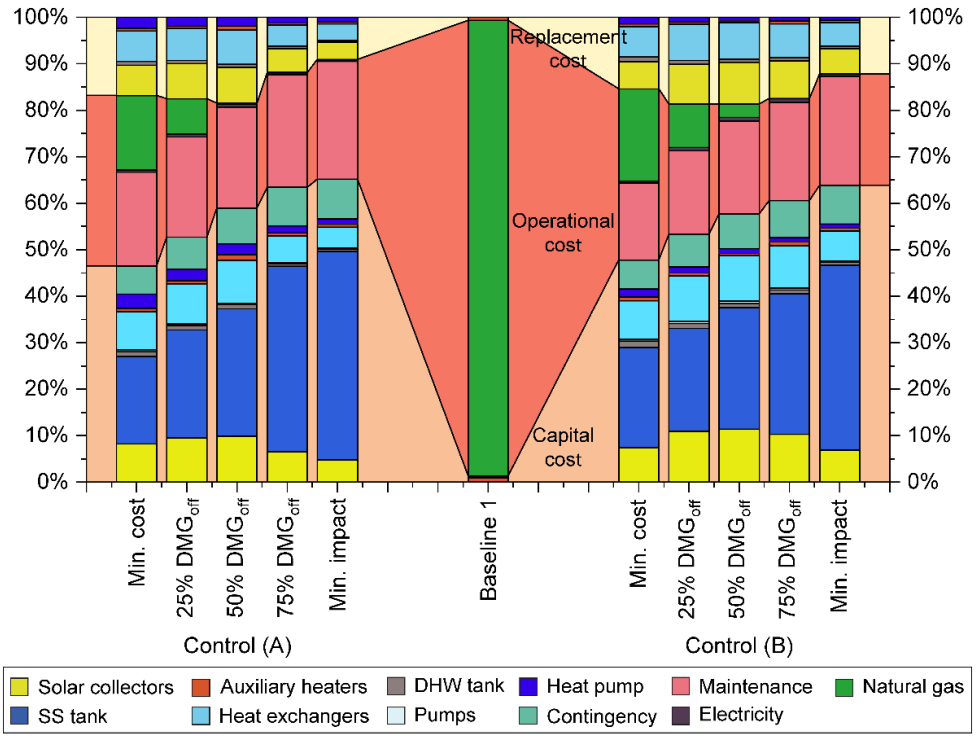

Figure IV-9: Breakdown of the $LCOH$ including the shares of initial capital cost, operational cost, and replacement cost for Pareto optimal solutions under HP control strategy (A) and (B) at the five optimal scenarios in comparison to baseline 1. These solutions cover the SH and DHW demands of 10 residential buildings located in Madrid.

Since the largest share of capital costs is associated with seasonal storage, it is worth evaluating how the heat pump affects the SST construction and insulation material requirements. As shown in Figure IV-10, the majority of the cost is due to the construction material required for the SST. In the case of the minimum cost solution, SDHS with a heat pump featured a higher amount of construction material and less insulation for the roof, wall, and ground when operated under control (B) compared to (A). The values tend to increase moving towards Min. impact solution. This change is expected since the insulation material, which can produce a

minimum environmental impact, is relatively expensive. The solutions under control (A) require even more insulation material to minimize the environmental impact.

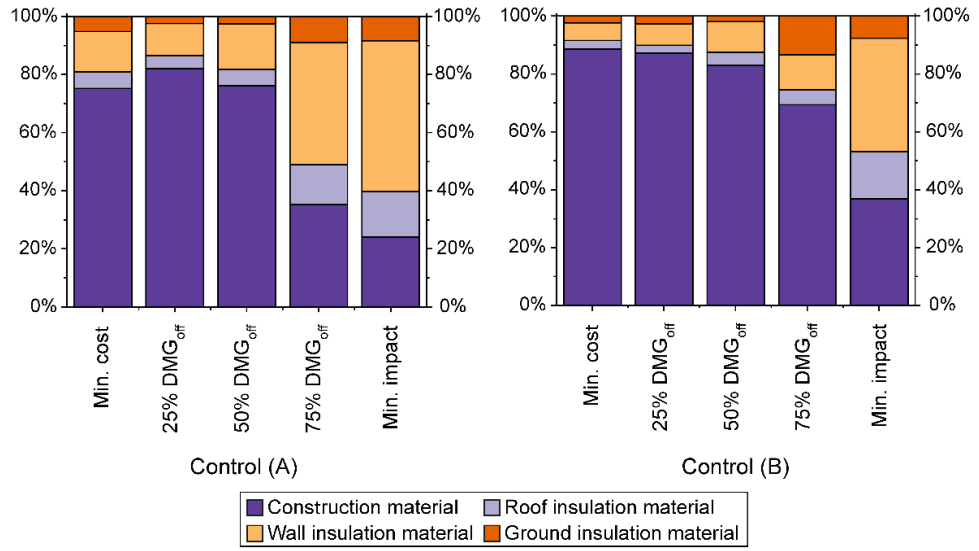

Figure IV-10: Cost breakdown for the SST under two different control systems in different damage scenarios.

IV.6.2.2 LCA performance analysis

A detailed analysis of the Pareto fronts in terms of the aggregated ReCiPe 2016 in comparison to the baseline 1 for the different damage scenarios is presented in Figure IV-11. In the baseline 1, the consumption of natural gas is responsible for almost 100% of the total impact. For the SDHS +HP configurations, the most significant impact contributors in both (A) and (B) are the solar collectors, natural gas, and seasonal storage tank.

In the case of control strategy (A), the natural gas is responsible for 66.6% and 44.6% share of total environmental impact for scenarios 1 and 2, respectively. When control (B) is applied, the impact of utilizing natural gas as a primary fuel is more prominent since it represents 75.23%, 49.3%, and 21.31% for scenarios 1, 2, and 3, respectively. Moreover, it reduces to a negligible share as we increment the environmental limits (scenarios 4 and 5). Concerning the environmental damage due to the renewable energy technologies used in our SDHS model, the impact of the solar collector increases significantly from 22% in scenario 1 to 70.9% in scenario 5 under the control setting (A). In the case of control (B), it increases from 16.7% to 75.4% (scenarios 1 to 5) as well. It can also be observed that the damage due to the SST shows similar patterns as the collectors. Since the types of construction materials used for the SST were included in the optimization process, its contribution

to the total environmental impact has been reduced which is clear from the scenario 4 and 5 in control (A) and scenario 5 in control (B). The impact of the heat pump integrated to SDHS is more prominent under the scheme (A) compared to that of (B) because of its higher fractional capacity. It is evident from Figure IV-11 that the consumption of electricity by the heat pump causes negligible environmental damage since the share of impact due to the consumption of electricity from the grid used to operate the heat pump and the other flow circulation pumps in the SDHS shows the equal distribution in both solutions. This also confirms the importance of the solar collectors, storage tank, and heat pump operating together to reduce the consumption of non-renewable energy sources. This type of analysis could be helpful in determining which carbon tax levels would be needed to push the market towards more renewable technologies.

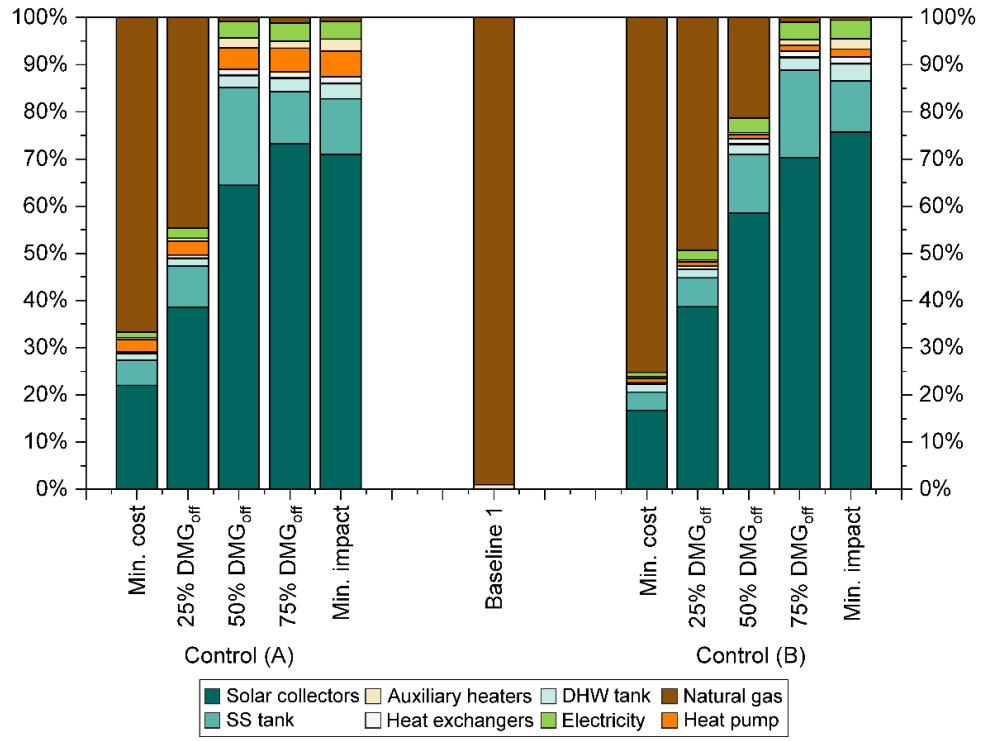

Figure IV-11: Breakdown for the aggregated ReCiPe 2016 of Pareto optimal solutions at different damage scenarios for the HP integrated with SDHS applied at control (A) and (B) in comparison to the baseline.

To track the environmental effect of combining heat pump with seasonal storage in a SDHS, Figure IV-12 displays the breakdown of the aggregated RCP value for the storage tank under control strategy (A) and (B). The construction of the SST leads to a considerable share of impact; nearly 100% in scenarios 4 and 5 under control (A) and scenario 5 under control (B), which depends on the optimized capacity of

the tank. On the other hand, the influence of various insulating materials used in the SST wall, roof, and ground in (A) is 67.4% in scenario 1, 51.9% in scenario 2, and 54.5% in scenario 3. In the case of control (B), the impact due to the insulation slightly reduces to 43% in scenario 1, 44.2% in scenario 2, and 48.2% in scenario 3. The optimization methodology selects the minimum value of the insulation material with minimum impact when we move towards the minimum impact solution. Therefore, in scenarios 4 and 5 under control (A) and scenario 5 under control (B), virtually zero environmental effects are caused by SST insulation. Consequently, the control scheme (B) appears to be marginally advantageous in terms of produced environmental impacts.

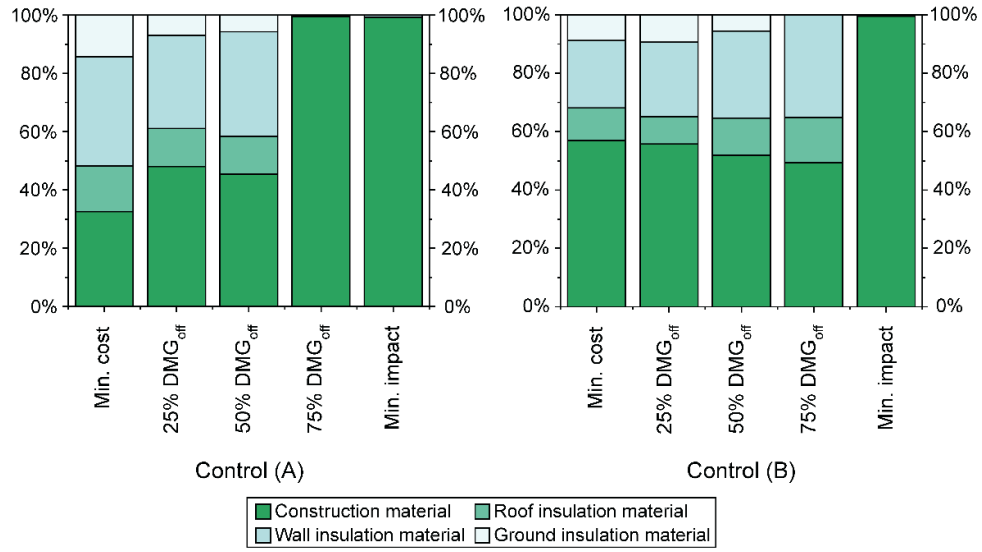

Figure IV-12: Breakdown for the aggregated ReCiPe 2016 for the SST at different control strategies under different damage scenarios.

IV.6.2.3 Energy performance analysis

Figure IV-13 presents the values of the energy performance indicators achieved by the combination of SDSH and HP with control strategy (A) and (B). As seen from the figure, both (A) and (B) provided almost similar results for $\eta_{COL}$with the change in scenarios except for the minimum cost solution. This shows a pleasant correspondence with the previously mentioned values of the solar collector area and the highest value of η_{COL}(72%) obtained in the scenario 1 under control (B) when the size of the collector field assumes the smallest value.

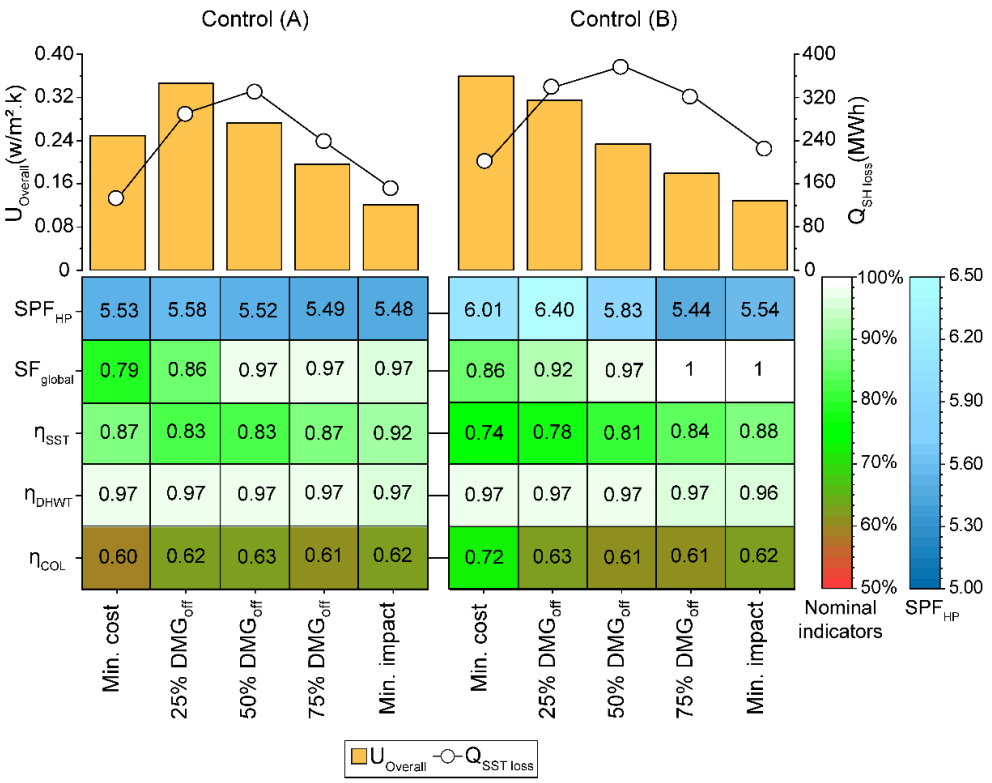

Figure IV-13: Thermal performance indicators for the optimal Pareto solutions of SDHS under HP control strategy (A) and (B). These designs satisfy the SH and DHW demand of the 10 residential buildings located in Madrid

The efficiency of the DHWT η_{DHWT} is very high (around 97%) for all scenarios since it is used as diurnal storage in the district heating network with a limited heat loss to the environment. Regarding the performance of the space heating circuit, under control (A), values of η_{SST} remain almost alike following the heat loss from the SST throughout the environmental damage scenarios, as seen in Figure IV-13. On the other hand, the overall heat loss coefficient of the SST in control (A) initially increases and then decreases. At the same time, in control (B), it diminishes consistently with increasing the limit of damage to the environment. This is due to the optimized geometry and materials used for the construction and insulation of the SST. The highest efficiency obtained for the SST is 92% for the Min. impact solution under control (A), which also has the minimum value of heat loss coefficient (0.075W/m^2). The efficiency of the storage is compromised under control (B) since this control setting uses the heat pump to stabilize the storage temperature reducing the use of insulation material for the SST, which in turn increases the heat loss. In terms of the solar fraction, it is improved from 79% in control (A) to 86% in control (B) under Min. cost-optimal scenario. For the rest of the scenarios, the SF_{global} rises progressively

with the increment in the environmental damage limits approaching almost 100% for the minimum impact solution. This can be explained with the expanded installation of renewable energy equipment in the district heating sector. The seasonal performance factor of the heat pump shows improvement under (B) compared to (A) when we look into the scenarios 1 to 3. The highest value of SPF_{HP} is 6.01 for the minimum cost solution in (B). However, when the methodology aims for the minimum environmental impact, the efficiency of the heat pump is compromised.

The next step in this analysis is the evaluation of the proposed design of SDHS operating under the superior control system (B) in comparison to a previously examined SDHS configuration without heat pump (Baseline 2) as presented by Abokersh et al. [42].

IV.6.3 The effect of integrating HP into SDHS

The Pareto optimal solutions under control (B) are compared with the results from Abokersh et al. [42](baseline 2) to establish the value addition made by the integration of the heat pump to SDHS while covering the SH and DHW demand of 10 residential buildings located in Madrid to achieve the 4GDH goals.

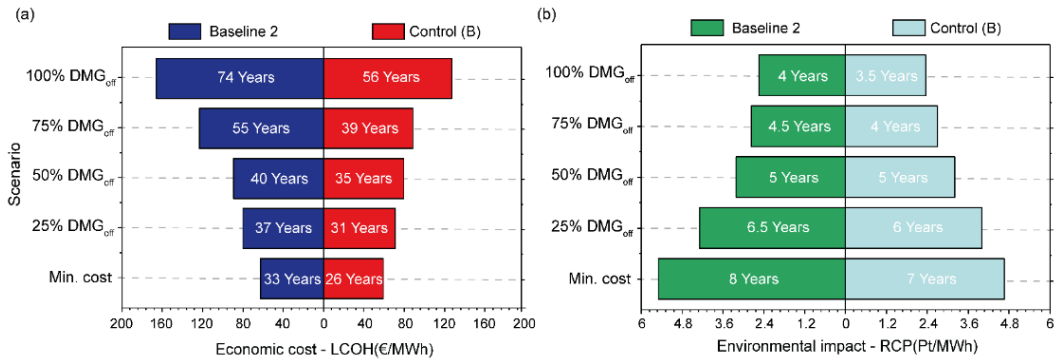

Figure IV-14: Various Pareto optimal solutions comprising of the objective functions for the HP integrated with SDHS under control strategies (B) in comparison to the baseline 2in terms of (a) the $LCOH$ and PB objectives, and (b) the RCP and $EPBP$ objectives.

It was observed in Figure IV-14(a) that coupling of a heat pump in between the solar collector and the seasonal storage tank could result in better cost-effectiveness for the SDHS network. The new configuration reduced the $LCOH$ from 62.5 €/MWh to 59.1 €/MWh (5.44%) in the case of the Min. cost solution. This is followed by the rest of the Pareto optimal solutions, which are also marginally cost-beneficial. Besides, the payback period of the new system configuration is significantly reduced under all damage scenarios. The Min. cost-optimal solution with the heat pump added to the SDHS has the lowest value of the payback period, i.e., 26 years in comparison to the baseline 2 scenario. However, this still very high payback period is due to two main

reasons; firstly, the low natural gas prices [72] which keep the operational cost of the natural gas boiler a competitive solution with the SDHS. Secondly, all the optimal solutions of the SDHS have a high solar fraction above 85%, which is the cause of a high investment cost due to the extensive usage for renewable energy components. Since the system lifetime is assumed to be 40 years, the Min. cost solution seems reasonable to adapt to implement the proposed SDHS with the control system (B) as a 4GDH system.

Regarding environmental sustainability, the values of environmental damage indicator RCP and $GPBP$for the HP integrated with SDHS are reasonably comparable with baseline 2, as shown in Figure IV-14(b). The optimal solution for minimum cost with a heat pump has an impact of 4.65 Pt/MWh with the largest $GPBP$ (7 years) against the baseline 2 with an impact of 5.49 Pt/MWh and $EPBP$ of 8 years. The environmental impact of both configurations reduces if moved towards the 100% damage limit. Hence, it can be concluded that the addition of the heat pump makes the SDHS more sustainable, although the heat pump runs on the electricity from the grid.

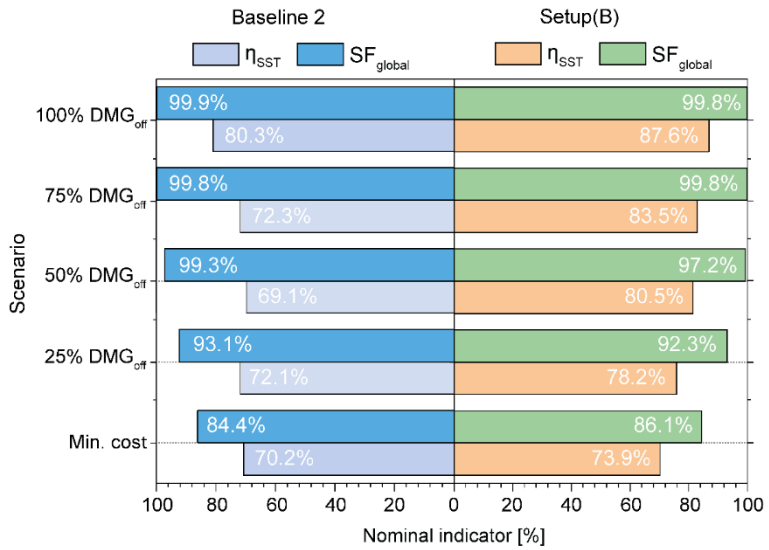

Figure IV-15: Thermal performance indicators for the optimal Pareto solutions for HP integrated with SDHS under control strategy (B) in comparison to baseline 2.

Based on the comparison presented in Figure IV-15, one can observe that the thermal efficiency of the seasonal storage tank in SDHS +HP is higher than that of baseline 2. The heat pump enhances the value of η_{SST} by 5% in damage scenario 1, 7.8% in scenario 2, 14.2% in scenario 3, 13.4% in scenario 4, and 8.3% in scenario 5 compared to baseline 2. Regarding the overall solar fraction of the system, only the Min. cost solution with an integrated heat pump shows a slightly higher value of SF_{global}(86.1%) than the baseline 2 (84.4%). All other optimal solutions (scenarios 2 to 5) have marginally less value of SF_{global} and remain energetically competitive with

the baseline 2 configuration. Therefore, if the Min. cost solution of the SDHS has to be chosen to establish the economic feasibility of a 4GDH network, the incorporation of the heat pump into the SDHS and seasonal storage with optimal control (B) proves to be a better decision in terms of energy efficiency as well.

The above analysis of the comparison between the HP integrated SDHS under control strategy (B), and the baseline 2 (without heat pump) shows again that the minimum cost solution is a favorable choice considering economic, environmental and energy performance. Hence, finally, we compare these two configurations using the optimized values of the decision variables in both cases, as shown in Table IV-3. In the heat supply circuit, by adding the heat pump, a reduction of 12.9% in the collector area is achieved compared to the baseline 2. This indicates that the heat pump is able to bring down the SDHS temperature levels to operate as a 4GDH and subsequently reduces the requirement to add more insulation materials, as shown in Figure IV-16.

Concerning the SH circuit, the volume of seasonal storage is increased from 4.96 m^3/(MWh·a) to 5.58 m^3/(MWh·a) (11.1%). However, the requirement of insulation materials is reduced significantly for the roof by 76.9%, 50% for the sidewalls, and 71.4% for the bottom of the SST due to the rule of the heat pump in reducing the SST temperature level. This reduction is reflected in the investment cost. This is followed by the change in the SST aspect ratio from 0.68 to 0.64. The optimization methodology selects the same type of materials for the construction and insulation of the SST. The heat pump did not have an impact on the size of the auxiliary heater required in the SH circuit as a backup. To supply the DHW demand using the HP+SDHS, the auxiliary heater is used more often than the baseline 2. This leads to an increase in terms of its fractional capacity (0.34 to 0.41) due to the limited capacity of the HP. The required volume of the DHWT remains the same, although the aspect ratio of the tank has differed.

The investment cost is reduced to 2.15 million Euros from 2.24 million Euros for the SHDH system equipped with the heat pump in the presented optimization results. The additional investment cost due to the heat pump does not affect the SDHS configuration. Instead, it helps to improve the overall system efficiency by lowering the capital investment on the solar collectors and the seasonal storage by 4% as compared to baseline 2. Furthermore, the operation cost is also decreased in the current study by 11.2% because of the lower operating temperatures yield. However, the replacement cost increases due to the use of the heat pump over the system lifetime.

Table IV-3: The Pareto minimum cost-optimal configuration and its relative cost breakdown for the HP integrated SDHS under control strategy (B) in comparison to baseline 2.

	Circuit Name	Parameter	Unit	Baseline 2	Control (B)
Decision variables	Supply Circuit	Heat demand	(MWh·a)	1913.4	1913.4
		A_{COL}	$m^2/(MWh \cdot a)$	0.54	0.47
		β_{COL}	º	45.4	47.3
		N_{COL}	-	4	4
		FC_{HP}	-	-	0.17
	SH circuit	V_{SST}	$m^3/(MWh \cdot a)$	4.96	5.58
		HDR	m/m	0.68	0.64
		d_{Roof}	m	0.52	0.12
		d_{Wall}	m	0.30	0.15
		d_{Gnd}	m	0.42	0.12
		λ_{con}	W/(m·K)	UHPC	UHPC
		λ_{ins}	W/(m·K)	FG	FG
		$\lambda_{ins\ gnd}$	W/(m·K)	FG	FG
		FC_{AUX1}	-	0.10	0.10
	DHW Circuit	V_{DWHT}	$m^3/(MWh \cdot a)$	0.12	0.12
		HDR_{DHWT}	m/m	1.80	1.63
		FC_{AUX2}	-	0.34	0.41
$LCOH$ parameters	Investment cost	C_C	Million Euros	2.24	2.15
	Operational cost	C_O	Million Euros	1.87	1.66
	Replacement cost	C_R	Million Euros	0.67	0.69

Additionally, Figure IV-16 shows the differences in temperature profiles within the solar thermal collectors and the seasonal storage tank over a year. Adding the heat pump under control strategy (B) has helped to keep the temperature low for the collector, especially during September, and it never exceeds 80ºC. In contrast, it goes up to 104.5ºC at baseline 2. Furthermore, the temperature inside the storage is also reduced to 85.4ºC in October compared to 87.6ºC in baseline 2. This lowers the temperature difference between the heat source (collector) and the heat sink (storage) for the heat pump resulting in a higher value of SST efficiency as well as a higher HP seasonal performance factor.

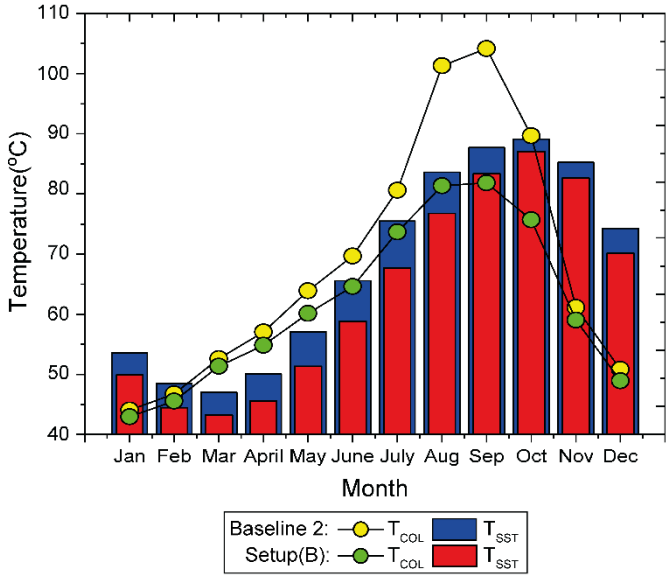

Figure IV-16: The monthly temperature profiles of the solar collector field and SST for the HP integrated with SDHS under control strategy (B) in comparison to baseline 2 for the minimum cost-optimal solution.

IV.6.4 The impact of heat pump in SDHS for reaching 4GDH targets

This section aims to answer the research question about whether the proposed configuration of SDHS enhanced with seasonal storage and heat pump for a district heating scenario can fulfill the target characteristics of a 4GDH system. The selected KPIs are based on the perspectives of three key stakeholders of district heating, as explained in section 3.4 and derived as a percentage of the target value of a 4GDH system for the minimum cost configuration of the SDHS among all the Pareto optimal points.

It is evident from Figure IV-17 that the energy KPIs have the potential to reach the 4GDH goals. Due to the implementation of the solar thermal collector with seasonal storage and heat pump technology using an optimal control strategy (B), the share of renewable energy, i.e. the solar fraction has been able to reach 86.1% of the total heating demand. This minimizes the use of fossil fuel for district heating and thus promotes a transition towards a low-carbon system. The coupling of the heat pump in order to directly supply the storage has resulted in a very high value of SPF_{HP} (6.01), although it is operated for small durations. This complies with the KPI target value by 100%. The temperature barrier for low-temperature district heating appears to be removed since the supply and return temperature in the proposed SDHS is maintained at 50/30°C. This is in line with the target temperature range of the 4GDH network by 80%, which is a major feature to be present in a 4GDH system. Concerning the seasonal storage integration into 4GDH, the temperature inside the storage tank is at 93.2% of the desired value. Nevertheless, the proposed model has

been entirely successful in keeping the collector temperature low. The efficiency of the storage is found less than the expected level due to the heat losses to the ambient. Overall, the technical suitability of the SDHS model is established to transform into a 4GDH system.

The financial KPIs in our study ($LCOH$) have shown that the cost at which the system must supply heat to the customers at 50°C is reduced by 34.2% compared to the local heat price for the natural gas-based district heating system. The reduction in the payback period is estimated to be about 35% as well. Hence, the SDHS carries potential economic benefits over the traditional district heat supply to be operated as a 4GDH for each potential district heating investor. This also highlights that the usage of low-temperature heat sources does not have financial disadvantages for the potential expansion of district heating networks into 4GDH. However, it calls for long-term financial commitments to become competitive.

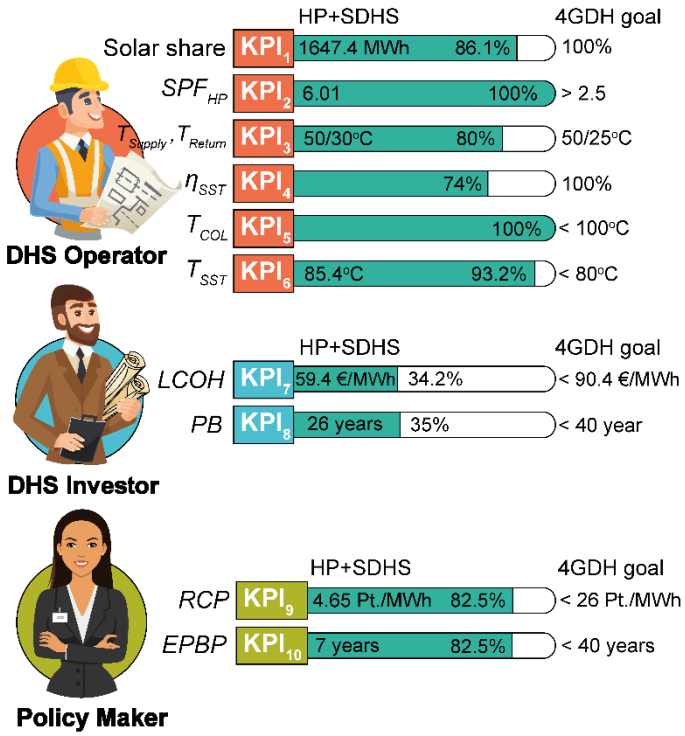

Figure IV-17: KPI achievement rates for the HP integrated with SDHS under control strategy (B) as a part of the 4GDH target.

When it comes to environmental impact and the policy decision-makers, the corresponding KPIs (RCP and $EPBP$) reflect that SDHS can be successful in reducing the adverse environmental effects of the natural gas-based conventional system by 82.5% while delivering energy for 40 years of operational lifetime. Therefore, the proposed configuration of SDHS can help to transform into a future 4GDH producing

a minimum carbon footprint. It also highlights the importance to orchestrate policies for deploying technologies as renewable as possible for building district heating systems in the future.

The overall discussion with KPIs thus indicates that the SDHS model presented in this study can successfully integrate low- temperature renewable heat source, i.e., solar thermal with seasonal and short-term storages with the help of an intelligently controlled heat pump. These technical improvements result in significant economic and sustainability motivations for the concerning stakeholders as compared to the traditional heat supply structures. Therefore, this configuration can be implemented as a 4GDH system in the future district energy systems.

With respect to potential district heating systems stakeholders, the KPIs mentioned above will allow them to have a better understanding of the business assets and to make informed decisions. For every KPI, however, not all the stakeholders have the same priority. DH companies interested in improving the thermal network would be more concerned about the energy and economic KPIs of 4GDH. The importance of environmentally friendly DH technologies typically goes unattended by both network operators and consumers at present. The environmental KPIs, however, provide the policymakers with valuable insight to encourage large-scale DH infrastructures. Furthermore, there may be incoherence between state and local governments with respect to energy policies. For this reason, it is expected that the introduction of sustainable technical solutions such as SDHS and transition towards the 4GDH would yield better results when local legislative authorities and DH operators/owners work together.

IV.7 Conclusion

This paper tends to optimize the performance of a heat pump (HP) enhanced solar assisted district heating system (SDHS) with seasonal storage to facilitate space heating (SH) and domestic hot water (DHW)for a hypothetical urban community located in Madrid, Spain. A multi-objective optimization methodology based on an artificial neural network (ANN) model is adopted through TRNSYS simulations. The objectives that are minimized in this study are cost and aggregated environmental impact while maximizing the energy efficiency of the SDHS model. Two different control strategies are applied to investigate the scope of improving the system stability and overall performance of the network to promote SDHS for implementation as a 4^{th} generation district heating (4GDH). To compare the performance of the proposed system, two baseline scenarios are presented; the conventional heating systems based on natural gas and an optimized SDHS model without integrating the heat pump. The following is a summary of our study's principal findings:

- The ANN model prediction is found to be highly accurate and hence used in our study to train and predict the performance of the SDHS model.

- Compared to the traditional district heating system fueled with natural gas, the estimated Min. cost-optimal solution for the configuration SDHS + HP achieves significant economic and environmental benefits. Under the control system (A), the life cycle cost is reduced to 72.1 €/MWh from 90.3 €/MWh while the environmental impact reduces by 80.6%. These values reduce further to 59.1 €/MWh and 82.5% when the control system (B) is applied. Also, control (B) has been able to outperform control (A) in reducing the consumption of grid electricity by the SDHS by 90%.
- Similar to the economic and environmental results, the energy efficiency of the solar thermal collectors and the solar fraction of the proposed configuration is higher when SDHS is operated under control setting (B) as well as the heat pump has a better seasonal performance factor. The efficiency of seasonal storage is decreased by 17.5% due to the increased amount of heat loss from the storage tank in comparison to control (A). Furthermore, the annual thermal energy profiles of the Min. cost Pareto optimized solutions show that the optimal control strategy (B) can build a better balance between the different heat sources, i.e., the solar collector, storage tanks, heat pump and auxiliary heaters leading to stable performance of the system. This highlights the effectiveness of control (B) to properly integrate a heat pump and seasonal thermal energy storage into a SDHS so that overall efficiency is improved.
- The techno-economic advantages of adding a heat pump into the SDHS with the aid of control strategy (B) is established further by comparing its performance with the second baseline system (SDHS without HP). The SDHS+HP configuration remarkably reduces the solar collector area and the SST insulation requirement, which causes the initial investment and operating cost to be reduced. This allows a return on the investment within the first 26 years of the project lifetime. The new configuration also lowers the temperature level of the collector and the SST, thereby raising the SH efficiency and total solar fraction. Considering the environmental impact, the SDHS+HP produces slightly lesser ecological damage. Thus, investing in a heat pump seems to be a smart policy. The cost associated with the heat pump is compensated by improved energy, economic and sustainable performance of the SDHS.
- The optimization methodology has resulted in several KPI scores for the SDHS, which are consistent with the target KPIs of the 4GDH concept. The combination of the solar thermal with seasonal storage for space heating along with a heat pump to stabilize the overall system performance is close enough to a 4GDH. The supply and return temperature of the SDHS is maintained at 50/30°C while covering 86.1%of the heat demand using renewable energy. Finally, it shows that even if the initial cost of introducing a SDHS+HP system may look like a financial bottleneck for investors, in the

long run, this new configuration has huge potential to generate revenue and as well as helping in decarbonizing the DH sector.

In conclusion, the presented research work shows SDHS assisted with HP can be an attractive energy solution that can lead to substantial techno-economic and environmental benefits over conventional heating systems if the influential design parameters are optimized using a smart control strategy. Furthermore, our study highlights the suitability of the combined configuration of solar thermal energy, seasonal storage, and heat pump as a 4GDH system. The results of this multi-perspective analysis can be used by the key stakeholders as a starting point to develop necessary business models. Future research should concentrate on optimizing the architecture of the thermal distribution grid and improving energy efficiency at the end-user. This will allow the full competitiveness of SDHS for the sustainable energy transition.

IV.8 Acknowledgements

The work is funded by the Spanish government RTI2018-093849-B-C31 and RTI2018-093849-B-C33. The authors would like to thank the Catalan Government for the quality accreditation given to their research group (GREiA - 2017 SGR 1537, AGACAPE - 2017 SGR 1409). GREiA is a certified agent TECNIO in the category of technology developers from the Government of Catalonia. This work is partially supported by ICREA under the ICREA Academia programme. This work is partially funded by the Ministerio de Ciencia, Innovación y Universidades – Agencia Estatal de Investigación (AEI) (RED2018-102431-T). This project has received funding from the European Union's Horizon 2020 research and innovation programme under the Marie Skłodowska-Curie grant agreement No. 713679 and from the Universitat Rovira i Virgili (URV).

IV.9 Nomenclature

A_{COL}	total aperture area of solar collectors (m^2/(MWh·a))
β_{COL}	inclination angle of the solar collectors (^{o})
C_C	total initial capital cost (€)
C_O	total discounted operational cost (€)
C_R	total discounted replacement cost (€)
$Cap_{heating}$	heating capacity of the HP (MW)
d_{con}	construction material thickness of the seasonal storage tank (m)
d_{Roof}	insulation material thickness for the seasonal storage tank roof (m)
d_{Wall}	insulation material thickness for the seasonal storage tank wall (m)

d_{Gnd}	insulation material thickness for the seasonal storage tank ground (m)
DAM_d	indicator result for damage category d
DAM_{off}	Indicator for the environmental damage limits
FC_{AUX}	contribution of the auxiliary heater as a percentage of the maximum heating load (-)
$f_c(x)$	original objective function [$LCOH$(x) or RCP(x)]
FC_{HP}	fraction capacity of the heat pump (-)
$g(x)$	inequality constraints
$h(x)$	equality constraints
h_{conv}	convective heat transfer coefficient to the air W/(m^2·K)
HDR	seasonal storage tank aspect ratio (m/m)
HDR_{DHWT}	domestic hot water storage aspect ratio (m/m)
k	number of regressors
$LCOH$	Levelized cost of heat (€/MWh)
$\dot{m}$	mass flowrate of the recirculating water pumps (kg/s)
n	sample size
N_{COL}	number of solar collectors in series
$\dot{P}_{heating}$	power drawn by the heat pump (MW)
$\dot{Q}_{SOL}$	useful energy rate received by the solar collector field (MW)
$\dot{Q}_{Useful}$	useful energy produced by the solar collector field (MW)
$\dot{Q}_{SST\ loss}$	heat loss rate through the seasonal storage tank (MW)
$\dot{Q}_{DHW\ loss}$	heat loss rate through the domestic hot water storage tank (MW)
$\dot{Q}_{HE}$	heat transfer rate through the heat exchanger (MW)
$\dot{Q}_{AUX}$	duty of auxiliary heater (MW)
$Q_{SH\ load}$	total space heating demand (MWh)
$Q_{DHWload}$	total domestic hot water demand (MWh)
$Q_{SST\ loss}$	total energy losses through the seasonal storage tank (MWh)
R	seasonal storage tank radius (m)
r	interest rate (%)
R_a	revenue of the system (€)
R^2-adj	adjusted coefficient of determination
RCP	ReCiPe 2016 aggregated impact factor (Pt/MWh)

SF_{DHW}	annual solar fraction for the DHW distribution circuit (%)
SF_{global}	overall solar fraction (%)
SF_{SH}	annual solar fraction for the SH distribution circuit (%)
SPF_{HP}	seasonal performance factor (SPF)of the heat pump
$T_{load,in}$	temperatures of the liquid entering on the load side (°C)
$T_{load,out}$	outlet temperatures of the load side (°C)
T_{Return}	return temperature of the district heating network (°C)
$T_{source,out}$	outlet temperatures of the source side (°C)
$T_{source,in}$	temperatures of the liquid entering on the source (°C)
T_{Supply}	supply temperature of the district heating network (°C)
$U_{Overall}$	overall heat loss coefficient of the seasonal storage tank (W/(m^2·K))
V_{DHWT}	volume of the domestic hot water tank (m^3/(MWh·a))
V_{SST}	volume of the seasonal storage tank (m^3/(MWh·a))
$y_{predict,i}$	predicted value
$y_{data,i}$	actual value

Greek symbols

η_{COL}	solar collector field efficiency (%)
η_{DHWT}	domestic hot water storage tank efficiency (%)
η_{SST}	efficiency of the seasonal storage tank
λ_{con}	construction material thermal conductivity of the seasonal storage tank (W/(m·K))
λ_{ins}	insulation material thermal conductivity for the seasonal storage tank roof and wall(W/(m·K))
λ_G	ground thermal conductivity (W/(m·K))
$\lambda_{ins\ gnd}$	insulation material thermal conductivity for the seasonal storage tank ground (W/(m·K))
δ_d	normalization factor for damage category d
ε_d	weighting factor for damage category d
ΔT_{SST}	temperature difference between the extracted and replaced water inside the space heating circuit
ΔT_{DHW}	temperature differences between the extracted and replaced water at storage tanks to cover the DHW load
ΔT_L	temperature difference between the exit and entrance of the auxiliary heater

Abbreviations

4GDH	4th Generation District Heating
ANN	Artificial Neural Network
AUX	Auxiliary Heater (fuelled by natural gas)
COL	solar collector field
DH	District Heating
DHW	Domestic Hot Water
DHWT	Domestic Hot Water Tank
EPBP	Environmental payback period
FG	Foam Glass gravel
GA	Generic Algorithm
HE	Heat Exchanger
HP	Heat Pump
HPC	High-Performance Concrete
KPI	Key Performance Index
LCA	Life Cycle Assessment
LCIA	Life Cycle Impact Assessment
MOO	Multi-Objective Optimization
MOGA	Multi-Objective Genetic Algorithm
MW	Mineral Wool
NC	Normal Concrete
P	Centrifugal pump
PB	Payback Period
SAHP	Solar Assisted Heat Pumps
SDHS	Solar Assisted District Heating System
SH	Space Heating
SST	Seasonal Storage Tank
STES	Seasonal Thermal Energy Storage
TES	Thermal Energy Storage
TRNSYS	Transient system simulation program
UHPC	Ultra-High-Performance Concrete
XPS	Extruded Polystyrene

Indices

d	damage category
i	elementary factor
k	equipment unit

IV.10 Appendix

This section contains the supplemental materials for the article “Flexible Heat Pump Integration to Improve Sustainable Transition Toward 4th Generation District Heating”. The Appendix is organized as follows. First, the methods are explained including the description of (i) The System component modeling, (ii) The components of the levelized cost of heat and (iii) Eco-environmental input parameters. Finally, the nomenclature and acronyms are described, and the list of references is provided.

IV.10.1 The System component modeling – SI 1

The major component models used are presented below:

- Flat-plate solar collector (type 1a): Modeling of flat–plate solar thermal collectors in TRNSYS was accomplished by using the component with an optical efficiency of 0.817 and a heat loss coefficient of 2.205 W/(m^2·K). This component is able to model the thermal performance of the solar collector. The useful heat gain (Q_{Useful}) from a collector of area A_{COL} takes the following form as obtained from [73]:

$$Q_{Useful} = A_{COL}F_r[G_t(\tau\alpha) - U_L(T_i - T_a)] \quad \text{Eq. IV-14}$$

  Here F_r is the collector heat removal factor. The parameters τ,α,G_t and $U_L$represent cover glazing transmittance, absorptance, irradiance and overall heat loss coefficient of solar collector, respectively. Temperature T_i is the heat transfer fluid input temperature and T_a is the ambient temperature. The heat removal factor F_r can be calculated as:

$$F_r = \frac{\dot{m}C_p}{A_{COL}U_L}[1 - \exp\left(-\frac{U_L\acute{F}A_{COL}}{\dot{m}C_p}\right)] \quad \text{Eq. IV-15}$$

  In the above equation, $\dot{m}$, C_p and $\acute{F}$ are the mass flow rate, specific heat and collector efficiency factor, respectively.

- Storage tanks (type 4c): To model SST and DHWT, this type is considered from TRNSYS component libraries. The TRNSYS model permits thermal stratification based on the value of volume segments. The energy supplied by the SST (Q_{SST}) can be calculated, as shown below [74]:

$$Q_{SST} = \int_0^t \dot{m}_{SH} C_p \Delta T_{SST} \quad \text{Eq. IV-16}$$

Here $\dot{m}_{SH}$ represents the mass flow rate of the water that passes through the SH distribution circuit, C_P is the specific heat, and ΔT_{SST} is the temperature difference between water going in and out of the SST to meet the SH requirement.

The performance of the SST depends greatly on the amount of heat losses through the top, sideways and bottom of the storage. Therefore, the Eq. IV-17 - Eq. IV-19 are used to estimate the heat loss coefficients of the SST, as suggested by Hadorn [75].

$$U_{Roof} = \frac{1}{\frac{d_{con}}{\lambda_{con}} + \frac{d_{Roof}}{\lambda_{ins}} + \frac{1}{h_{conv}}} \quad \text{Eq. IV-17}$$

$$U_{Wall} = \frac{1}{\frac{d_{con}}{\lambda_{con}} + \frac{d_{Wall}}{\lambda_{ins}} + \frac{1}{h_{conv}}} \quad \text{Eq. IV-18}$$

$$U_{Gnd} = \frac{2}{R^2}\left\{ a\left(\frac{\lambda_G}{\pi}\right)^2 . \ln\left[\frac{a}{a - \left(\frac{\pi R}{\lambda_G}\right)}\right] - \frac{R.\lambda_G}{\pi} \right\} \quad \text{Eq. IV-19}$$

Where: $$a = \frac{\pi R}{\lambda_G} + \frac{(d_{con} + d_{Gnd})}{\lambda_G} + \frac{d_{con}}{\lambda_{con}} + \frac{d_{Gnd}}{\lambda_{Gnd}}$$

In these above equations U_{Roof}, U_{Wall} ,and U_{Gnd} are the relative heat loss coefficients of the top, wall, and bottom of the SST. R is the SST radius, d_{con}represents the construction material thickness, whereas, d_{Roof}, d_{Wall} and d_{Gnd}represent the top, wall, and bottom surfaces insulation thicknesses of the SST, respectively. In addition, λ_{con}represents the thermal conductivity of the construction material, $\lambda_{ins}$and λ_{Gnd}represent the thermal conductivity of the insulating materials used for the roof, wall, and bottom surfaces of the SST, respectively. Parameter h_{conv} is the convective heat transfer coefficient to the air, and it is assumed to be 10 W/(m^2·K) for equations (3) to (5) [42]. The thermal conductivity of the ground λ_G is considered to be 3 W/(m·K).

The performance of the DHWT is assessed by its capacity to deliver energy (Q_{DHW}) and it can be expressed as [74]:

$$Q_{DHW} = \int_0^t \dot{m}_{DHW} C_p \Delta T_{DHW} \quad \text{Eq. IV-20}$$

The parameter $\dot{m}_{DHW}$ is the mass flow rate of the water re-circulated within the DHW distribution circuits, C_p is the specific heat capacity, and ΔT_{DHW} is the temperature variation between the supplied and returned water in the stratified storage tank for covering the DHW demand. The tank loss coefficient of DHWT is considered as 0.3125 W/(m²·K).

- Water-to-water heat pump (type 927): This model is supplied with normalized data files containing the manufacturer's catalogue data (WSHP-PRC026G-TRANE) for the heat capacity and power consumption for various operating temperatures. The amount of energy in time absorbed from the source fluid stream (Q_{abs}) by a heat pump operating in heating mode can be calculated by using Eq. (9) as shown below [76].

$$\dot{Q}_{abs} = Cap_{heating} - \dot{P}_{heating} \quad \text{Eq. IV-21}$$

Here $Cap_{heating}$ is the heating capacity of the HP, and $\dot{P}_{heating}$ is the power drawn by of the HP. The temperature of liquid exiting the source side of the heat pump ($T_{source,out}$) and temperature of liquid exiting the load side of the heat pump ($T_{load,out}$) can then be calculated using:

$$T_{source,out} = T_{source,in} - \frac{\dot{Q}_{abs}}{\dot{m}_{source} C_{p,source}} \quad \text{Eq. IV-22}$$

$$T_{load,out} = T_{load,in} - \frac{Cap_{heating}}{\dot{m}_{load} C_{p,load}} \quad \text{Eq. IV-23}$$

Here $T_{source,in}$ is the temperature of liquid entering the source side of the heat pump and $T_{load,in}$ is the temperature of liquid entering the load side of the heat pump. Meanwhile, the parameters $\dot{m}_{source}$, $C_{p,source}$, $\dot{m}_{load}$ and $C_{p,load}$ represent mass flow rate and specific heat of liquid stream.

- Auxiliary heaters (type 6): Traditional boilers that run on natural gas are used to maintain the required level of outlet temperature for distribution; one for the SH and another for the DHW. These boilers have an efficiency of 93% and are connected to the corresponding storage tanks in series. The auxiliary heating capacity (Q_{aux}) can be expressed in the following form:

$$\dot{Q}_{AUX} = \dot{m} C_p \Delta T_L \qquad \text{Eq. IV-24}$$

Where $\dot{m}$ is the mass flow rate of water that re-circulates within the SH and DHW distribution network while ΔT_L is the temperature difference of the water at the entrance and exit of the auxiliary heater.

- Heat exchanger (type 5b): A counter-flow heat exchanger with a heat transfer coefficient of 3942 W/(m^2·K) is selected.
- Flow circulation pump (type 3b): This component is a variable speed centrifugal pump. It forces the flow among the heat exchangers, collector, storage tanks, and heat pump base on an on/off signal generated by a differential controller.

The other supporting components are Tee-valves (Type 11h), inlet and outlet pipe ducts (Type 709), flow diverters (Type 11b), weather data processor (Type 15), time-dependent forcing functions for the heating and DHW demand profiles (Type 9), and controllers (Type 2).

IV.10.2 The components of the levelized cost of heat – SI 2

The overall initial cost of investment consists of several items such as the cost of the equipment purchase, installation, and transportation, including the cost of any contingencies and it can be expressed as follows [77]:

$$C_C = (1 + \alpha_{CF}) \sum_k (PEC_k . FBM_k) \qquad \text{Eq. IV-25}$$

Where PEC_k represents the purchase cost of equipment unit k, while the bare module factor FBM_k is responsible for the installation and transportation expense of unit k. α_{CF} denotes the contingency factor. The cost component PEC_k can be updated from the initial value in the base year A to the year of installation B based on the Chemical Engineering Plant Cost Index (CEPCI) using the following equation:

$$PEC_k = PEC_k^{yearA} \frac{CEPCI^{yearB}}{CEPCI^{yearA}} \qquad \forall k \qquad \text{Eq. IV-26}$$

The initial cost of purchasing unit k in year A (PEC_k^{yearA}) can be estimated for various equipment units using Eq. IV-27 - Eq. IV-31.

$$PEC_k^{yearA} = \alpha_k CAP_k^{\beta_k} \qquad \forall k = COL, DHW, AUX \qquad \text{Eq. IV-27}$$

$$PEC_k^{yearA} = \alpha_k (CAP_k^{\beta_k}) CAP_k \qquad \forall k = HP \qquad \text{Eq. IV-28}$$

$$PEC_k^{yearA} = CAP_k^{\beta_k} . 10^{[\alpha_k (log_{10} CAP_k)^{\beta_k}]} \qquad \forall k = HE_1, HE_2, HE_3 \qquad \text{Eq. IV-29}$$

$$PEC_k^{yearA} = \alpha_k \, ln\left(\frac{CAP_k}{1000}\right) + \beta_k \qquad \forall k = P_1, P_2, P_3, P_4 \qquad \text{Eq. IV-30}$$

$$PEC_k^{yearA} = Ins_{SST} + Con_{SST} \qquad \forall k = SST \qquad \text{Eq. IV-31}$$

Where:

$$Ins_{SST} = \alpha_k CAP_k^{\beta_k} \qquad \forall k = XPS, MW, FG$$

$$Con_{SST} = \alpha_k CAP_k^{\beta_k} \qquad \forall k = NC, HPC$$

$$Con_{SST} = \alpha_k e^{\left(\frac{\beta_k}{10^5} CAP_k\right)} \qquad \forall k = UHPC$$

Here α_k and β_k are the equipment cost parameters, CAP_k is responsible for the design variables of equipment unit k. The design variables are the area of the solar collector (A_{COL}), the volume of the fully stratified storage tanks (V_{SST}, V_{DHWT}), types of insulation materials used for the SST (XPS, MW, FG) which includes extruded polystyrene, mineral wool, and foam glass gravel, respectively, types of the SST construction material $(NC, HPC, UHPC)$ comprising of normal concrete, high-performance concrete, and ultra-high performance concrete, respectively, area of heat transfer for the heat exchangers $(A_{HE1}, A_{HE2}, A_{HE3})$, and the mass flow rates of discharge for the pumps $(\dot{m}_1, \dot{m}_2, \dot{m}_3, \dot{m}_4)$.The total operating cost (C_o) is the discounted summation of all annual operating costs and can be expressed as follows:

$$C_O = C_M PWF_M + C_P PWF_P + C_{AUX} PWF_{AUX} \qquad \text{Eq. IV-32}$$

Where the C_M indicate the annual maintenance, C_P is the electricity cost due to the recirculation pumps, and heat pump. While C_{AUX} is the energy cost of the auxiliary heaters (natural gas boilers). The term PWF reflects the present worth factor which is calculated for the specific cost of operation taking into account the inflation rate (i) and the rate of interest (r) over the lifetime of the proposed system. The cost of replacing several equipment units of the proposed SDHS can be estimated as shown below:

$$C_R = PVF_n \sum_k (PEC_k . FBM_k) \qquad \text{Eq. IV-33}$$

Here PVF_n is the present value factor of the future cash flows in the year n. The equipments which will incur a replacement cost in our study due to a high rate of

depreciation over the system's lifespan are the solar collectors, storage tank used for DHW, heat pump, heat exchangers, and auxiliary heaters.

IV.10.3 Eco-environmental input parameters – SI 3

The initial cost parameters are outlined in Table SIV-4. On the other hand, the annual maintenance costs are estimated to be 1.5% of its investment cost. Based on the EUROSTAT database [78], the natural gas and household electricity prices are 0.0526 and 0.1873 Euro/kWh, respectively. In addition, an inflation rate of 5.9% and 5% is selected for the natural gas and electricity, respectively. Aligning with Braungardt et al. [13] recommendation, an inflation rate of 2.3% is selected for the proposed system, whereas the discount rate is 3.5%.

Table SIV-4: The economic parameters for the initial cost of the heat pump integrated into SDHS

Unit	Options	α_k	β_k	CAP_k	Range	Base year	Ref.	FBM_k
Solar collector		974.2	0.8330	Aperture area (m^2)	4000-15,000	2007	[79]	1.00
Heat pump		2053.8	-0.348	Thermal power (kW)	600-100,000	2014	[50]	1.00
DHWT		3955	0.6500	Volume (m^3)	1-100,000	2007	[80]	1.00
Auxiliary heater		225.0	0.7460	Duty (kW)	600-10,000	2001	[77]	2.10
Heat exchanger		3.133	0.3310	Exchange area (m^2)	10-1000 m^2	2001	[77]	3.29
Pump (P_1, P_2)		389.0	283.2	Mass flow rate (kg/h)	15000-100,000	2009	[81]	3.24
Pump (P_3, P_4)		389.0	717.0	Mass flow rate (kg/h)	15000-100,000	2009	[81]	3.24
SST insulation	XPS	561.09	0.397	Material thickness (m)	0.05-0.8	2017	[82]	1.00
	MW	1902.7	0.942	Material thickness (m)	0.05-0.8	2018	[83]	1.00
	FG	311.41	0.968	Material thickness (m)	0.05-0.8	2014	[84]	1.00
STT construction	NC	4178.1	-0.394	Volume (m^3)	1-100,000	2000		1.00
	HPC	2575	-0.363	Volume (m^3)	1-100,000	2004	[85]	1.00
	$UHPC$	90.83	-3	Volume (m^3)	1-100,000	2004		1.00

On the other hand, the LCA input parameters are extracted from the Ecoinvent database [86]. This database categorizes the damage associated with the SDHS equipment based on the Recipe 2016 approach, a summary of the impact of different components in the SDHS is shown in Table S2.

Table SIV-5: The environmental impact of heat pump integrated SDHS equipment based on ReCiPe 2016

Unit	Option	Impact factor (ReCiPe 2016)
Solar collector		32.5 Pt/m^2
Heat pump		22.3 Pt/kW
DHWT		173.1 Pt/m^3
Auxiliary boiler		$1.57 \cdot 10^3$ Pt/kW
Heat exchanger		2.515 Pt/m^2
Pump		62.8 Pt/kW
SST insulation	XPS	0.773 Pt/kg
	MW	0.0016 Pt/kg
	FG	0.266 Pt/kg
SST construction	NC	0.008 Pt/kg
	HPC	0.002 Pt/kg
	$UHPC$	0.0206 Pt/kg
Natural gas		0.0245 Pt/kWh
Electricity		0.0380 Pt/kWh

IV.11 Reference

[1] EAA. Trends and projections in Europe 2019. 2019. doi:10.2800/51114.

[2] Lund H, Østergaard PA, Connolly D, Mathiesen BV. Smart energy and smart energy systems. Energy 2017. doi:10.1016/j.energy.2017.05.123.

[3] Lund H, Duic N, Østergaard PA, Mathiesen BV. Smart energy systems and 4th generation district heating. Energy 2016. doi:10.1016/j.energy.2016.07.105.

[4] Connolly D, Lund H, Mathiesen B V., Werner S, Möller B, Persson U, et al. Heat roadmap Europe: Combining district heating with heat savings to decarbonise the EU energy system. Energy Policy 2014. doi:10.1016/j.enpol.2013.10.035.

[5] Lund H, Duic N, Østergaard PA, Mathiesen BV. Future district heating systems and technologies: On the role of smart energy systems and 4th generation district heating. Energy 2018. doi:10.1016/j.energy.2018.09.115.

[6] Schmidt D, Kallert A, Blesl M, Svendsen S, Li H, Nord N, et al. Low Temperature District Heating for Future Energy Systems. Energy Procedia, 2017. doi:10.1016/j.egypro.2017.05.052.

[7] Buffa S, Cozzini M, D'Antoni M, Baratieri M, Fedrizzi R. 5th generation district heating and cooling systems: A review of existing cases in Europe. Renew Sustain Energy Rev 2019. doi:10.1016/j.rser.2018.12.059.

[8] Prando D, Prada A, Ochs F, Gasparella A, Baratieri M. Analysis of the energy and economic impact of cost-optimal buildings refurbishment on district heating systems. Sci Technol Built Environ 2015. doi:10.1080/23744731.2015.1040343.

[9] Li H, Nord N. Transition to the 4th generation district heating - Possibilities, bottlenecks, and challenges. Energy Procedia, 2018. doi:10.1016/j.egypro.2018.08.213.

[10] Lygnerud K. Business model changes in district heating: The impact of the technology shift from the third to the fourth generation. Energies 2019. doi:10.3390/en12091778.

[11] Guzzini A, Pellegrini M, Pelliconi E, Saccani C. Low temperature district heating: An expert opinion survey. Energies 2020. doi:10.3390/en13040810.

[12] Hmadi M, Mourtada A, Daou R. Forecasting the performance of a district solar thermal smart network in desert climate – A case study. Energy Convers Manag 2020;207:112521. doi:10.1016/j.enconman.2020.112521.

[13] Provasnek AK, Putz S. IEA SHC task 55: Towards the integration of large SHC systems into DHC networks. ISES Sol. World Congr. 2017 - IEA SHC Int. Conf. Sol. Heat. Cool. Build. Ind. 2017, Proc., 2017. doi:10.18086/swc.2017.06.10.

[14] Weiss W, Spörk-Dür M. Solar Heat Worldwide 2018. Global Market Development and Trends in 2017. Detailed Market Figures 2016. IEA Sol Heat Cool Program 2018. doi:10.1017/CBO9781107415324.004.

[15] Xu L, Torrens JI, Guo F, Yang X, Hensen JLM. Application of large underground seasonal thermal energy storage in district heating system: A model-based energy performance assessment of a pilot system in Chifeng, China. Appl Therm Eng 2018. doi:10.1016/j.applthermaleng.2018.03.047.

[16] Dahash A, Ochs F, Janetti MB, Streicher W. Advances in seasonal thermal energy storage for solar district heating applications: A critical review on large-scale hot-water tank and pit thermal energy storage systems. Appl Energy 2019;239:296–315. doi:10.1016/j.apenergy.2019.01.189.

[17] Hesaraki A, Holmberg S, Haghighat F. Seasonal thermal energy storage with heat pumps and low temperatures in building projects - A comparative review. Renew Sustain Energy Rev 2015;43:1199–213. doi:10.1016/j.rser.2014.12.002.

[18] Chwieduk DA. Solar-assisted heat pumps. Compr. Renew. Energy, 2012. doi:10.1016/B978-0-08-087872-0.00321-8.

[19] Marx R, Bauer D, Drueck H. Energy Efficient Integration of Heat Pumps into Solar District Heating Systems with Seasonal Thermal Energy Storage. Energy Procedia, 2014. doi:10.1016/j.egypro.2014.10.302.

[20] David A, Mathiesen BV, Averfalk H, Werner S, Lund H. Heat Roadmap Europe: Large-scale electric heat pumps in district heating systems. Energies 2017. doi:10.3390/en10040578.

[21] Tschopp D, Tian Z, Berberich M, Fan J, Perers B, Furbo S. Large-scale solar thermal systems in leading countries: A review and comparative study of Denmark, China, Germany and Austria. Appl Energy 2020;270:114997. doi:10.1016/j.apenergy.2020.114997.

[22] Garcia NP, Vatopoulos K, Lopez AP, Thiel C. Best available technologies for the heat and cooling market in the European Union. JRC Scientif and Policy Reports. 2012. doi:10.2790/5813.

[23] Song Z, Ji J, Cai J, Li Z, Gao Y. Performance prediction on a novel solar assisted heat pump with hybrid Fresnel PV plus TEG evaporator. Energy Convers Manag 2020;210:112651. doi:10.1016/j.enconman.2020.112651.

[24] Pardo García N, Zubi G, Pasaoglu G, Dufo-López R. Photovoltaic thermal hybrid solar collector and district heating configurations for a Central European multi-family house. Energy Convers Manag 2017;148:915–24. doi:10.1016/j.enconman.2017.05.065.

[25] Chaturvedi SK, Gagrani VD, Abdel-Salam TM. Solar-assisted heat pump - A sustainable system for low-temperature water heating applications. Energy Convers Manag 2014. doi:10.1016/j.enconman.2013.09.050.

[26] Sterling SJ, Collins MR. Feasibility analysis of an indirect heat pump assisted solar domestic hot water system. Appl Energy 2012. doi:10.1016/j.apenergy.2011.05.050.

[27] Kim T, Choi B Il, Han YS, Do KH. A comparative investigation of solar-assisted heat pumps with solar thermal collectors for a hot water supply system. Energy Convers Manag 2018. doi:10.1016/j.enconman.2018.07.035.

[28] Banister CJ, Collins MR. Development and performance of a dual tank solar-assisted heat pump system. Appl Energy 2015. doi:10.1016/j.apenergy.2015.03.130.

[29] Kim MH, Kim D, Heo J, Lee DW. Techno-economic analysis of hybrid renewable energy system with solar district heating for net zero energy community. Energy 2019. doi:10.1016/j.energy.2019.115916.

[30] Østergaard PA, Andersen AN. Economic feasibility of booster heat pumps in heat pump-based district heating systems. Energy 2018. doi:10.1016/j.energy.2018.05.076.

[31] Hirvonen J, ur Rehman H, Sirén K. Techno-economic optimization and analysis of a high latitude solar district heating system with seasonal storage, considering different community sizes. Sol Energy 2018;162:472–88. doi:10.1016/j.solener.2018.01.052.

[32] Rehman H ur, Hirvonen J, Sirén K. Performance comparison between optimized design of a centralized and semi-decentralized community size solar district heating system. Appl Energy 2018;229:1072–94. doi:10.1016/j.apenergy.2018.08.064.

[33] Khorasaninejad E, Hajabdollahi H. Thermo-economic and environmental optimization of solar assisted heat pump by using multi-objective particle swam algorithm. Energy 2014;72:680–90. doi:10.1016/j.energy.2014.05.095.

[34] Fazlollahi S, Becker G, Ashouri A, Maréchal F. Multi-objective, multi-period optimization of district energy systems: IV - A case study. Energy 2015;84:365–81. doi:10.1016/j.energy.2015.03.003.

[35] Kalogirou SA. Applications of artificial neural-networks for energy systems. Appl Energy 2000. doi:10.1016/S0306-2619(00)00005-2.

[36] Kumar R, Aggarwal RK, Sharma JD. Energy analysis of a building using artificial neural network: A review. Energy Build 2013. doi:10.1016/j.enbuild.2013.06.007.

[37] Wong SL, Wan KKW, Lam TNT. Artificial neural networks for energy analysis of office buildings with daylighting. Appl Energy 2010;87:551–7. doi:10.1016/j.apenergy.2009.06.028.

[38] Esen H, Inalli M, Sengur A, Esen M. Performance prediction of a ground-coupled heat pump system using artificial neural networks. Expert Syst Appl 2008. doi:10.1016/j.eswa.2007.08.081.

[39] Xia L, Ma Z, Kokogiannakis G, Wang Z, Wang S. A model-based design optimization strategy for ground source heat pump systems with integrated photovoltaic thermal collectors. Appl Energy 2018;214:178–90. doi:10.1016/j.apenergy.2018.01.067.

[40] Hirvonen J, ur Rehman H, Deb K, Sirén K. Neural network metamodelling in multi-objective optimization of a high latitude solar community. Sol Energy 2017. doi:10.1016/j.solener.2017.06.040.

[41] Tulus V, Abokersh MH, Cabeza LF, Vallès M, Jiménez L, Boer D. Economic and environmental potential for solar assisted central heating plants in the EU residential sector: Contribution to the 2030 climate and energy EU agenda. Appl Energy 2019. doi:10.1016/j.apenergy.2018.11.094.

[42] Abokersh MH, Vallès M, Cabeza LF, Boer D. A framework for the optimal integration of solar assisted district heating in different urban sized communities : A robust machine learning approach incorporating global sensitivity analysis. Appl Energy 2020;267:114903. doi:10.1016/j.apenergy.2020.114903.

[43] Rehman H ur, Hirvonen J, Sirén K. Influence of technical failures on the performance of an optimized community-size solar heating system in Nordic conditions. J Clean Prod 2018;175:624–40. doi:10.1016/j.jclepro.2017.12.088.

[44] United Nations Environment Programme, Solar Thermal Energy Technology Fact Sheet. 2014.

[45] Hobbi A, Siddiqui K. Optimal design of a forced circulation solar water heating system for a residential unit in cold climate using TRNSYS. Sol Energy 2009;83:700–14. doi:10.1016/j.solener.2008.10.018.

[46] Hui L, Edem NTK, Nolwenn LP, Lingai L. Evaluation of a seasonal storage system of solar energy for house heating using different absorption couples. Energy Convers Manag 2011;52:2427–36. doi:10.1016/j.enconman.2010.12.049.

[47] Lorenzo C, Narvarte L. Performance indicators of photovoltaic heat-pumps. Heliyon 2019;5:e02691. doi:10.1016/j.heliyon.2019.e02691.

[48] Hang Y, Qu M, Ukkusuri S. Optimizing the design of a solar cooling system using central composite design techniques. Energy Build 2011;43:988–94. doi:10.1016/j.enbuild.2010.12.024.

[49] Allouhi A, Agrouaz Y, Benzakour Amine M, Rehman S, Buker MS, Kousksou T, et al. Design optimization of a multi-temperature solar thermal heating system for an industrial process. Appl Energy 2017;206:382–92. doi:10.1016/j.apenergy.2017.08.196.

[50] Welsch B, Göllner-Völker L, Schulte DO, Bär K, Sass I, Schebek L. Environmental and economic assessment of borehole thermal energy storage in district heating systems. Appl Energy 2018;216:73–90. doi:10.1016/j.apenergy.2018.02.011.

[51] Gabbrielli R, Castrataro P, Del Medico F, Di Palo M, Lenzo B. Levelized cost of heat for linear Fresnel concentrated solar systems. Energy Procedia, 2014. doi:10.1016/j.egypro.2014.03.143.

[52] Kalogirou SA. Solar Energy Engineering: Processes and Systems. Second edi. Amsterdam: Elsevier Inc.; 2014. doi:10.1007/978-3-662-49120-1_32.

[53] Buonomano A, Calise F, Palombo A, Vicidomini M. Transient analysis , exergy and thermo-economic modelling of façade integrated photovoltaic / thermal solar collectors. Renew Energy 2019;137:109–26. doi:10.1016/j.renene.2017.11.060.

[54] Guillén-Gosálbez G, Caballero JA, Jiménez L. Application of Life Cycle Assessment to the Structural Optimization of Process Flowsheets. Ind Eng Chem Res 2008;47:777–89. doi:10.1016/S1570-7946(07)80218-5.

[55] Goedkoop M, Heijungs R, Huijbregts M, Schryver A De, Struijs J, Zelm R Van. ReCiPe 2008, A life cycle impact assessment method which comprises harmonised category indicators at the midpoint and the endpoint level. First edition. Report I: Characterisation. 2009.

[56] Gursel AP, Ostertag C. Comparative life-cycle impact assessment of concrete manufacturing in Singapore. Int J Life Cycle Assess 2017. doi:10.1007/s11367-016-1149-y.

[57] Li DHW, Lam TNT, Chan WWH, Mak AHL. Energy and cost analysis of semi-transparent photovoltaic in office buildings. Appl Energy 2009;86:722–9. doi:10.1016/j.apenergy.2008.08.009.

[58] Dammeier LC, Loriaux JM, Steinmann ZJN, Smits DA, Wijnant IL, Van Den Hurk B, et al. Space, Time, and Size Dependencies of Greenhouse Gas Payback Times of Wind Turbines in Northwestern Europe. Environ Sci Technol 2019;53:9289–97. doi:10.1021/acs.est.9b01030.

[59] Gibb D, Johnson M, Romaní J, Gasia J, Cabeza LF, Seitz A. Process integration of thermal energy storage systems – Evaluation methodology and case studies. Appl Energy 2018;230:750–60. doi:10.1016/j.apenergy.2018.09.001.

[60] Volkova A, Ma V, Siirde A. Methodology for evaluating the transition process dynamics towards 4th generation district heating networks 2018;150. doi:10.1016/j.energy.2018.02.123.

[61] Kucherenko S, Albrecht D, Saltelli A. Exploring multi-dimensional spaces: a Comparison of Latin Hypercube and Quasi Monte Carlo Sampling Techniques. 8th IMACS Semin. Monte Carlo methods, 2015, p. 1–32. doi:10.1016/j.ress.2017. 04.003.

[62] Bauer D, Marx R, Nußbicker-Lux J, Ochs F, Heidemann W, Müller-Steinhagen H. German central solar heating plants with seasonal heat storage. Sol Energy 2010;84:612–23. doi:10.1016/j.solener.2009.05.013.

[63] Solites. Guideline for Seasonal Thermal Energy Storage Systems in the Built Environment. Stuttgart: 2016.

[64] Konak A, Coit DW, Smith AE. Multi-objective optimization using genetic algorithms : A tutorial. Reliab Eng Syst Saf 2006;91:992–1007. doi:10.1016/j.ress.2005.11.018.

[65] Ibrahim D, Jobson M, Li J, Guillén-Gosálbez G. Optimization-based design of crude oil distillation units using surrogate column models and a support vector machine. Chem Eng Res Des 2018;134:212–25. doi:10.1016/j.cherd.2018.03.006.

[66] Deb K. Multiobjective Optimization Using Evolutionary Algorithms. New York, NY: John Wiley & Sons, Inc; 2001.

[67] Skiborowski M, Rautenberg M, Marquardt W. A Hybrid Evolutionary-Deterministic Optimization Approach for Conceptual Design. Ind Eng Chem Res 2015;54:10054–72. doi:10.1021/acs.iecr.5b01995.

[68] Institute for Energy Diversification and Saving - IDAE. Análisis del consumo

energético del sector residencial en España. INFORME FINAL; 2011.

[69] U.S. Department of Energy. EnergyPlus. Energy Simulation Software: Weather Data n.d. 2015.

[70] Guadalfajara M. Evaluación de centrales solares térmicas con acumulación estacional para el sector residencial en España. 2013. doi:10.1017/CBO9781107415324.004.

[71] Jordan U, Vajen K. DHWcalc: program to generate domestic hot water profiles with statistical means for user defined conditions. Proc. ISES Sol. World Congr., Orlando (US): n.d., p. 8–12.

[72] REN21. Renewables 2020 Global Status Report. 2020.

[73] Kalogirou SA. Solar thermal collectors and applications. Prog Energy Combust Sci 2004. doi:10.1016/j.pecs.2004.02.001.

[74] Duffie JA, Beckman WA. Wiley: Solar Engineering of Thermal Processes, 4th Edition - John A. Duffie, William A. Beckman. 2013.

[75] Hadorn J. Guide to Seasonal Heat Storage. SIA, Swiss Association of Engineers and Architects. Zurich: 1990.

[76] TESS – Thermal Energy Systems Specialists. TESSLibs 17: Component Libraries for the TRNSYS Simulation Environment, HVAC Library Mathematical Reference. vol. 06. 2014.

[77] Tulus V, Boer D, Cabeza LF, Jiménez L, Guillén-Gosálbez G. Enhanced thermal energy supply via central solar heating plants with seasonal storage: A multi-objective optimization approach. Appl Energy 2016;181:549–61. doi:10.1016/j.apenergy.2016.08.037.

[78] European Commision. EuroStat 2018. http://ec.europa.eu/eurostat/web/energy/data/database (accessed March 12, 2018).

[79] Ellehauge K PT. Solar heat storages in district heating networks. Energinet.dk, PREHEAT project no. 2006-2-6750. 2007.

[80] Schmidt T MD. Status of solar thermal seasonal storage in Germany. 2009.

[81] Calise F, Dentice d'Accadia M, Palombo A. Transient analysis and energy optimization of solar heating and cooling systems in various configurations. Sol Energy 2010;84:432–49. doi:10.1016/j.solener.2010.01.001.

[82] austrotherm. General price list. 2017. doi:10.5962/bhl.title.138707.

[83] Specialist Insulation Supplies Ltd. Prices list. 2018.

[84] GLAPOR-Schaumglasprodukte. GLAPOR PRICE LIST. Belgium: 2014.

[85] Reineck K, Greiner S, Reinhardt H. Dichte Heißwasser-Wärmespeicher aus ultrahochfestem Faserfeinkornbeton. Stuttgart: 2004.

[86] Ecoinvent. Eco invent 2017. https://www.ecoinvent.org/home.html (accessed March 12, 2018).

Chapter V

Thermal Energy Storage in Circular Economy

V. Thermal Energy Storage in Circular Economy

A Framework for Circular System Design: Application on Thermal Energy Storage

Mohamed Hany Abokersh [a], Masoud Norouzi [b], Dieter Boer [a], Luisa F.Cabeza [c], Gemma Casa [c], Cristina Prietod [e], Laureano Jiménez [b], Manel Vallès [a]

[a] Departament d'Enginyeria Mecànica, Universitat Rovira i Virgili, Av. Països Catalans 26, 43007, Tarragona, Spain

[b] Departament d'Enginyeria Química, Universitat Rovira i Virgili, Av. Països Catalans 26, 43007, Tarragona, Spain

[c] GREiA Research Group, Universitat de Lleida, Pere de Cabrera s/n, 25001, Lleida, Spain

[d] Abengoa, Energía Solar 1, 41014, Sevilla, Spain

[e] Department of Energy Engineering, University of Seville, Camino de los Descubrimientos s/n, 41092 Sevilla, Spain

E-mail addresses: mohamed.abokersh@urv.cat (M.H. Abokersh), masoud.norouzi@urv.cat (K. Norouzi), Dieter Boer (dieter.boer@urv.cat), luisaf.cabeza@udl.cat (L.F. Cabeza), greia@diei.udl.cat (Gemma Casa), cristina.prieto@abengoa.com (Cristina Prieto), laureano.jimenez@urv.cat (Laurean Jjimenez), manel.valles@urv.cat (Manel Valles)

V.1 Introduction

There are a new series of social hurdles, owing to the massive stress on organizational resources and the massive expansion of the worldwide population. The consumption of oil, food, water, components and other resources has risen, and suppliers are coping with this development [1]. The exponential progress of the world and the rapid growth of developing markets indicate that energy demand is growing, and costs have typically risen after the new century [2]. The European Union approved a new clean energy framework for a sustainable transition from fossil fuel usage to renewable energy following up the EU's 2030 greenhouse gases reduction

targets [3]. An important step to spread on the clean energy transition in the European Union and its Member States is renewable energy usage. Out of all renewable energy-based systems, the solar thermal system is the technology that can be expanded from residential applications to urban applications [4].

The concentrating solar power (CSP) plants are becoming the best option to produce clean thermal energy [5]. However, it presents a challenge as temporal fluctuations are experienced based on seasonality and daily patterns. However, this challenge can be overcome by implying energy storage, namely thermal energy storage [6]. The efficiency, as well as the flexibility of the thermal solar applications, can be greatly increased with the help of thermal energy storage systems (TES) where the excess energy produced by the system is stored and then used later when the thermal energy is needed [7]. It is one of the most common backup energy systems in the case of solar heating systems. Flexibility between supply and demand can be managed using the large scale TES and CSP [8]. The TES are classified into the following types on the basis of storage technologies [9]: (1) usage of chemical, which is known as chemical storage. (2) the use of phase change materials (PCM), which is known as latent heat storage (3) heat stored in the liquid media and solid media is known as sensible heat storage.

Due to favourable properties such as higher specific heat, lower cost, mechanical properties, and easy processing, concrete is the material often chosen for sensible heat storage at high temperatures [5]. Whereas for the liquid media, materials such as mineral oils, molten salts, and synthetic oils can be used [10]. Due to the density difference between the hot and cold fluids, the material maintains natural thermal stratification. Due to the heat of fusion, heat can be stored nearly isothermally in some materials using latent heat [11]. According to the temperature range and the application, the correct PCM should be chosen [12]. The correct PCM in each system has to be chosen depending on the application and its working temperature range [13].

According to a recent study by Palacios et al.[9], the publications regarding TES have increased exponentially. However, most of those publications have neglected the sustainability aspect and have only addressed the technical aspects such as (new control, new applications, new enhancement in technologies, and new materials) [14]. Following the IEA energy storage roadmap, the importance of TES was also highlighted, with a potential for CO_2 emissions reduction estimated to be 2.6 Gt [15]. Furthermore, A recent study shows that TES have significant environmental impacts [16]. One reason for the high impact is the absence for the closing of material loops in addition to the lack of sustainable redesigning concepts for thermal energy storage. Thus, a comprehensive environmental assessment such as life cycle assessment (LCA) [17] can be a key aspect to fulfil the European legislation [18] regarding the necessary decision support to minimize the environmental burdens associated with the utilization of the TES. Furthermore, technologies in integrated waste management

systems (WMS) such as waste treatment technologies and a combination of recycling and reused concept can also be useful in analyzing TES [19]. In this context, Guarino et al. [20] and Abokersh et al. [16] examined seasonal TES and its environmental impact in a complete district heating infrastructure. In addition, during the manufacturing and operation phase of the three different TES types for solar power plants, their impacts on the environment were compared by Oró et al.[21]. Furthermore, the LCA of two TES designs, namely indirect thermocline and indirect molten salt are compared by Heath et al. [22]. Most of the life cycle assessments of the TES have focused on the production, operation, as well as the end life as a single value [23]. Thus, all these studies did not focus on environmental analysis due to the potential of recycling and reuse of materials.

Regarding this limitation and to revise the current linear economy with a 'take disposition' model, the circular economy (CE) is one of the techniques endorsed by the United Nations Environmental Program (UNEP) and the Ellen MacArthur Foundation for decoupling [24,25]. The CE can be defined in large part as an industrial system that is intentionally and in terms of design restorative or regenerative. The Ellen MacArthur Foundation replaces the idea of end-of-life with reorganization and shifts to use of sustainable resources and eliminate utilization by a more advanced level of substance, processes, and business designs of chemical pollutants that impact reusability and waste reversion [26]. This substitutes the notion of a deficit with the regenerative framework to differentiate financial growth from the use of new environmental assets. There are numerous definitions of circular economy in the literature. CE can be explained with the help of 10 circular strategies. (R0: refuse, R1: rethink, R2: reduce, R3: reuse, R4: repair, R5: refurbish, R6: re-manufacture, R7: repurpose, R8: recycle, R9: recover, based on Potting et al.[27]. The CE has many links to sustainable development for economic prosperity, social equity, and environmental quality [28]. Globally, circularity can be achieved by implementing a clean cycle strategy which may start by improving material circularity through improving its environmental life cycle [29].

To assess CE, different methodologies have been proposed and applied, most prominently material flow analysis (MFA) and LCA [30,31]. MFA is a tool that helps to understand the flow of a waste management system as well as it is a starting point of the environmental assessment. Furthermore, the MFA reveal opportunities for improving and monitoring the recycling targets [32]. On the other hand, the LCA can be used to assess the system's environmental performance [21]. However, a complete LCA is laborious and complex as well [33]. Another approach is to use a shortened LCA form, also known as streamlined LCA [34]. Besides, Project PRO SUITE [35] has presented another approach that takes into account all activities and their effects on the economy, society, and environment. The assessment proposed by them is based on the five pillars which are (1) Impact on Exhaustible Resources, (2) Social Well-being, (3) Prosperity, (4) Natural Environment, and (5) Human Health.

However, the sustainability of TES has not been assessed using these methods. Following Cobo et al. [36], other assessment methodologies were proposed to assess CE including the life cycle costing [37], economic and environmental optimization [38], and the combination of MFA and LCA in multi-objective optimization [39]. Even though the previously mentioned strategies can be utilized for the appraisal of CE parts of the TES, an extensive and organized strategy for the frameworks that grasp CE features, while decreasing ecological effects for the TES, is as of now lacking.

This study's main goal is to develop a method for sustainable circular system design (SCSD) that ecologically assesses the sustainability of TES technologies. The method can be utilized to increase circularity and the sustainability of those derived measures. TES is included in this new CE approach of considering our actions, as energy is part of the concept. Going ahead, when developing TES and materials, CE principles should be considered. These principles are territorial ecology, "functionality" economy, reuse, second use, recycle, reparation, industrial, eco-design, and valorization. The technique draws from the pool of conceivable outcomes CE offers, minimal ecological damage, material quality aspects, product design considerations, circularity strategies within the production chain (R0-R9), and waste hierarchy.

The developed SCSD methodology will be tested on high-temperature TES technology using liquid media system with molten salt. Furthermore, SCSD embraces the analysis for the most intensive processes within TES technology through proposing the different ecological scenario including (i) increasing recycling rates, (ii) increasing the reuse rates, and (iii) a combination of both. The article's structure is as follows: A general outline of the SCSD methodology aspects is proposed in section 2. Section 3 describes the application of the methodology through high-temperature TES technology. Section 4 presents the article results and their relevant findings. The results summaries and work conclusion are shown in section 5.

V.2 The sustainable circular system design (SCSD) framework

The proposed methodology framework for evaluating the circularity of TES is illustrated in Figure V-1. The framework is structured in a 3-phases approach for sustainable evaluating of TES. The first phase (A) is mapping the overall waste movements and management procedures through introducing the material flow analysis (MFA) for TES bill of materials. Besides, it shows the residuals and contaminations need to be considered. Once this evaluation is implemented, the life cycle assessment (LCA) presents the environmental evaluation of the TES materials. In the second phase (B), the circularity metric is proposed to estimate product preservation through recycling and reuse techniques. The second step in phase (B) is to evaluate the overall sustainability of TES through combining the LCA indicator with the CE index. Finally, the third phase (C) offers a complete analysis for the effect of various scenarios on the TES circularity.

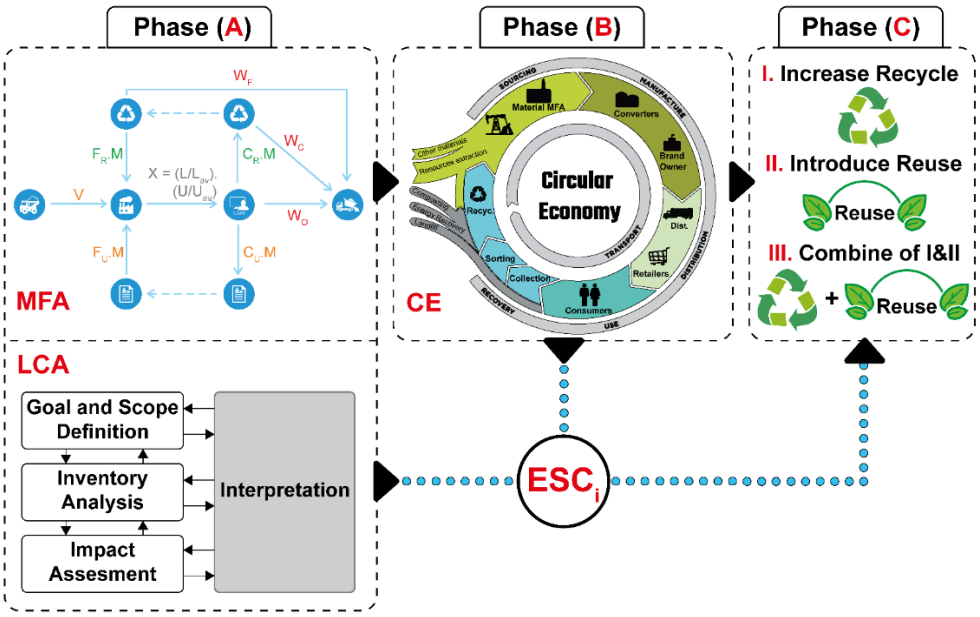

Figure V-1: The SCSD outlines

V.2.1 MFA/LCA assessment

This phase entails the environmental impact of the product (TES), where the proposed MFA/LCA module has been implemented following Haupt et al.[17] guidelines.

V.2.1.1 Material flow analysis (MFA)

The MFA offers the transfer factors for all residues processes in multiple entities that can be used for LCA calculations. To fabricate an input dependent model of waste management using LCAs, MFA can be used as the base. Knowledge of the transfer coefficients for all treatments (recycling, incineration, and landfilling) permits designing process inventories for arranging and reusing according to the MFA and ensures the preservation of the mass balance in the framework. MFA includes the comprehensive measurement of the content input and output flows into space at a time specified framework. The system in which input flows are equivalent to the output flows with addition to the accretion of substance in the system [40], as illustrated in Figure V-2, is handled as the black box.

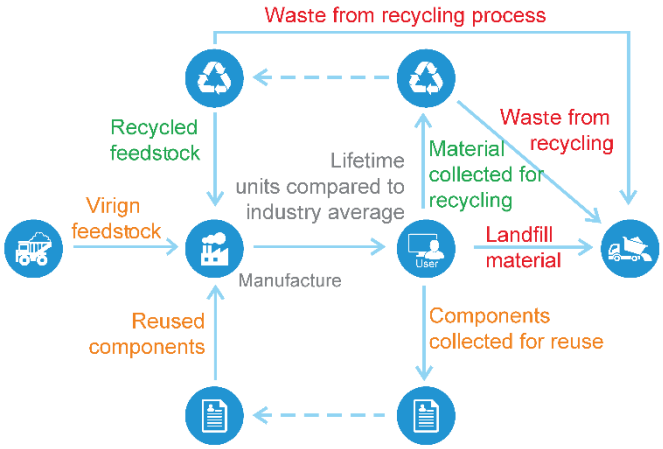

Figure V-2: Schematic representation for the MFA [41]

The MFA starts by establishing the boundaries of time and space. This strategy includes the examined process as an operation in the anthroposphere. The input flows involve all raw resources mined from nature, and the domestic extraction (DE). Hidden flows are products not evident from economic records but needed to produce the resource used at the end, for example, earth-removed products and overburdened mining materials or wood harvest reductions in forestry. Hidden flows, called environmental backpack or “Rucksack”, are measured by means of the Material Intensity per Unit of Service (MIPS) database, given by the Wuppertal Institute [42]. MIPS is a measuring unit designed by the Wuppertal Institute that monitors the material intensity of different products and services with respect to a particular product unit. MIPS measures how products are different from their normal extractions, as Ritthof et al. [43]. All content used is measured in relation to natural resource usages during the production, usage and recovery or disposal. The definition of the MIPS is based on the perception that the capacity for the product's environmental impact can be measured by the Material Input (MI) across its lifespan. Lesser raw materials utilized; lesser environmental impacts faced. As per Ritthof et al. [43], such items have their ecological impact as an intangible "ecological rucksack," i.e. as per the MIPS definition. The eco-backpack can be measured by extracting the product's total weight from the MI (Ecological Backpack = MI-net weight).

V.2.1.2 Life cycle assessment (LCA)

The LCA is a method for the environmental evaluation connected with material, products or operation under which resources, energy and atmosphere (from the cradle to the grave) are defined and quantified [44]. LCA contributes, including the

production, utilization and landfill process, for all resource and energy inputs and outputs of a product over its lifetime. The environmental impact measured by conducting an LCA practice must be transformed into a singular dimensionless value. The proposed procedure includes two sub-processes: standardization and weighting; two additional components of the LCA method of life-cycle impact assessment, as defined in the ISO 14044 International Standard [45]. Standardization is the magnitude measurement for the reference information of the section indicating findings. This will also help convey details on the relative value of the indicator's effects [46]. Weighting is a procedure using numerical variables to transform the findings of the impact category metrics, enabling the converted metrics to be aggregated further [47]. LCA intends to examine the unique influence of a product or service to the environmental burdens in its various life cycle phases. The ISO 14040:2006 and ISO 14044:2006 [45,48,49] sets out four interrelated measures: (1) Goal and scope definition; (2) inventory analysis; (3) impact assessment; (4) interpretation which identifies relevant issues and formulates recommendations. These phases are explained in detail in the next subsections.

a. Goal and scope definition

Three key regions, system borders, and impact groups are included in this process. The whole product development (cradle to grave idea) must be evaluated on the system border. The environmental effects of the impact groups are measured using the ReCiPe 2016 [50] impact value. Eighteen metrics of middle point effect are chosen and clustered in three groups of endpoint damage. They are classified in three categories: (i) ecosystem quality, (ii) Human health, and (iii) natural resources. These results are given in classifications of impact and by specific measures determine the environmental burden. The ReCiPe is a measure that is broadly utilized for comprehending damage. The decision-maker considers this kind of measure as more comprehensible than the so-called mid-point concept [4].

b. Inventory analysis

It takes into account input, performance and energy usage in connection with product in the second phase of the LCA sequence. In the impact evaluation step, they are further interpreted into waste and pollution. The material distribution and delivery to the factory are regarded during the entire project time. Besides the product effects and the energy usage (natural gas and electricity) in the framework, the product related reserves have been taken from the Ecoinvent 3.7 directory during its lifespan [51].

c. Impact assessment

The inventory records are transcribed into sustainability reports during this step. As already stated, three separate areas of harm are covered: the environment, health

care, and risk to infrastructure centered on the 2016 ReCiPe framework [50]. The assisted system classification may be carried out for the midpoints depending on the endpoints scale. The damage can be represented as follows numerically for each impact section.

$$IMP_e = \sum_i \theta_{ei}.LCI_i^{ToT} \quad \forall e \qquad \text{Eq. V-1}$$

Where LCI_i^{ToT} is the life cycle inventory related to production, resource logistics and plants execution, correlated with the primary flow *i*. θ_{ei} showed the damage material with respect to the elementary flow *i* impact factor *e*. This aspect encourages a connection between the inventory and the classifications of damage.

$$DAM_d = \sum_{e \in ID_d} IMP_e \quad \forall d \qquad \text{Eq. V-2}$$

$$RCP_d = \sum_d \delta_d \varepsilon_d DAM_d \quad \forall d \qquad \text{Eq. V-3}$$

Where ID_d describes a classification of endpoint effects in damage classification *d*. RCP is the standardized ReCiPe 2016 measure and δ_d, and ε_d are the specific weight and normalization elements. The element of normalization is calculated on the basis of the EU damage computations for land use and emissions calculations [52]. The weighting variables are calculated based on suggested values as described in the ReCiPe 2016 [53].

d. Interpretation

In addition to several suggestions that help improve system efficiency, this step offers an evaluation of the findings. In this sense, policymakers can recognize the weak points conveniently along the way, where additional effort must be made to decrease the environmental impact. Even so, there are no specific boundaries on how the decrease can be achieved. Besides, because of the range of possibilities accessible and differing targets (i.e. impact classifications) in many situations, assessment is highly complicated. The LCA findings can be implemented as variables in the statistical model in order to address these constraints.

V.2.1.3 MFA/LCA combination

Both MFA and LCA include production, use, and end-of-life of the products within the system, to allow for deriving measures at every step of the life cycle. The functional unit for both MFA and LCA should consider the service the investigated system provides over a determined time span [32]. The direct link between the MFA and the

LCA is established through the product-process-matrix proposed by Haupt et al.[17] where each process entails with a certain environmental impact.

Combining the MFA and LCA is used to facilitate waste management and provide environmental impact data on multiple situations of mass flow. The integration of regional MFA and LCA makes environmental assessment evaluations thus maintaining continuity between factors such as the transition parameters of MFA and LCA process models with consideration for the capacity constraints on waste management systems and the accessibility of waste resources. Besides, the input reliance on process output and the related environmental impacts may be observed, both for specific waste management processes like urban waste combustion and for alternate materials used as feedstocks.

V.2.2 Circular economy (CE) assessment

The CE aims to represent circularity of product consisting of product level Material Circularity Indicator (MCI). These structures then comprise a collection of products and materials, including functionality and interlinked behaviour. The 'ideals' of the CE should be correlated to all such metrics; (1) planning of the waste (2) product resilience by variety, (3) dependency on electricity from sustainable resources, (4) thought of "systems," and (5) wastes as fuel, are some of the recommendations that can be followed from comprehensive work carried out by the Ellen MacArthur Foundation [54].

This part concludes the advancement of a circularity evaluation method and the design composition. Part of these assessment is based on the methodological work undertaken on the 'circularity metrics – a guide to the calculation of circularity' by the Ellen MacArthur Foundation and Granta [25]. They established metrics that could be applied to designers as help for implementing choices, along with being utilized to various other ends, including acquisition choices and company assessment rates. The metrics rely mainly on non-renewable sources of technological cycles and resources. Since the research topic does not respond to Ellen MacArthur Foundation & Granta methods, further growth of a product evaluation technique is made.

V.2.2.1 Assessment methodology design

The MCI expresses the amount to which virgin feedstock is minimized, and, as contrasted to a similar industrially average product [55]. The MCI consists fundamentally of three main features: (1) mass of virgin raw materials used in the manufacturing phase, (2) mass of unrecoverable waste assigned to this product and (3) utility factor which represents the duration and severity of MCI usage of this product. Figure V-2 describes the numerous MCI parameters.

MCI_p is the fundamental step towards the product level material. A product's MCI can be classified by taking into consideration the product linear flow index (LFI) and the

factor $F(X)$, which is constructed as a function F of the utility X, which decides the impact of the product utility on its MCI. The formula of Ellen MacArthur and Granta [41] used for measuring the MCI for a material is:

$$MCI_P^* = 1 - LFI \cdot F(X) \quad \text{Eq. V-4}$$

$$MCI_p = \max\{0|MCI_P^*\} \quad \text{Eq. V-5}$$

V.2.2.2 Formulating product circulatory metric

The Ellen MacArthur Foundation & Granta [41] evaluation process is the guiding principle. The CE tests the degree to which linear flows have been reduced, and restoration flows amplified and how frequently and rigorously it is utilized contrasted with a comparable system-average product. The concept behind the CE is to analyze the application, features and outcomes. The materials and products, as also the linkages and the assembly of the structure, should be taken into account in the implementation of the CE independently. Products and materials are recovered in the market in technical intervals to the best appropriate standard and by replacements, maintenance, reuse, restoration, analysis, and recycle for as long as feasible. However, non-toxic materials in a wide range of applications are preserved. The development of CE is confined to the material's technology process. The organic process is not considered because the evaluation of this period is entirely different.

In developing the evaluation model, the first step is to develop a product level material circularity indicator (MCI) by evaluating the product's input, output, and effectiveness. The "theoretical" circularity attribute for a system without configurations and only the product itself may also be represented. The MCI will finally produce an MCI for a product for each material assessment. The input and output of materials include the content of virgin or non-virgin materials and then reusable or non-reusable materials.

V.2.2.3 Material circularity indicator (MCI)

The Circularity Indicator production for product depends on the assumption that construction is an ensemble of materials attached in a particular manner where every product has its circularity and characteristics. The basic principle for circularity is 100 % non-virgin content at end-of-life, and 100% recycled. The MCI for a product measures to what degree the linear flow has been mitigated, the restorative flow of basic elements amplified, and how much longer (often an estimate) the item is used particularly in comparison to the systemic layer valuation of the construct [55].

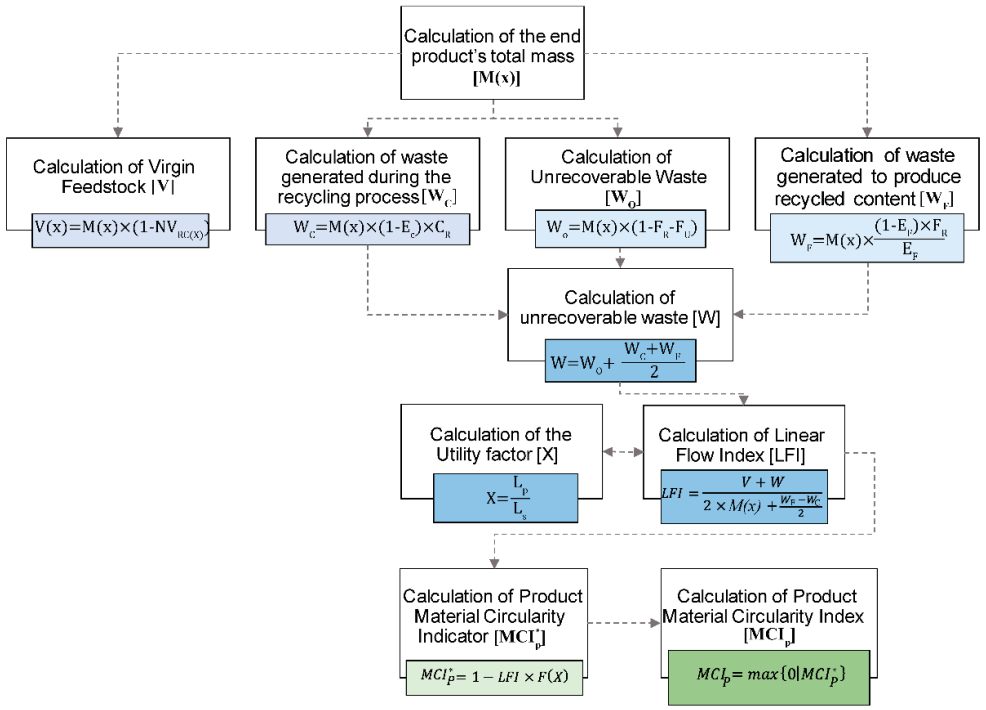

Figure V-3: The MCI Workflow [56]

The MCI is mainly focused on the following features (see also Figure V-3):

- Mass of virgin content in development.
- Mass of waste that is ascribed as unrecoverable after the operation.
- The utility factor X with the item's lifespan/ functional value.

These features are mainly utilized to calculate the Linear Flow Index and the Material Circularity Indicator (MCI_p).

For the determination of MCI, a differentiation between a fully linear product and a complete 100% circular product should be considered. From a single product perspective, it is considered a linear product when 100% of the virgin feedstock goes to the landfill. Furthermore, it is considered as a circular product when 100% non-virgin feedstock is utilized. All cumulative effects may be derived from this differentiation as an inference, which are the two extremes of MCI within a spectrum [0, 1], from 0% (linear) and 100% (circular).

In order to evaluate MCI_p, various materials as part of the final product, are required to be evaluated using comprehensive information of parts and specifications in a product. Thus, it is critical that the bill of material is a complete and fully accurate

material breakup. The MCI_p is established first by analyzing the input and output of the material and then by analyzing the utility factor of the product.

The amounts 'linear flow index' and 'material circularity measure' are successively explored in evaluating the products input, material performance, and utility factor.

a. Determination of the material input

As previously stated, there was a difference between virgin (raw material) or non-virgin (reused, revamped, repaired or rehabilitated) material production. All materials that are a part of a product may be applied to a production process, by Virgin Feedstock, Non-Virgin Feedstock, Fraction Recycled materials, and Fraction Remanufactured materials. A product is then produced with a variety of parts: subassemblies, sections and/or materials. A Bill of material can define all materials centered on the scale of specifics. The Material Circularity Indicator can summarize all materials input predicated on all subassemblies, elements, and/or materials (x).

The virgin materials feedstock is presented for every assembly, portion and/or material (x):

$$V(x) = M(x)(1 - NV_{RC(x)}) \quad \text{Eq. V-6}$$

Where $V(x)$ is a portion of virgin feedstock for each manufacturing process, $M(x)$ is the whole assembly mass, $NV_{RC(x)}$ is the feedstock component for each assembly from the non-virgin material.

The quantity of all distinct subsystems, materials or raw materials are the overall virgin component for a product (V):

$$V = \sum_x V(x) \quad \text{Eq. V-7}$$

If the Virgin Feedstock is equivalent to zero, the entire intake comes from a material that has a full circular input.

b. material performance evaluation

The material output is the target after the lifetime of the product. Again, the products reusable portion is the maximum amount of resources which are found for a second, a third or at least a next life without distinguishing between the reused, renovated, remanufactured and recycled item. The other alternative is to use it to produce energy or to detect when it is unable to consider taking the next lifespan.

A differentiation between the reusable percentage and the waste should be taken in this situation. The recovery of resources and/or deposition is then known as waste,

and the other proportion is seen to be reusable. The waste (W) in an incinerator (energy recovery) or goes to the landfill can be expressed as:

$$W = W_O + \frac{W_C + W_F}{2} \quad \text{Eq. V-8}$$

Where W_O is the unrecoverable waster amount, W_C waste generated to produce recycled content, and W_F is the waste generated during the recycling process. When the waste (W) is equivalent to 0, then it offers all materials a subsequent existence (second or subsequent existence), implying a circular output.

c. The material utility factor

The utility of a product is related to the materials and the product's lifetime. The period of the product's use phase (L_P) is the lifespan of a product. The period aspect reflects any decline (or increase) in waste streams for products that have a prolonged (or shorter) life cycle than certain products from various manufacturers over a given number of years. If a product's lifespan is doubled, waste is generated, and the virgin materials used every year are cut in half. The secondary element is the (L_{sys}) which is linked to the industrial lifespan of an industrial product. The determination of the X utility can be done as:

$$X = \frac{L_P}{L_{sys}} \quad \text{Eq. V-9}$$

This means that if a product's lifetime (L_P) is extended, a beneficial effect can be reflected in the utility. It is necessary to bring the product into perspective and to be part of a system that is either intensively or insufficiently utilized in the event of request adjustments (end of the deal or 'only' shifting requirements), and the ties to other products. A substance produced for excessive lives (utility X is significant), which ends up as energy rehabilitation or landfill, is not a circular but instead a gradual linear operation. There seems to be a debate between environmentally-efficiency and eco-effectiveness. Consequently, eco-efficiency, which reduces the need for resources, has a constructive significance for this highlighted scenario, in comparison with eco-efficiency, which has a negative connotation (to do good instead of less). The aim of eco-effectiveness is not to reduce the flow of material from cradle to grave, but to create cradle-to-cradle metabolisms that allow materials to sustain its role as a resource. The connection between economy and ecology is, therefore strengthened in a positive way. This tool could include either eco-efficient or eco-effective collectively with productivity, based on the prerequisites. Presumption of the highest longevity in good materials is the best option.

d. The linear flow index

The Linear Flow Index (LFI) stands for the portion of materials that have a linear flow where 100% of the virgin stock feed goes to the landfill or energy recovery units at the end of the material lifetime, and it can be expressed as follows:

$$LFI = \frac{(V + W)}{2M(x) + \frac{W_F - W_C}{2}} \quad \text{Eq. V-10}$$

If all the products are reused, remanufactured and/or recycled, the LFI is in the reverse direction, and the entire path is circular.

e. Determination of the material circularity indicator

By evaluating the input, value and performance, the material circularity measure of a material can now be calculated. The MCI is established for a product:

$$MCI_P^* = 1 - LFI \cdot F(X) \quad \text{Eq. V-11}$$

Where, LFI_P is the Linear Flow Index (from the Virgin Feedstock and Waste), $F(X)$ is the function of the utility factor X.

Where: $F(X) = \frac{a}{X}$ with a is a constant Eq. V-12

Ellen MacArthur Foundation [41] established a = 0.9. Accordingly, the usefulness of a product (e.g. through longer use) affects the MCI as it does reuse of materials which, in an amount of time (eco-efficiency), result to an equal amount of reduced virgin material use and waste not retrieved.

V.2.2.4 Development of the Environmental Sustainability and Circularity Assessment Indicator

The final phase is the interpretation of sustainability through combining their overall circularity and environmental impact. The circularity of the product is not taken into account in the LCA structure, and the MCI quantification structure does not take into account the ecological consequences of the respective manufacturing process. As already stated, efforts to increase the circularity of product may ultimately have negative environmental impacts; and efforts to mitigate the ecological consequences of the developed product may, then, theoretically contribute to a decline in circularity. Therefore, an index indicator is normalized and aggregated effects of the LCA as its base value (LCA_T) at the power of the value (1-MCI_p). Below you can find the equation defining the index [56]:

$$ESC_i = \frac{1}{LCA_T^{(1-MCI_p)}} \times 100 \qquad \text{Eq. V-13}$$

The Environmental effects of the analyzed product and its material index must be measured in order to measure the Environmental Sustainability and Circularity Indicator as defined over the last sections. Consequently, in terms of sustainable development and circularity, this technique can be used to grade the alternative options of a certain product. The ESC is various from 0% to 100% where the higher ESC value, the better it is contrasted with the lower-ranking indicators. An important factor of the ESC is that it follows the same system borders for either type of evaluation, environmental sustainability and circularity. It is an essential factor that requires the results of all tests to be combined into a single metric.

V.2.3 Development of scenarios

Following the SCDS approach for assessing the product technologies circularity based on using the MFA/LCA in the first phase and the CE in the second phase, three future scenarios were proposed and compared to the current product circularity situation (baseline scenario) to complete the SCDS approach. These scenarios can highlight the possible improvement potential in the WMS, including increasing the recycling and reuse rates in order to create new treatment pathways. It is important to keep in mind that the developed scenarios are ordered based on the level of required changes where the third scenario would introduce radical changes in the WMS, whereas other scenarios can present changes which can be attained in the near future.

V.2.3.1 Increase recycle rates scenario (Modest Scenario)

Due to the current low circularity for the TES materials, an option to increase recycling is proposed as an initiation to support the sustainable deployment for TES technologies in the near future. In the scenario, all materials entered the closed-loop recycling pathways where the recycling rates of the most relative environmental impact materials in TES technologies is increased by 70% following the EU 2030 target for waste management [57].

V.2.3.2 Increase low impact material usage (Medium Scenario)

In the reuse increment rates scenario, we would propose the EU 2030 targets of increasing the reuse rates of relative materials by 30%. This scenario can contribute to the reduction in TES raw materials extraction and subsequently increase its circularity. The selection of the reuse construction materials and their relative reuse efficiency is shown in the case study section.

V.2.3.3 Optimistic scenario

In the third scenario, we propose a combination of the two previous scenarios where the recycling rates are increased by 70% in parallel with reuse concept to contribute toward the EU 2030 targets. This scenario preserves an ambitious scenario where radical changes in climate change and human toxicity impacts can be reached by improving the current WMS situation.

V.3 SCSD application — TES cases studies

This paper demonstrates the developed approach by an application to high temperature TES technology. This TES have been engaged from the literature; this case has been built in a pilot plant scale following Abengoa Solar [58]. The functional unit for both the LCA and circularity assessment will be carried out per kWh of storage material. The proposed TES technologies used $NaNO_3$ and KNO_3 based molten salts to store sensible heat in the system [11].

V.3.1 Liquid media system description

Abengoa Solar developed a demonstration project using TES based on molten salt as liquid media storage [58] in Seville (Spain) as shown In Figure V-2. This project is proposed as an upgrade in their conventional parabolic trough commercial plants.

Figure V-4: A molten salt TES pilot plant located in Seville (Spain) [58]

The proposed Abengoa Solar TES consists of two molten salt storage tanks. The first storage (Hot Tank) holds the salt at a high temperature up to 388^{o}C, whereas the other storage (Cold Tank), holds the salt at a low temperature of 288^{o}C. Both tanks are identical in dimension and shape identical to avoid complexity. These tanks have a cylindrical shape with a diameter of 22.4 m and a height of 11 m. The volume of each tank is around 4335 m^3 as it needed to store 5500 tons of molten salt in order to store 600 MWh_{th}.

As shown in Figure V-3, the molten salt storage tanks are constructed into different layers. For the lateral walls (inside out): A stainless steel flexible protective liner is used, next is insulating firebricks' layer, a carbon steel made tank shell, an insulating layer of ceramic fiber, exterior insulation of ceramic fiber, and an aluminum sheet. The tank's bottom also has different layers, a stainless steel flexible protective liner, a layer of insulating firebricks, carbon steel tank shell, fine sand, insulating firebricks, foamglas®, reinforced concrete with a water-based cooling system, poor concrete, and foundation piles. The tank roof is also made up of different materials: a stainless steel flexible protective liner, ceramic fiber insulation, ellipsoid-shaped carbon steel sheet, and ceramic insulating material. The main characteristics of these storage tanks are shown in Table V-1.

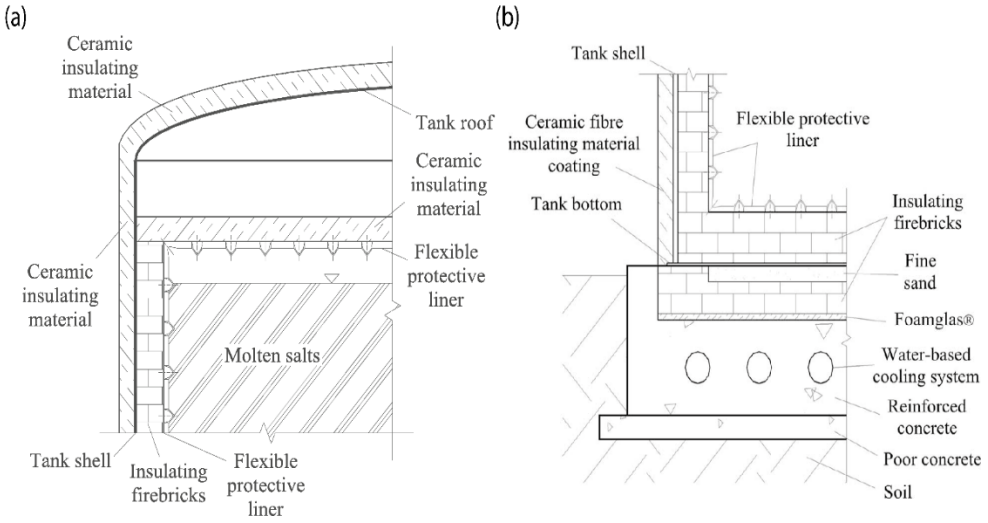

Figure V-5: A cross-section for the molten salts storage tank where:(a) roof & (b) construction base [58]

Several equipments are required in the TES where each molten salt tank is connected to an electric pump in addition to water cooling and heating systems. The temperature of the concrete base is maintained below 100ºC through the water-cooling system. While the salt solidification is prevented through the heating system. Furthermore, molten salts pumps are installed to transfer the salts between the hot and cold tanks.

Table V-1: The molten salt storage tanks characteristics [21]

	Units	Value
Diameter	m	22.4
Height	m	11
Storage unit volume	m^3	4335
Weight of steel	t	279
Lantern material insulation thickness	mm	125
Roof insulating thickness	mm	125
Foamglas® thickness	mm	40
Number of brick foundation	-	2
Number of brick vessel	-	1
Number of brick bottom	-	5

V.3.2 LCA and CE input data

The proposed methodology's application is illustrated through the molten salt TES where its material inventory is shown in Table V-2. Based on the proposed approach, the LCA includes the production, utilization, recycling, and landfill process, for all resource and energy inputs and outputs of a TES over its lifetime. The LCA data were retrieved from the Ecoinvent 3.7 database [59]. This database comprises the production, recycling and disposal stages of the proposed TES based on the ReCiPe 2016 methodology.

Table V-2: Material inventory during the manufacturing phase in the liquid media system [60].

Component	Units	Material Used
KNO_3	kg	3,300,000
$NaNO_3$	kg	2,200,000
Concrete	m^3	551.71
Poor Concrete	m^3	236.45
Sheet metal	m^2	3360.95
Firebricks	kg	1,271,756.92
Carbon steel	kg	554,052.81
Ceramic fibre	kg	10419.79
Aluminum sheet	m^2	1548.18
Sand	kg	417,726.27
Foamglas	kg	4256.08

A summary for the total normalized damage categories of the TES comprising three main stages: (i) material market, (ii) recycled waste market and (iii) disposal waste market is shown in Table V-3 where no data is found regarding the recycling of molten salt as well as firebricks, ceramic fibre, sand and foamglas. Moreover, the

CE of molten salt storage is estimated based on counting for the recycling and reuse rates in addition to their relative efficiency. Following Boer et al.[33], the value of recycled content and their relative efficiency in the molten salt storage varies between different materials inventory. On the other hand, with the lag of data regarding the reuse concept in the molten salt material inventory, we excluded from reuse from the initial scenario calculations.

Table V-4 shows a summary for the recycling rates of the TES material inventory which are extracted from CES Selector 2018 [61] whereas their relative efficiency is following the estimated values in Verberne work [55].

Table V-3: Total environmental life cycle impact at different life stages for molten salt TES represented in ReCiPe points (Pt) per characteristic dimension [59]

		Material stage		
Component	Unit	Material market	Recycled waste market	Waste final disposal
KNO_3	(Pt./kg)	0.38	-	0.0025
$NaNO_3$	(Pt./kg)	0.73	-	0.0025
Concrete	(Pt./m^3)	47.49	1.71	2.99
Poor Concrete	(Pt./m^3)	43.00	1.71	2.99
Sheet metal	(Pt./m^2)	0.36	0.01	0.001
Firebricks	(Pt./kg)	0.15	-	0.06
Carbon steel	(Pt./kg)	0.14	0.01	0.001
Ceramic fibre	(Pt./kg)	0.08	-	0.03
Aluminum sheet	(Pt./m^2)	0.62	0.02	0.01
Sand	(Pt./kg)	0.01	-	0.001
Foamglas	(Pt./kg)	0.45	-	0.01

Table V-4: The current recycling rates and their relative efficiency of the molten salt TES material inventory

Component	Recycling rate in current supply (%) [61]	Recycling efficiency (%) [55]
KNO_3	-	-
$NaNO_3$	-	-
Concrete	13%	90%
Poor Concrete	13%	90%
Sheet metal	39.9%	77.8%

Firebricks	-	-
Carbon steel	39.9%	77.8%
Ceramic fibre	16.5%	77.8%
Aluminum sheet	52.3%	77.8%
Sand	-	-
Foamglas	-	-

V.4 Results and discussion

V.4.1 Life Cycle Inventory

The life cycle inventory of the studied liquid (molten salts) thermal storage media per three damage categories (i) ecosystem quality, (ii) Human health, and (iii) natural resources, is detailed in Figure V-5. Furthermore, Table V-5 lists the calculated total environmental impact of the three material stages, including material market, recycled waste market, and waste final disposal in point per kilowatt-hour (Pt./kWh). As shown in Figure V-5 and Table V-5, the material market contributes to the highest portion of the total impact per whole life cycle of the system studied (5.27 Pt./kWh out of 5.53 Pt./kWh, accounting for 95% of the total environmental impact). According to the overall endpoint results, as indicated in Table V-5, the human health impacts receive greater consideration than natural resources and ecological impacts (59%).

Table V-5: Total impact of TES per material and lifecycle stage based on ReCiPe 2016 in Pt./kWh

	Ecosystem quality	Human health	Resources	Total per lifecycle stage
Material market	1.11	3.11	1.04	5.27
Recycled waste market	0.05	0.03	0.01	0.09
Waste final disposal	0.05	0.09	0.03	0.18
Total per material stage	1.21	3.24	1.09	5.53

As shown in Figure V-5, the storage material which is a mix of two molten salts ($NaNO_3$ and KNO_3), represents the highest impact on all three separate areas of damage as of human health, the environment, and risk to the natural resources, accounting for 83%, 89%, and 82% of the total impact, respectively. In general, 86% of the total impact is generated by the storage material, followed by firebricks and carbon steel accounting for 8% and 2% of the overall impact, respectively. The impact received from all other materials is less than 4%, being most of them insignificant. These differences in the impact between the salts and other materials of the system

are due to the high amount of storage material used (5500 ton). This observation implies that the main way to reduce overall impact would be to find more environmentally friendly materials to be substituted with these storage materials.

Figure V-6 also depicts that firebrick and aluminum sheets are the main contributors to the environmental impacts coming from waste final disposal and recycled waste market, respectively. These are related to the high mass of firebrick used (1272 ton) with its high disposal rate while the aluminum exhibits higher recyclability, and thus representing higher environmental impact originated from its recycled waste market.

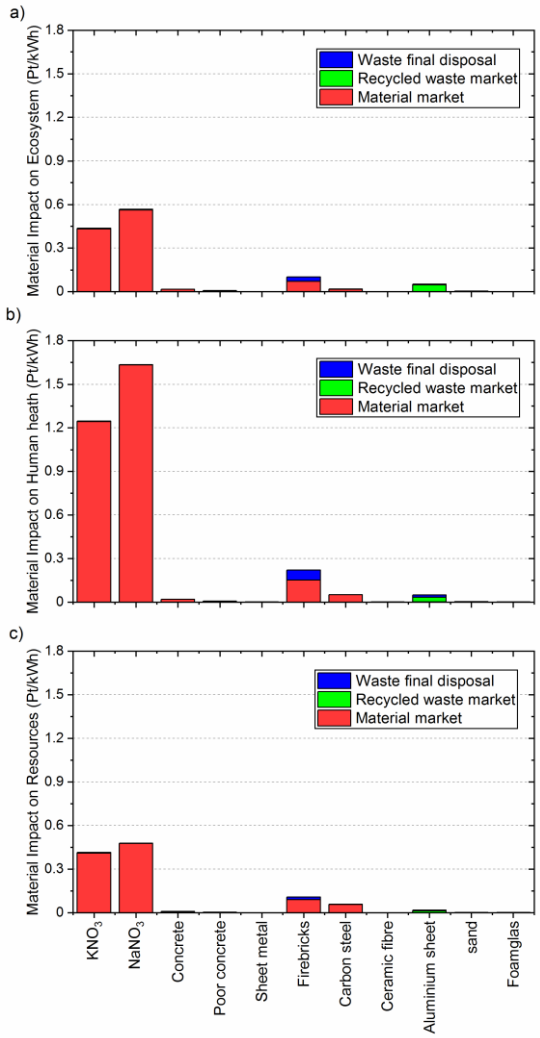

Figure V-6: The complete LCA for the TES with a capacity of 600 MWh. It includes the three damage categories:(a) ecosystem quality, (b) Human heath, and (c) Resources normalized to the storage capacity

Figure V-7 illustrates the LCA breakdown for all material stages including different damage category where the panel (a, d, and g) are depicted for the material market stage, while the recycle waste market stage is shown in panel (b, e, and h) and the waste final disposal is shown in panel (c, f, and i). As described in Section 3.2, the required inputs for quantifying the recycling of molten salts, firebricks, sand, and foamglas were not available, and therefore, there is no evaluation reported for their recycled waste market. Concerning the damage of different materials stages on the eight ecosystem quality categories considered in this study (panels a, b, and c), the natural land transformation and the climate change-ecosystems are affected more than the rest of the LCA impact categories.

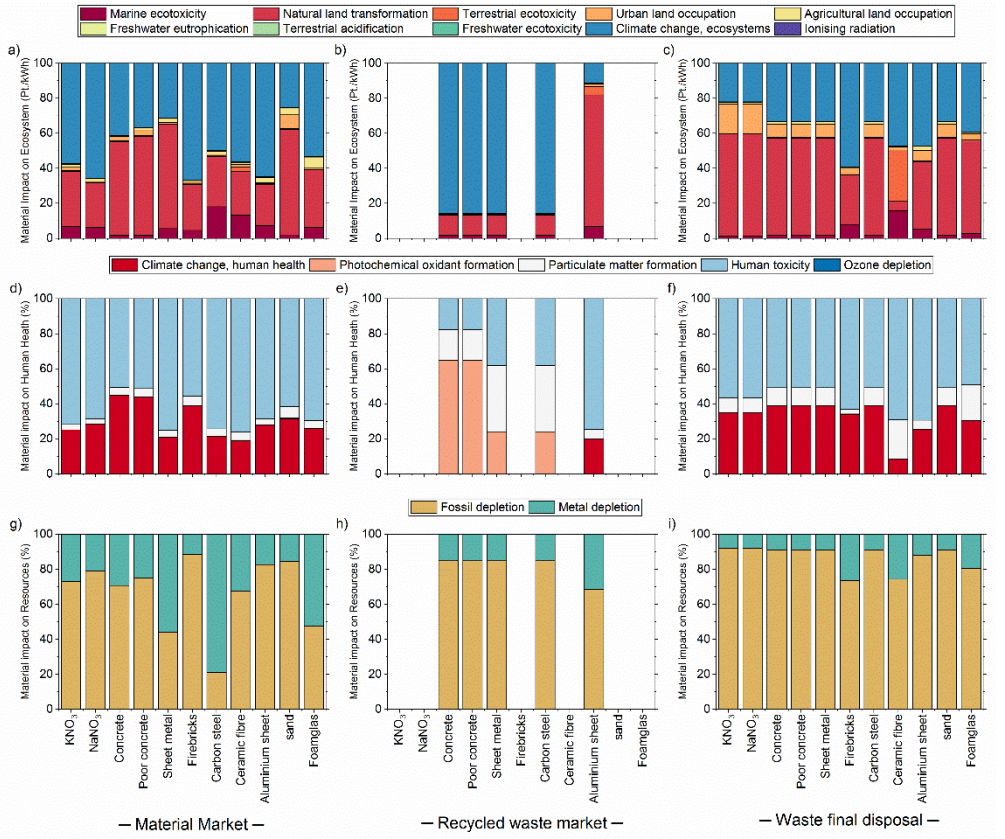

Figure V-7: LCA breakdown for the three material stages including the material market, the recycle waste market and the waste final disposal

Among different impact categories in human health damage area (Figure V-7- panels d, e, and f), human toxicity and climate change-human are the main affected ones. In case of damages on the resources (Figure V-7- panels g, h, and I), the material

impact on endpoint categories varies for each material, however, the fossil depletion is dominant for the material market as well as, namely, the end of life (disposal and recycling).

According to Table V-5, there is a substantial contribution from the molten salts affecting the human health damage area (52% of the overall LCA scores). This implies that human toxicity (i.e. emissions to soil, water, and air of substances that harm human health) and climate change-human health (i.e. emissions of greenhouse gases that cause an increase in temperature of the lower atmospheric layers with impact on human health) should be considered as the main two impact categories affected by molten salts TES systems.

V.4.2 MCI/ESC assessment

Figure V-8 shows the TES materials Sustainable Circular System Design (SCSD) indicators, including the product Material Circularity Index (MCI) and the Environmental Sustainability and Circularity indicator (ESC). Again, since no data was available on the recycling of molten salts ($NaNO_3$ and KNO_3), foamglas, sand, and firebrick, there are no data reported in panel (a) of Figure V-8. The level of MCI, ranging from 0% for the fully linear product to 100% for a fully circular product, which expresses the amount to which virgin feedstock is minimized as contrasted to a similar industrially average product [55]. The higher value of MCI, the higher level of circularity potential of the end-product is. Generally speaking, as shown in panel (a) of Figure V-8, currently the circularity of the TES materials is low (less than 50%). Among materials, metallic elements including aluminum sheet, stainless steel (sheet metal), and carbon steel, exhibit higher MCI than those reported for non-metallic materials. This is as to be expected since metallic materials are more favorable for recycling.

The value of ESC serves as an indicator to evaluate the integration of combined circularity (using MCI) and environmental sustainability (i.e. LCA scores) under a closed-loop product system perspective. As depicted in panel (b) of Figure V-8, the stainless steel (metal sheets), ceramic fiber, and aluminum sheets exhibit the top three highest ESCs (1.21%, 0.42%, and 0.26% respectively), representing the most environmentally sustainable and circular materials among all investigated ones. This is due to the low environmental impacts in the case of stainless steel and ceramic fiber, and relatively high MCI for the case of aluminum sheets.

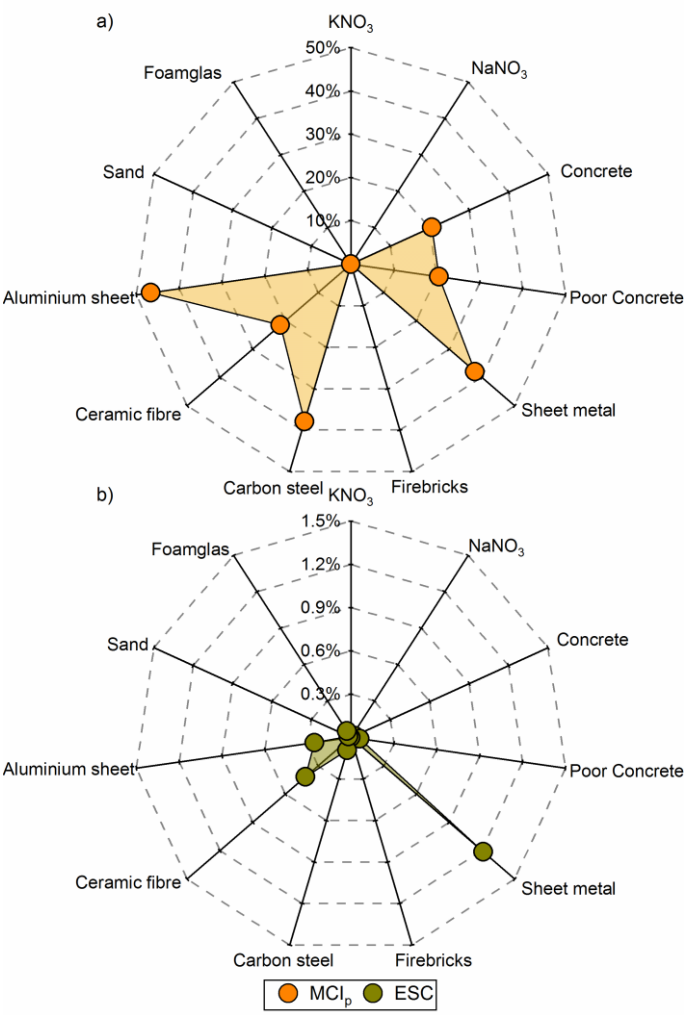

Figure V-8: The TES material SDSC indicators where (a) the material inventory circularity indicator (MCI) and (b) the combined environmental impact and circularity indicator (ESC)

V.4.3 The EU 2030 waste management scenarios analysis

V.4.3.1 Increase recycle rates scenario (Modest Scenario)

Figure V-9 shows the effect of increasing recycling rates by 70% on the SDCS indicators (e.g. MCI and ESC) of the investigated TES materials, following the EU

2030 target for waste management [57]. In this figure, those materials with missing data are the items with no data available on their circularity potential.

Increasing the recycling rate enhances the component circularity. As illustrated in Figure V-9 (panel a), the TES system modeled in this study exhibits a Material Circularity Index of 20.6% at the current situation, which can be escalated to 30.3% when the measures proposed by Modest Scenario are implemented. Aluminum sheets, carbon steel, and stainless steel (sheet metal) are the materials with the highest circularity. The reason behind this is that, as previously noted, aluminum -and metals in general- have high recycling potential as they can be recycled with very low loss of quality along with high energy saving in comparing to the primary production (for example, for recycling aluminum, only 5 percent of the energy needed for primary production is needed).

Concerning Environmental Sustainability and Circularity assessment indicator (ESC), the current situation represents the ESC of 0.23% while Scenario S1 suggests reaching 1.20% (Figure V-9 panel b). An increase in the recycling rates not only improves the circularity of the system but also decreases the total environmental impacts through reducing material disposal. Consequently, according to Equation 13, the ESC is improved for each material, and thus the overall ESC increases accordingly.

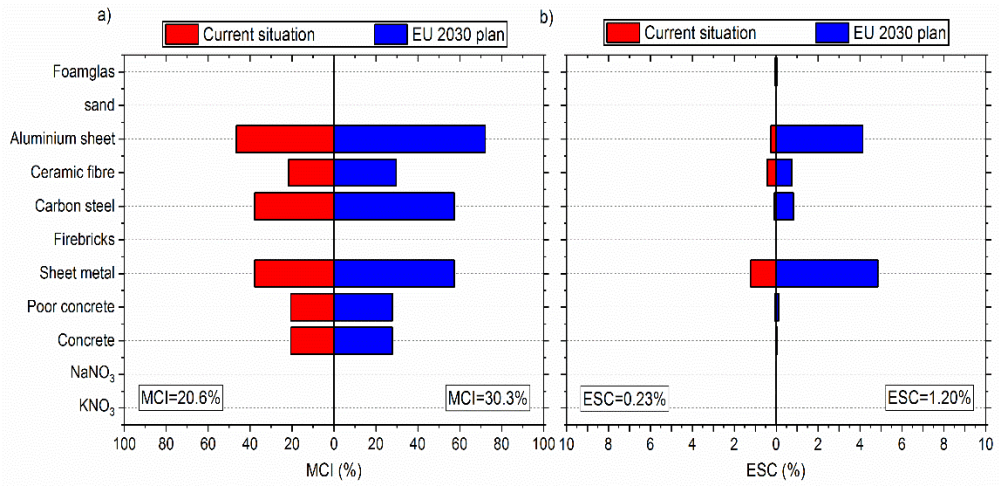

Figure V-9: The effect of increasing recycling rates by 70% on SDCS indicators where (a) MCI indicator and (b) ESC indicator

V.4.3.2 Increase reuse rate scenario (Medium Scenario)

Figure V-10 depicts the effect of increasing the reuse rates by 30% in the Medium Scenario, following the EU 2030 target for waste management, on the SDCS

indicators. Increasing the reuse rates of components and materials would increase the circularity of the system. As shown in Figure V-9 (panel a), the MCI of all materials as well as the overall system MCI of the Medium Scenario, are increased to a larger extent than the Modest Scenario, showing a higher circulatory improvement.

Moreover, comparing panels (b) of Figure V-9 and Figure V-10, it can be seen that the composite indicator of Environmental Sustainability and Circularity (ESC) is higher in the case of Medium Scenario. In other words, the introduction of fewer virgin materials into the production system (by increasing reuse rate, as in the Medium Scenario) can be more effective than decreasing disposal waste (by increasing recycling, as in Modest Scenario) from both the circularity point of view as well as the overall environmental impacts, accordingly, resulting to a more environmentally sustainable and circular outcome (i.e. ESC) in the Medium Scenario.

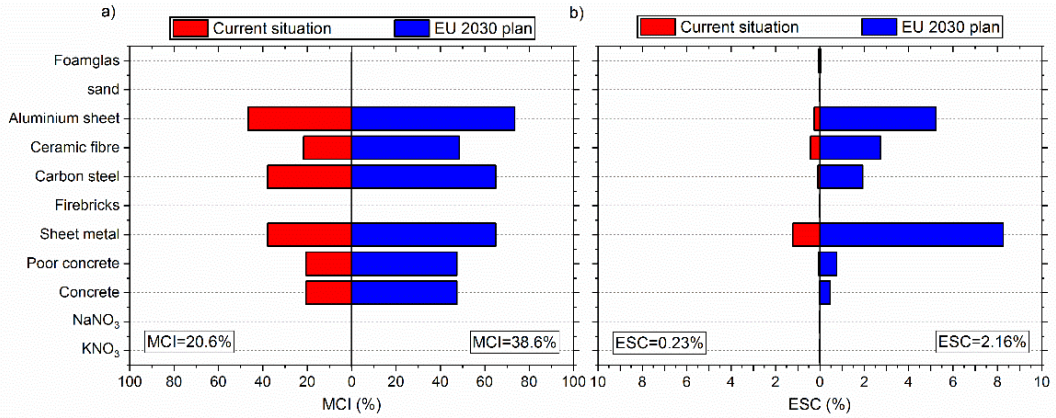

Figure V-10: The effect of increasing reuse rates by 30% on SDCS indicators where (a) MCI indicator and (b) ESC indicator

V.4.3.3 Increase recycle/reuse rates scenario (Optimistic scenario)

Figure V-11 depicts the effect of increasing simultaneously the recycling rates by 70% (i.e., Modest scenario) and the reuse rates by 30% (i.e., Medium scenario) on the SDCS indicators. As expected and is also shown in Figure V-11, a higher MCI can be reached in this scenario rather than Modest and Medium scenarios. Moreover, the changes to be applied to the current waste management systems (WMS) and the circular flow of the materials, leads to a noticeable increase in ESC, by 30 times compared to the current situation. Thus, *Optimistic scenario* represents the most environmentally sustainable and circular scenario among all the investigated ones. However, this scenario should be considered as an optimistic case since the implementation of this scenario requires applying radical changes to the current waste management system.

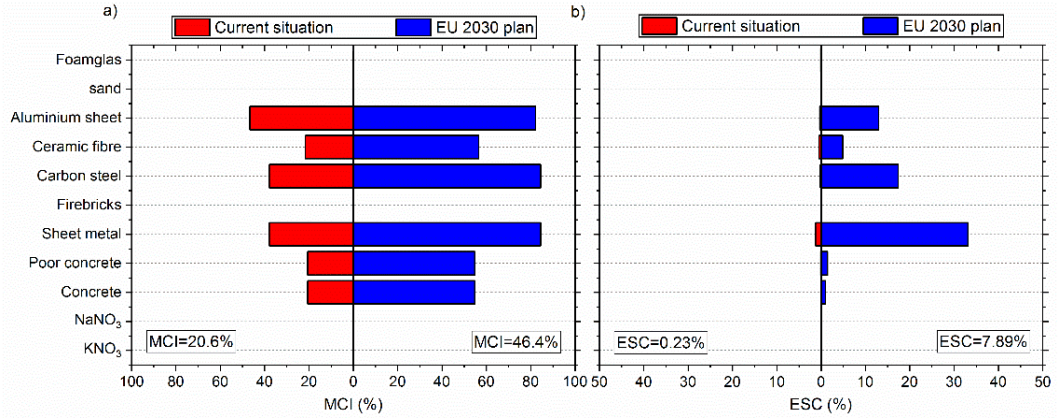

Figure V-11: The effect of increasing recycle/reuse rates by 70% & 30% on SDCS indicators where (a) MCI indicator and (b) ESC indicator

V.5 Conclusion

Conceptually the circular economy (CE) suggests that environmental pressures are closely related to material use, and to reduce the environmental pressures, it is required to circulate and use efficiently the materials in the system life cycle. However, it is a proven fact that CE activities do not necessarily contribute to decreased environmental pressures. Therefore, there is a need to consider a methodology that includes the key environmental flows to assess the contribution of CE to environmental sustainability.

In this paper, an extensive and organized strategy for the plan of frameworks that grasps the features of CE, while decreasing the ecological effects of TES systems, was developed. In so doing, an indicator that is defined as a relationship between the aggregated environmental impacts of the “cradle-to-grave” life cycle stage of TES and their product level Material Circularity Index, was utilized. To test the proposed methodology, three scenarios have been analyzed: (Modest scenario) increasing recycling rates by 70%; (Medium Scenario) increasing the reuse rates by 30%; and (Optimistic scenario) a combination of both scenarios Modest and Medium scenarios.

The circularity analysis showed that by increasing the recycling at the end of life (Modest scenario), increasing reuse rate leading to less use of virgin materials (Medium Scenario), and a combination of both (Optimistic scenario), the Material Circularity Index (MCI) moves from 20.6% for the current situation to 30.3%, 38.6%, and 46.4%, respectively. The results reveal that improving circularity generally reduces environmental impacts from the current situation by 15%, 18%, and 23% for Modest, Medium, and Optimistic scenarios, respectively.

The findings showed that the optimistic scenario represents the most environmentally sustainable and circular alternative with the ESC of 7.89%, where Modest and Medium scenarios exhibit ESC of 1.20% and 2.16%, respectively. For this specific

case study, these ESC results emphasize that achieving a CE goes beyond increasing reuse and recycling, particularly considering that to implement the most optimistic scenario, it is required to introduce radical changes in the waste management system. Major obstacles for a substantial increase of ESC is the extremely high share of noncircular materials, here the molten salts, accounting for 86% of overall LCA scores. Therefore, any effort to improve the circulatory and the environmental benefits of this TES system should be reached by using more environmentally friendly materials for storage material or attempt to enhance the circularity of the molten salt.

As a general concluding remark, the joint interpretation of MCI and LCA scores carried out using ESC indicator can provide a more appropriate ranking factor than evaluating environmental impacts and the level of circulatory of the products individually. This work also suggests that the integration of reusing and recycling at the initial design should be considered in order to achieve a more environmentally sustainable and circular result.

V.6 Acknowledgement

The authors would like to acknowledge financial support from the Spanish Ministry of Economy and Competitiveness RTI2018-093849-B-C31 and RTI2018-093849-B-C33 (MCIU/AEI/FEDER, UE), and thank the Catalan Government (2019 FI-B-00762). The authors would like to thank the Catalan Government for the quality accreditation given to their research group (GREiA - 2017 SGR 1537, AGACAPE – 2017 SGR 1409). GREiA is a certified agent TECNIO in the category of technology developers from the Government of Catalonia. This work is partially supported by ICREA under the ICREA Academia programme. This work is partially funded by the Ministerio de Ciencia, Innovación y Universidades – Agencia Estatal de Investigación (AEI) (RED2018-102431-T). This project has received funding from the European Union's Horizon 2020 research and innovation programme under the Marie Skłodowska-Curie grant agreement No. 713679 and from the Universitat Rovira i Virgili (URV).

V.7 Nomenclature

C_R	Fraction of mass of a product being collected to go to a recycling process
C_U	Fraction of mass of a product going to component reuse
DAM_d	Indicator result for damage category d
E_c	Efficiency of the recycling process used for the portion of product collected for recycling

E_f	Efficiency of the recycling process used to produce recycled feedstock for a product
F_R	Fraction of mass of a product's feedstock from recycled resources
F_U	Fraction of mass of a product's feedstock from reused resources
$F(X)$	Utility factor built as a function of the utility factor X
L	Actual average lifetime of a product
L_{av}	Actual average lifetime of an industry average product of the same type
LCA_T	Normalized and Weighted Results of the LCA
LFI	Linear Flow Index
L_p	Lifespan of a product
L_{sys}	lifespan of an industrial product
MCI	Material Circularity Indicator
MCI_p	Product Level Material Circularity Index
MCI_p^*	Material Circularity Indicator for a product
$M(x)$	Total Mass of the product x
PCI	Product Circularity Indicator
RCP	ReCiPe 2016 aggregated impact factor (Pt/MWh)
U	Actual average number of functional units achieved during the use phase of a product
U_{av}	Actual average number of functional units achieved during the use phase of an industry average product of the same type
W_c	Waste generated to produce recycled content (kg)
W	Waste generated during the recycling process (kg)
W_F	Waste generated during the recycling process (kg)
W_o	Unrecoverable waster amount (kg)
V	Overall virgin component for a product
$V(x)$	Virgin feedstock for the product x
X_i	Product Utility for product i

Greek symbols

δ_d	Normalization factor for damage category d
ε_d	Weighting factor for damage category d

Abbreviations

CE	Circular Economy
CSP	Concentrating solar power
ESC_i	Environmental Sustainability and Circularity Indicator
LCA	Life Cycle Assessment
$LCIA$	Life Cycle Impact Assessment
MFA	Material Flow Analysis
PCM	Phase Change Materials
SCSD	Sustainable Circular System Design
TES	Thermal Energy Storage
WMS	Waste Management System

Indices

d	damage category
i	elementary factor

V.8 References

[1] International Energy Agency, Key World Energy Statistics 2020, Paris, 2020. https://www.iea.org/reports/key-world-energy-statistics-2020.

[2] U.S. Energy Information Administration, International Energy Outlook 2016, 2016. https://doi.org/www.eia.gov/forecasts/ieo/pdf/0484(2016).pdf.

[3] European Commission, Clean energy for all Europeans, Luxembourg, 2019. https://doi.org/10.2833/9937.

[4] V. Tulus, M.H. Abokersh, L.F. Cabeza, M. Vallès, L. Jiménez, D. Boer, Economic and environmental potential for solar assisted central heating plants in the EU residential sector: Contribution to the 2030 climate and energy EU agenda, Appl. Energy. (2019). https://doi.org/10.1016/j.apenergy.2018.11.094.

[5] O. Achkari, A. El Fadar, Latest developments on TES and CSP technologies – Energy and environmental issues, applications and research trends, Appl. Therm. Eng. 167 (2020) 114806. https://doi.org/10.1016/j.applthermaleng.2019.114806.

[6] F. Ochs, A. Dahash, A. Tosatto, M. Bianchi Janetti, Techno-economic planning and construction of cost-effective large-scale hot water thermal energy storage for Renewable District heating systems, Renew. Energy. 150 (2020) 1165–1177. https://doi.org/10.1016/j.renene.2019.11.017.

[7] P. Sorknæs, Simulation method for a pit seasonal thermal energy storage system with a heat pump in a district heating system, Energy. 152 (2018) 533–538. https://doi.org/10.1016/j.energy.2018.03.152.

[8] A. Dahash, F. Ochs, M.B. Janetti, W. Streicher, Advances in seasonal thermal energy storage for solar district heating applications: A critical review on large-scale hot-water tank and pit thermal energy storage systems, Appl. Energy. 239 (2019) 296–315. https://doi.org/10.1016/j.apenergy.2019.01.189.

[9] A. Palacios, C. Barreneche, M.E. Navarro, Y. Ding, Thermal energy storage technologies for concentrated solar power – A review from a materials perspective, Renew. Energy. 156 (2020) 1244–1265. https://doi.org/10.1016/j.renene.2019.10.127.

[10] M. Abokersh, M. Osman, O. El-Baz, M. El-Morsi, O. Sharaf, Review on the Use of Phase Change Material in Domestic Solar Water Heating Systems, Int.

J. Energy Res. 42 (2018) 329–357. https://doi.org/10.1002/er.3765.

[11] C. Prieto, S. Fereres, F.J. Ruiz-Cabañas, A. Rodriguez-Sanchez, C. Montero, Carbonate molten salt solar thermal pilot facility: Plant design, commissioning and operation up to 700 °C, Renew. Energy. 151 (2020) 528–541. https://doi.org/10.1016/j.renene.2019.11.045.

[12] L. Qiu, Y. Ouyang, Y. Feng, X. Zhang, Review on micro/nano phase change materials for solar thermal applications, Renew. Energy. 140 (2019) 513–538. https://doi.org/10.1016/j.renene.2019.03.088.

[13] A. Crespo, C. Barreneche, M. Ibarra, W. Platzer, Latent thermal energy storage for solar process heat applications at medium-high temperatures – A review, Sol. Energy. 192 (2019) 3–34. https://doi.org/10.1016/j.solener.2018.06.101.

[14] A. Calderón, C. Barreneche, K. Hernández-Valle, E. Galindo, M. Segarra, A.I. Fernández, Where is Thermal Energy Storage (TES) research going? – A bibliometric analysis, Sol. Energy. 200 (2020) 37–50. https://doi.org/10.1016/j.solener.2019.01.050.

[15] P. Arce, M. Medrano, A. Gil, E. Oró, L.F. Cabeza, Overview of thermal energy storage (TES) potential energy savings and climate change mitigation in Spain and Europe, Appl. Energy. 88 (2011) 2764–2774. https://doi.org/10.1016/j.apenergy.2011.01.067.

[16] M.V. Abokersh, Mohamed Hany, Kangkana Saikia, Luisa F cabeza, Dieter Boer, Flexible heat pump integration to improve sustainable transition toward 4th generation district heating, Energy Convers. Manag. (2020).

[17] M. Haupt, T. Kägi, S. Hellweg, Modular life cycle assessment of municipal solid waste management, Waste Manag. 79 (2018) 815–827. https://doi.org/10.1016/j.wasman.2018.03.035.

[18] EU Commission, Waste Framework Directive 2008/98/EC of the European Parliament and of the Council, 2008.

[19] S.H. Gheewala, LCA of waste management systems — research opportunities, Int J Life Cycle Assess. 14 (2009) 589–590. https://doi.org/10.1007/s11367-009-0128-y.

[20] F. Guarino, S. Longo, C.H. Vermette, M. Cellura, Life cycle assessment of solar communities, Sol. Energy. 207 (2020) 209–217. https://doi.org/10.1016/j.solener.2020.06.089.

[21] E. Oró, A. Gil, A. de Gracia, D. Boer, L.F. Cabeza, Comparative life cycle assessment of thermal energy storage systems for solar power plants, Renew. Energy. 44 (2012). https://doi.org/10.1016/j.renene.2012.01.008.

[22] T. Decker, J. Burkhardt, Life Cycle assessment of thermal energy storage: two-tank indirect and thermocline, in: Am. Soc. Mech. Eng. (ASME). 3rd Int. Conf. Energy Sustain., California, 2009.

[23] D. Boer, M. Segarra, A.I. Fernández, M. Vallès, C. Mateu, L.F. Cabeza, Approach for the analysis of TES technologies aiming towards a circular economy: Case study of building-like cubicles, Renew. Energy. 150 (2020) 589–597. https://doi.org/10.1016/j.renene.2019.12.103.

[24] UNEP, Push to Pock up the Pace on the Circular Economy, 2018. http://www.resourcepanel.org/news-events/push-pick-pace-circular-%0Aeconomy.

[25] Ellen MacArtur Foundation, Towards the circular economy, London (UK), 2013.

[26] Ellen MacArthur foundation, Towards the Circular Economy - Part 3; Accelerating the scale-up across global supply chains, 2014.

[27] J. Potting, M. Hekkert, E. Worrell, A. Hanemaaijer, Circular Economy: Measuring innovation in the product chain, PBL Netherlands Assessment Agency, 2017.

[28] J. Kirchherr, D. Reike, M. Hekkert, Resources , Conservation & Recycling Conceptualizing the circular economy : An analysis of 114 definitions, 127 (2017) 221–232. https://doi.org/10.1016/j.resconrec.2017.09.005.

[29] U. Kral, L.S. Morf, D. Vyzinkarova, P.H. Brunner, Cycles and sinks : two key elements of a circular economy, J. Mater. Cycles Waste Manag. 0 (2018) 0. https://doi.org/10.1007/s10163-018-0786-6.

[30] S.O. Material, S. Web, H. Press, N. York, A. Nw, Emerging approaches, challenges and opportunities in life cycle assessment, Science (80-.). 80 (2014) 1109–1113. https://doi.org/10.1126/science.1248361.

[31] M. Haupt, M. Zschokke, How can LCA support the circular economy?—63rd discussion forum on life cycle assessment, Zurich, Switzerland, November 30, 2016, in: Int. J. Life Cycle Assess, The International Journal of Life Cycle Assessment, 2017. https://doi.org/10.1007/s11367-017-1267-1.

[32] M. Wiprächtiger, M. Haupt, N. Heeren, E. Waser, S. Hellweg, A framework for sustainable and circular system design: Development and application on thermal insulation materials, Resour. Conserv. Recycl. 154 (2020) 104631. https://doi.org/10.1016/j.resconrec.2019.104631.

[33] D. Boer, M. Segarra, A.I. Fernández, M. Vallès, C. Mateu, L.F. Cabeza, Approach for the analysis of TES technologies aiming towards a circular economy: Case study of building-like cubicles, Renew. Energy. 150 (2020) 589–597. https://doi.org/10.1016/j.renene.2019.12.103.

[34] M. Arena, G. Azzone, A. Conte, A streamlined LCA framework to support early decision making in vehicle development, J. Clean. Prod. 41 (2013) 105–113. https://doi.org/10.1016/j.jclepro.2012.09.031.

[35] PROSUITE, Development and application of standardized methodology for the PROspective SUstaInability assessment of TEchnologies, 2013.

[36] S. Cobo, A. Dominguez-ramos, A. Irabien, From linear to circular integrated waste management systems: A review ofmethodological approaches, Resour. Conserv. Recycl. 135 (2018) 279–295. https://doi.org/10.1016/j.resconrec.2017.08.003.

[37] V. Martinez-sanchez, M.A. Kromann, T. Fruergaard, Life cycle costing of waste management systems : Overview , calculation principles and case studies, Waste Manag. 36 (2015) 343–355. https://doi.org/10.1016/j.wasman.2014.10.033.

[38] M. Münster, H. Ravn, K. Hedegaard, N. Juul, M.L. Söderman, Economic and environmental optimization of waste treatment, 38 (2015) 486–495. https://doi.org/10.1016/j.wasman.2014.12.005.

[39] C. Vadenbo, S. Hellweg, G. Guillén-gosálbez, Multi-objective optimization of waste and resource management inindustrial networks – Part I: Model description, "Resources, Conserv. Recycl. 89 (2014) 52–63. https://doi.org/10.1016/j.resconrec.2014.05.010.

[40] European Communities, Economy-wide material flow accounts and derived indicators: a methodological guide, Luxembourg, 2001.

[41] Ellen Macarthur foundation, Circularity Indicators: An approach to Measuring Circularity, 2015. http://www.ellenmacarthurfoundation.org/circularity-indicators.

[42] Wuppertal Institute, Material intensity of materials, fuels, transport and

services. Version 2, 2003.

[43] M. Ritthoff, H. Rohn, C. Liedtke, Calculating MIPS: Resource productivity of products and services, Wuppertal, Germany, 2002. https://www.econstor.eu/bitstream/10419/59294/1/485276682.pdf.

[44] N.L. Nemerow, F.J. Agardy, P. Sullivan, J.A. Salvato, ENVIRONMENTAL ENGINEERING: Environmental Health and Safety for Municipal Infrastructure, Land Use and Planning, and Industry, 6th ed, John Wiley & Sons, Inc, 2009.

[45] International Organization for Standardization (ISO), ISO 14040: Environmental management - Life Cycle Assessment - Principles and framework, 2006. https://doi.org/10.1002/jtr.

[46] K. Mantalovas, G. Di Mino, The Sustainability of Reclaimed Asphalt as a Resource for Road Pavement Management through a Circular Economic Model, Sustainability. 11 (2019) 2234.

[47] International Organization for Standardization, SO 14040-Environmental Management—Life Cycle Assessment—Principles and Framework, Geneva, Switzerland, 2006.

[48] International Organization for Standardization (ISO), ISO 14041: Environmental Management - Life Cycle Assessment: Goal and Scope Definition and Inventory Analysis, 1997.

[49] International Organization for Standardization (ISO), ISO 14042:Environmental management - Life cycle assessment - Life cycle impact, 2000.

[50] M. Goedkoop, R. Heijungs, M. Huijbregts, A. De Schryver, J. Struijs, R. Van Zelm, ReCiPe: A LCIA method which comprises harmonised category indicators at the midpoint and the endpoint level. Report I: Characterisation 2008, 2009. https://doi.org/10.029/2003JD004283.

[51] B.P. Weidema, C. Bauer, R. Hischier, C. Mutel, T. Nemecek, J. Reinhard, C.O. Vadenbo, G. Wernet, Data quality guideline for the ecoinvent database version 3, 2013. http://www.ecoinvent.org/database/methodology-of-ecoinvent-3/methodology-of-ecoinvent-3.html.

[52] JRC European commission (JRC-IES), ILCD Handbook: Recommendations for Life Cycle Impact Assessment in the European context, 1st editio, Office of the European Union, Luxemburg, 2011. https://doi.org/10.278/33030.

[53] M.A.J. Huijbregts, Z.J.N. Steinmann, P.M.F. Elshout, G. Stam, F. Verones, M. Vieira, M. Zijp, A. Hollander, R. van Zelm, ReCiPe2016: a harmonised life cycle impact assessment method at midpoint and endpoint level, Int. J. Life Cycle Assess. 22 (2017) 138–147. https://doi.org/10.1007/s11367-016-1246-y.

[54] Ellen MacArthur Foundation, Growth within: a circular economy vision for a competitive europe, 2015.

[55] J.J.H. Verberne, Building circularity indicators - an approach for measuring circularity of a building, 2016. https://pure.tue.nl/ws/files/46934924/846733-1.pdf.

[56] K. Mantalovas, G. Di Mino, Integrating circularity in the sustainability assessment of asphalt mixtures, Sustain. 12 (2020) 9–12. https://doi.org/10.3390/su12020594.

[57] Eunomia, Support to the Waste Targets Review, Final Report to DG Environment of the European Commission, 2016. http://ec.europa.eu/environment/waste/pdf/target_review/Eunomia_support_waste_targets_review.pdf.

[58] C. Prieto, R. Osuna, A.I. Fernández, L.F. Cabeza, Thermal storage in a MW scale. Molten salt solar thermal pilot facility: Plant description and commissioning experiences, Renew. Energy. 99 (2016) 852–866. https://doi.org/10.1016/j.renene.2016.07.053.

[59] Ecoinvent, Eco invent, (2017). https://www.ecoinvent.org/home.html (accessed March 12, 2018).

[60] L. Miró, E. Oró, D. Boer, L.F. Cabeza, Embodied energy in thermal energy storage (TES) systems for high temperature applications, Appl. Energy. 137 (2015). https://doi.org/10.1016/j.apenergy.2014.06.062.

[61] Granta Design Ltd, CES Selector 2018, (2018).

Chapter VI

SDHS potential to achieve Zero Energy Buildings

VI. SDHS potential to achieve Zero Energy Buildings

Sustainable Insights on Emerging Solar District Heating Technologies to Boost the Nearly Zero Energy Building Concept

Mohamed Hany Abokersh [a], Sachin Gangwar [a], Marleen Spiekman [b], Manel Vallès [a], Laureano Jiménez [c], Dieter Boer [a*]

[a] Departament d'Enginyeria Mecànica, Universitat Rovira i Virgili, Av. Països Catalans 26, 43007 Tarragona, Spain

[b] Department of Building Physics and Systems, TNO, Leeghwaterstraat 44, Delft, the Netherlands

[c] Departament d'Enginyeria Química, Universitat Rovira i Virgili, Av. Països Catalans 26, 43007 Tarragona, Spain

** Corresponding author: Dieter.boer@urv.cat*

E-mail addresses: *mohamed.abokersh@urv.cat (M.H. Abokersh), sachin.gangwar@urv.cat (S. Gangwar), marleen.spiekman@tno.nl (M. Spiekman), laureano.jimenez@urv.cat (L. Jiménez), manel.valles@urv.cat (Manel Valles)*

Keywords: Solar assist district heating system; Nearly zero energy building; Life cycle assessment; Multi-objective optimization; Multi-criteria decision making; Sustainability targets

VI.1 Introduction

The world population is expected to consume 50% more energy by 2035 (compared to 1990) due to rapid growth in population, infrastructure, technology, and energy-intensive systems. This aspect has a direct impact on building energy consumption [1]. In the European Union (EU), building sector alone accounts for approximately 40% total energy consumption and 36% of the total CO_2 emissions [2]. Consequently, a more sustainable and climate oriented efficient building stock is needed to achieve climate-neutral Europe's goals by 2050. Corporations in the infrastructure industry face an urgent need to change their traditional practices in terms of energy access and its use to reduce the energy needs of building stocks. International bodies set guidelines to follow the nearly/net-zero energy building (NZEB) route. The NZEB concept is vastly interpreted as the utilization of renewable energy to satisfy building energy need. Sustainable energy authority of Ireland defines NZEB as '*a building that has a very high energy performance, and the nearly zero or very low amount of*

energy required should be covered to a very significant extent by energy from renewable sources, including energy from renewable sources produced on-site or nearby'[3]. However, communities worldwide have not yet reached a consensus on the definition [4]. National Renewable Energy Laboratory of the United States has classified NZEB as a range of buildings, e.g., from a building that offsets all of its energy needs from renewable energy resources available on-site' to a building that achieves an NZEB status through a combination of on-site renewables and off-site purchases of renewable energy credits [5]. The Energy Performance of Building Directive (EPBD) from the EU, requires all new buildings to be NZEB from 2021 and aims to achieve a highly decarbonized building stock by 2050 for existing and new buildings (Directives 2010/31/EU and 2018/844/UE) [6]. Driving forces for the rise of NZEBs have been explained in detail elsewhere [7], showing the social, economic and environmental benefits. To achieve this transition, centralized and decentralized renewable energy usage can contribute to push to net-zero energy buildings. Currently, Europe has 70% of the building stock needed by 2050 and improving the existing building stock's energy efficiency is an effective way to reduce energy demand [8], so this paper focuses on installable renewable energy solutions to satisfy the energy demand on building stock [9].

The transition of existing building blocks towards NZEB can be achieved by improving the building's energy efficiency, equipping the building block with renewable energy generation sources and connecting the building block with the district heating (DH) network. 4th generation district heating (4GDH) network is a promising concept to reduce high energy losses and installation and maintenance cost of previous generations district heating systems [10]. The high performance of 4GDH is attributed to its low-operation temperature (50–60°C). However, more research is required for broad implementation of 4GDH [11]. Use of renewable energy technology and DH networks can reduce the carbon footprint of the building block and, thus, building blocks with low carbon emission are called Low Carbon Buildings (LCB), building blocks with net-zero carbon emission called Net Zero Energy Building (NZEB). A plethora of research is available on the NZEB with different energy sources and different perspectives. While some of the researchers have used photovoltaics, solar thermal systems, geothermal systems [12], others have tried to measure the prospects of conventional smart energy systems and net metering [11]. While the research has been catching up to the target of carbon neutrality and NZEB concept [13], some researchers have also developed positive energy buildings (PEBs). PEB essentially means that the building or the building stock can satisfy its energy demand and be able to produce more energy to supply to the centralized district heating (DH) network (thermal energy) or the grid (electrical energy). Research in PEB is still in its nascent stage, and till now very few researchers have tried to make the transition from low carbon buildings to nearly zero energy buildings to positive energy buildings [14]. The concept of integrating smart energy systems to connect the building stock with grid and district heating network has also been studied [15] and the technical

feasibility of the building stock [16]. The smart energy system is a broader concept which suggests the load reduction on the electrical grid by connecting the demand to the respective energy networks (i.e., electricity demand to the electricity grid, heating demand to district heating networks, etc.). Smart energy system also incorporates the concept of net metering, thereby, addressing the component of direct financial benefit to the user for the implementation of such a system. The futuristic vision of high energy performance building stock can be achieved with smart energy system integration, especially in cold regions by connecting to 4GDH [17]. To implement EPBD regulations towards the NZEB transition, the Netherlands set the guidelines for achieving energy efficiency and the building's rating [6]. These indicators collectively form “EPC” (energy performance coefficient), which standardize the process of building energy efficiency rating [18].

Netherlands has a high potential for retrofit residential building stock and connects to renewable energy sources to reduce greenhouse gas emissions (GHG) [19]. Numerous efforts are being made to satisfy building energy consumption by renewable energy system installation (e.g., rooftop PV [20], geothermal heat pumps [21], solar-assisted heat pumps [22], passive heating and cooling [23]) Researchers have analyzed from the life cycle perspective [24] building integrated solutions with photovoltaics (PV) [25], increased renewable energy input with multiple systems [26], comprehensive solar energy solutions with PV and flat plate collectors [27] to satisfy the energy demand of the building and to assess the greenhouse gas emission. Extensive research has been done on case studies related to the application of photovoltaics [1], solar thermal applications [28] and technological design option for PV [29] in NZEBs and low carbon energy buildings. Given the environmental benefits associated with renewable energy utilization in buildings, a global rise has been observed in the area of NZEB and the low-carbon buildings (LCBs) application and research [4].

The availability of various green energy solutions has led to the adoption of different approaches by the researchers. In attempts to reach NZEB status, Dawood et al. [30] suggested a framework which includes the integration of energy simulation tools, national calculation methods and codes for low carbon buildings (LCB) and multi-criteria decision making (MCDM) to support the building design process. However, this framework was specifically addressing the architects for retrofitting. To emphasize the impact of various key areas researchers have also used MCDM: for energy systems design optimization to encounter load uncertainty [31], for building design optimization methods [32], for assessment and ranking of renewable energy technology [33] to point out the key decision-makers. Hang et al.[34] has summed up the findings of major agencies and researchers to move from low carbon buildings to NZEB: (i) assessing the energy and GHG emissions; (ii) optimizing the on-site and off-site distribution of renewable energy; (iii) answering low carbon buildings (LCB)

potentials through high-performance energy end-use devices and occupants' green behavior.

Achieving NZEB or PEB status for a building requires optimization of numerous variables (e.g. selection of an optimal renewable energy technology [35], optimizing building energy design [36], optimizing the use of energy-efficient material). [37]. Classical and metaheuristic optimization methods are not able to effectively optimize a large number of variables simultaneously as require large computational resources. Optimizing a multivariate objective function is difficult for non-confluent variables with mathematical programming, and some researchers use machine learning [38]. With the use of machine learning Rehman et al. [39] analyzed and optimized a building integrated photovoltaic panel, battery and use of electric vehicles in central European climatic condition, Han et al. [40] optimized the fault diagnosis of a building energy system, and Salah et al. [41] predicted the building energy performance to support deep energy retrofit. The use of machine learning by various researchers has been reviewed by Fathi et al. [42] in urban building energy performance forecasting, by Mishra [43] for structural health monitoring of heritage buildings, by Sun et al. [44] for building structural design and performance assessment, by Ayoub [45] to predict daylighting inside buildings and by Hong et al. [46] in the area of building life cycle. The use of machine learning in energy systems design, sizing and techno-economic analysis and environmental analysis to achieve NZEB targets is yet to be explored. We have used a machine learning approach based on artificial neural network (ANN) to optimize a multi-objective function that incorporating economic, environmental, and social variables. The robustness of these optimization approaches can be investigated with a global sensitivity analysis (GSA) against the uncertain parameters. GSA is an extensive tool to identify the major parameters causing uncertainty into an optimization model. Mavromtidis et al. [47] used GSA to determine the major causes of variation in economic and energy performance optimization of a distributed energy system. The use of GSA to provide the cushion against parameter uncertainty in energy system design is extensive [48]. Zhang et al have used GSA or key parameters identification of net-zero energy buildings for grid interaction optimization [49]. Hence, machine learning in conjugation with GSA is gaining popularity for energy systems optimization under uncertainty for NZEB.

The available literature on NZEB unanimously recommends the integration of renewable energy into the building footprints. Therefore, we aim to achieve the PEB targets by retrofitting a building stock situated in North-East Netherlands (Emmen). We are trying to achieve PEB status following the 4GDH principles to satisfy the heating and adding a rooftop PV system to meet the building stock's electricity demand. In addition, we connected the model to the electricity grid and centralized DH network.

Hence, this work's novelty lies in demonstrating the sustainable aspects for integrating 4GDH at various residential community sizes located in the Netherlands

to achieve NZEB targets. Additionally, this paper develops a MCDM framework based on optimal scenarios to support the selection of the most sustainable system design at various residential community size. This work suggests a roadmap for a transition from LCBs to PEBs with the integration of seasonal storage, heat pumps, PV, and smart energy systems. The structure of this article is as follows: section 2 shows a complete description of the 4GDH system and neighborhood demand. Section 3 describes the sustainable criteria to evaluate the DH performance. The ANN model's mathematical description and its coupling with a multi-objective optimization framework are presented and discussed in section 4. The post-analysis of the optimal solutions, including the MCDM and GSA, is shown in Section 5. Section 6 offers the required results and discussion. Finally, the work summary and conclusion are shown in section 7.

VI.2System Description

VI.2.1 Roof-mounted hybrid solar assisted district heating

A typology of solar assisted district heating system (SDHS) combined with heat pump (HP) is designed for a residential neighbourhood in the Netherlands to supply-demand loads of space heating (SH), domestic hot water (DHW) and electricity for the whole year as shown in Figure VI-1 schematically.

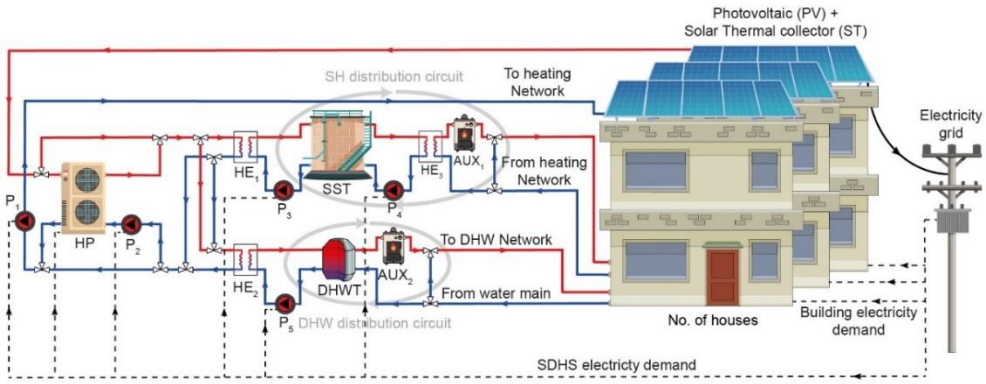

Figure VI-1: Schematic of roof-mounted hybrid solar assisted district heating network

This system primarily incorporates roof-mounted solar thermal collectors (ST) and photovoltaic panels (PV), a seasonal thermal storage tank (SST), a domestic hot water tank (DHWT), central water to water HP unit, and auxiliary heaters fueled by natural gas. From Figure VI-1. HP serves as a heat input source for both SST and DHWT. For this arrangement, heat collected via the ST is used to meet SH/DHW demand where the heat is transferred across the distribution network through heat exchangers using 'Y' valves. Contingent to operational mode, the heat produced by HP is either used for SH or DHW with potential to use it for SST heat charging. For

the winter season, the SST is used to satisfy SH demand, whereas short-term DHWT meets the daily DHW. It is noteworthy that the heat is supplied at low-temperature (50 °C) for space-heating, while the heat to DHW is supplied at higher-temperature (60 °C). Lastly, when solar collectors, HP and SST are not able to satisfy the heat load, the disparity is overcome via auxiliary heaters. On the other hand, the electricity demand comprising both the neighbour and SDHS electric equipment is covered by a combination of the on-grid roof-mounted PV panels and the electricity grid.

An efficient control strategy is adopted to meet the residential neighbourhood heating demand maximizing the use of solar energy and minimizing the network heat losses. Four modes of operation are planned considering the temperature levels of SDHS, which are enabled via on-off control switches. At the start:

1) In the first operational Mode or DHW operation mode, the heat obtained by ST is transported to the DHWT with the help of P_1, P_2 and P_5 pumps through HE_2. When the solar thermal energy is not enough to satisfy the demand in the DHW network, the auxiliary heater (AUX_2) is enabled. During DHW mode, the HP unit does not operate.
2) In the second mode, the SH gets initiated when a suitable level of temperature in DHWT (T_{DWT}) is reached while the temperature of the collector (T_{COL}) is at a higher temperature than the bottom of the SST (T_{SST}). In this mode of operation, P_1, P_2, P_3 pumps are used to transfer heat to SST from ST via HE_1.
3) In third operation mode, a concurrent operation of DHW and SH circuits gets initiated when the criteria for the DHW and SH operations are met, and $T_{SST} > T_{DHWT}$.

In the fourth mode of operation, HP operates if the solar thermal system fails to satisfy the heating demand. Thus, in this mode of operation, the HP is activated when the $T_{COL} < T_{SST}$ which, subsequently is less than the reference turn-on temperature of the heat pump (T_{ref}). Under the HP operation mode, the heat generated is transported to either SST or DHWT depending on the demand. In this case, the uncovered heat demand is met by using the auxiliary heaters as well. In cooperation with thermal SDHS part, the on-grid PV panels are integrated to reduce the purchased electricity from the supply grid while covering both the neighbourhood electric demand and SDHS electric equipment.

VI.2.2 TRNSYS simulation model

To model and analyse the SDHD system behaviour, TRNSYS 18 [50] has been used. This software uses partial differential equations and input constraints as limits for mass and energy conservation with defined boundary conditions. Due to the intrinsic dynamic nature of the system, it offers a realistic simulation of hybrid SDHS. In order to reduce the computational cost, the hybrid SDHS model has been simulated for three benchmarking operational years. The solution is then inferred over the project lifetime, assuming that weather data and demand profiles are constant over the project lifetime (40 years). This approach is inspired by the simulation models built by

Guadalfajara et al. [51], Tulus et al. [52] and Abokersh et al. [17], incorporating the hybrid solar circuits and its control schemes. Depicts the information flow diagram in detail for individual components, as shown in Figure VI-2 (Type – inside TRNSYS GUI).

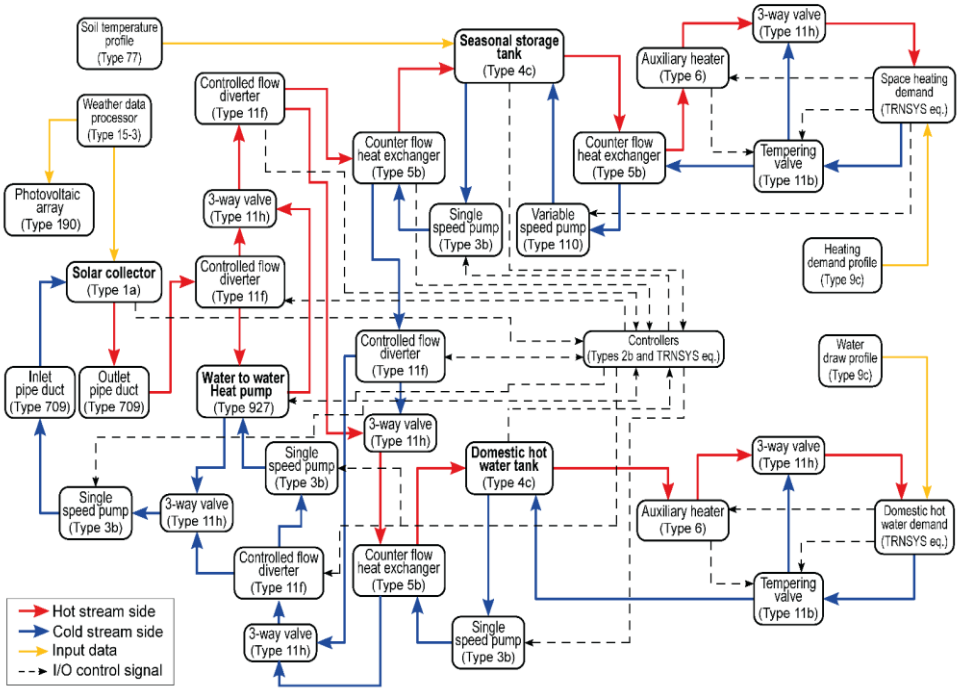

Figure VI-2: Info flow map of the SDHS system simulated in TRNSYS 18 with components and their interconnections

Each component has information boxes for component-specific parameters and input-output variables. We mainly have used following types: flat plate solar collectors (Type 1a) with an optical efficiency of 0.817, heat loss coefficient of 2.205 W/m^2·K; PV panel (Type 190) with a module conversion efficiency of 0.186; water to the water heat pump (Type 927); sensible storage tanks (Type 4c) with heat loss coefficient of 0.3125 W/m^2·K for the DHWT, respectively; counterflow heat exchangers (Type 5b) with overall heat transfer coefficient of 3.931 kW/m^2·K; and auxiliary heaters (Type 6) with an efficiency of 93%. The secondary model types are: single speed centrifugal pumps (Type 3b), inlet and outlet pipe ducts (Type 709), three-way valves (Type 11 h), controlled flow diverters (Type 11f), tempering valves (Type 11b), soil temperature profile for the SST (Type 77), weather data processor (Type 15-3), time-dependent forcing functions for the heating and DHW demand profiles (Type 9c), and controllers (Type 2b).

VI.2.3 Decentralized reference case (Base case)

In this setup, the heating demand (SH&DHW) of each building in the residential neighbourhood is satisfied through an individual air source heat pump (PUHZ-SW50VHA) with a Coefficient of performance equal 5 [18]. The heat pump compressor controller managed the required flow temperature based on the weather compensation routine and the zone setpoint (user adjusted). While the dwelling electric demand is met through the national grid. A schematic drawing for this decentralized system is shown in Figure VI-3.

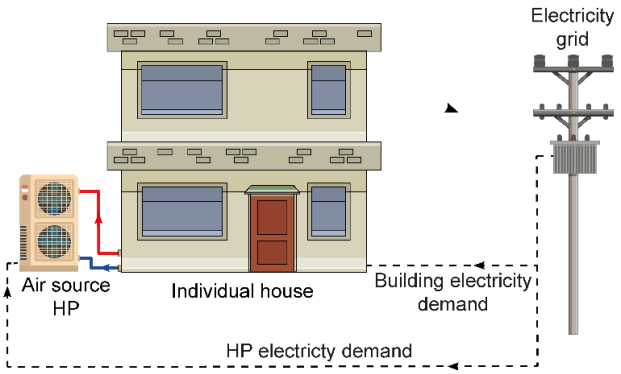

Figure VI-3: A schematic drawing for the decentralized air source heat connected to the supply grid to cover an individual house demand

VI.2.4 The neighbourhood description and demand profiles

The neighbourhood consists of 10 newly retrofitted houses located in Emmen, Netherlands [18]. The dwelling layout is shown in Figure VI-4, where each floor area is 60 m^2, and the ceiling height is 3 m.

Figure VI-4: General view for the Emmen dwelling

The considered dwelling has two external façades with a total area of 33.7 m^2, oriented to the East and West, whereas the opaque part represents 19.6 m^2. The outer walls of each dwelling are made of two primary walls which are made using hollow bricks coated with plaster and insulation layers. The interior partition walls, made of gypsum boards, are finished with light concrete. The floor is made of two surfaces; the main ground surface composed using layers of insulation material, concrete, and stones, whereas the inward surface of the ground floor is made of light concrete with gypsum boards. Moreover, the top roof surface composed of multiple layers of light concrete and plaster with insulation.

The solar radiation in Emmen (Netherlands) varies from 23 kWh/m^2 in December to 155 kWh/m^2 in August. In summer (May, Jun, July, August) the solar radiation is towards the upper range of solar irradiance range. The thermal demand of the neighborhood consists of an annual DHW demand (5.29 MWh/house) and an annual SH demand (4.14 MWh/house) which are covered by HP. Apart from the heat demand, the annual electricity demand (5.53 MWh/house) is currently supported by the electricity grid. The total energy demand and its monthly variation for the dwelling are plotted in Figure VI-5 alongside monthly solar radiation and average monthly ambient temperature. DHW and electricity demand is decreased in the months of winter due to reduced activities of occupants in these months while the space heating demand is significantly higher in winter due to low ambient temperatures and increased indoor occupant hours. Energy demand profiles (heat demand load for SH, DHW, and demand load for electricity) are provided as inputs variables for the time-dependent simulations of entire cases.

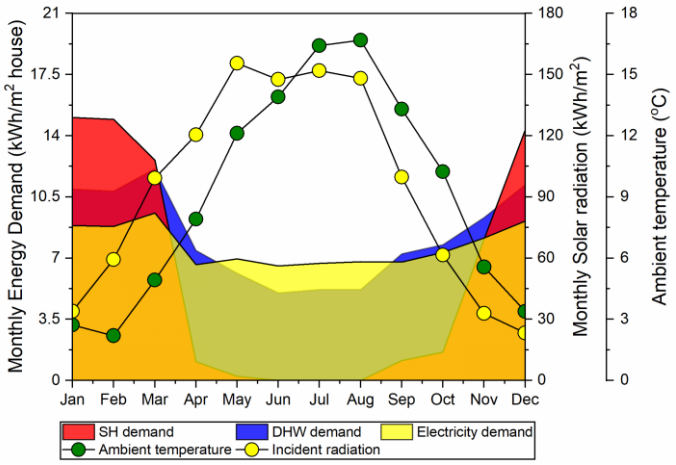

Figure VI-5: Monthly average energy demand profile, solar radiation profile and ambient temperature profile

VI.3SDHS sustainability assessment

In the context of nZEB, the developed framework assesses proposed SHDS based on four main criteria including the energy performance based on established energy

efficiency indicators for the dwelling, the social indicator for direct and indirect benefits of society, alongside economic performance and environmental impact throughout the system lifespan. A framework for the SDHS sustainability assessment criteria is shown in Figure VI-6.

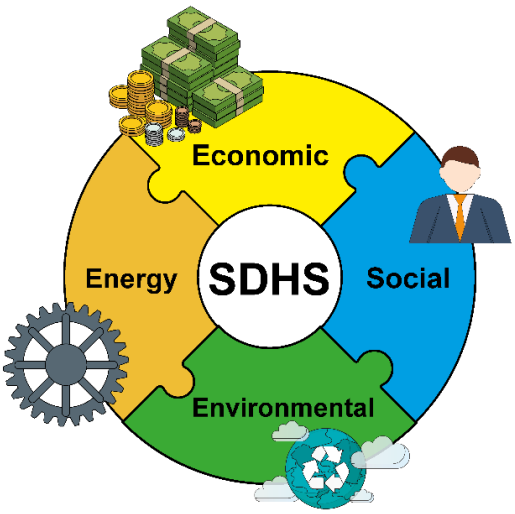

Figure VI-6: SDHS sustainability assessment criteria

VI.3.1 Energy indicators

The SDHS energy performance is evaluated through a couple of indicators to evaluated both its thermal and electric renewable energy equipment.

Firstly, the REF_{th} is the renewable energy fraction calculated for the on-site utilization of solar thermal energy for SH and DHW demand. It can be defined as a ratio between the total solar thermal energy used to the total thermal energy demand, as shown in Eq. VI-1 [55].

$$REF_{th} = 1 - (R_{HP} + R_{fuel}) \quad \text{Eq. VI-1}$$

Where:

$$R_{HP} = \frac{\int_0^t Cap_{heating}}{Q_{SH\ load} + Q_{DHW\ load}} \quad \text{Eq. VI-1.1}$$

$$R_{fuel} = \frac{\int_0^t \dot{Q}_{AUX_1} + \int_0^t \dot{Q}_{AUX_2}}{Q_{SH\ load} + Q_{DHW\ load}} \quad \text{Eq. VI-1.2}$$

Where $Cap_{heating}$ is the energy supplied by the heat pump. While the $\dot{Q}_{AUX_1}$ and $\dot{Q}_{AUX_2}$ are the energy provided by the auxiliary heaters to cover the SH load ($Q_{SH\ load}$) and DHW load ($Q_{DHW\ load}$) under the condition of insufficient solar energy.

In addition, solar electric energy is evaluated through the REF_{elec} which represent the energy fraction calculated for the on-site utilization of renewable electrical energy to satisfy the electricity demand of the neighbourhood, and It is calculated as following:

$$REF_{elec} = \frac{\int_0^t EC_{RE}}{Q_{electric\ load}} \quad \text{Eq. VI-2}$$

Where EC_{RE} is the generated electricity by the PV array, and $Q_{electric\ load}$ is the total electricity demand.

Besides evaluating the SDHS performance, it is important to assess the effect of the proposed SDHS to enhance the building energy performance to achieve a nearly zero energy consumption at both scales: individual buildings and community. In this context, Energy Performance Indicators (EPI) present an estimation for the energy performance of the building. This index is widely used in the Netherlands as '*Dutch energy label for dwellings'* [19]*,* and it is calculated as:

$$EPI = \frac{Q_{total}}{155A_{floor} + 106A_{loss} + 9560} \quad \text{Eq. VI-3}$$

Where: $Q_{total} = Q_{SH\ load} + Q_{DHW\ load} + Q_{AUX} + Q_{electric\ load} - \int_0^t EC_{RE} - \int_0^t EG_S$ Eq. VI-3.1

where Q_{total} is the total energy consumption in the building, whereas EG_S is the generated thermal energy cover by the solar thermal energy system. The values obtained from Eq. VI-3 are categorized corresponding to Dutch energy labels, as shown in Table VI-1, where the lowest Value of EPI indicates the highest building energy efficiency.

Table VI-1: Dutch energy labelling for building's energy performance

EPI	A++	A+	A	B	C	D	E	F	G
	<0.50	0.51 – 0.70	0.71 - 1.05	1.06 - 1.30	1.31 – 1.60	1.61 – 2.00	2.01- 2.40	2.40 – 2.90	>2.90

VI.3.2 Economic indicators

The net present cost (NPC) assess the life cycle cost (LCC) to evaluate the SDHS feasibility over the project lifespan [53]. The NPC is performed as a summation of the

capital cost (IC), the operational cost (OC), and the replacement cost (RC). A detailed description of NPC calculation is provided in the supplementary information - SI 1.

$$NPC = IC + OC + RC \quad \text{Eq. VI-4}$$

An alternative common approach to evaluate the economic feasibility is the payback period (PBT) which is the payback time of the proposed SDHS model, and it denotes the number of years taken by the proposed system to deliver the total life cycle cost [53]. It is calculated as the following:

$$PBT = \frac{NPC}{Annual\ cost\ saving} \quad \text{Eq. VI-5}$$

VI.3.3 Environmental indicators

The impact on environment of adding HP, SST and PV to SDHS system is determined using the life cycle approach (LCA) [54]. LCA can be performed using a variety of indicators to determine the environmental impact of any technology. For the developed SDHS system, we use the ReCiPe 2016 [55] framework to determine the environmental impact. The ReCiPe is among the widely used environmental indicator due to the methodological perspective, [56]. To calculate ReCiPe, Life Cycle Inventory Analysis (LCIA) data is transformed into endpoint scores, which are then categorized in three classes: human health, ecological systems, and resources depletion. Furthermore, theses damage classes are combined as a normalized indicator metric (RCP) for the SDHS conformation. The RCP can be expressed as:

$$RCP = \sum_{d} \delta_d \, \varepsilon_d DAM_d \qquad \forall d \quad \text{Eq. VI-6}$$

Where; DAM_d is endpoint score for damage category d. δ_d is a factor based on the use of extraction of material and use of land in the European setting to normalize endpoint data for different damage categories while ε_d is the weight factor based on values recommended in the ReCiPe 2016 framework. The data and environmental impact of SDHS components can be found in SI 2.

In addition, the environmental payback period (EPBP) is introduced to estimate the sustainability of the proposed SDHS model [17]. This indicator is estimated through calculating the total number of years required by the SDSH to replace the conventical system using the HP.

$$EPBP = \frac{RCP}{Annual\ RCP\ saving} \quad \text{Eq. VI-7}$$

VI.3.4 Social indicators

The proposed SDHS framework with the integration of multiple renewable energy technologies has a greater potential for providing social benefits improving the quality of life of the residents in the dwellings, providing more and better employment opportunities (EO).This value can be estimated as [57]:

$$EO = \lambda_{E.grid} E_{nom} + \lambda_{heat} Q_{nom,heat} + \lambda_{PV} Q_{nom,PV} \quad \text{Eq. VI-8}$$

Here $\lambda_{E.grid}$ = 0.61 persons/MW is the grid electricity coefficient, λ_{heat} = 0.38 persons/MW is the solar thermal collector coefficient, and λ_{PV} = 0.70 persons/MW is the PV module coefficient; all of them used to calculate the employment coefficients for technologies incorporated in the SDHS system [58]. E_{nom}, $Q_{nom,heat}$,and $Q_{nom,PV}$ are nominal capacities of the power plant, roof mounted solar thermal collectors and roof mounted PV module, respectively [57].

VI.4 Multi-objective optimization based on a surrogate model

Our objective is to enhance the economic and environmental performance of the proposed SDHS system. We used a surrogate modelling approach to implement multi-objective optimization on the SDHS system. The objective function is to minimize the net present cost and the environmental impact of a SDHS for a residential community while tracking its technical and social performance. In this work, we used surrogate models, which uses simulation results obtained with the TRNSYS model validated in section 3 to train a neural network to predict the thermal performance of the SDHS. Running the SDHS TRNSYS model with a feasible range of decision variables provides with a set of feasible scenarios that are used as training data set for the ANN. The trained ANN is then coupled to a genetic algorithm to devise a multi-objective optimization (MOO) function for minimizing NPC and RCP under several technical constraints.

VI.4.1 Data generation

Dataset development is a key aspect when developing a surrogate model, as a valid dataset obtained from a large number of simulations is used to train the surrogate model. For this work, data generation is performed by identifying the uncertain independent variables (inputs) and providing them to the TRNSYS simulation tool to obtain the dependent variables (outputs). In this work, the independent variables comprising the performance of the solar circuit, the SH distribution circuit and the DHW distribution circuit are used to create a combination of inputs to obtain the

sample point. More details regarding the data generation are introduced in Abokersh et al. [17].

VI.4.2 Surrogate model convergence

In developing a surrogate model, an intermediate step is developing a metamodel using ANN. In this work, the developed ANN metamodel's input layer has 14 neurons followed by 3 hidden layers. To implement the ANN model simulation, the Bayesian regularization algorithm is used with a learning rate of 0.001, and momentum mean of 0.004. ANN model structure is influenced by the approach adopted by Abokersh et al. [53] for good convergence. The ANN model's output layer has 21 variables that include thermal and electrical and thermal energy produced by solar collectors, energy supplied by SST, HP, and auxiliary heaters. The performance of the metamodel is verified using the performance metrics: (i) adjusted R^2 ($R^2-adj.$) and (ii) variation coefficient (CV). Equations (V-9) to (V-10) shows the mathematical form of R^2-adj and CV.

$$R^2 = 1 - \frac{\sum_{i=1}^{n}\left(y_{predict,i} - y_{data,i}\right)^2}{\sum_{i=1}^{n}\left(y_{data,i} - \overline{y}_{data}\right)^2} \quad \text{Eq. VI-9}$$

$$R^2 - Adj. = 1 - \frac{(1-R^2)(n-1)}{n-k-1} \quad \text{Eq. VI-10}$$

$$C.V(\%) = \sqrt{\frac{\sum_{i=1}^{n}\left(y_{predict,i} - y_{data,i}\right)^2}{\overline{y}_{data}}} \times 100 \quad \text{Eq. VI-11}$$

Here, $y_{predict,i}$ represents the value estimated at a time 'i', $y_{data,i}$ shows the value of output yat time 'i', n displays the sample size while k shows the total number of regressors used.

VI.4.3 Optimization algorithm and surrogate model integration

After developing the surrogate model, the next step is to incorporate the heuristic optimization techniques with the robust ANN model to solve a MOO problem. MOO framework deals with the physical constraints systems to solve the objective function of two or more conflicting nature objectives. In this case study, the energy performance of the system is optimized by aligning the environmental and economic system requirements. Ultimately, the residential community size's impact is also examined on the SDHS performance in an extended optimization problem. For the proposed SDHS system, the objective function to optimize the NPC and RCP is given as:

$$\begin{aligned} & min\ \{f_1(x), f_2(x)\} \\ & s.t.\ h(x) = 0 \\ & \quad g(x) \geq 0 \\ & lb_i \leq x_i \leq ub_i \qquad i \in \{1, \dots, 18\} \end{aligned} \qquad \text{Eq. VI-12}$$

Here, f_1 is NPC, f_2 is RCP, h represents equality constraints corresponding to the physics of physical systems solved in TRNSYS, and g denotes inequality constraints corresponding to technical evaluation of SDHS. Through these constraints, annual solar efficiency is maintained > 60%, REF_{th} is maintained > 50% as recommended by Bauer et al. [59] and Solites [60].

The solutions of multi-objective functions provide us with a non-dominated solution called Pareto solutions, which represent the optimal trade-off for the economic and environmental targets. To avoid obtaining sub-optimal solutions (which is probable in classical MOO using point by point search), an improved technique called Pareto-ranking [61] is utilized to refine the solutions for NPC and RCP.

The performance for SDHS has been examined for various community sizes (10, 25, 50, 100, and 500 houses) based on the decision variables explained in ensuing section.

VI.4.4 Decision variables and parameters

In the case study, 18 decision variables are used to formulate an optimization problem, including system components' relative alignment, structure, operating criteria and sizing. To categorize these variables, they are classified into 3 field circuits namely (i) supply (ii) SH (iii) DHW (Figure VI-7).

These decision variables are linked with mathematical equations to determine the equipment size for SDHS. The solar field circuit has 5 decision variables, i.e., area of photovoltaic panels (A_{PV}), area of solar thermal collector (A_{col}), inclination angle of solar collectors (β_{col}), number of solar thermal collectors in series (N_{col}), heat pump capacity as function of the maximum heat demand supplied (FC_{HP}), the turn on temperature of the heat pump (T_{ref}). The space heating circuit has 9 decision variables, i.e., volume of SST (V_{SST}), height to diameter ratio for SST (HDR), thickness of insulation for the wall (d_{wall}), roof (d_{roof}), and ground (d_{Gnd}), insulation material type represented by the conductivity of construction material (λ_{con}), roof and wall (λ_{ins}) and ground ($\lambda_{ins,gnd}$), and auxiliary heating unit capacity as a fraction of the maximum heating demand (FC_{AUX_1}). Finally, the domestic hot water circuit has 3 decision variables e.g. volume of DHWT (V_{DHW}), height to diameter ratio of DHWT (HDR_{DHWT}) and the fraction capacity supplied by the auxiliary unit as a percentage of the maximum heating load (FC_{AUX_2}).

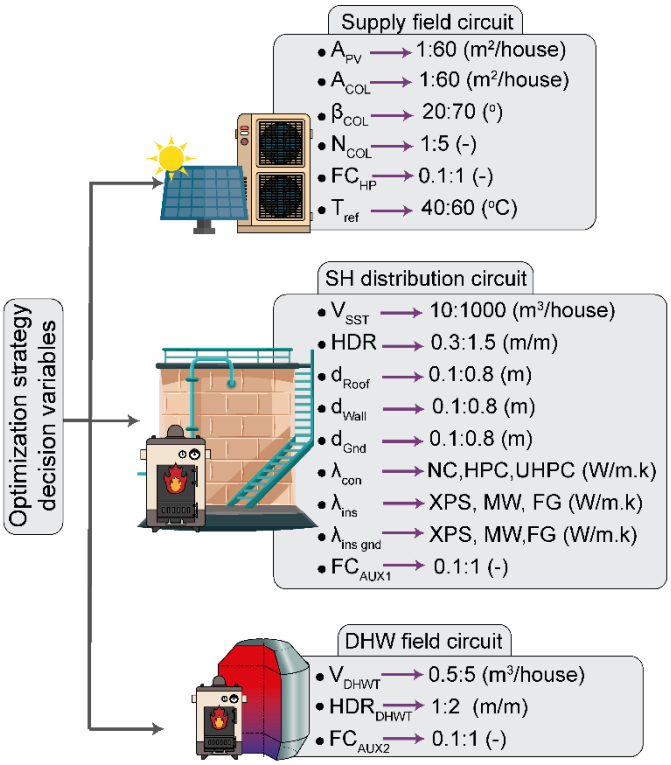

Figure VI-8: The decision variables in the SDHS optimization problem

VI.5 Optimal solutions post analysis

We have proposed a framework for the inclusive sustainability assessment of a solar assisted district heating system. The methodology framework is outlined in Figure VI-9. The framework starts with the simulation of SDHS in TRNSYS 18 and leads to defining most suited decision variables, their range and related output to showcase the thermal performance of the SDHS. To reduce the computational cost of the process, the TRNSYS model is coupled with MATLAB and an ANN with Bayesian optimization. Later, the multi-objective genetic algorithm (MOGA) is coupled with the neural network to perform the multi-objective optimization for economic and environmental objectives. MOO provides a Pareto frontier with the optimal solutions for different community sizes which are then subjected to multi-criteria decision making (MCDM) to facilitate the selection according to the needs/preferences of stakeholders. For MCDM, we used TOPSIS (Technique for Order of Preference by Similarity to Ideal Solution), which ranks the solutions based on the desired criteria. To illustrate the significance of uncertainty on the optimized objectives, we performed a global sensitivity analysis (GSA) [62].

VI.5.1 MCDM development for SDHS evaluation

VI.5.1.1 Indicators normalization

The indicators used for the sustainability evaluation vary in nature and value range. Before the applying the MCDM, we normalize the indicators to a common range [0,1]. We used a distance-based normalization (TOPSIS) for the MCDM[63]. The normalization method for the indicator being minimized is expressed in (Eq. VI-14 - Eq. VI-15), while for the indicator being maximized is expressed in Eq. VI-17.

$$v_{ij} = \frac{x_j^{min}}{\vec{x}_{ij}} \quad \text{Eq. VI-13}$$

$$x_j^{min} = min\left(\vec{x}_{ij}\right) \quad \text{Eq. VI-14}$$

$$v_{ij} = \frac{\vec{x}_{ij}}{x_j^{max}} \quad \text{Eq. VI-15}$$

$$x_j^{max} = \max\left(\vec{x}_{ij}\right) \quad \text{Eq. VI-16}$$

VI.5.1.2 Indicators weighting method

The importance of each criteria might be different for each stakeholder. There are subjective and objective methodologies to apply weighting factors [64]: objective methods are based on mathematical models and more suited for numerical data. One of the widely used objectives is entropy-based weighting approach, and it is easily adaptable [65]. Suppose, a set 'D' which represent our sustainability criteria characterized by a vector $d_j = (d_{j_1}, d_{j_2}, \dots, d_{j_m})$ in terms of normalized indicator 'i' is defined as:

$$D_j = \sum_{i=1}^{m} d_{ij_j} = 1,2, \dots, m \quad \text{Eq. VI-17}$$

Then, the entropy of j^{th} indicator is given by:

$$e_j = -\frac{1}{\ln(m)} \sum_{i=1}^{m} \frac{d_{ij}}{D_j} \ln \frac{d_{ij}}{D_j} \quad \text{Eq. VI-18}$$

In the end, normalized weight is calculated as:

$$w_j = \frac{1 - e_j}{\sum_{j=1}^{m}\left(1 - e_j\right)} \quad \text{Eq. VI-19}$$

VI.5.1.3 TOPSIS method

The TOPSIS algorithm, developed by Hwang et al. [66]. This method uses the normalized values obtained from Eq. VI-20 and assumes a distance-based criterion signifying that ideal solution lies at the shortest distance from the positive ideal solution and the longest distance from the negative ideal solution. The calculated distances are then compared to find out the best plausible solution. The advantage of TOPSIS is that it can provide a ranking of each solution for each criterion [67].

To determine the rank, first, we identify the positive ideal solution (A^+) and negative ideal solution (A^-) as below:

$$A^+ = \left\{\left(\underbrace{max}_{i} v_{ij} | j \in I\right), \left(\underbrace{min}_{i} v_{ij} | j \in I'\right), i = 1,2, \dots, m\right\} = \{v_1^+, v_2^+, \dots, v_m^+\} \quad \text{Eq. VI-20}$$

$$A^- = \left\{\left(\underbrace{min}_{i} v_{ij} | j \in I\right), \left(\underbrace{max}_{i} v_{ij} | j \in I'\right), i = 1,2, \dots, m\right\} = \{v_1^-, v_2^-, \dots, v_m^-\} \quad \text{Eq. VI-21}$$

Here, $I = \{j = 1, 2, \dots, n\}$ and $I' = \{j = 1, 2, \dots, n\}$ represents the sets of economic and environmental criterion. Then, we measure the Euclidean distance for each solution from positive and negative ideal solutions using following equations:

$$S_i^+ = \sqrt{\sum_{j=1}^{n} \left(v_{ij} - v_j^+\right)^2}, \qquad for\ i = 1,2, \dots, m \quad \text{Eq. VI-22}$$

$$S_i^- = \sqrt{\sum_{j=1}^{n} \left(v_{ij} - v_j^-\right)^2}, \qquad for\ i = 1,2, \dots, m \quad \text{Eq. VI-23}$$

Lastly, proximity index ($C_i \in [0;1]$ for $i = 1, 2, \dots, m$) is calculated to find the remoteness from the positive and negative ideal solutions for ranking, as:

$$C_i = \frac{S_j^-}{S_j^+ + S_j^-} \quad \text{Eq. VI-24}$$

VI.5.2 Global sensitivity analysis (GSA)

The final step of this methodology is to perform a sensitivity analysis to offer an understanding of the most sensitive system parameters. Given the advantage of GSA over LSA, a Bayesian-based GSA approach (BACCO) [68] is employed. This

approach can cover an extensive range of parameters with an interaction for their relative distribution under uncertainty. It also reduces the computational time compared to Monte-Carlo based GSA approach.

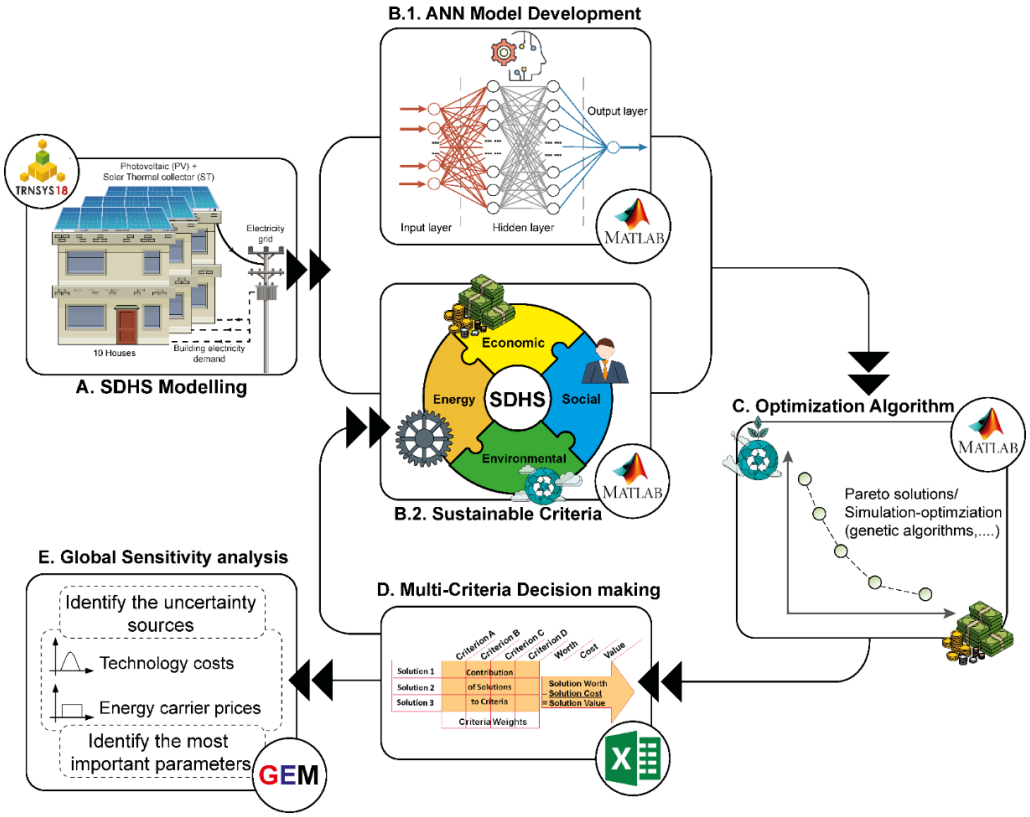

Figure VI-9: Framework for the inclusive, sustainable system optimization of SDHS

BACCO methodology has two main stages: (i) acting as emulator (statistical representative model) and (ii) uncertainty analysis. The emulator is trained with the data obtained from the simulation-optimization model. This dataset covers the feasible domain of solutions in a Latin hypercube design. Once the emulator is working, it is cross-validated to check its efficiency. The second stage covers the multidimensional domain of design variables to quantify the sensitivity of the parameters. The GSA is performed with respect to EPI, NPC, RCP, and EO in terms of percentage variation of each input to estimate the impact of ten economic decision variables. These variables comprise natural gas price (C_{ng}), uying (C_{el}) and selling to the grid electricity prices (S_{el}), atural gas (i_{ng}), electricity inflation rate (i_e), investment cost (IC), operational cost (OC), replacement cost (RC), in addition to system inflation (i) and discount rates (d).

VI.6Results and discussion

This work provides a sustainable insight on the applicability of surrogate modelling for the economic-environmental-social optimization of transient SDHS model. The surrogate model was used to optimize the SDHS framework for different community sizes ranging from 10 houses to 500 houses under different scenarios (i.e. scenario 1 - minimum cost, scenario 2 - 25% less environmental damage, scenario 3 - 50% less environmental damage, scenario 4 - 75% less environmental damage and scenario 5 - minimum environmental damage) addressing the impact on environment and project costing. The wide range of the decision variables produced multiple results which are discussed in the following sections. The first portion of the results and discussion section addresses the metamodel's fittingness for the SDHS framework optimization. The second portion sheds light on the SDHS optimization results for economic-environmental-social indicators and physical and technical constraints. In this section, optimal solutions are analyzed for all community sizes under each scenario. The third portion provides an insight into the ranking of the optimal solutions based on weighted criteria using multi-criteria-decision-making. The final portion checks the robustness of the metamodel using the global sensitivity analysis.

VI.6.1 Surrogate model convergence results

In this work, K-fold cross-validation strategy is adopted to fit the surrogate model. The 2048 samples (i.e., simulation results) are organized in k subsets [69]. The ANN model is trained with k-1 subsets while k subsets are used to test the trained model in each run. Table VI-2 displays a summary of the ANN model performance.

From the results shown in Table VI-2, the surrogate metamodel prediction agrees with TRNSYS simulation outputs where $C.V$ shows that model inaccuracy does not fall below 8.87% for any surrogate model output as the $R^2 - Adj.$. is always above 95.5% for any output through the ANN model. Hence, we can be confident about the ANN model's predictability for the proposed SDHS framework's thermal performance for the given training data range. The advantage of metamodeling offers the benefit of significantly reduced computational time over the conventional heuristic optimization techniques.

Table VI-2: Performance of ANN model in predicting the TRNSYS simulation output

	Solar circuit					SH circuit			DHW circuit		
	Q_{SOL}	Q_{PV}	Q_{Usefu}	Q_{abs}	P_{elec}	Q_{SST}	$Q_{SST\ los}$	Q_{AUX_1}	Q_{DHW}	$Q_{DHW\ lo}$	Q_{AUX_2}
$R^2 - Adj$	99.8%	99.7%	98.3%	97.7%	97.8%	99.5%	97.7%	99.2%	95.5%	98.9%	99.4%
$C.V$	1.98%	1.87%	3.97%	8.87	8.16%	2.87%	8.54%	8.15%	0.49%	2.70%	3.08%

VI.6.2 Multi-objective optimal solutions

Successfully tested ANN-based surrogate model is employed to optimize the economic and environmental performance of the proposed SDHS framework for various community sizes and under different scenarios. All the scenarios are compared to the base case (decentralized heat pump) explained in section 2. The first set of optimal results for the economic criteria are shown in Figure VI-10. Economic criterion (NPC) is simplified to €/m^2 for the considered building blocks. Base case has NPC at 66.6 €/m^{2,} which is constant for all the scenarios. For the smallest community size (10 houses), the optimal solution for scenario 1 (minimum cost) has an economic performance akin to base case equal to 70.1 €/m^2. The economic performance for 10 houses community size decreases with the decrease in environmental damage factor of SDHS as the NPC for scenario 5 (minimum environmental damage) is 125 €/m^2. However, as the community sizes increase from 10 to 25, 50, 100 and 500 houses, the economic performance increases significantly and proportionally. For 25 houses community sizes, the economic performance is improved for scenarios 1, 2, 3 and 4 by 32%, 28%, 23% and 12% respectively over the base case. While the scenario 5 has an unfavourable performance for 25 community size compared to the base case as the base case outperforms the former by 22%. For 50 houses community size, optimal SDHS solution surpasses the base case's economic performance for scenario 5 (minimum environmental damage) and has an NPC of 64.7 €/m^2. For community sizes higher than 50 houses, the proposed SDHS has economic and environmental solutions at par the base case for every scenario considered here. The best economic solution is obtained for the minimum cost scenario in 500 houses community (21 €/m^2). For scenario 4 and scenario 5, the economic performance is similar at NPC of 30.7 €/m^2.

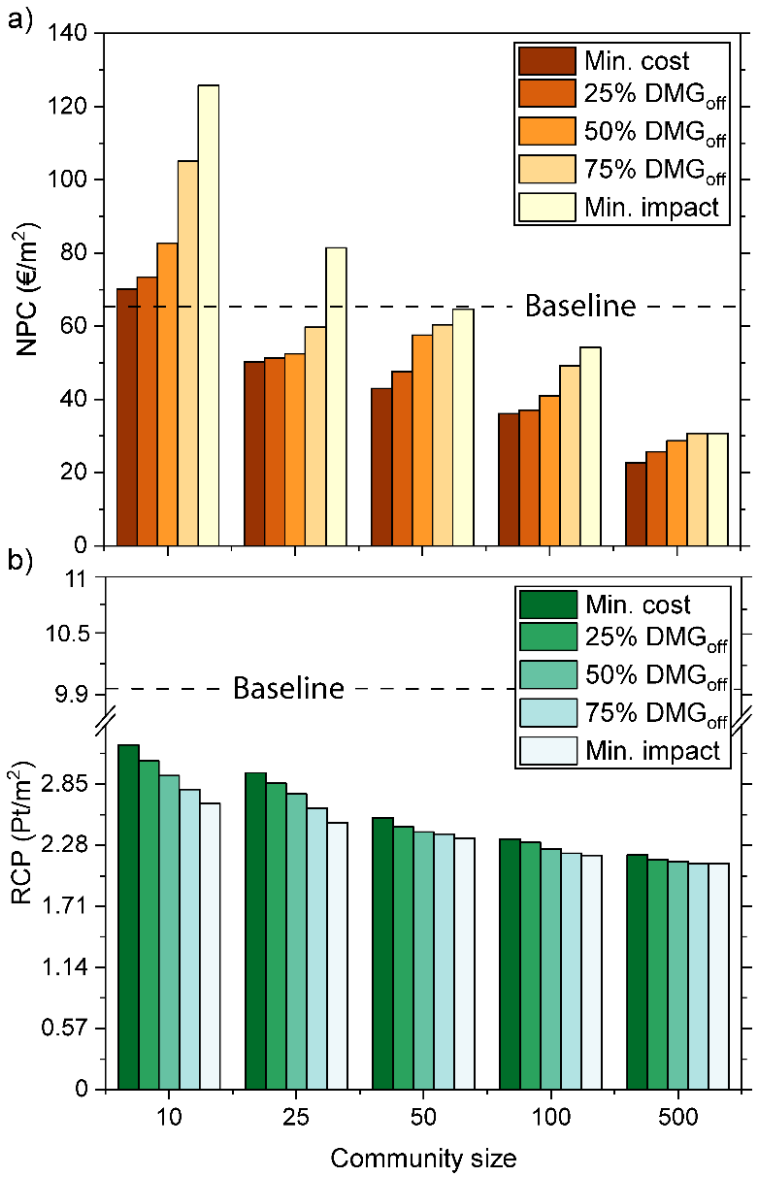

Figure VI-10. Optimal solutions of SDHS for various community sizes under different scenarios where (a) the economic criteria, whereas (b) the environmental criteria

Looking at the environmental damage factor in Figure VI-10, all the optimal solutions showed a better environmental performance compared to the base case which has RCP value of 10.1 Pt./m² while the least environmental friendly optimal solution is the minimum cost (scenario 1) for 10 houses community size which has a RCP value 3.2 Pt./m² giving 3 times better environmental performance compared to the base case.

Therefore, all the optimal solutions perform extremely well for environmental criterion against the base case. Like the economic performance, the environmental performance of the SDHS improves as we move to bigger community sizes. The case of 500 houses community gives the best environmental performance for scenario 4 and 5 with RCP value of 2.1 Pt./m^2 which shows 4 folds improvement over the base case's economic performance. Thus, we witness that the ANN model's optimal solutions have improved environmental and economic performance compared to this study's base case.

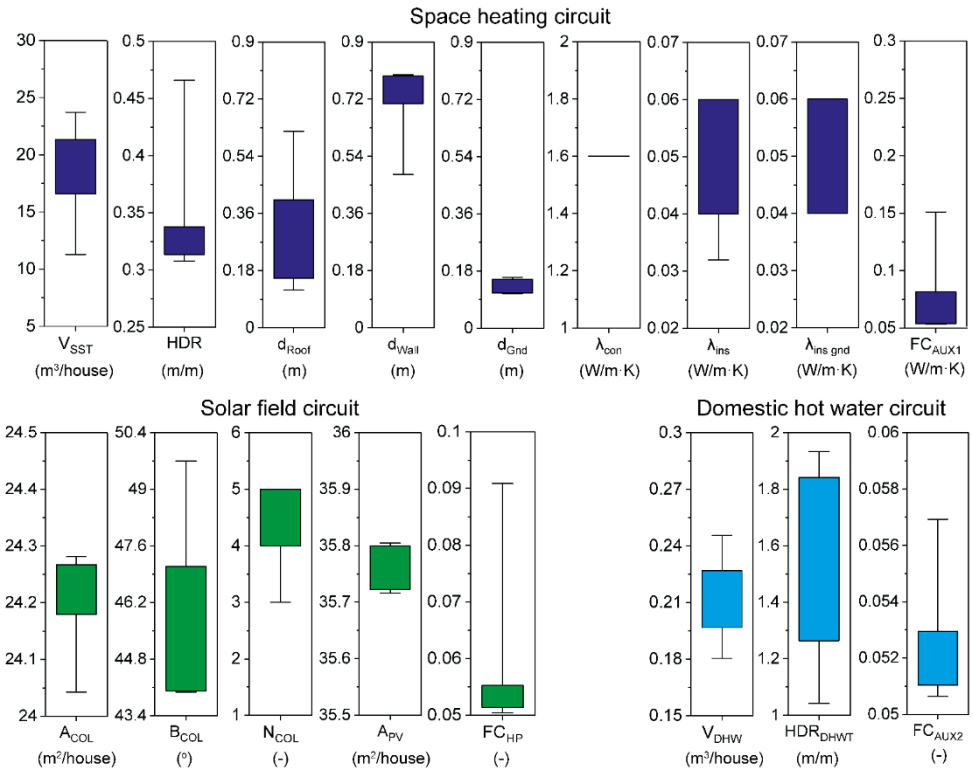

Figure VI-11. Guideline for key parameters values to design optimal SDHS solution under various scenarios

To arrive at the optimal solutions described above and depicted in Figure VI-10, the metamodel considers multiple decision variables for different scenarios and community sizes. The optimal design and sizing of the SDHS system also become an important consideration to achieve the desired economic and environmental performance. An in-depth analysis of the optimal solutions obtained from the ANN model provides us with a guideline for the SDHS system design and sizes of its components. SDHS was divided into three circuits, namely: (i) Space heating circuit,

(ii) Solar field circuit and (iii) Domestic hot water circuit. Each circuit consists of specific components to serve the specific purpose in the SDHS network. These decision variables vary due to multiple scenarios and provide a guideline to follow for optimal system design. This range of decision variables for optimal solutions has been shown in Figure VI-11, in the form of candles. Each candle has lower wick (representing minimum cost scenario), a center body (representing the scenario 2, 3 and 4) and the upper wick (representing minimum environmental damage scenario).

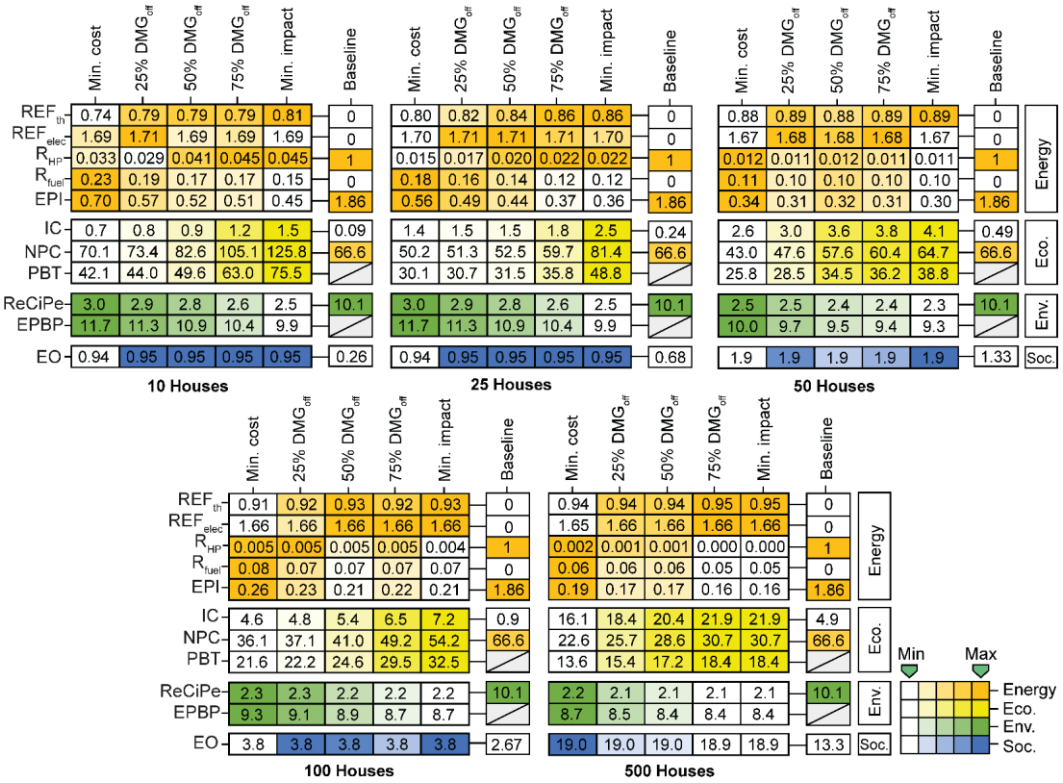

Figure VI-12. Key performance indicators for best ranked optimal solutions and base cases under different community sizes

To facilitate a comprehensive sustainable analysis of optimal SDHS solutions, a breakdown of the key performance indicators mentioned in section 3 is shown in Figure VI-12 for all 5 scenarios and the base case. The performance indicators are divided into 4 main categories: (i) Energy (ii) Economical (iii) Environmental, and (iv) Social. All scenario solutions perform better for the smallest community size of 10 houses than the base case for energy indicators. The performance of energy indicators improves from minimum cost scenario to minimize environmental damage scenario in general for all the community sizes, although the gradient for improvement from scenario 1 to scenario 5 is high for 10 houses community size. A comparison

between the scenario 1 and the base case for 10 houses shows 2.5 folds improved EPI performance (building energy performance grade = A+) for the optimal solution against the base case (building energy performance grade = D). In contrast, the optimal solution of scenario 5 has 4 times improved EPI performance over the base case to achieve a building energy performance grade A++. For social indicator, the 10-houses community size has 3.5 times improved performance for all the scenarios. As we move towards bigger community sizes, EPI's performance increases from 0.56 to 0.16 (NZEB), giving us a significant improvement range from 3 to 10 times in the energy performance over the base case for different scenarios. The building energy performance grade is reflected in the energy covered by the solar energy where the solar thermal fraction can increase from 80.8% on a community of 10 houses up to 95% on community size of 500 houses. On the other hand, the installed PV system provides extra electricity of around 70% for all community sizes to be sold to the national electricity grid, which can support the PEB state. Furthermore, the increment in solar energy usage with increasing the community size is reflected in the reduction of natural gas usage where it diminishes from 23% at the scenario 1 community size of 10 houses to only 5.6% under the same scenario at community size of 500 houses.

For economic indicators, the base case presents with an economical solution in the case of 10 houses community size, but optimal solutions have a better scope in the long term because of the PBT indicator. In contrast, the base case is depreciative and has no payback, optimal solutions have a payback and, therefore, provide a better option for long term planning. However, as we move to bigger community sizes, from 25 to 500 houses, economic indicators overcome the base case, and we find that for 50 houses community size even the most environment-friendly solution presents with better economic performance than that of the base case where the payback period is reduced to 26 years. Furthermore, with the movement toward a bigger community size of 500, the PBT can be reduced to 13.6 years. The environmental indicator has shown an improved performance for all the community sizes under all scenarios, where the environmental performance is improved from 11.7 years at community size of 10 houses to 8.4 years at community size of 500 houses. Similarly, the social indicator shows improved performance, for the optimal solutions over the base case, ranging from 1.3 times for 10 houses community size to 4 folds for 500 houses community size.

VI.6.3 Optimal solutions ranking based on MCDM

A large set of optimal solutions obtained from the ANN model under different scenarios for different community sizes provide stakeholders with multiple options to choose from. To facilitate the stakeholders' decision-making, a ranking system is developed using multi-criteria decision making. The criteria considered for this ranking system are energy, economic, environmental, social and a hybrid of all the criteria. A summary of indicators used for each criterion alongside their weightage

considered is shown in Table VI-3. A weighted entropy TOPSIS approach described in section 5.1 is used to rank the solutions under various scenarios.

Table VI-3. Weighted indicators to apply TOPSIS for MCDM

	Indicators	**Weights**
Energy	$(W_{REF_{th}}, W_{REF_{elec}}, W_{R_{HP}}, W_{R_{fuel}}, W_{EPI})$	(1.2%, 0%, 38.2%, 30.3%, 30.3%)
Economic	$(W_{IC}, W_{NPC}, W_{PBT})$	(43%, 28.5%, 28.5%)
Environmental	(W_{ReCiPe}, W_{ADSR})	(50%, 50%)
Social	(W_{EO})	(100%)
Hybrid system	$(W_{Energy}, W_{Economic}, W_{Environmental}, W_{Social})$	(28.8%, 67.8%, 3.2%, 0.2%)

The ranking of optimal solutions for different community sizes under the considered 5 scenarios is shown in Table VI-4. Under the assigned weightage, 50% DMG_{off} scenario gets priority for 10, 25 and 100 houses community size while it turns out 2nd ranked for 50 houses community and 3rd for 500 houses community. For 50 houses community size 25% DMG_{off} is best ranked while for 500 houses community 75% DMG_{off} is best ranked solution. It is worth noting that in 500 houses community, more environment-friendly solutions (i.e. scenario 4 and 5) make the top ranks by a clear margin and stand out as a clear choice for higher residential communities having 500 or more houses.

Table VI-4. Ranking of optimal solutions based on community size and scenario

Community size	**10 houses**		**25 houses**		**50 houses**		**100 houses**		**500 houses**	
Scenario	P_i	**Rank**	P_i	**Rank**	P_i	**Rank**	P_i	**Rank**	P_i	**Rank**
Min. cost	0.73	3	0.71	4	0.77	3	0.76	3	0.64	5
25% DMG_{off}	0.75	2	0.73	3	0.80	1	0.77	2	0.71	4
50% DMG_{off}	0.76	1	0.76	1	0.77	2	0.79	1	0.73	3
75% DMG_{off}	0.70	4	0.75	2	0.75	4	0.75	4	1.00	1
Min. impact	0.65	5	0.65	5	0.72	5	0.71	5	0.99	2

VI.6.3.1 Technical analysis

To analyze optimal solutions' thermal and energy performance, the technical analysis has been performed for optimal solutions. The thermal energy is used for space heating and hot water demands. As shown in Figure VI-13, the plots depict the energy demand and energy supplied (Q_{cov}) by the solar collectors (thermal and PV) for all the community sizes throughout the year. Space heating demand (kWh/m^2) is high for winter months (November, December, January and February). For November, December, and January, the proposed SDHS system can provide thermal energy to satisfy the demand in every community size fully. The SH demand is not met by Q_{cov} in the months of February and March for 10, 25 and 50 houses communities and the excess demand in these cases is satisfied by the auxiliary unit. The plot also shows that as the community size increases the Q_{cov} is able to cover more SH demand and for community size of 100 houses and above the SDHS can satisfy SH demand fully on its own suggesting a reduction in environmental damage with SDHS for bigger community sizes.

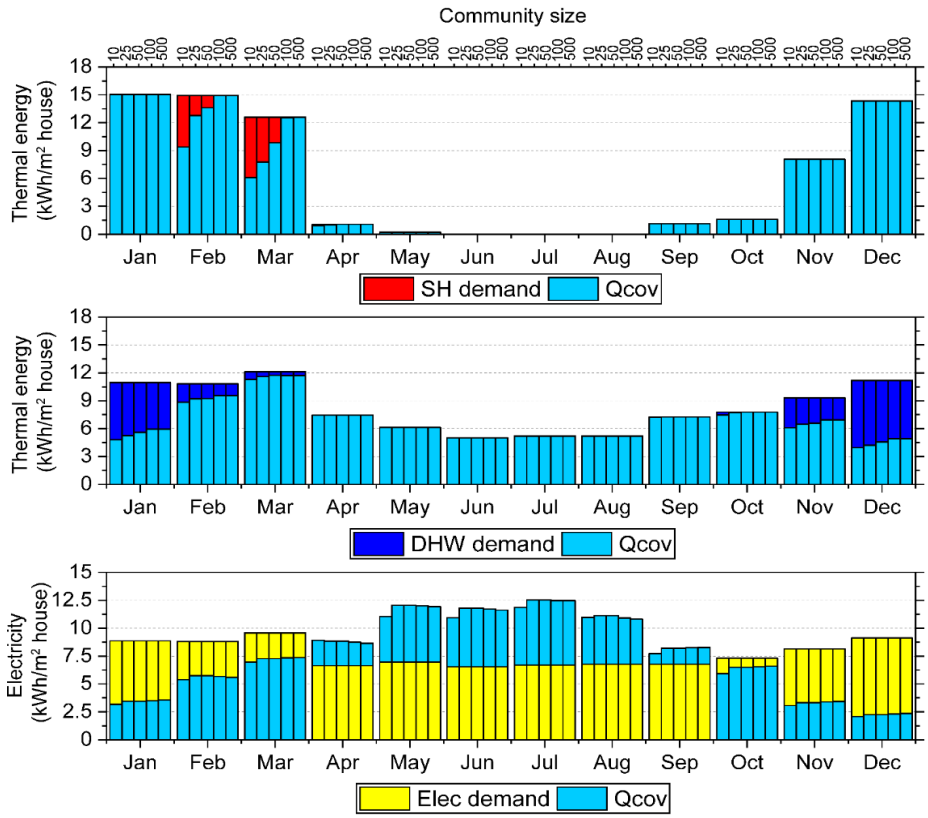

Figure VI-13. Energy demand and supply (per m^2) for all community sizes throughout the year

The DHW demand exists throughout the year, unlike SH demand. The DHW demand has 20% to 50% increase in the months of winter and Q_{cov} needs to be supplemented with auxiliary units to meet this extra demand for DHW. Q_{cov} shows a very small increasing gradient with the increase in community sizes, as shown in Figure VI-13. The electricity demand also has a similar nature as the SH and DHW demand over a year. Electricity demand is more in October, November, December, January, February and March than the Q_{cov} produced by PV panels for the all the community sizes. Therefore, the excess electricity demand is met by grid electricity through smart metering. In April, May, June, July and August, PV collectors' electricity is more than the demand. This extra production of electricity is supplied to grid through smart metering to earn credits. These results show the transition not only to the NZEB concept, but it can serve the transformation from LCB to PEB for community sizes ≥ 100 houses.

VI.6.3.2 Economic analysis

The economic performance of optimal solutions is further analyzed by breaking down the NPC into its various components.

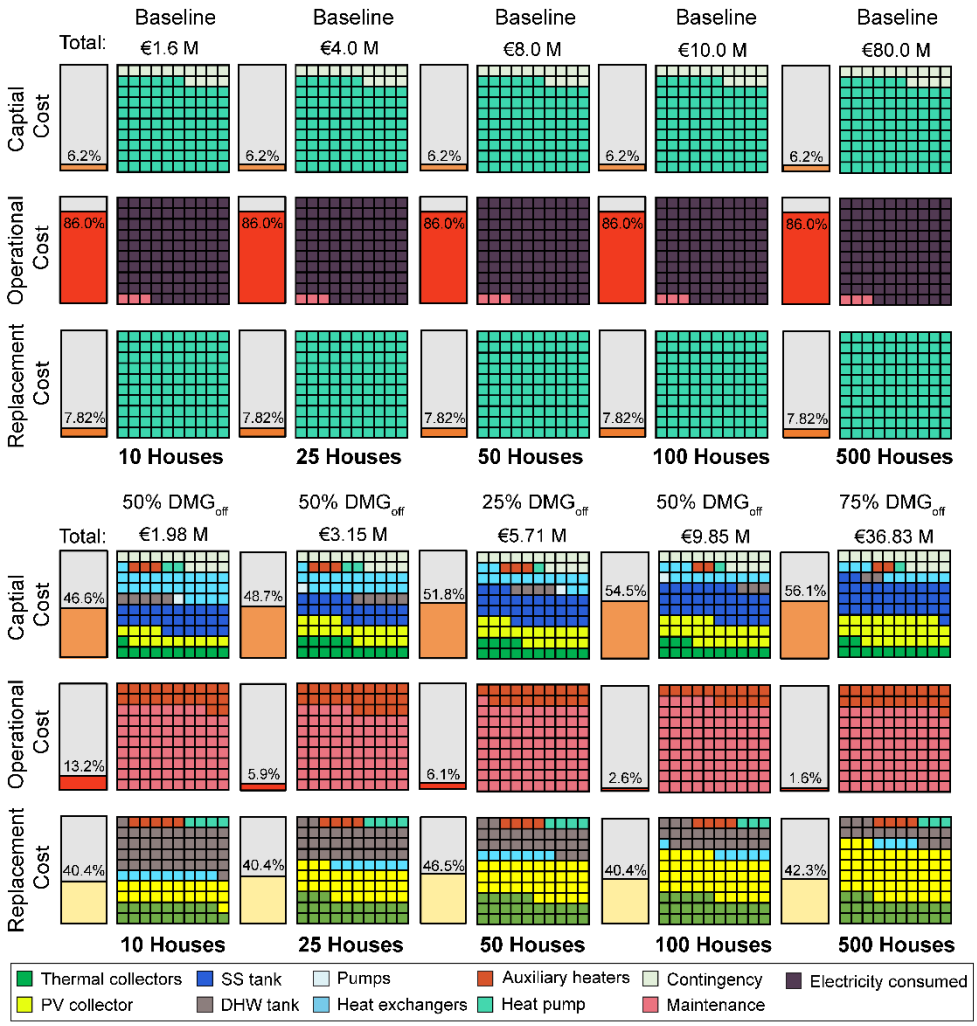

Figure VI-14. Cost analysis of optimal solutions for different community sizes compared to base case for respective community sizes

Figure VI-14 shows the cost distribution of SDHS components for the top-ranked solutions for every community size, mentioned in section Multi-objective *optimal solutions* Analysis of the cost components for the base case has a very low capital cost (6.2%) and replacement cost (7.8%) while the operational cost is extremely

high (86%) which makes the base case a depreciating project as each operational costs adds to the cost of the project.
On the other hand, for optimal solutions, the project's capital cost varies from 46.6% to 56.1%, operational cost varies from 13.2% to 1.6%, and replacement cost varies from 40.4% to 42.3%. The capital cost percentage of the optimal solutions increases as the community size increase because bigger community sizes corresponding to scenario 4 and scenario 5 (less environmental damage) have more infusion of renewable energy technology hence the high capital cost. The operational cost of the SDHS system reduces as we approach bigger community sizes while SDHS solution also provides more than 40% of the NPC as replacement costs which suggest that the depreciation of the SDHS project is reduced by at least 5-fold.

VI.6.3.3 Environmental analysis

The environmental indicator is an important part of this study. Therefore, a detailed analysis of optimal SDHS solutions is performed to see each ranked solution's environmental impact is constituting components.

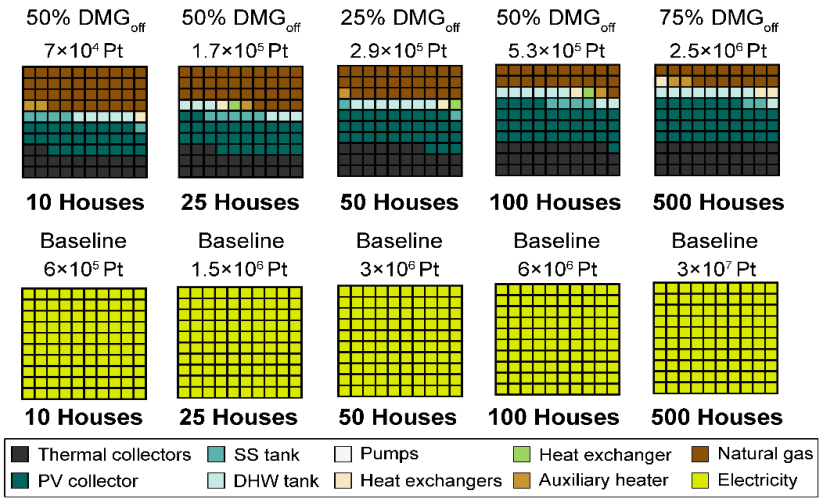

Figure VI-15. Comparison of results of environmental analysis under different optimal scenarios for various community sizes

Figure VI-15 shows the distribution of environmental damage caused by each component of the SDHS solutions compared to the base case below for the same community size. RCP points measure the environmental damage of each component. For the base case, the main cause of environmental damage is the electricity consumption from the grid. For 10 houses and 100 houses community sizes, under 50% DMG_{off} scenario, the environmental damage is almost 10 times

less than that of the base cases of same community sizes while it is comparable for 25 houses community size under the same scenario. For 25% DMG_{off} and 75% DMG_{off} scenario, environmental damage is more than 10 times less compared to the base cases for corresponding community sizes. Component wise environmental analysis of SDHS solutions provides us with a better understanding of the damage caused by each system. Figure VI-16, entails that as we increase the community size, environmental damage due to the consumption of natural gas reduces significantly as we see that in case of optimal SDHS system for 10 houses, the environmental damage caused by natural gas consumption is 38% of the total damage while that in case of 500 houses is 17%. The percentage of environmental damage due to solar collectors (PV + thermal) is the major constituent (49 % to 67%) for environmental impact for all SDHS solutions. A third major contributor to environmental damage in optimal solutions is SST, which constitutes 4% to 6% of total damage. Other components for environmental damage are auxiliary units (1% - 2%), heat exchangers (2%), DHW tank (2% - 3%) and pumps (1%). Following the above analysis, onsite constructed SST has a major influence on economic and environmental indicators. Therefore, a deeper analysis of the SST is performed, and Figure VI-17 depicts the finding of the analysis for SST.

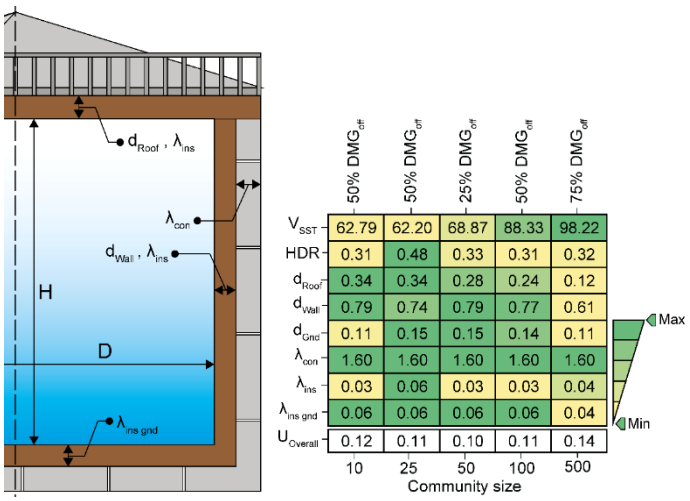

Figure VI-17: Design parameters of SST for various community size and optimal solution scenarios

The table in Figure VI-17 represents the optimized values for the different parameters of SST for each optimal solution. It is evident from the table that $U_{overall}$ = 0.14 W/m^2 is maximum for the optimal solution of the largest community size whereas SST of SDHS for 25 houses community has the lowest $U_{overall}$ = 0.10

W/m^2. ANN model optimizes the design parameters of SST to enhance the technical, economic and environmental performance of the SST. Optimal configurations of SST have listed in Figure VI-17 the variation in the parameter values aren't consistent with the increase in V_{SST} and community size where the d_{Roof} is around 0.34 m for community size of 10 house and it reduces to 0.12 m, and the d_{Wall} reduces from 0.79 m to 0.6 m. On the other hand, the d_{Gnd} stayed around 0.13 ± 0.02 m. For the SST construction material, the UHPC with λ_{con} = 1.6 W/m·K has a superiority over other construction materials due to its techno-economic and environmental benefits. Regarding the insulation materials, most of the optimal solutions insulate the SST ground using foam glass gravel with thermal conductivity of 0.06 W/m·K. In contrast, the SST walls use the foam glass only at the community size of 25 houses and other community sizes introduce extruded polystyrene usage due to its low price. The optimal size of SST for 500 houses community size solution has the most efficient and economical values of design parameters where the SST uses mineral wool in both walls and ground. Thermal performance and the SST's efficiency for the selected optimal solutions are plotted in Figure VI-18, where we see an increase in the SST efficiency performance of optimal solutions from 68.01% at 10 houses up to 89.7% at community size of 500 houses.

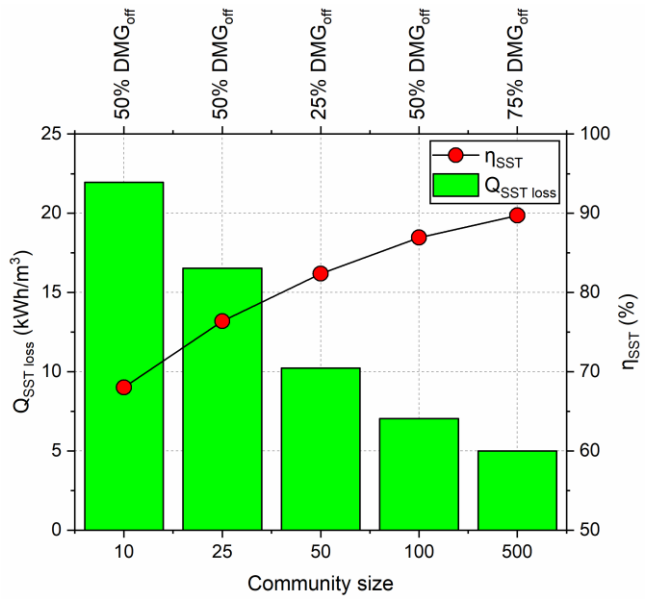

Figure VI-18: Thermal performance of SST with increased community sizes for optimal solutions

VI.6.4 GSA results

To understand the influence of critical parameters on the objective function, a global sensitivity analysis is performed. The analysis implies BACOO for its low computational cost. Here we have taken 10 houses community size minimum cost-optimal solution as the reference case to study the effects of parameters on the objective function. The reason to select the mentioned case for GSA is to have the closest economic performance to the base case. The parameters for BACOO analysis for GSA (as explained in section 5.2) includes prices of natural gas, electricity, inflation rate for gas and electricity, investment cost, replacement cost, operational cost and discount rate.

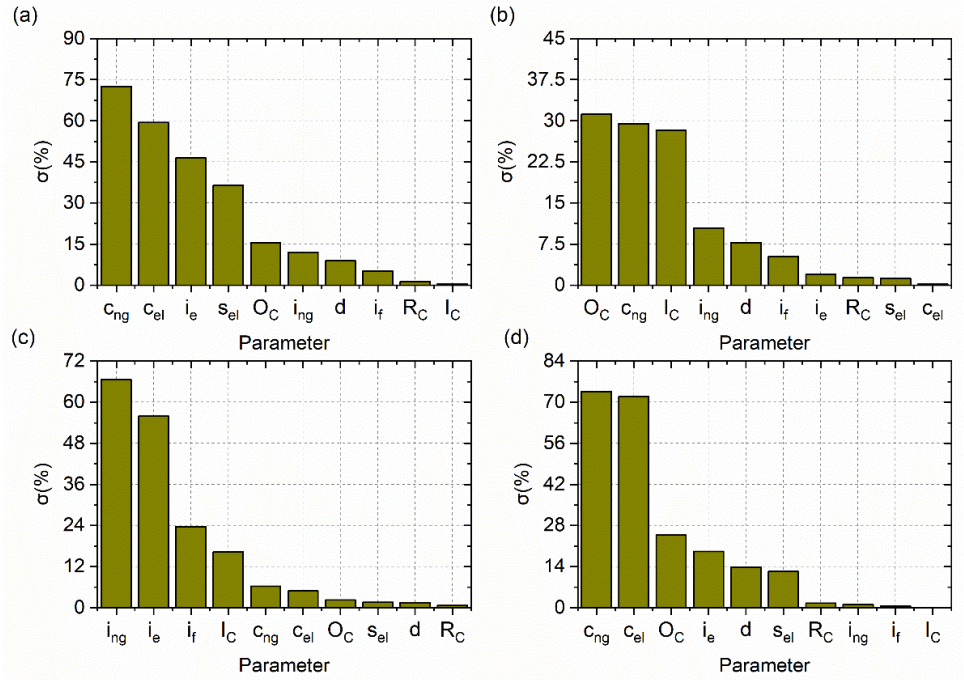

Figure VI-19: Results of the global sensitivity analysis following BACOO method to indicate the influence of critical parameters on (a) Energy indicator (b) Economic indicator (c) Environmental indicator and (d) Social indicator for minimum cost solution of 10 houses community size.

The effect of these parameters is shown in Figure VI-19 on energy performance Figure VI-19. a, economic performance Figure VI-19.b, environmental performance (Figure VI-19c) and on social performance (Figure VI-19d). Figure VI-19.a shows that energy performance presented by the EPI, which is highly affected by the cost of natural gas and electricity followed by inflation in electricity price, selling cost of electricity to the grid. The major factors affecting the economic performance

presented by NPC are the operational cost, price of natural gas and investment cost. An interesting observation was in the case of environmental performance where the inflation seemed to affect it greatly, and the other costs (investment, operational and salvation) have a tiny impact on the environment performance under uncertainty as shown in Figure VI-19c. Similarly, in Figure VI-19d, GSA for social performance indicated that variables like cost of natural gas and electricity have the extreme impact on social performance followed by operational cost, inflation in electricity price and discount rate. Hence, GSA's results cumulatively suggest that natural gas and electricity prices, operational cost, and inflation rates are the most critical factors to ensure the proposed SDHS system's expected performance.

VI.7Conclusion

This paper presents an investigation for the sustainable potential of solar assisted district heating system (SDHS) for retrofitted residential communities with different sizes located in Emmen, Netherlands to achieve Nearly Zero Energy Building (NZEB) concept. The work tends to optimize the performance of SDHS under energy, economic, environmental, and social criteria to facilitate the stakeholders in Europe regional network (ERN) in making the transition from low-carbon buildings (LCBs) to positive energy buildings (PEBs). In this context, a machine learning algorithm in cooperating TRSNYS is developed to simulate the SDHS thermal performance. A multi-objective optimization model is established to minimize the life cycle cost and environmental impact with consideration for maximizing the green energy use and social benefits. This ensures the system performance and implementation of the smart energy metering system for connecting to the grid. To estimate the SDHS system's performance from the perspective of sizing, different community sizes (10, 25, 50, 100, 500) were considered under 5 scenarios representing the effect of cost and environmental damage. A multi-criteria decision-making approach based on TOPSIS incorporating global sensitivity analysis (GSA) is proposed to help the stakeholders to see beyond the LCC and LCA based on selection criteria to choose the most appropriate scenario optimal solution for the desired community size and interpret the effect of various economic parameters on the sustainable performance of SDHS. The summary of the findings is the following:

- Compared to the existing base case (Decentralized heat pump), the minimum cost-optimal SDHS solution for 10 houses community size increases by 5.5 %, which failed to improve economic potential. However, the environmental performance improved 3.5 times, with 38% more social benefits.
- As the community size increases, more cost-effective and environment-friendly SDHS system. The most environment-friendly optimal SDHS solution for 500 community size is 50% more cost-effective, 4.5 times more environment friendly and has 1.5 times more social benefits compared to the 500 houses community size using the decentralized heat pump.

- The technical analysis of the optimal solution suggests that with the proposed SDHS system, it is possible to achieve a NZEB status for any community size with solar fraction up to 95% at 500 houses. However, it is possible to achieve PEB status only for a community size ≥ 50 houses due to its economic feasibility supported by 25 years of a payback period.
- Economic analysis of the optimal solutions suggests that seasonal storage tank has the biggest impact on the project cost of the SDHS model. In contrast, the environmental analysis shows that solar collectors (PV) constitute for the greatest part of environmental impact caused by any optimal SDHS solution.
- Global sensitivity analysis suggests that cumulatively a change in natural gas prices has the highest effect on the SDHS model's economic, environmental, and social performances.
- The adopted methodology has also resulted in providing a guideline for the SDHS system sizing with the optimal size range of SDHS system components.

This work concludes that SDHS provides an attractive energy sources option for cost-effectively transitioning to NZEB for medium to long term residential projects. Moreover, our proposed SDHS framework is in line with the 4GDH, which allows for the transition of existing buildings from LCBs to PEBs.

VI.8 Nomenclature

$Cap_{heating}$	Energy supplied by heat pump
C_c	Capital cost of the SDHS
C_O	Operational cost of SDHS
C_R	Replacement cost of SDHS
DAM_d	End point score for environmental damage category
EC_{RE}	Electricity generated by PV array
EG_S	electricity purchased from the grid
EO	Employment opportunity
LCC	Life cycle cost
NPC	Net present cost
PBT	Payback time
Q_{AUX}	Total thermal energy demand supplied by auxiliary units
$\dot{Q}_{AUX_1}$	Energy supplied by auxiliary heater 1
$\dot{Q}_{AUX_2}$	Energy supplied by auxiliary heater 2
$Q_{DHW\ load}$	Total thermal energy demand for hot water
$Q_{electric\ load}$	Total electricity demand
$Q_{SH\ load}$	Total thermal energy demand for space heating
Q_{total}	Total energy consumption
R_{fuel}	Ratio of total energy supplied by fossil fuels

RCP	Normalized indicator metric for environmental damage
REF_{elec}	Renewable energy fraction for electrical energy
REF_{th}	renewable energy fraction for thermal energy
R_{HP}	Ratio of total energy supplied by heat pump

Abbreviations

ANN	Artificial neural network
DHWT	Domestic hot water tank
EPBP	Energy performance building parameter
EPI	Energy performance indicators
GSA	Global sensitivity analysis
HP	Heat pump
IC	Investment cost
LCIA	Life Cycle Inventory Analysis
MCDM	Multi criteria decision making
NZEB	Net zero energy building
PEB	Positive energy building
PV	photovoltaic
SDHS	Solar assisted district heating system
SST	Seasonal storage tank

VI.9 Appendix

VI.9.1 The components of the of net present cost – SI.1

The overall initial cost of investment consists of several items such as the cost of the equipment purchase, installation, and transportation, including the cost of any contingencies and it can be expressed as follows [53]:

$$IC = (1 + \alpha_{CF}) \sum_{k} (PEC_k . FBM_k) \qquad \text{Eq. VI-25}$$

Where PEC_k represents the purchase cost of equipment unit k, while the bare module factor FBM_k is responsible for the installation and transportation expense of unit k. α_{CF} denotes the contingency factor. The cost component PEC_k can be updated from the initial value in the base year A to the year of installation B based on the Chemical Engineering Plant Cost Index (CEPCI) using the following equation:

$$PEC_k = PEC_k^{yearA} \frac{CEPCI^{yearB}}{CEPCI^{yearA}} \qquad \forall k \qquad \text{Eq. VI-26}$$

The initial cost of purchasing unit k in year A (PEC_k^{yearA}) can be estimated for various equipment units using Eq. VI-27 - Eq. VI-31.

$$PEC_k^{yearA} = \alpha_k CAP_k^{\beta_k} \qquad \forall k = COL, PV, DHW, AUX \qquad \text{Eq. VI-27}$$

$$PEC_k^{yearA} = \alpha_k (CAP_k^{\beta_k}) CAP_k \qquad \forall k = HP \qquad \text{Eq. VI-28}$$

$$PEC_k^{yearA} = CAP_k^{\beta_k}.10^{[\alpha_k (log_{10} CAP_k)^{\beta_k}]} \qquad \forall k = HE_1, HE_2, HE_3 \qquad \text{Eq. VI-29}$$

$$PEC_k^{yearA} = \alpha_k \, ln\left(\frac{CAP_k}{1000}\right) + \beta_k \qquad \forall k = P_1, P_2, P_3, P_4 \qquad \text{Eq. VI-30}$$

$$PEC_k^{yearA} = Ins_{SST} + Con_{SST} \qquad \forall k = SST \qquad \text{Eq. VI-31}$$

Where:

$$Ins_{SST} = \alpha_k CAP_k^{\beta_k} \qquad \forall k = XPS, MW, FG \qquad \text{Eq. VI-31.1}$$

$$Con_{SST} = \alpha_k CAP_k^{\beta_k} \qquad \forall k = NC, HPC \qquad \text{Eq. VI-31.2}$$

$$Con_{SST} = \alpha_k e^{\left(\frac{\beta_k}{10^5} CAP_k\right)} \qquad \forall k = UHPC \qquad \text{Eq. VI-31.3}$$

Here α_k and β_k are the equipment cost parameters, CAP_k is responsible for the design variables of equipment unit k. The design variables are the area of the solar collector (A_{COL}), the volume of the fully stratified storage tanks (V_{SST}, V_{DHWT}), types of insulation materials used for the SST (XPS, MW, FG) which includes extruded polystyrene, mineral wool, and foam glass gravel, respectively, types of the SST construction material ($NC, HPC, UHPC$) comprising of normal concrete, high-performance concrete, and ultra-high performance concrete, respectively, area of heat transfer for the heat exchangers (A_{HE1}, A_{HE2}, A_{HE3}), and the mass flow rates of discharge for the pumps ($\dot{m}_1, \dot{m}_2, \dot{m}_3$, $\dot{m}_4$).The total operating cost (C_o) is the discounted summation of all annual operating costs and can be expressed as follows:

$$OC = C_M PWF_M + C_P PWF_P + C_{AUX} PWF_{AUX} \qquad \text{Eq. VI-32}$$

Where the C_M indicate the annual maintenance, C_P is the electricity cost due to the recirculation pumps, and heat pump. While C_{AUX} is the energy cost of the auxiliary heaters (natural gas boilers). The term PWF reflects the present worth factor which is calculated for the specific cost of operation taking into account the inflation rate (i) and the rate of interest (r) over the lifetime of the proposed system. The cost of replacing several equipment units of the proposed SDHS can be estimated as shown below:

$$RC = PVF_n \sum_k (PEC_k . FBM_k) \qquad \text{Eq. VI-33}$$

Here PVF_n is the present value factor of the future cash flows in the year n. The equipments which will incur a replacement cost in our study due to a high rate of

depreciation over the system's lifespan are the solar collectors, storage tank used for DHW, heat pump, heat exchangers, and auxiliary heaters.

VI.9.2 Eco-environmental input parameters – SI.2

The initial cost parameters are outlined in Table SIV-4. On the other hand, the annual maintenance costs are estimated to be 1.5% of its investment cost. Based on the EUROSTAT database [74], the natural gas and household electricity prices are 0.0526 and 0.1873 Euro/kWh, respectively.

Table VI-5: The economic parameters for the initial cost of the heat pump integrated into SDHS

Unit	**Options**	**α_k**	**β_k**	**CAP_k**	**Base year**	**Ref.**	**FBM_k**
Solar collector		974.2	0.8330	Aperture area (m^2)	2007	[71]	1.00
Photovoltaic panels		300	1	Aperture area (m^2)	2016		1.00
Heat pump		2053.8	-0.348	Thermal power (kW)	2014	[72]	1.00
DHWT		3955	0.6500	Volume (m^3)	2007	[73]	1.00
Auxiliary heater		225.0	0.7460	Duty (kW)	2001	[52]	2.10
Heat exchanger		3.133	0.3310	Exchange area (m^2)	2001	[52]	3.29
Pump (P_1, P_2)		389.0	283.2	Mass flow rate (kg/h)	2009	[74]	3.24
Pump (P_3, P_4)		389.0	717.0	Mass flow rate (kg/h)	2009	[74]	3.24
SST insulation	XPS	561.09	0.397	Material thickness (m)	2017	[75]	1.00
	MW	1902.7	0.942	Material thickness (m)	2018	[76]	1.00
	FG	311.41	0.968	Material thickness (m)	2014	[77]	1.00
SST construction	NC	4178.1	-0.394	Volume (m^3)	2000		1.00
	HPC	2575	-0.363	Volume (m^3)	2004	[78]	1.00
	$UHPC$	90.83	-3	Volume (m^3)	2004		1.00

In addition, an inflation rate of 5.9% and 5% is selected for the natural gas and electricity, respectively. Aligning with Braungardt et al. [13] recommendation, an inflation rate of 2.3% is selected for the proposed system, whereas the discount rate is 3.5%.

On the other hand, the LCA input parameters are extracted from the Ecoinvent database [79]. This database categorizes the damage associated with the SDHS equipment based on the Recipe 2016 approach, a summary of the impact of different components in the SDHS is shown in Table S2.

Table VI-6: The environmental impact of heat pump integrated SDHS equipment based on ReCiPe 2016

Unit	Option	Impact factor (ReCiPe 2016)
Solar collector		32.5 Pt/m^2
Photovoltaic panels		26.3 Pt/m^2
Heat pump		22.3 Pt/kW
DHWT		173.1 Pt/m^3
Auxiliary boiler		$1.57 \cdot 10^3$ Pt/kW
Heat exchanger		2.515 Pt/m^2
Pump		62.8 Pt/kW
SST insulation	XPS	0.773 Pt/kg
	MW	0.0016 Pt/kg
	FG	0.266 Pt/kg
SST construction	NC	0.008 Pt/kg
	HPC	0.002 Pt/kg
	$UHPC$	0.0206 Pt/kg
Natural gas		0.0245 Pt/kWh
Electricity		0.0380 Pt/kWh

VI.10 References

[1] Ghosh A. Potential of building integrated and attached/applied photovoltaic (BIPV/BAPV) for adaptive less energy-hungry building's skin: A comprehensive Review. J Clean Prod 2020;276:123343. doi:10.1016/j.jclepro.2020.123343.

[2] Abokersh M, Vallès M, F. Cabeza L, Boer D. A Multicriteria Approach to Evaluate Solar Assisted District Heating in the German Market. 14th Int. Conf. Energy Sustain., ASME; 2020. doi:10.1115/ES2020-1668.

[3] Nearly Zero Energy Building Standard | Business & Public Sector | SEAI n.d.

[4] Luo T, Tan Y, Langston C, Xue X. Mapping the knowledge roadmap of low carbon building: A scientometric analysis. Energy Build 2019;194:163–76. doi:10.1016/j.enbuild.2019.03.050.

[5] Ely Lecture RT, Nicholas Stern B, Anderson D, Bowen A, Catovsky S, Diamond P, et al. The Economics of Climate Change. vol. 98. 2008.

[6] Commission E. 2 Energy efficiency state of non-profit housing stock in the Netherlands 2020:61–82.

[7] Lai X, Liu J, Shi Q, Georgiev G, Wu G. Driving forces for low carbon technology innovation in the building industry: A critical review. Renew Sustain Energy Rev 2017;74:299–315. doi:10.1016/j.rser.2017.02.044.

[8] Al Dakheel J, Del Pero C, Aste N, Leonforte F. Smart buildings features and key performance indicators: A review. Sustain Cities Soc 2020;61:102328. doi:10.1016/j.scs.2020.102328.

[9] Hamburg A, Kuusk K, Mikola A, Kalamees T. Realisation of energy performance targets of an old apartment building renovated to nZEB. Energy 2020;194:116874. doi:10.1016/j.energy.2019.116874.

[10] Lund H, Duic N, Østergaard PA, Mathiesen BV. Future district heating systems and technologies: On the role of smart energy systems and 4th generation district heating. Energy 2018. doi:10.1016/j.energy.2018.09.115.

[11] Li H, Nord N. Transition to the 4th generation district heating - Possibilities, bottlenecks, and challenges. Energy Procedia, 2018. doi:10.1016/j.egypro.2018.08.213.

[12] Gondal IA. Prospects of Shallow geothermal systems in HVAC for NZEB. Energy Built Environ 2020. doi:10.1016/j.enbenv.2020.09.007.

[13] Grillone B, Danov S, Sumper A, Cipriano J, Mor G. A review of deterministic and data-driven methods to quantify energy efficiency savings and to predict retrofitting scenarios in buildings. Renew Sustain Energy Rev 2020;131:110027. doi:10.1016/j.rser.2020.110027.

[14] Magrini A, Lentini G, Cuman S, Bodrato A, Marenco L. From nearly zero energy buildings (NZEB) to positive energy buildings (PEB): The next

challenge - The most recent European trends with some notes on the energy analysis of a forerunner PEB example. Dev Built Environ 2020;3:100019. doi:10.1016/j.dibe.2020.100019.

[15] Behzadi A, Arabkoohsar A, Yang Y. Optimization and dynamic techno-economic analysis of a novel PVT-based smart building energy system. Appl Therm Eng 2020;181:115926. doi:10.1016/j.applthermaleng.2020.115926.

[16] Behzadi A, Arabkoohsar A. Feasibility study of a smart building energy system comprising solar PV/T panels and a heat storage unit. Energy 2020;210:118528. doi:10.1016/j.energy.2020.118528.

[17] Abokersh, Mohamed Hany, Kangkana Saikia, Luisa F cabeza, Dieter Boer MV. Flexible heat pump integration to improve sustainable transition toward 4th generation district heating. Energy Convers Manag 2020.

[18] Hany M, Spiekman M, Vijlbrief O, Goch TAJ Van, Vall M, Boer D. A real-time diagnostic tool for evaluating the thermal performance of nearly zero energy buildings 2021;281. doi:10.1016/j.apenergy.2020.116091.

[19] Majcen D, Itard LCM, Visscher H. Theoretical vs. actual energy consumption of labelled dwellings in the Netherlands: Discrepancies and policy implications. Energy Policy 2013;54:125–36. doi:10.1016/j.enpol.2012.11.008.

[20] Hong T, Lee M, Koo C, Jeong K, Kim J. Development of a method for estimating the rooftop solar photovoltaic (PV) potential by analyzing the available rooftop area using Hillshade analysis. Appl Energy 2017;194:320–32. doi:10.1016/j.apenergy.2016.07.001.

[21] Jeong J, Hong T, Kim J, Chae M, Ji C. Multi-criteria analysis of a self-consumption strategy for building sectors focused on ground source heat pump systems. J Clean Prod 2018;186:68–80. doi:10.1016/j.jclepro.2018.03.121.

[22] Rehman H ur, Hirvonen J, Sirén K. Performance comparison between optimized design of a centralized and semi-decentralized community size solar district heating system. Appl Energy 2018;229:1072–94. doi:10.1016/j.apenergy.2018.08.064.

[23] Cao X, Dai X, Liu J. Building energy-consumption status worldwide and the state-of-the-art technologies for zero-energy buildings during the past decade. Energy Build 2016;128:198–213. doi:10.1016/j.enbuild.2016.06.089.

[24] Marszal AJ, Heiselberg P, Lund Jensen R, Nørgaard J. On-site or off-site renewable energy supply options? Life cycle cost analysis of a Net Zero Energy Building in Denmark. Renew Energy 2012;44:154–65. doi:10.1016/j.renene.2012.01.079.

[25] Susan S, Wardhani D. Building integrated photovoltaic as GREENSHIP'S on site renewable energy tool. Results Eng 2020;7:100153. doi:10.1016/j.rineng.2020.100153.

[26] Song J, Oh SD, Song SJ. Effect of increased building-integrated renewable energy on building energy portfolio and energy flows in an urban district of Korea. Energy 2019;189:116132. doi:10.1016/j.energy.2019.116132.

[27] Barone G, Buonomano A, Forzano C, Giuzio GF, Palombo A. Passive and active performance assessment of building integrated hybrid solar photovoltaic/thermal collector prototypes: Energy, comfort, and economic analyses. Energy 2020;209:118435. doi:10.1016/j.energy.2020.118435.

[28] Li G, Xuan Q, Akram MW, Golizadeh Akhlaghi Y, Liu H, Shittu S. Building integrated solar concentrating systems: A review. Appl Energy 2020;260:114288. doi:10.1016/j.apenergy.2019.114288.

[29] Kuhn TE, Erban C, Heinrich M, Eisenlohr J, Ensslen F, Neuhaus DH. Review of Technological Design Options for Building Integrated Photovoltaics (BIPV). Energy Build 2020:110381. doi:10.1016/j.enbuild.2020.110381.

[30] Dawood S, Crosbie T, Dawood N, Lord R. Designing low carbon buildings: A framework to reduce energy consumption and embed the use of renewables. Sustain Cities Soc 2013;8:63–71. doi:10.1016/j.scs.2013.01.005.

[31] Sun Y, Huang P, Huang G. A multi-criteria system design optimization for net zero energy buildings under uncertainties. Energy Build 2015;97:196–204. doi:10.1016/j.enbuild.2015.04.008.

[32] Mokhtara C, Negrou B, Settou N, Gouareh A, Settou B. Pathways to plus-energy buildings in Algeria: Design optimization method based on GIS and multi-criteria decision-making. Energy Procedia, vol. 162, Elsevier Ltd; 2019, p. 171–80. doi:10.1016/j.egypro.2019.04.019.

[33] Laguna Salvad L, Villeneuve E, Masson D. Decision making in near zero energy building refurbishment: A technology alternatives ranking tool. IFAC-PapersOnLine 2019;52:313–8. doi:10.1016/j.ifacol.2019.11.196.

[34] Chang Y, Wei Y. The utilization of renewable energy for low-carbon buildings. Renewable-Energy-Driven Futur., Elsevier; 2021, p. 289–309. doi:10.1016/B978-0-12-820539-6.00009-1.

[35] Pinamonti M, Baggio P. Energy and economic optimization of solar-assisted heat pump systems with storage technologies for heating and cooling in residential buildings. Renew Energy 2020;157:90–9. doi:10.1016/j.renene.2020.04.121.

[36] Li H, Wang S. Coordinated optimal design of zero/low energy buildings and their energy systems based on multi-stage design optimization. Energy 2019;189:116202. doi:10.1016/j.energy.2019.116202.

[37] Zhou Y, Zheng S, Liu Z, Wen T, Ding Z, Yan J, et al. Passive and active phase change materials integrated building energy systems with advanced machine-learning based climate-adaptive designs, intelligent operations, uncertainty-based analysis and optimisations: A state-of-the-art review. Renew Sustain Energy Rev 2020;130:109889. doi:10.1016/j.rser.2020.109889.

[38] Bengio Y, Lodi A, Prouvost A. Machine learning for combinatorial optimization: A methodological tour d'horizon. Eur J Oper Res 2020. doi:10.1016/j.ejor.2020.07.063.

[39] Rehman H ur, Korvola T, Abdurafikov R, Laakko T, Hasan A, Reda F. Data analysis of a monitored building using machine learning and optimization of integrated photovoltaic panel, battery and electric vehicles in a Central European climatic condition. Energy Convers Manag 2020;221:113206. doi:10.1016/j.enconman.2020.113206.

[40] Han H, Zhang Z, Cui X, Meng Q. Ensemble learning with member optimization for fault diagnosis of a building energy system. Energy Build 2020;226:110351. doi:10.1016/j.enbuild.2020.110351.

[41] Seyedzadeh S, Pour Rahimian F, Oliver S, Rodriguez S, Glesk I. Machine learning modelling for predicting non-domestic buildings energy performance: A model to support deep energy retrofit decision-making. Appl Energy 2020;279:115908. doi:10.1016/j.apenergy.2020.115908.

[42] Fathi S, Srinivasan R, Fenner A, Fathi S. Machine learning applications in urban building energy performance forecasting: A systematic review. Renew Sustain Energy Rev 2020;133:110287. doi:10.1016/j.rser.2020.110287.

[43] Mishra M. Machine learning techniques for structural health monitoring of heritage buildings: A state-of-the-art review and case studies. J Cult Herit 2020. doi:10.1016/j.culher.2020.09.005.

[44] Sun H, Burton H V., Huang H. Machine Learning Applications for Building Structural Design and Performance Assessment: State-of-the-Art Review. J Build Eng 2020;33:101816. doi:10.1016/j.jobe.2020.101816.

[45] Ayoub M. A review on machine learning algorithms to predict daylighting inside buildings. Sol Energy 2020;202:249–75. doi:10.1016/j.solener.2020.03.104.

[46] Hong T, Wang Z, Luo X, Zhang W. State-of-the-art on research and applications of machine learning in the building life cycle. Energy Build 2020;212:109831. doi:10.1016/j.enbuild.2020.109831.

[47] Mavromatidis G, Orehounig K, Carmeliet J. Uncertainty and global sensitivity analysis for the optimal design of distributed energy systems. Appl Energy 2018;214:219–38. doi:10.1016/j.apenergy.2018.01.062.

[48] You C, Kim J. Optimal design and global sensitivity analysis of a 100% renewable energy sources based smart energy network for electrified and hydrogen cities. Energy Convers Manag 2020;223:113252. doi:10.1016/j.enconman.2020.113252.

[49] Zhang Y, Zhang X, Huang P, Sun Y. Global sensitivity analysis for key parameters identification of net-zero energy buildings for grid interaction optimization. Appl Energy 2020;279:115820. doi:10.1016/j.apenergy.2020.115820.

[50] Klein SA et al. TRNSYS Version. 18, Solar Energy Laboratory, University of Wisconsin-Madison, Website: <http://sel.me.wisc.edu/ trnsys> 2004.

[51] De Guadalfajara M, Lozano MA, Serra LM. Evaluation of the potential of large solar heating plants in Spain. Energy Procedia 2012;30:839–48. doi:10.1016/j.egypro.2012.11.095.

[52] Tulus V, Boer D, Cabeza LF, Jiménez L, Guillén-Gosálbez G. Enhanced thermal energy supply via central solar heating plants with seasonal storage: A multi-objective optimization approach. Appl Energy 2016;181:549–61. doi:10.1016/j.apenergy.2016.08.037.

[53] Abokersh MH, Vallès M, Cabeza LF, Boer D. A framework for the optimal integration of solar assisted district heating in different urban sized communities : A robust machine learning approach incorporating global sensitivity analysis. Appl Energy 2020;267:114903. doi:10.1016/j.apenergy.2020.114903.

[54] Guillen-Gosalbez G, Caballero J #x ;. A, Esteller LJ, Gadalla M. Application of life cycle assessment to the structural optimization of process flowsheets. Comput Aided Chem Eng 2007;24:1163–8. doi:10.1016/S1570-7946(07)80218-5.

[55] Huijbregts MAJ, Steinmann ZJN, Elshout PMF, Stam G, Verones F, Vieira M, et al. ReCiPe2016: a harmonised life cycle impact assessment method at midpoint and endpoint level. Int J Life Cycle Assess 2017;22:138–47. doi:10.1007/s11367-016-1246-y.

[56] Gursel AP, Ostertag C. Comparative life-cycle impact assessment of concrete manufacturing in Singapore. Int J Life Cycle Assess 2017. doi:10.1007/s11367-016-1149-y.

[57] Chen Y, Wang J, Lund PD. Sustainability evaluation and sensitivity analysis of district heating systems coupled to geothermal and solar resources. Energy Convers Manag 2020;220:113084. doi:10.1016/j.enconman.2020.113084.

[58] Cameron L, Van Der Zwaan B. Employment factors for wind and solar energy technologies: A literature review. Renew Sustain Energy Rev 2015;45:160–72. doi:10.1016/j.rser.2015.01.001.

[59] Bauer D, Marx R, Nußbicker-Lux J, Ochs F, Heidemann W, Müller-Steinhagen H. German central solar heating plants with seasonal heat storage. Sol Energy 2010;84:612–23. doi:10.1016/j.solener.2009.05.013.

[60] A Multiobjective Simplex Method. Multicriteria Optim., Springer-Verlag; 2005, p. 171–96. doi:10.1007/3-540-27659-9_7.

[61] Nö K, Niedenfü Hr S, Beyß Id M, Wiechert Id W. A Pareto approach to resolve the conflict between information gain and experimental costs: Multiple-criteria design of carbon labeling experiments 2018. doi:10.1371/journal.pcbi.1006533.

[62] Saltelli A, Annoni P. How to avoid a perfunctory sensitivity analysis. Environ

Model Softw 2010;25:1508–17. doi:10.1016/j.envsoft.2010.04.012.

[63] Lior N. Sustainability as the quantitative norm for water desalination impacts 2017. doi:10.1016/j.desal.2016.08.008.

[64] Campos-Guzmán V, García-Cáscales MS, Espinosa N, Urbina A. Life Cycle Analysis with Multi-Criteria Decision Making: A review of approaches for the sustainability evaluation of renewable energy technologies. Renew Sustain Energy Rev 2019;104:343–66. doi:10.1016/j.rser.2019.01.031.

[65] Bhowmik C, Gangwar S, Bhowmik S, Ray A. Selection of energy-efficient material: An entropy–TOPSIS approach. vol. 584. 2018. doi:10.1007/978-981-10-5699-4_4.

[66] Hwang C-L, Yoon K. Methods for Multiple Attribute Decision Making, 1981, p. 58–191. doi:10.1007/978-3-642-48318-9_3.

[67] Sari F. Forest fire susceptibility mapping via multi-criteria decision analysis techniques for Mugla, Turkey: A comparative analysis of VIKOR and TOPSIS. For Ecol Manage 2021;480:118644. doi:10.1016/j.foreco.2020.118644.

[68] Qin X, Wang H, Li Y, Li Y, McConkey B, Lemke R, et al. A long-term sensitivity analysis of the denitrification and decomposition model. Environ Model Softw 2013;43:26–36. doi:10.1016/j.envsoft.2013.01.005.

[69] Abokersh MH, Vallès M, Jiménez L, Boer D. Cost-Effective Processes of Solar District Heating System Based on Optimal Artificial Neural Network. vol. 48. 2020. doi:10.1016/B978-0-12-823377-1.50068-9.

[70] European Commision. EuroStat 2018. http://ec.europa.eu/eurostat/web/energy/data/database (accessed March 12, 2018).

[71] Ellehauge K PT. Solar heat storages in district heating networks. Energinet.dk, PREHEAT project no. 2006-2-6750. 2007.

[72] Welsch B, Göllner-Völker L, Schulte DO, Bär K, Sass I, Schebek L. Environmental and economic assessment of borehole thermal energy storage in district heating systems. Appl Energy 2018;216:73–90. doi:10.1016/j.apenergy.2018.02.011.

[73] Schmidt T MD. Status of solar thermal seasonal storage in Germany. 2009.

[74] Calise F, Dentice d'Accadia M, Palombo A. Transient analysis and energy optimization of solar heating and cooling systems in various configurations. Sol Energy 2010;84:432–49. doi:10.1016/j.solener.2010.01.001.

[75] austrotherm. General price list. 2017. doi:10.5962/bhl.title.138707.

[76] Specialist Insulation Supplies Ltd. Prices list. 2018.

[77] GLAPOR-Schaumglasprodukte. GLAPOR PRICE LIST. Belgium: 2014.

[78] Reineck K, Greiner S, Reinhardt H. Dichte Heißwasser-Wärmespeicher aus

ultrahochfestem Faserfeinkornbeton. Stuttgart: 2004.

[79] Ecoinvent. Eco invent 2017. https://www.ecoinvent.org/home.html (accessed March 12, 2018).

Chapter VII

Allocation for Nearly Zero Energy Building Constraints

VII. Allocation for Nearly Zero Energy Building Constraints

A real-time diagnostic tool for evaluating the thermal performance of nearly zero energy buildings

Mohamed Hany Abokersh [a], Marleen Spiekman [b], Olav Vijlbrief [b], T.A.J. van Goch [c], Manel Vallès [a], Dieter Boer [a,*]

[a] Departament d'Enginyeria Mecànica, Universitat Rovira i Virgili, Av. Països Catalans 26, 43007 Tarragona, Spain

[b] Department of Building Physics and Systems, TNO, Leeghwaterstraat 44, Delft, the Netherlands

[c] BAM Bouw en Techniek, Bunnik, the Netherlands

** Corresponding author: Dieter.boer@urv.cat*

E-mail addresses: mohamed.abokersh@urv.cat (*M.H. Abokersh),* marleen.spiekman@tno.nl *(Marleen Spiekman*), olav.vijlbrief@tno.nl *(O. Vijlbrief),* dennis.van.goch@bam.com (*T.A.J. van Goch),* manel.valles@urv.cat *(Manel Valles)*

Keywords: Nearly Zero Energy Building; Building performance simulation; Occupant behaviors; Bayesian calibration; Monte Carlo uncertainty analysis; Global sensitivity analysis

VII.1 Introduction

From the Brundtland Report "Our Common Future" in 1987 [1] to UN Climate Conference of Parties, 21 of 2015 through the Kyoto Protocol stipulation in 1997, the increase of awareness regarding the sustainability can be identified on a global level. A vital footstep to spread on the sustainable communities concept relies on the

energy efficiency in the building sector. A fraction of 40% of the total energy utilized in the Union [2] and 36% of the total emissions of CO_2 come from the buildings [3]. Thus, in the building sector, the EU environmental and energy policy has progressed, and it has covered the sustainability and resource efficiency for reducing the CO_2 emissions and energy consumption [4]. The objective of the European Commission is to reduce the CO_2 emissions from the building sector in 2050 by 88-91% compared to CO_2 emission 1990 levels [5].

The Netherlands is working on increasing the energy efficiency of buildings since 1975. They are limiting the transmission losses by controlling the insulation values [6]. In 1995,'EPC' (Energy Performance Coefficient) was added to these limits. It is a non-dimensional quantity that uses the energy required for space heating, cooling, hot water, humidification, and lighting as an indicator of energy performance. The ratio of calculated energy demand to a standard energy performance yields the Dutch EPC calculation where the total heated area of the dwelling and the heat transfer surface defines the standardized energy performance [7]. In 1996, the value of EPC was set to 1.4 that could be achieved through the construction techniques. In 1998, the value of EPC was reduced to 1.2. It was further reduced to 1.0 in 2000, 0.8 in 2006, and 0.6 in 2011. With the introduction of the concept of the nearly zero energy buildings (nZEB), the EPC value was further reduced to 0.4 in 2015 [8].

The estimation of the heating systems impact and the accurate size of the renewable energy system with mutually and multiple different design criteria are the biggest challenges during the design of nZEB [9]. That is why; the literature has focused on learning the thermal performance of these buildings. In the research papers, the objective is achieved through the monitoring studies as given in [10] or through the model simulations as provided in [11,12]. The thermal performance of a building helps in foreseeing the consequence of the renovation measures of potential energy, and then, recognizing the optimized option for energy, comfort as well as addressing the economic issues [2].

In this context, building energy simulation (BES) can be utilized for studying the behavior of the nZEBs under many engineering and design conditions, such as thermal properties of the building [13], occupant's behavior [14], different weather conditions [15], as well as energy supply systems [16]. There are several uncertainties and driving factors involved in building performance. Such aspects require detailed inputs to the BES tool for modelling the thermal performance. Software such as EnergyPlus, BLAST, TRNSYS, practices a transient method to simulate the cooling and heating loads of the building. Such tools require modelling expertise and professional knowledge because they provide reliable, detailed, and sophisticated modelling and simulations dynamically inherent into the calculations [17]. Another type of simulations is the Black box or statistical approach [18]. This approach is used in the case of incomplete information about the building. This approach uses the measured data for the identification of the parameters and selects

a mathematical model (ARMAX, polynomial, transfer function) to represent the thermal behavior of the building [19]. The generation of the training database by using the simulation engines is the major challenge of this method because it consumes significant computational resources. Heuristic optimization has the same issues when it is used for the identification of the objective function specified in relation to the building energy use, the thermal comfort level, and economic benefits [20].

Apart from the above-described approaches, research has been conducted to define a lighter modeling method that can be utilized for the comparative study of the energy use and building heating and cooling loads. In one of these researches, RC (resistance and capacitance) model is used for modelling the building thermal behavior; this approach works on the phenomenon of electrical analogue [21]. In this context, researchers have indicted the RC model for modelling the building's thermal reaction under the effect of outdoor and indoor thermal conditions. Berthoua et al.[22] simulated the heating and cooling needs of a multi-zone office building by using four RC models with different complexity. From the simulation results, it was observed that the two-order 6R2C semi-physical model is the best-compromised model out of all the tested models. The accuracy of the model for predicting the indoor air temperature and thermal needs during the cooling and heating periods was around 84%. Terés-Zubiaga et al.[23] used monitored data and developed a sophisticated RC model for the dwelling. In the first stage, an empty social housing dwelling was monitored for 3 months to analyze its thermal performance. Afterwards, the monitored data was used for the development of the proposed model. The development of the model and some of the results are evaluated and presented later. Asadi et al. [24] worked on the development of a multi-objective mathematical model that assists the stakeholders in making decisions regarding the energy-minimizing cost-effectively. They evaluate the effectiveness of all the combinations of the retrofit actions on a simultaneous basis by using an RC model. Liao and Dexter [25] simulated the dynamic behavior of the existing heating system by developing a second-order RC physical model. The results illustrated that the simple low-order RC model had been verified to have a good performance in modeling the heating and cooling need of a simple building that usually has one zone or single-use. The shortcoming of the RC model is that it presents the performance for a shorter period, such as a few days to several weeks. In this way, the long-term prediction is not possible from the RC model. Moreover, the simplified models show a lag in quantifications of occupant behaviors, building operations, and dynamic behavior of weather conditions. These factors strongly influence the RC network's performance [26]. Thus, the energy savings output from simulation models of existing buildings has indicated discrepancies often significant in some cases (up to 100% differences), between BES model-predicted and the actual metered building energy use [27].

In this context, the researchers have conducted several ways to reduce the variations between the real-time energy measurements and the model results. A detailed audit

is conducted to get a real insight into the different characteristics of the building. It was the primary approach used for the calibration of the energy model [28]. All the parameters that affect the energy performance of the building must be included in these characteristics. Some of the essential parameters are material properties, building geometry, lighting and equipment schedules, and type of schedule and occupancy [29]. This approach is constructive for the correction of the model, but it involves many uncertainties, and it consumes a lot of time [27]. Because of these issues, statistical analysis methods such as Bayesian method is utilized to perform uncertainty analysis (UA) and calibrate the energy model [30]. For instance, Booth et al. [31] used the macro-level data to calibrate micro-level models by utilizing the Bayesian method. Bayesian inferences and a combination of regression models were used for the estimation of the average consumption intensity. Bayesian methods can illustrate the uncertainties involved in the consumption intensities, and that is why they are known as bottom-up methods. In simple words, the Bayesian approach predicts the range of consumption level with decent probability because it works on the basis of the detailed measured data.

By involving UA into the calculations, many other studies are convinced to use this method for the calibration of the energy model [32]. Over the last few decades, sensitivity analysis (SA) [33], optimization search algorithms [34], and objective penalty function [35] are utilized for calibrating the energy models. Monetti et al. [36] have presented an optimization-based calibration procedure. They used GenOpt [37] for developing a simulation-based optimization algorithm that minimized the variations in the simulation results and the measured data to calibrate the energy model. In another paper, Reddy and Sun [35] calibrated a building energy model by utilizing an analytical optimization approach. There were four steps in their calibration procedure: sensitivity analysis, identifiability analysis, optimization, and uncertainty analysis. The sensitivity analysis performed by them was very comprehensive, and their results contain the occupant's behavior during the calibration of the buildings.

Liu and Henze [38] calibrated the building energy model by utilizing a common optimization outline and GenOpt. They majorly focused on cooling loads. They exhibited that the model can perform energy model calibration with appropriate accuracy. However, for reducing the optimization problem dimensions, the number of parameters were kept lower. Therefore, occupants' behaviors' effect in the context of different factors of consumption is not undertaken in this study. As evidenced from the literature review, the majority of these researches focused on quantifying the uncertainty associate with building energy model based on the time-independent approach with ignoring the temporal variation for some parameters. In other words, the underlying occupancy behavior and weather variation are estimated in a deterministic manner instead of considering its stochastic nature [39,40].

In practice, the construction companies that lead the development of nZEB in the Netherlands indicate a substantial obstacle to guarantee the nZEB performance and

thus to improve their market position. An additional challenge is that the guarantee of building data quality where monitoring a thousand of homes simultaneously isn't feasible since sensors may not function properly and it can be out of budget. Therefore, the need for a generic approach to monitor and guarantee the building performance is essential. Furthermore, this approach should be based on minimal monitoring data for individual homes to find out what is the cause for the current situation of the deviations between the actual and expected performance as analyses based on wrong data lead to wrong conclusions, wrong decisions, extra costs and loss of support.

Following the challenges facing the construction companies and the limitations associate with various strategies for BES regarding the verification and calibration processes, this study aims to propose a methodology framework to address these shortcomings via the following contributions:

i. The Development of a Multizone RC-Network on an hourly base. This model offers an extended period prediction for the heating demands and indoor air temperature with quantifications for the occupant behaviors as well the dynamic behavior of weather conditions and building operations.
ii. Trace the limitations associated with the current building energy models calibration through considering the temporal variation associate with the climate change projections and the occupant behaviors in the calibration process.
iii. The development of a modelling scheme for defining the difference between the predicted and actual energy and indoor performance at an individual nZEB based on uncertainty analysis (UA) incorporating Bayesian optimization to minimize the required monitoring data.
iv. The application of the proposed framework is demonstrated through a case study to insight the uncertainty importance using a global sensitivity analysis approach (GSA).

Hence, the main novelty is to develop a diagnostic tool to guarantee and proactively maintain the indoor climate performance of nZEBs with consideration for the temporal variation associate with the climate data and occupant behavior during the operation stage of the building. Furthermore, with the data analysis model based on UA incorporating GSA, additional knowledge in the future can be added to the builders, installers and occupants, which can bridge the nZEB concept with the client anticipations. The structure of the paper is: (i) The methodology for developing a Multizone RC-Network incorporating the Bayesian optimization for calibration purposes is given in Section 2. In addition, it shows the quantification for Uncertainty Characterization (UC) based on global sensitivity analysis approach. (ii) The case study of the paper for nZEB diagnostic tool is given in Section 3. (iii) The paper's results regarding the developed framework performance are presented and discussed in Section 4. Finally, (iv) the concluding marks are given in Section 5 can

be useful for the construction and installation companies working with buildings performance diagnosis.

VII.2 Methodology structure

Figure VII-1 shows the outlines of the proposed methodology framework for diagnosing nZEB energy performance which consist of two main phases.

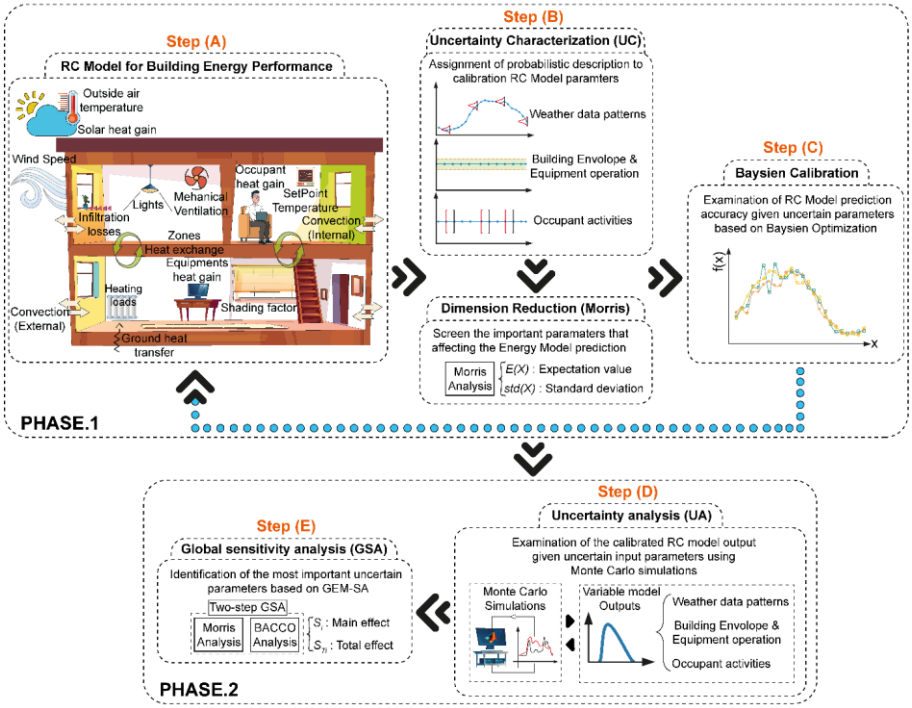

Figure VII-1: General workflow for the diagnostic tool of nZEB energy performance

Phase 1 includes the development of RC model and its calibration where step (A) consists of the development of a RC model for building energy performance. This model includes different building thermal properties, occupancy behavior, as well as the supply energy systems. In step (B), the Uncertainty Characterization (UC) that contains the uncertain RC model parameters are identified and described in a probabilistic manner. Once the RC model uncertain parameters are quantified, the dimension reduction is implemented to screen the important parameters that affect the energy model prediction. In step (C), the Bayesian calibration is carried out to minimize the gap between the field observations and the RC-Network simulations output. On the other hand, phase 2 comprises the estimation for the uncertainty associate with calibrated RC model and the parameters responsible for these uncertainties. Therefore, in step (D), Monte Carlo (MC) simulations are used to

perform uncertainty analysis (UA) to estimate the variation in the RC Network output. In the end, step (E) provides the two-step Global Sensitivity Analysis (GSA) to highlight the important effects of uncertain on the energy performance of the nZEB.

VII.2.1 RC Model formulation

The core of the RC model relies on two-node model (6R2C) thermal-electric analogy that is programmed in MATLAB. This approach based on adapting the electric analog to simulate the thermal performance of multi zones dwelling in a dynamic manner. The RC model follows the Kirchhoff's law which is able to provide the temperature and the heat flow rate at each simulation time step [20].

The key parameters for the heat transfer in the modelling approach are $\emptyset_{int}$(internal heat gain by occupants and appliances, in kW) , $\emptyset_{H}$ (heat flow rate sourced from the heaters based on heat pump, in kW), $\emptyset_{exch}$ (exchange heat flow rate with other zones, in kW), $\emptyset_{sol}$ (heat flow rate sourced from solar, in kW), $\emptyset_{neigh}$ (heat flow rate exchange with the neighbour, in kW), $\emptyset_{vent}$ (ventilation and infiltration losses of the zone, in kW), $\emptyset_{trans}$ (heat flow rate transmitted through the windows, in kW) and $\emptyset_{gnd}$, (heat loss to the ground, in kW). All energy flows through Zone ith are indicated in Figure VII-2, where the blue dashed rectangle describes the inner and outer node.

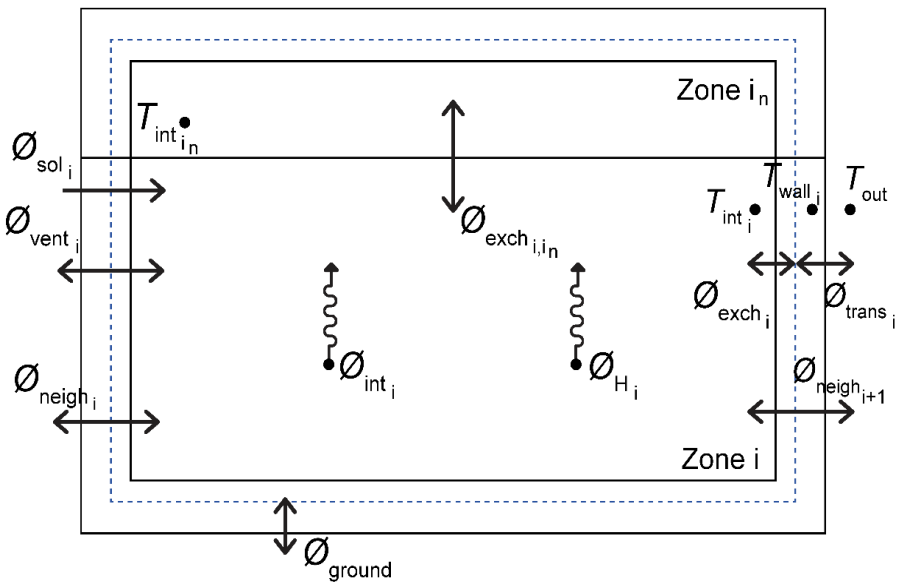

Figure VII-2: Energy Flow Through Zone ith and its interaction with the surrounding

The basic idea of the proposed model relies on two specific thermal mass nodes. The first node is typically consisting of the indoor envelopes thicknesses including the walls, floor, and roof and it counts to a few centimetres in addition to the furniture.

This part of the thermal mass is called the 'indoor mass', C_{int}. While the second node states for the heat exchange between the indoor thermal mass and the ambient through the R_{exch}, and it is called the 'outdoor mass', C_{wall}. The thermal capacity of the air is neglected since it is relatively small compared to the indoor walls' capacity. The RC Network representing the building by the two thermal masses is illustrated in Figure VII-3. For estimating the total thermal mass of the building, a simplified formula derived using volume and density of the building materials is utilized, and it can be expressed as following [41]:

$$C = \alpha . V^{\beta} . f_c \qquad \text{Eq. VII-1}$$

where α & β coefficients are 0.18 and 0.92, respectively. While f_c is a correction factor which is defined as the ratio between the indoor mass and the total mass, which is initially set to 0.3.

To better take into account the heat transmitted through the envelope in each zone, the proposed model has three temperature nodes which are T_{int} (indoor zone temperature, in °C), T_{wall} (envelope zone temperature, in °C), and T_{out} (outdoor temperature, in °C). It can be described based on stochastic differential equations in the following way:

$$\frac{dT_{int_i}}{dt} = \frac{1}{C_{int_i}} (\emptyset_{int_i} + \emptyset_{sol_i} + \emptyset_{vent_i} - \emptyset_{exch_i} + \emptyset_{exch_{i,i_n}} + \emptyset_{neigh_i} + \emptyset_{neigh_{i+1}} + \emptyset_{H_i}) \qquad \text{Eq. VII-2}$$

Where:

$$\emptyset_{vent_i} = UA_{vent_i}(T_{out} - T_{int_i}) \qquad \text{Eq. VII-2.1}$$

$$\emptyset_{exch_i} = UA_{exch_i}(T_{int_i} - T_{wall_i}) \qquad \text{Eq. VII-2.2}$$

$$\emptyset_{exch_{i,\,i_n}} = UA_{exch_{i,\,i_n}} \left(T_{int_{i_n}} - T_{int_i}\right) \qquad \text{Eq. VII-2.3}$$

$$\emptyset_{neigh_i} = UA_{neigh_i}(T_{neigh_i} - T_{int_i}) \qquad \text{Eq. VII-2.4}$$

$$\emptyset_{neigh_{i+1}} = UA_{neigh_{i+1}}(T_{neigh_{i+1}} - T_{int_i}) \qquad \text{Eq. VII-2.5}$$

$$\frac{dT_{wall_i}}{dt} = \frac{1}{C_{wall_i}} (\emptyset_{trans_i} + \emptyset_{ground} + \emptyset_{exch_i}) \qquad \text{Eq. VII-3}$$

Where:

$$\emptyset_{ground_i} = UA_{gnd_i} \left((T_{ground} + T_{out})/2 - T_{wall_i}\right) \qquad \text{Eq. VII-3.1}$$

$$\emptyset_{trans_i} = UA_{trans_i}(T_{out} - T_{wall_i}) \qquad \text{Eq. VII-3.2}$$

In general, the inverse of the heat loss coefficient (U) through different building skin is used to represent the thermal resistances in the proposed model. For the internal temperature node, the solar and internal heat gains tend to raise the indoor zone temperature. While the ventilation, infiltration and conduction heat losses tend to reduce it. The conduction heat losses to the ambient are represented through the sum of the R_{exch}. R_{exch_n} is presented to represents the transfer of heat between the floor and internal walls if the zone thermal coupling will be considered. Moreover, the

ventilation and infiltration losses of the building are represented by the thermal resistance R_{vent}. On the other hand, the heat flow in the envelope zone temperature node is made up of the sum of the heat flow rate transmitted to the ground R_{ground}, windows R_{trans} and ambient R_{exch}.

In the proposed method, the internal heat gain is counting for heat gains by occupants, appliances, and lighting devices where occupants heat gain is estimated based on a schedule for the number of occupants in each zone. In order to incorporate the heat gain caused by the appliance, the net electricity consumption for the dwelling is determined by using the measured data of the electricity consumption from the grid, generation from PV panels, electricity consumption by a heat pump and the surplus electricity fed to the grid from the PV panels.

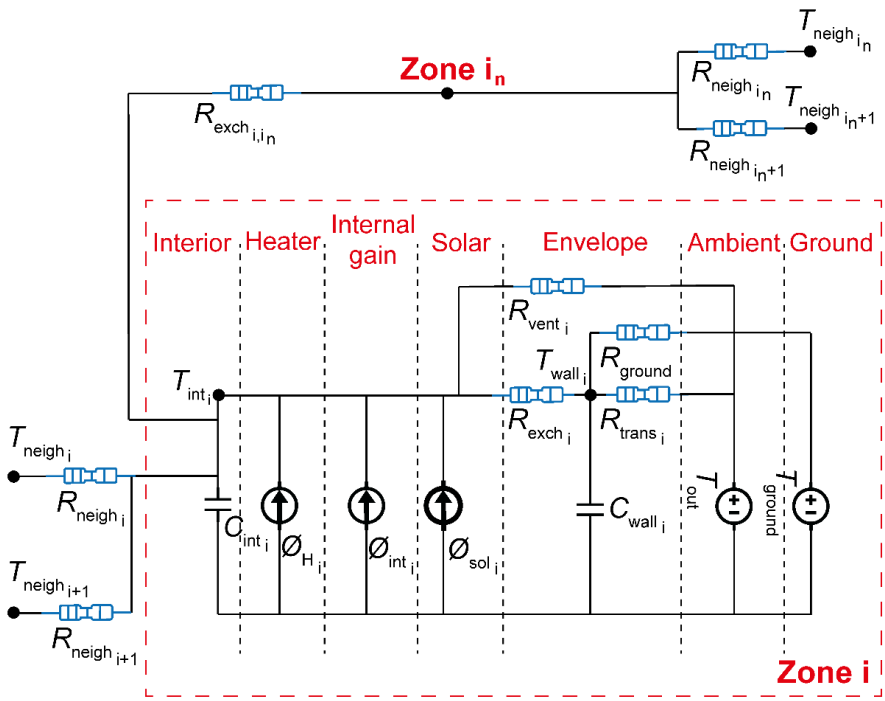

Figure VII-3: Thermal network for the simplified model of Multizone dwelling

In calculating solar gains, solar radiation is not always perpendicularly oriented on the window. Thus solar fraction factor (sf) is introduced to covert the solar radiation on a horizontal surface to a vertical surface, and it can be expressed as [42]:

$$\emptyset_{sol} = f_{shading}.Q_{sol}.A_{glass}.sf.G_{value} \quad \text{Eq. VII-4}$$

Where Q_{sol} is the amount of global solar radiation as a function of envelope shading reduction factor $f_{shading}$, effective solar collecting area A_{glass}, and G_{value} is the solar energy transmittance.

Based on the measured data, mechanical ventilation, and the natural ventilation comprising infiltration and occupant behavior regarding opening/closing windows and doors are quantified. For mechanical ventilation, it can be easily seen that it varies depending on the position of ventilation. However, there is no specific sensor data to obtain the ventilation position. Therefore, the energy consumption of the mechanical ventilation for all dwellings is used to estimate the position of ventilation in each zone, and subsequently, the mechanical ventilation volumetric flow rate.

For the occupant behavior regarding the windows and doors opening, the volumetric flow rate through windows that are opened on a single side is estimated through counting for the fresh air into buildings based on the pressure difference across the window, and it can be expressed as [43]:

$$q(t) = Opening\ sensor(t).C_d.A\big(\theta(t)\big).\sqrt{\frac{2|\Delta P_{th}(t)|}{\rho}} \quad \text{Eq. VII-5}$$

where: $\Delta P_{th}(t) = \frac{1}{2}\rho.C_p.V_{wind}(t)^2$

Where C_d is the discharge airflow rate coefficient, which represents the fractional loss of airflow due to windows' geometry. $A\big(\theta(t)\big)$ is the window opening area only for the ingoing airflow, and it is a share of the total operable building's window area depending on the windows open percentage 'θ' at the given time 't', ρ is the air density, and ΔP_{th} is the difference of pressure across the window opening. The ΔP_{th} across the window opening is approximated estimated as a function of the local air velocity 'V_{wind}', for a given configuration of the building at a given time 't', and C_p is the wind pressure coefficient [44].

The volumetric airflow through infiltration can be modeled by Power Law below which is the function of an air pressure differential across a building envelope and the flow characteristic of the shell.

$$Q_v = C_v * \Delta P^n \quad \text{Eq. VII-6}$$

where C_v is air permeability coefficient, ΔP is pressure difference and n flow exponent. Theoretically, the flow exponent lies between n = 1 and n=0.5. n=1 shows the fully developed laminar airflow and n = 0.5 given the fully developed turbulent airflow. Measured infiltration rate ($Q_{v_{10}}$) for the dwelling is 1 l/s.m^2 at 10 Pa pressure

difference. Then $Q_{v_{10}}$ is extrapolated back to more typical pressures inside dwellings (1-5 Pa). The pressure difference inside the dwelling is assumed 1 Pa, and the n is assumed 0.5 in this model. Although the pressure difference inside the dwelling changes over the year based on wind orientation and wind speed, however, it is assumed constant in this model.

Finally, we estimate the energy provided by the heat pump. Firstly the temporary temperatures are calculated for the next time step by state Eq. VII-2 and Eq. VII-3. After that, the required heating powers for each zone are calculated based on setpoint zone temperatures (T_{set_i}) and temporary temperatures. Then the heating capacity is evenly distributed based on the heating needs in each zone. Finally, the temperatures in the next time step are calculated based on adjusted heating powers for each zone.

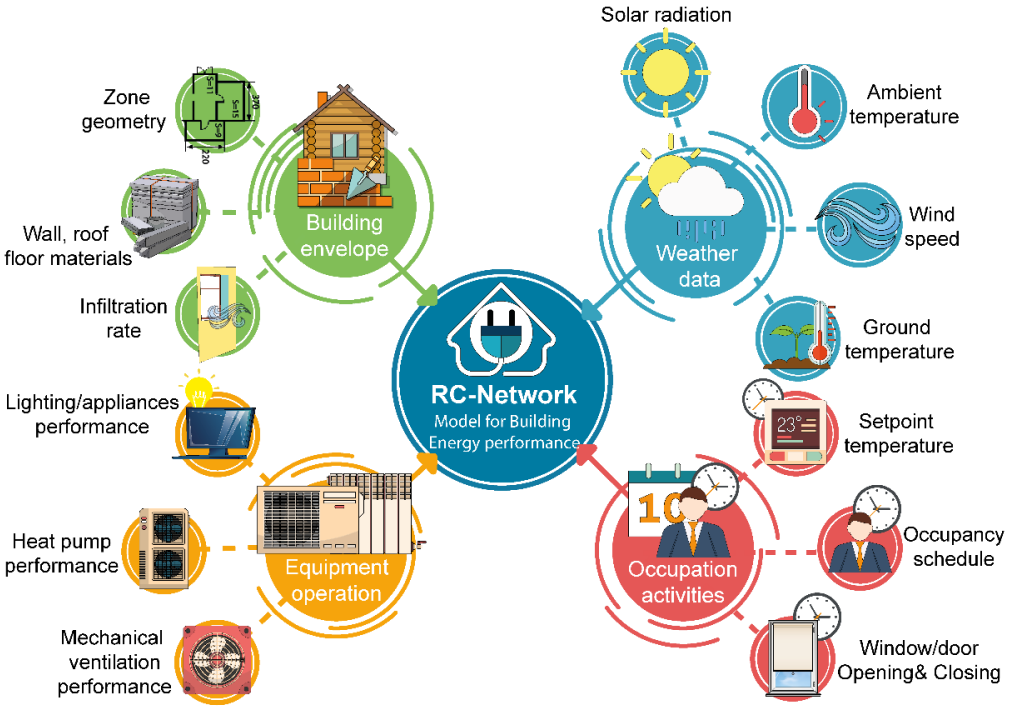

Figure VII-4: A flow chart for the RC Model inputs

A flowchart summarizes the RC model inputs is shown in Figure VII-4. This model is using the hourly bases for the metrological data, including the hourly-radiation on a horizontal surface, hourly-outdoor temperature, hourly wind speed, and average ground temperature. In terms of the building's envelopes, the zone geometry, the infiltration rates as well the building envelopes comprising the walls, floors and roof materials are defined. For the occupant behavior impact on the building performance, the RC model uses the hourly-setpoint temperature, the daily occupancy schedule,

and the hourly-opening/closing schedules for windows and doors. Finally, in terms of the equipment operation, the mechanical ventilation performance as well the heat pump performance and energy consumed by lighting and appliances are considered as inputs in the developed model.

VII.2.2 Calibration of the building model

In the building industry, the simplified simulation models is a common approach used for the analysis of the building performance [45]. However, there are a lot of variations between the actual consumption of real buildings and the simulation results. Therefore, these models can be calibrated to identify savings and analyze retrofit options for supporting the investments grade Energy Conversion Measures [46]. When the forward energy simulation program that involves various numerical inputs are calibrated against the building energy data, a highly under-determined problem occurs with non-unique solutions [45]. Kaplan et al. [47], have noticed that sensitivity issues and the exact solutions of the calibration problems have primary significance in the field of the calibration. According to another perspective, a dynamic matching between the measured values and the computed data over one year is required for the calibration. Calibration cannot be performed at a static one at one condition [48].

To understand the concept of model calibration, model uncertainty is essential to understand, especially, for the indeterminate models of complex systems. The recent BES studies have neglected this vital issue, and it is not considered in any validation criteria of BES [27]. Østergård et al. [49] have classified the different uncertainty sources in BES as follows:

- **Specification Uncertainty:** occurs because of the inaccurate and incomplete specifications of the modelled building. Plant schedules, HVAC specifications, geometry, system, and material properties, etc. are the exposed model parameters that are included in the specification uncertainty.
- **Modelling Uncertainty:** It occurs because of the assumptions and simplifications of the complex models. These assumptions can be hidden from the tool (calculation algorithms) or maybe explicit to the modeler.
- **Scenario Uncertainty:** It occurs because of the external conditions that are imposed on the building. For instance, occupant's behavior and outdoor climate conditions.

In the current study, we are considering only the specification uncertainty and scenario uncertainty associated with the RC-model, and they are classified into four main categories comprises climate input data, building envelope, equipment system, and occupant behavior.

VII.2.3 Uncertainty characterization (UC)

Uncertainty Characterization (UC) identifies the uncertain parameters associate with the RC model development and assign a mathematical description for their uncertainty. The uncertain parameters can be classified based on their time dependency, as shown in Figure VII-5. In the time-independent uncertain parameters, the uncertainty associated with these parameters is constant over its whole simulation period. While the time-dependent uncertain parameters are temporal variables where they change at the time step of each simulation. The parameter uncertainty is described through the probabilistic methods. These probabilistic methods consider each parameter as a random variable by following the probability density function (PDF) [50]. Coakley et al. [27] gave a review of different UC approaches for describing the uncertain parameters of BES models. The next sections of the report discuss the UC approaches that are used for all the parameter categories of BES model. At each zone of the RC Model, 18 different uncertain parameters are found.

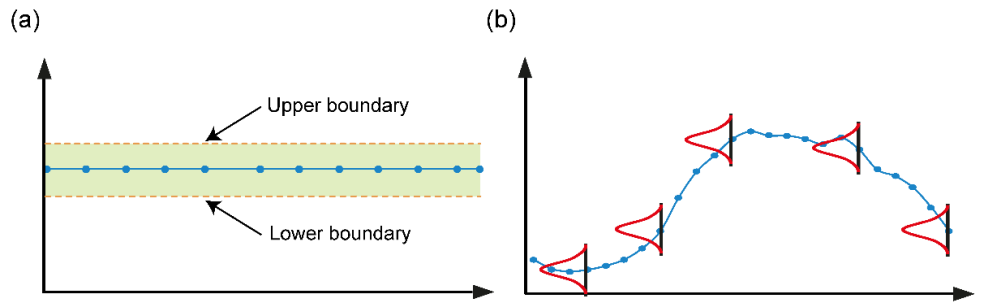

Figure VII-5: Types of uncertain parameters: (a) time-independent parameters, (b) time-dependent parameter

a. Climate input data

Due to weather nature, there are high uncertainties in weather data. It further causes variations in building energy usage. In BES, Finkelstein-Schafer method is used for applying the chosen meteorological year from actual weather data over several decades [51]. Currently, concerns have arisen that a single weather file (that consists of 8760 hours values) does not contain sufficient and reliable information on credible weather conditions. In this way, it can't be reliable for assessing the building energy performance [52]. The simulated energy consumption based on typical weather data is not able to represent the weather data for actual meteorological years. Furthermore, historical weather conditions do not affect building performance. However, future climate affects building performance. Most of the weather data that is obtained from the historical data do not help forecast the building energy usage in

the future [53]. The uncertainty associated with the weather data comprises; the solar radiation 'Q_{sol}', wind speed 'V_{wind}', the ambient temperature 'T_{out}', and ground temperature 'T_{ground}'.

Kaplanis and Kaplani [54] performed an outstanding analysis regarding solar radiation uncertainty. They used their observed data for analyzing the stochastic characteristics of global solar radiation based on an hourly basis. They deduct the following conclusions from their study:

- In hourly global solar radiation, the fluctuation is high in winter and lower in summer.
- In a day, the fluctuations are higher in the morning and late afternoon and lower around the solar noon.
- The normal distribution is experienced in hourly solar radiation.

A summary of the probability distribution of hourly global solar radiation is shown in Table VII-1. For depicting the frequency distribution of wind speed, probability density function (PDF) is a widely used technique. Several PDF approaches are proposed for wind speed estimation [55]. Among all the PDF approaches for wind energy, Weibull distribution is the most reliable and authentic approach [56]. It is illustrated in Table VII-1. Moreover, for the ground and ambient temperatures, a normal distribution is used by applying the mean equal to normal values as given in Table VII-1 [57,58].

b. Building envelope

The windows properties, building insulation materials thickness, and other properties such as building thermal correction factor and infiltration rate are the building envelope properties that affect the BES model's performance. The differences between the design specifications and the construction outcomes cause uncertainties in the insulation materials' thickness and subsequently changes its insulation capacity. Wei Tiana et al. [53] followed the assumption that the parameter of materials thickness follows a normal distribution that contains a standard deviation of 5% of the mean value. Gaussian distribution is used for describing different parameters such as U-value of windows 'U_{glass}', G-value of windows 'G_{value}', and shading factor reflecting the blinds effect '$f_{shading}$', and they were described based on a Gaussian distribution [59–61]. For the infiltration rate that depends on the construction quality, weather conditions, function of age, and building use [44]. It is counted as one of the most uncertain parameters because it is not easy to determine in buildings [62]. In this study, a Normal distribution that contains a standard deviation of 12.5% of its mean is considered. Finally, for the f_{c_i} at zone i which as always unknown parameters in the RC model, we assume it as a uniform distribution ranged between

10% and 90%. A summary for the uncertainty associated with the building envelopes parameters is shown in Table VII-1.

c. Equipment system

Based on the manufacturer data, engineering judgement, and experience and recommendations of Smith et al. [63], the systematic and random uncertainty values for the heat recovery efficiency 'η_{fan}' are taken as ±0.5% of its mean value. Following the recommendation by Zhang [61], the uncertainty associated with the mechanical ventilation '$vent._i$' at zone i is considered as a normal distribution with a standard deviation 2.5% of its mean value.

d. Occupant behavior

The relationship between the thermal performance of a building and its occupant behavior has emerged as an essential topic for research [64]. Occupant behavior is capable of introducing significant uncertainties in BES [65]. The detailed studies have shown that occupancy behavior in comparable buildings can lead to different energy consumption [26,66].

Most of the energy building simulation programs consider the factors linked to the occupant's behavior as deterministic by allowing the users to postulate fixed temporal schedules for occupancy-related variables, such as zone-heating set points, occupants, and closing/opening of the windows. These schedules can be easily implemented, but they are not responsible for the human behavior's stochastic nature or its interaction with the indoor environment of the buildings [53]. Following Sun et al. [67] recommendation, normal distributions are assigned to the occupant schedule '$Occup_{sch_i}$' and their relative internal heat gain '$Occup_{int_i}$' at zone i with a standard deviation 25% of its mean value. Furthermore, the same distribution is used with zone setpoint temperature 'T_{set_i}' at zone i with a 14% standard deviation to its mean value [53]. Finally, the angle of opening/closing the windows and doors 'θ_i' at zone i are of the most controversial issues regarding the BES. We assume that the fraction of opening windows is following a uniform distribution ranged between 1% and 90% with an initial value of 10%. In reality, many other occupant behaviors parameters such as the opening/closing windows schedule can contribute significantly to the BES performance especially in the nZEB case. However, due to the lack of information regarding the uncertainty associates with such these parameters, we define them only in a deterministic manner. A summary of the uncertainty associated with the occupant behavior parameters is shown in Table VII-1.

Table VII-1: Parameter-uncertainty distributions affecting the RC model performance

Parameter category	Uncertain parameter	Time frame	Probability distribution	Ref.
Input climate data	Q_{sol}	November–April, 9:00 am–3:00 pm	$N(\mu, 0.12\mu)$	[54]
		November–April, the rest of the day	$N(\mu, 0.25\mu)$	
		May–October, 9:00 am–3:00 pm	$N(\mu, 0.03\mu)$	
		May–October, the rest of the day	$N(\mu, 0.08\mu)$	
	V_{wind}	Time-dependent	$Wei(1.6,4.6)$	[56]
	T_{out}	Time-dependent	$N(\mu, 0.067\mu)$	[57]
	T_{ground}	Time-dependent	$N(\mu, 0.01\mu)$	[58]
Building envelope	RC_{roof}	Time-independent	$N(\mu, 0.05\mu)$	[53]
	RC_{floor}	Time-independent	$N(\mu, 0.05\mu)$	[53]
	RC_{facade}	Time-independent	$N(\mu, 0.05\mu)$	[53]
	U_{glass}	Time-independent	$N(\mu, 0.004\mu)$	[59]
	G_{value}	Time-independent	$N(\mu, 0.006\mu)$	[60]
	$f_{shading}$	Time-dependent	$N(\mu, 0.25\mu)$	[61]
	$Infl._i$	Time-independent	$N(\mu, 0.0125\mu)$	[61]
	f_{c_i}	Time-independent	$U(1\%, 90\%)$	-
Equipment system	η_{fan}	Time-independent	$U(75\%, 85\%)$	[63]
	$vent._i$	Time-independent	$N(\mu, 0.025\mu)$	[61]
Occupant behavior	$Occup_{sch}$	Time-dependent	$N(\mu, 0.25\mu)$	[67]
	$Occup_{int}$	Time-dependent	$N(\mu, 0.25\mu)$	[67]
	θ_i	Time-dependent	$U(0\%, 90\%)$	-
	T_{set_i}	Time-dependent	$N(\mu, 0.14\mu)$	[53]

VII.2.4 Dimension reduction using Morris analysis

The dimension reduction strategy is used to identify the key uncertain parameters out of various uncertainty variables given in Table VII-1, which influence the performance of the BES based on RC model. It facilitates an accurate prediction within the BES performance. As shown in Figure VII-6, the first step of the dimension reduction technique is to generate an input matrix. It is generated by grouping the design parameters on the basis of the distribution of the parameters with consideration of its time-dependent nature.

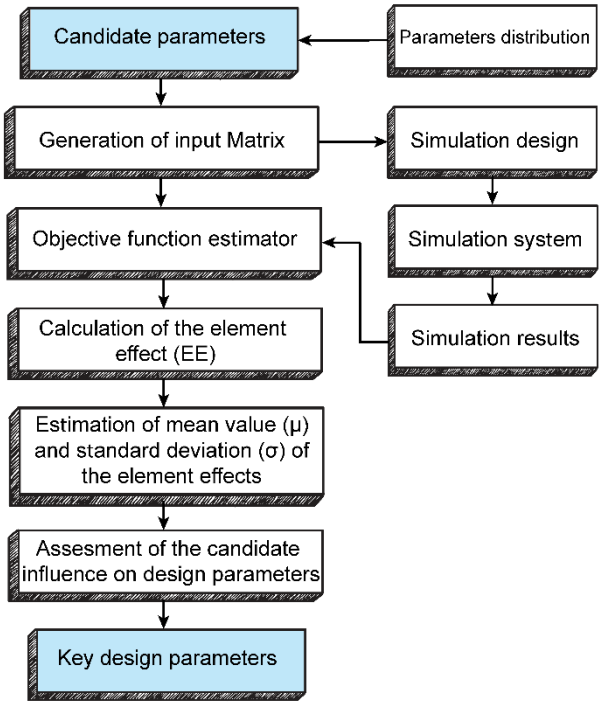

Figure VII-6: Dimension reduction process

The simulation scenarios are designed by using the input matrix. The design is used for determining the BES performance data based on the simulation of RC model as given in section 2.1. The simulation results were then used to calculate the zone temperature and its thermal energy consumption to generate the element effects, and the mean values and standard deviations of the element effects. The final step was to compare the standard deviations and mean values for determining the effect of each uncertain parameter so that the key uncertain parameters can be found out.

Morris global sensitivity analysis is a dimension reduction process that is used in this study. It offers the handling of large samples at low computational costs. Furthermore, it helps achieve optimized cooperation between efficiency and accuracy [68]. The following equation is used for determining the minimum number of required simulations in Morris analysis [69].

$$N_s = r(k+1) \qquad \text{Eq. VII-7}$$

Where N_s is the number of total simulations, r is the number of elementary effects per parameter, and k represents the number of design parameters.

From Morris analysis, two sensitivity indicators, i.e. mean value (μ) and standard deviation (σ) of the absolute values of the elementary effects as defined in Eq. VII-8 and Eq. VII-9 respectively [69]. The input parameter's influence on the output value can be determined with the help of the mean value. Moreover, the interactions among the non-linear effects or the parameters can be determined with the help of the standard deviation. A plane (μ, σ) is used for presenting these methods in Morris analysis. The presentation of the plane also helps in comparing their relative influence [70].

$$\mu = \sum_{i=1}^{r} |EE_i|/r \qquad \text{Eq. VII-8}$$

$$\sigma = \sqrt{\sum_{i=1}^{r} |EE_i - \mu|^2/r} \qquad \text{Eq. VII-9}$$

where EE is the elementary effect, and r shows the total number of elementary effects for each parameter.

The elementary effect EE is derived from a model $y = y(x1, \dots, xj)$ with j input parameters, i.e. $x_1, \dots, x_j$. The EE for the i^{th} input parameter at the k^{th} sampling point is calculated by Eq. VII-10.

$$EE_i^{(k)} = \frac{y\left(x_1^{(k)}, x_2^{(k)}, \dots., x_{i-1}^{(k)}, x_i^{(k)} + \Delta, x_{i+1}^{(k)}, \dots, x_j^{(k)}\right) - y(x_1^{(k)}, \dots, x_j^{(k)})}{\Delta} \qquad \text{Eq. VII-10}$$

The proper sampling of each input variable within its defined range is required for the success of the Morris sensitivity analysis. This study used the Latin hypercube sampling method that can generate a specific amount of discretized values within the range of every parameter. This method helps improve the efficiency of the Morris method [71].

VII.2.5 Bayesian optimization

Following the proposed framework, the Bayesian calibration [72] tends to incorporate the uncertainty of the parameters in the calibration process, and correct any inadequacy associate with them to keep the difference between the model prediction and observed values minimum.

In this study, a Bayesian approach is used for calibrating the uncertain parameters θ. The calibration of energy simulation models is performed in accordance with the building specifications and the observed data y. The calibration process aims to find the closest match between the observed data and the energy simulation data by deriving the values for θ. The method of Bayesian calibration (mathematical formulation) devised by Kennedy and O'Hagan [73] is used in this study. Three types of uncertainties are captured by the statistical formula: (i) discrepancy between the true behavior of building and the simulation model, (ii) parameter uncertainty in the energy simulation model, and (iii) errors because of the observations. Known conditions x are used for quantifying these uncertainties. Eq. VII-11 gives the relationship between the model outputs and the observations:

$$y(x) = \eta(x, \theta) + \delta(x) + \varepsilon(x) \qquad \text{Eq. VII-11}$$

$y(x)$ denotes the observations, the simulation model outputs that are computed at the given conditions x are given by $\eta(x, \theta)$. Known occupancy and external temperatures are examples of the known input conditions x. Even with the help of the calibration parameters, simulated models cannot perfectly predict the energy consumption of a building. Indeed, building energy models are based on approximations of the heat transfer processes occurring in a building. $\delta(x)$ represents the discrepancies between the physical behavior and simulated behavior of the building. This term helps in the over-estimation of the calibration values. It also indicates the shortages of the energy model. All the errors that occur during the recording of observations are given by $\varepsilon(x)$.

In the Bayesian paradigm, expert judgement is used for assigning the prior distributions $p(\theta)$ to the uncertain parameters. Several sources can be used for deriving it. Observations obtained from the formal set up are used for updating the prior distributions. In this system, the chances of obtaining observations from the simulated model drive the updating process of the prior distributions. As a result of this, plausible distributions of calibration parameters that are also known as posterior distributions are collected.

For characterizing the performance of the developed model, the accuracy is evaluated by utilizing a group of performance metric of the metamodel. Following standard evaluation measures are included in the performance metrics: (i) R-squared

(R^2), (ii) Coefficient of Variation ($C.V$), and (iii) Symmetric mean absolute percentage error ($SMAPE$), their formulas are expressed in Eq. VII-12 to Eq. VII-14.

$$R^2 = 1 - \frac{\sum_{i=1}^{n}\left(y_{predict,i} - y_{data,i}\right)^2}{\sum_{i=1}^{n}\left(y_{data,i} - \overline{y}_{data}\right)^2} \quad \text{Eq. VII-12}$$

$$C.V(\%) = \sqrt{\frac{\sum_{i=1}^{n}\left(y_{predict,i} - y_{data,i}\right)^2}{\overline{y}_{data}}} \times 100 \quad \text{Eq. VII-13}$$

$$SMAPE(\%) = \frac{1}{n}\sum_{t=1}^{n}\frac{\left|y_{data} - y_{predict}\right|}{\left(\left|y_{predict}\right| + \left|y_{data}\right|\right)/2} \times 100 \quad \text{Eq. VII-14}$$

In the above equations, $y_{predict,i}$ gives the predicted value at time point i. $y_{data,i}$ is the actual value at time point i, n represents the total number of the data points, and k gives the number of regressors. There are two main reasons for which the $C.V$ is used as an objective function in the model set. The first reason is that its index allows to determine how well a model fits the data by capturing offsetting errors between measured and simulated data. Therefore, it does not suffer from the cancellation effect [27]. The second reason is the recommendation of ASHRAE for using $C.V$ in evaluating the BES models [74].

VII.2.6 Uncertainty analysis (UA)

The uncertainty analysis requires two basic functions; the deterministic model $y = g(x)$ of the inspected system (section 2.1) and a probabilistic framework for the uncertain variables of the model (Section 2.2.1), The initial step of UA is to generate N samples for every k uncertain variables by utilizing their probability distributions. Then, the samples are kept in a matrix $\boldsymbol{X}$ Eq. VII-15. The j^{th} sample of a parameter X_i is given by $x_{i,j}$ based on Latin hyper cube design, In the space-filling design, we consider the range [0,1] divided into N intervals of the equal length $1/N$. One point is selected at random from each interval forming a sequence of N points in $H^1\ \{1\}, 1, .., i\ x\ i = N$. Similarly, but independently we construct another sequence $\{x_i^2\}, 1, .., i\ x\ i = N$. The two sequences $\{x_i^1\}, 1, .., i\ x\ i = N\ and\ \{x_i^2\}, 1, .., i\ x\ i = N$ can be paired to populate a bidimensional space. These N pairs can in turn randomly be combined with the N values of $\{x_i^3\}, 1, \ldots, i\ x\ i = N$ to form N triplets, and so on until an n-dimensional sequence of N is formed. The Latin hypercube has better space-filling properties than another random sampling since it allows us to obtain a full distribution of the output in less time than Monte Carlo; that is why; it is used for sampling from the parameter distribution [71].

$$\boldsymbol{X} = \begin{bmatrix} x_{1,1} & x_{2,1} & \cdots & x_{k,1} \\ x_{1,2} & x_{2,2} & \cdots & x_{k,1} \\ \vdots & \vdots & \ddots & \vdots \\ x_{1,N} & x_{2,N} & \cdots & x_{k,N} \end{bmatrix} \quad \text{Eq. VII-15}$$

After developing the sample matrix, the next step is to evaluate N Monte Carlo of the deterministic model. It is evaluated one per row of a matrix to get the model response, $\boldsymbol{y}$, see Eq. VII-16. The uncertainty impact can be quantified through the evaluation of the statistical and variability characteristics.

$$\boldsymbol{y} = \begin{bmatrix} y_1 \\ y_2 \\ \vdots \\ y_N \end{bmatrix} = \begin{bmatrix} g(x_{1,1}, x_{2,1}, \ldots\ldots, x_{k,1}) \\ g(x_{1,2}, x_{2,2}, \ldots\ldots, x_{k,2}) \\ \vdots \\ g(x_{1,N}, x_{2,N}, \ldots\ldots, x_{k,N}) \end{bmatrix} \quad \text{Eq. VII-16}$$

While using the Monte Carlo simulations, a random question arises regarding the number of iterations for the sufficient accuracy of the results. Based on the availability of the competitional resources, 10,000 simulations are selected as a thumb rule for the current study.

VII.2.7 Sensitivity analysis (SA) for building performance

After identifying the uncertainty associate with the parameters in the calibrated BES model based on Monte Carlo simulations, SA is performed to identify the most influential uncertain parameters in the building performance. The main output indicators are; the total energy thermal consumption at each building zone (Q_{Heat}) and the total over/underheating hours ($t_{o/u}$) in which the operating temperature at each zone gets out of the thermal comfort conditions (20:24 ^{o}C) identified by the ISO7730 [75].

Given the drawbacks in the local sensitivity analysis approach [76], a two-step global sensitivity analysis (GSA) approach is proposed in this study, as shown in Figure VII-7. In the first step, the Morris analysis is applied to screen the insignificant uncertain parameters and rank them in a low computational cost, as mentioned in Eq. VII-7 in terms of two objective outputs (Q_{Heat} and $t_{o/u}$). Noting that this ranking and screening phase is only qualitative approach, thus it cannot quantify the important of each parameter. Following this limitation, another GSA technique is proposed in the second step to provide more quantitative information regarding the uncertain investigated parameters.

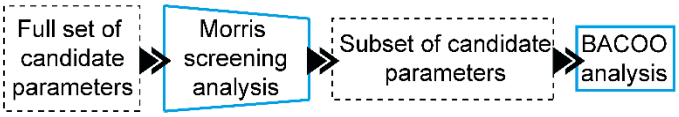

Figure VII-7: Two-steps GSA approach including screening phase (first step) based on Morris analysis and a second step using BACOO method using the subset of candidate parameters from the first step

In the second step, the Bayesian analysis of computer code outputs (BACCO) [73] is employed. The advantage of this method includes investigating a full range of the input parameters and their distribution. In addition, it offers a substantial declination in the computational cost compared to other GSA methods [77]. The BACCO approach has two main key stages. In the first stage, a set of training data are utilized to develop a statistical model derived from the RC model simulations. The training data tends to cover the whole problem domain based in a multidimensional filling algorithm (Latin hypercube design). In order to verify the model accuracy, cross-validation is applied to the developed model. In the second stage, the statistical model is proposed to in quantifying the importance of parameters in interest and their relative interaction due to its low computational expenses [78].

VII.3 Case study

VII.3.1 Building general description

The application of the proposed framework is illustrated through a two-story dwelling located in a district of Emmen at the Netherlands. A layout for the dwelling is shown in Figure VII-8 where the total floor area is 60 $m^{2,}$ and the ceiling height is 3 m. The considered dwelling has two external façades with a total area of 33.7 m^2, oriented to the East and West, whereas the opaque part represents 19.6 m^2. The first floor consists of living room, kitchen and the entrance. While the second floor has 3 bedrooms, one storage room, one bathroom and the hallway.

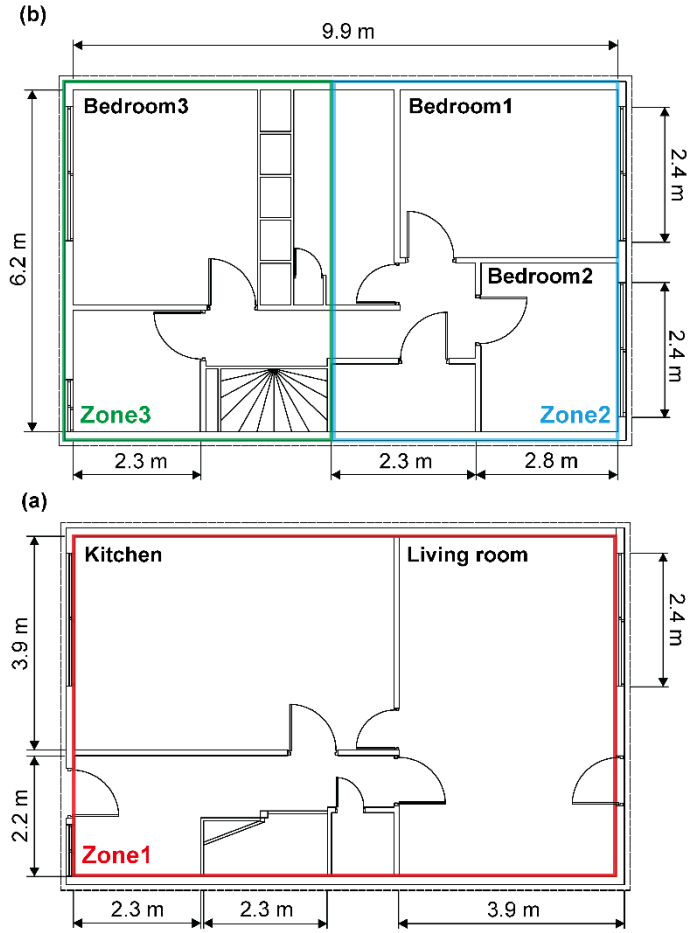

Figure VII-8: A layout for the two-story Emmen's dwelling: (a) first floor (Zone 1) highlighted in red, and (b) second floor (Zone 2&3) highlighted in blue and green, respectively

A 3-zone model is applied in Emmen's dwelling. The first floor is an open kitchen and living room with two temperature sensors. Therefore, as it is seen in Figure VII-8 all first floor is defined as Zone 1. All bedrooms have temperature sensors, and the orientation of the bedrooms is different. Whereas bedroom 1 and 2 face towards the west and bedroom 3 faces towards east. Moreover, it can be possible that 2 bedrooms are heated, and one is unheated and vice versa. Therefore, to distinguish the conditioned and unconditioned area and for the more accurate consideration of the solar gain, floor 2 is divided into 2 zones as it is seen in Figure VII-8 60% of the total floor area is considered as Zone 2, and the rest is Zone 3.

VII.3.2 Building construction feature

This building is a newly renovated home where all insulation of roof, floor, walls and glazing are reconstructed in passive level to enhance the dwelling energy-efficiency. The external walls are composed of two main walls; the outer walls comprise hollow bricks covered with layer insulation and plaster. While the inner walls are gypsum boards over light concrete. The ground surface composed of two main surfaces; the ground surface which comprises stones, concrete and insulation materials, whereas the inner floor surface composed of light concrete, and floor layer over gypsum boards. Finally, for the roof surface, it composes of three layers, including concrete and plaster over insulation materials.

As far as the windows are in concern, double-glazing windows with a total area of 12.1 m^2 are constructed in the western façade and 11 m^2 for the eastern façade. A summary of the construction material properties is shown in Table VII-2.

Table VII-2: Thermal properties of the building envelopes

Parameter name	Unit	Value
RC_{roof}	[m^2K/W]	5
RC_{floor}	[m^2K/W]	5
RC_{facade}	[m^2K/W]	4.7
U_{glass}	[W/m^2K]	1.1
G_{value}	-	0.7

VII.3.3 RC Model boundary conditions

For the development of the RC model, several monitoring data are required to trace the occupant behavior and equipment operation effects in the development of an accurate predictive model. The acquisition was performed for nine months (September 2017 to May 2018). This data collection guarantees to provide a quality data set during the whole heating period (autumn, winter and spring). On the other hand, the summer period was excluded in the data acquisition process since these dwelling doesn't have a cooling system. Thus, the summer period does not influence the annual energy thermal consumption of the building. The dwelling measurements were carried out while the dwelling was occupied in order to reflect the occupant behavior interaction with the dwelling. The measurement was taken within 10 min frequency and integrated over 1 hour, which is a more suitable frequency for building measurements over long periods. The measurement comprises the climate input data, the equipment operation and occupant activities.

VII.3.4 Climate input data

To obtain real-time weather data for the dwelling, the climate data are obtained from a KNMI weather station. The nearest KNMI weather station to the dwellings in Emmen is in the Hoogeveen (STN:279, LON(east):6.574, LAT(north):52.750, ALT(m):15.80) which is approximately 25-30 km away from the dwellings. The monthly average ambient temperature and its relative incident solar radiation on a horizontal surface are shown in Figure VI-10.

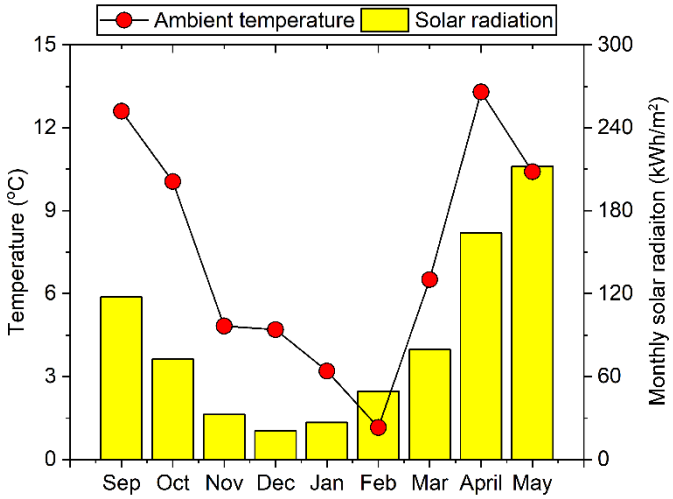

Figure VII-9: The climate conditions in the dwelling in Emmen from September 2017 to May 2018

In addition, the wind speed, as well, was extracted from the KNMI weather data. While the wind pressure coefficient on the building envelope is assumed to be 0.1. On the contrary, the ground temperature data is not available in the KNMI weather data file. Therefore T_{ground} is assumed as 10 °C and constant during the all year (although it varies from 7 °C to 13 °C during the year). However, the dwellings have a crawlspace which is naturally ventilated. Therefore, the average of the ground and outside temperature $\left(\frac{T_{ground}+T_{out}}{2}\right)$ is used in the model to calculate the transmission loss through the ground floor. Finally, to consider the shading by surrounding objects and the dwelling itself, the shading factor ($f_{shading}$) is introduced. The monthly shading factor values are in Table VII-3.

Table VII-3: Monthly shading factor

Month	Sep	Oct	Nov	Dec	Jan	Feb	Mar	April	May
Shading factor [%]	0.3	0.5	0.5	0.5	0.5	0.5	0.5	0.5	0.3

VII.3.5 Equipment operation

The building is heated up through radiators on all levels that are primarily provided by an air source heat pump (PUHZ-SW50VHA). The heat pump compressor controller managed the required flow rate based on the thermostats and the zone setpoint (user adjusted). Therefore, a variation in the heat pump performance factor (COP) is recognized with the variation in the ambient air temperature where the observed COP is up to 5, More details regarding the heat pump model is found in SI. Base on the time-dependent of the COP and its relative heat pump electricity consumption ($HP\ Power_{electric}$), the thermal heat pump power ($HP\ Power_{thermal}$) is estimated as following:

$$HP\ Power_{thermal} = COP(time) * HP\ Power_{electric} \quad \text{Eq. VII-17}$$

As shown in Figure VII-10, the maximum monthly thermal energy consumption occurs during February (1028.9 kWh_{th}).

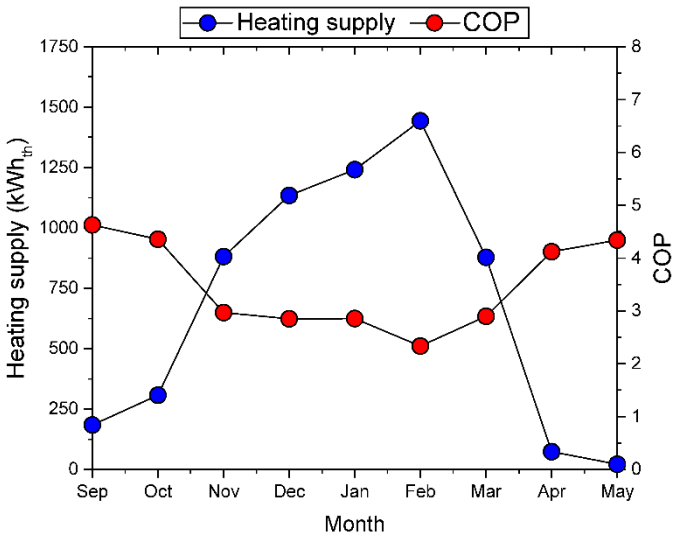

Figure VII-10: The pump heat performance during the heating period

For the mechanical ventilation, the hourly flow rate at each zone is estimated through the measurement of ventilation position throughout the operation period, and flow rate for the different ventilation positions at all the three zones. Since there is no specific sensor data to obtain the ventilation position, the energy consumption of the heat-recovery/ventilation for all dwelling is utilized for ventilation position. The mechanical ventilation system has three main positions during its operation, as

shown in Figure VII-11-(a). The relative heat recover, and the mechanical ventilation flow rate at each zone is shown in Figure VII-11-(b),(c),(d).

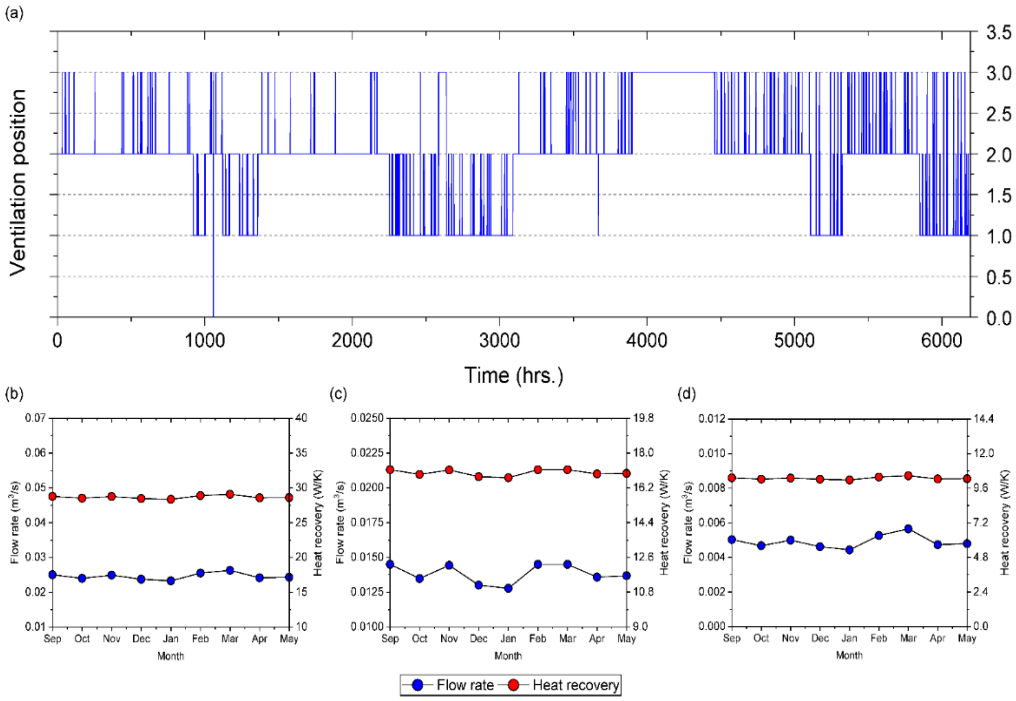

Figure VII-11: The mechanical ventilation position throughout the heating season aligning with its relative flow rates and heating recovers at each zone where; (a) The mechanical ventilation position, whereas (b), (c) and (d) mechanical ventilation flow rate and its relative heat recovery in Zone 1, 2 and 3, respectively

VII.3.6 Occupant activities

Since the occupant activities have a significant effect in the building energy performance, the measurements are taken under normal operating conditions in order to calculate the thermal response of the building under the different possible realistic operating conditions accurately. The occupant activities, including the setpoint temperature, the occupancy schedule, neighbour temperature and open/closing of window and doors are utilized as inputs in the developed RC model.

Occupancy data and their relative internal heat gain for each zone-type were determined based on human resources interviews, personnel counts, and multiple day/night occupancy surveys, as shown in Table VII-4. Furthermore, the internal heat gain is estimated to be 100 W per person during daylight and 70 W per person during night period where the distribution of occupants is 75% in zone 1 and 25 % in zone

2&3 during the daylight. While this percentage changes to 0% for zone 1 and 100% in zone 2&3 during the night period.

Table VII-4: Occupancy schedules for dwelling in Emmen

	Sunday	Monday	Tuesday	Wednesday	Thursday	Friday	Saturday
Morning (08:00 - 13:00)	5	3	3	3	3	3	5
Afternoon (13:00 - 18:00)	5	5	5	5	5	5	5
Evening (18:00 - 23:00)	5	5	5	5	5	5	5
Night (23:00 - 08:00)	5	5	5	5	5	5	5

In the dwelling at Emmen, the opening sensors are available in all windows and doors. Thereby, it is possible to detect when the window and door are closed or open. The results of opening sensors are available for Emmen's dwelling in Figure VII-12. The opening and closing windows/doors operation include the detection of its opening and its relative period where 1 means that the window/door is opened for 1 hour while zero represent a complete closing for an hour.

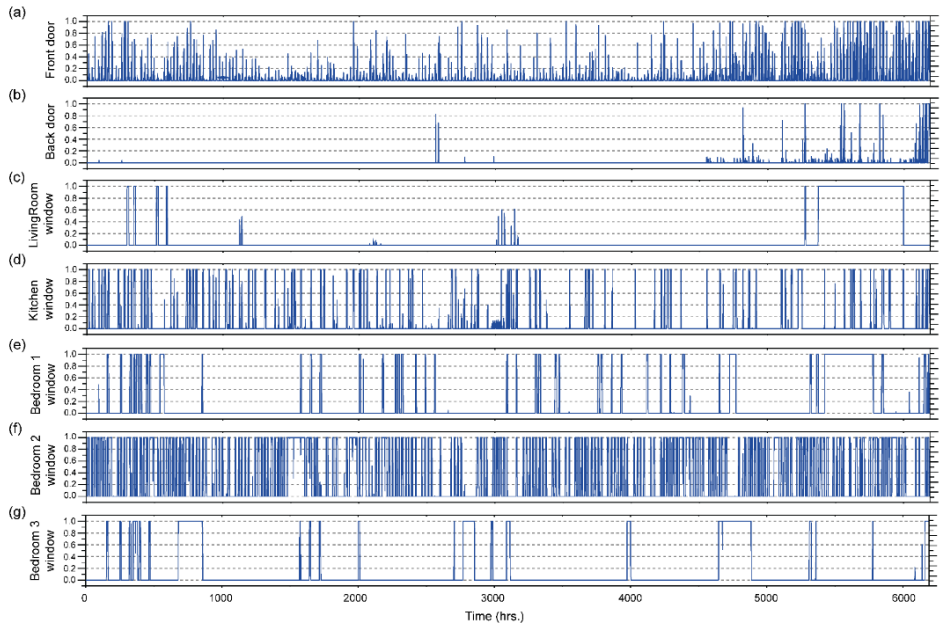

Figure VII-12: Windows and doors opening schedule for dwelling in Emmen

In addition to the occupancy and window operation schedules, the neighbour temperature is projected based on it is the neighbour's indoor temperature. It is used to calculate the heat loss or gain through the neighbour/s. Finally, the heating set-point temperature is also measured for zone 1, and it is utilized to calculate the required heating power. In contrast, the setpoint temperature for zone 2&3 is considered in a fixed proportional band to zone 1. A summary for the utilized equipment in the measurements and their error is shown in Table VII-5.

Table VII-5: Measurement equipment and their relative error

	Sensor Name	**Measurement error**
Temperature	Wireless M-Bus - CMa12w	0.2 degrees
Power	Energy meter - SDM630	< 1% of range / Power factor 0.01
Open/close windows	Window Sensor - FGK-101	NONE / Binary sensor
Weather data	KNMI (Dutch national weather institute)	

VII.4 Result and discussion

The results in the current study are divided into three main parts. The first part depicts the calibration of the RC model based on the Bayesian optimization approach incorporating Morris analysis for dimension reduction. The main purpose of this phase is first to define the most relevant uncertain parameters in the RC model and then calibrate them with consideration for the temporal variation (Time dependency) inherent in the relative uncertain parameters. Once the RC model performance is verified and calibrated in terms of the energy performance and zones temperature, the second part purposes a quantification for the uncertainty associate with RC model based on Monte Carlo simulations. Finally, a two-steps global sensitivity analysis is purposed to express the contribution of the uncertain parameters to the variation in the dwelling performance adequately.

VII.4.1 Model calibration

VII.4.2 Dimension reduction results

In order to carry out the dimension reduction based on Morris analysis for the developed RC model, 31 uncertain candidates are select for the three zones in Emmen's dwelling, as shown in Table VII-6. The Morris analysis in this stage is utilized to estimate all parameters that affect the accuracy of the RC model performance in terms of predicting the total thermal energy consumption and the zones temperatures. Given a total number of parameters k =31, the number of elementary effects r is selected as 100, leading to $r(k+1) = 3200$ model

performance evaluation. For all candidate design parameters, the performance of Morris analysis was quantified based on the mean value (μ) for the element effect and the standard deviation (σ) for its potential for interaction with other parameters.

Table VII-6: Candidate uncertain parameters at Emmen zones classification based on the parameter category

	Uncertain parameter			
Parameter category	Whole building	Zone 1	Zone 2	Zone 3
Input climate data	1. Q_{sol}	-	-	-
	2. V_{wind}	-	-	-
	3. T_{out}	-	-	-
	4. T_{ground}	-	-	-
Building envelope	5. RC_{roof}	-	-	-
	6. RC_{floor}	-	-	-
	7. RC_{facade}	-	-	-
	8. U_{glass}	-	-	-
	9. G_{value}	-	-	-
	10. $f_{shading}$	-	-	-
	-	11. $Infl._1$	12. $Infl._2$	13. $Infl._3$
	-	14. f_{c_1}	15. f_{c_2}	16. f_{c_3}
Equipment system	17. η_{fan}	-	-	-
	-	18. $vent._1$	19. $vent._2$	20. $vent._3$
Occupant behavior	21. $Occup_{sch}$	-	-	-
	22. $Occup_{int}$	-	-	-
	-	23. $\theta_{Living\ room}$	27. $\theta_{Bedroom\ 1}$	29. $\theta_{Bedroom\ 3}$
	-	24. $\theta_{Kitchen}$	28. $\theta_{Bedroom\ 2}$	-
	-	25. $\theta_{Entrance}$	-	-
	-	26. θ_{Exit}	-	-
	-	-	30. T_{set_2}	31. T_{set_3}

All the Morris analysis results for the total thermal energy consumption and temperature at each zone are shown in Figure VII-13. In the plot analysis, we consider the most 14 influential parameters from the Morris method and label them according to their μ and σ values. The important parameters are marked with circles, whereas the remain parameters are considered less important and marked with X. For the prediction of the total thermal energy consumption, it can be seen that the infiltration rate in zone 2 (i.e. factor 12) followed by the infiltration rate in zone 1 (i.e. factor 11) are the most influential parameters due to their high μ. While the correction factor of thermal mass fraction in zone 1 (i.e. factor 14) followed by the window opening angle

of kitchen room (i.e. factor 24) have the highest possibility for interactions with other parameters due to their high σ. In term of the temperature at zone 1, the window G-value (i.e. factor 9) and the correction factor of thermal mass fraction in zone 1 (i.e. factor.14) are the most influential parameters since they have the highest μ and σ. This is followed by the infiltration rate in zone 1 (i.e. factor 11). Furthermore, the window opening angle of kitchen room (i.e. factor 24) followed by wind speed (i.e. factor 2) have a high potential for interaction with other parameters due to their high σ. For the temperature prediction in zone 2, the correction factor of thermal mass fraction in zone 2 (i.e. factor.15), followed by the window G-value (i.e. factor 9) and the infiltration rate in zone 2 (i.e. factor 12) have the highest influence in the temperature in Zone 2. Furthermore, the window opening angle of bedroom 1 (i.e. factor 27) have high interaction potential. Finally, for the temperature in zone 3, the most influential parameter is the correction factor of thermal mass fraction in zone 3 (i.e. factor.16). The second most influential parameter is the window G-value (i.e. factor 9), followed by the window opening angle of bedroom 3 (i.e. factor 29). Noting that occupant behavior has a significant impact on the performance of the model accuracy, as mentioned by [64].

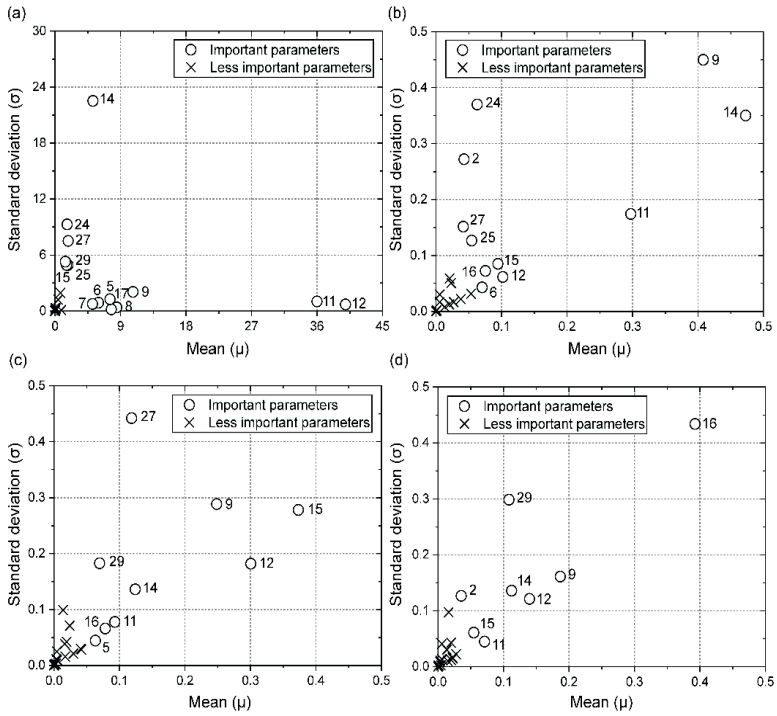

Figure VII-13: Results of the Morris sensitivity analysis to evaluate the parameters affect the RC model accuracy in predicting; (a) the total thermal energy consumption, (b) temperature at zone 1, (c) temperature at zone 2, and (d) temperature at zone 3

Therefore, including more occupant behavior parameters such as opening/closing window schedule can significantly change the contribution of each uncertain parameter to the model accuracy. However, due to the lack of extensive knowledge regarding the uncertainty associate with these parameters, we keep them as deterministic parameters.

The remaining uncertain parameters can be considered as the parameters with a less impact on the prediction of the RC model performance, and they set as constant values (see Table VII-7) based on the case study data entry mentioned in section 3.

Table VII-7: Low sensitivity parameters and values used

Parameter	**Value**
1. Q_{sol}	KNMI weather station
3. T_{out}	KNMI weather station
4. T_{ground}	10 ^{o}C
10. $f_{shading}$	Monthly shading factor (Table VII-3)
13. $Infl._3$	0.31 l/s
18. $vent._1$ / 19. $vent._2$ / 20. $vent._3$	Ventilation position profile (Figure VII-11)
21. $Occup_{sch}$	Occupant questionnaire (Table VII-4)
22. $Occup_{int}$	100 W (daylight) & 70 W (night)
23. $\theta_{Living\ room}$ / 26. θ_{Exit} / 28. $\theta_{Bedroom\ 2}$	10%
30. T_{set_2} / 31. T_{set_3}	T_{set_1} profile

VII.4.3 RC Model setting (Bayesian optimization)

Following the screening phase using Morris analysis to eliminate the less important uncertain parameters, the Bayesian optimization is proposed in this stage to calibrate and produce an accurate RC model that can predict the dwelling thermal energy consumption as well as the zones temperature more accurate. Based on 500 iterations in the Bayesian model, the optimal values for uncertain parameters are estimated for the time-independent and dependent uncertainty parameters.

A summary of the time-independent parameters is shown in Figure VII-14. For the building envelope parameters, a large diversion from the initial construction materials design is observed in the optimal parameters where the thermal resistances are higher by 38% and 34% for the roof and floor surfaces, respectively. While the thermal resistances of the façade surface is lower by 17% from its initial value. The difference between the initial and the Bayesian optimal values are due to the aging and the difference between the design specifications and the construction outcomes. For the windows construction properties, a limited deviation is detected for the U_{glass} where

it is lower by 19% from the initial values, whereas the G_{value} is higher by 32%. In terms of the infiltration rates, the deviation between the initial value and optimal estimate values is about 80% for zone 1 and 43.3% for zone 2. This deviation in the infiltration rate is a function of several parameters comprising the construction quality, the building use as well as the weather conditions. For the equipment operation presented by the η_{fan}, a deviation of 5% is estimate from the equipment specification. Finally, for the correction of the thermal mass parameter, this value was set to 0.3 for all zones. However, a big deviation from the initial values is observed for all f_c where the optimal value is 0.81, 0.14 and 0.45 for zone 1, 2 and 3, respectively.

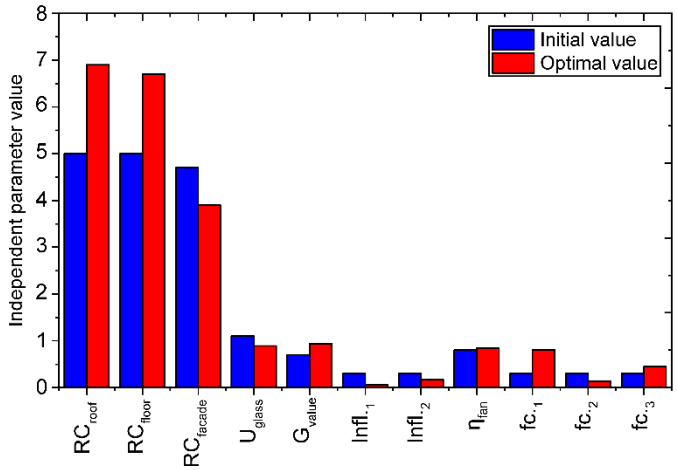

Figure VII-14: The initial vs optimal values for time-independent parameters

On the other hand, a summary of the time-dependent uncertain parameters is illustrated in Figure VII-15. For the wind speed, the optimal scenario over the 36 weeks (heating seasons) has a limited difference from the data extracted from the KNMI weather station. The maximum deviation is about 9% in week 24 (February). While for the parameters related to the opening angle of windows and doors 'θ_i', a big deviation is indicated in all windows and doors from the initial proposed values. This deviation is expected since the θ_i is one of the most controversial uncertain parameters in the BES models. For the $\theta_{Entrance}$, the angle of opening is stayed around 45.5%±3.5 for the whole 36 weeks. Moreover, the windows $\theta_{Kitchen}$, $\theta_{Bedroom\ 1}$, $\theta_{Bedroom\ 3}$ stay around for the 45%±3 over all the operation period.

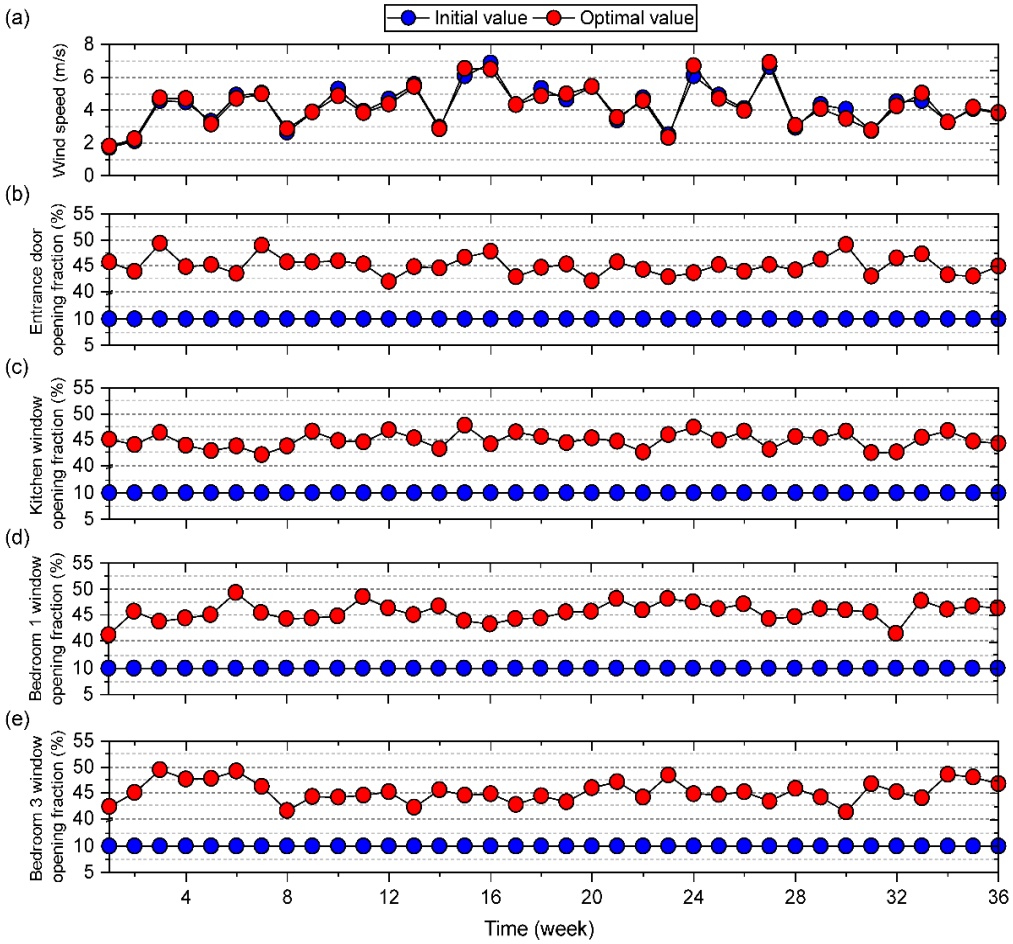

Figure VII-15: The initial vs optimal values for time-dependent parameters

VII.4.4 Calibration performance

Following the calibrated parameters based on the Bayesian optimization approach, the developed RC network for the digital dwelling using zone thermal coupling method is compared with the measured hourly data of 9 months of operation (heating seasons). The developed model performance is validated in terms of the indoor air temperature at the three investigated zones and the cumulative thermal energy consumption by the dwelling. According to the indoor air temperature profiles shown in Figure VII-16, a good agreement is indicated between the prediction of the RC model and the indoor measured temperatures at all the dwelling zones. In zone 1, the $C.V$ is 3.63% and $SMAPE$ is 5.04%. While the maximum error of 4.5 ^{o}C is indicated during the end of the spring season (April). For upper floor (Zone 2 and 3), a higher error is indicated within the RC model prediction for indoor temperature where the C.V is 5.53%, and 7.03% for zones 2, and 3, respectively. While the SMAPE stayed

around 3.54% and 4.35% for both zones 2 and 3, respectively. Furthermore, the maximum error of around 9 °C for the prediction of the indoor temperature is zone 2, and 3 is indicated during the winter season (end January).

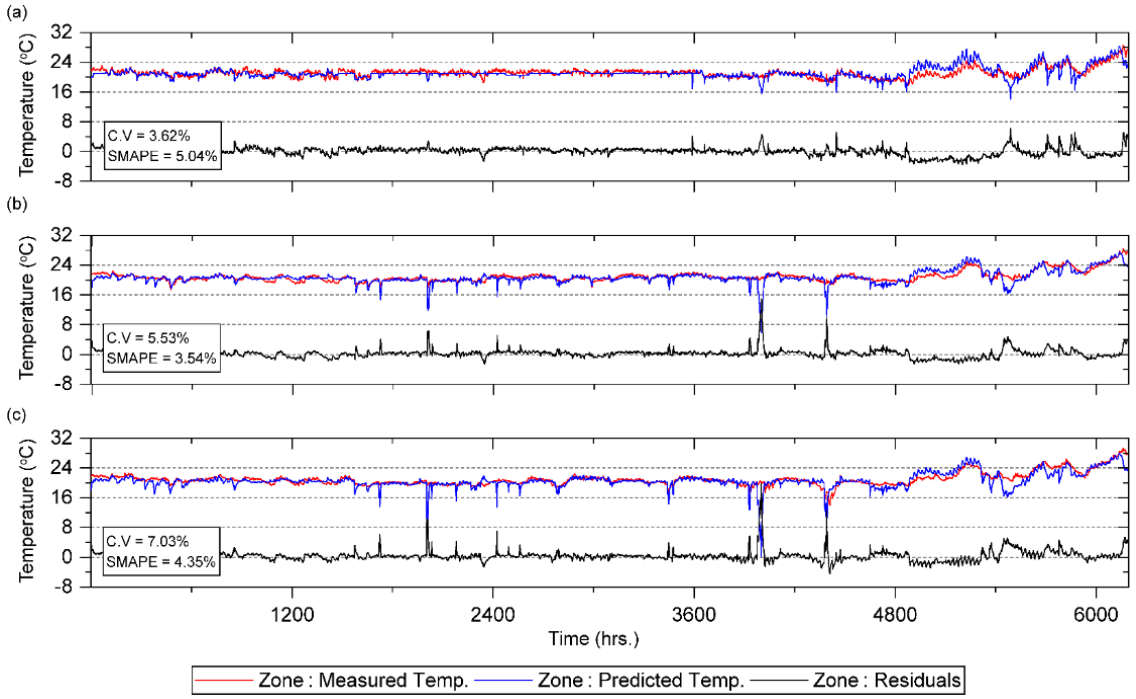

Figure VII-16: Hourly indoor air temperature in °C for the RC model prediction in comparison to the Emmen's dwelling monitoring data

Figure VII-17 represents the cumulative heating demand results of the RC model in the Emmen's dwelling during 9 months of operation. In this plot, the results of the RC model (Predicted $Q_{heat\ total}$) are compared to the measured heating demand for dwellings (Measured $Q_{heat\ total}$). A good performance is indicated in the RC model for the prediction of the $Q_{heat\ total}$ where the predicted value is 4.05 MWh with an error of 2.2% from the measured $Q_{heat\ total}$. In addition, the C.V and SMAPE show that the prediction error doesn't excess 2%. Finally, the residual analysis shows that the maximum cumulative thermal energy consumption difference between the measured and the predicted $Q_{heat\ total}$ is around 0.25 MWh.

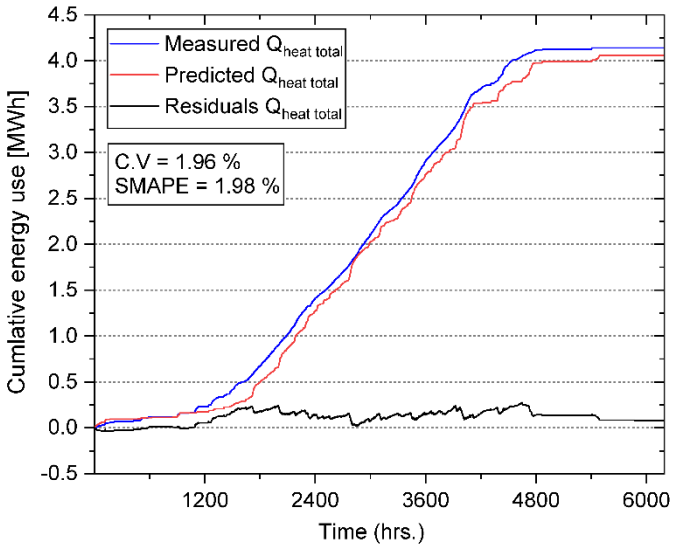

Figure VII-17: The predicted cumulative thermal energy consumption at Emmen's dwelling in comparison to the monitoring data

In order to test the performance of the RC model at a different scale of prediction, the energy signature results for the Emmen's dwelling is presented in Figure VII-18.

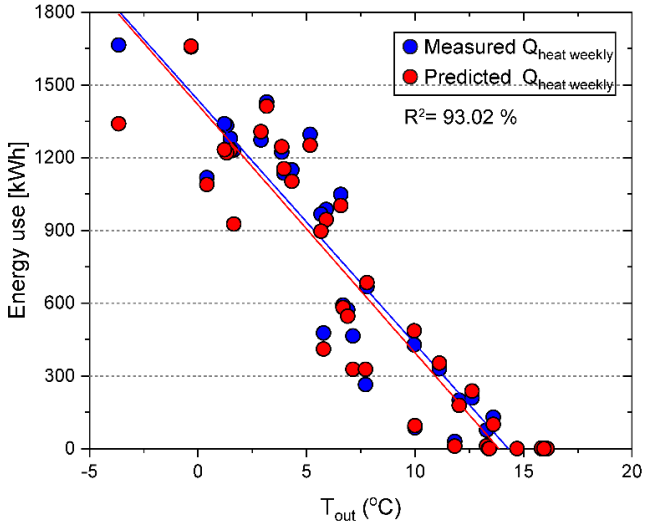

Figure VII-18: The weekly predicted vs. measured energy signature for the Emmen's dwelling

In this plot, the results of the RC model (predicted thermal power) are compared to the measured thermal power of dwellings. The energy demand and the outdoor

temperature is averaged on a weekly basis. The dots in the figure represent the data points, and the lines are obtained from these data points by fitting where the energy demand decreases with the increase in outside temperature. The results confirm an agreement between the measured and predicted weekly thermal power where the R^2 equal to 93%. The validation of the hourly indoor air temperature and the building thermal energy performance reflect the ability of our methodology approach cover the limitation associate with the RC models in predicting the thermal energy performance for a long-term period successfully.

VII.4.5 Uncertainty analysis (UA) results

In recent years, several contractors in Netherlands (e.g. Van Wijnen and BAM) offer energy-neutral housing in both the construction market and existing construction market. However, there is a burden of proof with the builder for zero on the gauge of the housing due to the uncertainty associate with the performance of the building. This burden increases due to the residents who have not yet confidence regarding the building performance guarantees. Therefore, it is important to guarantee of performance of these building independently on uncertain dwelling parameters. The long-term guarantee of the quality of the home, both in terms of thermal energy consumption and indoor climate, will lead to forecast the demand for these homes, and subsequently will boost energy savings of the housing, both new construction and renovation.

In this context, once the RC model is calibrated, and its performance is validated in comparison to the monitoring data. The UA based on Monte Carlo simulations is performed to quantify the uncertainty associate with the performance of the developed digital dwelling in terms of the indoor temperature at each zone and the total thermal energy consumption which is reflected in the building energy efficiency rating. For the UA step of the methodology, 10,000 MC evaluations of the developed model are performed using the uncertain parameters proposed in Table VII-6.

Figure VII-19 illustrates the variation in the zone indoor temperature using the blue plots and its relative $t_{o/u}$ using the dotted circles. In zone 1, a limited variation is indicated in the indoor temperature throughout the heating operation seasons where the maximum variation reveals by the end of the operation period (May). This limited variation is reflected in $t_{o/u}$ in which the zone indoor temperature gets out of the thermal comfort conditions mentioned by ISO7730 [75].The over/underheating hours varies between 1147 hrs to 1730 hrs throughout 9 months of operation. In zone 2, almost the same behavior is indicated as zone 1 except for two regions. First during weeks between 10 and 18 (November and December). While the second region appears by the end of the operation (May) where a limited variation in the indoor zone temperature is indicated in comparison to zone 1. This variation is reflected in the $t_{o/u}$ and it ranged between 1624 hrs. and 2606 hrs. Besides, zone 3 follows the zone 1 as well as 2 behaviors with a larger range of variation in the indoor temperature, especially during the winter season. This variation expansion is reflected in $t_{o/u}$ and

it varies between 2044 hrs. and 3292 hrs. In general, the increment in the $t_{o/u}$ associated with zone 2 and 3 demonstrates a high impact for the uncertain parameters on the thermal comfort conditions at these zones.

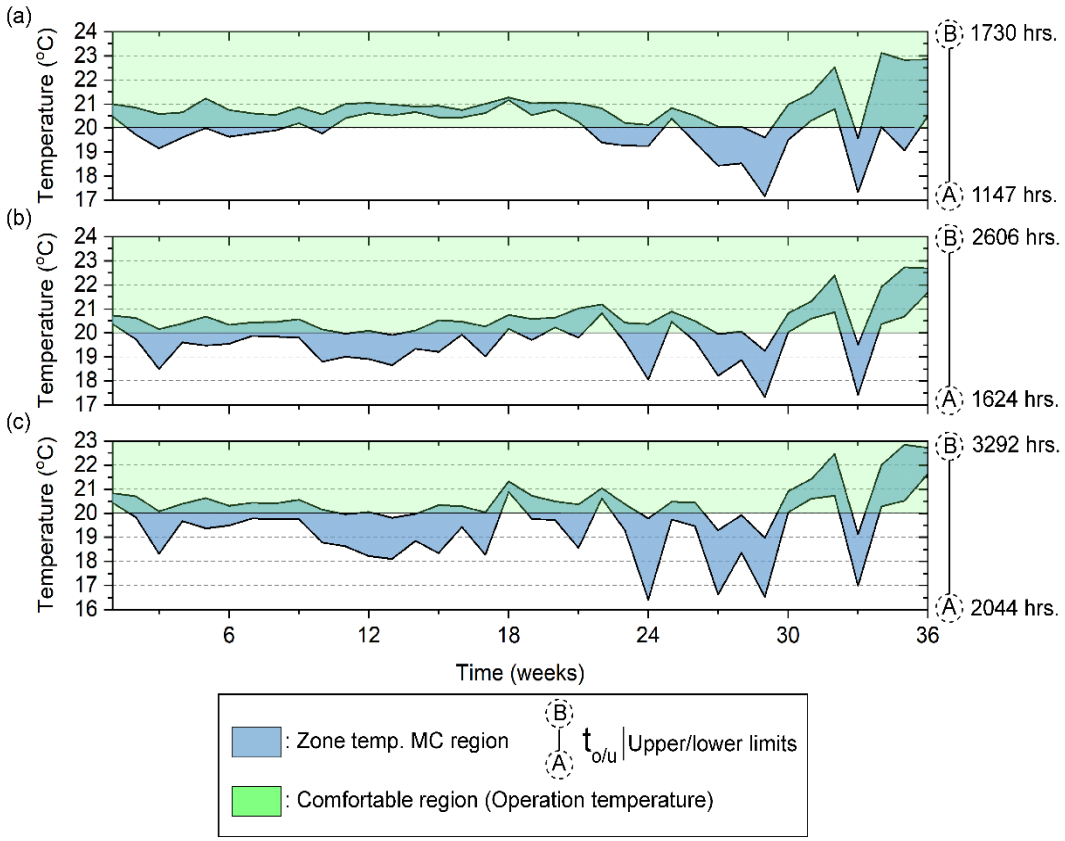

Figure VII-19: The indoor temperature range at different zones based on the UA where (a) indoor temperature in zone 1, (b) indoor temperature in zone 2, (c) indoor temperature in zone 3. The blue filled areas represent a range for the indoor temperature at different zone under uncertainty, the light green region represents the temperature thermal comfort conditions (20:24 °C), and the dotted circles between A and B anchor points represent the upper and lower limited number of hours out of the thermal comfort conditions

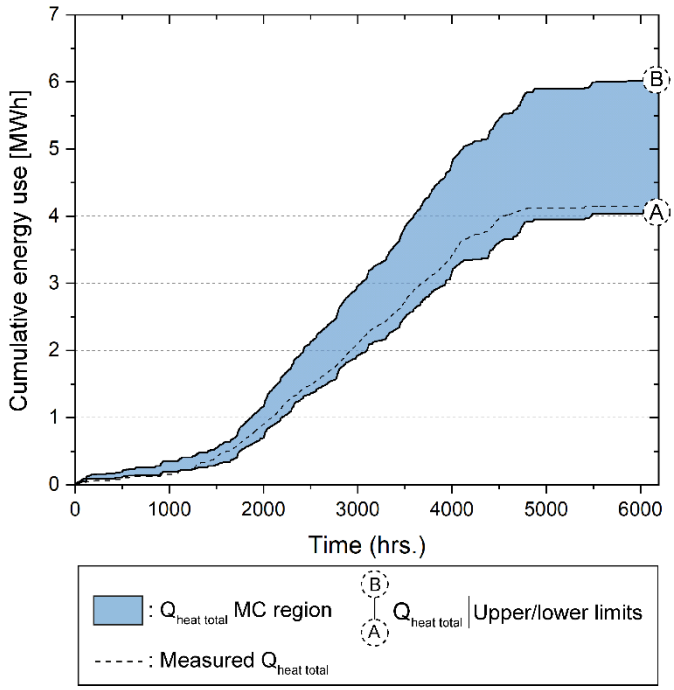

Figure VII-20: The total thermal energy consumption variation range where the dotted circles between A and B anchor points represent the upper and lower limits. The blue filled areas represent a variation range for total thermal energy consumption vs the monitoring data in dotted line

Figure VII-20 illustrates the variation in the total dwelling thermal energy consumption ($Q_{heat\ total}$) using the blue plots and the dotted circles. The UA shows a significant impact for the uncertain parameters in the thermal energy building performance where the $Q_{heat\ total}$ ranges between the 4.03 MWh (67 kWh/m^2/yr) to 6.01 MWh (100 kWh/m^2/yr) due to the uncertainty associate with climate data, the building envelope and occupant behavior. Accordingly, the high thermal energy consumption due to the possibility of uncertainty can decline the motivate the prospective owners or new tenants of the building to purchase or rent the building and subsequently reduce the market for energy-efficient renovation [79].

VII.4.6 Global sensitivity analysis results

The UA results demonstrated the significant effects of uncertainty on the RC model output scopes comprising the indoor zone temperature and its relative $t_{o/u}$ and $Q_{heat\ total}$. The GSA is able to produce additional understanding by recognizing the uncertain parameters that are majorly accountable for the output variations. The GSA technique can be used for investigating the main sources behind the variability in the RC model output. In this paper, the GSA technique is used for identifying the

significant factors that are related to the variations in the total thermal energy consumption and indoor zone temperature, as shown in following figure.

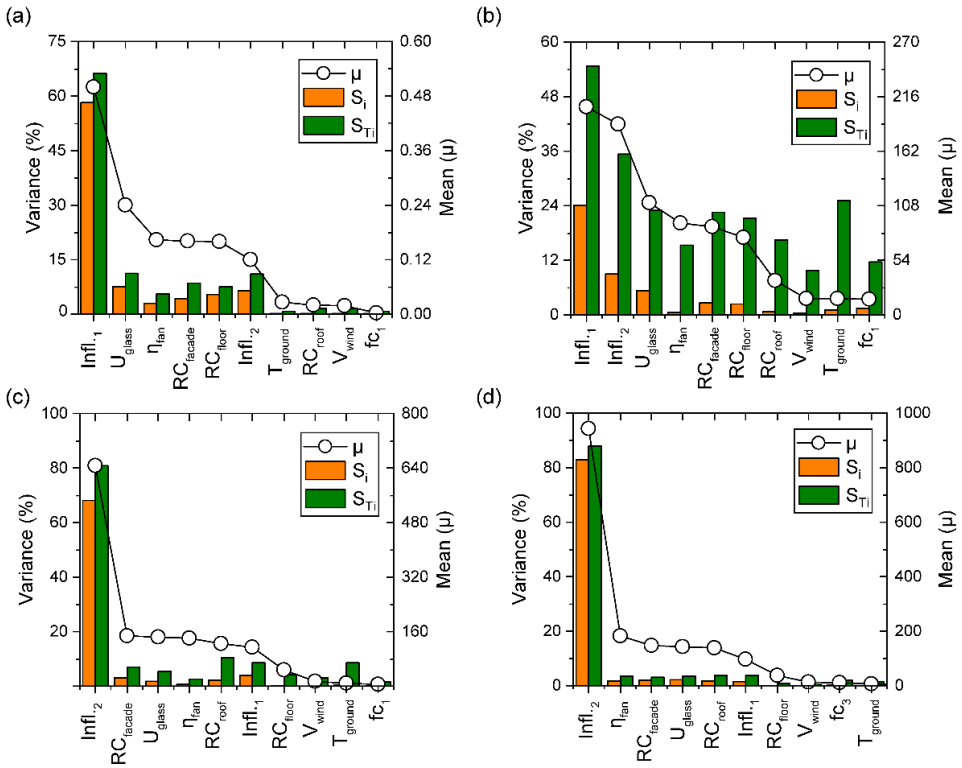

Figure VII-21: The Morris analysis mean and the BACCO analysis method indices to specify the most influencing uncertain parameters with regards to the Emmen's dwelling where (a) the total thermal energy consumption in the Emmen's dwelling, (b) $t_{o/u}$ at zone 1, (c) $t_{o/u}$ at zone 2, (d) $t_{o/u}$ at zone 3

According to Table VII-6, there are total 31 uncertain parameters in the two-step GSA, the Morris analysis setting is selected, as mentioned in section 4.1.1. Then, for the ten most influential parameters, 400 sample points are used for the BACCO analysis. Latin hypercube sampling design is used for obtaining these sample points. The analysis is performed by formulating the sensitivity analysis problem and then using the Gaussian Emulator Machine Sensitivity Analysis Software (GEM-SA).

In each graph, μ value is used for presenting and ranking the ten most uncertainty parameters obtained from the Morris method. The BACCO analysis is quantified based on the main effect (S_i) and the total effect (S_{Ti}). The initial observation of the graphs revealed the fact that the ranking of parameters obtained from the Morris method is in accordance with the BACCO analysis results where the μ value and the BACCO main effect (S_i) follow the same decreasing trend. Therefore, the Morris

method is applicable for performing the GSA analysis in case of the quantitative ranking. Although the essential parameters are identified with the help of the Morris method, the BACCO analysis tells about the contribution of these parameters towards the output's variance that is also given by adding the first-order indices and total-order indices.

For the thermal energy consumption in the dwelling ($Q_{heat\ total}$). The total effect indices are almost following the first-order effect indices in the BACCO analysis where the infiltration rate in zone 1 is the most significant parameter in the building performance, followed by the U_{glass}. In addition, the total effect indices showed a noticeable effect for the infiltration rate in zone 2 followed by the building envelope materials of the floor and façade (RC_{floor}, RC_{facade}). In terms of the $t_{o/u}$ at zone 1, the total effect indices show that the infiltration rate at zone 1&2 are the most influential parameters followed by the T_{ground} and building envelope characterization comprising the U_{glass}, RC_{floor} and RC_{facade}. On the other hand, the $t_{o/u}$ in the zone, 2&3 is only affected by the infiltration rate in zone 2. In general, the two-step GSA encompass a significant influence for the air tightness represented by the infiltration rate at each zone. This influence is a function of various parameters, including the building age, construction materials, weather conditions and building use. Since in the current study, the parameters related to the climate conditions and building construction are already included in the sensitivity analysis, which approve the building performance independency on these parameters. Therefore, the uncertain parameters regarding the building use presented by opening/closing doors& windows for natural ventilation may be responsible for the significant impact for the infiltration rate.

In general, the minimum ventilation rate should be around 41 L/s based on the Dutch standard (NEN 1087) [80]. However, it completely changes with the occupant behavior (opening/closing window schedule). The lack of extensive knowledge regarding such these parameters present a constraint in the performance of our framework when we preform uncertainty analysis. It can significantly change the contribution of each uncertain parameter to the model energy performance. Therefore, we keep them as deterministic parameters. Besides the most important parameters, the GSA results also showed that the uncertainty associate with the occupant behavior including the occupant schedule and zone temperature setting have less impact on the performance of the dwelling in terms of the $Q_{heat\ total}$ and $t_{o/u}$ objectives. In general, the two-step GSA is a valuable decision support technique that can offer the builders and construction companies an evaluation for the main drivers of the uncertainty associate the dwelling performance.

VII.5 Conclusion

Improving the building energy efficiency is widely considered as a promising technique to meet the European Commission 2050 targets in reducing the CO_2 emission. In Netherland, Association of Dutch Municipalities is working on expanding this concept through the introduction of the nearly zero energy building (nZEB) approach [81]. However, the construction companies that lead the development of nZEB in the Netherlands indicate a substantial obstacle to guarantee the nZEB performance and thus to improve their market position. This work tends to propose a methodology framework to benefit the guarantee and assist proactively in maintaining the indoor climate performance of nZEBs. This methodology is implemented through developing a calibrated RC (resistance and capacitance) model for estimating the building energy performance. The first step in the calibration process is the dimension reduction strategy using Morris sensitivity analysis to estimate the influential parameters that contribute to the proposed model accuracy. Then the calibration process is implemented based on Bayesian optimization with consideration for the temporal variation associate with the climate data as well as the occupant behavior. Once the calibrated model is established, the uncertainty analysis (UA) incorporating global sensitivity analysis (GSA) is performed to quantify and assess the uncertainty associate with the performance of the developed digital dwelling. In this context, the developed methodology is applied for a newly renovated two-story home located in a district of Emmen at the Netherlands to close the gap between the initial retrofitting design and the monitoring operation throughout the heating seasons (9 months), a summary of the methodology framework key findings is the following:

- The Morris sensitivity analysis for the RC model accuracy drivers shows that the infiltration rates are main drivers for the prediction of the energy performance. While the indoor temperature zones mainly depend on the zone correction factor of the thermal mass fraction.
- The developed digital dwelling based on RC model illustrates a high accuracy in predicting the dwelling performance where the model offers a prediction accuracy of 2.2% for the total thermal energy consumption. Moreover, the developed model provides acceptable estimations for the indoor zone temperature with $C.V$ of 7.03%.
- The UA results show a large variation associate with digital dwelling output due to uncertain parameters including the climate data, the building envelope and occupant behavior. The uncertainty associates with indoor temperature can increase the over/underheating hours up to 3292 hrs. While the uncertainty associates with total thermal energy consumption can change the building performance from 4.03 MWh (67 kWh/m^2/yr) to 6.01 MWh (100 kWh/m^2/yr) .
- Finally, the GSA based on the Morris analysis and BACCO analysis reveals that the variation in building energy performance is due to the infiltration rates

followed by the construction properties comprising the U_{glass}, RC_{floor} and RC_{facade}. Without losing the generality of the results, including more in parameters regarding the occupant behavior can contribute significantly to the GSA results.

In the real application, the developed methodology can serve as a diagnostic tool to improve and guarantee the performance of nZEB buildings during its operation stage which can be useful for the construction and installation companies to maintain the performance of their products proactively. Furthermore, it can promote a clear statement toward the EU approach to sustainable development.

VII.6 Acknowledgements

The work is funded by the Spanish government RTI2018-093849-B-C33 (MCIU/AEI/FEDER, UE). This work is supported by the Ministerio de Ciencia, Innovación y Universidades – Agencia Estatal de Investigación (AEI) (RED2018-102431-T). This project has received funding from the European Union's Horizon 2020 research and innovation programme under the Marie Skłodowska-Curie grant agreement No. 713679 and from the Universitat Rovira i Virgili (URV). In addition, this work was part of the Dutch project TKI Optimaal and co-funded by TKI Urban Energy from the Surcharge for Top Consortia for Knowledge and Innovation (TKIs) of the Ministry of Economic Affairs of the Netherlands.

VII.7 Nomenclature

$A(\theta(t))$	window opening area only for the ingoing airflow (m^2)
A_{glass}	effective solar collecting area (m^2)
$C.V$	coefficient of variation (%)
C_d	discharge airflow rate coefficient
C_p	wind pressure coefficient
C_v	air permeability coefficient
C	total thermal mass of the building (kW)
C_{int}	indoor thermal mass (kW)
C_{wall}	outdoor thermal mass (kW)
EE	elementary effect
f_c	correction factor of the thermal mass
$f_{shading}$	envelope shading reduction factor
G_{value}	solar energy transmittance (-)
$Infl._i$	Infiltration rate at zone i (m^3/s)
n	flow exponent
N_s	number of total simulations
$Occup_{sch_i}$	occupant schedule at zone i
$Occup_{int_i}$	internal heat gain at zone i (kWh)
ΔP	air pressure differential across a building envelope (Pa)

ΔP_{th}	difference of pressure across the window opening (Pa)
Q_{sol}	amount of global solar radiation (W/m^2)
Q_v	calculated volumetric airflow through infiltration (m^3/s)
$Q_{v_{10}}$	measured volumetric airflow through infiltration (m^3/s)
Q_{Heat}	total thermal energy consumption at each building zone (kWh)
r	number of elementary effects per parameter
R^2	R-squared (%)
RC_{roof}	thermal resistance of the roof (m^2·K/W)
RC_{floor}	thermal resistance of the floor(m^2·K/W)
RC_{facade}	thermal resistance of the façade (m^2·K/W)
sf	solar fraction factor
$SMAPE$	symmetric mean absolute percentage error (%)
T_{int}	indoor zone temperature (ºC)
T_{ground}	ground temperature (ºC)
T_{wall}	envelope zone temperature (ºC)
T_{out}	outdoor temperature (ºC
T_{neigh}	neighbour temperature (ºC)
T_{set_i}	setpoint zone temperatures (ºC)
t	operation time (hour)
$t_{o/u}$	total over/underheating hours
U	heat loss coefficient (W/m^2·K)
U_{glass}	U-value of windows W/(m^2·K)
$vent._i$	mechanical ventilation at zone i (m^3/s)
'V_{wind}'	local air velocity (m/s)
$y_{data,i}$	actual value at time point i
$y_{predict,i}$	predicted value at time point i

Greek symbol

η_{fan}	heat recovery efficiency (%)
μ	mean value
θ	opening/closing the windows and doors (º)
σ	standard deviation
ρ	air density (m^3/kg)
$Ø_{int}$	internal heat gain by occupants and appliances (kW)
$Ø_H$	heat flow rate sourced from the heaters based on heat pump (kW)
$Ø_{exch}$	exchange heat flow rate with other zones (kW)
$Ø_{sol}$	heat flow rate sourced from solar (kW)
$Ø_{vent}$	ventilation and infiltration losses (kW)
$Ø_{neigh}$	heat flow rate exchange with the neighbour (kW)

$\emptyset_{trans}$	heat flow rate transmitted through the windows (kW)
$\emptyset_{gnd}$	heat loss to the ground (kW)

Abbreviations

BACCO	Bayesian analysis of computer code outputs
BES	Building energy simulation
COP	Heat pump performance factor
EPC	Energy Performance Coefficient
GEM-SA	Gaussian Emulator Machine Sensitivity Analysis Software
GSA	Global sensitivity analysis
MC	Monte Carlo
nZEB	Nearly zero energy building
PDF	Probability density function
RC	Resistance and capacitance
SA	Sensitivity analysis
UA	Uncertainty analysis
UC	Uncertainty Characterization

VII.8 Appendix. Supplementary information – SI

The building is heated up through radiators on all levels that are primarily provided by an air source heat pump (PUHZ-SW50VHA). Table S1 shows the heating capacity and the coefficient of performance (COP) of the heat pump (HP) which is taken from the data book for the nominal operating conditions at 45 °C outlet temperature of the water. In this table, it can be observed that COP is limited by 5.

Table S1. Heat Pump Specification

Outside temperature [^{o}C]	Capacity [kW]	COP
-15	3.15	1.46
-10	4	1.77
-7	4.4	1.98
2	5	2.47
7	6	3.32
12	7.07	3.63
15	7.54	3.89
20	8.04	4.19
25	8.54	4.49
30	9.04	4.79
35	9.54	5.09

Therefore, a variation in the COP is recognized with the variation in the outside temperature. Figure S1 represents the time-dependent COP data in the first plot

which is used for calculating heat pump thermal power. Furthermore, the second plot represents the variation of COP with the variation in the outside temperature.

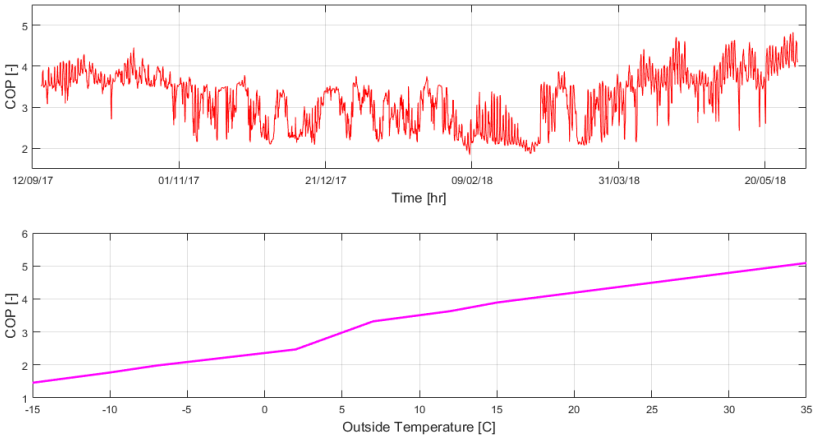

Figure VII-S1: Heat pump performance factor and its relative outside temperature

Finally, the measured heat pump electricity consumption data and the time-dependent COP data in first plot of Figure S2 is utilized to estimate the thermal power of the heat pump through the following formula ($HP\ Power_{thermal} = COP(time) * HP\ Power_{electric}$), where the thermal power of heat pump is obtained and it is represented in the second plot.

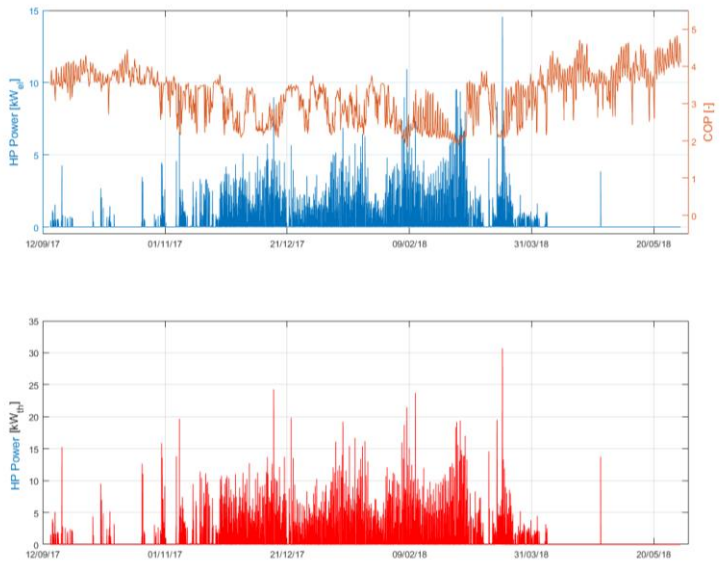

Figure VII-S2: The electric and thermal heat pump power

VII.9 References

[1] G. Brundtland, M. Khalid, S. Agnelli, S. Al-Athel, B. Chidzero, L. Fadika, V.Hauff, I. Lang, M. Shijun MM de B. The Brundtland Report: “Our Common Future.” vol. 4. 1988. doi:10.1080/07488008808408783.

[2] European Energy Agency. Final energy consumption by sector and fuel. Denmark: 2017. doi:CSI 027/ENER 016.

[3] European Environment Agency. Annual European Union greenhouse gasinventory 1990–2016 and inventory report 2018. Copenhagen: 2018.

[4] Dodd N, Donatello S, Garbarino E, Gama Caldas M. Identifying macro-objectives for the life cycle environmental performance and resource efficiency of EU buildings. 2015. doi:10.2791/975886.

[5] European Commission 6317. Towards an Integrated Strategic Energy Technology (SET) Plan: Accelerating the European Energy System Transformation. vol. 151. 2015. doi:10.1145/3132847.3132886.

[6] Boot PA. Energy efficiency obligations in the Netherlands: A role for white certificates? 2009.

[7] NEN (Nederlands Normalisatie-instituut). NEN7120+C2 Energieprestatie van gebouwen –Bepalingsmethode. 2017.

[8] Beuken R. mplementing the Energy Performance of Buildings Directive (EPBD) - Netherlands Country Report 2012. 2012.

[9] Lu Y, Wang S, Yan C, Huang Z. Robust optimal design of renewable energy system in nearly/net zero energy buildings under uncertainties. Appl Energy 2017;187:62–71. doi:10.1016/j.apenergy.2016.11.042.

[10] Guerra-Santin O, Tweed C, Jenkins H, Jiang S. Monitoring the performance of low energy dwellings: Two UK case studies. Energy Build 2013;64:32–40. doi:10.1016/j.enbuild.2013.04.002.

[11] Stazi F, Vegliò A, Di Perna C, Munafò P. Experimental comparison between 3 different traditional wall constructions and dynamic simulations to identify optimal thermal insulation strategies. Energy Build 2013;60:429–41. doi:10.1016/j.enbuild.2013.01.032.

[12] Terés-Zubiaga J, Campos-Celador A, González-Pino I, Escudero-Revilla C. Energy and economic assessment of the envelope retrofitting in residential buildings in Northern Spain. Energy Build 2015;86:194–202. doi:10.1016/j.enbuild.2014.10.018.

[13] Hillary J, Walsh E, Shah A, Zhou R, Walsh P. Guidelines for developing

efficient thermal conduction and storage models within building energy simulations. Energy 2017;125:211–22. doi:10.1016/j.energy.2017.02.127.

[14] Monteiro H, Fernández JE, Freire F. Comparative life-cycle energy analysis of a new and an existing house: The significance of occupant's habits, building systems and embodied energy. Sustain Cities Soc 2016;26:507–18. doi:10.1016/j.scs.2016.06.002.

[15] Spandagos C, Ng TL. Equivalent full-load hours for assessing climate change impact on building cooling and heating energy consumption in large Asian cities. Appl Energy 2017;189:352–68. doi:10.1016/j.apenergy.2016.12.039.

[16] Shen P, Lior N. Vulnerability to climate change impacts of present renewable energy systems designed for achieving net-zero energy buildings. Energy 2016;114:1288–305. doi:10.1016/j.energy.2016.07.078.

[17] Bertagnolio S. Evidence-based Model Calibration for Efficient Building EnergyServices. University of Liège, 2012.

[18] Eisenhower B, O'Neill Z, Narayanan S, Fonoberov VA, Mezić I. A methodology for meta-model based optimization in building energy models. Energy Build 2012;47:292–301. doi:10.1016/j.enbuild.2011.12.001.

[19] Jiménez MJ, Madsen H, Andersen KK. Identification of the main thermal characteristics of building components using MATLAB. Build Environ 2008;43:170–80. doi:10.1016/j.buildenv.2006.10.030.

[20] Shen P, Braham W, Yi Y. Development of a lightweight building simulation tool using simplified zone thermal coupling for fast parametric study. Appl Energy 2018;223:188–214. doi:10.1016/j.apenergy.2018.04.039.

[21] Ji Y, Xu P, Duan P, Lu X. Estimating hourly cooling load in commercial buildings using a thermal network model and electricity submetering data 2016;169:309–23.

[22] Berthou T, Stabat P, Salvazet R, Marchio D. Development and validation of a gray box model to predict thermal behavior of occupied office buildings. Energy Build 2014;74:91–100. doi:10.1016/j.enbuild.2014.01.038.

[23] Terés-Zubiaga J, Escudero C, García-Gafaro C, Sala JM. Methodology for evaluating the energy renovation effects on the thermal performance of social housing buildings: Monitoring study and grey box model development. Energy Build 2015;102:390–405. doi:10.1016/j.enbuild.2015.06.010.

[24] Asadi E, Da Silva MG, Antunes CH, Dias L. Multi-objective optimization for building retrofit strategies: A model and an application. Energy Build 2012;44:81–7. doi:10.1016/j.enbuild.2011.10.016.

[25] Liao Z, Dexter AL. A simplified physical model for estimating the average air temperature in multi-zone heating systems. Build Environ 2004;39:1013–22. doi:10.1016/j.buildenv.2004.01.034.

[26] De Wilde P. The gap between predicted and measured energy performance of buildings: A framework for investigation. Autom Constr 2014;41:40–9. doi:10.1016/j.autcon.2014.02.009.

[27] Coakley D, Raftery P, Keane M. A review of methods to match building energy simulation models to measured data. Renew Sustain Energy Rev 2014;37:123–41. doi:10.1016/j.rser.2014.05.007.

[28] Asadi S, Mostavi E, Boussaa D, Indaganti M. Building energy model calibration using automated optimization-based algorithm. Energy Build 2019;198:106–14. doi:10.1016/j.enbuild.2019.06.001.

[29] Lam KP, Zhao J, Ydstie EB, Wirick J, Qi M, Park J. An energyplus whole building energy model calibration method for office buildings using occupant behavior data mining and empirical data. 2014 ASHRAE/IBPSA-USA Build. Simul. Conf., 2014, p. 160–7.

[30] Riddle M, Muehleisen RT. A guide to Bayesian calibration of building energy models. 2014 ASHRAE/IBPSA-USA Build Simul Conf 2014:276–83. doi:10.13140/2.1.1674.9127.

[31] Booth AT, Choudhary R, Spiegelhalter DJ. A hierarchical bayesian framework for calibrating micro-level models with macro-level data. J Build Perform Simul 2013;6:293–318. doi:10.1080/19401493.2012.723750.

[32] Wang S, Sun X, Lall U. A hierarchical Bayesian regression model for predicting summer residential electricity demand across the U.S.A. Energy 2017;140:601–11. doi:10.1016/j.energy.2017.08.076.

[33] Eisenhower B, O'Neill Z, A. Fonoberov V, Mezic I. Uncertainty and sensitivity decomposition of building energy models. J Build Perform Simul 2012;5:1–18. doi:10.1080/1940149YYxxxxxxxx.

[34] Yang T, Pan Y, Mao J, Wang Y, Huang Z. An automated optimization method for calibrating building energy simulation models with measured data: Orientation and a case study. Appl Energy 2016;179:1220–31. doi:10.1016/j.apenergy.2016.07.084.

[35] Sun J, Reddy TA. Calibration of building energy simulation programs using the analytic optimization approach (RP-1051). HVAC R Res 2006;12:177–96. doi:10.1080/10789669.2006.10391173.

[36] Monetti V, Davin E, Fabrizio E, André P, Filippi M. Calibration of building

energy simulation models based on optimization: A case study. Energy Procedia 2015;78:2971–6. doi:10.1016/j.egypro.2015.11.693.

[37] Wetter M. GenOpt. Generic Optimization Program. User Manual. California: 2011. doi:10.2172/962948.

[38] Liu S, Henze GP. Calibration of building models for supervisory control of commercial buildings. IBPSA 2005 - Int Build Perform Simul Assoc 2005 2005:641–8.

[39] Stoppel CM, Leite F. Integrating probabilistic methods for describing occupant presence with building energy simulation models. Energy Build 2014;68:99–107. doi:10.1016/j.enbuild.2013.08.042.

[40] Neill ZO, Niu F. Uncertainty and sensitivity analysis of spatio-temporal occupant behaviors on residential building energy usage utilizing Karhunen-ve expansion Lo e. Build Environ 2017;115:157–72. doi:10.1016/j.buildenv.2017.01.025.

[41] Koene FGH, Bakker LG, Lanceta D, Narmsara S. SIMPLIFIED BUILDING MODEL OF DISTRICTS. Fifth Ger. IBPSA Conf., Aachen: RWTH Aachen University; 2014, p. 152–9.

[42] Heo Y. BAYESIAN CALIBRATION OF BUILDING ENERGY MODELS FOR ENERGY RETROFIT DECISION-MAKING UNDER UNCERTAINTY. Georgia Institute of Technology, 2011.

[43] Larsen TS, Heiselberg P. Single-sided natural ventilation driven by wind pressure and temperature difference 2008;40:1031–40. doi:10.1016/j.enbuild.2006.07.012.

[44] Heo Y, Choudhary R, Augenbroe GA. Calibration of building energy models for retrofit analysis under uncertainty 2012;47:550–60. doi:10.1016/j.enbuild.2011.12.029.

[45] Mustafaraj G, Marini D, Costa A, Keane M. Model calibration for building energy efficiency simulation 2014;130:72–85. doi:10.1016/j.apenergy.2014.05.019.

[46] Raftery P, Keane M, Costa A. Calibrating whole building energy models : Detailed case study using hourly measured data. Energy Build 2011;43:3666–79. doi:10.1016/j.enbuild.2011.09.039.

[47] Kaplan MB, McFerran J, Jansen J PR. Reconciliation of a DOE2.1c model with monitored end-use data for a small office building. ASHRAE Trans, 1990, p. 981–93.

[48] Reddy TA MI. Procedures for reconciling computer-calculated results with measured energy data. Research Project 1051-RP. 2006.

[49] Østergård T, Jensen RL, Maagaard SE. Building simulations supporting decision making in early design – A review. Renew Sustain Energy Rev 2016;61:187–201. doi:10.1016/j.rser.2016.03.045.

[50] Chowdhury S, Champagne P, Mclellan PJ. Uncertainty characterization approaches for risk assessment of DBPs in drinking water : A review. J Environ Manage 2009;90:1680–91. doi:10.1016/j.jenvman.2008.12.014.

[51] Eames M, Ramallo-gonzalez AP, Wood M. An update of the UK ' s test reference year : The implications of a revised climate on building design. Build Serv Eng 2015;37:316–33. doi:10.1177/0143624415605626.

[52] Hong T, Chang W, Lin H. A fresh look at weather impact on peak electricity demand and energy use of buildings using 30-year actual weather data. Appl Energy 2013;111:333–50. doi:10.1016/j.apenergy.2013.05.019.

[53] Heo Y, Wilde P De, Li Z, Yan D, Park CS. A review of uncertainty analysis in building energy assessment. Renew Sustain Energy Rev 2018;93:285–301. doi:10.1016/j.rser.2018.05.029.

[54] Kaplanis SÃ, Kaplani E. A model to predict expected mean and stochastic hourly global solar radiation I (h ; n j) values 2007;32:1414–25. doi:10.1016/j.renene.2006.06.014.

[55] Vela S. A review of wind speed probability distributions used in wind energy analysis Case studies in the Canary Islands 2009;13:933–55. doi:10.1016/j.rser.2008.05.005.

[56] Cai YP, Huang GH, Yang ZF, Lin QG, Tan Q. Community-scale renewable energy systems planning under uncertainty — An interval chance-constrained programming approach 2009;13:721–35. doi:10.1016/j.rser.2008.01.008.

[57] Huang P, Huang G, Wang Y. HVAC system design under peak load prediction uncertainty using multiple-criterion decision making technique. Energy Build 2015;91:26–36. doi:10.1016/j.enbuild.2015.01.026.

[58] Silva AS, Ghisi E. Uncertainty analysis of user behaviour and physical parameters in residential building performance simulation. Energy Build 2014;76:381–91. doi:10.1016/j.enbuild.2014.03.001.

[59] CORRADO V, MECHRI HE. Uncertainty and Sensitivity Analysis for Building Energy Rating. J Build Phys 2009;00. doi:10.1177/1744259109104884.

[60] Hoes P, Hensen JLM, Loomans MGLC, Vries B De, Bourgeois D. User

behavior in whole building simulation 2009;41:295–302. doi:10.1016/j.enbuild.2008.09.008.

[61] Zhang S, Sun Y, Cheng Y, Huang P, Olaide M, Lin Z. Response-surface-model-based system sizing for Nearly / Net zero energy buildings under uncertainty. Appl Energy 2018;228:1020–31. doi:10.1016/j.apenergy.2018.06.156.

[62] Tian W. Identification of key factors for uncertainty in the prediction of the thermal performance of an office building under climate change 2009:157–74. doi:10.1007/s12273-009-9116-1.

[63] Smith A, Luck R, Mago PJ. Analysis of a combined cooling , heating , and power system model under different operating strategies with input and model data uncertainty. Energy Build 2010;42:2231–40. doi:10.1016/j.enbuild.2010.07.019.

[64] Hong T, Taylor-lange SC, Oca SD, Yan D, Corgnati SP. Advances in research and applications of energy-related occupant behavior in buildings ☪. Energy Build 2016;116:694–702. doi:10.1016/j.enbuild.2015.11.052.

[65] Re F, Manfren M, Chiara L, Luigi A, Ciribini C, Angelis E De. Probabilistic behavioral modeling in building performance simulation : A Monte Carlo approach. Energy Build 2017;148:128–41. doi:10.1016/j.enbuild.2017.05.013.

[66] Bahaj ASÃ, James PAB. Urban energy generation : The added value of photovoltaics in social housing 2007;11:2121–36. doi:10.1016/j.rser.2006.03.007.

[67] Sun Y, Huang P, Huang G. A multi-criteria system design optimization for net zero energy buildings under uncertainties. Energy Build 2015;97:196–204. doi:10.1016/j.enbuild.2015.04.008.

[68] Tian W. A review of sensitivity analysis methods in building energy analysis. Renew Sustain Energy Rev 2013;20:411–9. doi:10.1016/j.rser.2012.12.014.

[69] Saltelli A, Tarantola S, Campolongo F RM. Sensitivity analysis in practice: a guide to assessing scientific models. John Wiley & Sons, Inc; 2004.

[70] Sohier H, Piet-lahanier H, Farges J. Acta Astronautica Analysis and optimization of an air-launch-to-orbit separation. Acta Astronaut 2015;108:18–29. doi:10.1016/j.actaastro.2014.11.043.

[71] Kucherenko S, Albrecht D, Saltelli A. Exploring multi-dimensional spaces: a Comparison of Latin Hypercube and Quasi Monte Carlo Sampling Techniques. 8th IMACS Semin. Monte Carlo methods, 2015, p. 1–32.

doi:10.1016/j.ress.2017. 04.003.

[72] Chong A, Menberg K. Guidelines for the Bayesian calibration of building energy models. Energy Build 2018;174:527–47.

[73] Kennedy MC, O'Hagan A, Higgins N. Bayesian Analysis of Computer Code Outputs. Quant Methods Curr Environ Issues 2011:227–43. doi:10.1007/978-1-4471-0657-9_11.

[74] Amasyali K, El-gohary NM. A review of data-driven building energy consumption prediction studies 2018;81:1192–205. doi:10.1016/j.rser.2017.04.095.

[75] ISO. Moderate thermal environments- Determination of the PMV and PPD indices and specification of the conditions for thermal comfort: ISO7730. 1994.

[76] Abokersh MH, Vallès M, Cabeza LF, Boer D. A framework for the optimal integration of solar assisted district heating in different urban sized communities : A robust machine learning approach incorporating global sensitivity analysis. Appl Energy 2020;267:114903. doi:10.1016/j.apenergy.2020.114903.

[77] Uusitalo L, Lehikoinen A, Helle I, Myrberg K. An overview of methods to evaluate uncertainty of deterministic models in decision support. Environ Model Softw 2015;63:24–31. doi:10.1016/j.envsoft.2014.09.017.

[78] Petropoulos G, Wooster MJ, Carlson TN, Kennedy MC, Scholze M. A global Bayesian sensitivity analysis of the 1d SimSphere soil-vegetation-atmospheric transfer (SVAT) model using Gaussian model emulation. Ecol Modell 2009;220:2427–40. doi:10.1016/j.ecolmodel.2009.06.006.

[79] Koo C, Hong T, Lee M, Seon Park H. Development of a new energy efficiency rating system for existing residential buildings. Energy Policy 2014;68:218–31. doi:10.1016/j.enpol.2013.12.068.

[80] NEN. NEN 1087:2001- Ventilatie van gebouwen: Bepalingsmethoden voor nieuwbouw. 2001.

[81] Zeiler W, Gvozdenović K, de Bont K, Maassen W. Toward cost-effective nearly zero energy buildings: The Dutch Situation. Sci Technol Built Environ 2016;22:911–27. doi:10.1080/23744731.2016.1187552.

Chapter VII

APPENDIX

VIII. APPENDIX

VIII.1 List of publications

Click on the icons below to go to the author's profiles.

Author's ORCID: orcid.org/0000-0002-0215-5167

VIII.1.1 Research articles

[1]. MH Abokersh, S Gangwar, M Spiekman, M Vallès, L Jiménez, LF Cabeza, D Boer, "Sustainable Insights on Emerging Solar District Heating Technologies to Boost the Nearly Zero Energy Building Concept," Renewable Energy, May 2021, (Under review). Area: Energy engineering and Power technology/Renewable Energy, sustainability, and environment (Q1). Impact Factor: 6.274.

[2] MH Abokersh, M Norouzi, M Vallès, LF Cabeza, C Prieto, D Boer, "A Framework for Sustainable Evaluation of Thermal Energy Storage in Circular Economy", Renewable Energy, May 2021, (Under review). Area: Renewable Energy, sustainability, and environment (Q1). DOI: 10.1016/j.renene.2021.04.136. Impact Factor: 6.274.

[3]. MH Abokersh, K Saikia, LF Cabeza, D Boer, M Vallès, "Techno-Economic Analysis for Control Strategies of Heat Pump Integrated into Solar District Heating System," Journal of Energy Storage, September 2020, (Under review). Area: Energy engineering and Power technology (Q1). Impact Factor: 3.76.

[4]. MH Abokersh, M Spiekman, O Vijlbrief, M Vallès, D Boer, "A Real-time Diagnostic Tool for Evaluating the Thermal Performance of Nearly Zero Energy buildings," Applied Energy, January 2021, vol.281. Area: Energy / Building and construction (Q1). DOI: 10.1016/j.apenergy.2020.116091. Impact Factor: 8.84.

[5]. MH Abokersh, LF Cabeza, D Boer, M Vallès, "Flexible Heat Pump Integration to Improve the Sustainable Transition Toward 4th Generation District Heating," Energy Conversion and Management Journal, December 2020, vol.225. Area: Energy engineering and Power technology/Renewable Energy, sustainability, and environment (Q1). DOI: 10.1016/j.enconman.2020.113379. Impact Factor: 8.208.

[6]. MH Abokersh, M Vallès, LF Cabeza, D Boer, "A Framework for the Optimal Integration of Solar Assisted District Heating in Different Urban Sized Communities: A Robust Machine Learning Approach Incorporating Global Sensitivity Analysis". Applied Energy, June 2020, vol.267. Area: Renewable Energy, sustainability, and environment (Q1). DOI: 10.1016/j.apenergy.2020.114903. Impact Factor: 8.84.

[7]. V Tulus, MH Abokersh, LF Cabeza, M Vallès, L Jiménez, D Boer, "Economic and Environmental Potential for Solar Assisted Central Heating Plants in the EU Residential Sector: Contribution to the 2030 Climate and Energy EU Agenda," Applied Energy, February 2019, vol.236. Area: Renewable Energy, sustainability, and environment (Q1). DOI: 10.1016/j.apenergy.2018.11.094. Impact Factor: 8.84.

VIII.1.2 Book Chapters

[1]. Dieter Boer, MH Abokersh, "Sustainability aspects of Thermal Energy Storage," Encyclopedia of Energy Storage, Elsevier, 2020. DOI: 10.1016/B978-0-12-819723-3.00003-2.

[2]. MH Abokersh, M Vallès, L Jiménez, D Boer, "Cost-Effective Processes of Solar District Heating System Based on Optimal Artificial Neural Network". Computer Aided Chemical Engineering, 2020, Vol. 48, 403-408, DOI: 10.1016/B978-0-12-823377-1.50068-9.

VIII.2 Scientific conferences participations

VIII.2.1 Oral communications

[1]. MH Abokersh, LF Cabeza, M Vallès, D Boer "An insight into challenges associate with seasonal storage in solar district heating systems," ENERSTOCK 2021, June 2021.

[2]. MH Abokersh, LF Cabeza, M Vallès, D Boer, "A Multicriteria Approach to Evaluate Solar Assisted District Heating in the German Market," 14th International Conference on Energy Sustainability (ASME 2020), June 2020. DOI: 10.1115/ES2020-1668.

[3]. MH Abokersh, M Vallès, L Jiménez, D Boer, "Cost-Effective Processes of Solar District Heating System Based on Optimal Artificial Neural Network," 30th European Symposium on Computer Aided Process Engineering (ESCAPE 2020), May 2020. DOI: 10.1016/B978-0-12-823377-1.50068-9.

[4]. MH Abokersh, M Vallès, LF Cabeza, D Boer, "Challenges Associated with the Construction and Operation of Seasonal Storage for A Small Solar District Heating

System: A Multi-Objective Optimization Approach," 14th International Renewable Energy Storage Conference (IRES 2020), March 2020. DOI: 10.2991/ahe.k.210202.023.

[5]. MH Abokersh, V Tulus, LF Cabeza, M Vallès, L Jiménez, D Boer, "A Sustainable Pathway for the Deployment of Central Solar Heating Plant Coupled with Seasonal Storage in Spain," XI National and II International Engineering Thermodynamics Congress (CNIT 11), June 2019.

VIII.2.2 Poster presentations

[1]. MH Abokersh, M Vallès, LF Cabeza, D Boer, "The Community Size Effect on the Techno-Economic Performance of Solar District Heating Systems," 14th International Renewable Energy Storage Conference (IRES 2020), March 2020. DOI: 10.2991/ahe.k.210202.021.

[2]. MH Abokersh, M Vallès, D Boer. "Tackling the challenges facing the deployment of solar assisted central heating plants in Mediterranean conditions: A multi-objective optimization approach," URV doctoral day, May 2019.

VIII.3 Master thesis co-supervision

Title: "The potential barriers for the Solar-assisted Heat Pump: From Building to Neighbourhood Scale", JF Fernández, Supervisors: D Boer, MH Abokersh, Master of Industrial Engineering, Universitat Rovira i Virgili (2019-2020).

VIII.APPENDIX

UNIVERSITAT ROVIRA I VIRGILI
DECISION MAKING TOOLS FOR SUSTAINABLE TRANSITION TOWARD LOW CARBON ENERGY TECHNOLOGIES IN THE RESIDENTIAL SECTOR
Mohamed Abokersh

UNIVERSITAT ROVIRA i VIRGILI

Decision Making Tools for Sustainable Transition Toward Low Carbon Energy Technologies in the Residential Sector

Aligning with the ambitious EU 2030 climate and energy package for cutting the greenhouse emissions and replacing conventional heat sources through the presence of renewable energy share to achieve net-zero-energy community, the stakeholders at residential sector are facing several technical, economic, and environmental issues to meet the EU targets in the near future.

This thesis is focusing on two key structural transformations needed for sustainable transition towards clean energy production: the low carbon energy technologies problem represented by the solar district heating systems coupled with seasonal energy storage, and its application to achieve Nearly Zero Energy Buildings. The Tackling for these challenges is instigated through using design and optimization of clean energy systems incorporated with machine learning and data analysis to develop Computer-Aided Process Engineering tools. These tools would help in addressing the stakeholder's challenges, thus contributing to the transition towards a more sustainable future.